

1. Report No. FHWA/TX-13/0-6152-2	2. Government Accession No.	3. Recipient's Catalog No.	
4. Title and Subtitle SHEAR IN HIGH STRENGTH CONCRETE BRIDGE GIRDERS: TECHNICAL REPORT		5. Report Date Published: April 2013	
		6. Performing Organization Code	
7. Author(s) Emad L. Labib, Hemant B. Dhonde, Rachel Howser, Y. L. Mo, Thomas T. C. Hsu, and Ashraf Ayoub		8. Performing Organization Report No. Report 0-6152-2	
9. Performing Organization Name and Address Department of Civil & Environmental Engineering Cullen College of Engineering University of Houston 4800 Calhoun Road Houston, TX 77204-4003		10. Work Unit No. (TRAIS)	
		11. Contract or Grant No. Project 0-6152	
12. Sponsoring Agency Name and Address Texas Department of Transportation Research and Technology Implementation Office P. O. Box 5080 Austin, Texas 78763-5080		13. Type of Report and Period Covered Technical Report September 2008–August 2012	
		14. Sponsoring Agency Code	
15. Supplementary Notes Project performed in cooperation with the Texas Department of Transportation and the Federal Highway Administration Project Title: Shear in High Strength Concrete Bridge Girders URL: http://tti.tamu.edu/documents/0-6152-2.pdf			
16. Abstract <p>Prestressed Concrete (PC) I-girders are used extensively as the primary superstructure components in Texas highway bridges. A simple semi-empirical equation was developed at the University of Houston (UH) to predict the shear strength of PC I-girders with normal strength concrete through the project TxDOT 0-4759. The UH-developed equation is a function of shear span to effective depth ratio, concrete strength, web area and amount of transverse steel. This report intends to (1) validate the UH-developed equation for high strength concrete by testing ten 25-foot long full-scale PC I-girders with different concrete strength. (2) validate the UH-developed equation for different sizes of PC girders and studying the possibility of having premature failure due to local failure in end zone.</p> <p>Ten modified Tx28 PC girders were tested for the first objective. The girders were divided into three groups (namely Groups A, C and F) based on the concrete compressive strength. Group A consisted of two girders with a concrete compressive strength of 7000 psi. Group F had four girders with a concrete compressive strength of 13000 psi and Group C included four girders with a compressive strength 16,000 psi. Girders in Group A were designed to have a balanced condition in shear. A pair of girders each belonging to Group F and Group C were designed to have a balanced condition while remaining girders were designed as over-reinforced sections. Each group of the PC girders was tested with different shear span to effective depth ratio so as to get two types of shear failure modes, i.e., web-shear and flexure-shear. The validity of the proposed UH-developed equation was ascertained using the girders test results. UH-developed equation was found to accurately predict the ultimate shear strength of PC girders having concrete strength up to 17,000 psi with enough ductility.</p> <p>Six PC girders of Tx-series with three different sizes were tested for the second objective. The girders were divided into three groups (namely Groups D, E and G) based on the girder depth. The test data shows that the PC girders of the new Tx-series has no cracks under service loads and can reach the maximum shear capacity without having a shear bond failure. Also, these girders' test results ensured the validity of the UH-developed equations for PC girders with different sizes.</p> <p>Simulation of Concrete Structures (SCS), a finite element program recently developed at UH, was used to predict the shear behavior of the tested girders. Analytical results presented in this report proved the validity of SCS to predict the behavior of PC girders with different concrete strength up to 17,000 psi and with different depth up to 70 inches.</p>			
17. Key Word Girders, Constitutive Laws, Shear Provisions, Prestressed Concrete, High-Strength Concrete, Membrane Elements, Full-Scale Tests, Design Equation, End Zone, Bond Failure, Slip		18. Distribution Statement No restrictions. This document is available to the public through NTIS: National Technical Information Service Alexandria, Virginia 22312 www.ntis.gov and University of Houston, Houston, Texas 77204 www.egr.uh.edu/structuralallab/	
19. Security Classif. (of this report) Unclassified	20. Security Classif. (of this page) Unclassified	21. No. of Pages 300	22. Price

SHEAR IN HIGH STRENGTH CONCRETE BRIDGE GIRDERS: TECHNICAL REPORT

by

Emad L. Labib
Research Assistant

Hemant B. Dhonde
Research Assistant Professor

Rachel Howser
Research Assistant

Y. L. Mo
Professor

Thomas T. C. Hsu
Moore Professor

and

Ashraf Ayoub
Associate Professor

Technical Report 0-6152-2

Project 0-6152

Project Title Shear in High Strength Concrete Bridge Girders

Performed in cooperation with the
Texas Department of Transportation
and the
Federal Highway Administration

Published: April 2013

Department of Civil and Environmental Engineering
University of Houston
Houston, Texas

Disclaimer

This research was performed in cooperation with the Texas Department of Transportation and the U.S. Department of Transportation, Federal Highway Administration. The contents of this report reflect the views of the authors, who are responsible for the facts and accuracy of the data presented herein. The contents do not necessarily reflect the official view or policies of the FHWA or TxDOT. This report does not constitute a standard, specification, or regulation, nor is it intended for construction, bidding, or permit purposes. Trade names were used solely for information and not product endorsement.

Acknowledgments

This research, Project 0-6152, was conducted in cooperation with the Texas Department of Transportation and the U.S. Department of Transportation, Federal Highway Administration. The project monitoring committee consisted of Kenneth Ozuna (Project Coordinator), Mathew Connelly (Project Director), Wade Odell (Research Engineer), John Holt (Member), Albert Fan (Member), Yongqian Lin (Member), Nicholas Horiszny (Member).

The researchers would like to thank the Texas Concrete Company, Victoria, Texas, the Flexicore of Texas Company, Houston, Texas, and Texas Concrete Partners, Elm Mott, Texas for continued co-operation during this project.

TABLE OF CONTENTS

List of Figures	x
List of Tables	xv
Chapter 1 Introduction	1
1.1. Overview of Research	1
1.2. Research Significance	3
1.3. Objectives of Research	5
1.4. Outline of Report	6
Chapter 2 Literature Review	9
2.1. High Strength Concrete	9
2.2. Shear Design Provisions of Prestressed Girders in Current Codes	10
2.2.1. Shear Provisions of ACI Building Code	10
2.2.2. Shear Provisions of AASHTO LRFD Specifications	12
2.3. Shear Design Provisions of Prestressed Girders at University of Houston	13
2.4. Shear Tests of PC Girders in Literature	19
2.5. Shear-bond Studies and Background in Literature	26
2.6. Transverse Reinforcement in End Zone in Pretension Prestressed Girders	28
2.7. Effect of Top Flange Geometry on the Shear Behavior	29
2.8. Background on Used Finite Element Model	30
2.8.1. ConcreteL01	31
2.8.2. SteelZ01	34
2.8.3. TendonL01	36
Part I: Maximum Shear Strength As A Function of Concrete Strength	39
Chapter 3 Experimental Program To Study Maximum Shear Strength As A	
 Function of Concrete Strength	41
3.1. Introduction	41
3.2. Tested Girders	41
3.3. Manufacturing of Test Girders	55
3.4. Test Set-up	58
3.5. Instrumentation	59
Chapter 4 Analysis of Maximum Shear Strength	67
4.1. Introduction	67
4.2. Experimental Results of Group A Girders with $f'_c \cong 7,000 \text{ psi}$	67
4.2.1. Girder A1	67
4.2.2. Girder A2	73
4.3. Experimental Results of Group F Girders with $f'_c \cong 13,000 \text{ psi}$	81
4.3.1. Girder F1	81
4.3.2. Girder F2	87
4.3.3. Girder F3	96
4.3.4. Girder F4	102

4.4.	Experimental Results of Group C Girders with $f'_c \cong 16,000 \text{ psi}$	110
4.4.1.	Girder C1	110
4.4.2.	Girder C2	118
4.4.3.	Girder C3	126
4.4.4.	Girder C4	133
4.5.	Maximum Shear Strength for High Strength Concrete Prestressed Girders	141
4.6.	Steel and Concrete Shear Contributions	143
Chapter 5	Simulation of Prestressed Concrete I-Girders Failed in Shear	147
5.1.	Introduction	147
5.2.	Analytical Model	148
5.3.	Finite Element Model of Girders with Web Shear Failure	150
5.4.	Finite Element Model of Girders with Flexure Shear Failure	157
5.5.	Finite Element Model of Girders with Flexure Failure	160
Part II:	Study of Shear Bond Failure	163
Chapter 6	Experimental Program to Study Shear-Bond Failure	165
6.1.	Introduction	165
6.2.	Tested Girders and Studied Objective	165
6.3.	Manufacturing of Test Girders	180
6.4.	Test Set-up	183
6.5.	Instrumentation	185
Chapter 7	Shear-Bond Failures versus Web-Shear Failure	195
7.1.	Introduction	195
7.2.	Experimental Results of Group G Girders	195
7.2.1.	Girder G1	195
7.2.2.	Girder G2	203
7.3.	Experimental Results of Group D Girders	210
7.3.1.	Girder D1	210
7.3.2.	Girder D2	217
7.4.	Experimental Results of Group E Girders	224
7.4.1.	Girder E1	224
7.4.2.	Girder E2	231
7.5.	Service Load vs. Cracking Load	237
7.6.	Discussion of Shear Force vs. Tendon Slip Curves	237
7.7.	Maximum Shear Strength	239
7.8.	Maximum Shear Strength vs. AASHTO LRFD (2010)	239
7.9.	Proposed Equation for Concrete Contribution in End Zone	240
Chapter 8	Simulation of Full Scale Prestressed Concrete I-Girders Failed in Shear	243
8.1.	Introduction	243
8.2.	Analytical Model	243
8.3.	Finite Element Model of Group G Girders	244
8.4.	Finite Element Model of Group D Girders	249
8.5.	Finite Element Model of Group E Girders	254
8.6.	Finite Element Analysis Using Fiber Elements	259

Chapter 9	Design Recommendation and Design Examples	261
9.1.	Introduction	261
9.2.	Design Recommendation	261
9.3.	Design Examples	264
9.3.1.	Example 1	264
9.3.2.	Example 2	268
Chapter 10	Conclusions	273
10.1.	Final Summary	273
10.2.	Major Conclusions	274
10.3.	Suggestions for Future Work	275
References		277

LIST OF FIGURES

Fig. 1.1 Prestressed Concrete I-Girders	2
Fig. 1.2 Shear Failure Modes in I-Girders	2
Fig. 1.3 Variation of Maximum Shear Strength $V_{n,max}$ with Concrete Strength f'_c	4
Fig. 1.4 Experimental Program Specimens Matrix.....	5
Fig. 2.1 Determination of Number of Stirrups for Contribution of Steel V_s According to ACI 318 (2011).....	11
Fig. 2.2 Loov's Analytical Model Used for Calculating Shear Capacities of Beams.....	16
Fig. 2.3 Determination of Number of Stirrups for Contribution of Steel V_s	18
Fig. 2.4 ConcreteL01 Material Module	31
Fig. 2.5 Cyclic Smeared Stress-Strain Curve of Embedded Mild Steel Bars (Mansour 2001).....	35
Fig. 2.6 SteelZ01 Material Module.....	36
Fig. 2.7 TendonL01 Material Module.....	37
Fig. 3.1 Layout of Tx54 Girders with 8 inches Top Deck	42
Fig. 3.2 Full Scale and Scaled Down Cross-Sections	42
Fig. 3.3 Cross-Section and Reinforcement Details for Modified Tx28 Girders	44
Fig. 3.4 Cross-Section and Reinforcement Details for Modified Tx28 Girders C2 and C4	44
Fig. 3.5 Detailed Longitudinal Cross-Section for Girder A1	47
Fig. 3.6 Detailed Longitudinal Cross-Section for Girder A2.....	48
Fig. 3.7 Detailed Longitudinal Cross-Section for Girder F1	49
Fig. 3.8 Detailed Longitudinal Cross-Section for Girder F2	50
Fig. 3.9 Detailed Longitudinal Cross-Section for Girder F3	51
Fig. 3.10 Detailed Longitudinal Cross-Section for Girder F4	52
Fig. 3.11 Detailed Longitudinal Cross-Section for Girder C1	52
Fig. 3.12 Detailed Longitudinal Cross-Section for Girder C2.....	53
Fig. 3.13 Detailed Longitudinal Cross-Section for Girder C3.....	53
Fig. 3.14 Detailed Longitudinal Cross-Section for Girder C4.....	54
Fig. 3.15 Reinforcement Cage for a Typical Girder	55
Fig. 3.16 Styro-Foam Forms with LVDT Rods	56
Fig. 3.17 Installation of Styro-Foam Forms.....	56
Fig. 3.18 Set-up of Steel Side Forms for Girders.....	56
Fig. 3.19 Concrete Placement Using a Hopper	57
Fig. 3.20 Removing Styro-Foam Forms from the Girders.....	57
Fig. 3.21 Test Setup for Girders.....	58
Fig. 3.22 LVDT Rosette Installed on Girders.....	60
Fig. 4.1 Shear Force vs. Girder Deflection Curves for Girder A1	68
Fig. 4.2 Shear Crack Pattern and Failure Mode of Girder A1	69
Fig. 4.3 Shear Force vs. Concrete Smeared Strains Curves for Girder A1	71
Fig. 4.4 Shear Force vs. Local Transverse Tensile Strain of Girder A1	72
Fig. 4.5 Shear Force vs. Girder Deflection Curves for Girder A2	73

Fig. 4.6 Shear Crack Pattern and Failure Mode of Girder A2	74
Fig. 4.7 Shear Force vs. Concrete Smeared Strains Curves for Girder A2 – First Run.....	77
Fig. 4.8 Shear Force vs. Local Transverse Tensile Strain of Girder A2 – First Run	78
Fig. 4.9 Shear Force vs. Concrete Smeared Strains Curves for Girder A2 – Second Run	79
Fig. 4.10 Shear Force vs. Local Transverse Tensile Strain of Girder A2 - Second Run	80
Fig. 4.11 Shear Force vs. Girder Deflection Curves for Girder F1.....	81
Fig. 4.12 Shear Crack Pattern and Failure Mode of Girder F1	83
Fig. 4.13 Shear Force vs. Concrete Smeared Strains Curves for Girder F1 –First Run.....	84
Fig. 4.14 Shear Force vs. Local Transverse Tensile Strain of Girder F1 – First Run.....	85
Fig. 4.15 Shear Force vs. Concrete Smeared Strains Curves for Girder F1 – Second Run	86
Fig. 4.16 Shear Force vs. Girder Deflection Curves for Girder F2.....	87
Fig. 4.17 Shear Crack Pattern and Failure Mode of Girder F2	90
Fig. 4.18 Shear Force vs. Concrete Smeared Strains Curves for Girder F2 – First Run.....	91
Fig. 4.19 Shear Force vs. Local Transverse Tensile Strain of Girder F2 – First Run.....	92
Fig. 4.20 Shear Force vs. Concrete Smeared Strains of Girder F2 – Second Run.....	93
Fig. 4.21 Shear Force vs. Local Transverse Tensile Strain of Girder F2 – Second Run	94
Fig. 4.22 Shear Force vs. Concrete Smeared Strains of Girder F2 – Third Run.....	95
Fig. 4.23 Shear Force vs. Girder Deflection Curves for Girder F3.....	96
Fig. 4.24 Shear Crack Pattern and Failure Mode of Girder F3	98
Fig. 4.25 Shear Force vs. Concrete Smeared Strains of Girder F3- First Run.....	99
Fig. 4.26 Shear Force vs. Local Transverse Tensile Strain of Girder F3- First Run	100
Fig. 4.27 Shear Force vs. Concrete Smeared Strains of Girder F3- Second Run	101
Fig. 4.28 Shear Force vs. Girder Deflection Curves for Girder F4.....	102
Fig. 4.29 Shear Crack Pattern and Failure Mode of Girder F4	105
Fig. 4.30 Shear Force vs. Concrete Smeared Strains Curves for Girder F4 – First Run.....	106
Fig. 4.31 Shear Force vs. Local Transverse Tensile Strain of Girder F4 – First Run.....	107
Fig. 4.32 Shear Force vs. Concrete Smeared Strains Curves for Girder F4 – Second Run	108
Fig. 4.33 Shear Force vs. Local Transverse Tensile Strain of Girder F4 – Second Run	109
Fig. 4.34 Shear force vs. Net Deflection Curve for Girder C1	111
Fig. 4.35 Shear Crack Pattern and Failure Mode of Girder C1.....	113
Fig. 4.36 Shear Force vs. Concrete Smeared Strains of Girder C1- First Run	114
Fig. 4.37 Shear Force vs. Local Transverse Tensile Strain of Girder C1 – First Run	115
Fig. 4.38 Shear Force vs. Concrete Smeared Strains Curves for Girder C1 – Second Run.....	116
Fig. 4.39 Shear Force vs. Local Transverse Tensile Strain of Girder C1 – Second Run.....	117
Fig. 4.40 Shear Force vs. Girder Deflection Curves for Girder C2	118
Fig. 4.41 Shear Crack Pattern and Failure Mode of Girder C2.....	121
Fig. 4.42 Shear Force vs. Concrete Smeared Strains Curves for Girder C2 – First Run	122
Fig. 4.43 Shear Force vs. Local Transverse Tensile Strain of Girder C2 – First Run	123
Fig. 4.44 Shear Force vs. Concrete Smeared Strains Curves for Girder C2 – Second Run.....	124
Fig. 4.45 Shear Force vs. Local Transverse Tensile Strain of Girder C2 – Second Run.....	125
Fig. 4.46 Shear Force vs. Girder Deflection Curves for Girder C3	126
Fig. 4.47 Shear Crack Pattern and Failure Mode of Girder C3.....	128
Fig. 4.48 Shear Force vs. Concrete Smeared Strains Curves for Girder C3 – First Run	129
Fig. 4.49 Shear Force vs. Local Transverse Tensile Strain of Girder C3 – First Run	130

Fig. 4.50 Shear Force vs. Concrete Smeared Strains Curves for Girder C3 – Second Run.....	131
Fig. 4.51 Shear Force vs. Local Transverse Tensile Strain of Girder C3 – Second Run.....	132
Fig. 4.52 Shear Force vs. Girder Deflection Curves for Girder C4	133
Fig. 4.53 Shear Crack Pattern and Failure Mode of Girder C4.....	136
Fig. 4.54 Shear Force vs. Concrete Smeared Strains Curves for Girder C4 – First Run	137
Fig. 4.55 Shear Force vs. Local Transverse Tensile Strain of Girder C4 – First Run	138
Fig. 4.56 Shear Force vs. Concrete Smeared Strains Curves for Girder C4 – Second Run.....	139
Fig. 4.57 Shear Force vs. Local Transverse Tensile Strain of Girder C4 –Second Run.....	140
Fig. 4.58 Variation of Normalized Ultimate Shear Strength with Concrete Strength.....	142
Fig. 4.59 Variation of the Normalized Concrete Shear Contribution with Shear Span to Effective Depth Ratio a/d for Girders.....	144
Fig. 5.1 Experimental and Analytical Cross Section for Girders A1, A2, F1 to F4, C1, and C3	149
Fig. 5.2 Experimental and Analytical Cross Section for Girders C2 and C4.....	149
Fig. 5.3 Finite Element Mesh of Girder Specimens A1, F1, F3, C1, and C3	151
Fig. 5.4 Finite Element Mesh of Girder Specimens A2.....	151
Fig. 5.5 Finite Element Mesh of Girder Specimen F4.....	152
Fig. 5.6 Section Discretization of NonlinearBeamColumn Elements for Web Shear Girder.....	152
Fig. 5.7 Analytical and Experimental Load-Deflection Curves of Girder A1	153
Fig. 5.8 Analytical and Experimental Load-Deflection Curves of Girder F1.....	154
Fig. 5.9 Analytical and Experimental Load-Deflection Curves of Girder F3.....	154
Fig. 5.10 Analytical and Experimental Load-Deflection Curves of GirderC1	155
Fig. 5.11 Analytical and Experimental Load-Deflection Curves of Girder C3	155
Fig. 5.12 Analytical and Experimental Load-Deflection Curves of Girder A2	156
Fig. 5.13 Analytical and Experimental Load-Deflection Curves of Girder F4.....	156
Fig. 5.14 Finite Element Mesh of Girder Specimens C2 and C4.....	158
Fig. 5.15 Section Discretization of NonlinearBeamColumn Elements for Girder Specimens C2 and C4.....	158
Fig. 5.16 Analytical and Experimental Load-Deflection Curves of Girder C2	159
Fig. 5.17 Analytical and Experimental Load-Deflection Curves of Girder C4	159
Fig. 5.18 Finite Element Mesh of Girder Specimen F2.....	161
Fig. 5.19 Section Discretization of NonlinearBeamColumn Elements for Girder Specimen F2.....	161
Fig. 5.20 Analytical and Experimental Load-Deflection Curves of Girder F2.....	162
Fig. 6.1 Concrete Dimensions and Reinforcement Details for Girder G1	168
Fig. 6.2 Detailed Longitudinal Cross-Sections for Girder G1	169
Fig. 6.3 Concrete Dimensions and Reinforcement Details for Girder D1	170
Fig. 6.4 Detailed Longitudinal Cross-Section for Girder D1.....	171
Fig. 6.5 Concrete Dimensions and Reinforcement Details for Girder E1.....	172
Fig. 6.6 Detailed Longitudinal Cross-Section for Girder E1	173
Fig. 6.7 Concrete Dimensions and Reinforcement Details for Girder G2	174
Fig. 6.8 Detailed Longitudinal Cross-section for Girder G2	175
Fig. 6.9 Concrete Dimensions and Reinforcement Details for Girder D2	176
Fig. 6.10 Detailed Longitudinal Cross-Section for Girder D2.....	177
Fig. 6.11 Concrete Dimensions and Reinforcement Details for Girder E2.....	178
Fig. 6.12 Detailed Longitudinal Cross-Section for Girder E2	179

Fig. 6.13 Reinforcement Cage for a Typical Girder	181
Fig. 6.14 Coupling Nuts Fixed in Steel Forms	181
Fig. 6.15 Concrete Placement Using a Hopper	181
Fig. 6.16 Bed Vibrator Attached to Steel Forms.....	182
Fig. 6.17 Reinforcement Cage for Top Slab	182
Fig. 6.18 Test Setup for Girders.....	183
Fig. 6.19 Details of Loading Set-up	184
Fig. 6.20 Details of Support.....	185
Fig. 6.21 LVDT Rosette Installed on Girders.....	188
Fig. 6.22 LVDTs Names on Selected Tendons to Measure Slip	192
Fig. 6.23 LVDTs to Measure Slip.....	193
Fig. 7.1 Shear Force vs. Beam Deflection Curves for Girder G1	196
Fig. 7.2 Shear Crack Pattern and Failure Mode of Girder G1	198
Fig. 7.3 Shear Force vs. Tendons Slip Curves for Girder G1-North	199
Fig. 7.4 Shear Force vs. Tendons Slip Curves for Girder G1-South	199
Fig. 7.5 Shear Force vs. Concrete Smeared Strains Curves for Girder G1 (North End Test).....	200
Fig. 7.6 Shear Force vs. Concrete Smeared Strains Curves for Girder G1 (South End Test).....	201
Fig. 7.7 Shear Force vs. Local Transverse Tensile Strain of Girder G1 (South End Test).....	202
Fig. 7.8 Shear Force vs. Beam Deflection Curves for Girder G2	203
Fig. 7.9 Shear Crack Pattern and Failure Mode of Girder G2	205
Fig. 7.10 Shear Force vs. Tendons Slip Curves for Girder G2-North.....	206
Fig. 7.11 Shear Force vs. Tendons Slip Curves for Girder G2-South	206
Fig. 7.12 Shear Force vs. Concrete Smeared Strains Curves for Girder G2 (North End Test).....	207
Fig. 7.13 Shear Force vs. Concrete Smeared Strains Curves for Girder G2 (South End Test).....	208
Fig. 7.14 Shear Force vs. Local Transverse Tensile Strain of Girder G2	209
Fig. 7.15 Shear Force vs. Beam Deflection Curves for Girder D1	210
Fig. 7.16 Shear Crack Pattern and Failure Mode of Girder D1	212
Fig. 7.17 Shear Force vs. Tendons Slip Curves for Girder D1-South	213
Fig. 7.18 Shear Force vs. Tendons Slip Curves for Girder D1-North.....	213
Fig. 7.19 Shear Force vs. Concrete Smeared Strains Curves for Girder D1 (South End Test).....	214
Fig. 7.20 Shear Force vs. Concrete Smeared Strains Curves for Girder D1 (North End Test).....	215
Fig. 7.21 Shear Force vs. Local Transverse Tensile Strain of Girder D1	216
Fig. 7.22 Shear Force vs. Girder Deflection Curves for Girder D2	217
Fig. 7.23 Shear Crack Pattern and Failure Mode of Girder D2	219
Fig. 7.24 Shear Force vs. Tendons Slip Curves for Girder D2-South	220
Fig. 7.25 Shear Force vs. Tendons Slip Curves for Girder D2-North.....	220
Fig. 7.26 Shear Force vs. Concrete Smeared Strains Curves for Girder D2 (South End Test).....	221
Fig. 7.27 Shear Force vs. Concrete Smeared Strains Curves for Girder D2 (North End Test).....	222
Fig. 7.28 Shear Force vs. Local Transverse Tensile Strain of Girder D2	223
Fig. 7.29 Shear Force vs. Girder Deflection Curves for Girder E1.....	224
Fig. 7.30 Shear Crack Pattern and Failure Mode of Girder E1	225
Fig. 7.31 Shear Force vs. Tendons Slip Curves for Girder E1-South.....	226
Fig. 7.32 Shear Force vs. Tendons Slip Curves for Girder E1-North.....	226
Fig. 7.33 Shear Force vs. Concrete Smeared Strains Curves for Girder E1 (South End Test).....	228

Fig. 7.34 Shear Force vs. Concrete Smeared Strains Curves for Girder E1 (North End Test)	229
Fig. 7.35 Shear Force vs. Local Transverse Tensile Strain of Girder E1	230
Fig. 7.36 Shear Force vs. Girder Deflection Curves for Girder E2	231
Fig. 7.37 Shear Crack Pattern and Failure Mode of Girder E2	233
Fig. 7.38 Shear Force vs. Tendons Slip Curves for Girder E2-South	234
Fig. 7.39 Shear Force vs. Concrete Smeared Strains Curves for Girder E2 (South End Test)	235
Fig. 7.40 Shear Force vs. Local Transverse Tensile Strain of Girder E2	236
Fig. 7.41 Variation of the Normalized Concrete Shear Contribution with Shear Span to Effective Depth Ratio a/d for Girders	242
Fig. 8.1 Experimental and Analytical Cross Section for Girder G1	245
Fig. 8.2 Experimental and Analytical Cross Section for Girder G2	245
Fig. 8.3 Finite Element Mesh of Girder Specimen G1	246
Fig. 8.4 Finite Element Mesh of Girder Specimen G2	246
Fig. 8.5 Section Discretization of NonlinearBeamColumn Elements for Girder Specimens G1 and G2	247
Fig. 8.6 Analytical and Experimental Load-Deflection Curves of Girder G1	248
Fig. 8.7 Analytical and Experimental Load-Deflection Curves of Girder G2	248
Fig. 8.8 Experimental and Analytical Cross Section for Girder D1	250
Fig. 8.9 Experimental and Analytical Cross Section for Girder D2	250
Fig. 8.10 Finite Element Mesh of Girder Specimens D1 and D2	251
Fig. 8.11 Section Discretization of NonlinearBeamColumn Elements for Girder Specimens D1 and D2	252
Fig. 8.12 Analytical and Experimental Load-Deflection Curves of Girder D1	253
Fig. 8.13 Analytical and Experimental Load-Deflection Curves of Girder D2	253
Fig. 8.14 Experimental and Analytical Cross Section for Girder E1	254
Fig. 8.15 Experimental and Analytical Cross Section for Girder E2	255
Fig. 8.16 Finite Element Mesh of Girder Specimens E1 and E2	256
Fig. 8.17 Section Discretization of NonlinearBeamColumn Elements for Girder Specimens E1 and E2	257
Fig. 8.18 Analytical and Experimental Load-Deflection Curves of Girder E1	258
Fig. 8.19. Analytical and Experimental Load-Deflection Curves of Girder E2	258
Fig. 9.1. Flowchart for UH Shear Design Procedure	263

LIST OF TABLES

Table 3.1 Concrete Mix Proportions Used for Casting Girders.....	43
Table 3.2 Reinforcement Details for Modified Tx28 Girders.....	46
Table 3.3 Strain Gauges Names and Locations.....	60
Table 3.4 LVDTs Names and Locations.....	63
Table 4.1 Test Variables and Ultimate Shear Strength of Girders.....	141
Table 4.2 Calculations of Steel and Concrete Shear Contribution.....	145
Table 6.1 Additional End Zone Reinforcement.....	167
Table 6.2 Strain Gauges Names and Locations	186
Table 6.3 LVDTs Names and Locations.....	189
Table 7.1 Experimental Cracking Load vs. Service Load	237
Table 7.2 Test Variables and Ultimate Shear Strength of Girders.....	239
Table 7.3 Test Variables and Ultimate Shear Strength of Girders.....	240
Table 7.4 Calculations of Steel and Concrete Shear Contribution.....	241
Table 9.1 Full Design of Tx28.....	267
Table 9.2 Full Design of Tx62.....	271

CHAPTER 1 INTRODUCTION

1.1. Overview of Research

The idea of prestressed concrete (PC) structures was first developed and applied by Eugene Freyssinet in France at the beginning of 1900s through the Bernard Arch of 1908 and the bridge over the Allier River at Le Veudre, designed in 1907 and completed in 1912 (Freyssinet 1949). The primary purpose of using PC was to eliminate/reduce cracking at service load and to fully utilize the capacity of high-strength steel. After the Second World War, PC became prevalent due to the needs of reconstruction and the availability of high-strength steel. Today, PC has become the predominant material in highway bridge construction. It is also widely used in the construction of buildings, offshore structures, nuclear reactor vessels, etc.

The developments in new materials and technology in recent years have made it possible to construct and assemble long-span prestressed concrete girders. The use of high strength concrete has gained wide acceptance in the PC industry. Standardization in the design and manufacturing of the precast bridge components has optimized bridge design. Bridge superstructure elements such as the I-girders, double tee and box girders are generally plant-produced precast and prestressed concrete products inheriting the advantages of economy, durability, low maintenance and assured quality. The most commonly used precast/prestressed concrete girder for short-to-medium-spans is the I-girder as shown in Fig. 1.1. An I-girder consists of a top and a bottom flanges with a slender web joining the flanges. The bottom flange and some portion of the web-bottom are reinforced with prestressing tendons; thus the bottom and top flanges build up the flexural strength. The web is reinforced with vertical (transverse) deformed reinforcing bars (rebars), referred to as stirrups, which contribute toward the shear strength of the girder.

In the design of PC girders, an adequate margin of safety must be provided against various modes of failure. Shear failures, the subject of this research work, are generally considered hazardous because the failures could be brittle, giving little or no warning. Shear failures in such girders are generally encountered at two locations as shown in Fig. 1.2: (1) web shear failure near the supports where shear is large and bending moment is small, and (2) flexural-shear failure near the one-third or quarter points of the span where both shear and bending are large or

where the bridge girders are continuous over supports which are generally critical in flexural shear.



Fig. 1.1 Prestressed Concrete I-Girders

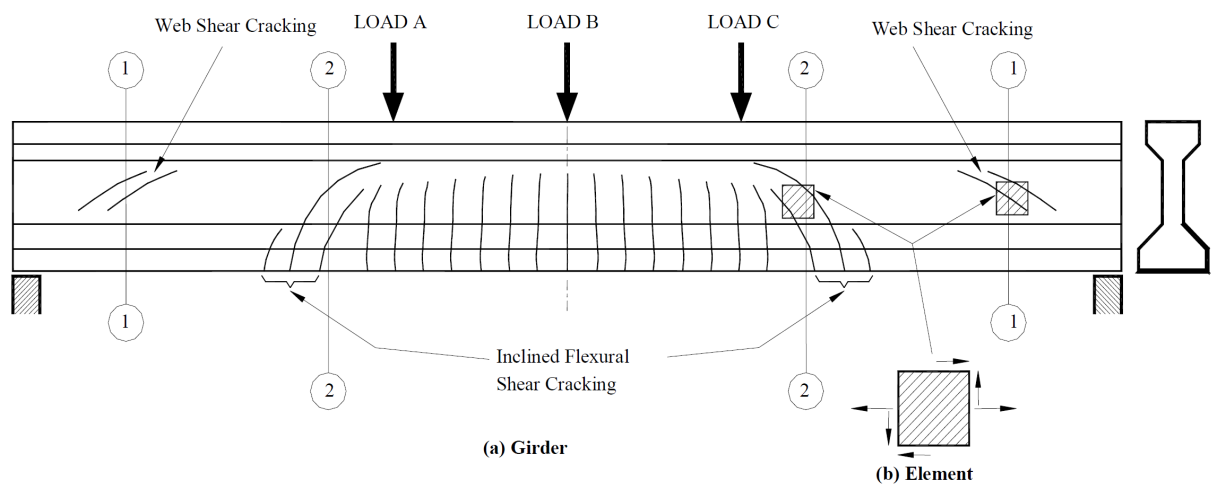


Fig. 1.2 Shear Failure Modes in I-Girders

In addition, two types of failures can occur at each of these two locations. When moderate amounts of web reinforcement are provided, failures are predominantly caused by yielding of the steel leading to some degree of ductility. However, when excessive amounts of web reinforcement are provided, failures are caused by the crushing of the concrete and the failure mode could be very brittle. Thus, there are four possible failures modes in a PC girder: (1) web-shear failure near the support with yielding of steel, (2) Arch-rib failure near the support due to crushing of concrete, (3) flexural-shear failure within the span due to yielding of steel, and (4)

compression-shear failure within the span due to crushing of concrete. In view of the four shear failure modes, the most effective way to associate all the above failure modes with design would be to develop a simple design equation based on a rational theory calibrated by experimental results. It is also essential to implement the analytical models into finite element programs in order to provide an effective tool for the prediction of shear behavior.

This research intends to address one of the most troublesome problems in prestressed concrete, namely shear. All the guidelines for shear design, such as American Concrete Institute (ACI) Codes (ACI 2011) and American Association of State Highway Transportation Officials (AASHTO) Specifications (AASHTO 2010), are complicated and have severe limitations. The problem arises from their deficiency to predict the behavior of PC structures under shear action and the various modes of shear failures. The primary focus of this research would be to develop a simple shear design provisions applicable for high strength concrete PC girders and able to prevent premature failure due to shear-bond failure in end zone of pre-tensioned PC girders.

1.2. Research Significance

High strength concrete (HSC, i.e., concrete compressive strength $f'_c > 8,000$ psi) is increasingly being used in highway bridges to enable PC girders of a given size to support larger loads or longer span. Even if it is not specified, it is frequently provided by the contractor to speed concrete strength development. In the past decade, the National Cooperative Highway Research Program (NCHRP) and the Federal Highway Administration (FHWA) have supported several research projects to extend the application of HSC to highway bridges. To date, design provisions for HSC have been successfully proposed for the AASHTO Load and Resistance Factor Design (LRFD) Bridge Design Specifications (2010) in the areas of axial loads, bending and bond. For shear, the new section 5.8.3.4.3 of the AASHTO LRFD (2010) Specifications allows engineers to return to the pre-1994 shear provisions which were based on the ACI Code based on the recommendations of NCHRP Report 549 (Hawkins et al., 2005).

Both shear design provisions in the ACI Code and the AASHTO Specifications are derived empirically for normal strength concrete (up to 8000 psi) only. Because of their empirical origins and complicated expressions, it is nearly impossible to extend the current design provisions for application to HSC. Recently, a rational approach was developed at the University of Houston to estimate the maximum shear strength based on the extensive studies of two-dimensional (2D)

membrane elements using the Universal Panel Tester available at the University of Houston (Laskar et al. 2010).

Fig. 1.3 plots the maximum shear strength, $V_{n,max}$, as given in four available codes or recommendations (AASHTO 2007, ACI 318 2008, NCHRP 579 2007, and Laskar et al. 2010) as a function of concrete strength f'_c , and compares these shear provisions to shear beam tests available in the literature (Bennett and Balasooriya 1971, Rangan 1991 and Ma et al. 2000).

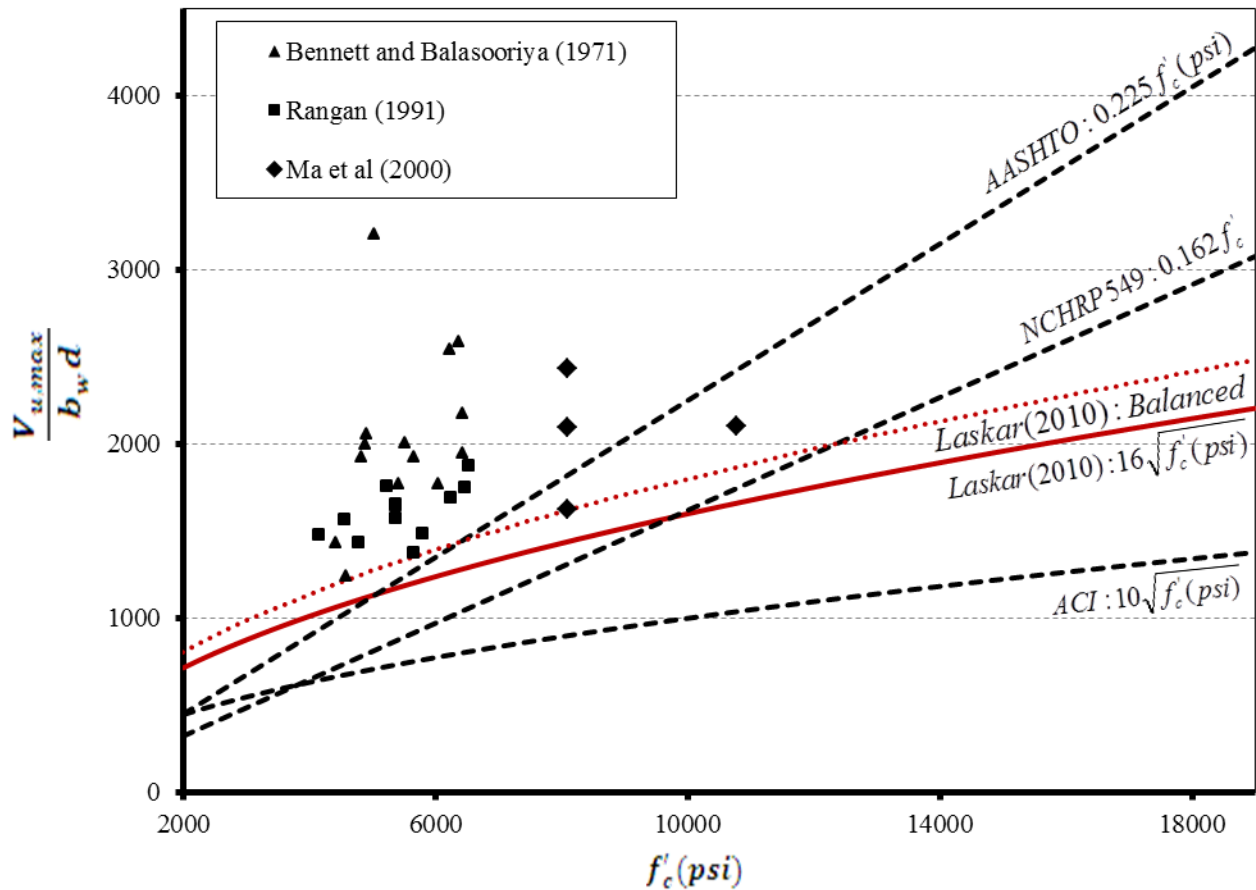


Fig. 1.3 Variation of Maximum Shear Strength $V_{n,max}$ with Concrete Strength f'_c

Fig. 1.3 highlights the two basic problems in the shear design of prestressed beams with high strength concrete. First, the shear provisions in the codes and recommendations vary drastically, especially in the regions of high strength concrete. For a concrete strength f'_c of 14,500 psi, AASHTO Specifications allows a $V_{n,max}$ value to be 2.5 times that in the ACI Code. Second,

there is a dearth of data points for shear girder tests with concrete strength greater than 8000 psi. Hence, shear beam tests with high strength concrete are necessary to be investigated.

1.3. Objectives of Research

This research has two main objectives. The first objective is to develop a design provision for the maximum shear strength of HSC in PC girders and a finite element analysis program able to predict the shear behavior of the PC girders with different concrete strengths. The second objective is to investigate premature bond slippage of prestressing tendons at the end regions of PC girders. Fig. 1.4 shows the experimental program specimens matrix.

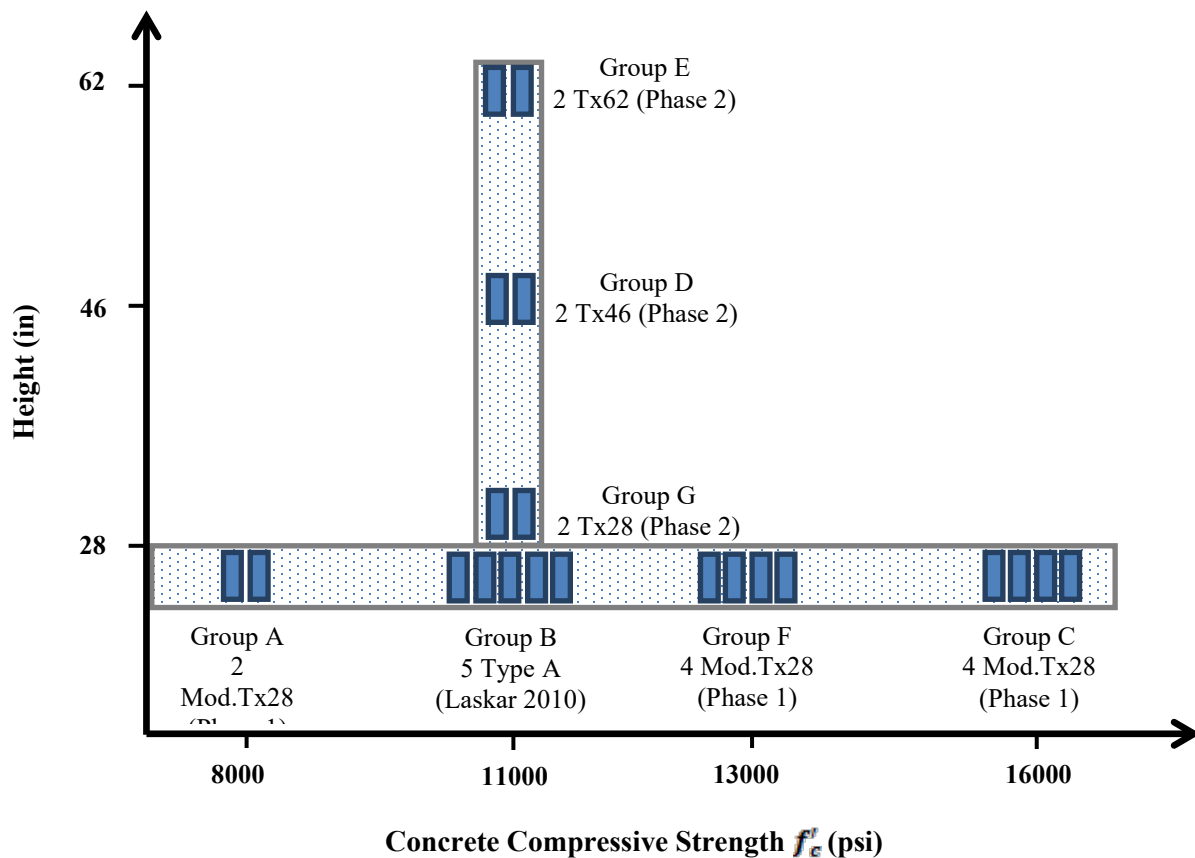


Fig. 1.4 Experimental Program Specimens Matrix

A total 15 specimens are tested for the first objective. Five specimens in Group B (TxDOT Type A girders) have been tested previously at University of Houston by Laskar in 2010. Another 10 specimens divided into 3 groups namely A, F, and C based on their concrete compressive strength, are required to be tested to acquire experimental data points for shear design. In addition, six full size girders with different heights and the same concrete strength will

be tested to investigate premature bond slippage of prestressing tendons at the end regions of PC girders and its effect on the web-shear capacity of the girder.

1.4. Outline of Report

This report is divided into 10 chapters, which can be summarized as follow:

Chapter 1 introduces the problem statement and outlines the objective of the research.

Chapter 2 includes a comprehensive literature review about the shear provisions in current codes. The tested prestressed concrete girders and the used concrete strength in literature are discussed. A brief literature review of developing high strength concrete and its characteristics are presented. The shear bond characteristics and the design limitation due to this phenomenon are also reviewed. Finally the Cyclic Softened Membrane Model for Prestressed Concrete (CSMM-PC), which is the most recent constitutive models of PC developed at the University of Houston, and the object-oriented finite element framework OpenSees (Fenves 2005), which has been used as a framework to create a nonlinear finite element program to simulate the behavior of the tested girder in this research work, are introduced.

Chapter 3 describes the experimental program to study the maximum shear strength as a function of concrete strength. This includes designing and manufacturing the tested girders, studied parameters, test set-up, and used instruments.

Chapter 4 introduces the general experimental results including load deflection curves for both ends of all girders reported in Chapter 3, the ultimate shear capacity for each end, and the measured smeared and local strains for each end of the girder. The analysis of the experimental results to estimate the concrete and the steel contributions to the shear capacity of the girder is presented. This analysis is used to validate the University of Houston proposed design equations for high strength concrete.

Chapter 5 contains the results from using the finite element program in simulating the behavior of tested girders to validate the capability of the finite element program Simulation of Concrete Structures (SCS) (Hsu and Mo 2010) in predicting the behavior of prestressed high strength concrete structures under monotonic loading. The analytical and experimental load-deflection curves are compared and presented.

Chapter 6 describes the experimental program to study shear-bond failure and premature failure in end zones (D-region) of PC girders. This includes designing and manufacturing the tested girders, studied parameters, test set-up, and used instruments.

Chapter 7 introduces the general experimental results including load deflection curves for all girders reported in Chapter 5, the ultimate shear capacity, the measured local strains, and the measured bond slip in selected tendons. The analysis of the experimental results to estimate the concrete and the steel contributions to the shear capacity of the girder is presented. This analysis is used to validate the University of Houston proposed design equations for the end zone of PC girders (D-region).

Chapter 8 contains the results from using finite element program SCS in simulating the behavior of tested girders in Chapter 6 to validate the capability of the finite element program SCS (Hsu and Mo 2010) in predicting the behavior of the end region of prestressed high strength concrete structures under monotonic loading if there is no shear-bond failure. The analytical and experimental load-deflection curves are compared and presented in this chapter.

Chapter 9 summarizes the new design provision for estimating the shear capacity of PC girders. Design examples are prepared to illustrate the application of the new shear equation for prestressed concrete girders.

Finally, Chapter 10 gives the conclusions of this research and the recommendations for further study.

CHAPTER 2 LITERATURE REVIEW

2.1. High Strength Concrete

The concrete strength is governed by the weakest of the strength of the coarse aggregate, the strength of the mortar, and the mortar-to-aggregate bond (Myers and Carrasquillo 1999). This concept of the weakest component controlling the strength of the concrete is referred to as the “Three Link Chain” concrete theory.

The strength of the mortar is affected by the used water-to-cement ratio and how rich the mortar is, in other words, decreasing the water content and increasing the cementitious materials content increase the concrete strength.

The concept of using low water-to-cement ratios to develop high strength concrete has been well known for many years. Water-cementitious material ratios by weight for high-strength concretes typically have ranged from 0.27 to 0.50, (ACI committee 363R-92 1997). The optimal ratio is the balance between densifying the paste and supplying sufficient water for hydration of cement particles. The quantity of liquid admixtures, particularly high-range water reducers, sometimes has been included in the water-cementitious material ratio.

Most mix designs for high strength concrete (HSC) use a combination of cement and fly ash and sometimes silica fume as binder. Using silica fume in the highway bridge girder industry in the state of Texas is not economical because it is not available inside the state, which makes delivery too costly. Thus fly ash is the available and cheap mineral admixtures to enrich the mortar. Fly ash has been referred to as Portland cement without the calcium. When fly ash is added to a mix, it reacts with the free calcium to form additional cementitious material.

Fly ash also helps in decreasing the hydration temperature during casting caused by the huge amount of cement used in the mix. Fly ashes contain almost spherical particles, which can serve as ball bearings and improve workability. High fly ash contents and the omission of silica fume are a possible solution for providing more workable mixes. Since fly ash increases workability, the superplasticizer dosage has to be adjusted to prevent segregation, which affects the dispersion of coarse and fine aggregates.

High-strength concretes have some characteristics and engineering properties that are different from those of lower-strength concretes. Recently, many researchers conducted several experimental programs including tests of high strength concrete behavior under flexure, axial compression, and combined axial and flexure, as well as under the shear actions. For example, Rizkalla et al. (2009) conducted an experimental program to study material properties of PC members. When the experimental results were compared with AASHTO LRFD, they found that high strength concrete has lower modulus of rupture and that the predicted nominal flexural resistance using the current LRFD specifications is less conservative and less accurate.

With identical shear provisions, ACI 318 (2011) and AASHTO LRFD (2010), provisions have severe limitations and empirical backgrounds for high strength concrete applications. The next section presents brief discussion about the shear design procedure in both codes.

2.2. Shear Design Provisions of Prestressed Girders in Current Codes

As stated in Chapter 1, the shear design provisions in the current codes (ACI 318 (2011) and AASHTO LRFD (2010)) are empirical, complicated, and have severe limitations. A brief description of the shear design provisions of the ACI Building Code (2011) and AASHTO Specifications (2010) are given in Sections 2.2.1 and 2.2.2 respectively.

2.2.1. Shear Provisions of ACI Building Code

As per the provisions of the ACI Building Code (2011), the factored shear force at any section of a PC member, V_u , should be less than the nominal shear strength, V_n , times the factor of safety, ϕ . The nominal shear strength, V_n , is calculated as the summation of the nominal shear strengths provided by concrete, V_c , and steel, V_s .

For prestressed members with effective prestress force not less than 40 percent of the tensile strength of flexural reinforcement, the shear strength provided by concrete can be calculated as

$$V_c = \left(0.6\lambda\sqrt{f'_c} + 700 \frac{V_u d_p}{M_u} \right) b_w d \quad (2.1)$$

It is allowed also to take the shear strength provided by concrete as the lesser of web-shear cracking strength, V_{cw} , and flexure-shear cracking strength, V_{ci} , where:

$$V_{cw} = (3.5\lambda\sqrt{f'_c} + 0.3f_{ps})b_w d_p + V_p \quad (2.2)$$

$$V_{ci} = 0.6\lambda\sqrt{f'_c}b_w d_p + V_d + \frac{V_i M_{crs}}{M_{max}} \quad (2.3)$$

$$M_{crs} = \frac{1}{y_t} (6\lambda\sqrt{f'_c} + f_{ps} - f_d) \quad (2.4)$$

The web-shear cracking begins when the principal tensile stresses exceed the tensile strength of the concrete, but the flexure-shear cracking initiates by flexural cracking and develops when the combined shear and tensile stress exceeds the tensile strength of concrete. This shows clearly that the concrete contribution to the shear strength in ACI provision depends on the tensile strength of the concrete. In general it is recommended that the concrete contribution V_c not to be taken less than $2\sqrt{f'_c}b_w d$.

The nominal shear strength provided by transverse steel, V_s , is calculated based on the number of stirrups cut by the shear crack which is assumed to be on 45° angle as shown in Fig. 2.1. Thus, the steel contribution can be calculated as:

$$V_s = A_v f_y \frac{d}{s} \quad (2.5)$$

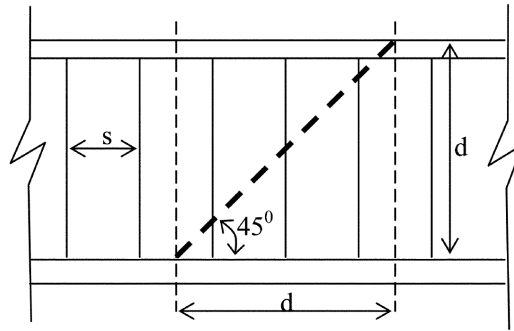


Fig. 2.1 Determination of Number of Stirrups for Contribution of Steel V_s According to ACI 318 (2011)

ACI specifies that the contribution of transverse steel to shear should not be taken greater than $8\sqrt{f'_c}b_wd$ to ensure steel yields before concrete crushes at ultimate load and have enough alerting time before the failure occurs.

On the other hand, ACI specifies minimum requirement for the area of transverse steel to prevent brittle failure at cracking load as:

$$A_{v,min} = 0.75\sqrt{f'_c} \frac{b_ws}{f_{yt}} \quad (2.6)$$

$$A_{v,min} = \frac{A_{ps}f_{pu}s}{80 f_{yt}d} \sqrt{\frac{d}{b_w}} \quad (2.7)$$

2.2.2. *Shear Provisions of AASHTO LRFD Specifications*

The nominal shear resistance, V_n , of a PC member is given as the summation of the nominal shear resistances due to concrete, V_c , the nominal shear resistance due to steel, V_s , and the component of the effective prestressing force, V_p , in the direction of the applied shear.

To ensure that the concrete in the web of the beam will not crush prior to yielding of the transverse reinforcement, the upper limit of, V_n , is recommended as:

$$V_n < 0.25 f'_c b_w d_v \quad (2.8)$$

where: $d_v = 0.80 \times d$

The nominal shear strength provided by concrete, V_c , in the general procedure is calculated as:

$$V_c = 0.0316\beta\sqrt{f'_c(ksi)}b_vd_v \quad (2.9)$$

The nominal shear strength provided by steel, V_s , is calculated as:

$$V_s = \frac{A_v f_y d_v \cot\theta}{s} \quad (2.10)$$

AASHTO LRFD (2007) assumed that the shear stresses are not uniform over the depth of the web. Thus the parameters β and θ were given in tables and graphs as functioned in the longitudinal strain ϵ_x at the middle of the web. AASHTO LRFD (2010) assumes a uniform distribution of concrete shear stresses over depth d_v . Thus, parameters β and θ are given in Eqs. 2.11 and 2.12 as functioned in the longitudinal strain ϵ_s at the middle of the web in the case of sections with at least the minimum transverse reinforcement recommended, where:

$$\beta = \frac{4.8}{1 + 750 \epsilon_s} \quad (2.11)$$

$$\theta = 29 + 3500 \epsilon_s \quad (2.12)$$

$$\epsilon_s = \frac{\left(\frac{|M_u|}{d_v} + 0.5N_u + |V_u - V_p| - A_{ps}f_{po} \right)}{E_s A_s + E_p A_{ps}} \quad (2.13)$$

In the case of sections without transverse reinforcement or with transverse reinforcement less than the minimum requirements, the factor β becomes a function in the crack spacing parameter, s_{xe} , where:

$$s_{xe} = s_x \frac{1.38}{a_g + 0.63} \quad (2.14)$$

where: 12 in. $< s_{xe} < 80$ in. and s_x is the lesser of either d_v or the maximum distance

between layers of longitudinal crack control reinforcement

the area of the reinforcement in each layer is not less than $0.003b_v s_x$

2.3. Shear Design Provisions of Prestressed Girders at University of Houston

The shear behavior and strength of the PC I-beam girders depends mainly on the web. The web can be considered as 2-D membrane element. For many years, the shear research group at the University of Houston (UH) has been working on understanding the behavior and strength of the 2D membrane element subjected to shear using the Universal Panel Tester.

Using the universal panel tester, a Rotating-Angle Softened-Truss Model (RA-STM) was developed at UH (Belarbi and Hsu 1994; 1995; Pang and Hsu 1995), which truly treated the cracked reinforced concrete as a smeared, continuous material. This model, like other models that are based on the rotating-angle, could not logically produce the concrete contribution because shear stresses could not exist along the rotating-angle cracks. In order to predict the “concrete contribution,” Hsu and his colleagues (Pang and Hsu 1996; Hsu and Zhang 1996; Zhang and Hsu 1998) proposed the Fixed-Angle Softened-Truss Model (FA-STM). In FA-STM the direction of cracks is assumed to be perpendicular to the principal applied tensile stresses at initial cracking rather than following the rotating cracks. The constitutive laws of concrete are set in the principal coordinates of the applied stresses at initial cracking. The only shortcoming of FA-STM is that it is more complicated than RA-STM because of the complexity in the stress-strain relation of concrete in shear.

Recently, the research group at UH tried to utilize their previous experience and clear understanding of the behavior of 2D element in shear to better estimate the shear capacity of PC girders. Laskar (2009 and 2010) used the softened truss model (Zhang and Hsu, 1998) to express the maximum shear strength $V_{n,max}$ as:

$$V_{n,max} = \sigma_2^c b_w (0.9d) \sin \alpha_1 \cos \alpha_1 \quad (2.15)$$

where: σ_2^c is the compression strength of the concrete struts

(0.9d) is the height of the truss measured from the centroid of the steel to the centroid of the compression zone.

α_1 is the angle of the normal to failure surface with respect to the longitudinal axis of the beam ($\alpha_1 = 45^\circ$ when an element is subjected to pure shear).

In order to develop an expression for $V_{n,max}$ that is applicable to the whole range of concrete strengths from 3,000 psi to 14,500 psi, Zhang and Hsu (1998) tested full-sized reinforced concrete (RC) panel elements (55 in. x 55 in. x 7 in.) with concrete strengths up to 14,500 psi. Zhang and Hsu (1998) summarized the extensive panel tests at UH and showed that the strength of the concrete struts in the principal compressive direction is “softened” by the perpendicular principal tensile strain $\bar{\epsilon}_1$. Thus the resulted strength of the concrete struts is function in the

concrete compressive strength f'_c and the principal tensile strain $\bar{\epsilon}_1$. Thus the maximum shear strength, $V_{n,max}$, can be given by:

$$V_{n,max} = 5.8\sqrt{f'_c(MPa)} \cdot f(\bar{\epsilon}_1) \cdot b_w \cdot (0.9d) \cdot (0.5) \quad (2.16)$$

Equation 2.16 shows that max $V_{n,max}$ is a function of $\sqrt{f'_c}$ for concrete compressive strength f'_c up to 14,500 psi. Equation 2.16 was simplified as:

$$V_{n,max} = C_1\sqrt{f'_c(MPa)} \cdot b_w \cdot d \quad (2.17)$$

where C_1 is a constant which was determined by calibrating the balance condition constant C_b based on the shear tests of prestressed beams available in literature and was found to be taken 1.5. Since the balance condition assumes the steel yields at the same moment concrete crushes ensuring ductile shear failure constant C_1 has to be less than the balance condition constant C_b . Thus, constant C_1 was decided to be taken equal to 1.33. Then the maximum shear strength $V_{n,max}$ can be given by:

$$V_{n,max} = 1.33\sqrt{f'_c(MPa)}b_wd \quad (2.18)$$

$$V_{n,max} = 16\sqrt{f'_c(ksi)}b_wd \quad (2.19)$$

The maximum shear strength $V_{n,max}$ in the case of prestressed girders with only straight tendons is the summation of concrete contribution V_c and steel contribution V_s .

$$V_{n,max} = V_c + V_s \quad (2.20)$$

Laskar (2007) used the shear friction concept put forth by Loov (2002) and the available tests on prestressed beams in literature to develop a rational equation for the estimation of the concrete contribution, V_c . According to Loov's shear model, the contribution of concrete to the shear capacity of the beams stems from the shear stress of the concrete along a failure crack indicated by the inclined force "S" as shown in Fig. 2.2. This concept is very different from the existing design methods (ACI 2011 and AASHTO 2010), which assume that the concrete

contribution to the shear capacity of beams arises from the tensile stress across the shear failure cracks.

Assuming the failure surface to be an inclined plane, and taking the force equilibrium of the free body along the crack direction, as shown in Fig. 2.2, the shear capacity of the beam, V , can be calculated as:

$$V = \frac{S - T \sin \alpha_1}{\cos \alpha_1} + \sum F_v \quad (2.21)$$

where: $\sum F_v$ is the “contribution of steel in shear” denoted as V_s and simply it is the summation of the vertical forces in stirrups intersected by the failure crack at the ultimate shear load.

T is the tensile force in the main flexural reinforcement at the ultimate shear load of the beam.

α_1 is the angle between the normal to the failure crack and the longitudinal axis.

The term $\frac{S - T \sin \alpha_1}{\cos \alpha_1}$ in Eq. 2.21 is the “contribution of concrete in shear,” V_c . In order to avoid the excessive complexity involved in the calculation of S , T , and α_1 , the V_c term was directly derived from tests in literature.

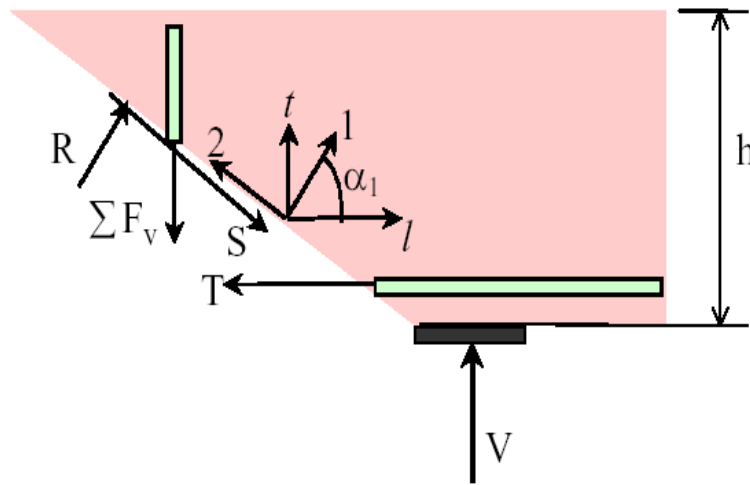


Fig. 2.2 Loov's Analytical Model Used for Calculating Shear Capacities of Beams

Since the study of Reinforced Concrete (RC) shear elements with concrete strengths up to 14,500 psi (Zhang and Hsu 1998), it was observed that the softened compressive strength of concrete struts is proportional to $\sqrt{f'_c}$. Also, from the test results of tested beams B1 to B5 by Laskar et al. (2007 and 2010), the concrete contribution V_c was observed to be a strong function of the a/d ratio. Based on the analysis of tested beams and those which are in the literature, Laskar et al. (2010) presented a new and simple equation to predict the concrete contribution V_c as follows in US Customary units:

$$V_c = \frac{14}{(a/d)^{0.7}} \sqrt{f'_c (\text{psi})} b_w d \leq 10 \sqrt{f'_c} b_w d \quad (2.22)$$

where:

b_w = width of the web of beam, inches.

a = shear span, inches, and

d = effective depth from the centroid of the tendons to the top compression fiber of the beam, inches. The value of d is not taken to be less than 80% of the total beam depth.

Research has shown that the maximum shear capacity of the beams is not affected by the amount of prestressing force (Lyngberg 1976), especially in the case of the straight tendons. The steel contribution, V_s , must be based on the observed failure shear crack. For design, the failure crack can simply be assumed to be inclined at an angle of 45° , similar to the ACI Code. The assumption of a 45° failure shear crack has also been supported by a study of shear energy dissipations in the failure zone (Laskar 2009). In Laskar et al. (2007 and 2010), a more realistic concept of seeking a path of minimum shear resistance among a series of individual stirrups is used, as shown in Fig. 2.3. The minimum number of stirrups intersecting the minimum shear resistance line at 45° is taken as $[(d/s) - 1]$. This differs from the ACI Code procedure, which is based on the concept of smearing the stirrups, resulting in an average number of stirrups, d/s , crossing the 45° shear crack. Hence, the steel contribution in shear can be calculated as follows:

$$V_s = A_v f_y \left(\frac{d}{s} - 1 \right) \quad (2.23)$$

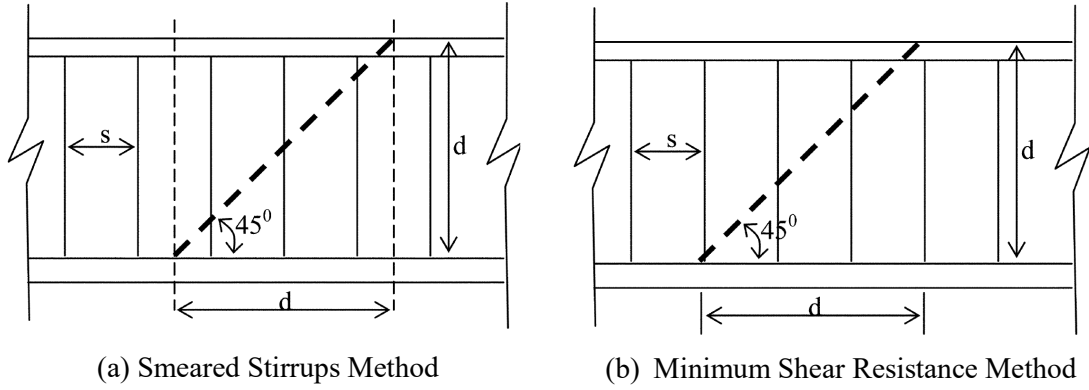


Fig. 2.3 Determination of Number of Stirrups for Contribution of Steel V_s

Minimum shear reinforcement, $A_{v,min}$, in beams is required to prevent the brittle failure of the girders due to the fracture of the shear reinforcement shortly after the formation of the inclined shear cracks. Based on literature review, Laskar et al. (2010) proposed the following equations for $A_{v,min}$:

$$A_{v,min} = \frac{0.75 \sqrt{f'_c (psi)} b_w s}{f_y}, \text{ for } \frac{a}{d} \leq 2 \text{ and } \frac{a}{d} \geq 4 \quad (2.24)$$

$$A_{v,min} = \frac{1.5 \sqrt{f'_c (psi)} b_w s}{f_y}, \text{ for } 2 < \frac{a}{d} < 4 \quad (2.25)$$

$$A_{v,min} \geq \frac{50 b_w s}{f_y} \quad (2.26)$$

2.4. Shear Tests of PC Girders in Literature

This section briefly describes tests on prestressed concrete beams carried out by researchers all over the world. The major conclusions drawn from the individual series of tests are mentioned.

Billet and Appleton (1954) tested 26-12 inches deep PC I-beams without any web reinforcement. The range of the concrete compressive strength at time of test varies from 3,000 to 8,200 psi. Twenty-one of these beams failed in flexure, either by crushing of concrete after excessive elongation of reinforcement or by crushing of concrete while steel stress were still in the elastic range. Three beams were balanced-design between shear and flexural failure, and two beams failed prematurely due to bond failure. Using the test results, the authors studied the effect of three major variables, namely percentage of transverse steel, amount of prestress, and concrete strength on deflections, cracking and ultimate loads of the beams. They found that bond and shear failures may occur, either of which will result in an ultimate load less than the computed flexure capacity.

Zwoyer and Siess (1954) tested 34 simply-supported rectangular PC beams without web reinforcement. The beams had a rectangular cross section 6 inches wide and 12 inches deep. The test variables included applied prestress, percentage and type of transverse steel, concrete strength, and ratio of shear span to effective depth (i.e., a/d ratio) of the beams. The compressive strength of the used concrete ranged from 2,890 to 7,990 psi. The authors developed a hypothesis of failure based on the test results. The hypothesis provided a basis for a method of analysis able to predict the shear strength of PC beams similar to the ones tested. The method of analysis presented in this study could also be applied to ordinary reinforced concrete beams.

Hernandez (1958) tested 38 simply supported prestressed I-beams, symmetrically loaded by either one or two concentrated loads on a span of 9 ft. with concrete compressive strength from 2,310 to 4,660 psi. A hypothesis was developed to quantitatively explain the mechanism of failure of these beams and an expression was proposed to determine the amount of web reinforcement for a “balanced design” based on the variable which seemed to be most significant in the test results.

Hicks (1958) investigated the effect of shear-span and concrete strength on the shear resistance of prestressed I-beam without web reinforcement, having an overall depth of

10 inches. The average concrete compressive strength at 28 days was 6,000 to 7,000 psi. Four types of failure were observed in these tests, namely shear distortion, diagonal compression, diagonal tension, and flexural. From the tests, the authors were able to establish the limits of the shear span to effective depth ratio within which each type of failure occurred.

MacGregor et al. (1960) tested 87 prestressed beams having a depth of 12 inches and 4 different types of cross-sections. While some of the beams had rectangular cross-sections, others were I-beams with different web thickness. Cold-drawn and stress-relieved high tensile strength wires were used as prestressing steel, which were either horizontal or draped. The concrete compressive strength of the used concrete varied from 2,400 to 7,625 psi. The amount of shear reinforcement in the beams was also varied. Another variable that was studied was the shear span at which the beams were loaded. The tests clearly demonstrated the two types of shear cracks that develop in prestressed beams, namely web shear crack and flexural shear cracks. It was concluded that the presence of web reinforcement improved both the strength and ductility of beams failing in shear. However, maximum strength and ductility were obtained in the beams in the case of flexural failures. It was thus recommended that prestressed concrete beams should be provided with sufficient web reinforcement to ensure flexural failures. The results of these tests were used to develop the shear design provisions of the ACI Building Code.

Mattock and Kaar (1961) tested 15 single span PC I-girders with a tied down cantilever at one end. The girders had an overall depth of 22.5 inches with 3 inches overlying slab continuous over the girder supports. The concrete compressive strength for the girder and the deck slab varied from 6,070 to 6,860 psi and from 2,270 to 3,490 psi, respectively. The girders were loaded by three point loads located at a variable distance from the support to simulate the distribution of axle loads of a standard moving design vehicle. By suitably varying the tie-down force at the end of the cantilever independent of the vehicle loads, it was possible to simulate the conditions that would exist in a two-span continuous girder. The ultimate shear strengths of the girders were not influenced adversely by flexural cracking in the interior support regions. The test results for the continuous girders were found to be in excellent agreement with those of simply supported single-span prestressed girders and were used to develop shear design recommendations for prestressed concrete girders.

Bruce (1962) conducted an extensive investigation of the behavior of prestressed concrete beams with concrete compressive strength from 2,790 to 3,950 psi subjected to combined bending and shear and developed a method for predicting the strength of beams in shear or in combined bending and shear, and for the design of web reinforcement to prevent failure in any but a flexural mode.

McClarnon et al. (1962) tested 28 prestressed beams having an overall depth of approximately 12 inches without any web reinforcements. Six of these specimens were I-sections while the others had a rectangular cross section. The range of the used compressive strength of the concrete was from 5,060 to 6,460 psi. The authors used the test results to study the effect of the length of overhang, the effect of existing inclined cracks and the effect of the manner of loading on the behavior of these beams. The test results showed that for 12 inches deep beams an overhang of 24 inches provided adequate embedment for the reinforcement. Under reloading conditions, ultimate strengths of beams were observed to be lower than conventionally loaded beams by 11 to 17 percent.

Evans and Schumacher (1963) tested 54 simply supported prestressed beams without web reinforcement, loaded with 2 symmetrically placed concentric loads to investigate the influence of amount of longitudinal reinforcement, length of shear span, shape of beam cross section, and curing method. The range of the concrete compressive strength was from 3,480 to 7,300 psi. Based on the test results, expressions were presented for load capacity in shear-compression failure, diagonal cracking failure mode, and web-crushing following diagonal cracking failure mode. It was concluded that for prestressed concrete beams without shear reinforcement the lesser of the shear-compression and diagonal cracking load governed the failure of the beams.

Arthur (1965) tested 50 PC I-beams and concluded that failure in these beams should be considered to have occurred when the diagonal web-cracking in shear ensued in the beams. The concrete compressive strength was from 2,500 to 10,050 psi. Although many of the beams tested carried a shear load greater than the shear cracking load, the failure load could not be predicted. An expression was developed to predict the diagonal web-cracking shear force, which showed satisfactory agreement with other test results.

Hanson and Hulsbos (1965) tested 18 PC I-beams having an overall depth of 18 inches. The concrete compressive strength was from 5,400 to 6,410 psi. The shear span to effective depth

ratio of the specimens ranged from 2.54 to 6.34 and the percentage of shear reinforcement varied from 0 to 1.22 percent. Seven of the eighteen specimens failed in shear while the remaining failed in flexure. From the test results, the authors confirmed that the ultimate shear that can be carried by the concrete is equal to the shear force at the state of inclined web-cracking.

Kar (1969) experimentally studied the ultimate strength of PC beams without any web reinforcement undergoing two types of shear failure, namely shear-compression and web-crushing. The concrete compressive strength was from 4,039 to 5,642 psi. Four different types of cross sections were tested. Two types of rectangular cross-sections had dimension of 5 inches x 10 inches and 4 inches x 8 inches were tested. Two types of I-section having an overall depth of 12 inches were also tested. The tests revealed that the shear-compression failure of PC beams is not always associated with the development of limiting strain at the top concrete fiber. In this mode of shear failure, the concrete compression zone is either crushed or ruptured along the diagonal crack. However, these tests could not well establish the location and pattern of diagonal cracks associated with shear failure due to web crushing and the influence of the a/d ratio on such failure mode.

Bennett and Balasooriya (1971) tested a series of 26 PC I-beams to investigate the upper limit of the shear strength associated with inclined compressive failure of the web. The concrete compressive strength was from 4,420 to 6,420 psi. The test variables included cross-section, web reinforcement, prestress, and shear span of the specimens. Two different types of cross-sections were tested, one having a depth of 10 inches and the other having an overall depth of 18 inches. The results of these tests showed that the behavior of the beams at failure could be represented by a truss formed by the stirrups and the concrete compression struts in the web and was further strengthened by the flanges of the beam.

Mahgoub (1975) tested 58-12 inches deep prestressed concrete I-beams without web reinforcement, under one or two-point loading. The concrete compressive strength had a range from 6,350 to 9,300 psi. Based on the test results, an expression was derived for predicting the inclined cracking load and comparison was made with other published expressions. Other published test results were found to be in good agreement with the derived expression.

Lyngberg (1976) tested a series of 9-24 inches deep PC beams to investigate the effect of upper limit of shear strength, associated with inclined compressive failure of the web. The

concrete compressive strength had a range from 3,730 to 4,920 psi. The cross-section, web reinforcement, flexural ultimate moment, and shear span were kept constant in all the specimens. The number of prestressing tendons and amounts of flexural non-prestressed steel were varied. Two of their test beams did not have any prestressing tendons and could be considered as reinforced concrete beams. The results showed that the failure load was not influenced by the presence of prestress and could be accurately predicted by a rigid plastic model.

Elzanaty et al. (1986) experimentally investigated the shear strengths of 34 prestressed concrete beams, half of which were designed for flexural-shear cracking and the other half for web-shear cracking. The used concrete had a compressive strength varying from 5,800 to 10,700 psi. In each of these two sets of beams, nine beams were without web reinforcement while eight had web reinforcement in the form of vertical stirrups. The test variables studied in these specimens were concrete strength, longitudinal prestressed and non-prestressed steel ratios, shear span-to-depth ratio, amount of prestress force, and amount of web reinforcement. Test results were compared with 1983 ACI Building Code (ACI 318-83) recommendations. It was observed that ACI 318-83 Code equations for cracking load gave conservative results for all concrete strengths. For beams with stirrups, the code equations for total shear strength were also conservative, but the degree of safety depended on several parameters, including concrete strength, that were not adequately considered by the ACI 318-83 Code equations.

Robertson and Durrani (1987) studied the effectiveness of plane sheets of welded wire fabric as shear reinforcement in prestressed concrete T-beams having an overall depth of 20 inches. The studied specimens had a concrete compressive strength from 5,720 to 6,688 psi. The test variables were the type (smooth or deformed) and the amount of (size and spacing) welded wire fabric used as shear reinforcement and the anchorage condition at the ends of the vertical wires. The effectiveness of the welded wire fabric against the individual stirrups was also studied. The test results showed that the use of welded wire reinforcement as shear reinforcement is convenient and its performance is as good as the individual stirrups. The study also showed that the minimum capacity of shear reinforcement specified by the ACI Code can be satisfied by an amount of reinforcement smaller than that currently required, without affecting the ductility of the beams. The contribution of concrete to the shear strength of beams was on an average 40 percent greater than the ACI Code predictions.

Kaufman and Ramirez (1988) tested six high strength concrete beams AASHTO Type I and II that have an overall depth of 28 inches and 36 inches, respectively. The concrete strength in the specimens ranged from 8,340 psi to 9,090 psi. The results of these tests showed that shear tension failures are associated with a potentially serious detailing problem and the ACI and AASHTO shear provisions at that time were conservative in properly detailing the members.

Rangan (1991) tested 12 prestressed concrete beams having a height of 24 inches and concrete strength varying from 4,160 psi to 6,530 psi. The beams, with large amounts of transverse steel and thin webs, were over-reinforced in shear to produce web crushing failure before the yielding of steel. The experimental strengths were compared with the upper limit on shear strength given in the ACI Building Code (ACI 318-83 1983) as well the Australian (AS 3600-1988) and the Canadian Standards (CAN3-A23.3-M84). The code proposals were always found to be conservative.

Shahawy and Batchelor (1996) conducted an extensive laboratory testing program to investigate the shear strength of prestressed concrete girders. Twenty full-scale AASHTO Type II prestressed concrete girders 44 inches in deep were tested. The average concrete compressive strength in all the beams was 7,000 psi. The main variables in the test program were the amounts of shear reinforcement and the shear span. The shear strengths obtained from the tests were compared with the predictions based on the AASHTO Standard (1989) Specifications for Highway Bridges and the AASHTO LRFD (1994) Specifications. The results showed that the AASHTO Standard (1989) Specifications gave a much better prediction of the shear strengths of the girders than the LRFD provisions, indicating that the latter requires some examination and modification to enhance reliability.

Ma et al. (2001) observed that the upper shear limit specified by the AASHTO Standard (1996) Specifications and the AASHTO LRFD (1998) Specifications may differ by as much as 100% and showed the limit on shear capacity specified by the AASHTO LRFD Specifications through full-scale tests. Two 43 inches deep NU1100 I-girders were tested with different types of shear reinforcement at the two ends of the beams. The used concrete in the two girders had a compressive strength 8,100 and 10,780 psi. Other major variables in the beams were draped tendons versus shielded tendons. The tests showed that anchorage of the longitudinal flexural prestressing tendons at member ends is a key factor to reach the actual shear strengths of beams.

Lack of proper anchorage could lead to a “shear/bond” failure with 25% less strength than actual web-crushing failure with perfectly anchored tendons.

Teoh et al. (2002) conducted an experimental investigation on 6-28 inches PC I-beams have low stirrup ratios with concrete strengths ranging from 6,240 to 14,500 psi. Tests results indicated that the reserved shear strength of PC beams (i.e., the strength in excess of the cracking strength of the beams) depends on the discrete number of stirrups intercepted by the inclined failure cracks in the beams. Using the reserved shear strength as a measure of safety, the researchers found the ACI (1999) and Canadian code (1994) provisions, with respect to the minimum shear reinforcement to be inadequate in guaranteeing a satisfactory margin of safety in the PC beams.

NCHRP 579 (2007) reported the tests of 10 bulb-tree prestressed girders made of HSC up to 18,000 psi. The girders were simply-supported on a span of 50 ft and subjected to a uniform load. The cross-section had a height of 6 ft-1 in. and a thin web of 6 in. The small bottom flange had a width of 26 in. and a vertical thickness just sufficient to enclose 42 prestressed tendons. The failure patterns of the University of Illinois Urbana-Champaign (UIUC) girders revealed that most of them failed due to premature anchorage-related failure at the ends rather than due to shear failure in the web. Concrete crushing or splitting occurred at the intersection between the web and the bottom flange and spread from the end surface toward the mid-span of the girder. Such a local anchorage failure in the D-region occurred prior to the web-crushing shear failure. Hence, the load carrying capacities of many UIUC specimens could be used to provide experimental data for developing the provision to prevent end failures. However, these tests could not be used to develop the design provision for $V_{n,max}$ for high strength concrete. These results were published later in Kushma et al. (2008).

Laskar et al. (2007 and 2010), carried out tests on 5 full-scale TxDOT Type-A girders, which were 25 ft. long with concrete strength between 9,370 to 10,800 psi, to study their behavior in web shear and flexural shear failures, at UH. Three of the five girders (Girders B1, B2 and B3) were designed to fail in web shear, whereas the remaining two (Girders B4 and B5) were designed to fail in flexural shear mode. One web shear girder (Girder B3) and one flexural shear girder (Girder B5) had draped prestressing tendons. Three girders (B1, B4, and B5) had a minimum transverse steel ratio (0.17%), while the other two girders (B2 and B3) had a

transverse steel ratio of 0.95%. The girders were symmetrically loaded using two hydraulic actuators. The loads from the actuators were applied at 3 feet from the supports (both at north and south supports) to induce web-shear failure in girders B1, B2, and B3, giving a shear span to depth ratio (a/d) of 1.6. Girders B4 and B5 were loaded at 8 feet from the supports, at either ends, giving an a/d ratio of 4.3 to achieve flexural-shear failure. Analysis of the girders was performed using the constitutive laws of prestressed concrete developed from the prestressed concrete panels tested in the Universal Panel Tester at UH. A new and simple equation for shear design of prestressed girders was developed based on the test results and experimental findings in the literature.

2.5. Shear-bond Studies and Background in Literature

A series of load tests on AASHTO Type II girders conducted by Shahawy and Batchelor (1996) showed that tendon slip, the bond slip of prestressing tendons within the anchorage length, reduces the shear strength in girders with shear span-to-depth ratios (a/d ratios) varying from 1.37 to 1.52. Tests results carried out by Ma et al. (2001) concluded that the “shear-bond” failure load is 25% less than the “web-crushing” failure load of the end with fully anchored tendons using shear span-to-depth ratios (a/d ratios) 1.16 to 1.28.

Many factors affecting the bond stress between the tendon and the surrounding concrete are found. Adhesion, friction, and mechanical resistance are the major mechanical factors affect the transfer bond. These factors in turn depend on several factors.

Adhesion depends mainly on the tendon surface condition. Janney (1963), and Holmberg and Lindgren (1970) note transfer lengths of rusted tendon approximately $1/2$ to $2/3$ of those of un-rusted tendons. The failure of the adhesion between concrete and tendon surface results in the first bond slip. Hanson and Kaar (1959) recommend that design criteria should be governed by first bond slip rather than by final bond failure.

Frictional bond stresses requires radial compressive stresses which has been attributed to a number of mechanisms. The most well-known is the Hoyer Effect (Hoyer and Friedrich 1939), which is a radial expansion in the tendon due to the longitudinal contraction. This Poisson expansion induces compression perpendicular to the steel-concrete interface. Stocker and Sozen

(1970) stated that the small changes in the tendon cross-section cause a wedging upon movement of the tendon relative to the concrete.

Mechanical resistance, or interlock, stems from the axial component of bearing stress between the tendon and the surrounding concrete those results from the helical shape of the seven-wire tendon. Hanson and Kaar (1959) said that the additional capacity provided by mechanical interlock often provides an extra margin of safety, but it is too unreliable to count on.

Abrishami and Mitchell (1993) performed several pullout tests introducing a simple test method to determine the bond stress-versus-slip response for pretensioned tendon embedded in concrete along both the transfer length and the flexure bond length. The prestressing steel used in this study was seven-wire tendon. The nominal diameters of the tendon sizes used were (0.375, 0.50, 0.60 in). For each size of tendon, three specimens were tested to determine bond characteristics along the transfer length and three specimens were used to examine the bond response along the flexural bond length. They found that after bond failure, the flexure bond specimen exhibits more ductile response, while the transfer length test exhibits more brittle bond failure.

Yerlici and Özturan (2000) conducted an eccentric pullout tests under monotonic loading on high-performance concrete specimens. The concrete strength was between 8,702 to 13,053 psi. The results indicated that the bond strength between reinforcement and concrete increased with increasing concrete strength, cover thickness, and amount of web reinforcement, while it decreased with increasing bar size.

Barnes et al. (2003) indicate a definite trend in which transfer lengths tend to decrease in inverse proportion to the square root of the concrete strength at release. A “best fit” line reported by the authors includes the square root of the concrete strength at release in the denominator. Concrete with higher compressive strength from 10,000 to 12,000 psi results in transfer lengths that are about 25 percent shorter than that in concrete with normal compressive strength from 6,000 to 8,000 psi.

NCHRP 603 (2008) reported that some of the variables that affect bond are currently included in the AASHTO LRFD Bridge Design Specifications (2007) while some are not. In the area of transfer length and development length of prestressing tendon, specifications do not account for variables such as concrete strength, tendon size, “top bar” effects, epoxy coating,

bond quality of individual tendon samples, confining reinforcement, tendon spacing, and structural behavior issues. The effect of the shear-bond-interaction, as a structural behavior issue, on the shear behavior of the end region of the pretension prestressed concrete girders is investigated in the current research work.

2.6. Transverse Reinforcement in End Zone in Pretension Prestressed Girders

Cracks are frequently observed at the ends of pretensioned concrete members at the time of prestress transfer, especially in narrow-stemmed members such as I-girders and inverted-tee girders. These cracks are caused primarily by the concentration of prestressing forces at the time of prestress release. They are commonly horizontal and occur near the junction of the bottom flange and web. Some diagonal cracks are also observed higher up on the web.

In the early 1960s, Marshall and Mattock (1962) developed a simple design equation for the required area end zone reinforcement. The semi-empirical equation was based on testing of 14 pretensioned girders whose depths ranged from 22.5 to 25.0 inches. The splitting reinforcement area A_s is given by the following equation:

$$A_s = 0.021 \left(\frac{P_i h}{f_s l_t} \right) \quad (2.27)$$

where: h = girder depth

l_t = transfer length

This equation was deemed accurate for girders whose geometries satisfied $\frac{h}{l_t} \leq 2$ and yielded conservative designs for $\frac{h}{l_t} > 2$. The end zone stirrups are distributed uniformly over a length equal to one-fifth of the girder depth.

Because it is common for the pretension prestressed girders to have a total height of 50 inches, and the transfer length is proven to be 50 times the diameter, which is usually 0.5 in., the AASHTO LRFD (2010) Specifications takes $\frac{h}{l_t} = 2$ which results in that 4 percent of the total prestressing force should be used as the tensile force in the vertical reinforcement at the end zone of a girder, where:

$$A_s = 0.04 \frac{P_i}{f_s} \quad (2.28)$$

AASHTO LRFD (2010) further stipulates that this vertical reinforcement is designed for a stress of 20,000 psi and placed within a distance from the end equal to one-fourth of the girder depth, $h/4$. AASHTO Standard (1996) Specifications contains essentially the same provisions but it requires putting the reinforcement within a distance from the end equal to one-fourth of the girder effective depth, $d/4$.

Tuan et al. (2004) conducted an experimental program of two phases. In Phase I, the stresses and strains in the end zone vertical reinforcement of various girders designed in accordance with AASHTO LRFD (2002) Specifications were measured and analyzed. In Phase II, new end zone reinforcement details were proposed, tested, and evaluated. Phase I research work concluded that the maximum stress in the end zone reinforcement varied between 200 and 12,900 psi. The maximum stresses in the end zone reinforcement were less than the allowable design stress of 20,000 psi provided by the AASHTO LRFD (2002) Specifications. Also, it was observed that only the reinforcement located $h/8$ from the end of the member experienced significant stress. There was some stress applied to the reinforcement located $h/8$ to $h/2$ from the end. Beyond that zone, tensile stresses in the splitting reinforcement were very small. In Phase II the research team proposed an innovated way to reinforce the end zone by taking half the required area of vertical reinforcement by AASHTO LRFD (2002) specifications and condensing it within $h/8$ from the girder end. The remaining half was redistributed within the next zone with a length $3h/8$. In other words, they recommend distributing the end reinforcement within a total distance $h/2$ from the end of the girder rather than $h/4$ according to AASHTO LRFD (2010).

2.7. Effect of Top Flange Geometry on the Shear Behavior

As it was mentioned before, the I-girders are the most widely used in casting bridge prestressed girders. The main difference between the I-girder and T-girder is the presence of the bottom flange. The bottom flange provides more area to accommodate more tendons, which in turn optimize the flexure behavior. The effect of the top flange is the same in I-girders and T-girders, especially on the ultimate shear capacity. Most of the shear design provisions for prestressed concrete girders are taking into consideration only the web area. Many researchers studied the effect of the top flange in reinforced concrete girders.

Zararis et al. (2006) studied the shear strength of reinforced concrete T-Girders, and their study showed that the shear strength of T-girders is much higher than the shear strength of rectangular girders of their web. This is solely due to the increase of the compression zone.

Giaccio et al. (2002) tested 15 reinforced concrete T-girders with depth 305 mm. The girders had a different width and thickness of flanges. This study has shown that the effectiveness of the ratio of the flange width to web width, $\frac{b_f}{b_w}$, on the shear strength of a point-loaded reinforced concrete T-girder is dependent on the ratio of flange depth to effective depth, $\frac{d_f}{d_o}$. For the geometric ratios used in the experiments in this study, it is suggested that as long as the ratio $\frac{d_f}{d_o}$ is above 0.25, then the increase in shear resistance for a given increase in $\frac{b_f}{b_w}$ is independent of $\frac{d_f}{d_o}$, provided that a girder shear failure mechanism is displayed.

Pansuk and Sato (2007) tested 2 small girders with total height 13.75 inches. The first girder had a rectangular cross-section. The second girders had a T-section with a web dimension equal to the rectangular girder. They conclude that the increase in the flange width of a T-girder gives higher shear capacity with a nonlinear relationship for the T-girder with shear reinforcement. In the case of a T-girder without shear reinforcement, the width of the flange has almost no effect on shear capacity. Using the data from this research work and the data available in literature, the effect of the geometry of the top flange on the shear capacity of the pretension prestressed I-girders will be more understood.

2.8. Background on Used Finite Element Model

Laskar (2009) developed the Cyclic Softened Membrane Model for Prestressed Concrete (CSMM-PC) based on the Softened Membrane Model for Prestressed Concrete (SMM-PC) (Wang 2006) and the Cyclic Softened Membrane Model (CSMM) (Mansour 2001). The capability of CSMM-PC to predict the monotonic and cyclic shear behavior of the prestressed concrete elements has been proven. Three uniaxial material models are used. The concrete model ConcreteL01 and the tendon model TendonL01 have been created based on the uniaxial constitutive relationships of concrete and prestressing tendons in the CSMM-PC. The steel model SteelZ01 (Zhong 2005) has been previously created based on the uniaxial constitutive relationships of steel in CSMM (Mansour 2001). Since the constitutive relationships of steel in

CSMM and CSMM-PC are same, the previously developed steel model SteelZ01 is still valid. All these models were implemented into the OpenSees framework forming a Finite element program called Simulation of Concrete Structures (SCS). The three models mentioned before are listed in the following sections.

2.8.1. ConcreteL01

The concrete module ConcreteL01 was developed according to the monotonic uniaxial concrete model in SMM-PC and the cyclic uniaxial concrete model in CSMM. The model is a cyclic uniaxial concrete model with consideration of the softening effect due to the perpendicular tensile strain on the concrete struts. The initial stress in concrete due to prestressing is also taken into account. The stress-strain curves used in ConcreteL01 are illustrated in Fig. 2.4.

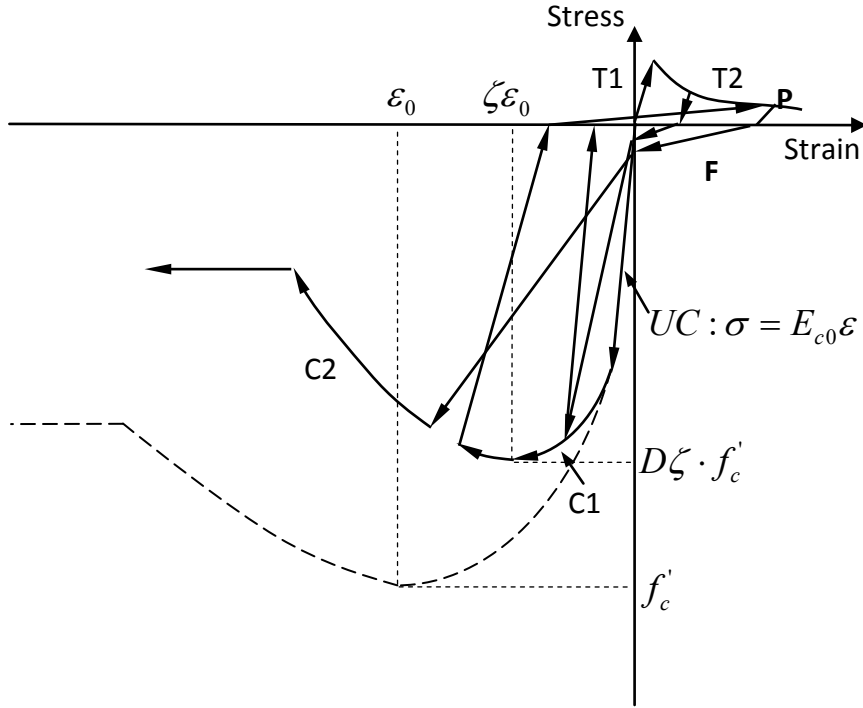


Fig. 2.4 ConcreteL01 Material Module

The envelopes of ConcreteL01 model in compression and tension are the same as those of the concrete constitutive model in SMM-PC. The equations defining the envelopes and the stress-strain relationships during unloading and reloading are expressed in following sections.

2.8.1.1. Compression Envelope

The stress-strain relationships of concrete in compression are given as:

$$(Stage\ C1)\ \sigma^c = D\zeta f'_c \left[2 \left(\frac{\bar{\varepsilon}}{\zeta \varepsilon_s} \right) - \left(\frac{\bar{\varepsilon}}{\zeta \varepsilon_s} \right)^2 \right] \leq k D f'_c \left(\frac{\bar{\varepsilon}}{\varepsilon_s} \right), \quad 0 \leq |\bar{\varepsilon}| \leq |\zeta \varepsilon_s| \quad (2.29)$$

$$(Stage\ C1)\ \sigma^c = D\zeta f'_c \left[1 - \left(\frac{\bar{\varepsilon}/\varepsilon_s - 1}{4/\zeta - 1} \right)^2 \right], \quad |\bar{\varepsilon}| > |\zeta \varepsilon_s| \quad (2.30)$$

where:

$$\zeta = \frac{5.8}{\sqrt{f'_c (MPa)}} \frac{1}{\sqrt{1 + 400 \bar{\varepsilon}_T}} \left(1 - \frac{|\beta|}{24} \right) \overbrace{\left(1.15 + \frac{|\beta| (0.09|\beta| - 1)}{6} \right)}^{w_p \leq 0.9} \quad (2.31)$$

$$D = 1 - 0.4 \frac{\varepsilon'_s}{\varepsilon_s} \leq 1.0 \quad (2.32)$$

$$\beta = \frac{1}{2} \tan^{-1} \left[\frac{\gamma_{12}}{(\varepsilon_1 - \varepsilon_2)} \right] \quad (2.33)$$

$$(Stage\ UC)\ \sigma^c = E'_c \bar{\varepsilon} + \sigma_{ci}, \quad \text{if } \varepsilon_{ci} \leq \bar{\varepsilon} < 0 \quad (2.34)$$

where: E'_c = decompression modulus of concrete = $E_{co} = \frac{k f'_c}{\varepsilon_s}$

k = a constant introduced to impose an upper slope $E_{co} = \frac{k f'_c}{\varepsilon_s}$ at the initial portion of the compressive stress-strain relationship of concrete. Taking $k = 1.4$ makes the slope E_{co} lower than $\frac{2f'_c}{\varepsilon_s}$, the initial slope at origin of a parabolic curve.

2.8.1.2. Tension Envelope

The stress-strain relationships of concrete in tension are given as:

$$(Stage\ T1) \quad \sigma^c = E_c^n(\bar{\varepsilon} + \bar{\varepsilon}_{ci}), \text{ if } 0 \leq \bar{\varepsilon} < \varepsilon_{cr} \quad (2.35)$$

Where E_c^n = modulus of concrete in tension before cracking given by the slope of the line joining the point representing the end of decompression of the stress-strain curve to the cracking tensile stress of concrete, f_{cr} (given by $0.31\sqrt{f'_c}$ (MPa)) corresponding to a strain of 0.00008.

$$(Stage\ T2) \quad \sigma^c = f_{cr} \left(\frac{\varepsilon_{cr}}{\bar{\varepsilon} + \bar{\varepsilon}_{ci}} \right)^{0.4}, \text{ if } \bar{\varepsilon} > \varepsilon_{cr} \quad (2.36)$$

2.8.1.3. Unloading and Reloading

The unloading and reloading paths defined in the concrete constitutive model in CSMM were simplified in ConcreteL01 as shown in Fig. 2.4. The unloading and reloading paths from the ascending branch of the compressive envelope are simplified as one straight line and the slope is taken as the modulus of concrete E_{co} . The slope of the unloading and reloading paths from the descending branch of the compressive envelope is simplified as one straight line with a slope of $0.8 E_{co}$. The slopes of the unloading and reloading paths in tension are dependent on the stage of closing of the cracks. During the partial closing of the concrete cracks (region represented by “P” in Fig. 2.4) the slope of the unloading and reloading curve is given by the slope of the straight line joining the unloading point on the envelope curve to the point having a compressive stress of $0.2 f_{cr}$ and a strain equal to one-third of the strain at the unloading point on the descending envelope curve in tension. During the full closing of the concrete cracks (region represented by “F” in Fig. 2.4) the slope of the unloading and reloading curve is given by the slope of the straight line joining the following two points: the first point has a compressive stress of $0.2 f_{cr}$ and a strain equal to one-third of the strain at the unloading point on the descending envelope curve in tension; the second point has a strain of 0 and a stress given by the difference of a compressive stress of $1.5 f_{cr}$ and a tensile stress of 0.8 times the stress at the unloading point on the descending envelope curve in tension.

After the full closure of the cracks, the slope of the stress-strain curves in the compression region depends on the compression history in the previous cycle. If the compressive stress in the previous cycle is less than the peak compressive stress, the slope of the stress-strain curve is given by the slope of the straight line joining the point representing the full closing of the cracks to the unloading point on the ascending envelope curve in compression. If the compressive stress in the previous cycle is greater than the peak compressive stress, the slope of the stress-strain curve is given by 93% of the slope of the straight line joining the point representing the full closing of the cracks to the unloading point on the descending envelope curve in compression.

2.8.2. *SteelZ01*

Fig. 2.5 incorporates both the envelope and the unloading/reloading pattern of uniaxial constitutive relationships of embedded mild steel (Mansour 2001) in the CSMM and CSMM-PC. The equations for the envelope are given as:

$$(Stage\ 1T)\ f_s = E_s \bar{\varepsilon}_s, \text{ if } \bar{\varepsilon}_s \leq \bar{\varepsilon}_n \quad (2.37)$$

$$(Stage\ 2T)\ f_s = f_y \left[(0.91 - 2B) + \left(0.02 + 0.25B \frac{\bar{\varepsilon}_s}{\varepsilon_y} \right) \right], \text{ if } \bar{\varepsilon}_s > \bar{\varepsilon}_n \quad (2.38)$$

$$\text{where } B = \frac{1}{\rho} \left(\frac{f_{cr}}{f_y} \right)^{1.5} \text{ and } \rho \geq 0.15\% \quad (2.39)$$

$$\bar{\varepsilon}_n = \varepsilon_y (0.93 - 2B) \quad (2.40)$$

$$(Stage\ 2C)\ f_s = -f_y, \quad (2.41)$$

The nonlinear unloading and reloading paths are described in Eqs. 2.42 to 2.45.

$$(Stage\ 3\ and\ Stage\ 4)\ \bar{\varepsilon}_s - \bar{\varepsilon}_{si} = \frac{f_s - f_i}{E_s} \left[1 + A^{-R} \left| \frac{f_s - f_i}{f_y} \right|^{R-1} \right], \quad (2.42)$$

$$\text{where } A = 1.9 k_p^{-0.1} \quad (2.43)$$

$$R = 10k_p^{-0.2} \quad (2.44)$$

$$k_p = \frac{\bar{\epsilon}_p}{\bar{\epsilon}_n} \quad (2.45)$$

In Fig. 2.6, the dashed curves are the unloading and reloading paths defined by the CSMM, and the solid curves are the linear simplifications implemented in SteelZ01. Two turning points, (ϵ_{m1}, f_{m1}) and (ϵ_{m2}, f_{m2}) in Fig. 2.6, are selected as the points at which $f_{m1} = \pm 0.65f_y$ and $f_{m2} = 0$, and ϵ_{m1} and ϵ_{m2} are calculated by substituting f_{m1} and f_{m2} into f_s of Eq. 2.41, respectively. Once the turning points are determined, the stress of the point on the line segments is a linear function of the strains and stresses of the turning points and can be easily calculated from a given strain. In this way, the iteration is bypassed with acceptable deviation from the original curves. To calculate A and R in Eqs. 2.43 and 2.44 default values of the coefficients are set as 1.9 and 10 as shown in the equations. The values of these coefficients can be changed.

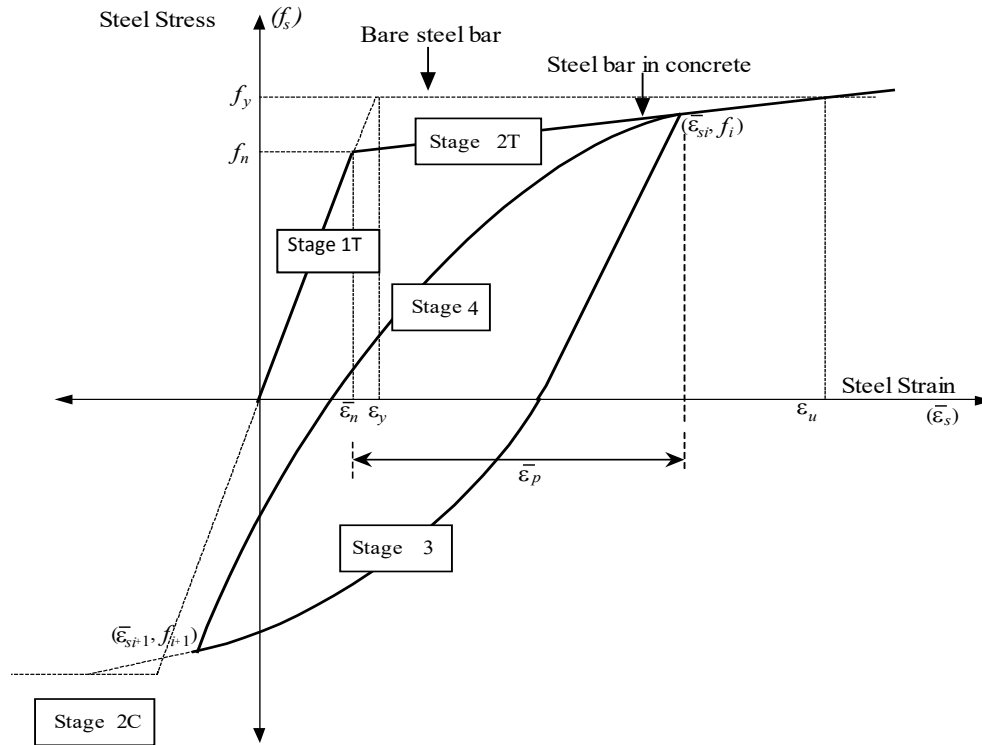


Fig. 2.5 Cyclic Smeared Stress-Strain Curve of Embedded Mild Steel Bars (Mansour 2001)

2.8.3. TendonL01

The tendon module TendonL01 is illustrated in Fig. 2.7. It incorporates the envelope for the uniaxial constitutive relationships of embedded prestressing tendons in the SMM-PC. The equations for the envelope in tension are given as Eqs. 2.46 and 2.47.

$$f_{ps} = E_{ps} \bar{\epsilon}_s, \quad \bar{\epsilon}_s < \frac{0.7 f_{pu}}{E_{ps}}, \quad (2.46)$$

$$f_{ps} = \frac{E_{ps}'' \bar{\epsilon}_s}{\left[1 + \left(\frac{E_{ps}'' \bar{\epsilon}_s}{f_{pu}'} \right)^5 \right]^{\frac{1}{5}}}, \quad \bar{\epsilon}_s \geq \frac{0.7 f_{pu}}{E_{ps}}, \quad (2.47)$$

Where: E_{ps} = elastic modulus of prestressing tendons taken as 200 GPa (29000 ksi).

f_{pu} = ultimate strength of prestressing tendons taken as 1862 MPa (270 ksi).

E_{ps}'' = Young's modulus of prestressing tendons, used in plastic region (Eq. 2.47), taken as 209 GPa (30345 ksi) (Wang, 2006).

f_{pu}' = reduced strength of prestressing tendons taken as 1793 MPa (260 ksi).

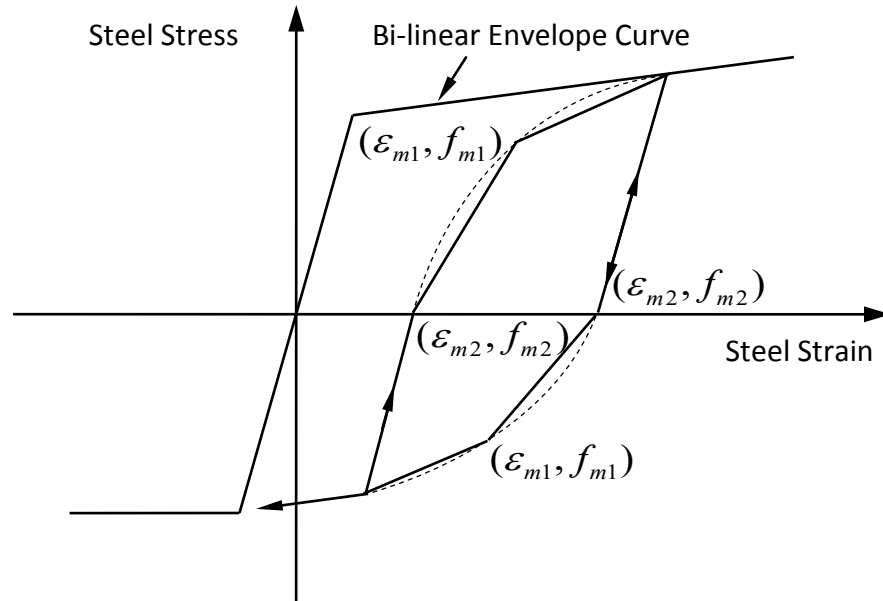


Fig. 2.6 SteelZ01 Material Module

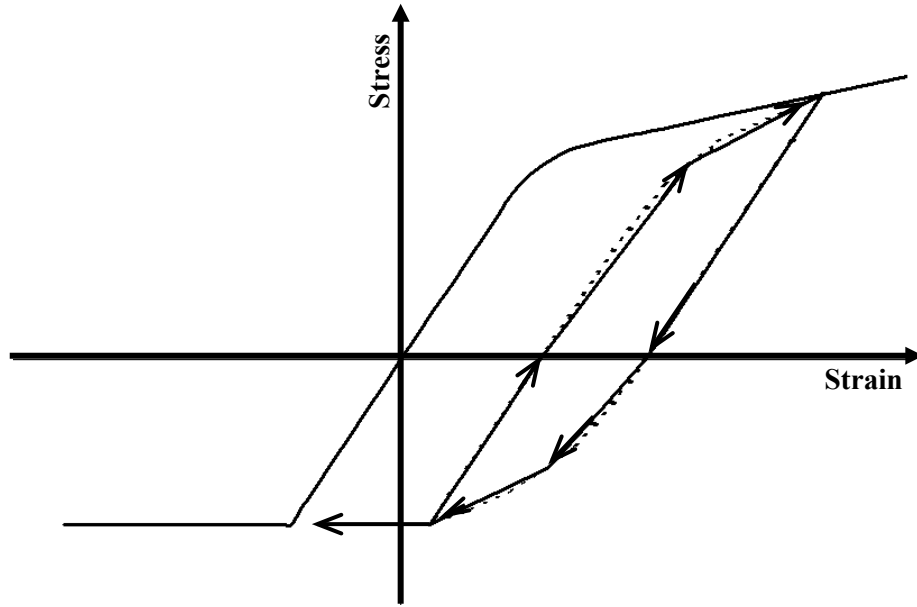


Fig. 2.7 TendonL01 Material Module

However the equations for the compression envelope were the same as the ones used for SteelZ01 module. Even the nonlinear unloading and reloading paths for module SteelZ01 was also used for creating module TendonL01. So the module developed for TendonL01 differs from the SteelZ01 module mainly in the constitutive relationships in the tensile envelope. The constitutive relationships in tension, compression, and unloading and reloading for TendonL01 module are shown in Fig. 2.7.

Then Laskar (2009) used the previous constitutive laws to develop a membrane element PCPlaneStress and implemented this element in OpenSees frame to be used to predict the shear behavior of structural elements such as pretensioned prestressed girders behavior under vertical loads and prestressed columns behavior under lateral loads. The fiber element already available in the OpenSees framework was used to resist any normal forces due to the flexure behavior. Five girders have been tested previously at University of Houston were simulated to validate this model. As it was mentioned before these girders had a concrete strength 9,370 to 10,800 psi.

In this research work, 10 prestressed concrete girders with high strength concrete up to 17,000 psi with different amount of transverse steel and shear span to depth ratio are simulated to validate these constitutive models of prestressed concrete.

PART I: MAXIMUM SHEAR STRENGTH AS A FUNCTION OF CONCRETE STRENGTH

CHAPTER 3 EXPERIMENTAL PROGRAM TO STUDY MAXIMUM SHEAR STRENGTH AS A FUNCTION OF CONCRETE STRENGTH

3.1. Introduction

Several variables affect the shear behavior of prestressed concrete girders, such as concrete strength, girder height, percentage of transverse steel, and shear span to effective depth ratio a/d . In this chapter tests on ten 25 feet long prestressed concrete girders (groups A, F and C shown in Fig. 1.4) are reported to study maximum shear strength, $V_{n,max}$, as a function of concrete compressive strength, f'_c , having different percentage of transverse steel, ρ_v , and different shear span to effective depth ratio, a/d .

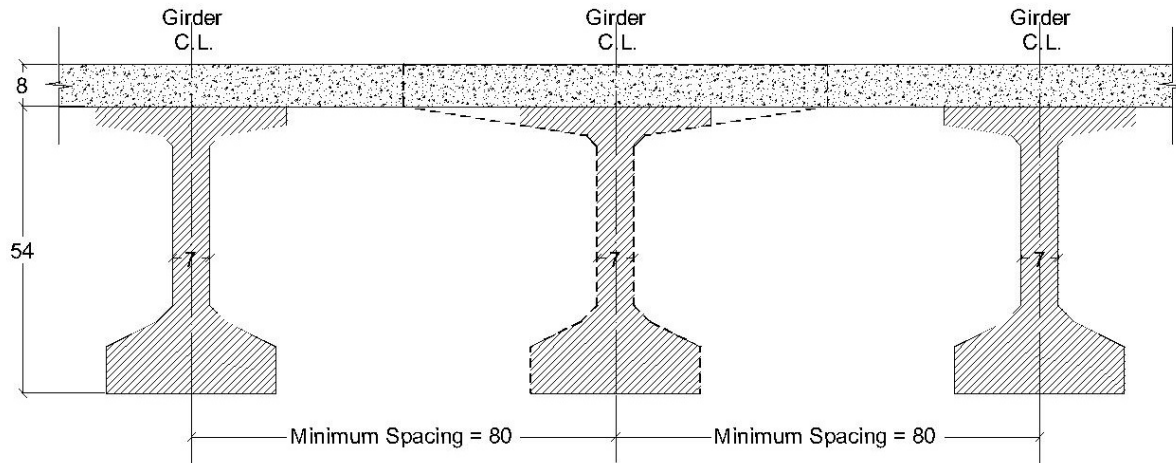
3.2. Tested Girders

Tx-series of PC girders are currently used by TxDOT for the construction of highway bridges in state of Texas. All Tx-series girders have a web thickness of 7 inches and depths ranging from 28 to 72 inches. The Tx28 girder has a wide web compared to its shallow depth, making the web relatively stouter/compact. The Tx70 girder has a relative thin web compared to its huge depth, making the web very slender with high chance to have end zone failure.

Hence, to ensure shear failure without any local failure in the end regions, it was decided to study Tx54 in this research. Typically Tx-series girders have a top slab with a typical thickness 8 inches and the minimum spacing between girders is 80 inches, as shown in Fig. 3.1. In this research an internal Tx54 was considered with a top slab 80 inches wide, as shown in Fig. 3.2. The resulting girder cross-section was scaled down to 43% to form the “modified Tx28” girder. The cross-section of the modified Tx28 girder is shown in Fig. 3.2.

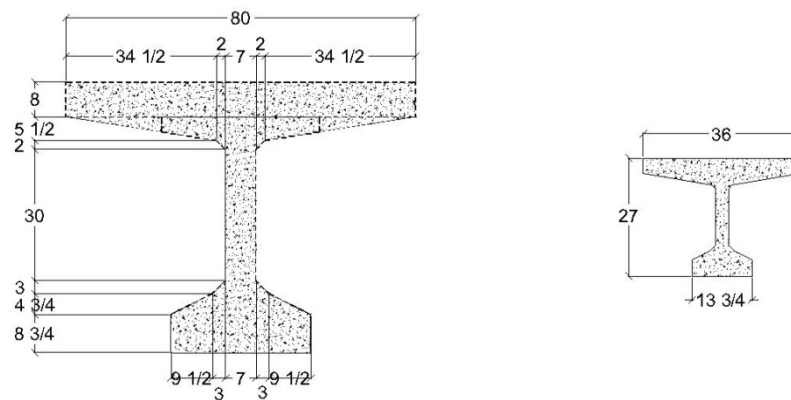
Ten full-scale modified Tx28 girders – with a length of 25 feet were tested at UH under this research work. Two “Group A” Girders (A1 and A2) with concrete compressive strength of $f'_c \cong 7,000 \text{ psi}$; four “Group F” Girders (F1 to F4) with concrete compressive strength of $f'_c \cong 13,000 \text{ psi}$; and four “Group C” Girders (C1 to C4) with concrete compressive strength of $f'_c \cong 16,000 \text{ psi}$ were investigated in this research. Table 3.1 shows the various concrete mix proportions used for casting the girders belonging to these three groups. The first two concrete

mixes (i.e., for Groups A and F) were produced in the Texas Concrete Company precast plant in Victoria, Texas, while the concrete mix for Group C was produced in the Flexicore of Texas precast plant in Houston, Texas.



(All Dimensions are in Inches)

Fig. 3.1 Layout of Tx54 Girders with 8 inches Top Deck



(All Dimensions are in Inches)

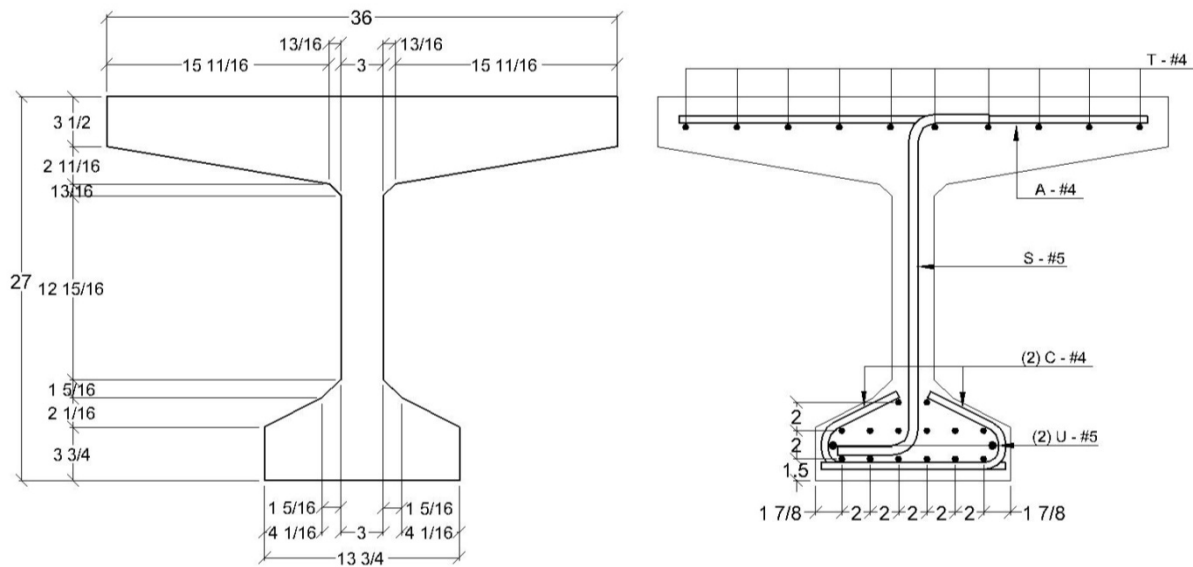
Fig. 3.2 Full Scale and Scaled Down Cross-Sections

Table 3.1 Concrete Mix Proportions Used for Casting Girders

Materials (lb/yd³)	Group A	Group F	Group C
Cement Type-III	368	519	700
Fly Ash Type-F	150	248	200
Cementitious Content	518	767	900
Fine Aggregate	1156	1156	1070
Coarse Aggregate	2200 ¹	1899 ¹	2200 ²
Coarse Aggregate/Fine Aggregate Ratio	1.91	1.64	2.06
Water	180	230	240
Water/Cement Ratio	0.49	0.43	0.34
Water/Cementitious Materials Ratio	0.35	0.30	0.27
Superplasticizer (fl.oz./cwt)	-	9.6 ³	12.8 ⁴
Retarder (fl.oz./cwt)	-	1	4
Slump (inches)	6.5	8.5	10.50
Targeted Min. 28 th Day Strength (psi)	8000	10500	16000
Actual Average Strength (psi) ⁵	7000	13000	16000

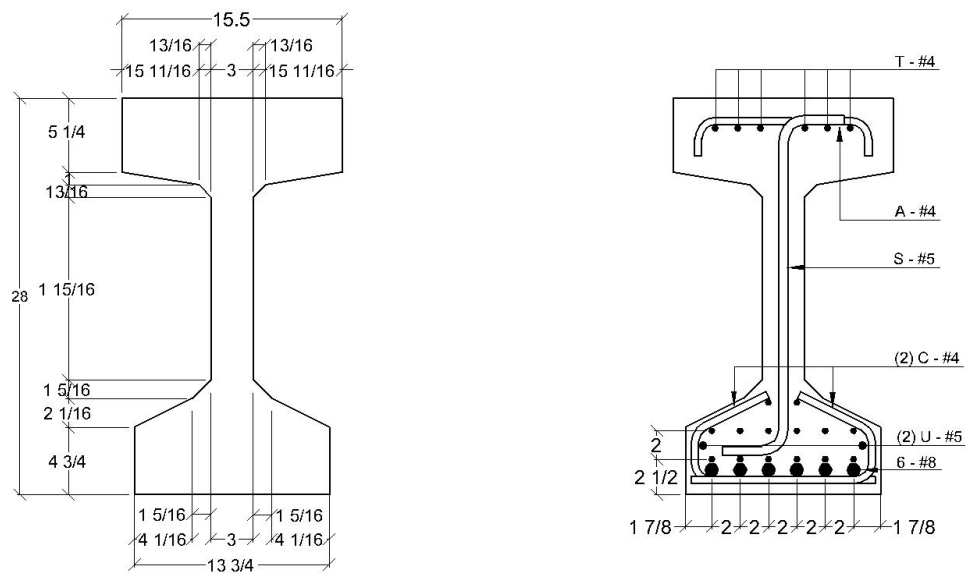
1- ¾ in. rounded river-bed; 2- ¾ in. Dolomite, Burnet, Texas; 3– BASF (Glenium7700); 4- Sika (ViscoCrete2110); 1 lb/yd³ = 0.593 kg/m³ ; 5- At the testing day

In this research, different shear span to depth ratio was used for different concrete strength. The test results of girders made with different concrete strength will be used to investigate the validity of the equations proposed by Laskar et al. (2010) to predict both concrete and steel shear contributions at different shear span to depth ratios (**a/d**) of a girder with any concrete compressive strength. Girders A1, F1, F3, C1, and C3 were designed having the cross section shown in Fig. 3.3 with shear span to effective depth ratio of 1.77 to study the web shear behavior. Girders A2, F2, F4, C2, and C4 were designed with higher shear span to effective depth ratio in attempting to study the flexural shear behavior. Girders A2, F2, and F4 were designed having the cross section shown in Fig. 3.3, while girders C2 and C4 were designed having the cross section in Fig. 3.4. The locations of the applied loads and support reactions are shown in Figs. 3.5 to 3.9.



(All Dimensions are in Inches)

Fig. 3.3 Cross-Section and Reinforcement Details for Modified Tx28 Girders



(All Dimensions are in Inches)

Fig. 3.4 Cross-Section and Reinforcement Details for Modified Tx28 Girders C2 and C4

When shear force is applied on a 2D RC Element, both concrete and steel contribute to resist the applied shear force. If the cross section is designed to be at balanced condition, this means that the steel yields at the same time the concrete crushes giving the limit for design. If the concrete crushes before the steel yields, the cross-section is said to be designed as over-reinforced, and the mode of failure is brittle. On the other hand if the steel yields before the concrete crushes, the cross-section is designed to be under-reinforced, and the resulting mode of failure is ductile. Thus, in order to achieve a ductile failure mode, the girder cross-section must be designed to be under-reinforced.

In this study, structural behavior of girders under web-shear and flexure-shear failure modes was investigated with balanced and over-reinforced cross-sections. Girders A1, A2, F1, F2, C1, and C2 were designed at balanced condition while Girders F3, F4, C3, and C4 were designed to have over-reinforced cross-sections. The web of all girders was reinforced in the transverse direction with one legged stirrups namely called S rebars which is fabricated using #5 mild steel bars with ultimate tensile strength 60,000 psi.

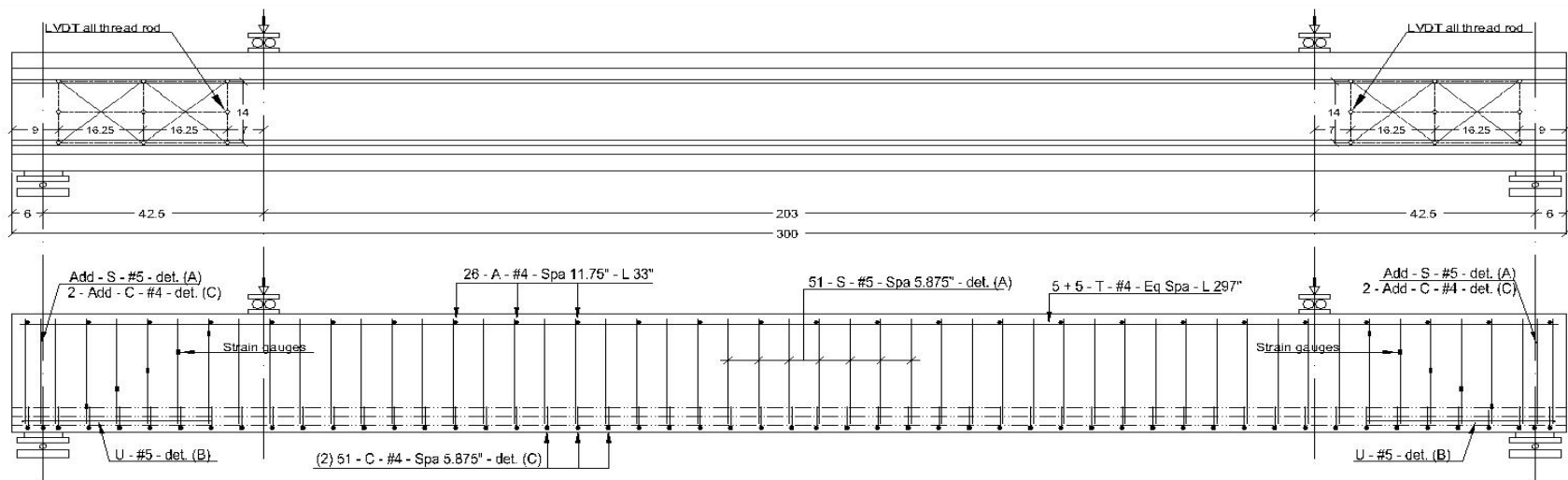
In addition to the transverse direction reinforcement, #5 bar was used for U rebars which were designed to resist the end zone bearing, spalling, and bursting stresses. #4 bar was used for C, A, and T rebars; where C rebars were designed to confine concrete and act as secondary reinforcements in the bottom flange, while A and T rebars were designed to be the lateral and longitudinal flexural reinforcement in the top flange. The fully detailed longitudinal cross-section for all the girders is shown in Figs.3.5 to 3.9.

For flexural resistance, Groups A and F, fourteen 0.5-in. diameter, seven-wire, low-relaxation prestressed straight tendons were used, while in Group C, a 0.5-in. diameter oversize, seven-wire, low-relaxation straight tendons were used to increase the bending moment capacity ensuring shear failure of the girders. The prestressing tendons had an ultimate tensile strength of 270 ksi. The locations of prestressing tendons and different types of reinforcing steel in the tested girders are shown in Fig. 3.3 and Fig. 3.4. Table 3.2 presents the reinforcement details for all the tested girders.

Table 3.2 Reinforcement Details for Modified Tx28 Girders

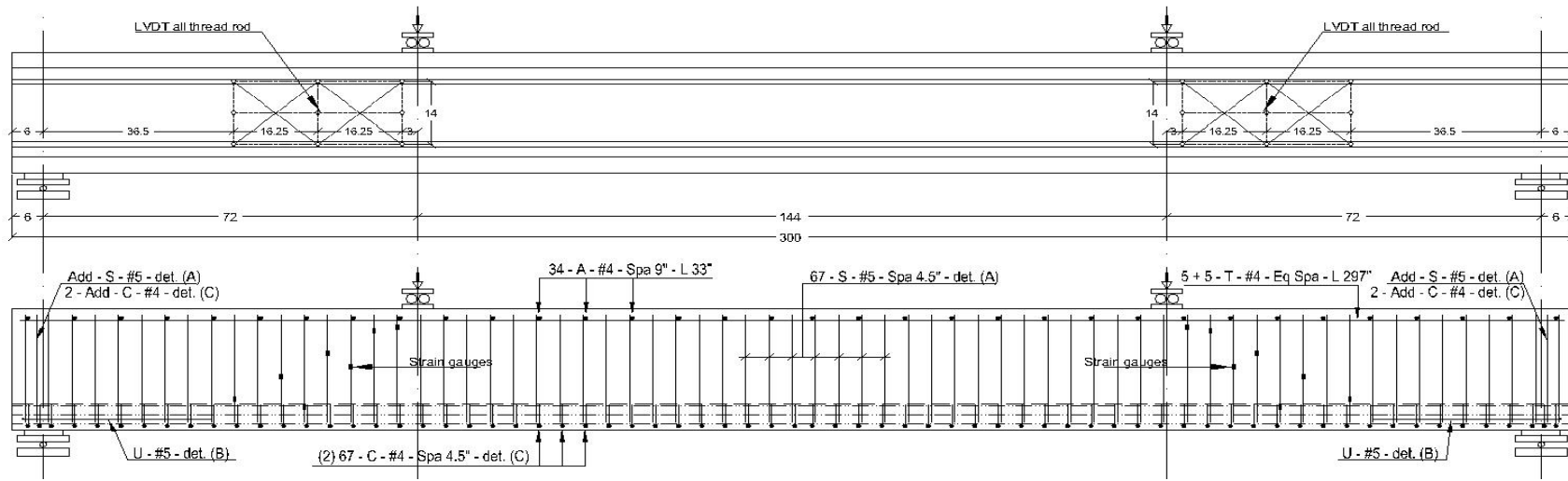
Girder	Tendons		Mild Steel Reinforcement								
	Nos.	Dia. (in.)	Transverse Steel (#5) “S”-Rebar		Top Flange Flexural Steel (#4)				Bottom Flange Flexural Steel		
			Sp.	Ratio (%)	Longitudinal Direction “T”-Rebar		Lateral Direction “A”-Rebar		Extra Flexural Steel	Confinement Steel (#4) “C”-Rebar	
					Nos.	Sp.	Nos.	Sp.		Nos.	Sp.
A1	14	0.5	5.875	1.76	10	3.5	26	11.75	-	106	5.875
A2	14	0.5	4.5	2.30	10	3.5	34	9	-	138	4.5
F1	14	0.5	5.5	1.88	10	3.5	28	11	-	114	5.5
F2	14	0.5	4	2.58	10	3.5	38	8	-	154	4
F3	14	0.5	4.25	2.43	10	3.5	36	8.5	-	146	4.25
F4	14	0.5	3.125	3.31	10	3.5	32	9.75	-	196	3.25
C1	14	0.5*	4	2.58	10	3.5	27	12	-	154	4
C2	14	0.5*	3.25	3.18	6	1.5	32	9.75	6 # 8	96	6.5
C3	14	0.5*	3	3.44	10	3.5	27	12	-	100	6
C4	14	0.5*	2.5	4.13	6	1.5	30	7.5	6 # 8	120	5

* - Oversize Sp. – Spacing c/c (inches) Nos. – Total Number of rebars



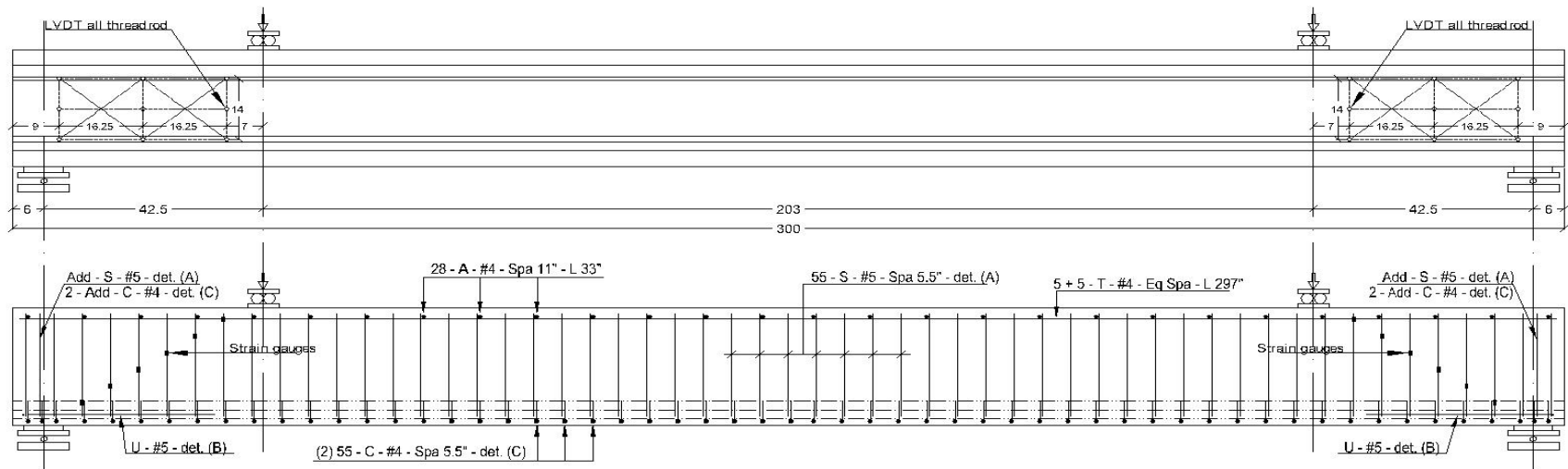
(All Dimensions are in Inches)

Fig. 3.5 Detailed Longitudinal Cross-Section for Girder A1



(All Dimensions are in Inches)

Fig. 3.6 Detailed Longitudinal Cross-Section for Girder A2



(All Dimensions are in Inches)

Fig. 3.7 Detailed Longitudinal Cross-Section for Girder F1

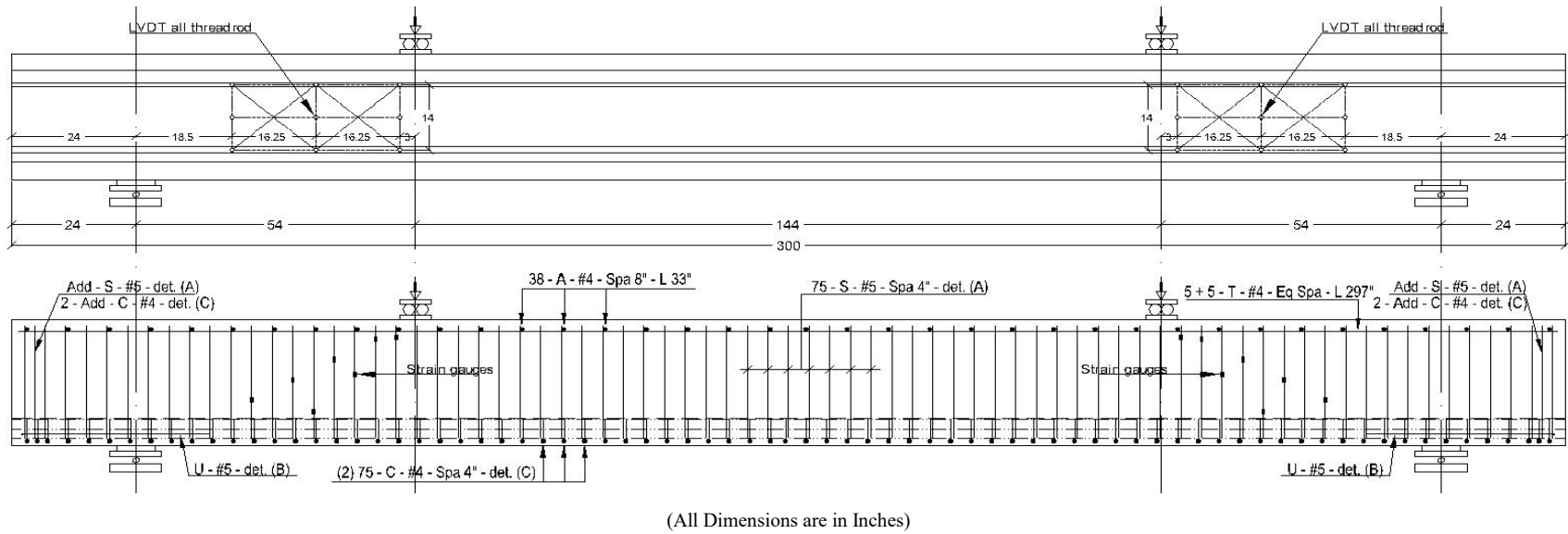
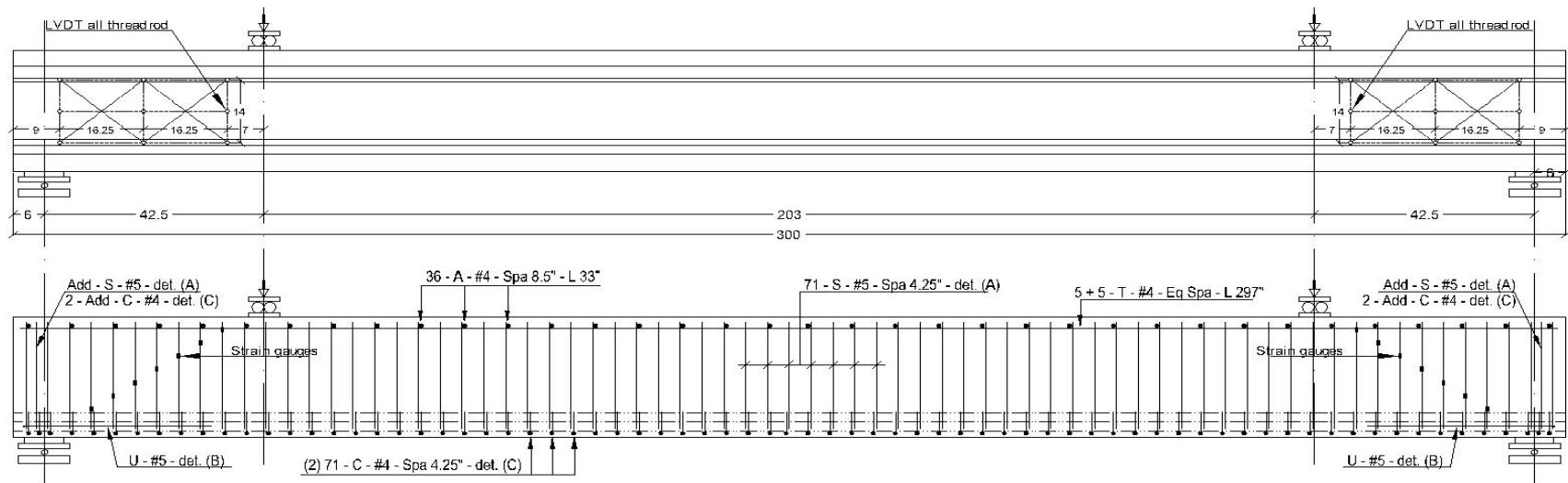
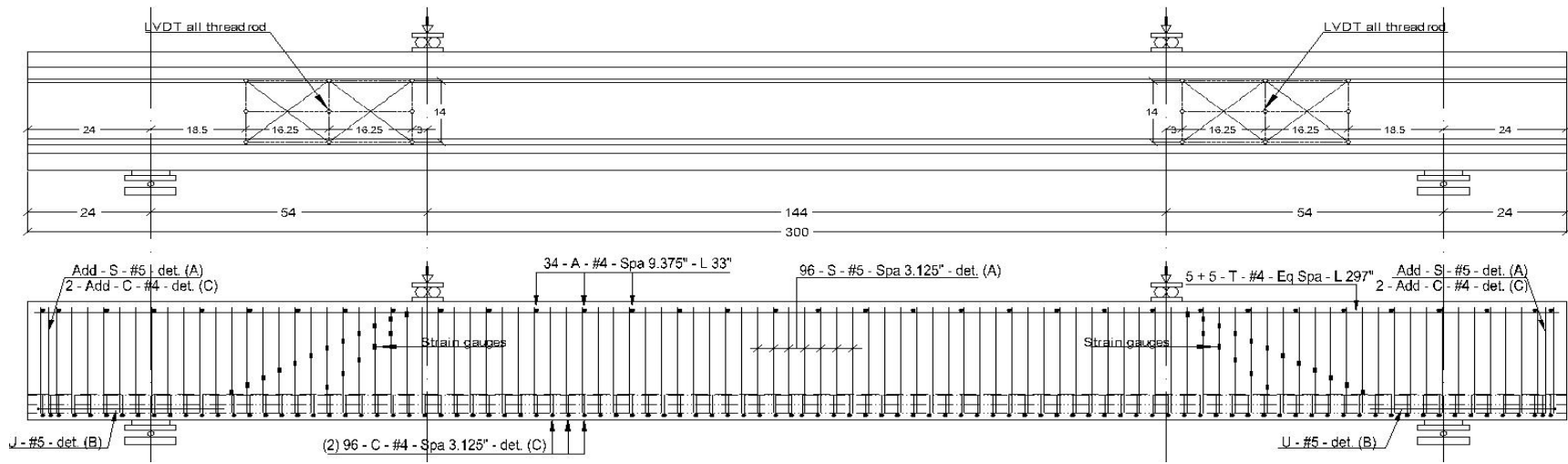


Fig. 3.8 Detailed Longitudinal Cross-Section for Girder F2



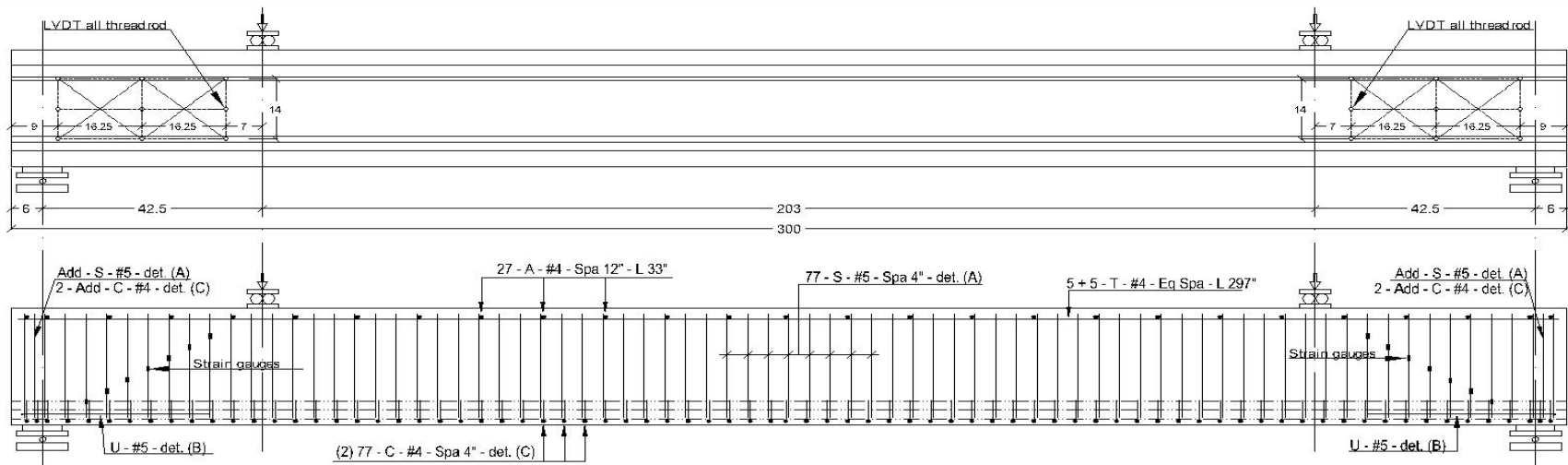
(All Dimensions are in Inches)

Fig. 3.9 Detailed Longitudinal Cross-Section for Girder F3



(All Dimensions are in Inches)

Fig. 3.10 Detailed Longitudinal Cross-Section for Girder F4



(All Dimensions are in Inches)

Fig. 3.11 Detailed Longitudinal Cross-Section for Girder C1

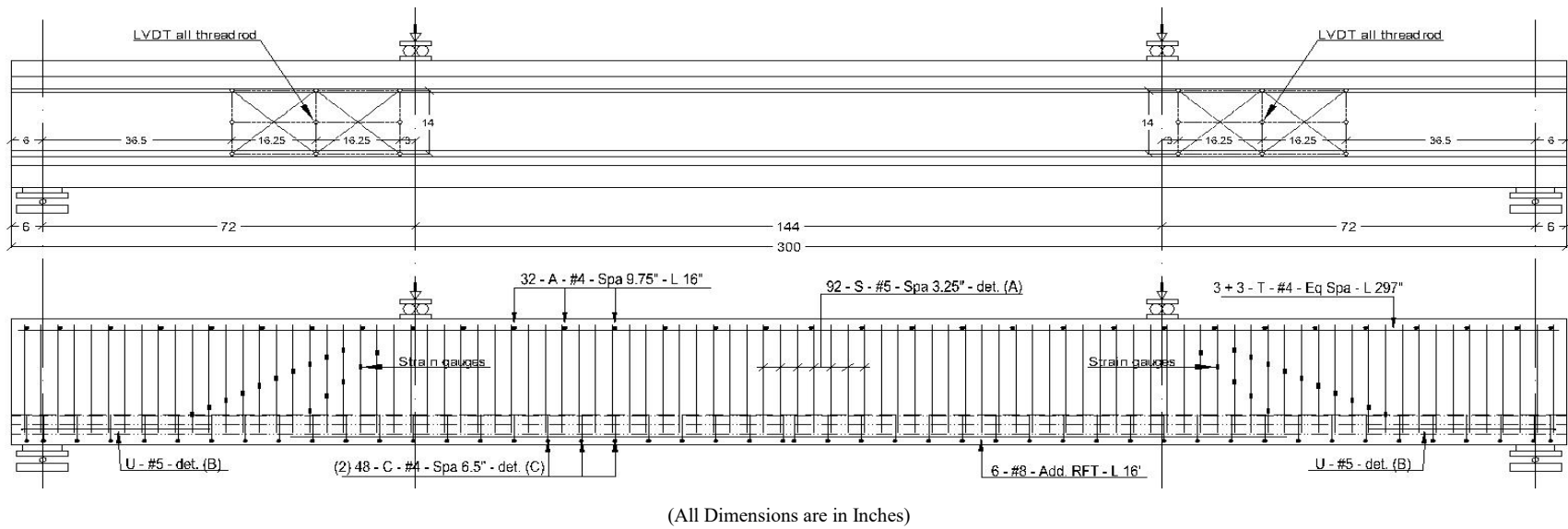


Fig. 3.12 Detailed Longitudinal Cross-Section for Girder C2

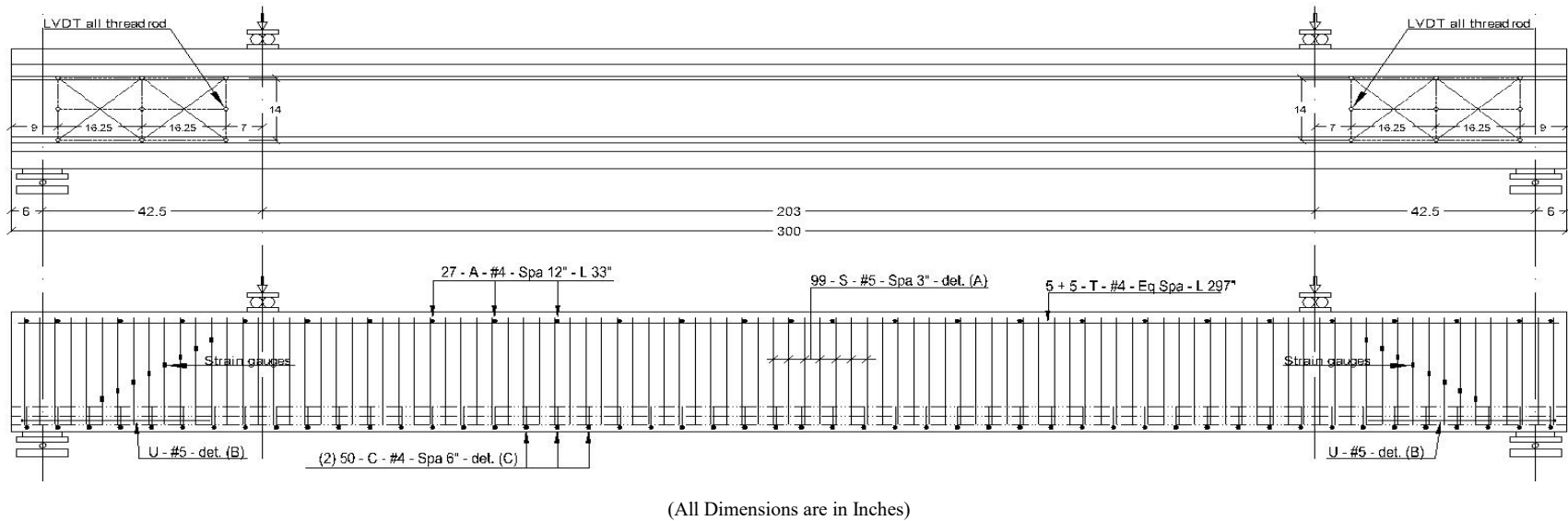
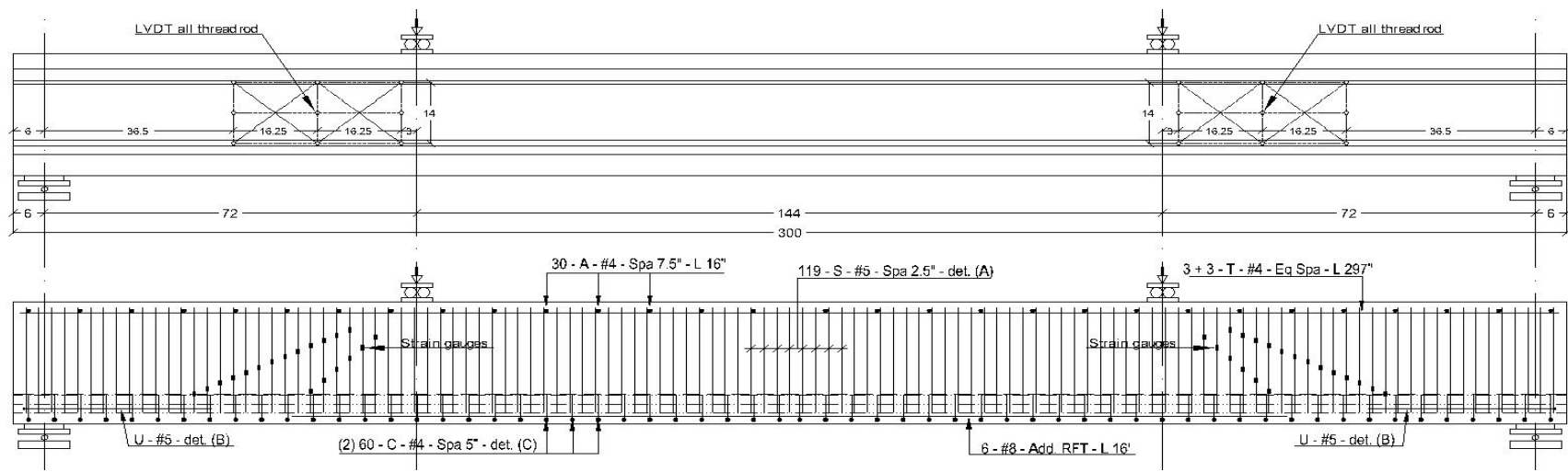


Fig. 3.13 Detailed Longitudinal Cross-Section for Girder C3



(All Dimensions are in Inches)

Fig. 3.14 Detailed Longitudinal Cross-Section for Girder C4

3.3. Manufacturing of Test Girders

The 10 girders have been manufactured at two different companies. The girders belonging to the Groups A and F were cast at Texas Concrete Company, Victoria, Texas, in July 2009. Group C girders were cast at Flexicore of Texas, Pearland, Texas, in June 2010. The prestressing tendons were pretensioned by hydraulic jacks placed in a prestressing steel platform/bed. Transverse steel, including the rebars were instrumented with strain gauges, along with all the other confining and flexural reinforcements were installed in the girders. Fig. 3.15 shows the reinforcement cage of a typical girder.



Fig. 3.15 Reinforcement Cage for a Typical Girder

Specially designed side forms made of styro-foam as shown in Fig. 3.16 and Fig. 3.17 were used to form the required cross-sectional shape of Modified-Tx28 girder. Standard vertical steel side forms rigidly fixed to the prestressing-bed were used to hold the styro-foam forms in place Fig. 3.18.

Steel rods of 6 in. length were installed in the web of each girder on the sides at pre-determined locations as depicted in Fig. 3.16. These steel rods were used to mount the Linear Variable Displacement Transformer (LVDT), which served as instrumentation to measure the average strains in the girders during the load testing.



Fig. 3.16 Styro-Foam Forms with LVDT Rods



Fig. 3.17 Installation of Styro-Foam Forms



Fig. 3.18 Set-up of Steel Side Forms for Girders

The concrete mix was prepared in a plant mixer, transported to the casting site, and deposited into the formworks using a mobile hopper as shown in Fig. 3.19. During casting, spud vibrators were used to compact the concrete. Standard concrete cylinders were cast per each girder. Just prior to the actual girder tests, the concrete cylinders were tested to get the representative concrete compressive strength of the girder. One day after casting the girders, the prestressing tendons were slowly released, and the girders were transported to the storage yard to remove the formwork, as shown in Fig. 3.20.



Fig. 3.19 Concrete Placement Using a Hopper



Fig. 3.20 Removing Styro-Foam Forms from the Girders

3.4. Test Set-up

The girders were subjected to vertical loading up to their maximum shear capacity in a specially built steel loading frame, as shown in Fig. 3.21. Two of the four actuators (namely actuator B and actuator C), each attached to a vertical steel frame, were used to apply the vertical loads on the girders. Each of these two actuators had a capacity of 320 kips in compression. Actuator frames B and C were installed on the north and south end of the girder, respectively. These two actuator frames were sitting on top of two WF18×97 girders, bolted securely to the strong floor. The two WF18×97 girders were 20 ft. long and spaced at 87 in. center to center. Girder was positioned in the middle of this spacing width on top of two load cells placed at north and south ends. The load cells of 500 kips capacity were sitting on top of the steel pedestals fixed to the strong floor. On top of the load cells, bearing plates to support the girders were placed with a roller on the north end and a hinge on the south end, thus allowing the girder to rotate freely at the supports and to expand freely along its length. The actuators were provided with bracings for their lateral stability.



Fig. 3.21 Test Setup for Girders

The position of vertical loads and load-cell supports for all girders of Group A, F, and C are shown in Figs. 3.3 to 3.7. Compressive loads from actuators B and C were applied at 42.5 inches from either supports (i.e., north and south supports) to have $a/d = 1.77$ for Girders A1, F1, F3, C1 and C3. Similarly, actuator loads for Girders F2 and F4 were applied at 54 inches from either supports to have $a/d = 2.25$. Girders A2, C2 and C4 were loaded at 72 inches from the supports to have $a/d = 3.00$. Actuator loads were applied through a roller assembly consisting of two 6

inches x 12 inches x 2 inches thick hardened steel bearing plates and two hardened steel rollers of 2 inches diameter and 12 inches in length, so as to ensure uniform and frictionless load transfer from actuators on to the girder surface. All the bearing plates and rollers were heat-treated to maximum possible hardness, in order to minimize local deformations. Lead sheets were also used between the load bearing plates and girder surface to aid uniform loading. The applied loads and displacements through the actuators were precisely controlled by the MTS “MultiFlex” System. Each girder was first loaded using actuators B and C under a load-control mode at the rate of 2 kips/min. As soon as the slope of load vs. displacement curve for girder being tested dropped, the actuator control-mode was switched to a displacement-control at the rate of 0.2 inch/hour until shear failure occurred at either end of the girder. The displacement-control mode was essential in capturing the ductility or brittleness behavior of the girder failing in shear.

3.5. Instrumentation

Strains in both transverse steel and concrete were measured as load was applied on the girders. Electrical-resistance foil-type strain gauges were installed on transverse steel rebars (i.e., shear steel reinforcement) to measure local maximum strains at critical locations in the girders during the load tests. The strain gauge data obtained during the load tests were used to ascertain the number of transverse steel rebars that may have yielded at the failure shear load.

Girders which were designed to fail in web-shear had strain gauges installed on transverse rebars along the line joining the points of applied load and the load-cell support, i.e., at an angle of about 32°. Girders that were designed to fail in flexure-shear had the strain gauges installed on transverse rebars along two lines representing anticipated shear crack direction in the web. The first line was at 45° to the horizontal as per ACI (2008) code recommendations, and the second line at an angle “ θ ” based on the AASHTO LRFD Specification (2007). Table 3.3 shows the strain gauges’ names and locations in each girder.

To measure the average or smeared strain in concrete within the expected failure region of the girder web, a set of 10 Linear Voltage Differential Transformers (LVDTs) were used in a rosette formation as shown in Fig. 3.22, on both faces (i.e., west and east) and either end of the girder. Table 3.4 shows the names and locations of each LVDT measurement relative to the support and the loading point.

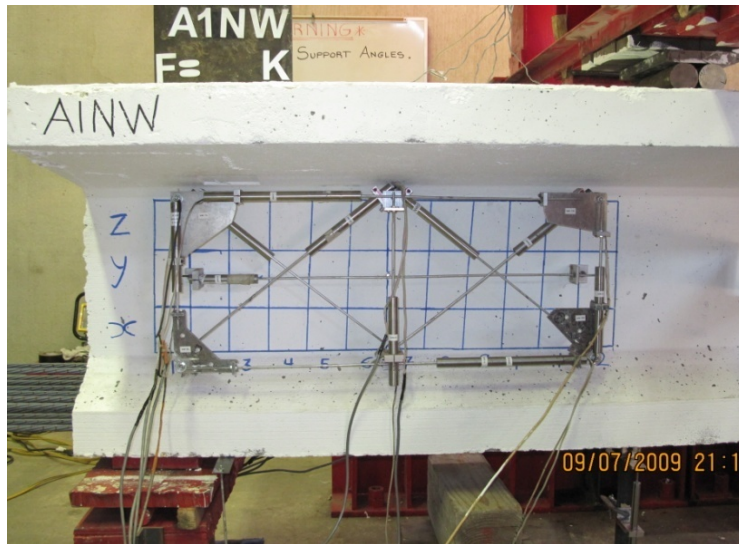


Fig. 3.22 LVDT Rosette Installed on Girders

Table 3.3 Stain Gauges Names and Locations

	North	South
A1		
A2		

Table 3.3-Cont. Stain Gauges Names and Locations

	North	South
F1		
F2		
F3		
F4		

Table 3.3-Cont. Stain Gauges Names and Locations

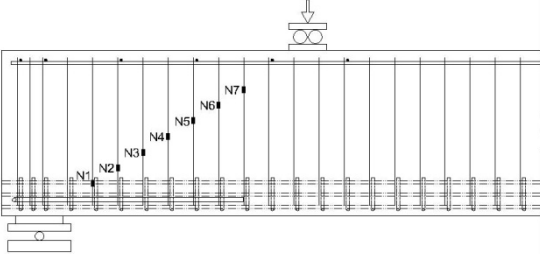
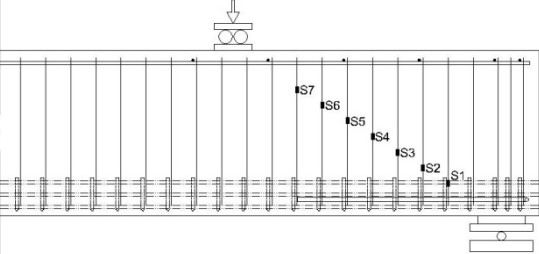
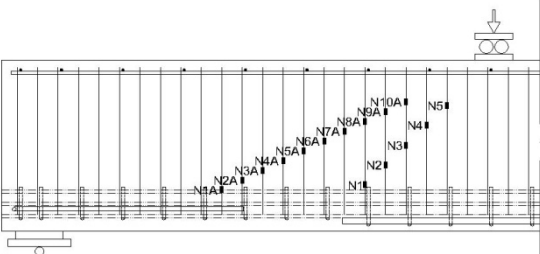
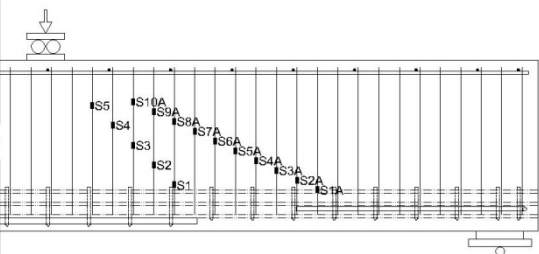
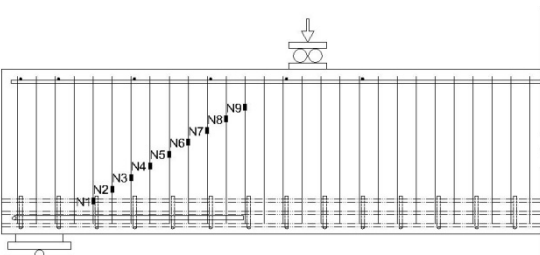
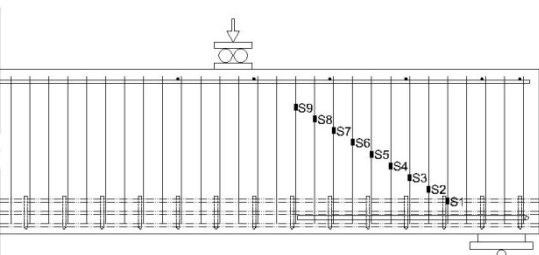
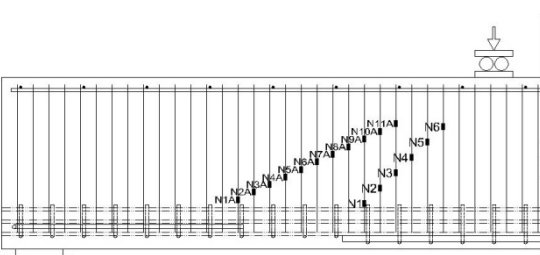
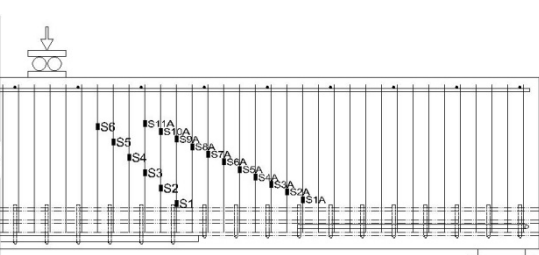
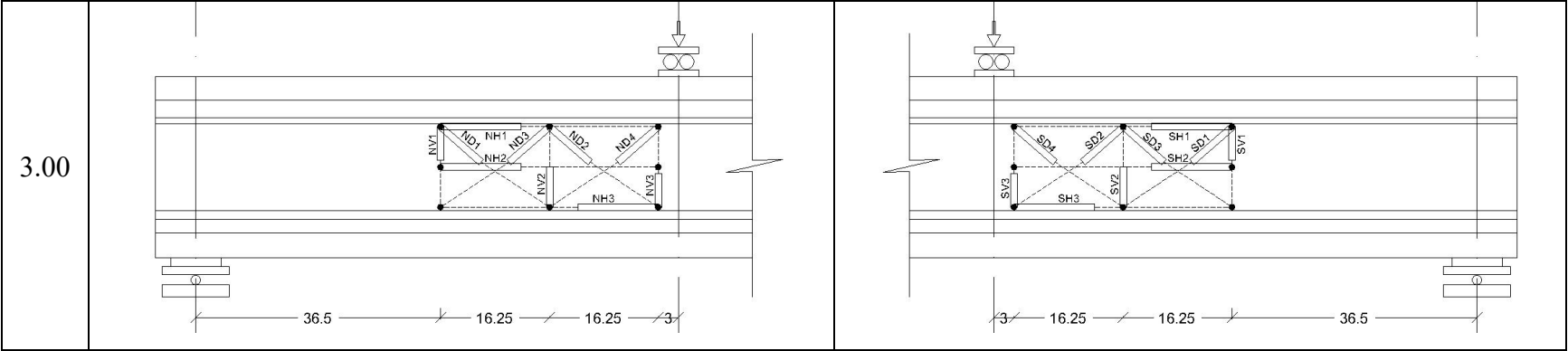
	North	South
C1		
C2		
C3		
C4		

Table 3.4 LVDTs Names and Locations

a/d	North	South
1.77		
2.25		



Six LVDTs placed under the girder were used to measure the vertical displacement, i.e., deflection of the girder during the test. Two of the six LVDTs were positioned under the applied load while the other four were located on both sides of each support to measure the total and net displacements of the girder, respectively. On average, each girder was instrumented with 44 LVDTs and several strain gauges. Data from all the above discussed sensors was continuously monitored and stored by HBM “Spider-8” Data Acquisition System. Shear and flexure cracks formed on the girder during the load test were regularly marked on the grid. Shear crack widths were measured at different load intervals using a handheld microscope having a 0.001 in. measuring precision.

CHAPTER 4 ANALYSIS OF MAXIMUM SHEAR STRENGTH

4.1. Introduction

Ten designed and manufactured girders described in Chapter 3 were tested using the test set-up mentioned in Section 3.4. Two data points for the *ultimate shear strength* were obtained from each girder test, i.e., at the north and south ends of each girder.

This chapter presents the experimental results at both ends of each girder. It includes the shear load versus net deflection curves. Each girder's net deflection was obtained by subtracting the measured deflection by the LVDT placed underneath the girder at the locations of the actuators minus the support settlement measured by the LVDT placed beside the support during test. The test procedure, the mode of failure for each girder, the transverse steel local strain, and the concrete smeared strains in the studied zone measured during the test are presented and discussed. Photos for the crack pattern and the failure at both ends of each girder are presented as well. The maximum shear strength of each end of the girders is presented and compared to the maximum shear strength predicted by the current codes and the UH-proposed equation (Laskar 2010) to validate the UH-proposed equation for different concrete strength. The concrete and transverse steel contributions to the maximum shear strength of each end are calculated. The calculated concrete contribution is used to validate the capability of the UH-proposed equation (Laskar 2010) to predict the concrete contribution for different concrete strength.

4.2. Experimental Results of Group A Girders with $f'_c \cong 7,000$ psi

Group A consists of two girders with concrete compressive strength around 7,000 psi. Both girders had a transverse reinforcement ratio at balanced condition. The two girders in this group have been designed with different shear span to effective depth ratio a/d intending to study both the web shear and flexure shear in normal strength concrete.

4.2.1. Girder A1

This girder was loaded simultaneously at both ends with $a/d = 1.77$. The first shear crack appeared at the south end at a shear load of 40 kips, and on the north end at a shear load of 48 kips, which is clearly shown on the load deflection curves shown in Fig. 4.1. Fig.4.2 (a) and

(b) show that the first crack on the south end had more length than that observed on the north end during the test and both of them are joining the loading point and the support. Having longer crack at lower load at the south end implies weakness of the south end, which resulted in a failure in the south end at a lower shear load than that reached at the north end, as shown in Fig. 4.2 (e) and (f).

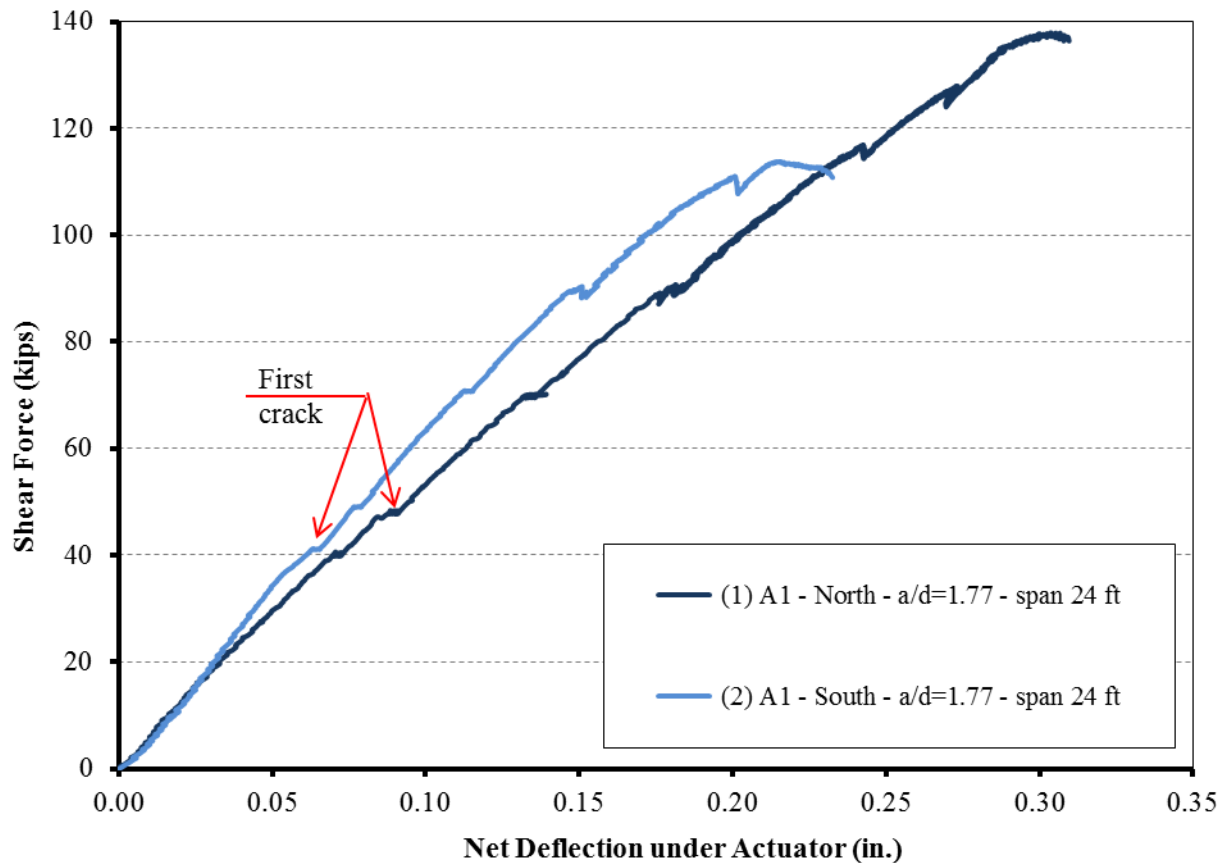
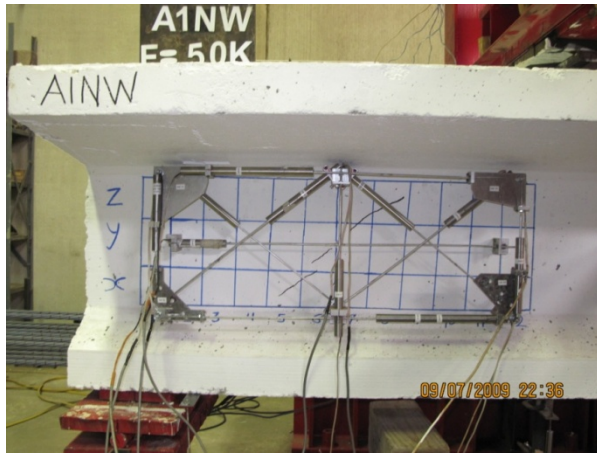


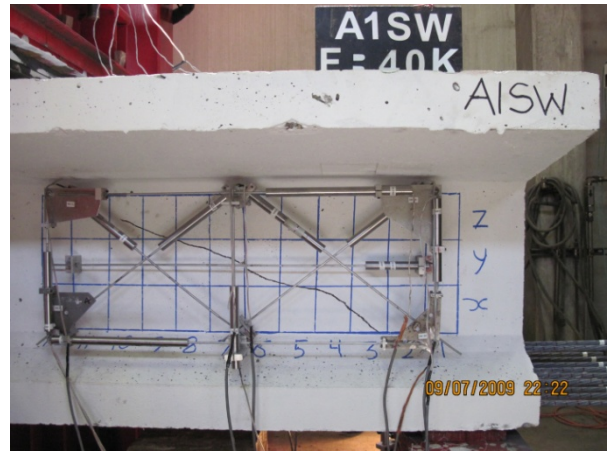
Fig. 4.1 Shear Force vs. Girder Deflection Curves for Girder A1

North End

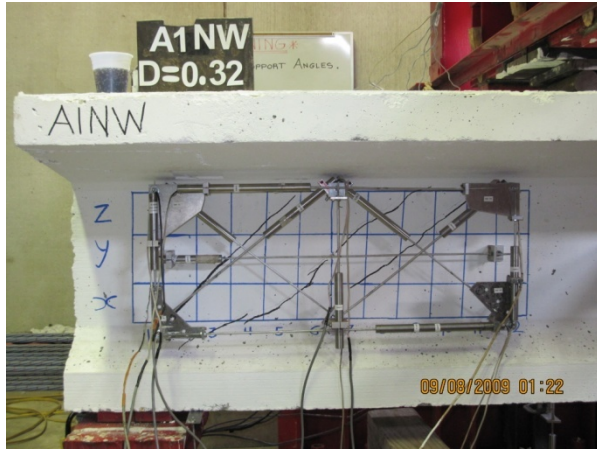


(a) First shear crack at 48 kips

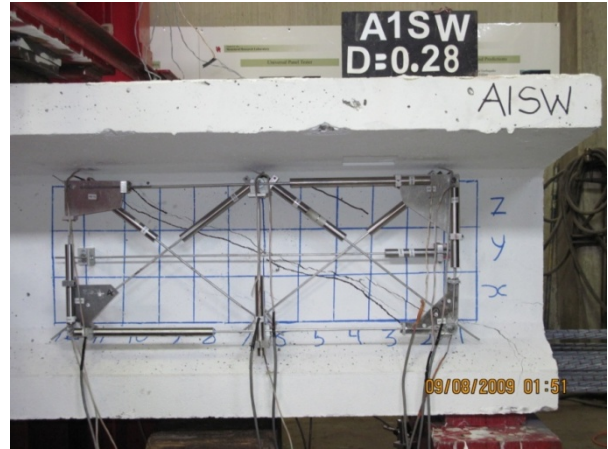
South End



(b) First shear crack at 40 kips



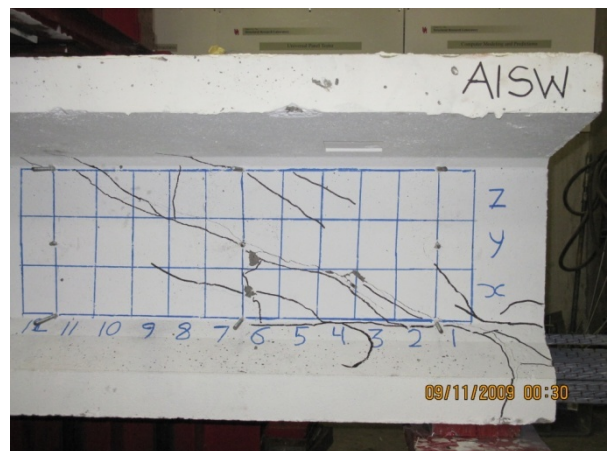
(c) Shear crack pattern before failure



(d) Shear crack pattern before failure



(e) Shear failure at 138.21 kips



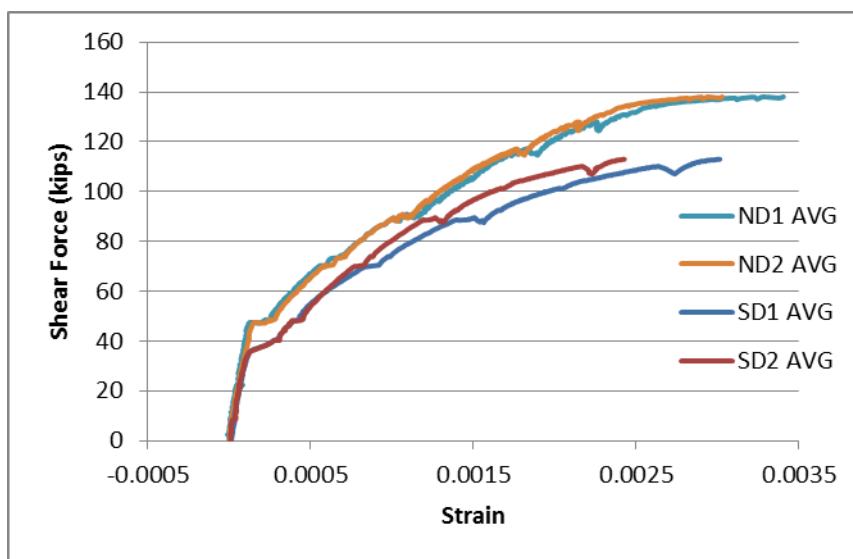
(f) Shear failure at 112.96 kips

Fig. 4.2 Shear Crack Pattern and Failure Mode of Girder A1

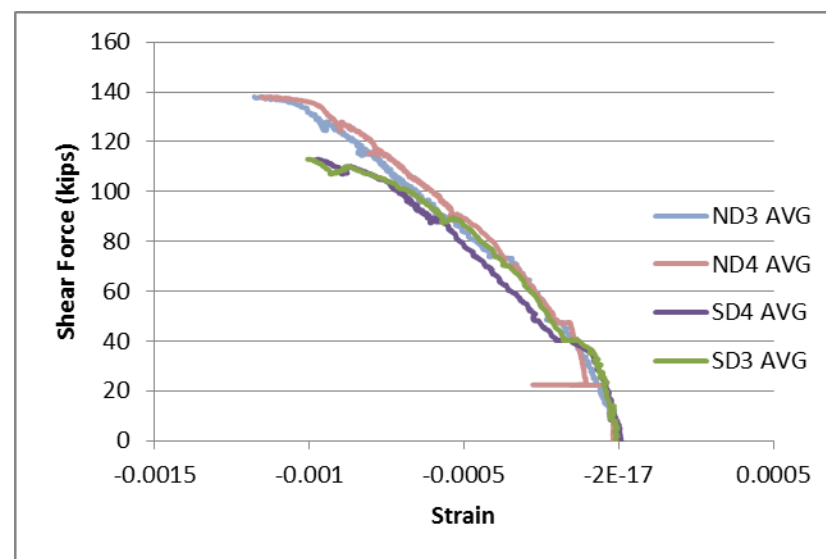
Fig. 4.3 shows the plot of shear force versus average smeared strains measured by LVDTs in all directions for Girder A1. The measured smeared strains in all directions at both ends had the same stiffness before cracking. Although the south side cracked first, both ends had the same post cracking stiffness until an applied shear load of 100 kips, after which the south end started to lose its stiffness inducing a web shear failure at 112.96 kips. Because the failure of the south end did not affect the stability of the girder, the north end was tested until it failed at a shear load of 138.21 kips. At the failure of each end, the smeared compressive strain in the concrete struts was 0.0012 and 0.0010 in average, while the smeared tensile strain across the cracks was 0.0032 and 0.0027 at the north and south ends in average, respectively, as shown in Fig. 4.3 (a) and (b). Web shear failure was clearly visible through the crushing of concrete struts in the web area of Girder A1.

Fig. 4.3 (c) shows the plot of shear force versus the smeared tensile strain in the transverse direction. LVDTs V1 and V3, which are close to the support and the loading point, respectively, show a very minor strain. This is due to missing the main cracks in the studied zone as can be seen in Fig. 4.2 (c) and (d). The transverse smeared strain at the middle of the studied zone by LVDT V2 gives a peak value at an ultimate of 0.0038 and 0.0030 at the north and the south end, respectively.

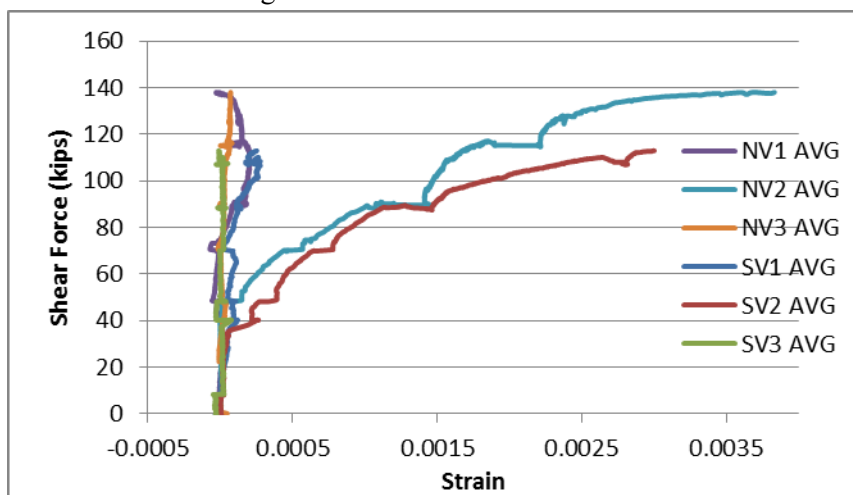
Fig. 4.4 shows the plot of shear force and local tensile strain in the transverse steel rebars measured by strain gauges in Girder A1. The collected data during the test could not provide strong evidence about the strain of the transverse steel at the south end because of missing the zero reading at the beginning of loading. For the north end, the obtained profile of the local strain measured by strain gauge number 5, which was close to the top flange, had a flat plateau indicating reaching the yield strain before crushing of concrete. This suggests that the other rebars that intersected the main shear crack at the middle of the web also yielded.



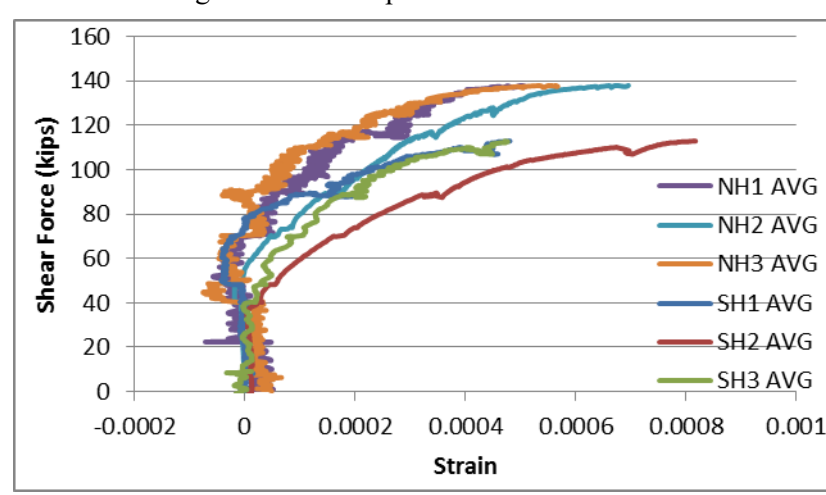
a - Average smeared tensile strain across Cracks



b - Average smeared compressive strain in concrete struts

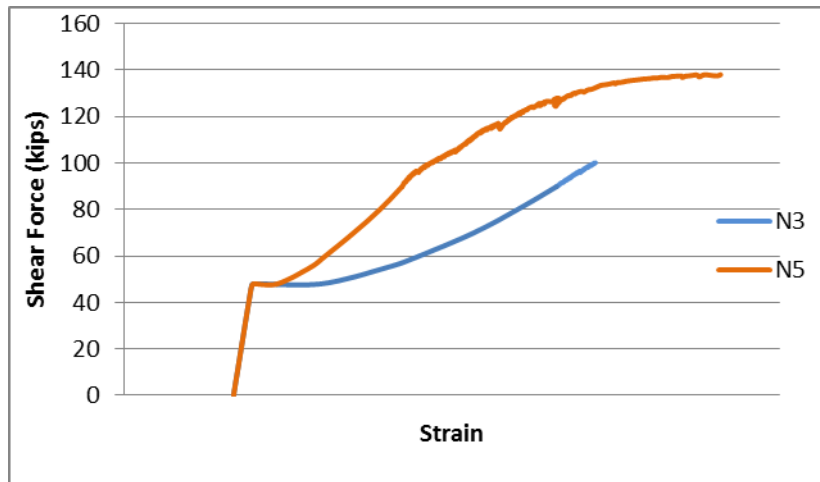


c - Average transverse smeared strain

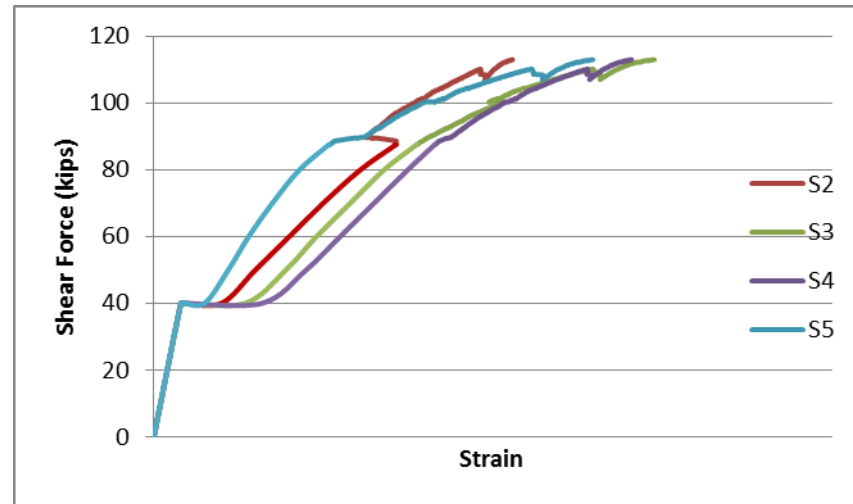


d - Average longitudinal smeared strain

Fig. 4.3 Shear Force vs. Concrete Smeared Strains Curves for Girder A1



a - North strain gauges



b – South strain gauges

Fig. 4.4 Shear Force vs. Local Transverse Tensile Strain of Girder A1

4.2.2. Girder A2

To study the effect of the shear span to depth ratio on the shear behavior and the ultimate shear capacity, this girder was loaded simultaneously having shear span to depth ratio a/d equal to 3.00. Fig. 4.5 shows the shear force versus net deflection curves for both the north and the south ends, which reflects the identical behavior of both ends starting from the appearance of the first shear crack at both ends at a load of 56 kips shown in Fig. 4.6 (a) and (b).

Fig. 4.7 shows the smeared strains measured by LVDTs' rosette at the north and south ends during the first run. Fig. 4.8 shows the plots of shear force and local tensile strain in the transverse steel bars measured by strain gauges located along 45° and 29.7° (AASHTO angles) on both ends of Girder A2 during the same run.

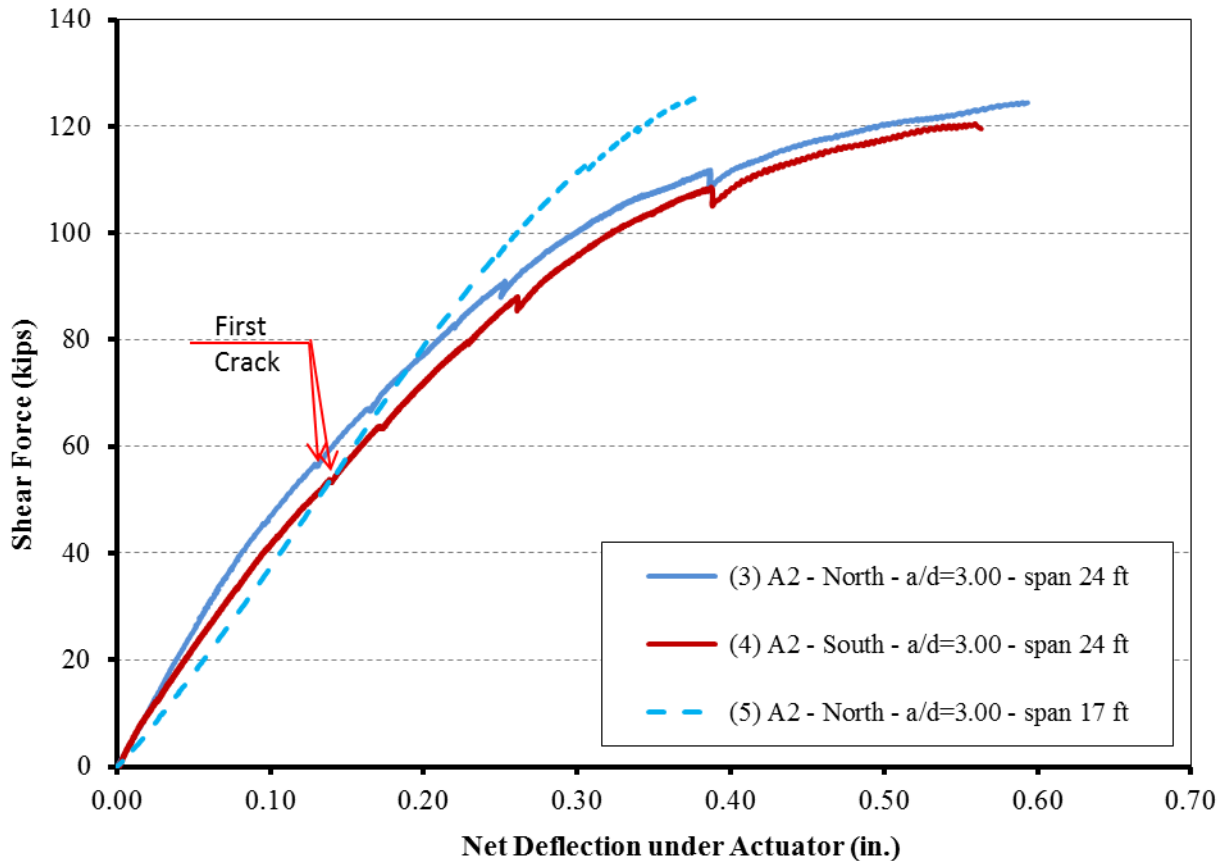


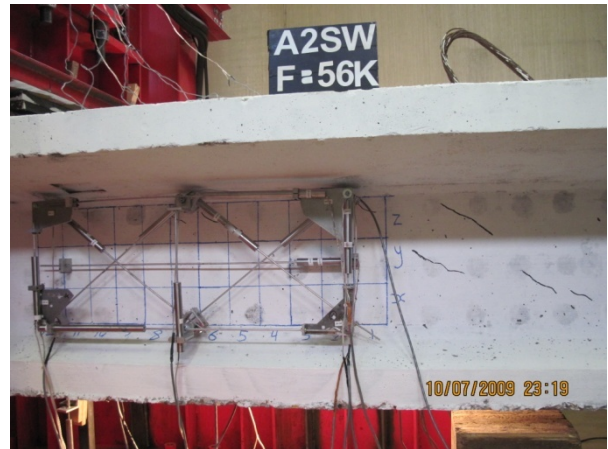
Fig. 4.5 Shear Force vs. Girder Deflection Curves for Girder A2

North End



(a) First shear crack at 56 kips

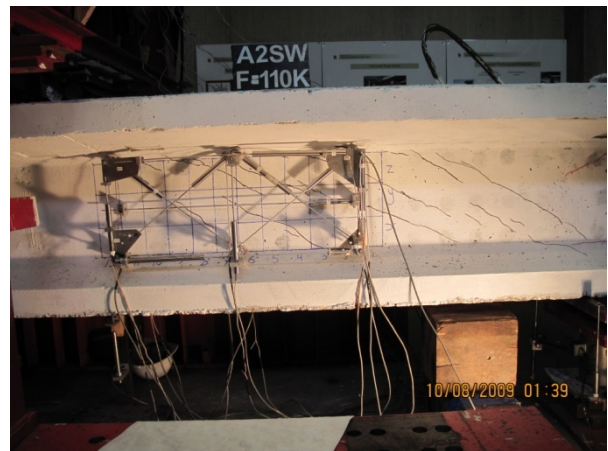
South End



(b) First shear crack at 56 kips



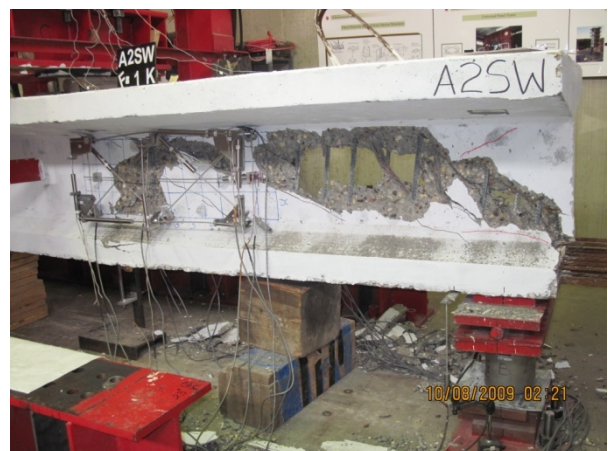
(c) Shear crack pattern before failure



(d) Shear crack pattern before failure



(e) Shear failure at 125.60 kips



(f) Shear failure at 120.40 kips

Fig. 4.6 Shear Crack Pattern and Failure Mode of Girder A2

It can be seen from Fig. 4.7 that the smeared strains at both the girder ends had the same trend, but they are higher at the south end than that measured at the north end for a given load. The higher smeared tensile strains across the cracks and in the transverse and longitudinal directions at the south end allowed the concrete struts to have higher smeared compressive strain. Generally, the smeared compressive strain measured by LVDT D3 is higher than that measured by LVDT D4, which indicates that the failure starts in the closer rosette to the support. The smeared compressive strain measured by LVDT D3 was 0.0013 at the south end, while it was 0.0009 at the north end, which induced a failure at the south end at a shear load of 120.4 kips, while the corresponding shear load at the north end was 124.49 kips.

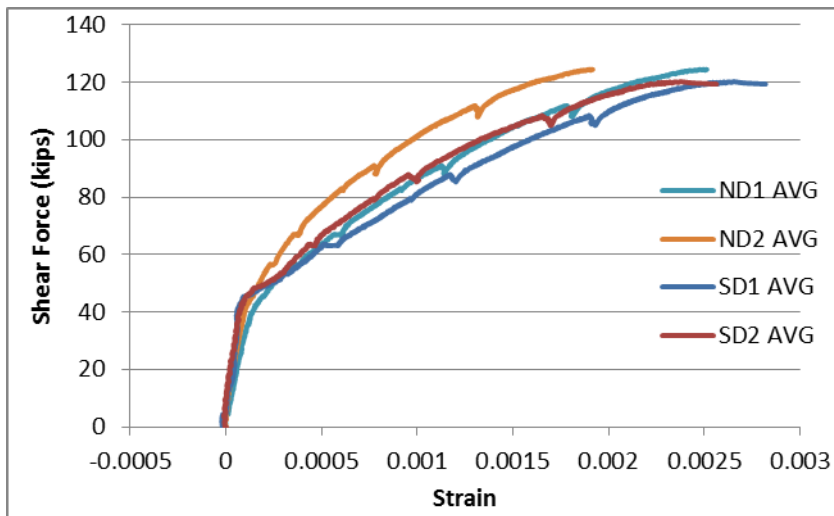
The smeared transverse tensile strains at the middle of the studied zone increased rapidly compared to the strain measured by the LVDTs, which was close to the support, Fig. 4.7(c). This notes that the strain is larger in the transverse steel within the central portion of the studied zone than other locations. This may be due to the intersection of the shear crack at the location of the central vertical LVDTs. The smeared tensile strain readings from the LVDT V3, which was close to the loading point, at both the north and south ends were relatively small because they missed the main shear crack, as can be seen in Fig. 4.6 (c) and (d).

Similarly, from Fig. 4.8, it can be seen that the local rebar tensile strains were higher at the middle of the web. By comparing the maximum strain measured by a strain gauges located along 45° and 29.7° (AASHTO angle), it can be seen that the transverse rebars yielded along the 45° line. Thus, it is appropriate to consider the 45° line in Eq. (4.1.4) as the line of minimum shear resistance offered by the transverse rebars to estimate the contribution of rebars in shear.

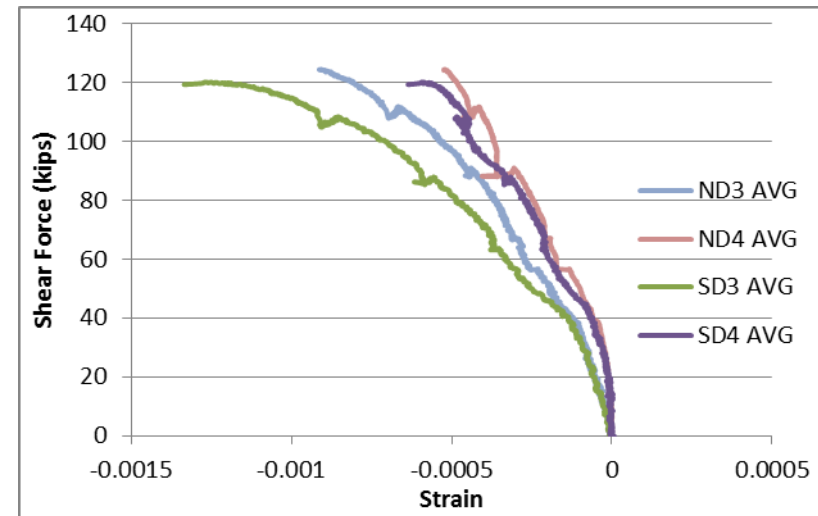
Although the shear span to effective depth ratio (a/d) for this girder was 3.00, multiple shear cracks were formed throughout the web, i.e., fanning out from the support point toward the loading point as seen in Fig. 4.6 (c) to (d). The girder did not show any flexure cracks during the test. This may be because the flexure cracking load was significantly higher owing to the huge prestressing force, while the web shear strength was controlling. Fig. 4.7(d) shows that the tensile smeared strain in the longitudinal direction of the web was very small comparing to that of Girder A1 in Fig. 4.3(d), which emphasized the web shear failure as the final mode of failure for Girder A2.

After the failure of the south end, the south load cell was moved toward the north end yielding a net span of 17 feet. The north end was reloaded until failure at a shear load of 125.60 kips having a smeared compressive strain 0.0010 at the location of LVDT D3, as shown in Fig. 4.9 (b), which is less than the compressive strain at the south end. This indicates that the maximum compressive strain might be missed because of being out of the studied zone. Fig. 4.6 (e) shows that the failure was due to a crushing of concrete near the support. However, the smeared tensile strains across the cracks and in the transverse and longitudinal directions were slightly less than that obtained in the first test.

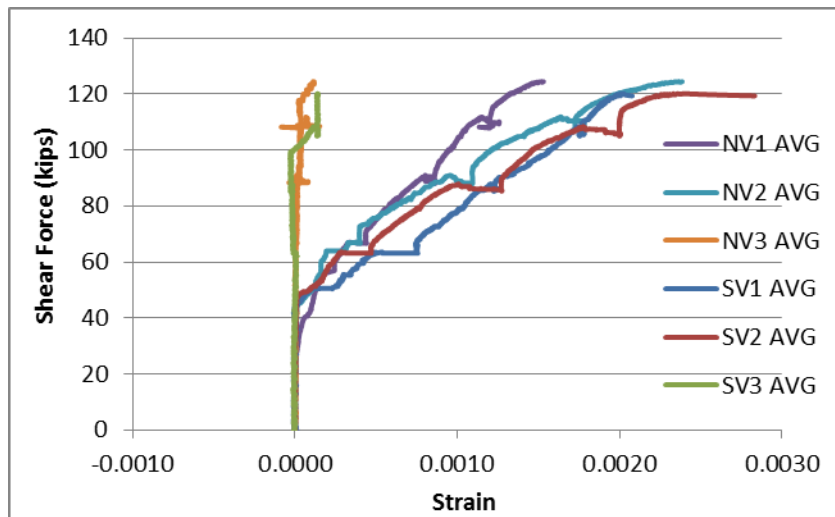
Fig. 4.10 presents the local strain in the transverse rebars measured by strain gauges. Smaller values of strain are measured by these strain gauges in the second run. This might be due to the residual strain because of reaching the yield strain during the first test.



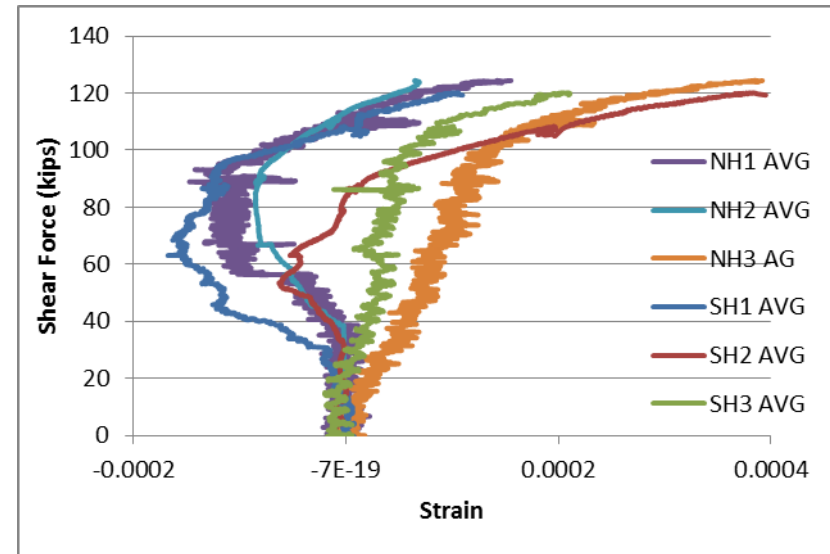
a - Average smeared tensile strain across Cracks



b - Average smeared compressive strain in concrete struts

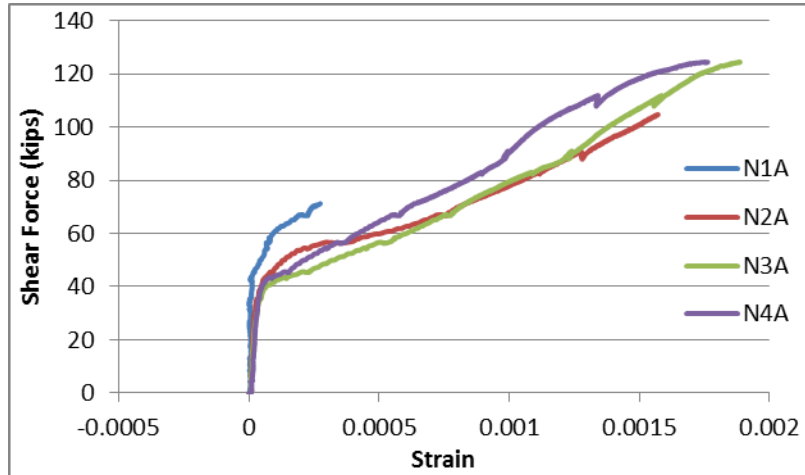


c - Average transverse smeared strain

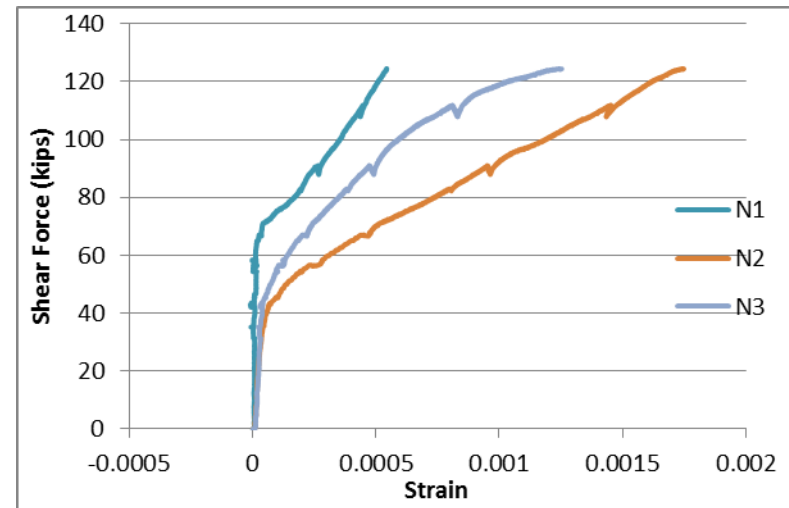


d - Average longitudinal smeared strain

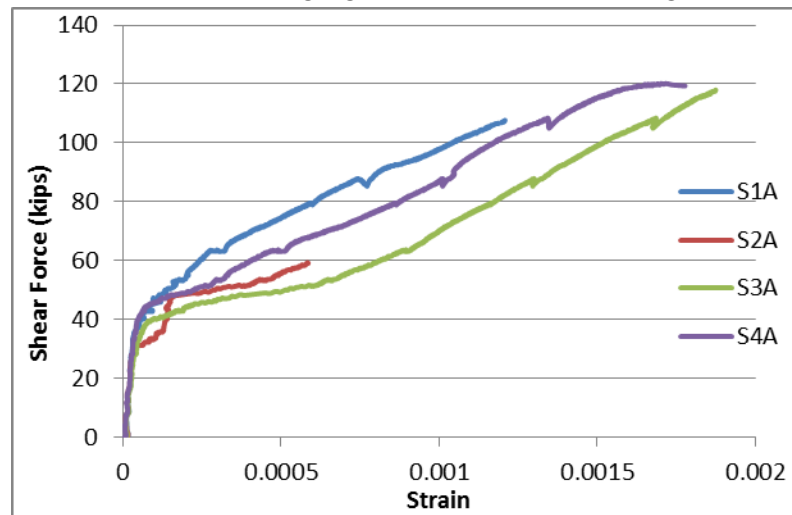
Fig. 4.7 Shear Force vs. Concrete Smeared Strains Curves for Girder A2 – First Run



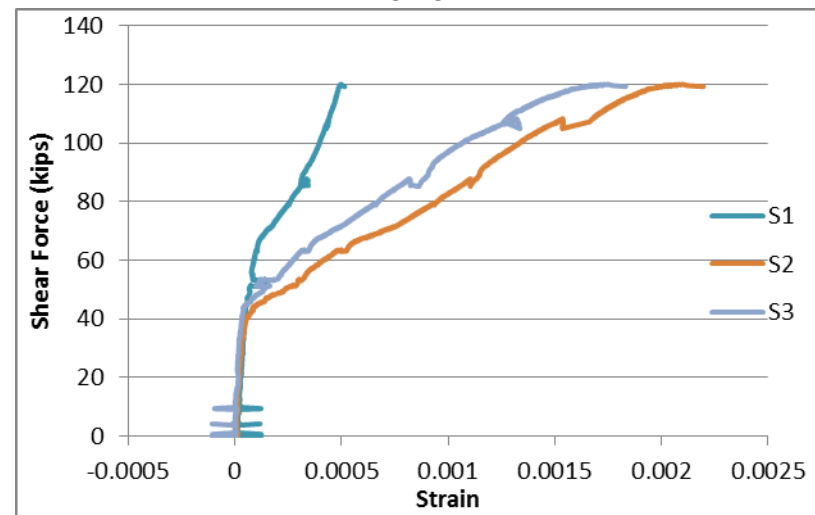
a - North strain gauges located at AASHTO angle



b - North strain gauges located at 45°

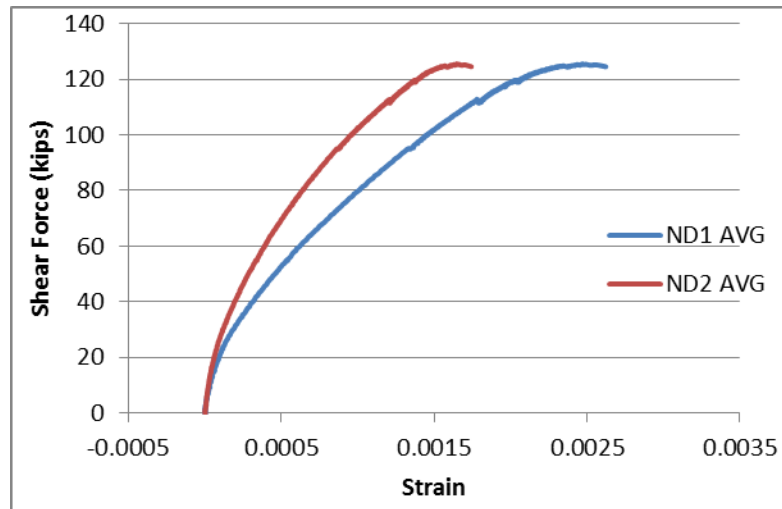


c - South strain gauges located at AASHTO angle

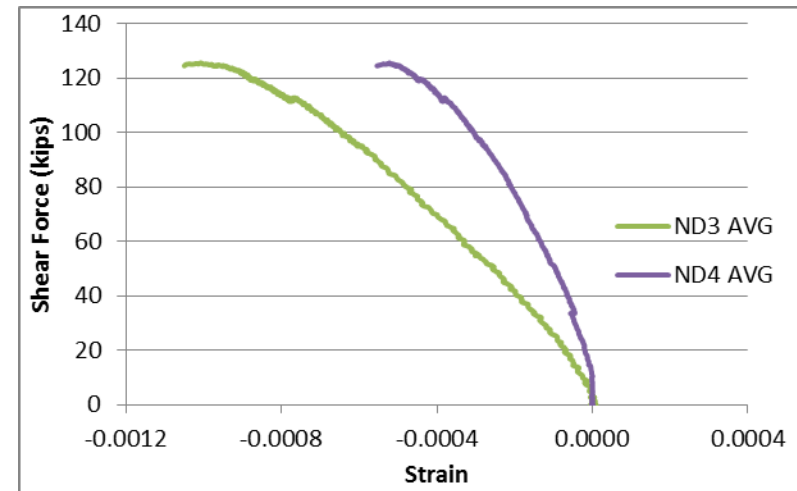


d - South strain gauges located at 45°

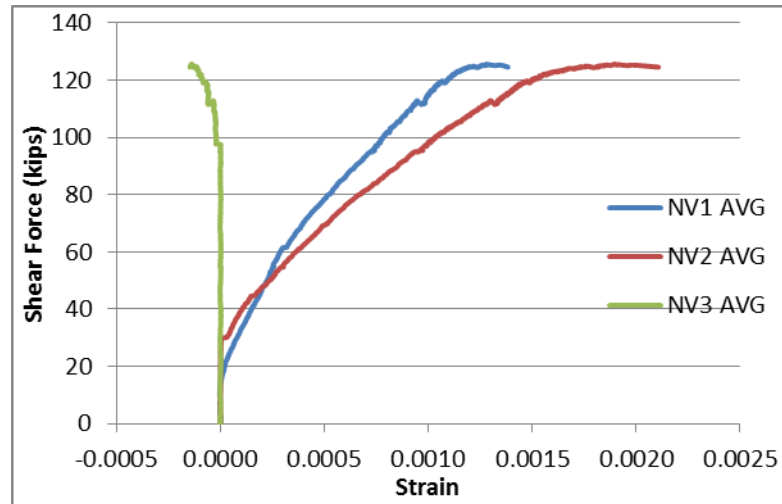
Fig. 4.8 Shear Force vs. Local Transverse Tensile Strain of Girder A2 – First Run



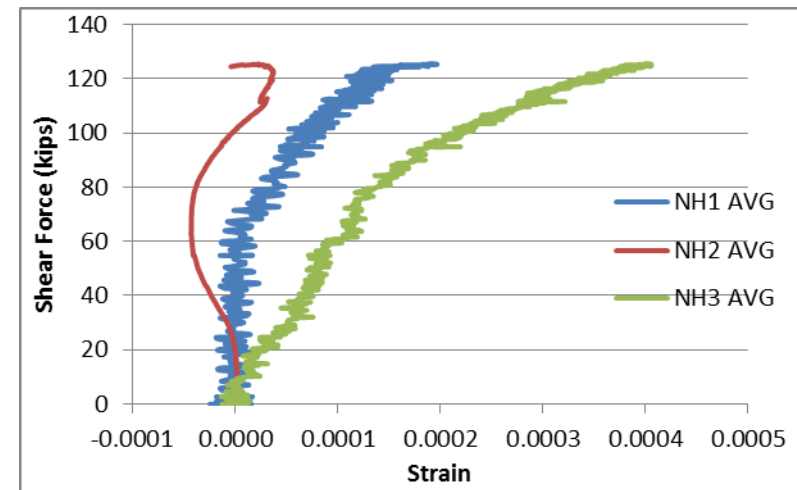
a - Average smeared tensile strain across Cracks



b - Average smeared compressive strain in concrete struts

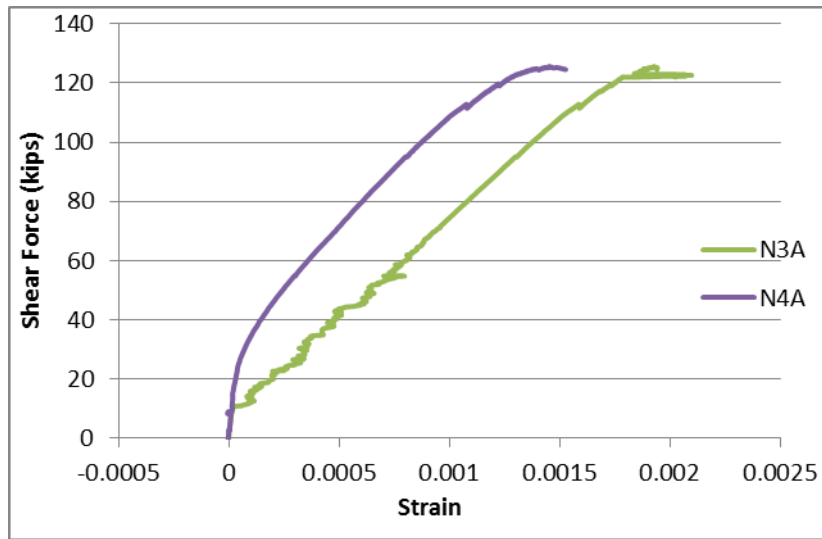


c - Average transverse smeared strain

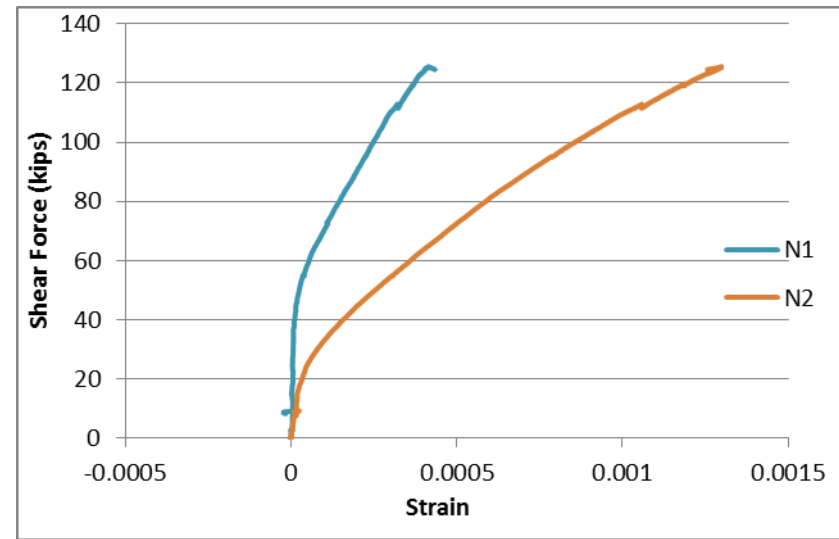


d - Average longitudinal smeared strain

Fig. 4.9 Shear Force vs. Concrete Smeared Strains Curves for Girder A2 – Second Run



a - North strain gauges located at AASHTO angle



b – north strain gauges located at 45°

Fig. 4.10 Shear Force vs. Local Transverse Tensile Strain of Girder A2 - Second Run

4.3. Experimental Results of Group F Girders with $f'_c \cong 13,000$ psi

Group F includes four girders with concrete compressive strength around 13,000 psi. Girders F1 and F2 are designed having transverse steel close to balanced condition, while F3 and F4 are designed to be over-reinforced in transverse direction. The four girders in this group have been designed with different shear span to effective depth ratio a/d .

4.3.1. Girder F1

Girder F1 was loaded simultaneously at both ends with shear span to effective depth ratio $a/d = 1.77$, as shown in Fig. 4.11. The first shear cracks appeared at both the girder ends at the same time under a shear load of 70 kips, Fig. 4.12 (a) and (b). The first crack happened on the line between the loading and reaction points. The cracking load is very clearly shown on all the LVDTs' data.

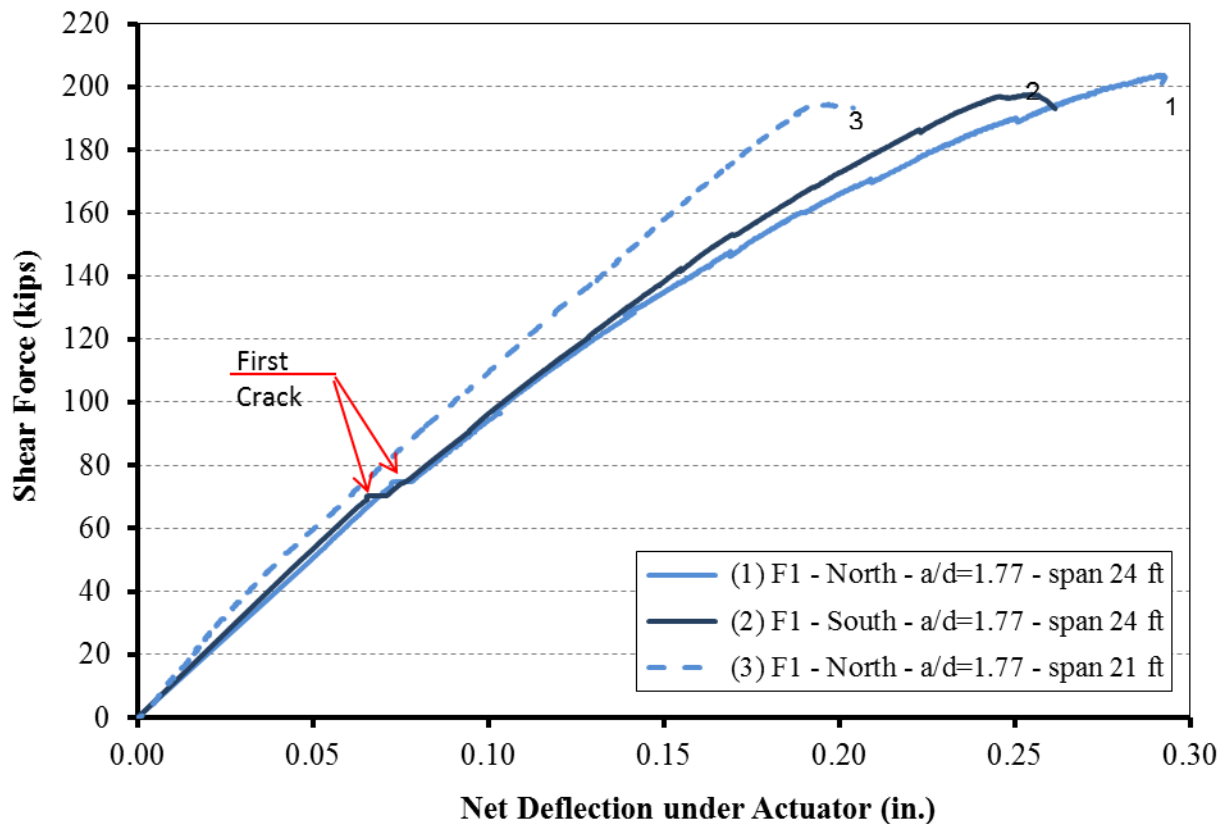


Fig. 4.11 Shear Force vs. Girder Deflection Curves for Girder F1

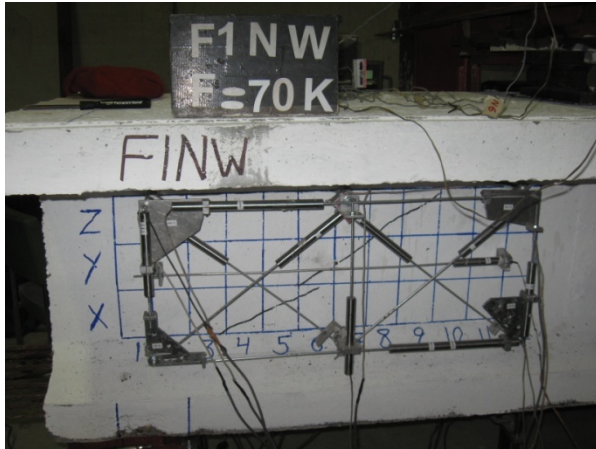
With increasing the applied loads at both ends, the south end had more shear cracks than the north end, as shown in Fig. 4.12 (c) to (d), having an average smeared strain across cracks slightly higher on the south end with maximum strain at peak equal 0.0025 and 0.0029 at the north end and south end respectively, as shown in Fig. 4.13 (a) and (c). This would have softened the south end more than the north, which leads to the web failure of the south end before the north end under a shear load of 197.69 kips, as shown in Fig. 4.12 (f), having a maximum smeared compressive strain close to the support (measured by SD3) of 0.0010. The corresponding shear load at the north end was 202.90 kips, and the maximum smeared compressive strain at the north end was 0.0012 and was closer to the loading point (measured by ND4).

Fig. 4.13 (c) shows the smeared transverse strain measured by the vertical LVDTs installed on the web at both the girder ends during the first test run. For a given shear force, the south end had a higher smeared transverse strain than the north end due to having more cracks at the south end resulting in a smeared transverse strain at peak equal 0.0040 and 0.0028 at the middle of studied zones at south and north ends respectively. The readings from the LVDTs V1 and V3, being close to the support and loading point respectively, were significantly smaller because they missed the main shear crack, as can be seen in Fig. 4.12 (c) and (d).

The local strain in the transverse rebars measured by strain gauges at the south and north ends can be shown in Fig. 4.14. The strain data strongly suggests that all the rebars inside the web intersecting the shear cracks yielded. Strain gauge #6 showed compression strain in the rebar because it was located very close to the loading point inside the top flange.

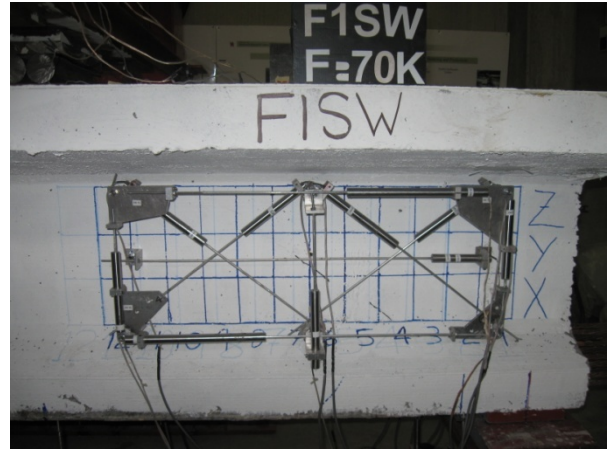
After the failure of the south end, the south support was moved to get a net girder span of 21 ft., and the north end was retested and failed finally in web-shear shown in Fig. 4.11, at 194.55 kips shear force, (Curve 3 in Fig. 4.4). In the second test of the north end the smeared compressive strain nearby the loading point reached 0.0013 (measured by D4), Fig. 4.15(b) causing more damage close to the loading point, Fig. 4.12(e), and the smeared tensile strain across the crack was limited to 0.0022, which is less than that reached in the first test because of the residual strain after the first test. The same with the smeared transverse strain at the middle of studied zone was limited to 0.0020, which is also less than that reached in the first test. Since most the strain gauges stopped working during the first test or reached the yield point, their data during the second run was not reliable.

North End

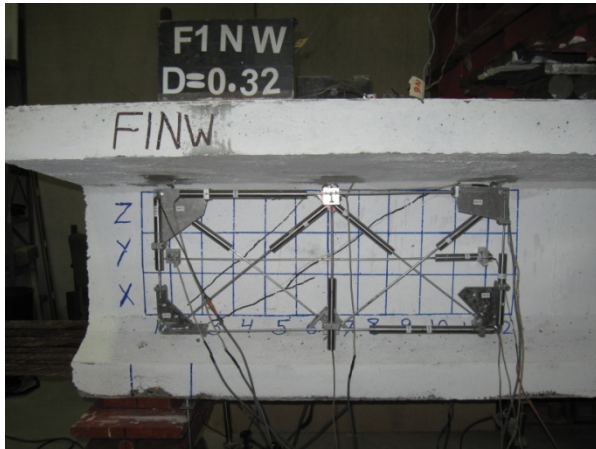


(a) First shear crack at 70 kips

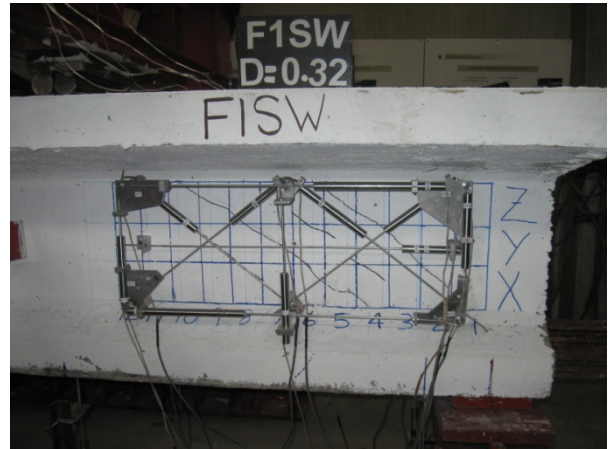
South End



(b) First shear crack at 70 kips



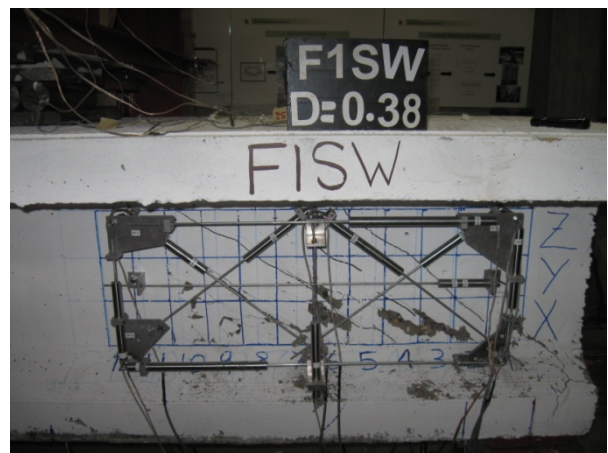
(c) Shear crack pattern before failure



(d) Shear crack pattern before failure

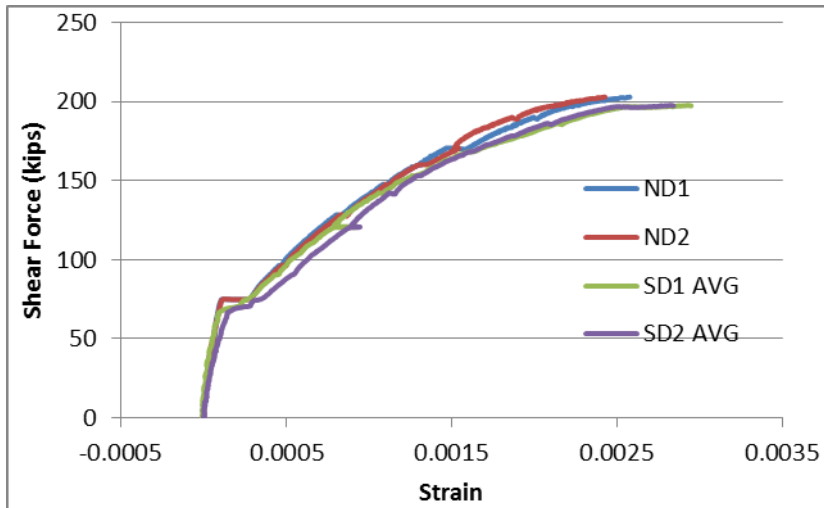


(e) Shear failure at 202.90 kips

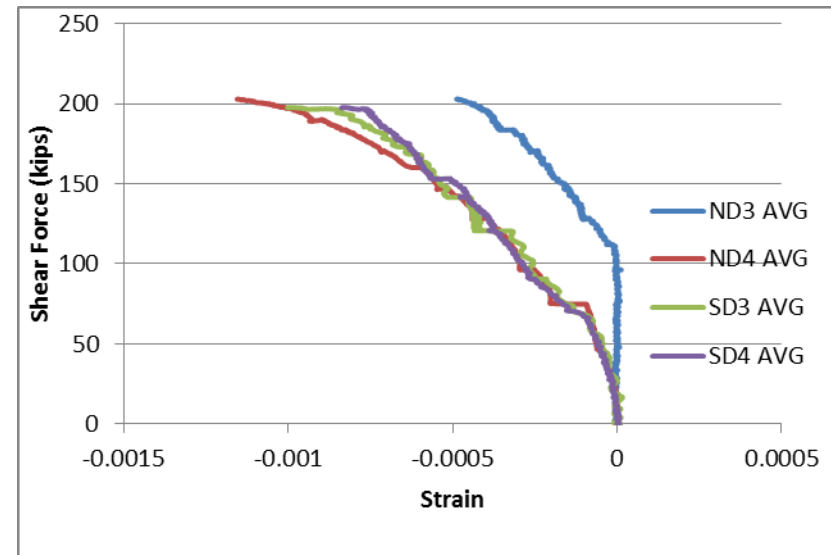


(f) Shear failure at 197.69 kips

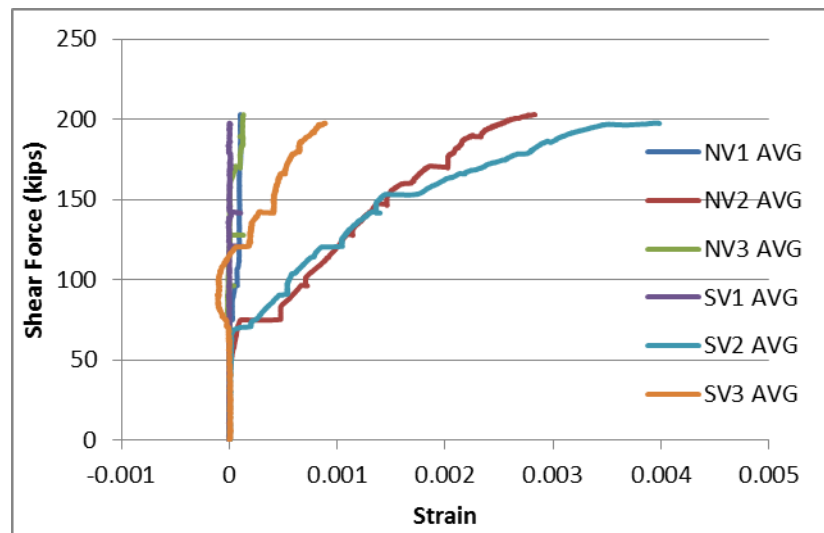
Fig. 4.12 Shear Crack Pattern and Failure Mode of Girder F1



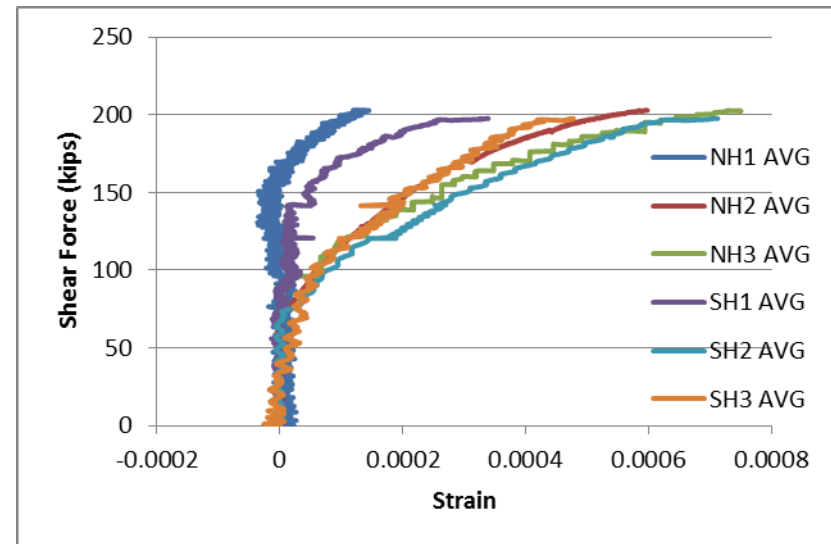
a - Average smeared tensile strain across Cracks



b - Average smeared compressive strain in concrete struts

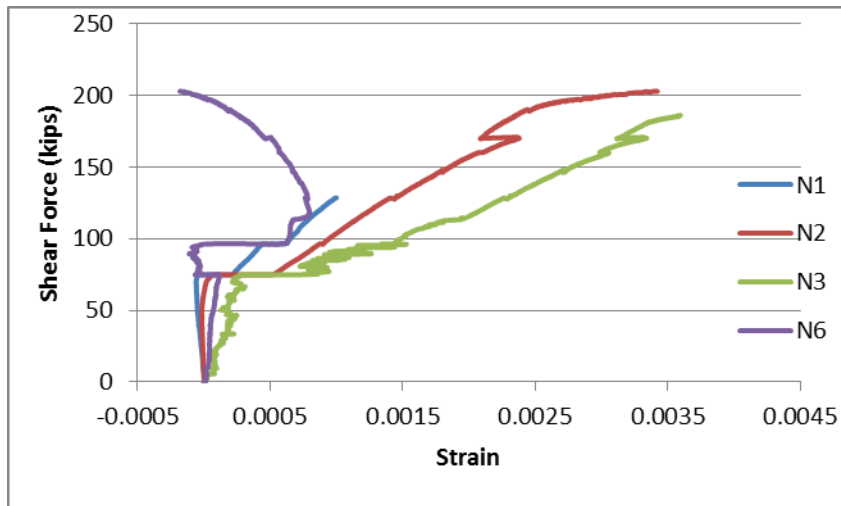


c - Average transverse smeared strain

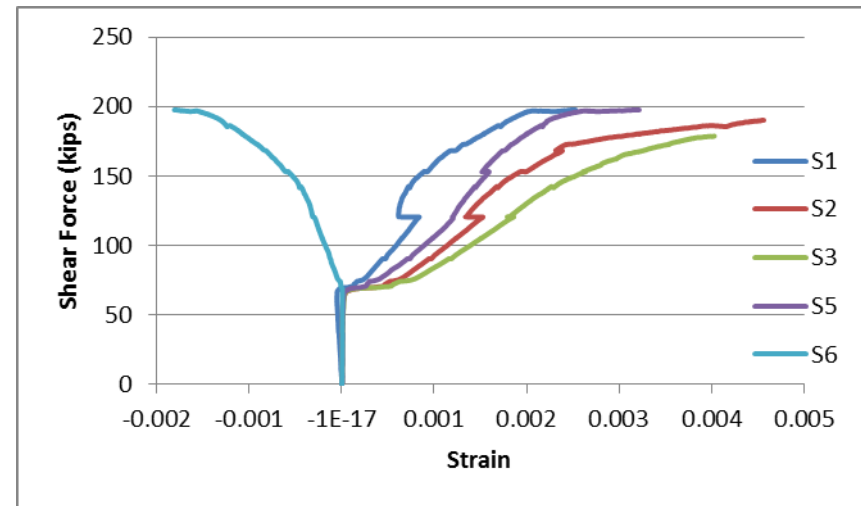


d - Average longitudinal smeared strain

Fig. 4.13 Shear Force vs. Concrete Smeared Strains Curves for Girder F1 –First Run

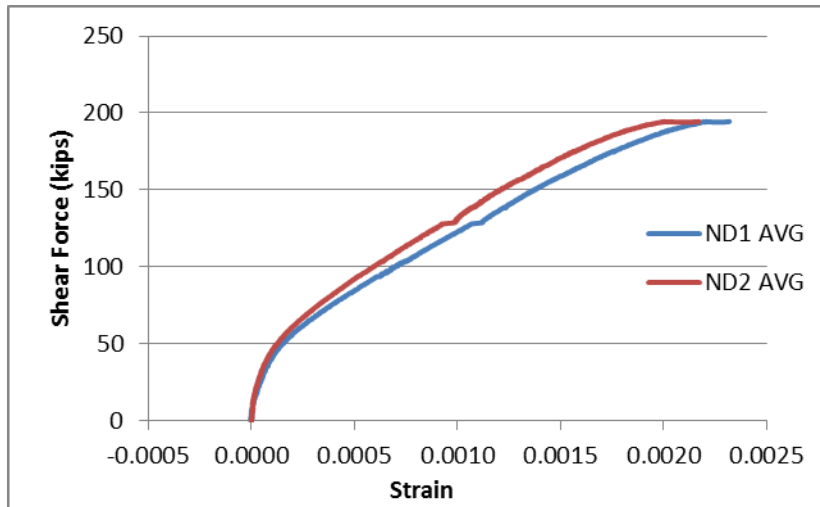


a - North strain gauges

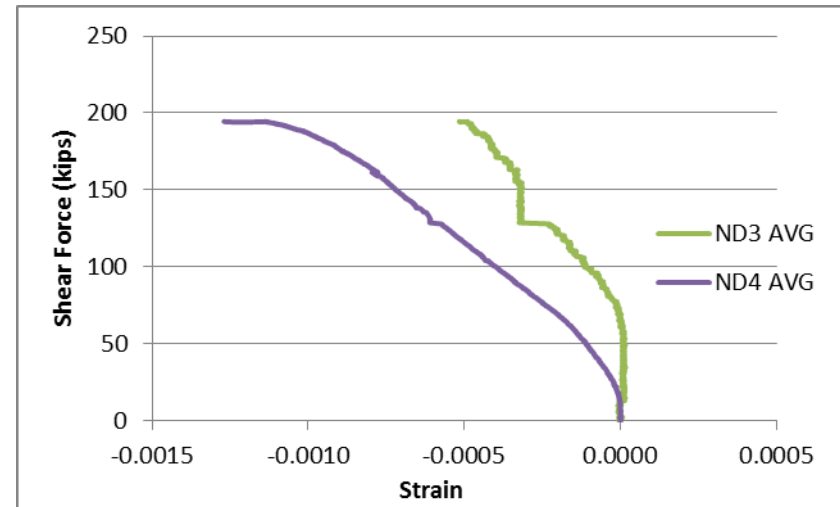


b - South strain gauges

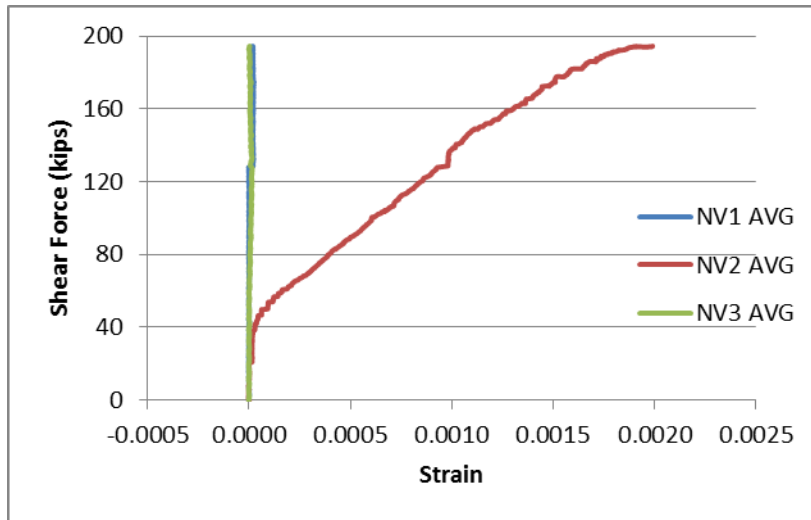
Fig. 4.14 Shear Force vs. Local Transverse Tensile Strain of Girder F1 – First Run



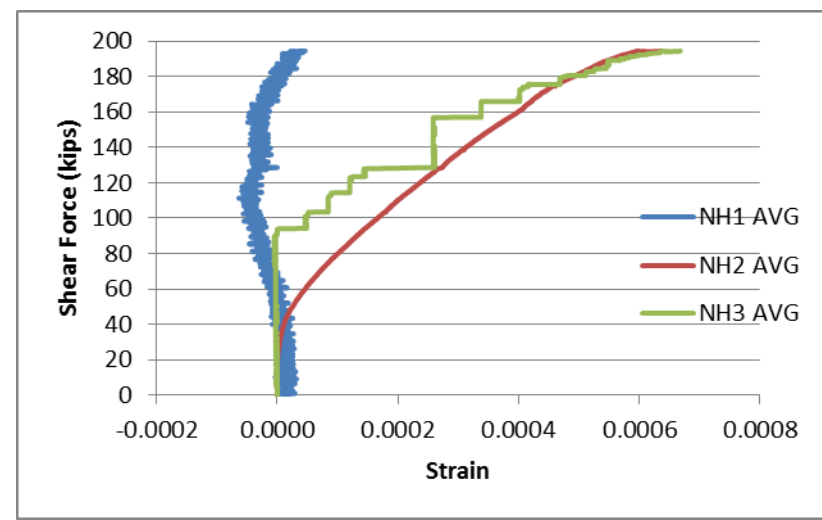
a - Average smeared tensile strain across Cracks



b - Average smeared compressive strain in concrete struts



c - Average transverse smeared strain



d - Average longitudinal smeared strain

Fig. 4.15 Shear Force vs. Concrete Smeared Strains Curves for Girder F1 – Second Run

4.3.2. Girder F2

Girder F2 was tested to fail in flexure shear mode with shear span to effective depth ratio $a/d = 3.00$. The first shear cracks appeared at 63 kips at both ends of the girder, as seen in Fig. 4.17(a) and (b). With increasing the applied load both ends behaved identically. This can be observed from the recorded smeared strains in the different directions. Thus, the curve No (1) in Fig. 4.16 represents the shear load versus the net deflection for both ends.

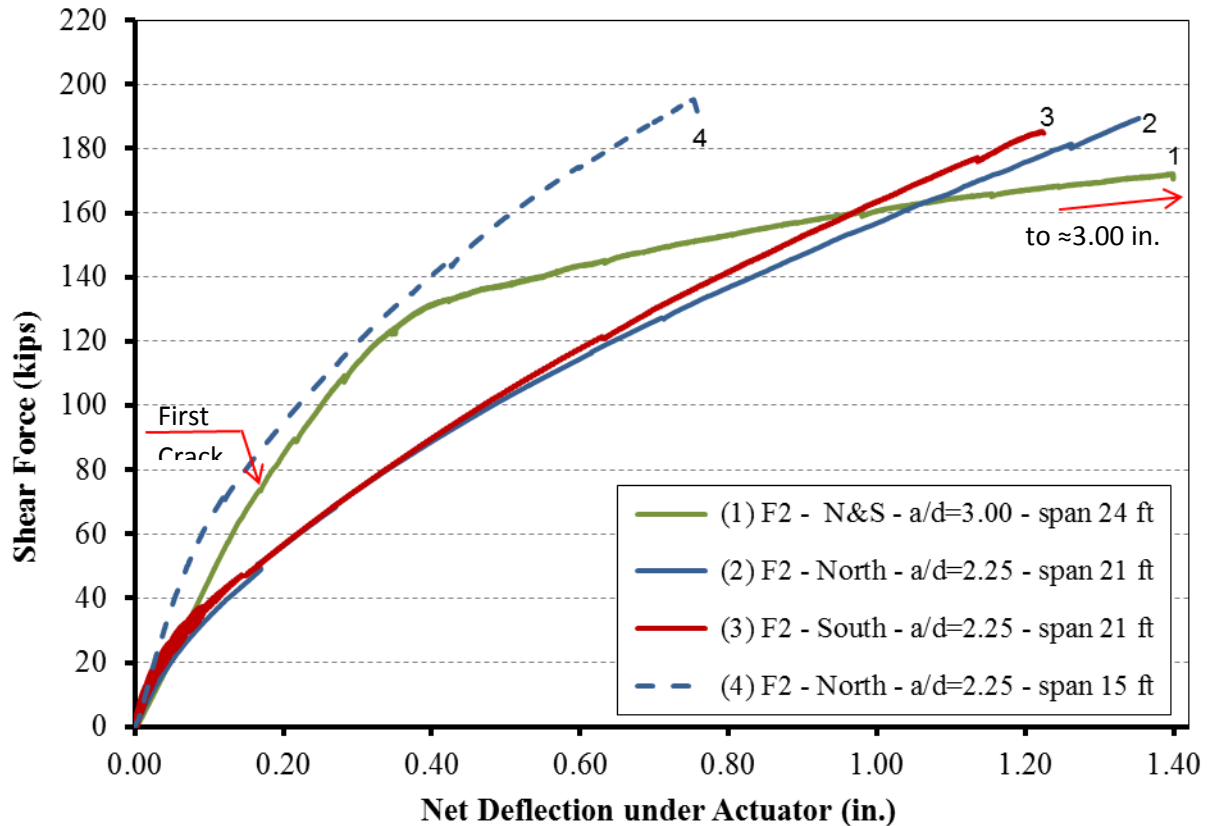


Fig. 4.16 Shear Force vs. Girder Deflection Curves for Girder F2

During loading, flexure shear cracks initiated at both the ends of the girder causing a significant increase in the horizontal smeared tensile strain comparing to that in Girder F1, which failed previously in web shear. Because of the significant increase in the concrete strength, the shear strength increased more significantly than its flexure capacity. In spite of having a smeared tensile strain across cracks 0.0042 and 0.0038 in average at north and south ends respectively, Fig. 4.18(a), the peak smeared compressive strain in concrete struts was only 0.0008 and 0.0009 in average at north and south ends, respectively, as shown in Fig. 4.18(b), which indicated the impossibility of having crushing of concrete struts before flexure failure. Because the flexure

failure is not our objective in this research work, it was decided to hold the test and to diminish the shear span to have smaller shear-span-to-depth ratio ensure a shear failure.

Fig. 4.18(c) shows the smeared transverse tensile strain measured by vertical LVDTs during first test. It can be seen that the smeared strain measured by the LVDTs V1 and V2 are identical at both the girder ends having an average peak smeared transverse strain 0.0022 and 0.0020 at the north and the south ends, respectively. The readings from the LVDT V3, which were closer to the loading point, at both ends of the girder were very small. Fig. 4.19 shows the strain gauges data representing the local strains in the transverse steel rebars at both ends of the girder. Generally, it can be seen that the tensile strain was higher at the middle of the web than in the flanges. The maximum strain measured along 28.5° (AASHTO angle) and 45° lines were almost the same and indicated the yielding of the transverse steel.

After stopping the test, the shear span to depth ratio a/d was reduced to be 2.25 to ensure a shear failure. The new girder span 21 ft. was used to retest the Girder F2. The girder reloaded simultaneously having the reduced shear-span-to-depth ratio at both ends. The smeared tensile strains across crack were identical having an average strain at peak of 0.0027 and 0.0025 at the north and the south ends respectively, as shown in Fig. 4.20 (a).

Fig. 4.20 (b) presents the smeared compressive strains measured at two locations throughout the study zone. It can be seen that the smeared compressive strain was higher closer to the support, indicating where the failure started. Thus, the concrete struts formed on the web in previous test crushed at the south end at a maximum smeared compressive strain of 0.0010 close to the support, indicating web shear failure at a shear force of 185.35 kips, while the corresponding load at the north end was 189.13 kips (Curves 2 and 3 in Fig. 4.16), and the maximum smeared compressive strain at the north end was 0.0009. During this test the flexure cracks did not open up, and hence did not contribute toward the ultimate failure of the girder at either end. This can be demonstrated by the small tensile smeared strain measured in the longitudinal direction compared to that recorded during the first test, Figs. 4.18 (d) and 4.20 (d).

The smeared transverse tensile strain measured by vertical LVDTs during the second test had the same trend as the first test, as shown in Fig. 4.20(c). The readings from the LVDT V3, which was closer to the loading point, at both ends of the girder were very small. It can be seen

that the smeared strain measured by the LVDTs V1 and V2 are close at both the girder ends having an average peak smeared transverse strain 0.0012 and 0.0014 at the north and the south ends respectively, which is less than the peak in previous test. This might happen due to the residual strain due to the yield of the transverse steel in previous test. For the same reason, the local strains measured by strain gauges at both ends of the girder have values less than yield strain, as shown in Fig. 4.21.

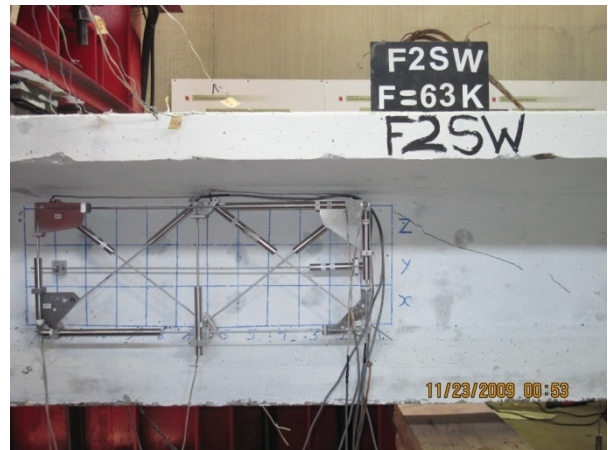
After the failure of the south end, the south load cell was moved to get a net girder span of 15 ft., and the north end was retested having the same shear span to depth ratio equals 2.25. The north end finally failed at 195.24 kips shear force, (Curve 4 in Fig. 4.16), having maximum smeared compressive strain 0.0011 closer to the support, Fig. 4.22(b).

North End

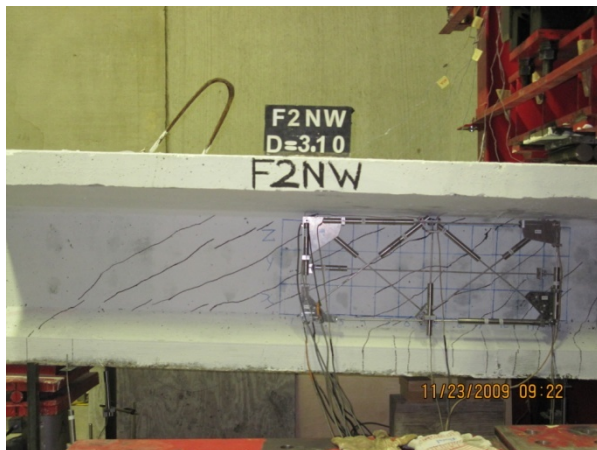


(a) First shear crack at 63 kips

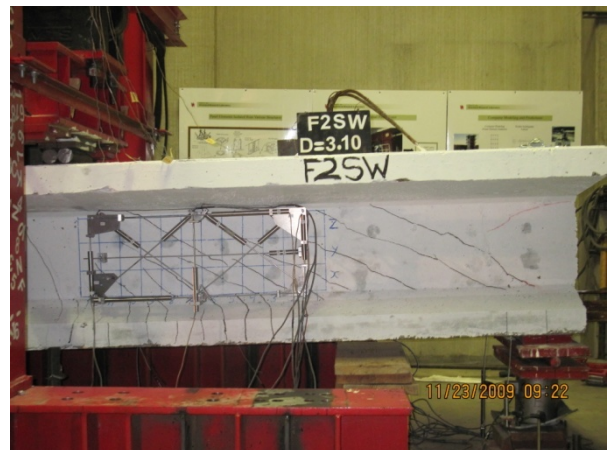
South End



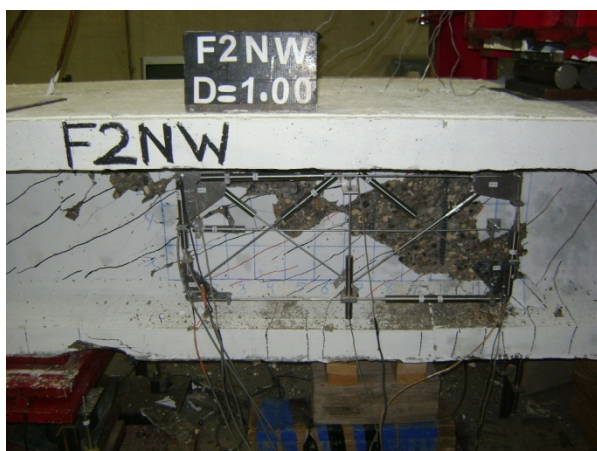
(b) First shear crack at 63 kips



(c) Shear crack pattern before failure



(d) Shear crack pattern before failure

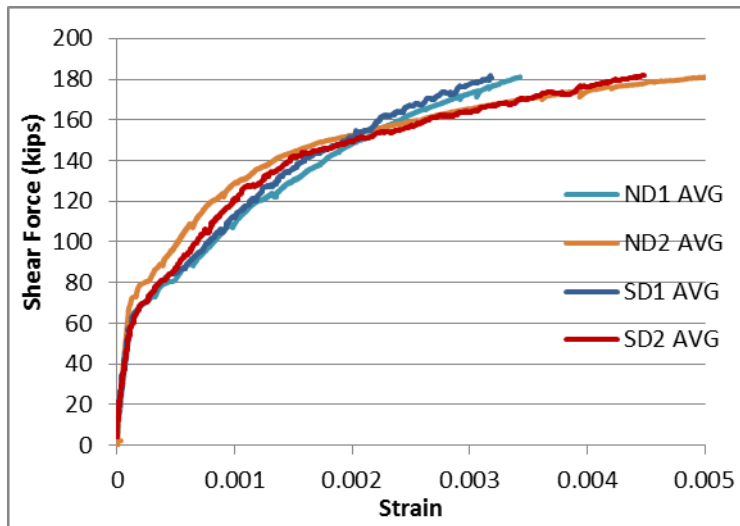


(e) Shear failure at 195.24 kips

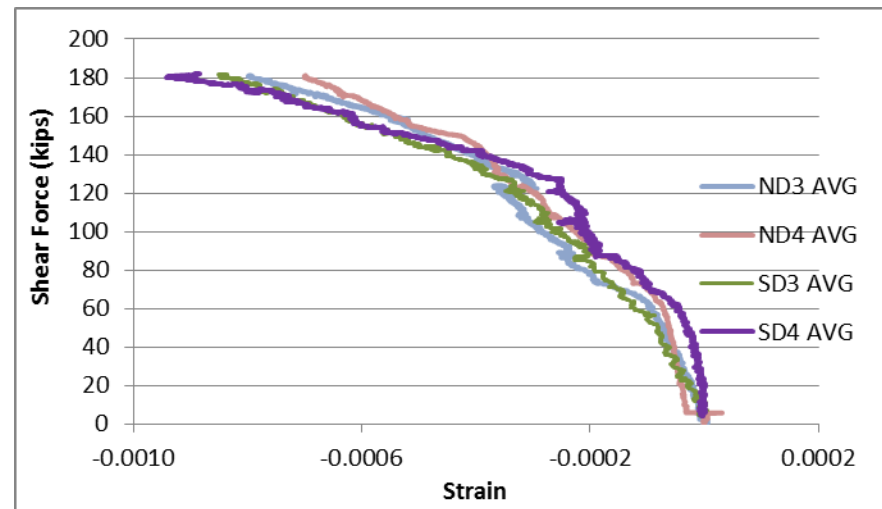


(f) Shear failure at 185.35 kips

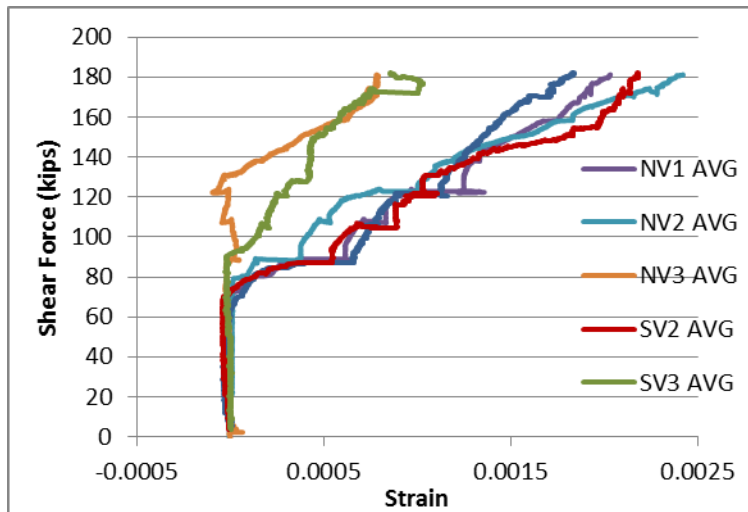
Fig. 4.17 Shear Crack Pattern and Failure Mode of Girder F2



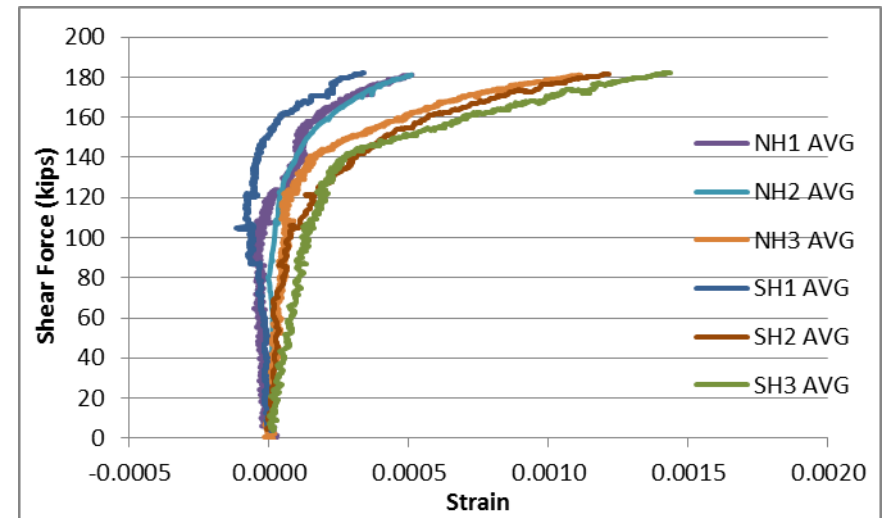
a - Average smeared tensile strain across Cracks



b - Average smeared compressive strain in concrete struts

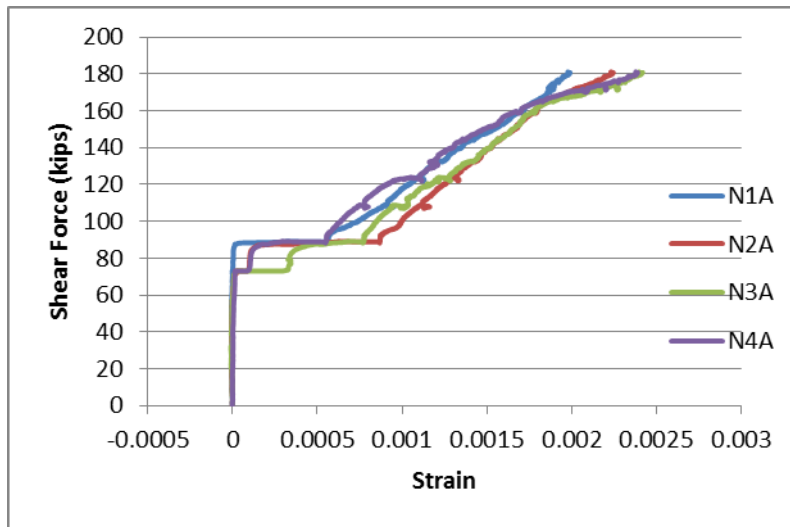


c - Average transverse smeared strain

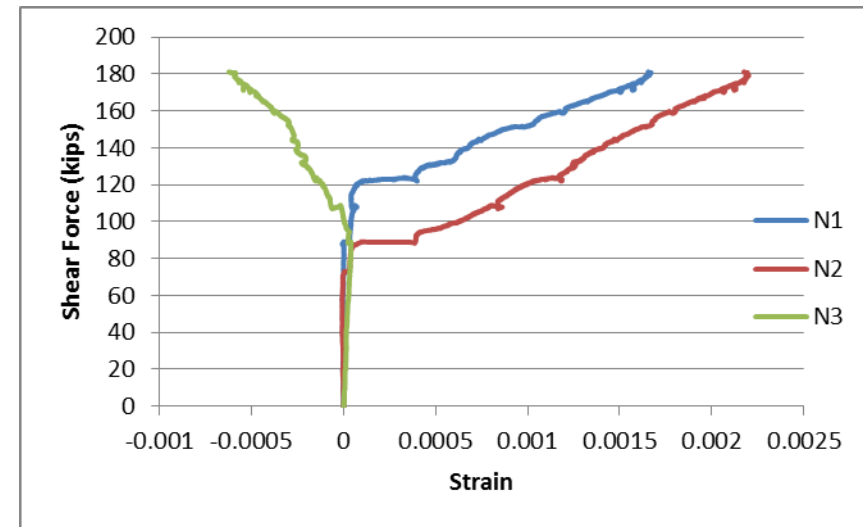


d - Average longitudinal smeared strain

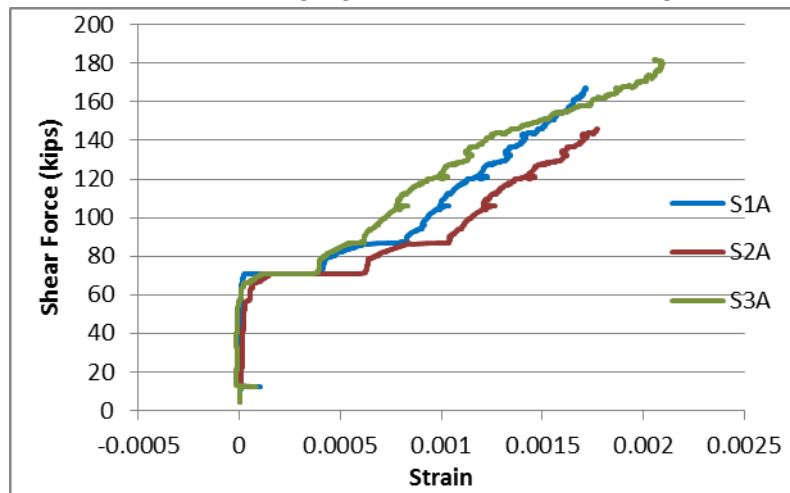
Fig. 4.18 Shear Force vs. Concrete Smeared Strains Curves for Girder F2 – First Run



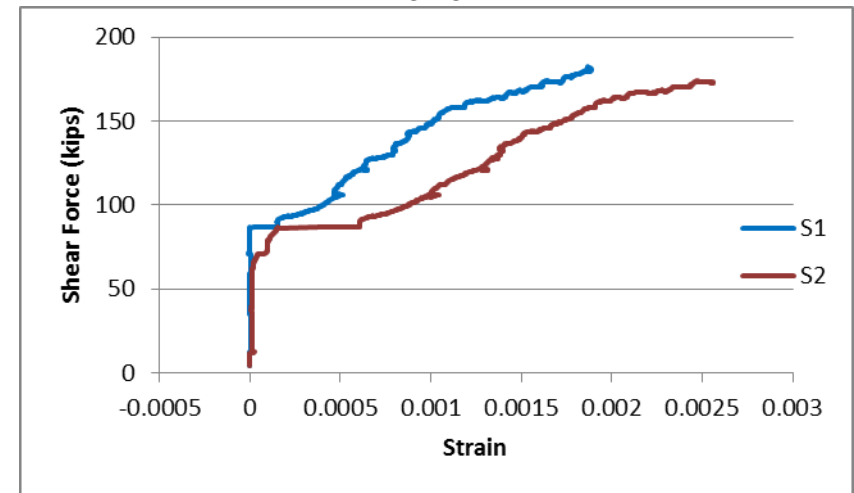
a - North strain gauges located at AASHTO angle



b - North strain gauges located at 45°

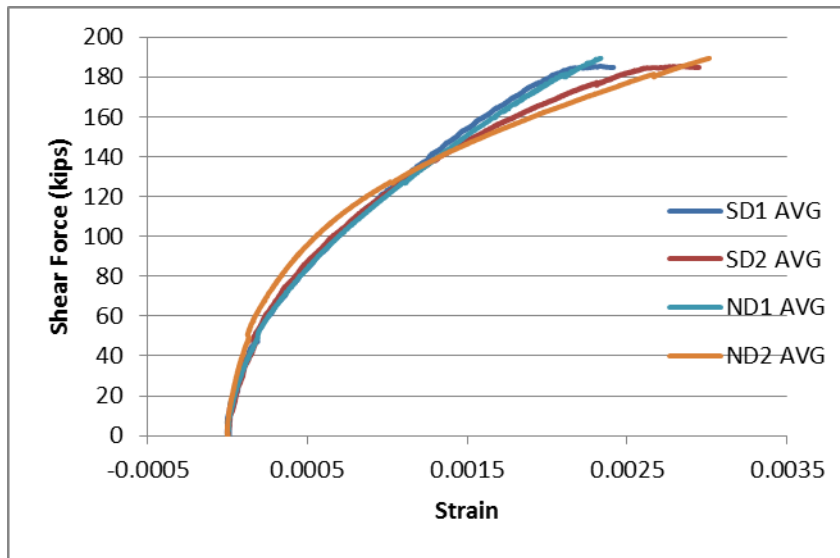


c - South strain gauges located at AASHTO angle

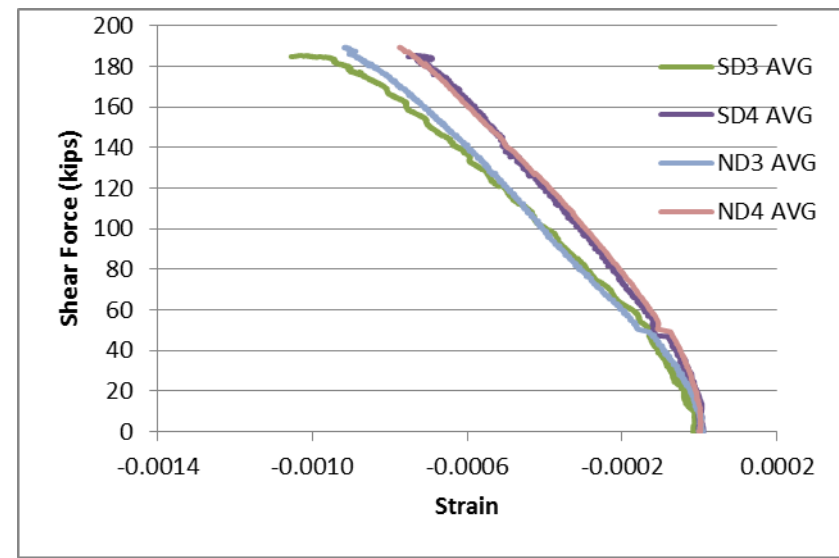


d - South strain gauges located at 45°

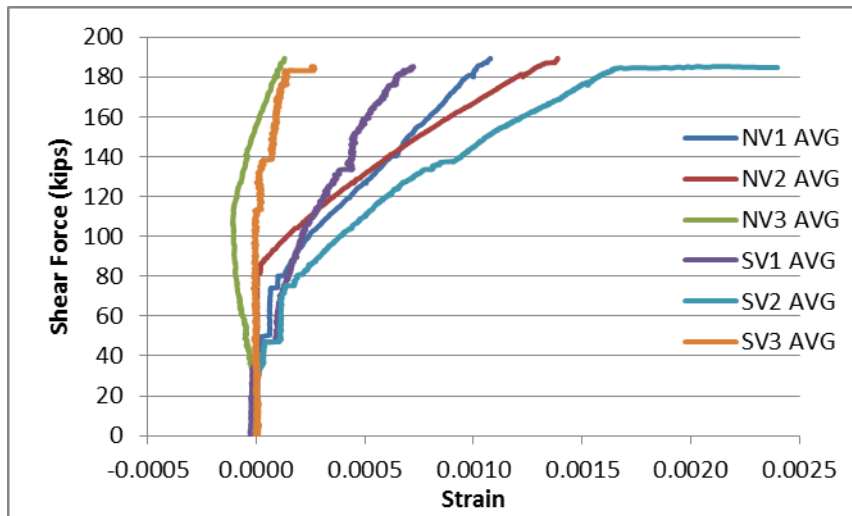
Fig. 4.19 Shear Force vs. Local Transverse Tensile Strain of Girder F2 – First Run



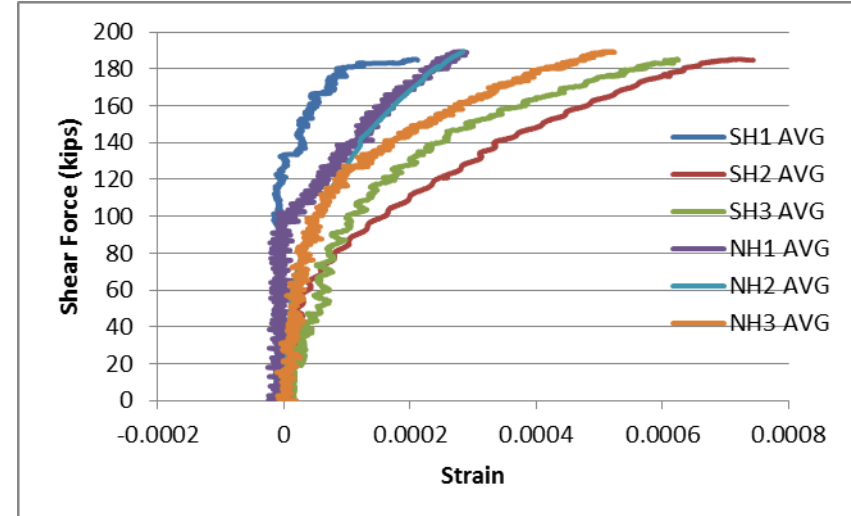
a - Average smeared tensile strain across Cracks



b - Average smeared compressive strain in concrete struts

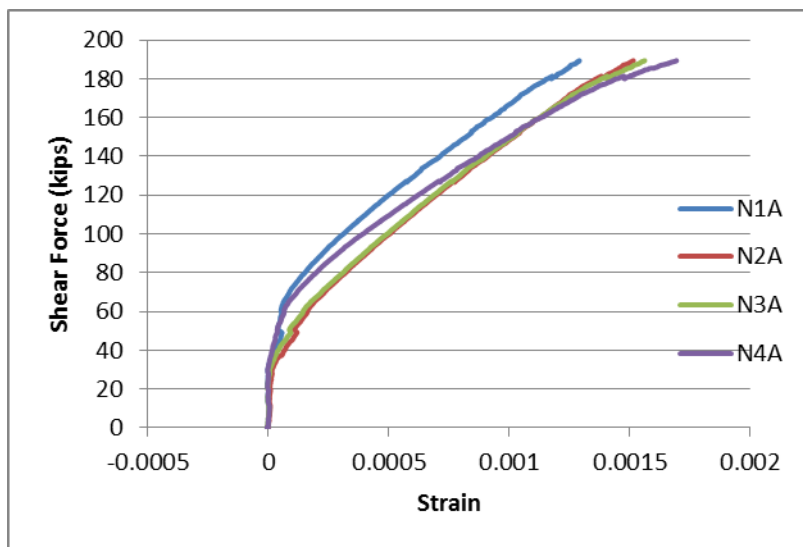


c - Average transverse smeared strain

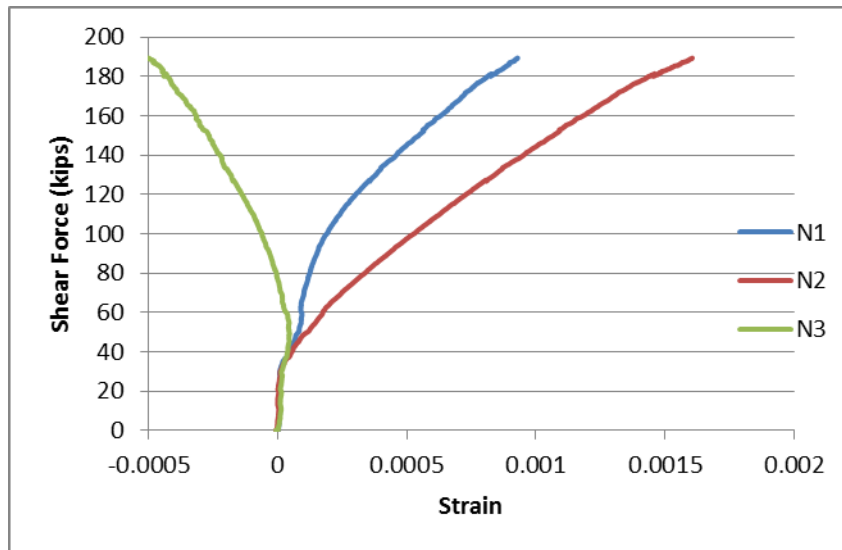


d - Average longitudinal smeared strain

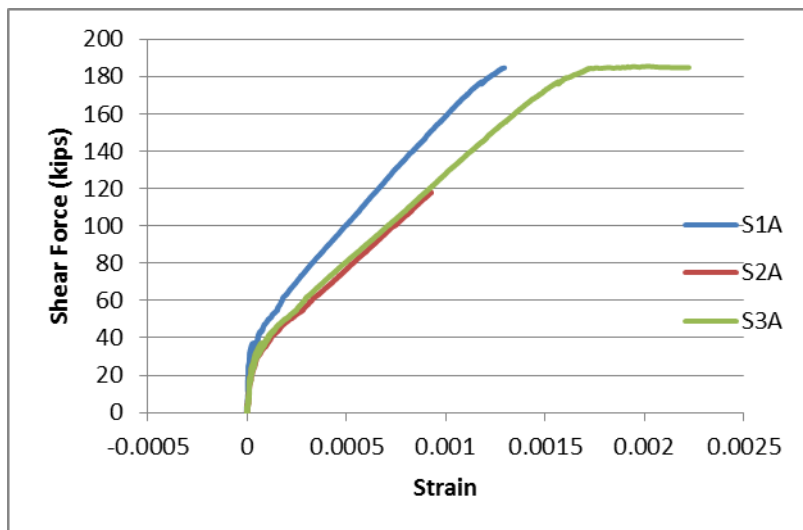
Fig. 4.20 Shear Force vs. Concrete Smeared Strains of Girder F2 – Second Run



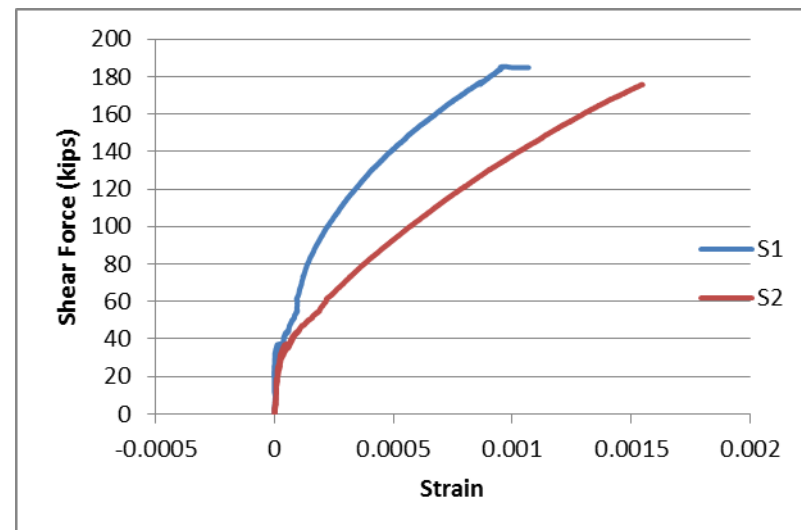
a - North strain gauges located at AASHTO angle



b – North strain gauges located at 45°

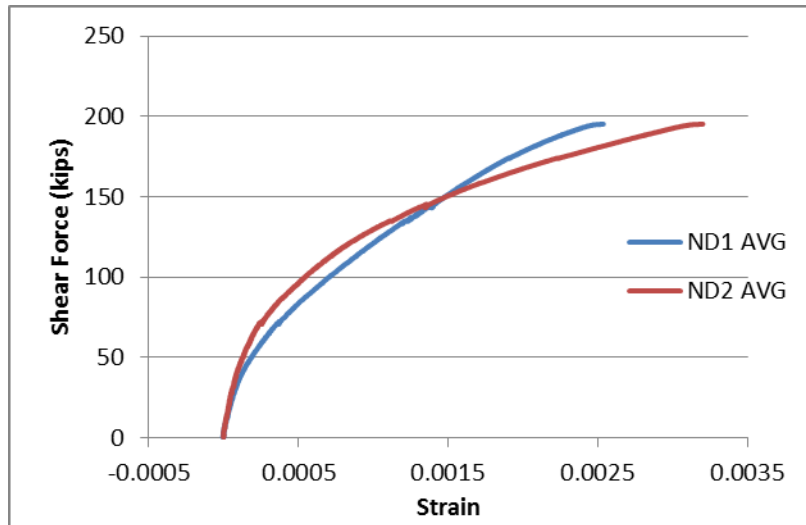


c - South strain gauges located at AASHTO angle

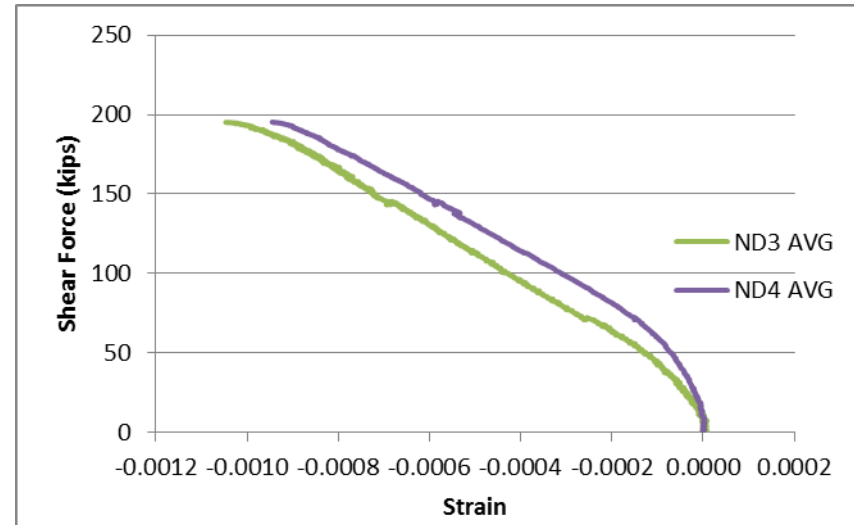


d – South strain gauges located at 45°

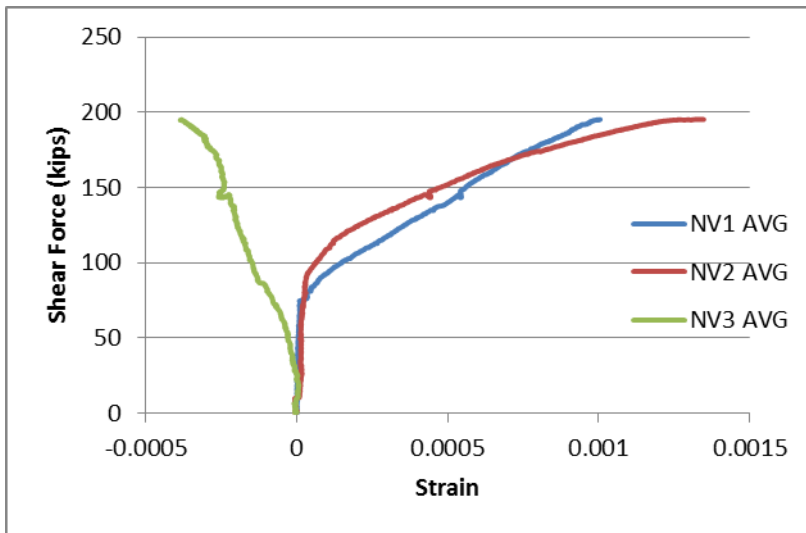
Fig. 4.21 Shear Force vs. Local Transverse Tensile Strain of Girder F2 – Second Run



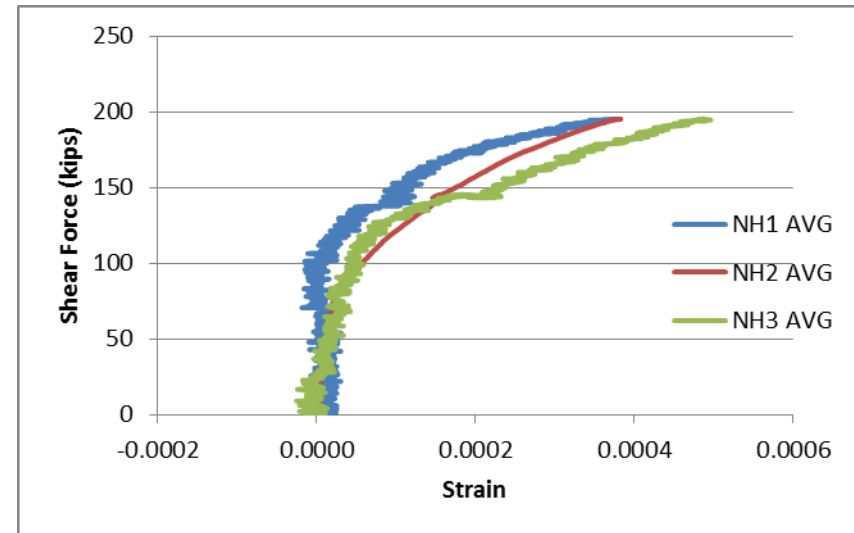
a - Average smeared tensile strain across Cracks



b - Average smeared compressive strain in concrete struts



c - Average transverse smeared strain



d - Average longitudinal smeared strain

Fig. 4.22 Shear Force vs. Concrete Smeared Strains of Girder F2 – Third Run

4.3.3. Girder F3

Girder F3 was designed to fail in web shear mode with shear span to effective depth ratio $a/d = 1.77$. Fig. 4.23 shows the shear load versus net deflection curves at both north and south ends during the first test as well as at the north end in the second test. The first shear crack appeared at both the ends of the girder at the same time under a shear load of 70 kips on the line between the loading and reaction points, as shown in Fig. 4.24 (a) and (b). The smeared strains measured at the north and south ends demonstrated the identical behavior of both ends starting from the cracking load.

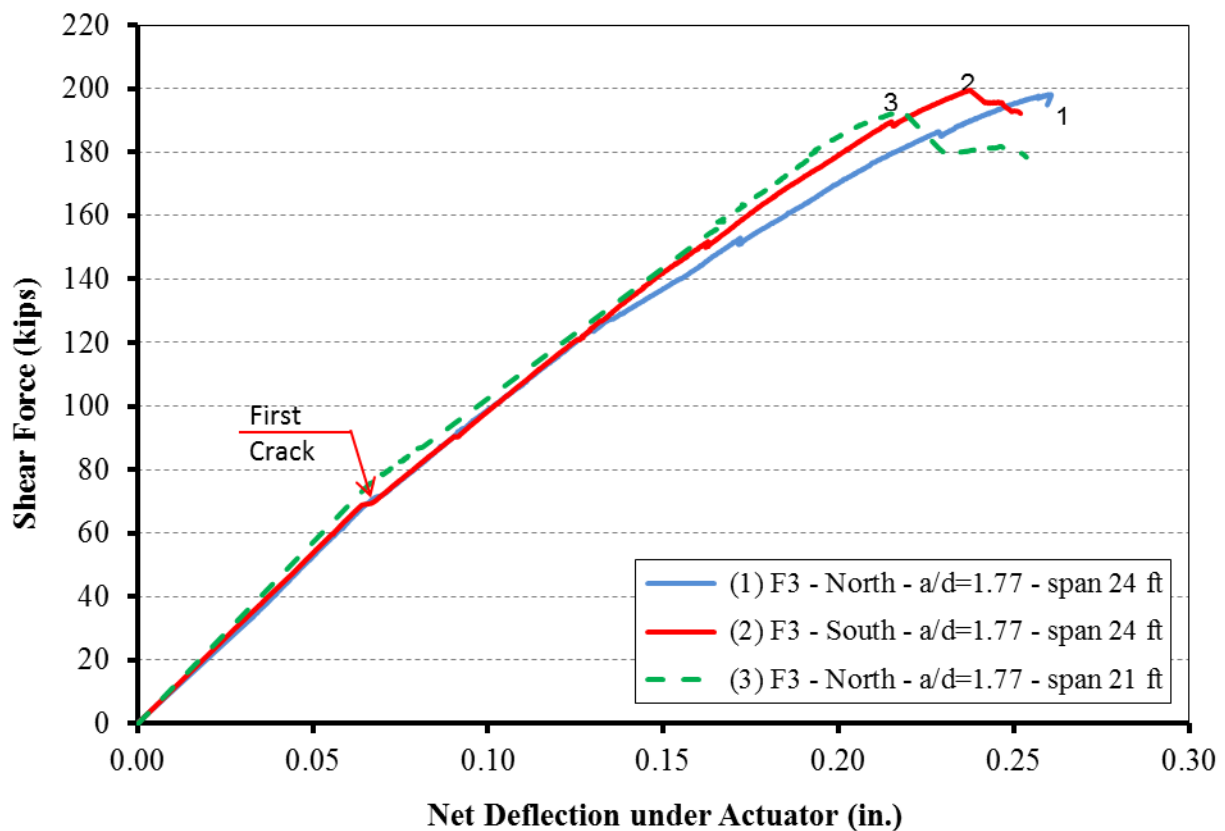


Fig. 4.23 Shear Force vs. Girder Deflection Curves for Girder F3

Although the average smeared tensile strain across cracks was 0.0022 at both the north and south ends, as shown in Fig. 4.25(a), with increasing the applied load the south end had higher smeared compressive strain closer to the support measured by LVDT D3 while the higher smeared compressive strain at the north end was measured by LVDT D4, i.e., closer to the loading point, as shown in Fig. 4.25(b). Thus, the south end failed under a shear load of

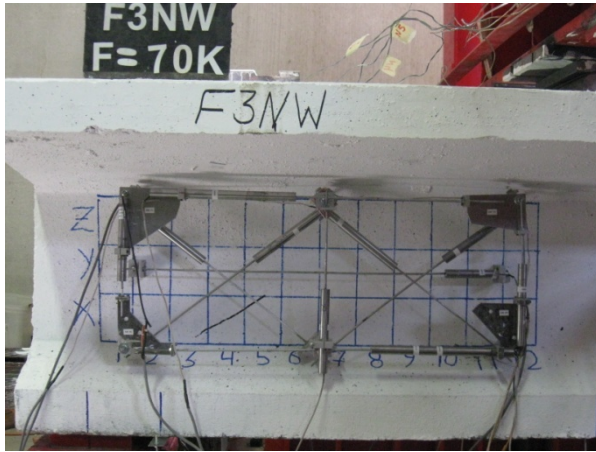
199.55 kips having a smeared compressive strain 0.0014 in average throughout the studied zone at the south end, while the corresponding shear force at the north end was 197.31 kips with a smeared compressive strain 0.0010 in average throughout the studied zone at the north end.

Fig. 4.25 (c) shows the smeared strain measured by the vertical LVDT installed in the web at both the ends of Girder F3. The plot shows that the smeared vertical strains in the transverse direction at the middle of the studied zone were identical at both ends of the girder. The readings from the LVDTs V1 and V3, which were close to the support and the loading points, respectively, were relatively small, as the shear crack did not intersect these LVDTs. The maximum smeared tensile strains recorded by LVDT V2 were 0.0021 and 0.0023 at the north and south ends respectively, which exceeds the yield strain of a bare steel bar. The local strain in the transverse rebars measured by strain gauges at both ends can be seen in Fig. 4.26. The results from the strain gauges in both ends were almost the same. The strain data strongly suggests that almost all the rebars inside the web intersecting the shear cracks yielded.

The behavior of both ends was not identical only in the transverse direction but also in the longitudinal direction. Fig. 4.25(d) shows that the maximum strain was developed at the middle height of the web while it still very small at the interface between flanges and the web.

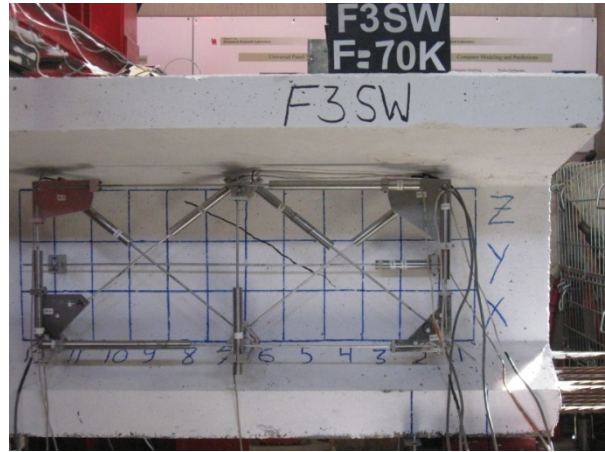
Consequently, after the failure of the south end, the girder was reloaded after moving the support toward the interior at the failed south end giving a net girder span of 21 ft. The north end of the girder failed at a shear force of 192.93 kips (Curve 3 in Fig. 4.23). The shear failure in the web was inclined along a line joining the point of loading and the point of support. Typical of a web shear failure, the concrete struts formed between the shear cracks crushed at failure, as shown in Fig. 4.24 (e), having a maximum smeared compressive strain of 0.0011 closer to the support, as shown in Fig. 4.27 (b). The smeared strains measured across the cracks and in the transverse and longitudinal directions were very close to that have been measured during the first test, as shown in Figs 4.25 and 4.27. Since most the strain gauges reached the yielding strain in the first test, the obtained readings in the second test was less because of the residual strains due to the yielding of the transverse steel.

North End

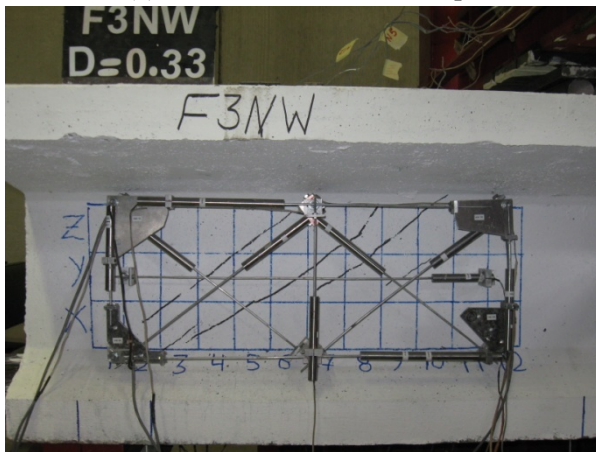


(a) First shear crack at 70 kips

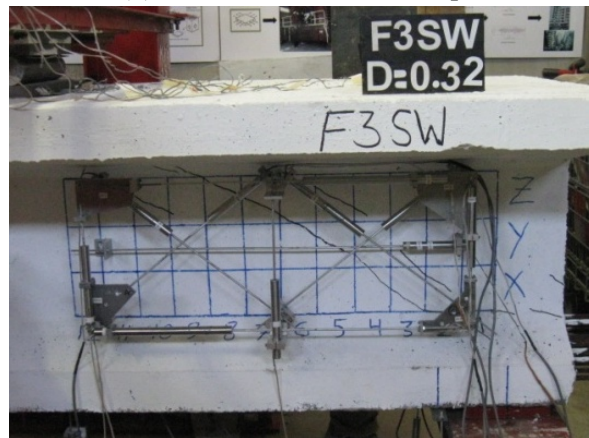
South End



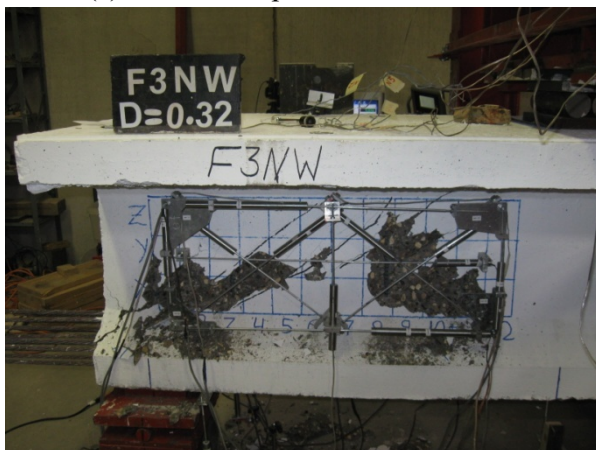
(b) First shear crack at 70 kips



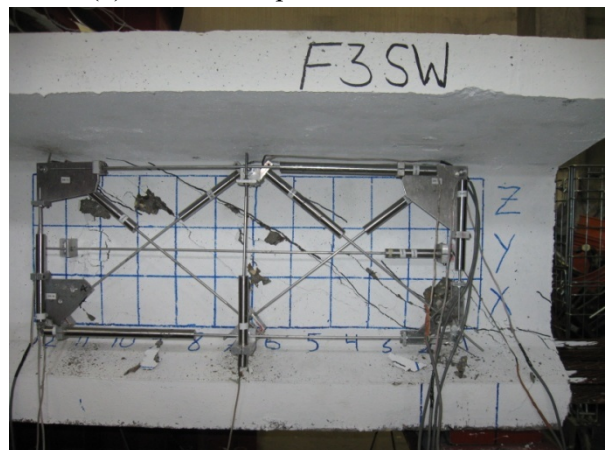
(c) Shear crack pattern before failure



(d) Shear crack pattern before failure

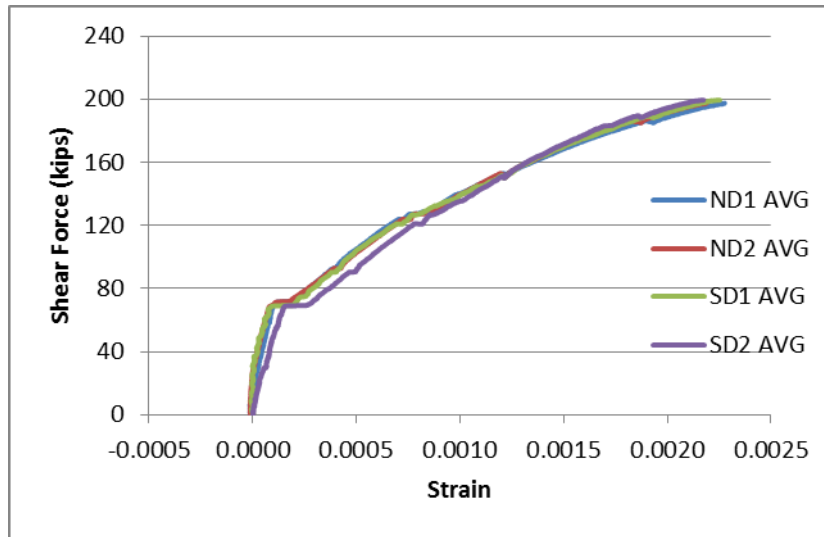


(e) Shear failure at 198.17 kips

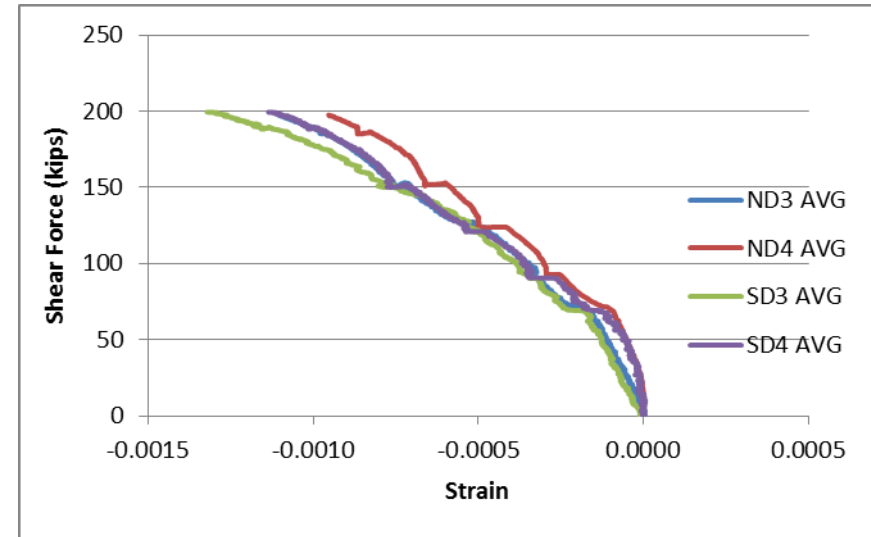


(f) Shear failure at 199.55 kips

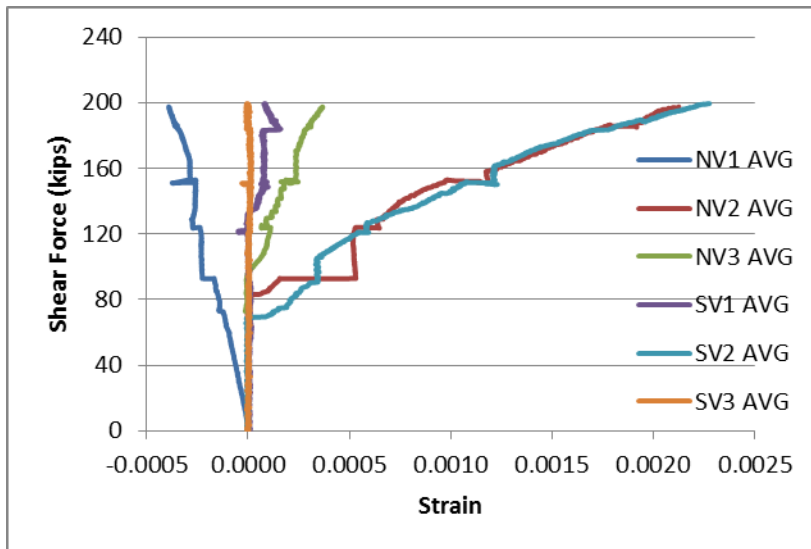
Fig. 4.24 Shear Crack Pattern and Failure Mode of Girder F3



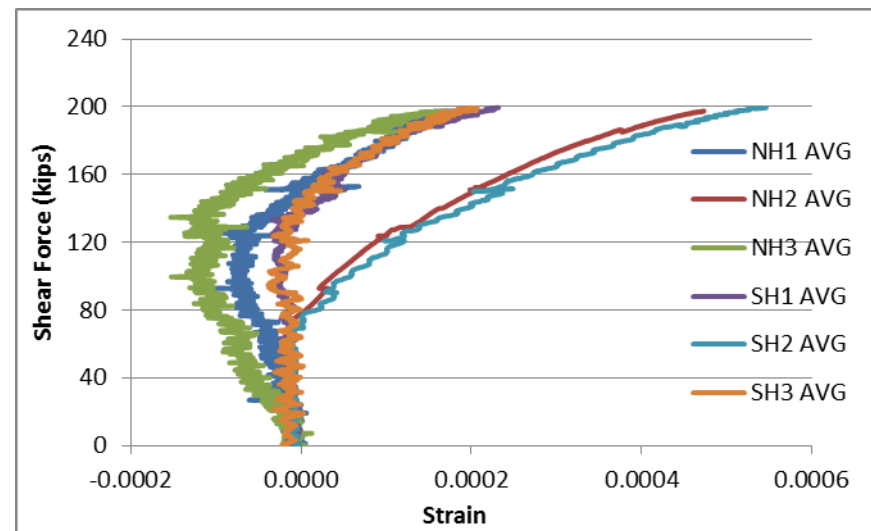
a - Average smeared tensile strain across Cracks



b - Average smeared compressive strain in concrete struts

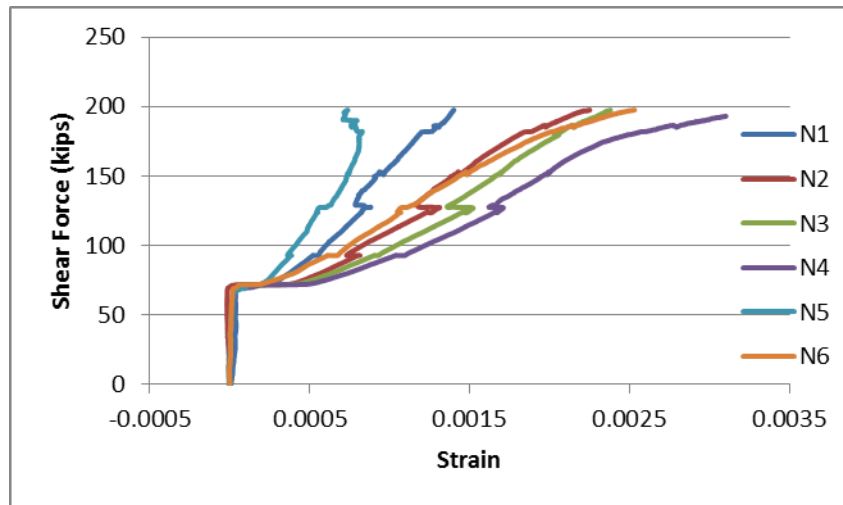


c - Average transverse smeared strain

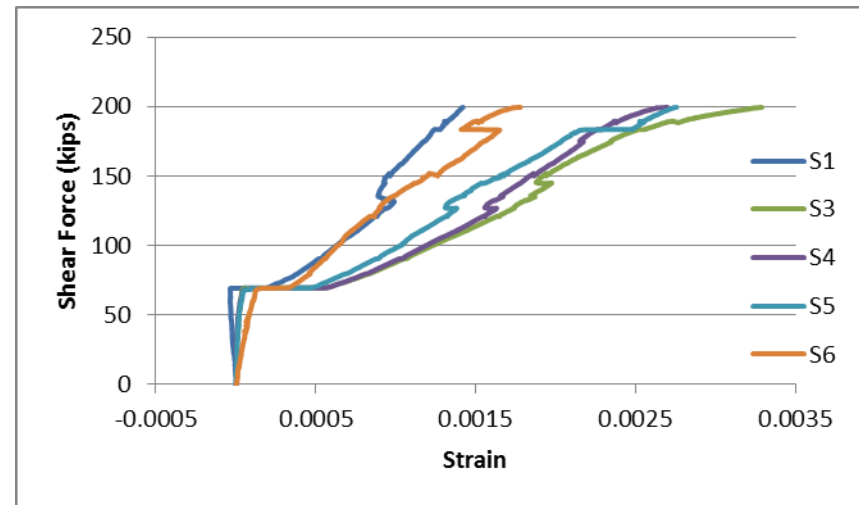


d - Average longitudinal smeared strain

Fig. 4.25 Shear Force vs. Concrete Smeared Strains of Girder F3- First Run

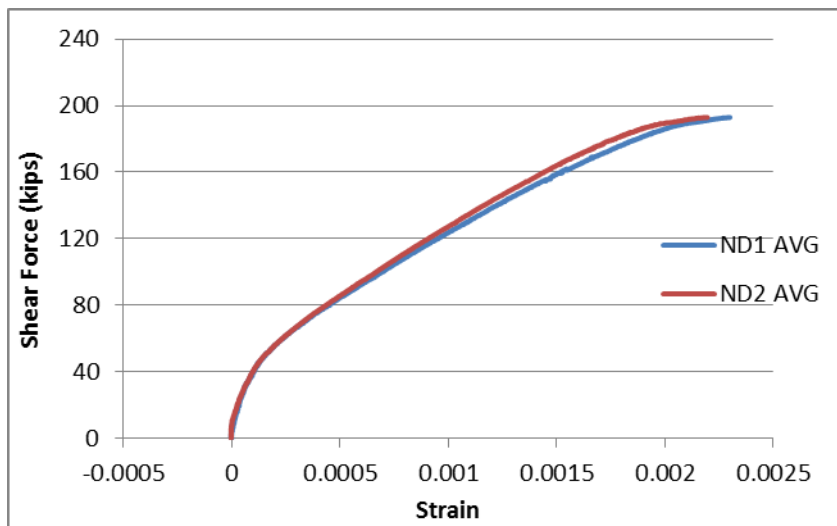


a - North strain gauges

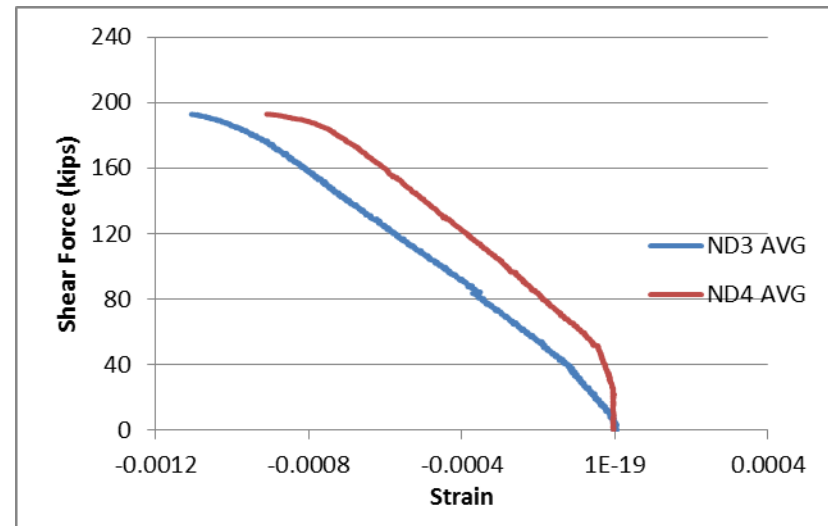


b - South strain gauges

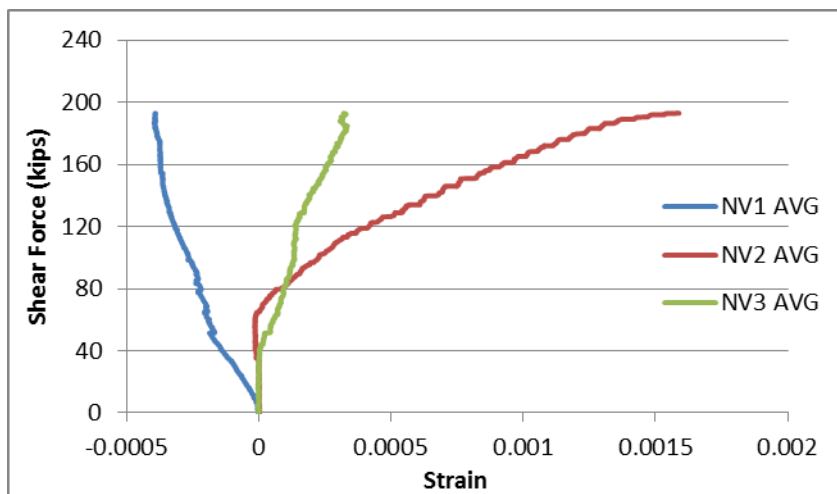
Fig. 4.26 Shear Force vs. Local Transverse Tensile Strain of Girder F3- First Run



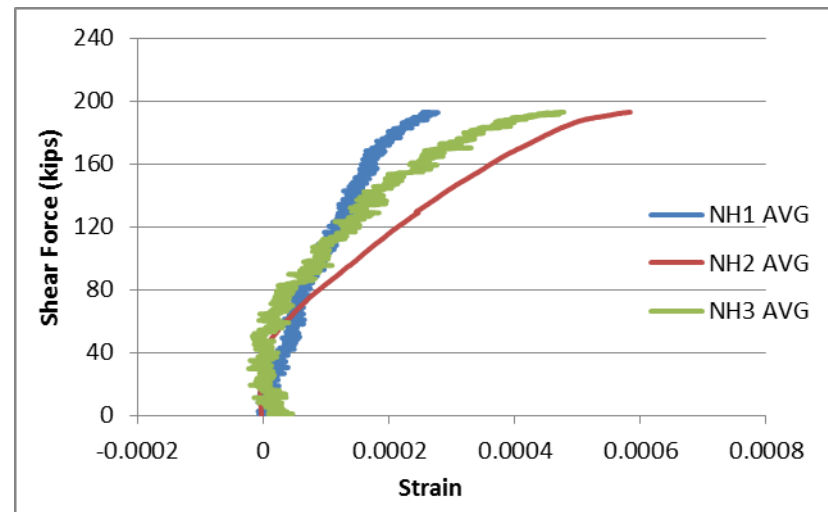
a - Average smeared tensile strain across Cracks



b - Average smeared compressive strain in concrete struts



c - Average transverse smeared strain



d - Average longitudinal smeared strain

Fig. 4.27 Shear Force vs. Concrete Smeared Strains of Girder F3- Second Run

4.3.4. Girder F4

Girder F4 was tested to fail in flexure shear mode with shear span to effective depth ratio $a/d = 2.25$. The first shear crack appeared at 58 kips and 67 kips at north and south ends of the girder, respectively, as can be seen from the load deflection curves in Fig. 4.28. The first cracks appeared at the same location shown in Fig. 4.29 (a) and (b).

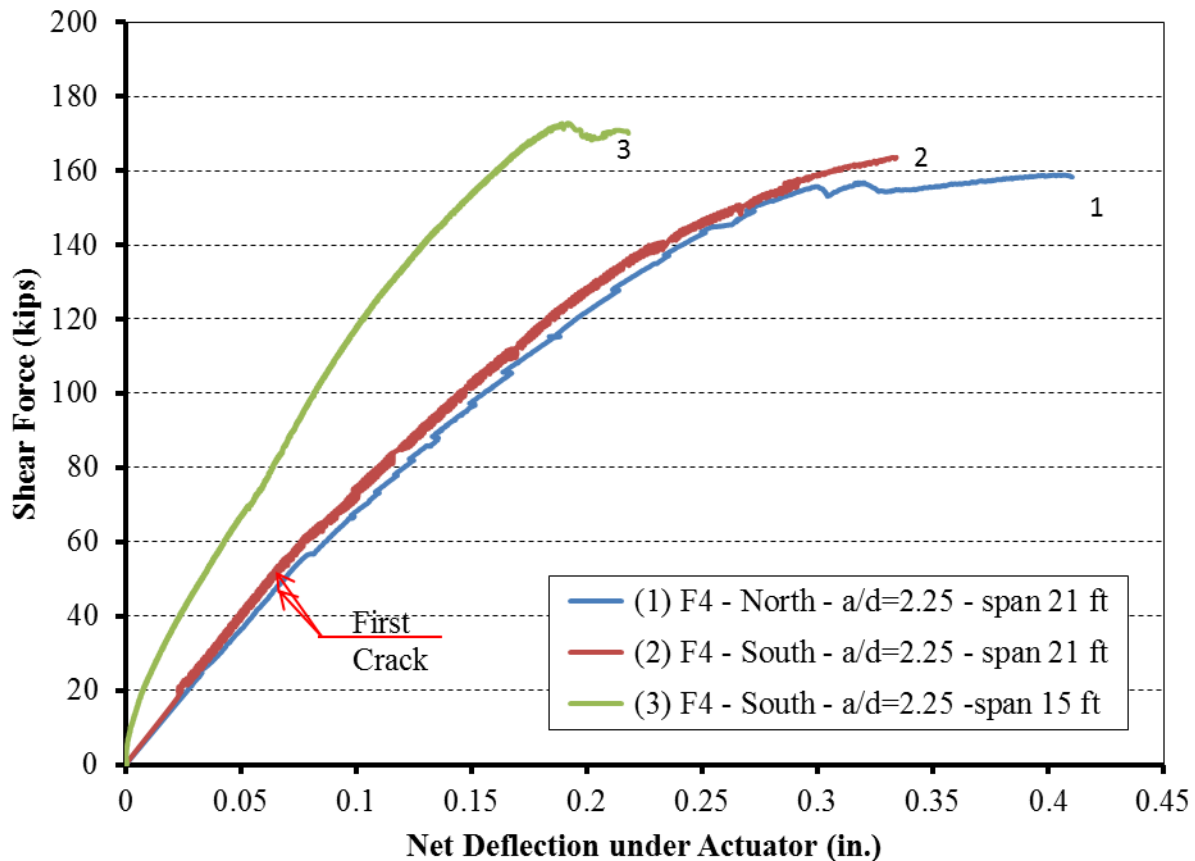


Fig. 4.28 Shear Force vs. Girder Deflection Curves for Girder F4

Fig. 4.30 shows the plot of the variation of smeared concrete strains with applied shear load at both ends of Girder F4. It should be notice that this girder is over-reinforced in shear, and it has enough flexural extra capacity which cannot be reached before occurrence of shear failure. In spite of that, the smeared strains versus shear force at the north end exhibits very ductile behavior in the first test before failure. During the test, when the applied shear load at the north end reached 155.69 kips, the concrete struts formed in the web crushed having a higher compressive smeared strain closer to the support (measured by LVDT D3) and equal to 0.0008.

This crushing harshly affected the stiffness, but the huge percentage of steel used in the transverse direction helped the web to resist more load until reaching the ultimate shear load of 158.80 kips. Although the load did not have a significant increase, losing the stiffness caused a significant increase in the net deflection measured under the north actuators as well as the smeared strains of the north end. This pseudo ductility should not mislead the understanding of the shear behavior of this girder. Although the maximum shear capacity of 158.80 kips will be used as the shear strength of the north end of Girder F4, the peak value of all the smeared and local strains should be taken at the shear strength of 155.69 kips.

In addition to the pseudo ductility at the north end, Fig. 4.30 (a) and (b) shows that the south end was stiffer than the north end. This can explain the reason of having the first crack at the north end at a lower shear load than the south end. The maximum compressive strain at the south end was recorded by LVDT D4 as 0.0007, while the maximum smeared tensile strain across the crack was the same at both ends and equal to 0.0020.

From Fig. 4.30 (c), it can be seen that the smeared strain measured by the LVDTs V1 and V2 are almost identical at the south end of the girder. The north end had more cracks crossing LVDT V2 shown in Fig. 4.29 (c) and (d), which is giving higher smeared strain value at a given shear load. The maximum transverse smeared tensile strain was 0.0020 and 0.0014 at the middle of the studied zone at the north and the south end, respectively. The reading from the LVDT V3, which was closer to the loading point, was comparatively small, as it was not intercepted by the shear crack. The web shear behavior and failure of Girder F4 can be supported by the smeared tensile strain in the longitudinal direction of the web which did not exceed 0.0004 at both ends, as shown in Fig. 4.30 (d).

The local strain in the transverse rebars measured by strain gauges at the north and south ends can be seen in Fig. 4.31. Generally, it can be seen that the tensile strain was higher at the middle of the web than in the flanges. The average strain measured along the 28.5° (AASHTO angle), coinciding with the line joining the support point and the loading point, was higher than the average strain measured along the 45° line. At the moment of the concrete struts crushing, the average strain measured along the 28.5° (AASHTO angle) was $0.7 \epsilon_y$, while the average strain measured along the 45° line was only $0.55 \epsilon_y$. Thus an average strain of $0.7 \epsilon_y$ in the transverse

steel will be used in the calculation of steel contribution toward the shear capacity of the girder in the later section of this chapter.

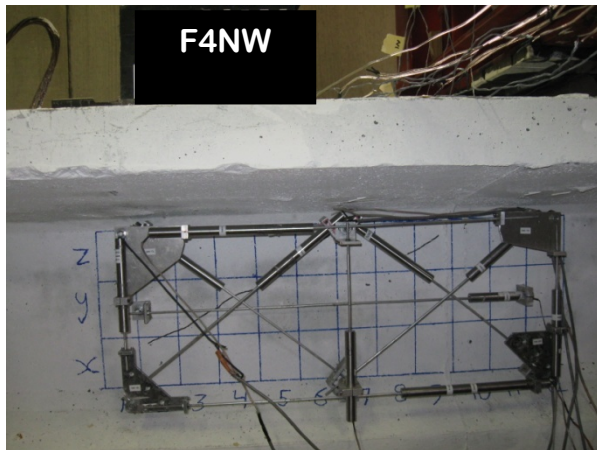
Consequently, the girder was reloaded after moving the support toward the interior at the failed north end. Fig. 4.32 shows the same phenomena of having a flat plateau after reaching the peak, which will be handled in the same way as the north end. At the peak shear load the south end also demonstrated a web shear mode of failure, Fig. 4.29(e), under shear load of 172.83 kips, having a maximum smeared compressive strain of 0.0009 in the concrete struts closer to the support, as shown in Fig. 4.32 (b), while the smeared tensile strain in the perpendicular direction of these struts was 0.0021, as shown in Fig. 4.32(a).

The maximum transverse smeared tensile strain was 0.0018 at the middle of the studied zone at the south end, as shown in Fig. 4.32 (c), which is higher than that measured in the first load with the same ratio of increase in the applied shear load. The reading from the LVDT V3, which was closer to the loading point, was comparatively small since it was not intercepted by the shear crack.

Similar to the north end, the web shear behavior and failure of Girder F4 can be supported by the smeared tensile strain in the longitudinal direction of the web, which did not exceed 0.0004 at both ends, as shown in Fig. 4.32 (d).

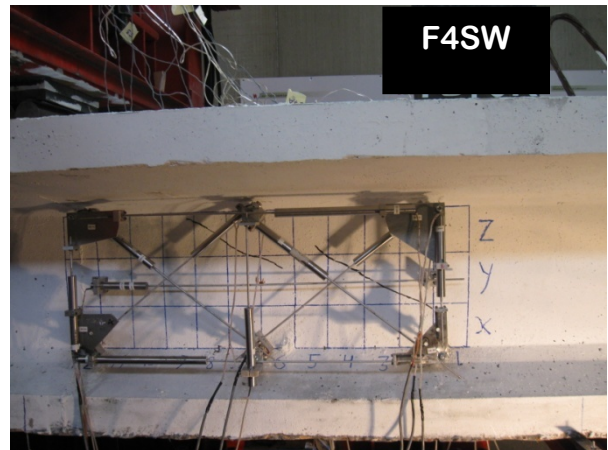
At the ultimate shear load, the average strain measured along the 28.5° (AASHTO angle) line was the same and equal to $0.7 \epsilon_y$, as shown in Fig. 4.33 (a), while the average strain measured along the 45° line was only $0.55 \epsilon_y$, as shown in Fig. 4.33 (b). Thus an average strain of $0.7 \epsilon_y$ in the transverse steel will be used in the calculation of steel contribution toward the shear capacity of the girder in the later section of this chapter.

North End

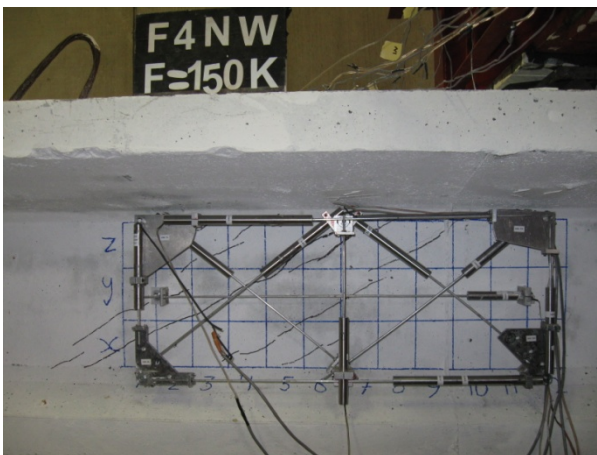


(a) First shear crack at 58 kips

South End



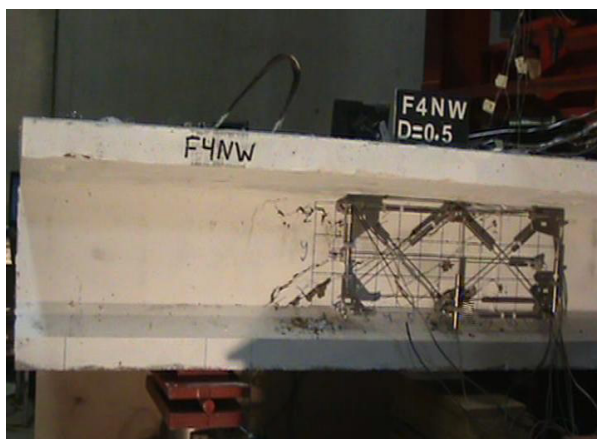
(b) First shear crack at 67 kips



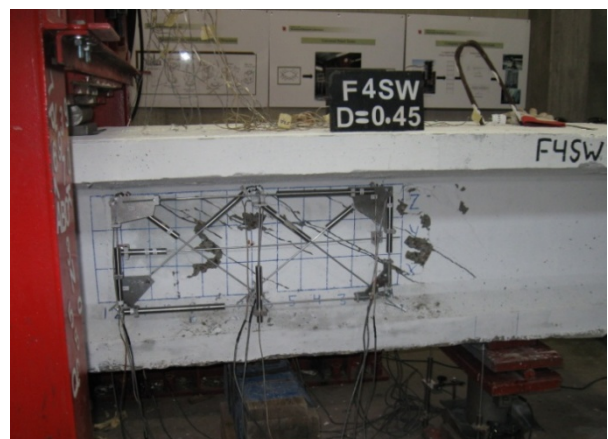
(c) Shear crack pattern before failure



(d) Shear crack pattern before failure

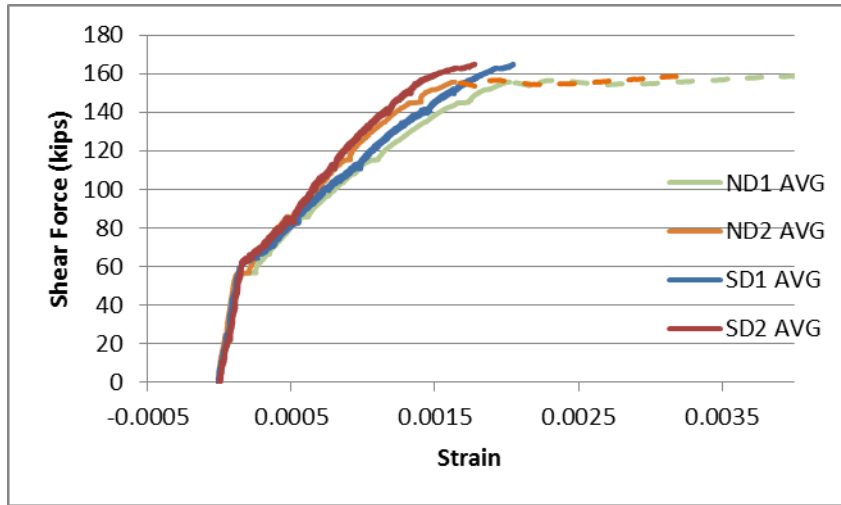


(e) Shear failure at 158.80 kips

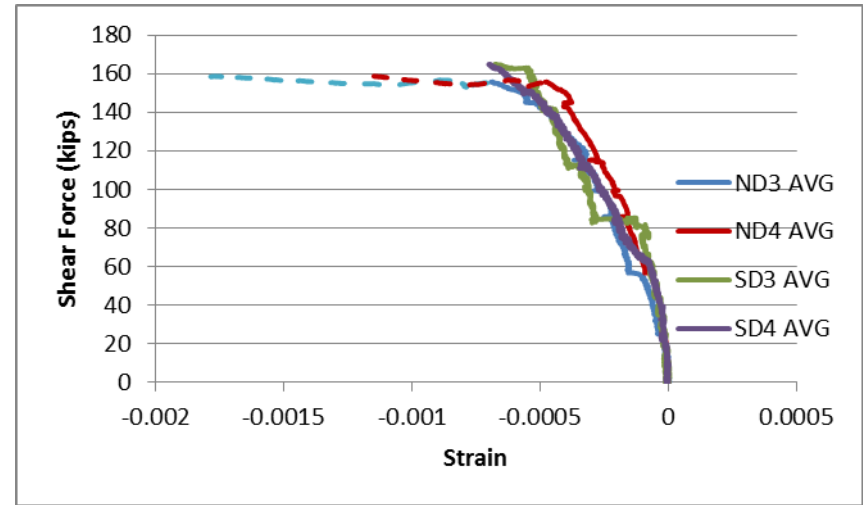


(f) Shear failure at 172.83 kips

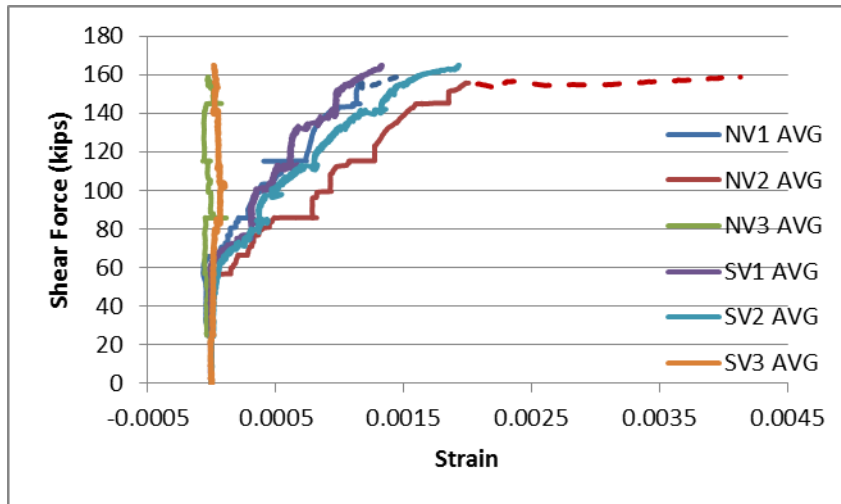
Fig. 4.29 Shear Crack Pattern and Failure Mode of Girder F4



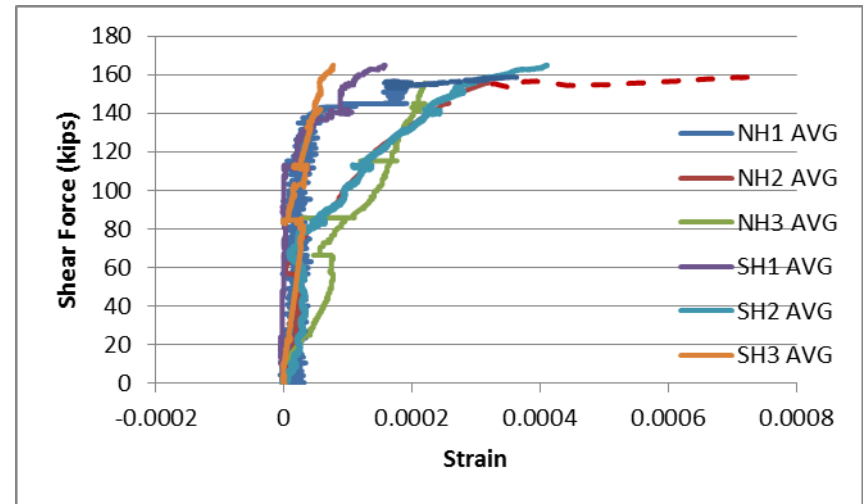
a - Average smeared tensile strain across Cracks



b - Average smeared compressive strain in concrete struts

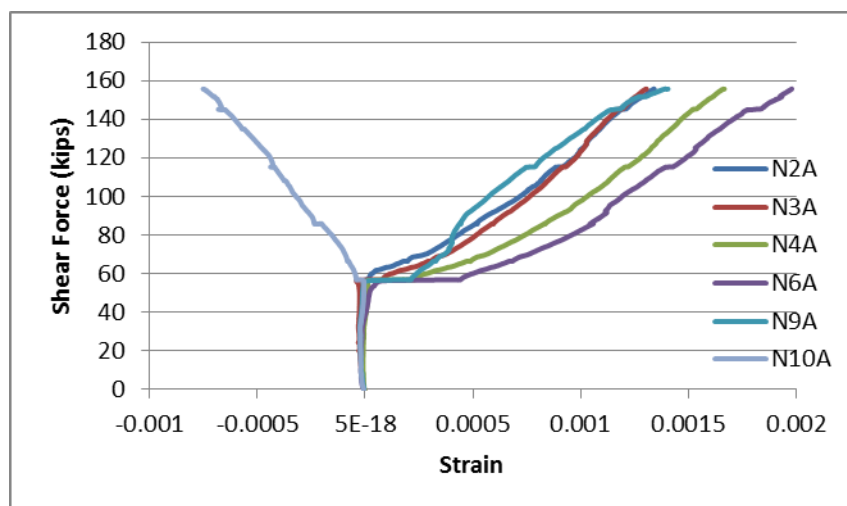


c - Average transverse smeared strain

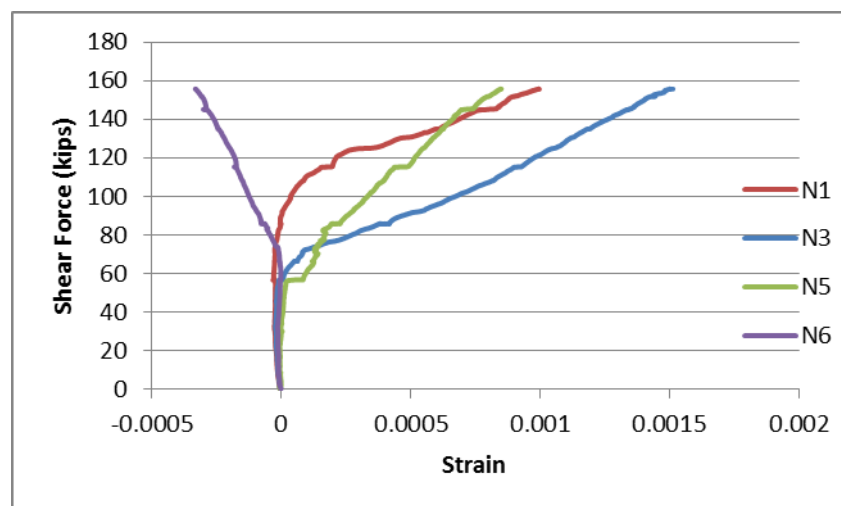


d - Average longitudinal smeared strain

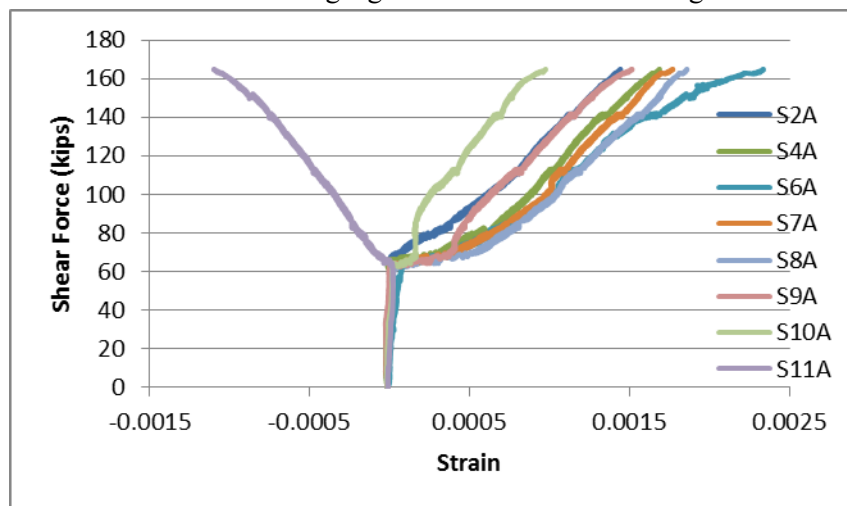
Fig. 4.30 Shear Force vs. Concrete Smeared Strains Curves for Girder F4 – First Run



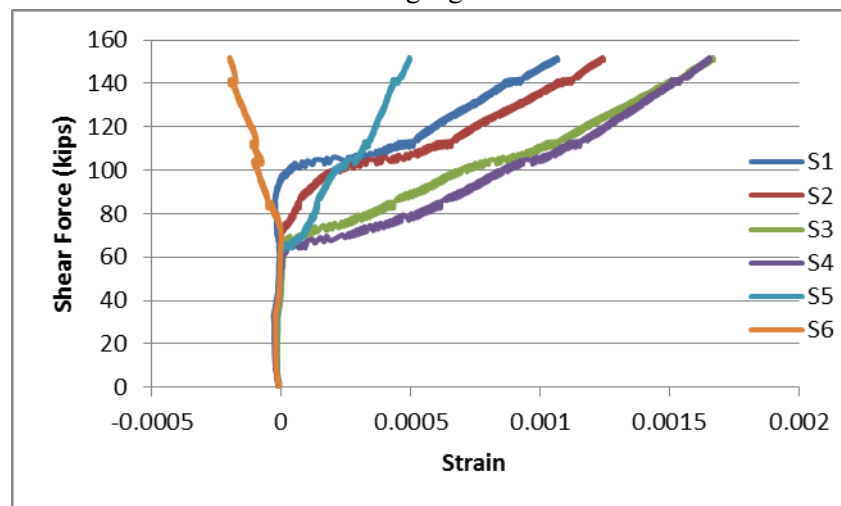
a - North strain gauges located at AASHTO angle



b – North strain gauges located at 45°

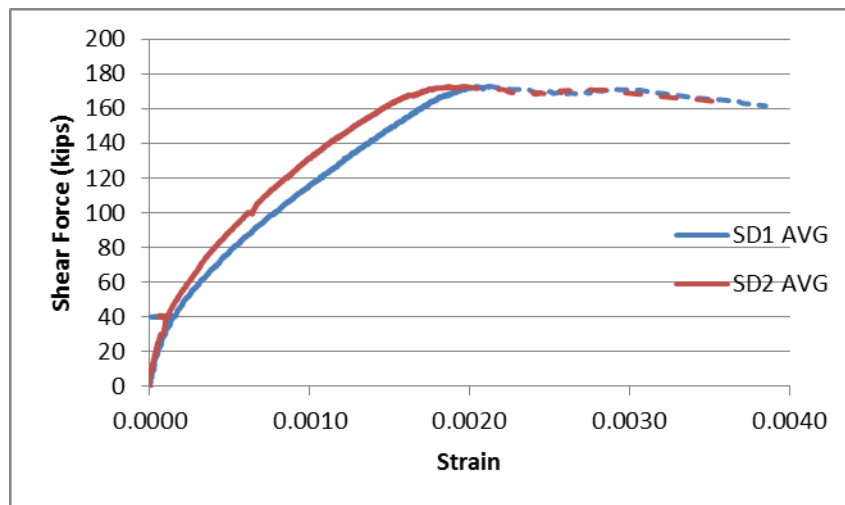


c - South strain gauges located at AASHTO angle

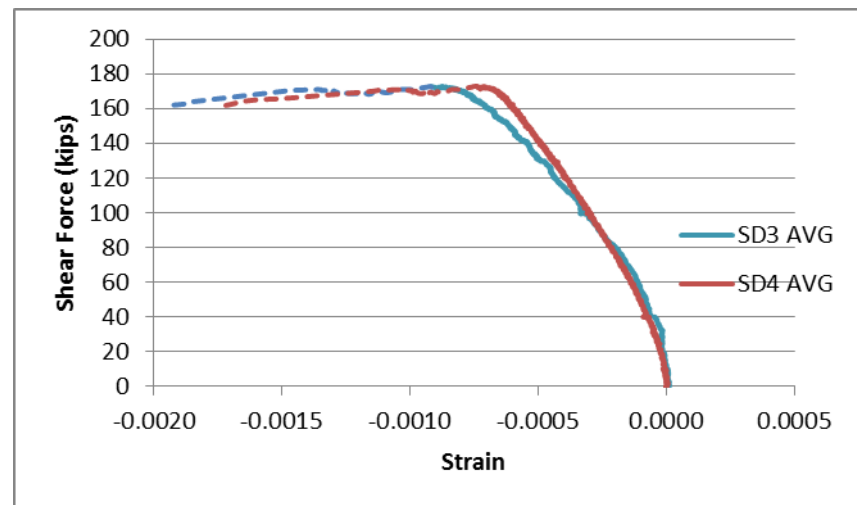


d – South strain gauges located at 45°

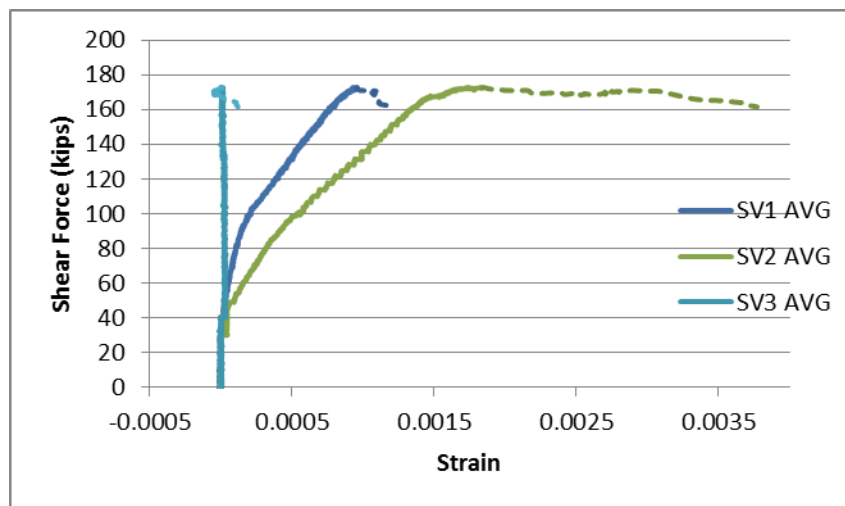
Fig. 4.31 Shear Force vs. Local Transverse Tensile Strain of Girder F4 – First Run



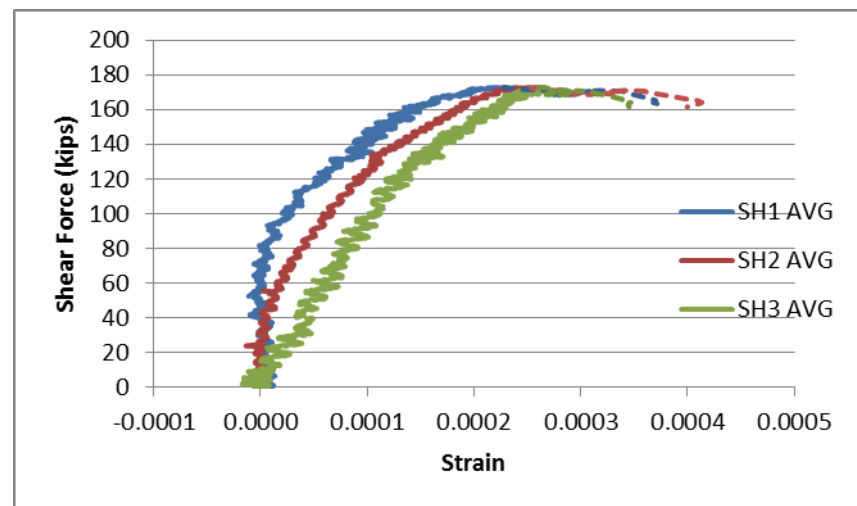
a - Average smeared tensile strain across Cracks



b - Average smeared compressive strain in concrete struts

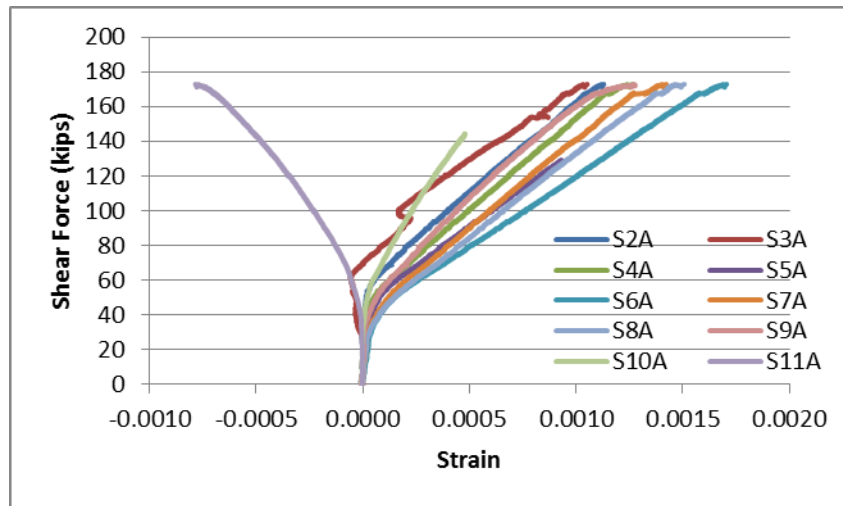


c - Average transverse smeared strain

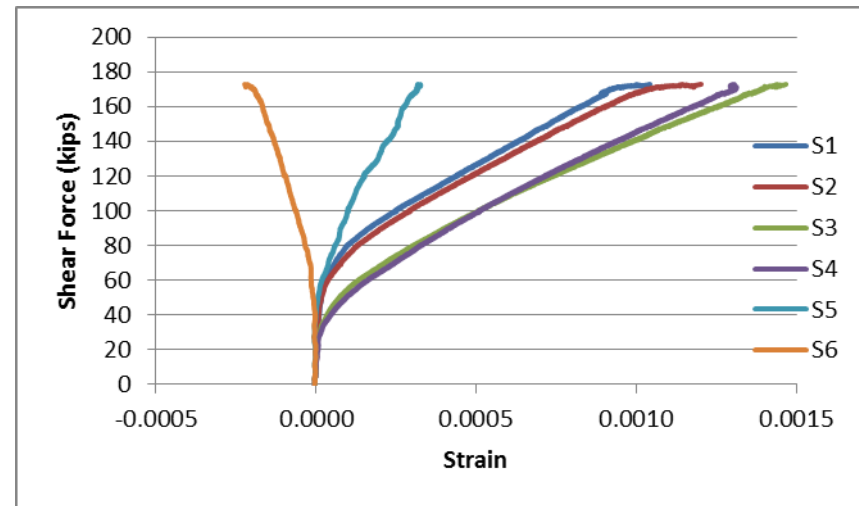


d - Average longitudinal smeared strain

Fig. 4.32 Shear Force vs. Concrete Smeared Strains Curves for Girder F4 – Second Run



a - South strain gauges located at AASHTO angle



b – South strain gauges located at 45°

Fig. 4.33 Shear Force vs. Local Transverse Tensile Strain of Girder F4 – Second Run

4.4. Experimental Results of Group C Girders with $f'_c \cong 16,000$ psi

Group C includes four girders. Girders C1 and C3 are designed to be tested to study web shear failure similar to Girders F1 and F3 in the previous group but with higher concrete strength around 16,000 psi. Girders C2 and C4 had a different cross-section with a reduced width of top flange and are designed to have a flexural-shear failure. Girders C1 and C2 are designed having transverse steel at the balanced condition, while girders C3 and C4 are designed to be over-reinforced. The four girders in this group have been designed with different shear span to effective depth ratio a/d .

4.4.1. Girder C1

As a girder designed to fail in web shear, Girder C1 had a span to effective depth ratio $a/d = 1.77$. Fig. 4.34 presents the shear load versus net deflection curves at both the north and the south ends during the first test and at the north end during the second run. The first shear cracks appeared at 75 kips at both ends of the girder with the crack line connecting the loading point and the reaction point, as shown in Fig. 4.35(a) and (b), which increased the crack width rapidly with increasing of the shear force.

Due to a malfunction in the data acquisition system that did not allow the computer to record more than three decimals, it was not possible to plot all the LVDT results. Fig. 4.36 (a) and (b) shows approximate curves for the smeared tensile strain across the shear cracks and the smeared compressive strain in the concrete struts at both the north and south ends. It shows that Girder C1 failed first at the south end under a shear force of 168.50 kips when the smeared compressive strain in the concrete struts exceeds 0.0010, while the corresponding force at the north end was 169.02 kips, (Curves 1 and 2 in Fig. 4.34). The smeared tensile strain on the north end was higher, but at both ends it exceeds 0.0020.

The available data showed the same trend of the vertical LVDTs in previous girders. The highest smeared tensile strain was at the middle of the studied zones. The available data indicated that the smeared tensile strain in the longitudinal direction at the middle of the web at both ends was between 0.0005 and 0.0010, which should be expected to be closer to 0.0005 as a web shear girder.

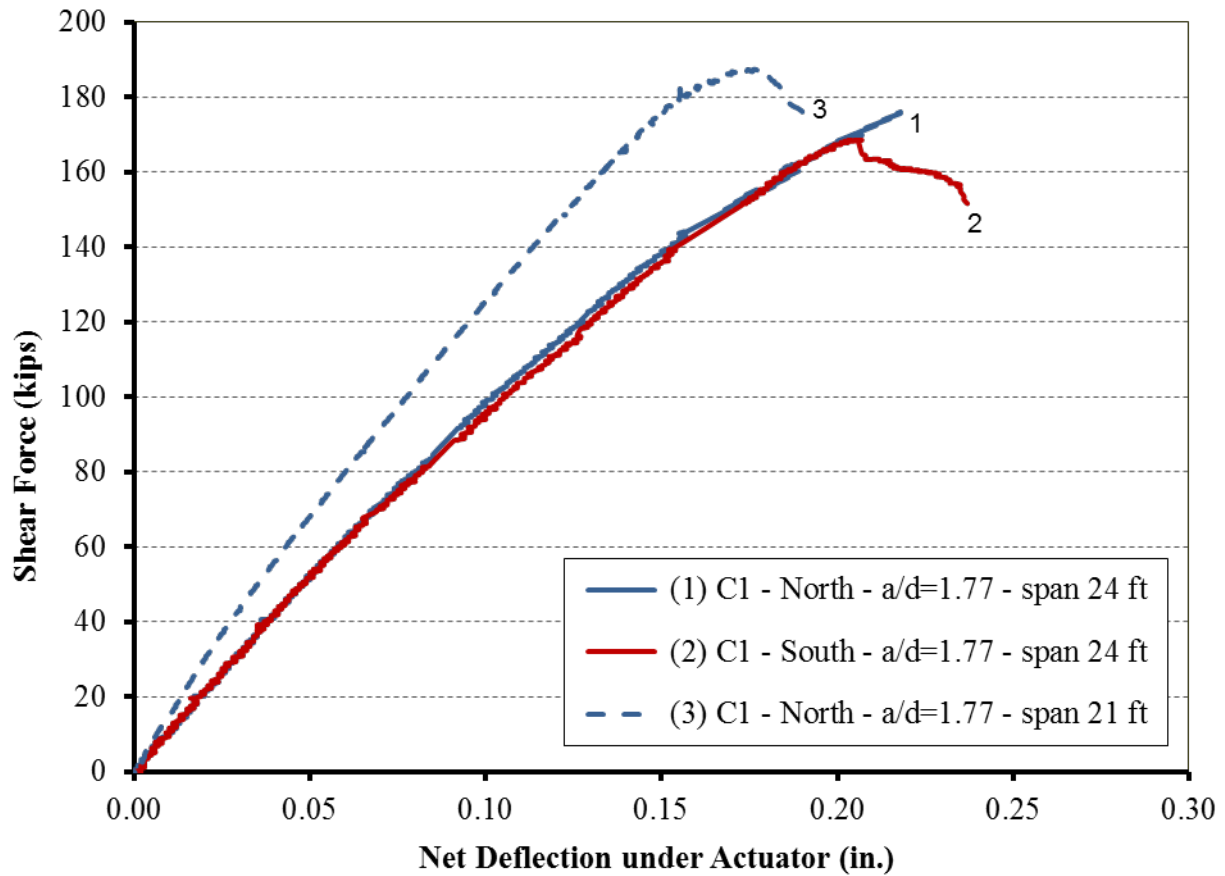


Fig. 4.34 Shear force vs. Net Deflection Curve for Girder C1

The local strain in the transverse rebars measured by strain gauges at both the south and the north ends can be shown in Fig. 4.37. During the first run, the average strain for the rebars inside the web (SG2 to SG6) intersecting the shear cracks was $0.80 \epsilon_y$ and $0.85 \epsilon_y$ for the north and south end, respectively. The first run resulted in a failure at the south end. During retesting the north end the average strain for the rebars reached $0.90 \epsilon_y$.

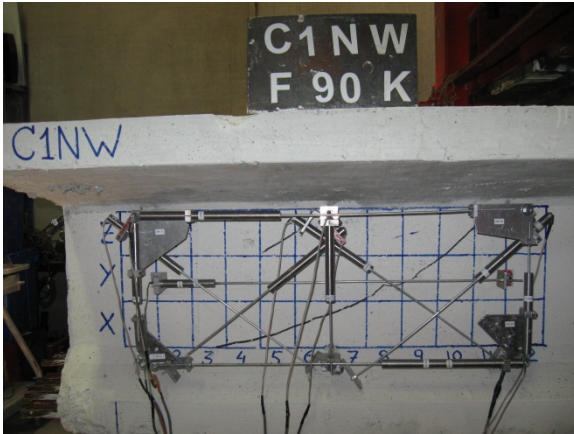
After the failure of the south end, the south support was moved to get a net girder span of 21 ft., and the north end was retested and failed finally at 187.50 kips, (Curve 3 in Fig. 4.34), having a smeared compressive strain in concrete struts of 0.0014 in average throughout the studied zone, shown in Fig. 4.38 (b). The smeared tensile strain across crack was 0.0029 in average, shown in Fig. 4.38 (a).

Fig. 4.38 (c) shows that the transverse smeared tensile strain was 0.0025 at the middle of the studied zone at the north end. The readings from LVDTs V1 and V3, which were close to the support and the loading points, respectively, were very small, as the shear crack did not intersect these LVDTs, as shown in Fig. 4.35(c).

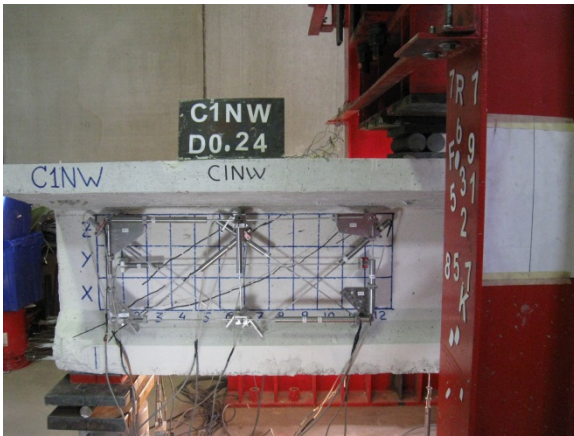
Fig. 4.39 (d) shows that the longitudinal smeared tensile strain was higher than what was predicted for a web shear girder. The reading from LVDT H1 was very small being the top of the web where fewer cracks intersected it.

It can be seen that capacity of Girder C1 is very close to the capacity of Girders F1 and F3 in the previous group, although it has higher concrete strength. This might happen due to a lack of compaction during the casting of the girder.

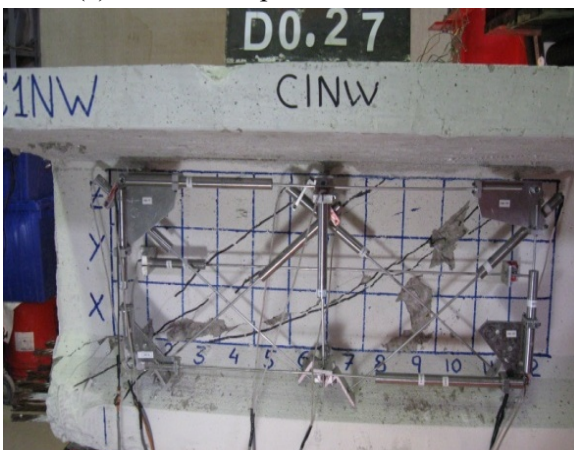
North End



(a) First shear crack at 75 kips



(c) Shear crack pattern before failure



(e) Shear failure at 187.50 kips

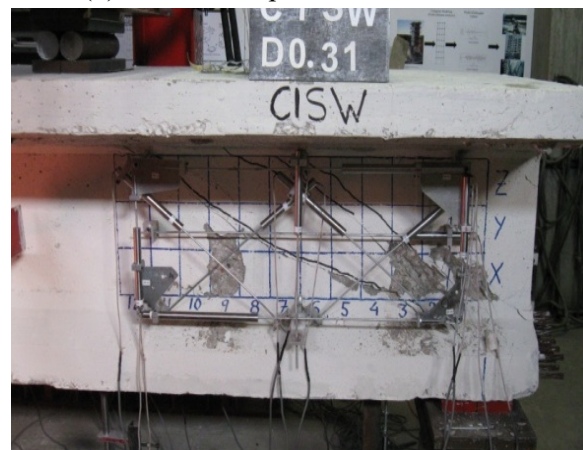
South End



(b) First shear crack at 75 kips

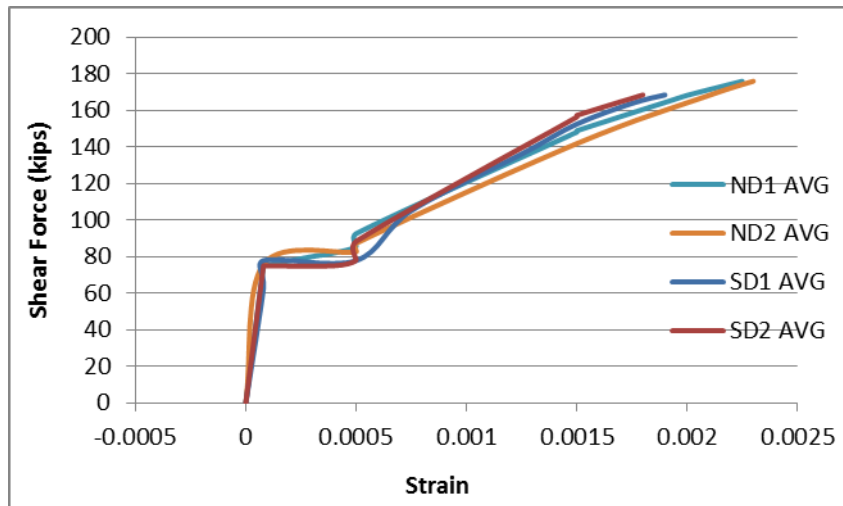


(d) Shear crack pattern before failure

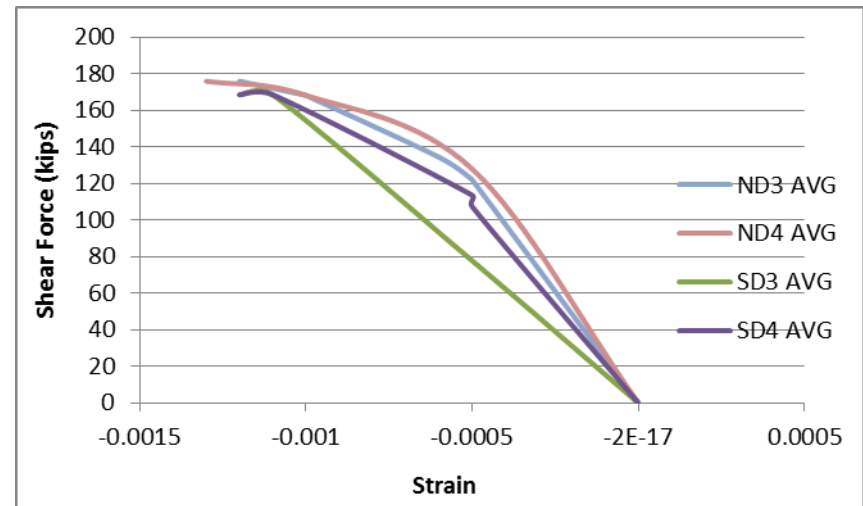


(f) Shear failure at 168.50 kips

Fig. 4.35 Shear Crack Pattern and Failure Mode of Girder C1

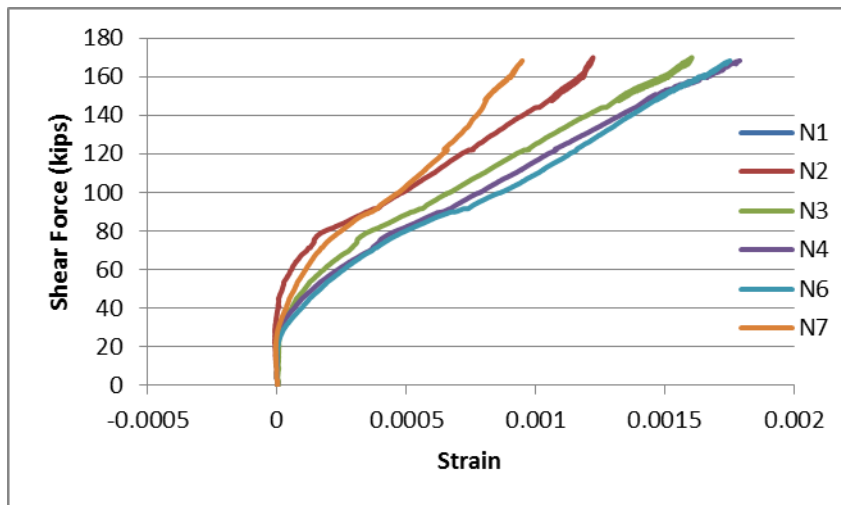


a - Average smeared tensile strain across Cracks

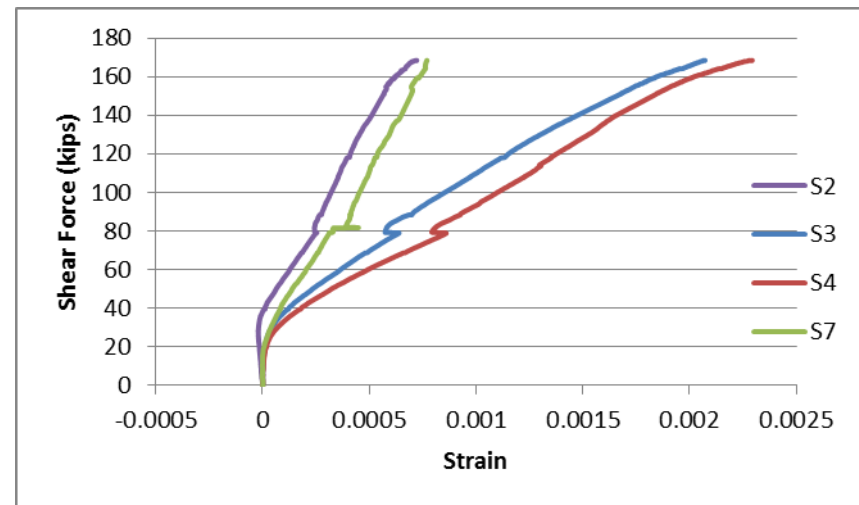


b - Average smeared compressive strain in concrete struts

Fig. 4.36 Shear Force vs. Concrete Smeared Strains of Girder C1- First Run

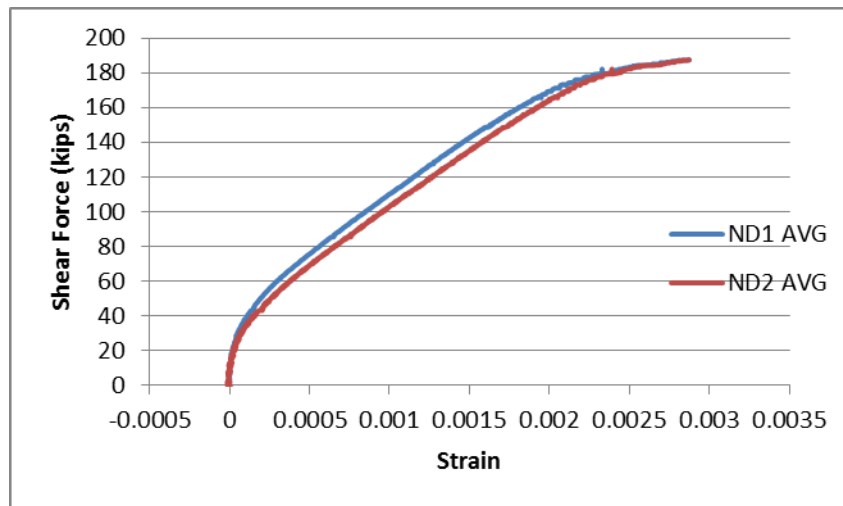


a - North strain gauges

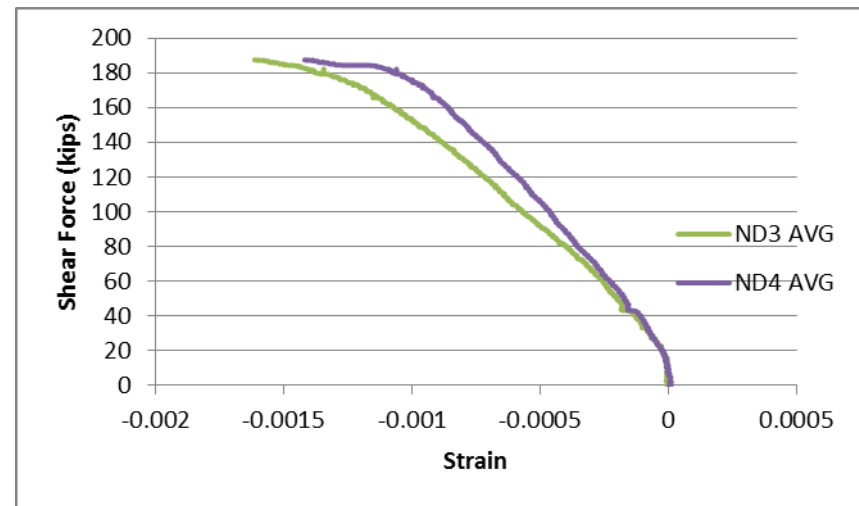


b - South strain gauges

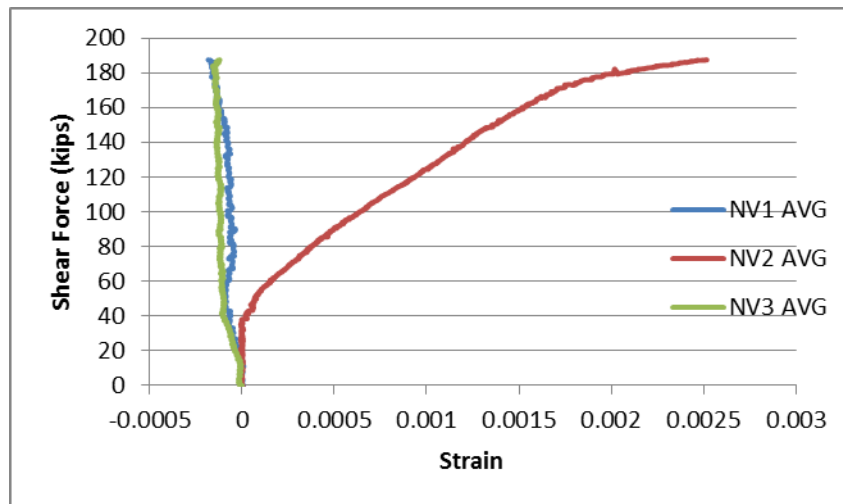
Fig. 4.37 Shear Force vs. Local Transverse Tensile Strain of Girder C1 – First Run



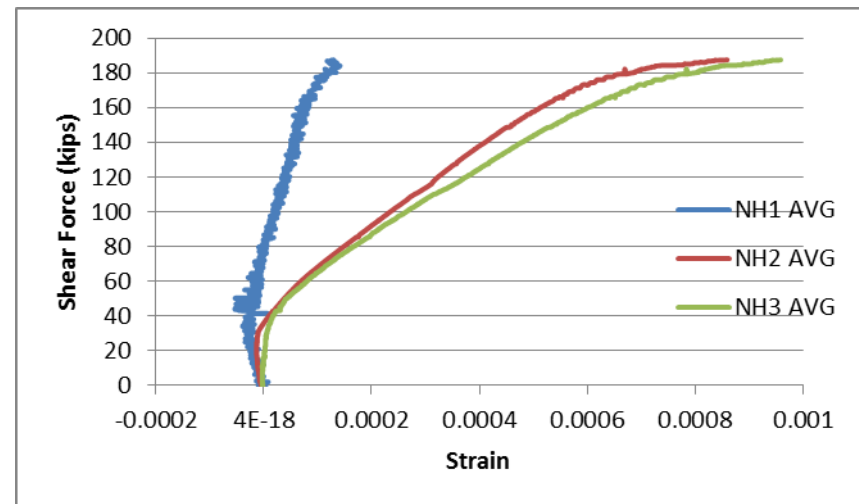
a - Average smeared tensile strain across Cracks



b - Average smeared compressive strain in concrete struts

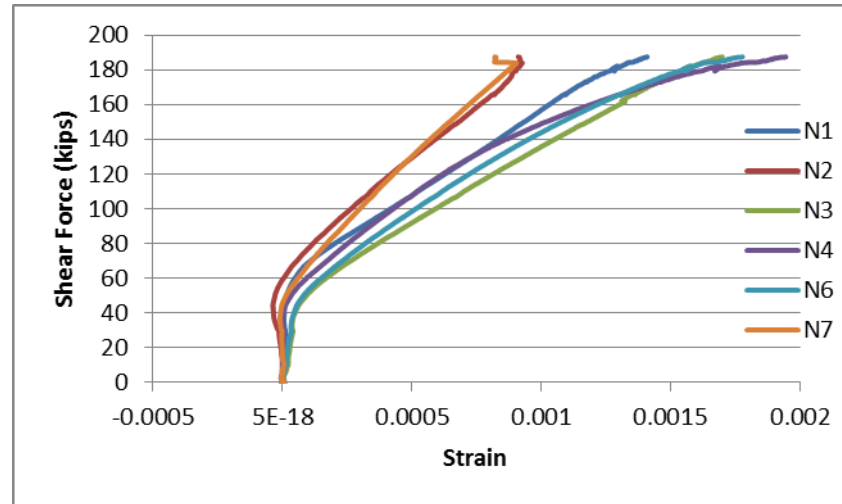


c - Average transverse smeared strain



d - Average longitudinal smeared strain

Fig. 4.38 Shear Force vs. Concrete Smeared Strains Curves for Girder C1 – Second Run



North strain gauges

Fig. 4.39 Shear Force vs. Local Transverse Tensile Strain of Girder C1 – Second Run

4.4.2. Girder C2

Girder C2 was tested to fail in the flexure shear mode with a shear span to effective depth ratio $a/d = 3.00$. Fig.4.40 shows the plot of shear force and corresponding girder net deflection during the first and second tests. The first shear crack appeared at 60 and 53 kips at the north and south ends of the girder, respectively, as shown in Fig. 4.41(a) and (b). By increasing the applied loads on both ends, new shear cracks have been shown in the web, as shown in Fig. 4.41 (c) and (d). Owing to a casting problem at the south end of this girder having concrete with higher water-to-cement ratio and higher slump than the north end, and the cracks developed more during the test at the south end, which resulted finally in a failure at the south end first. Also, some flexure cracks have been shown in the bottom flange. Flexure cracks in the bottom flange demonstrated that the girder was going to fail in flexural shear.

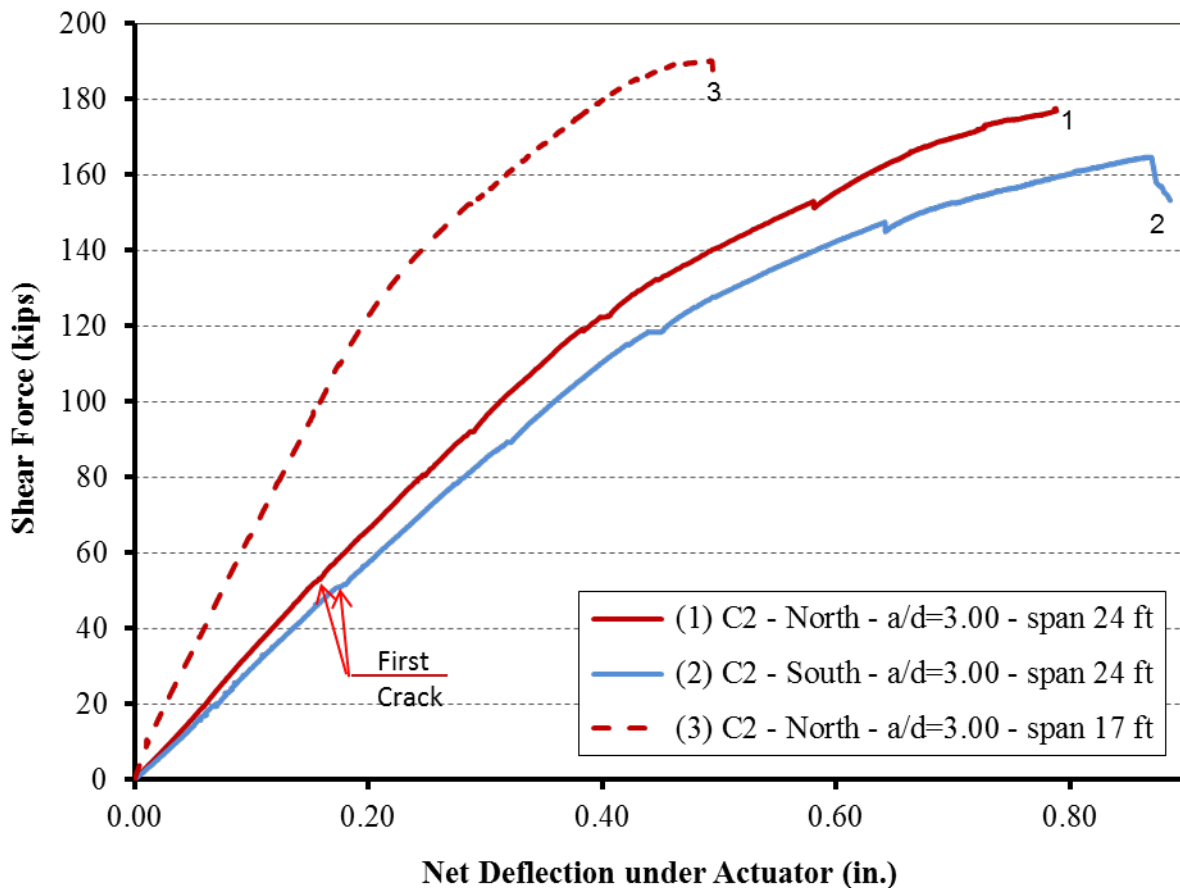


Fig. 4.40 Shear Force vs. Girder Deflection Curves for Girder C2

Due to the different concrete properties at both ends, the stiffness of all the presented curves in Fig. 4.42 is different. It is always less at the south end. For a given shear force load, the measured smeared strain always higher at the south end. Fig. 4.42(a) show that the smeared tensile strain was 0.0024 and 0.0028 in average at the north and the south ends, respectively. Finally, the girder failed first at the south end at a shear load of 164.60 kips having a maximum smeared compressive strain 0.0011, while the corresponding load at the north end was 176.90 kips with maximum smeared compressive strain 0.0008, as shown in Fig. 4.42 (b).

Fig. 4.42 (c) shows the smeared tensile strain in the transverse direction at both ends. It can be seen that the smeared strain was around 0.0016 in average throughout the studied zone at both ends. The smeared strain at the middle of the studied zone at the south end had a higher value of 0.0026 comparing to 0.0019 at the middle of the studied zone at the north end. Although in average the smeared tensile strain was very close at both ends, the strain measured by LVDTs V1 and V2 at the north end are very close, which did not happen at the south end. This is a sign of the non-uniformity of the concrete properties at the south end, which resulted in a more destructive failure at the south end with a lower shear load, as shown in Fig. 4.41 (e) and (f). As usual, the readings from the LVDT V3, which was closer to the loading point, at both ends of the girder were very small because of missing most of the shear cracks.

Figure 4.42 (d) shows the smeared tensile strain measure in the longitudinal direction, where considerable smeared tensile strain was measured by LVDTs H2 and H3. LVDT H1, being at the top of the web, is giving a small compressive strain due to the effect of the flexural action.

The local strain in the transverse steel at both the north and south ends has a similar behavior, as shown in Fig. 4.43. At the failure of the south end, the average strain measured through 26.2° (AASHTO angle) was around $0.85 \epsilon_y$ at both ends, while the average strain measured along the 45° was around $0.70 \epsilon_y$ and $0.78 \epsilon_y$ at the north and south ends, respectively.

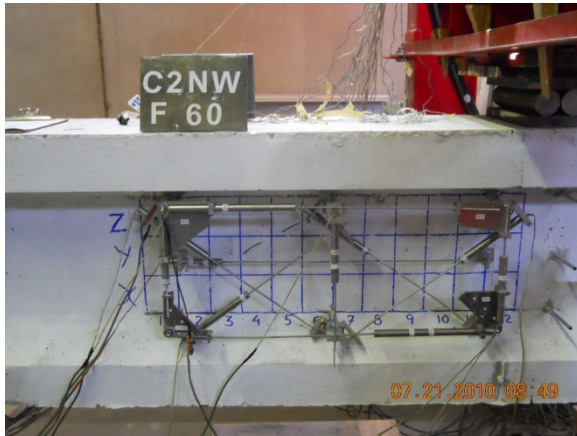
After the failure of the south end, the south load cell was moved after the failed zone to get a net girder span of 17 ft., and the north end was retested and failed also in flexural shear at a shear force of 190.10 kips, (Curve 3 in Fig. 4.40). While the smeared tensile strain was uniform throughout the studied zone having an average strain of 0.0032 at the peak shear load, the

maximum smeared compressive strain was measured by LVDT D3, and it reached 0.0013 at its peak. Fig. 4.44 (a) and (b). Fig. 4.44 (c) shows the smeared tensile strain in the transverse direction with very similar behavior until the load was near the peak load. Closer to the peak the tensile strains started to develop more at the middle of the studied zone that resulted in a maximum strain of 0.002 at the peak, which is almost the same strain obtained during the first run.

Again the flexure shear failure of Girder C2 can be demonstrated clearly by the smeared tensile strain in the longitudinal direction, as shown in Fig. 4.44 (d). Due to the effect of the flexural action, LVDTs H2 and H3 exhibit a significant tensile strain, while LVDT H1, being at the top of the web, is demonstrating a small compressive strain.

During re-testing the north end the strain gauges at the 26.2° (AASHTO angle) measured only an average strain of $0.70 \epsilon_y$, which is less than the average measured in the first test, while the average strain measures along the 45° was only $0.65 \epsilon_y$, as shown in Fig 4.45. This is not true because the failure load of the north end was higher by 15% than the failure load of the south end. By assuming that the strain in the transverse rebars should increase by the same increasing ratio of the shear force, it could be presumed that the steel had almost an average strain of yielding.

North End

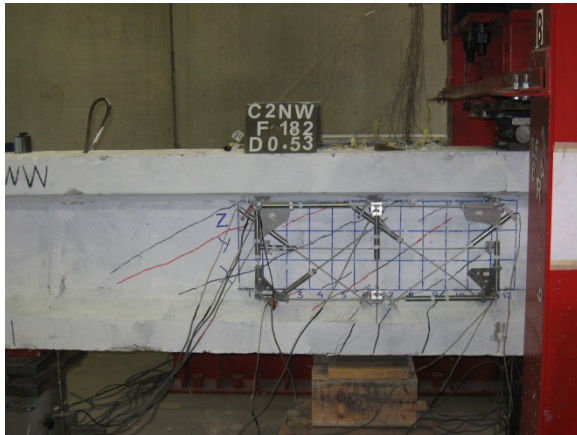


(a) First shear crack at 60 kips

South End



(b) First shear crack at 53 kips



(c) Shear crack pattern before failure



(d) Shear crack pattern before failure

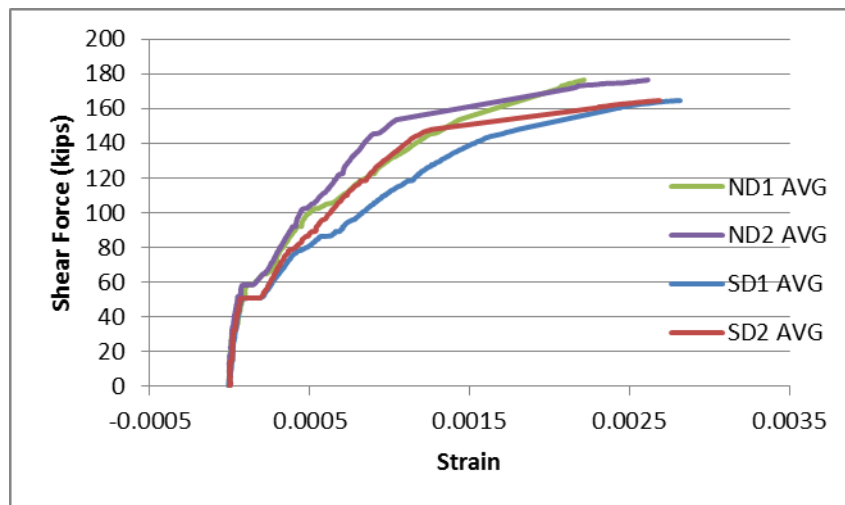


(e) Shear failure at 190.10 kips

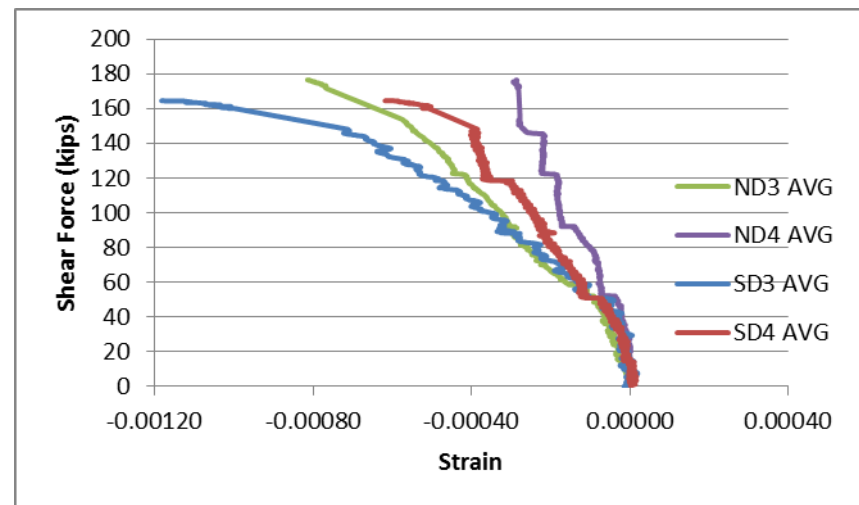


(f) Shear failure at 164.60 kips

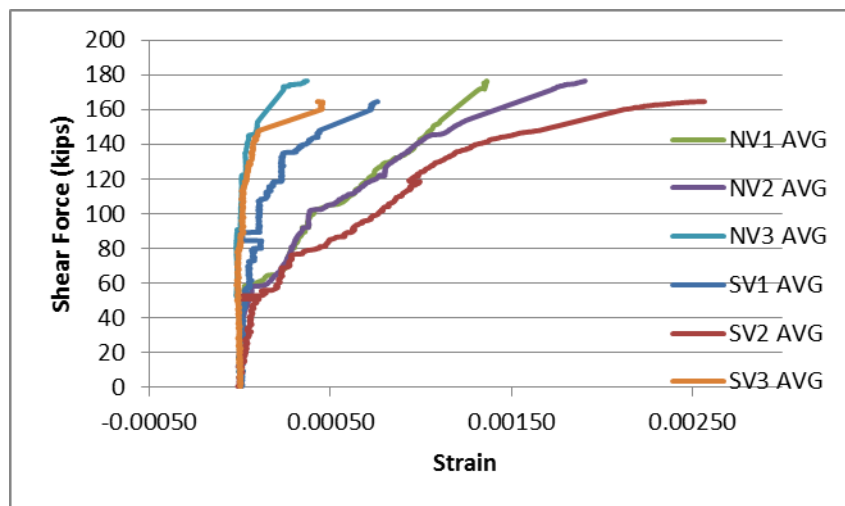
Fig. 4.41 Shear Crack Pattern and Failure Mode of Girder C2



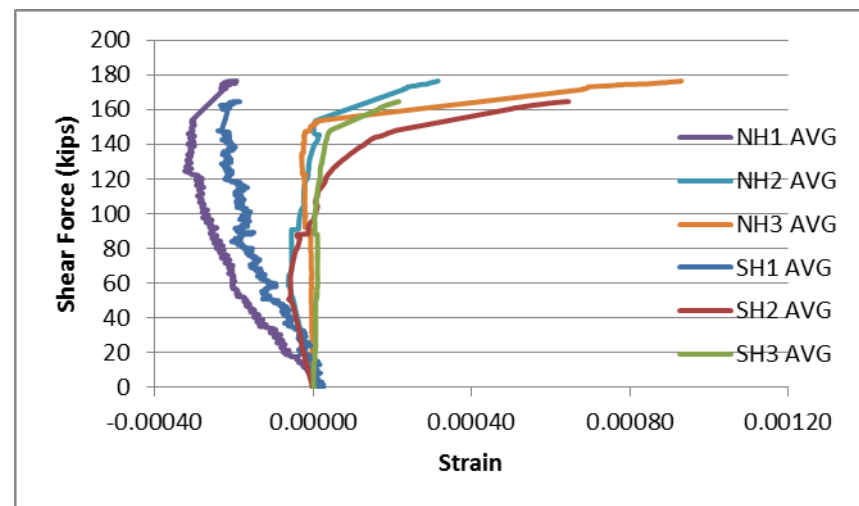
a - Average smeared tensile strain across Cracks



b - Average smeared compressive strain in concrete struts

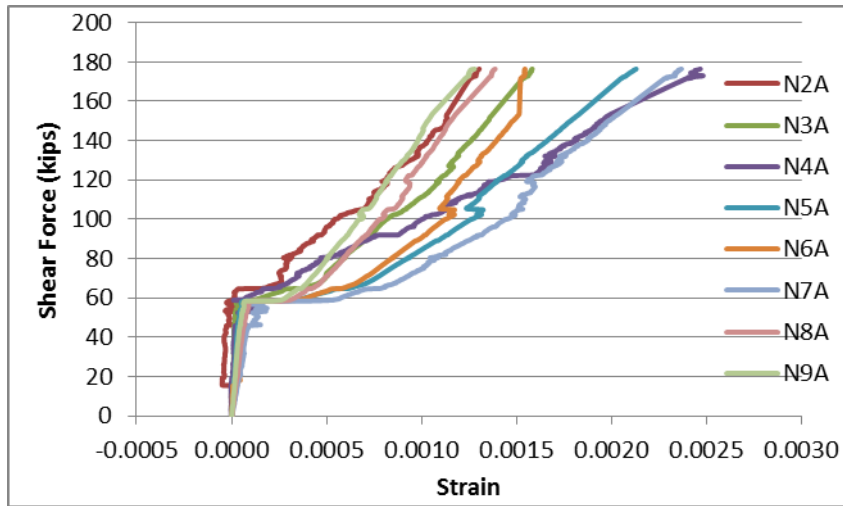


c - Average transverse smeared strain

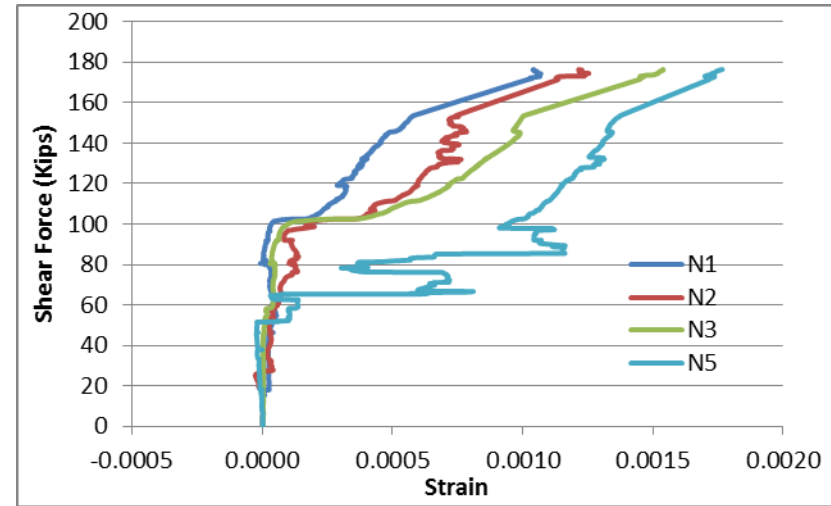


d - Average longitudinal smeared strain

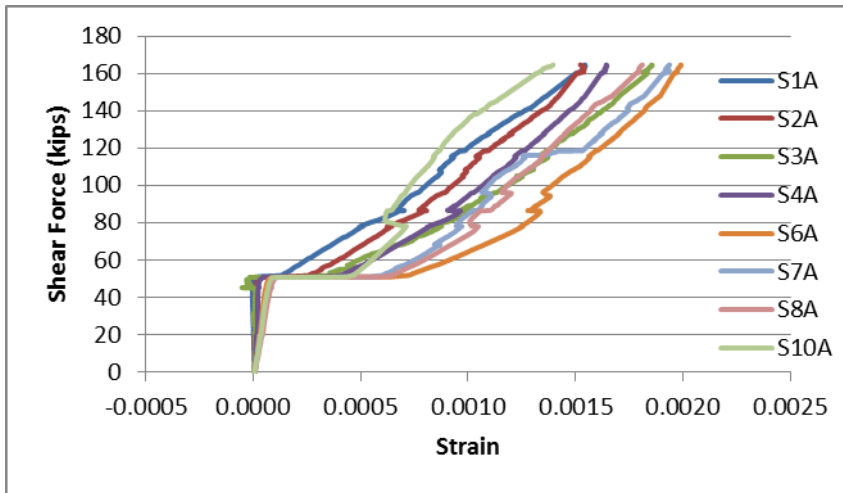
Fig. 4.42 Shear Force vs. Concrete Smeared Strains Curves for Girder C2 – First Run



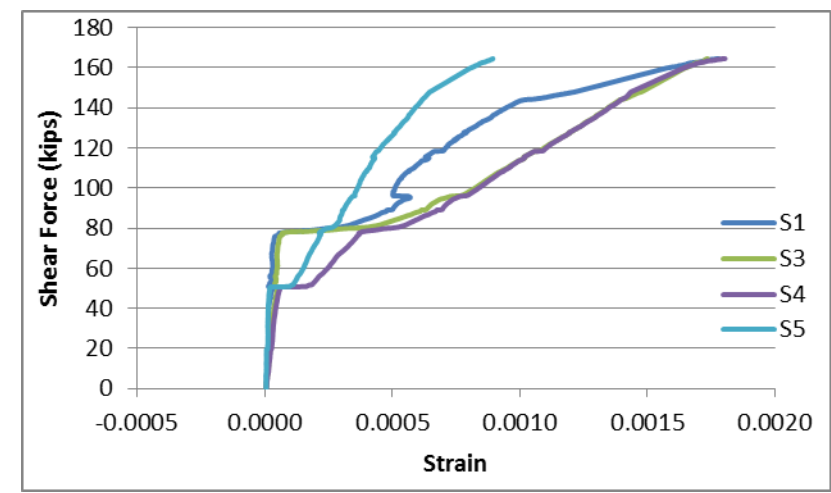
a - North strain gauges located at AASHTO angle



b – North strain gauges located at 45°

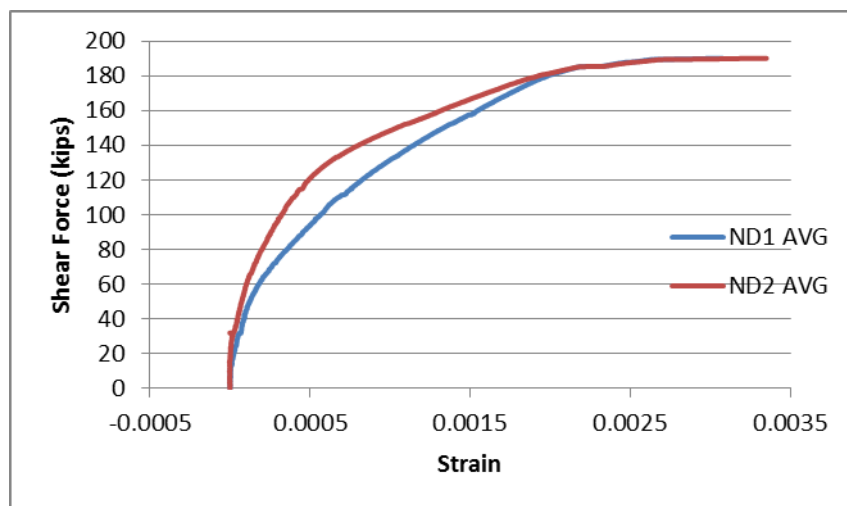


c - South strain gauges located at AASHTO angle

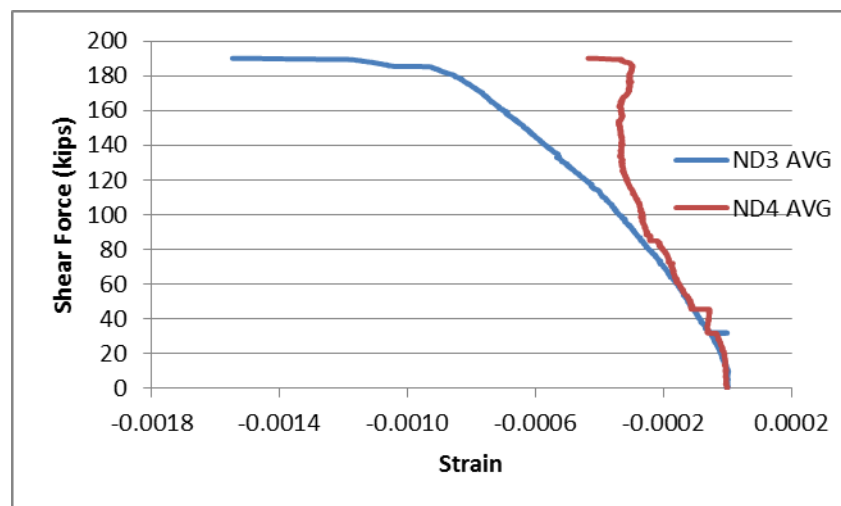


d – South strain gauges located at 45°

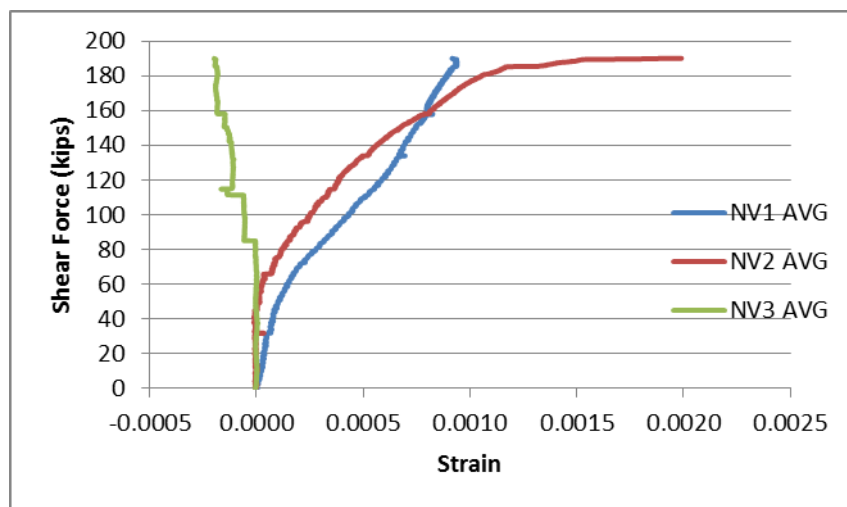
Fig. 4.43 Shear Force vs. Local Transverse Tensile Strain of Girder C2 – First Run



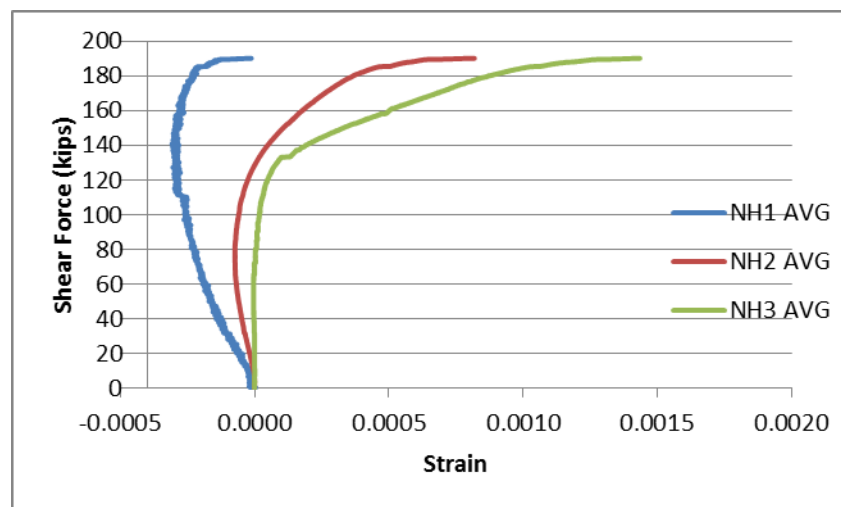
a - Average smeared tensile strain across Cracks



b - Average smeared compressive strain in concrete struts

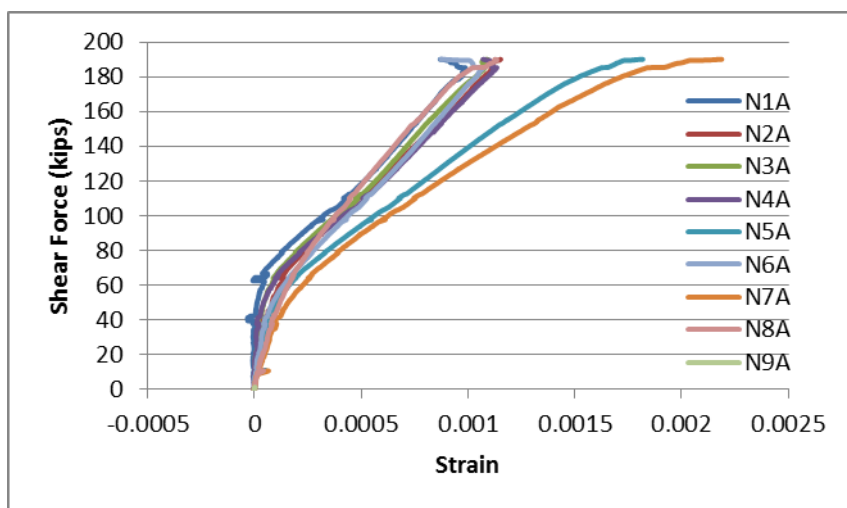


c - Average transverse smeared strain

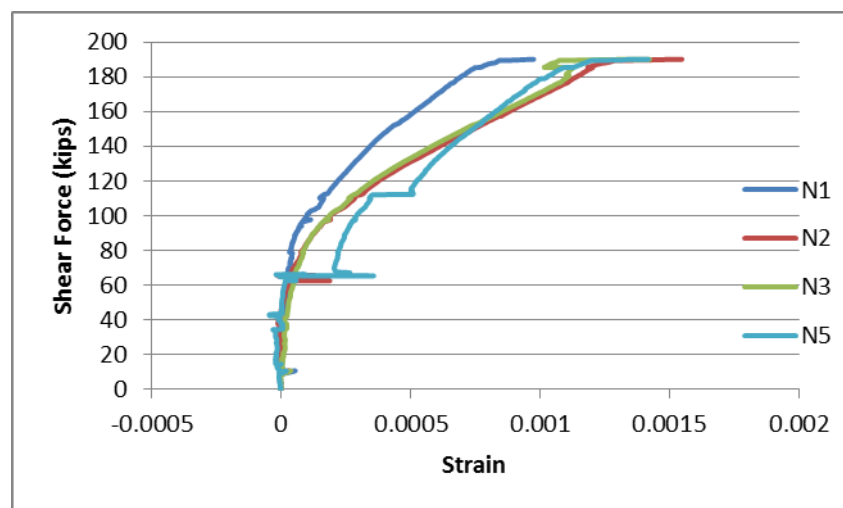


d - Average longitudinal smeared strain

Fig. 4.44 Shear Force vs. Concrete Smeared Strains Curves for Girder C2 – Second Run



a - North strain gauges located at AASHTO angle



b – North strain gauges located at 45°

Fig. 4.45 Shear Force vs. Local Transverse Tensile Strain of Girder C2 – Second Run

4.4.3. Girder C3

Girder C3 was tested to fail in web shear mode with a shear span to effective depth ratio $a/d = 1.77$. The first shear crack appeared at the north end was observed at 71 kips, and it is reflected on the shear load versus net deflection, shown in Fig. 4.46-curve 1, while the first crack was observed at the south end at 75 kips, which did not affect the load deflection curve, as shown in Fig. 4.46-curve 2. Fig. 4.47(a) and (b) show the first shear crack at each end of Girder C3.

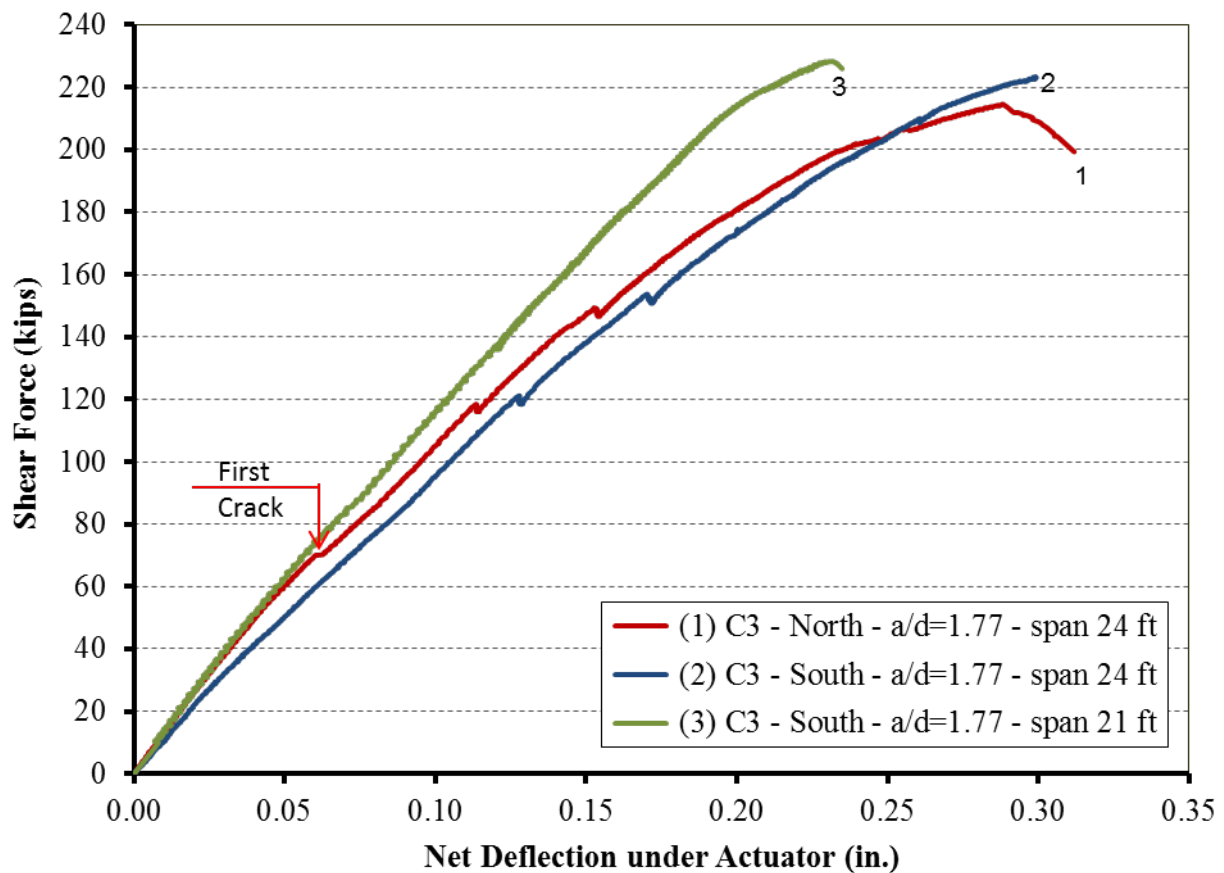


Fig. 4.46 Shear Force vs. Girder Deflection Curves for Girder C3

By increasing the shear force, the first shear crack extended and became wider and more cracks appeared at the north end closer to the support than at the south end, as shown in Fig. 4.47(c) and (d). However, the smeared tensile strain in average over the entire studied zone was 0.0022 and 0.0021 at the north end and the south end respectively, as shown in Fig. 4.48 (a). Fig. 4.48 (b) shows that the smeared compressive strain in concrete struts was higher at the north

end resulting in a web shear failure under a shear force of 214.44 kips, shown in Fig. 4.47 (e), due to a maximum smeared compressive strain of 0.0011 close to the support (measured by LVDT D3), while the force at the south end was 222.06 kips, with smeared compressive strain not larger than 0.0009.

Fig. 4.48 (c) shows the smeared transverse strain measured by the vertical LVDTs installed on the web at both the girder ends during the first test run. For a given shear force, the north end had higher smeared transverse strain than the south end due to having more cracks until a shear load of 180 kips. After that, the behavior was identical having a smeared transverse strain at peak equal to 0.0022 and 0.0024 at the middle of the studied zones at the north and south ends respectively. The readings from the LVDTs V1 and V3, being close to the support and loading point respectively, were significantly smaller because they missed the main shear crack, as can be seen in Fig. 4.47 (c) and (d).

The local strain in the transverse rebars measured by strain gauges at the south and north ends can be shown in Fig. 4.49. The rebars inside the web intersecting the shear cracks at the north end had an average strain of $0.90 \epsilon_y$, while those rebars inside the web intersecting the shear cracks at the south end had only an average strain of $0.75 \epsilon_y$.

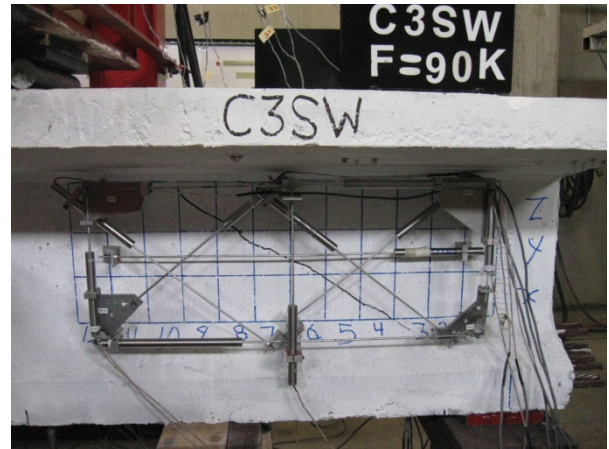
After the failure of the south end, the south support was moved to get a net girder span of 21 ft., and the south end was retested and failed finally in web-shear, as shown in Fig. 4.47(f), at 228.24 kips shear force, (Curve 3 in Fig. 4.46). In the second test of the south end, the smeared compressive strain nearby the support reached 0.0013 (measured by LVDT D3), as shown in Fig. 4.50(b), and the smeared tensile strain in the perpendicular direction at that region was 0.0033, as shown in Fig. 4.50(a). The measurement of the smeared transverse strain at the middle of studied zone was 0.0037, as shown in Fig. 4.50(c). The increase in the local strain measured by the strain gauges was not as large as in the smeared transverse tensile strain. The average local strain indicated that the average strain in the transverse steel reached $0.90 \epsilon_y$ at failure.

North End



(a) First shear crack at 71 kips

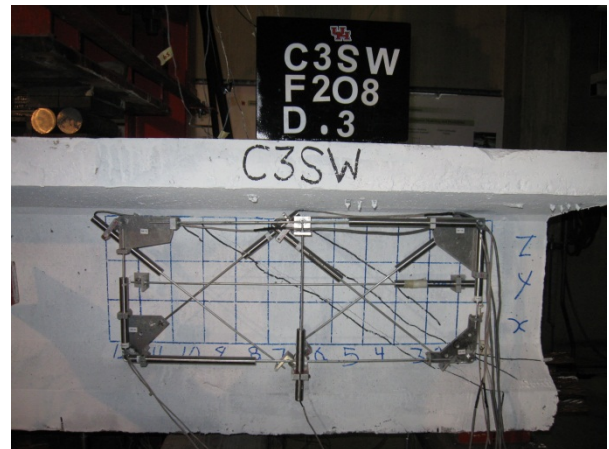
South End



(b) First shear crack at 75 kips



(c) Shear crack pattern before failure



(d) Shear crack pattern before failure

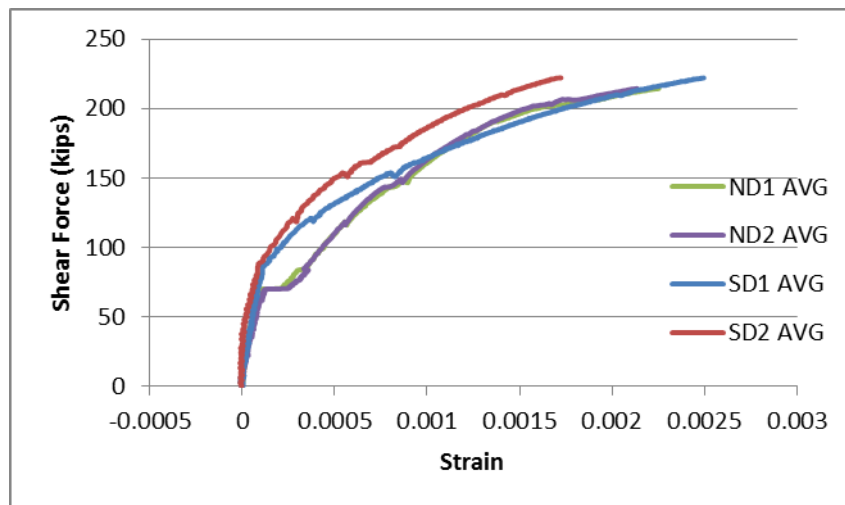


(e) Shear failure at 214.44 kips

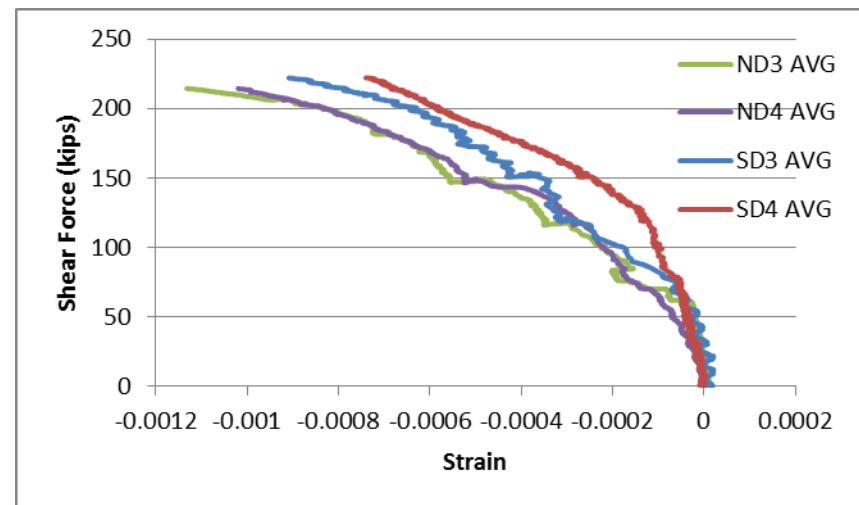


(f) Shear failure at 228.24 kips

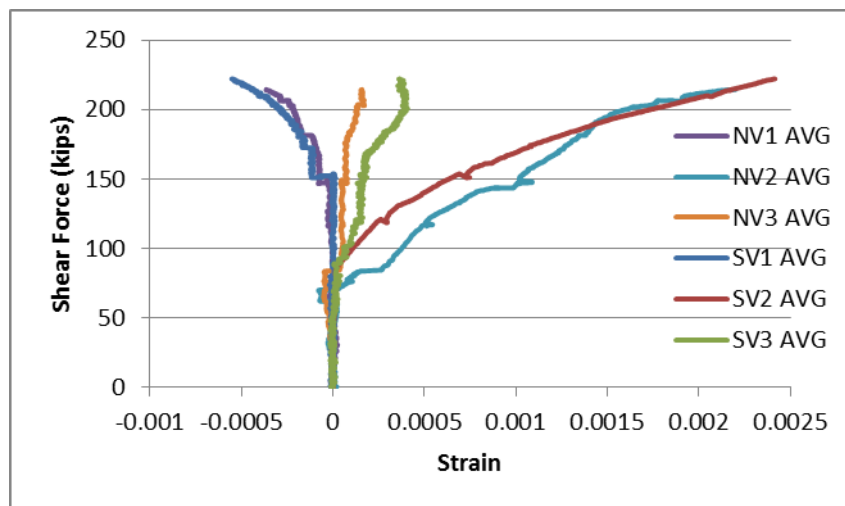
Fig. 4.47 Shear Crack Pattern and Failure Mode of Girder C3



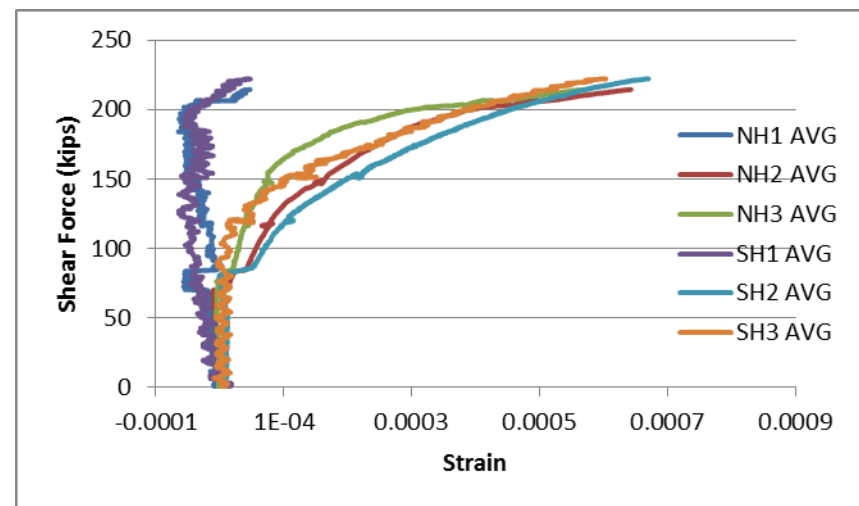
a - Average smeared tensile strain across Cracks



b - Average smeared compressive strain in concrete struts

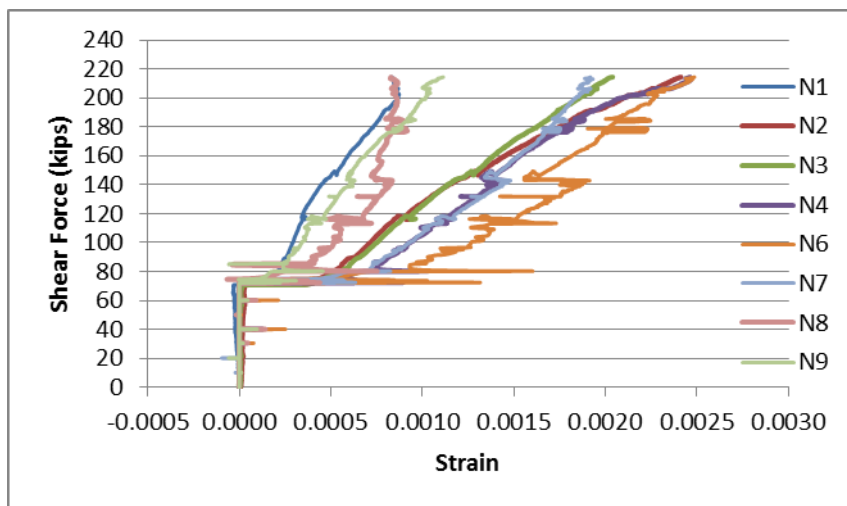


c - Average transverse smeared strain

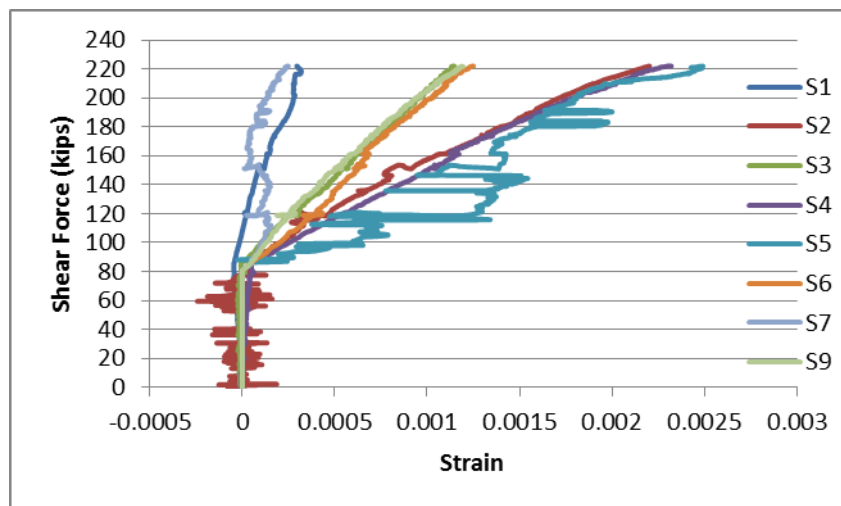


d - Average longitudinal smeared strain

Fig. 4.48 Shear Force vs. Concrete Smeared Strains Curves for Girder C3 – First Run

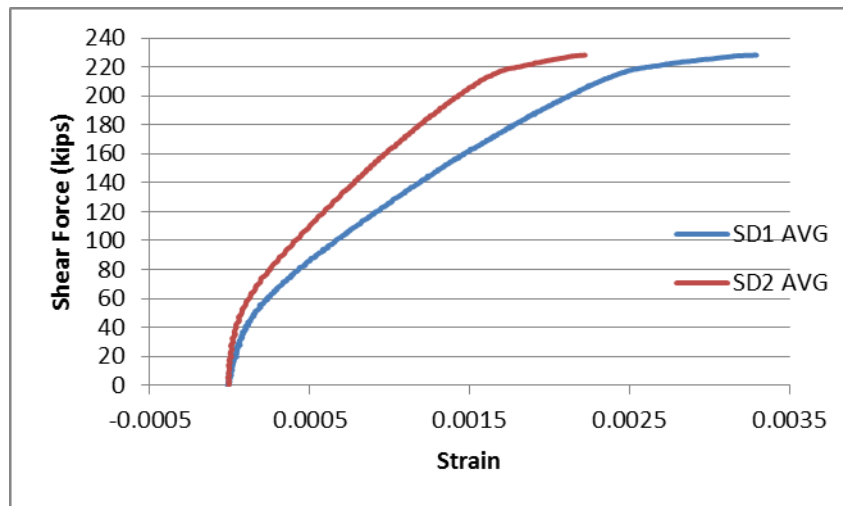


a - North strain gauges

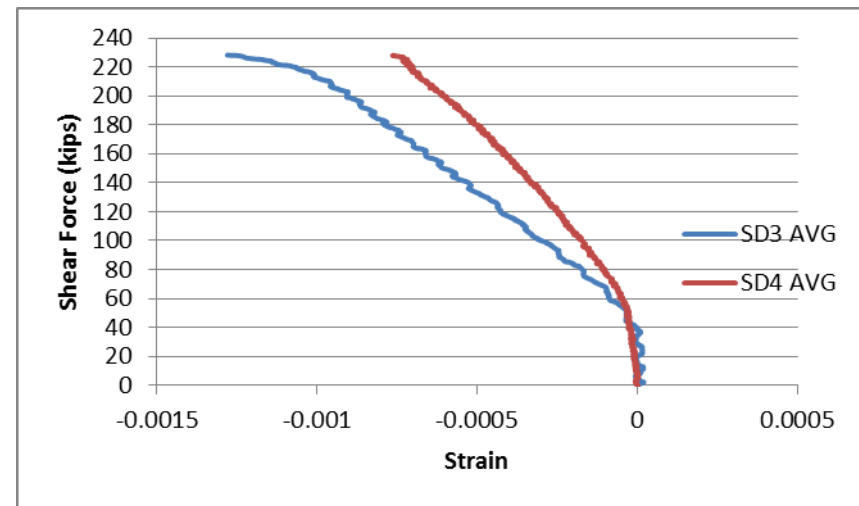


b - South strain gauges

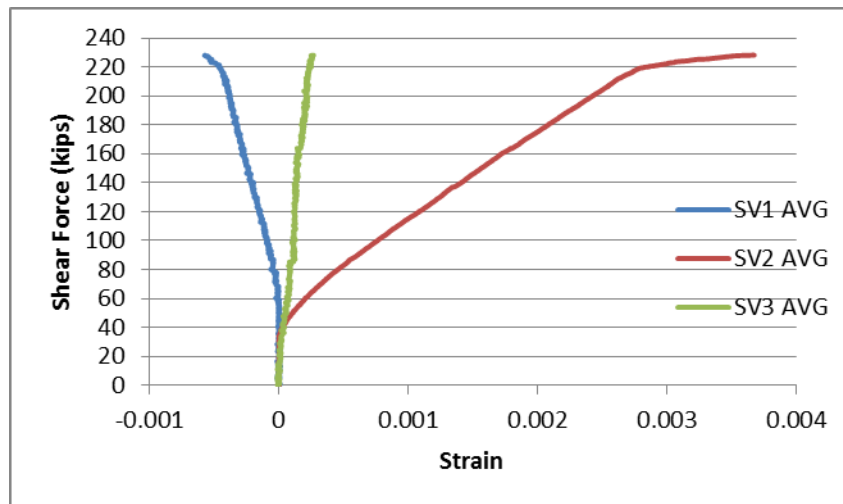
Fig. 4.49 Shear Force vs. Local Transverse Tensile Strain of Girder C3 – First Run



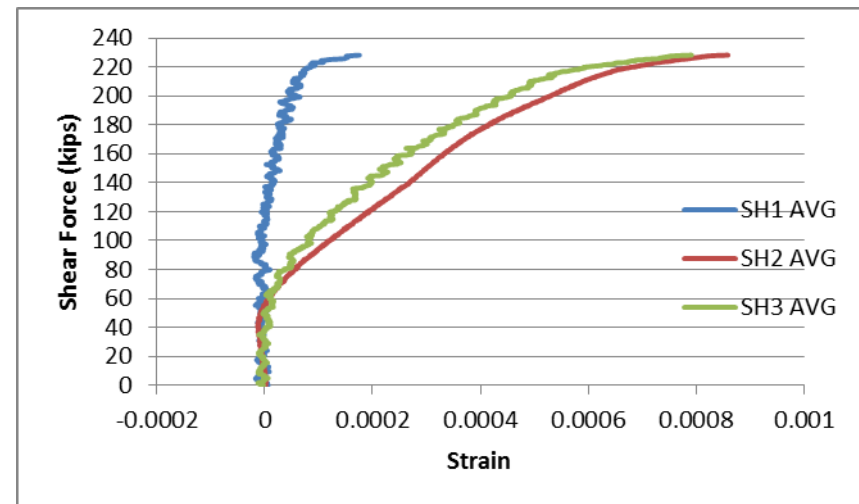
a - Average smeared tensile strain across Cracks



b - Average smeared compressive strain in concrete struts

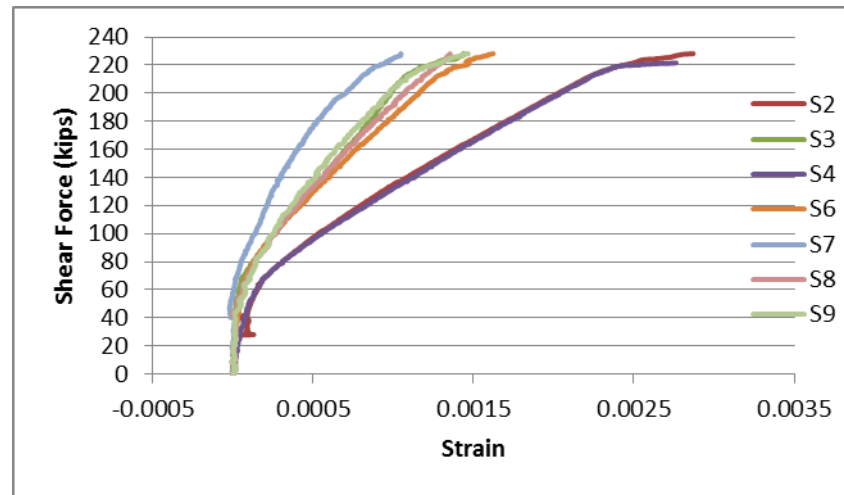


c - Average transverse smeared strain



d - Average longitudinal smeared strain

Fig. 4.50 Shear Force vs. Concrete Smeared Strains Curves for Girder C3 – Second Run



South strain gauges

Fig. 4.51 Shear Force vs. Local Transverse Tensile Strain of Girder C3 – Second Run

4.4.4. Girder C4

Then Girder C4 was tested similar to Girder C2 by loading it at both ends simultaneously using a shear-span-to-depth ratio of 3.00. Fig. 4.52 shows the shear load versus net deflection at both ends during the first test until the failure of the south end, and at the north end during the second test. The first shear crack appeared at 65 kips at the north end of the girder, as shown in Fig. 4.53 (a). Due to improper behavior of the south loading actuator at the beginning of the test, a huge load was applied in a few seconds causing the south end to have multiple cracks in the studied zone, as shown in Fig. 4.53(b), and with increasing the load, new crack appeared closer to the loading point. These multiple cracks affected the initial stiffness of the south end and also the web behavior monitored the LVDT rosette posted on the web, as shown in Fig. 4.54.

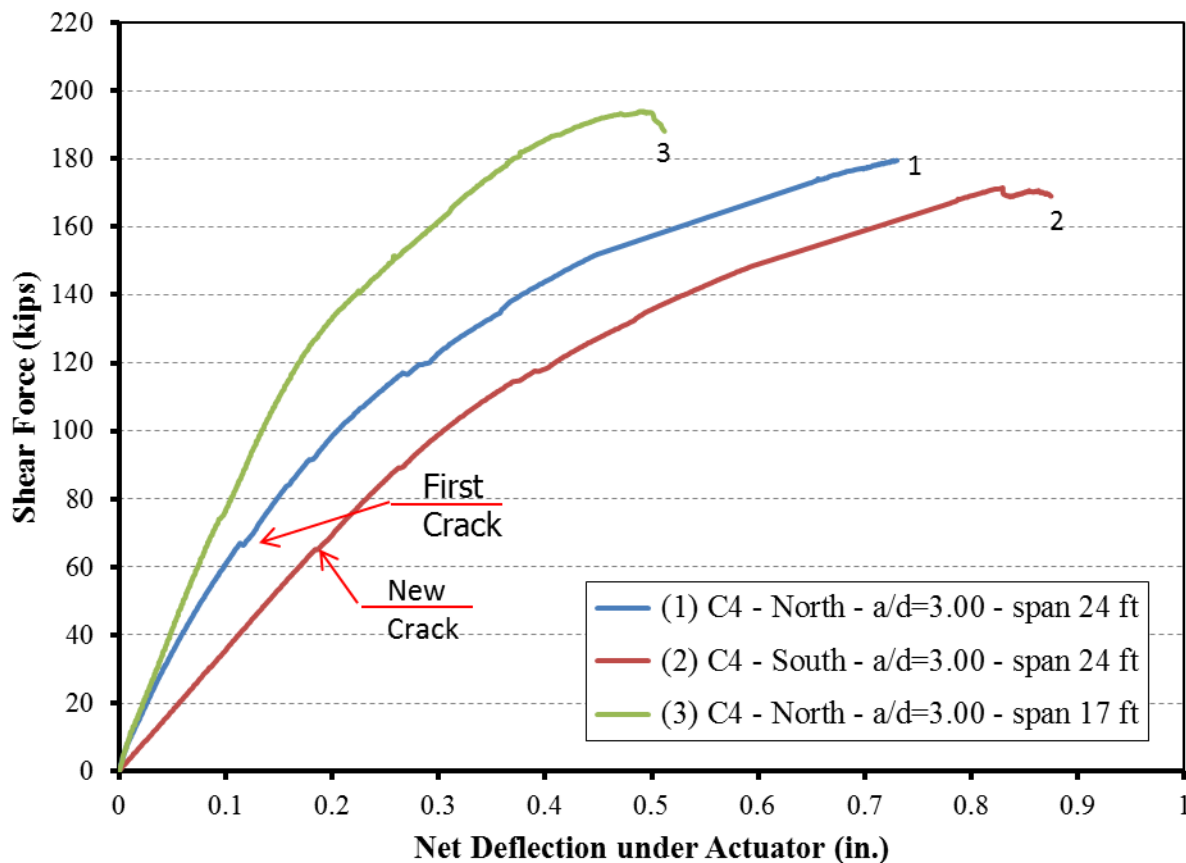


Fig. 4.52 Shear Force vs. Girder Deflection Curves for Girder C4

However, the first test ended with a flexure shear failure at the south end under a shear load of 171.50 kips, as shown in Fig. 4.53 (e), due to having a maximum smeared compressive strain of 0.0012 measured by LVDT D3, while the corresponding force at the north end was 177.30 kips, with a maximum smeared compressive strain at the same location of 0.0007, as shown in Fig. 4.54 (b). However, the average smeared tensile strains across cracks throughout the studied zone at the peak shear load were very close and having a value of 0.0022 and 0.0024 at the north and south ends respectively, as shown in Fig. 4.54(a).

The smeared tensile strain in the transverse direction was different at both ends, as shown in Fig. 4.54 (c). The smeared transverse tensile strain measured at the south end was much less than those at the north end. The behavior of the north end matches the behavior obtained from previous girders with the same shear span to depth ratio. The smeared strain measured by LVDTs V1 and V2 are very close having an average of 0.0017 at the peak. The readings from the LVDT V3, which was closer to the loading point, was very small because of missing the main cracks.

The same with the strain gauges reading, shown in Fig. 4.55. The readings from the strain gauges at the south end are less than those measured at the north end. This can be explained with the sudden increase in the measured strains at the north end at cracking. Because of the pre-existence of cracks at the south end, this increase in strains is missed. Thus, the strain gauge readings from the north end will be used to estimate the steel contribution to the shear capacity of both ends. From the data presented in Fig. 4.55 (a) and (b), at the failure of the south end, the average strain measured through 26.2° (AASHTO angle) at north end was around $0.70 \epsilon_y$, while the average strain measured along the 45° was around $0.50 \epsilon_y$ at the north end.

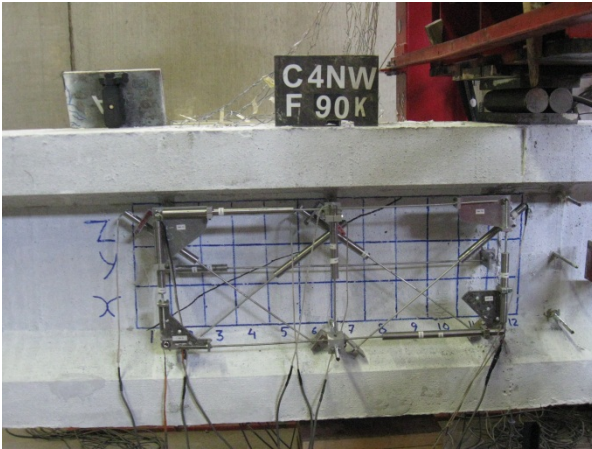
The smeared tensile strain in the longitudinal direction, as shown in Fig. 4.54 (d), had almost the same values at the peak load. Although it is very clear that the north end was much stiffer than the south end.

Consequently, the girder was reloaded after moving the south support toward the interior at the failed end to yield a test span of 17 ft., and the north end was retested and failed at 194 kips, (Curve 3 in Fig 4.52), as shown in Fig. 4.53(f). The maximum smeared compressive strain in the concrete struts was 0.0012 measured by LVDT D3, as shown in Fig. 4.56 (b).

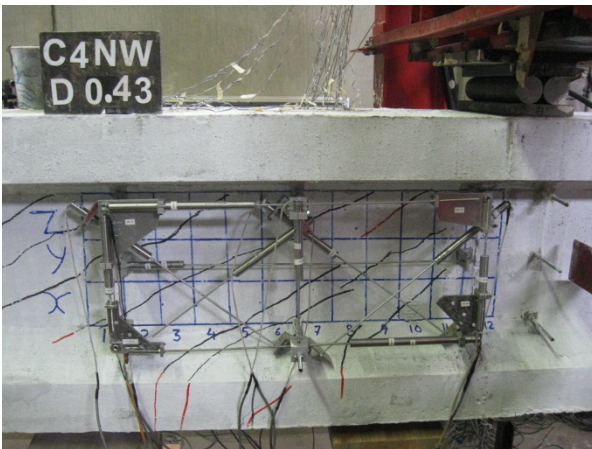
The maximum smeared tensile strain in the transverse direction at the middle of the studied zone was 0.0018, as shown in Fig. 4.56 (c), which is almost the same as what was recorded in the first test. This can be adequate support that the readings from strain gauges during the second test are reliable. Fig. 4.57 (a) and (b), at the failure of north end, the average strain measured through 26.2° (AASHTO angle) was around $0.70 \epsilon_y$, while the average strain measured along the 45° was around $0.55 \epsilon_y$ at the north end.

The flexure shear failure was demonstrated on both ends with existence of flexure cracks in the bottom flange, which initiated with very small width and increased in width with increasing the load. These cracks on the north end were observed during the second test and it was found that these cracks re-opened with increasing the load and causing an obvious flexural-shear failure.

North End



(a) First shear crack at 65 kips

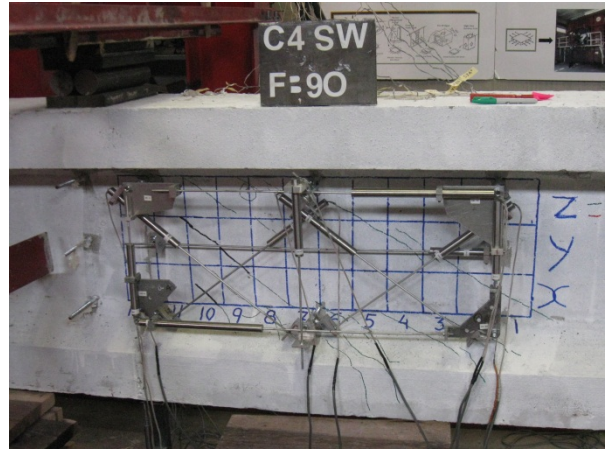


(c) Shear crack pattern before failure

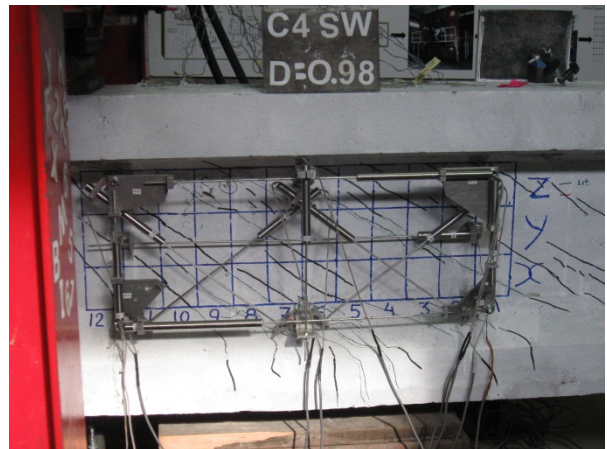


(e) Shear failure at 194 kips

South End



(b) Multiple cracks before test

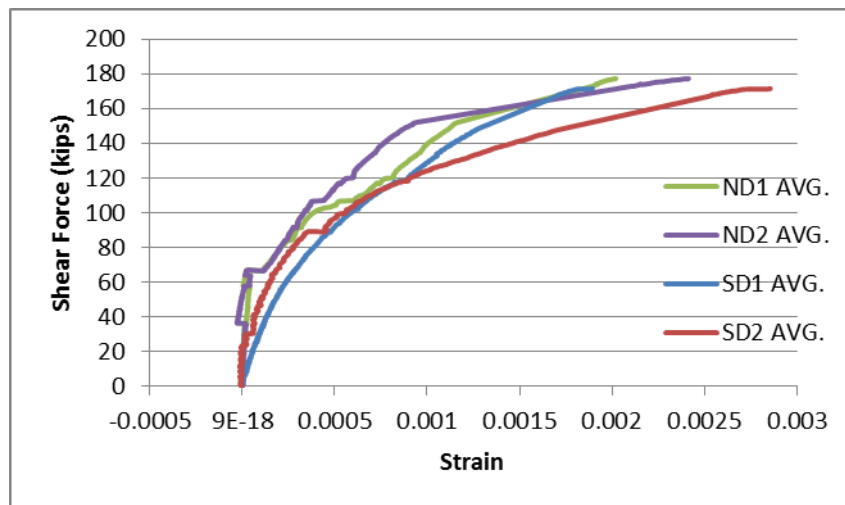


(d) Shear crack pattern before failure

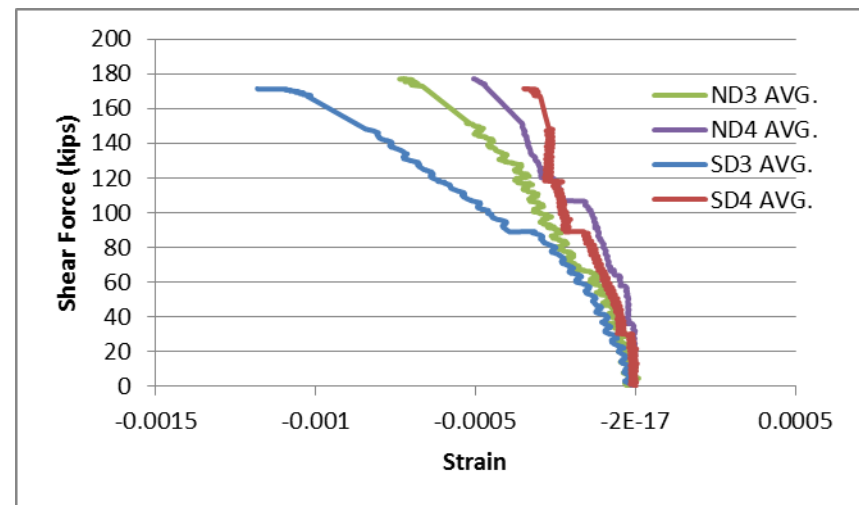


(f) Shear failure at 171.50 kips

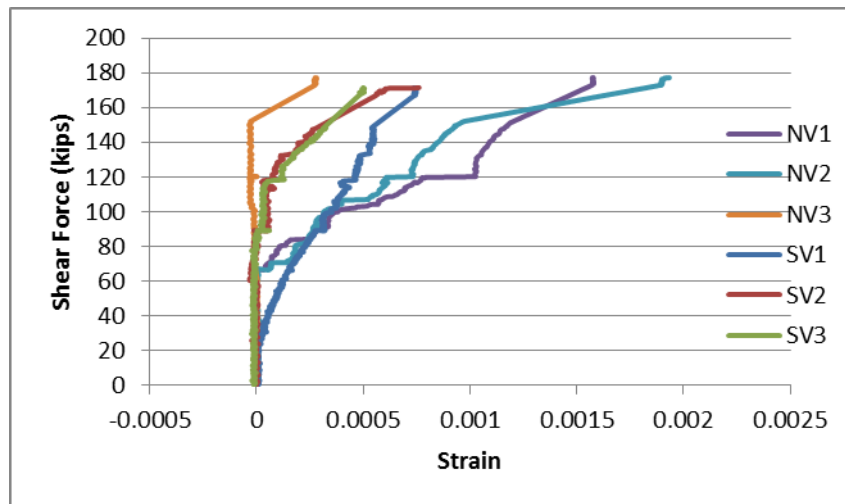
Fig. 4.53 Shear Crack Pattern and Failure Mode of Girder C4



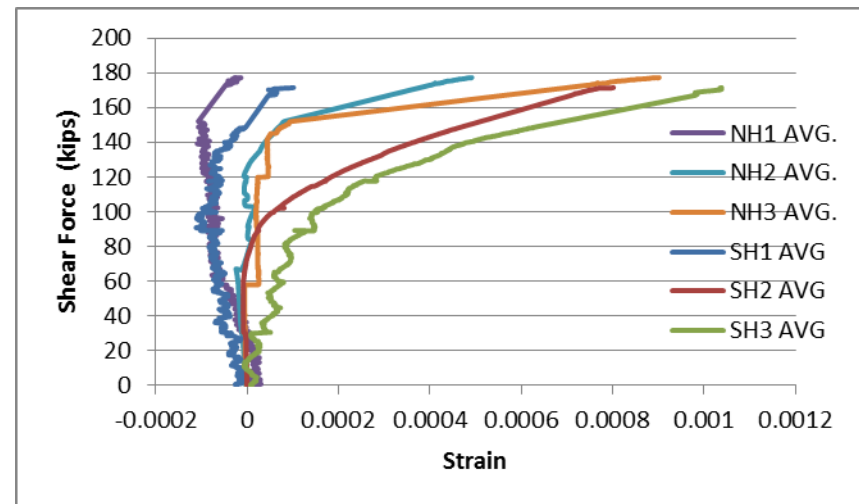
a - Average smeared tensile strain across Cracks



b - Average smeared compressive strain in concrete struts

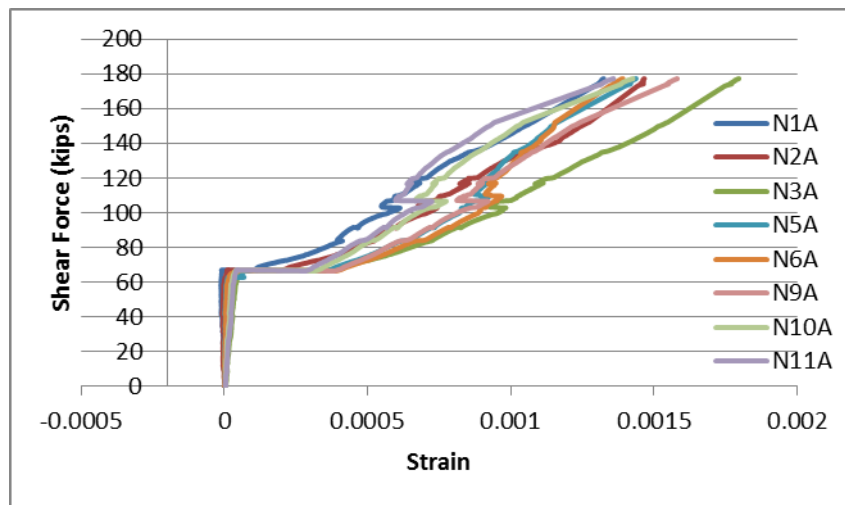


c - Average transverse smeared strain

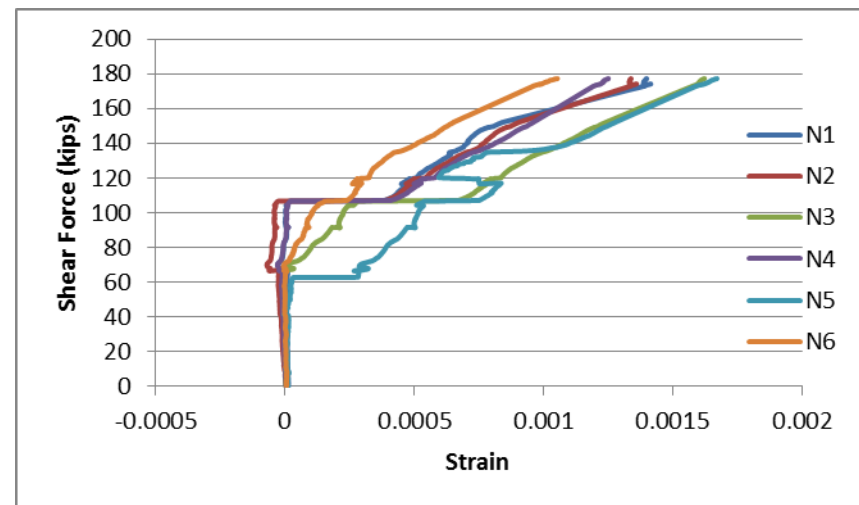


d - Average longitudinal smeared strain

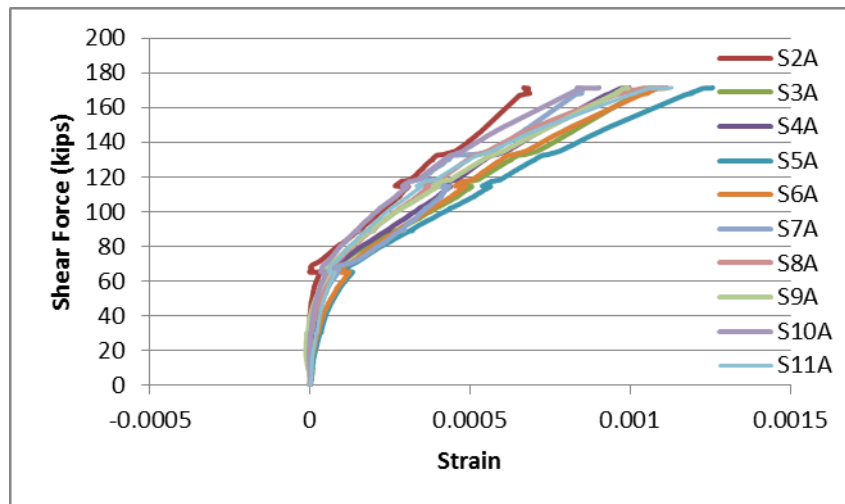
Fig. 4.54 Shear Force vs. Concrete Smeared Strains Curves for Girder C4 – First Run



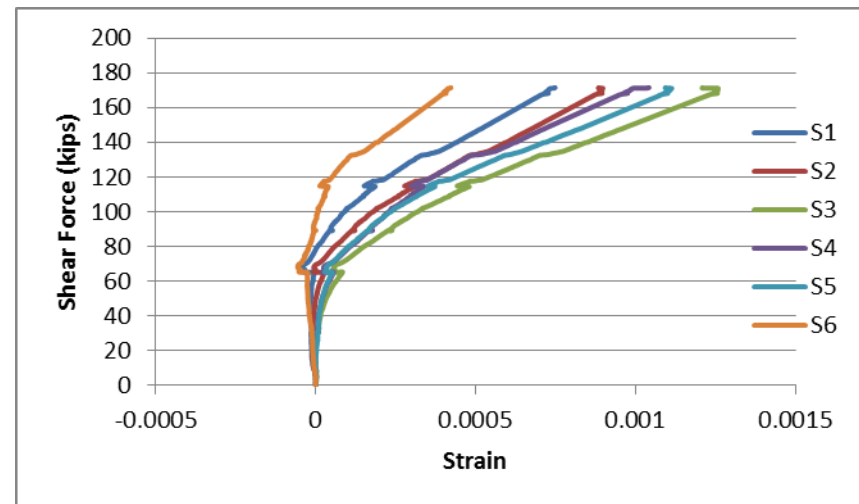
a - North strain gauges located at AASHTO angle



b - North strain gauges located at 45°

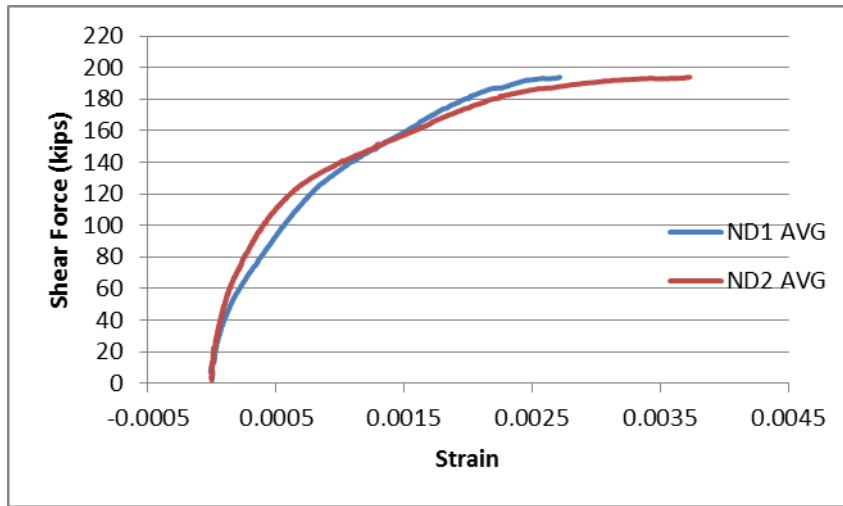


c - South strain gauges located at AASHTO angle

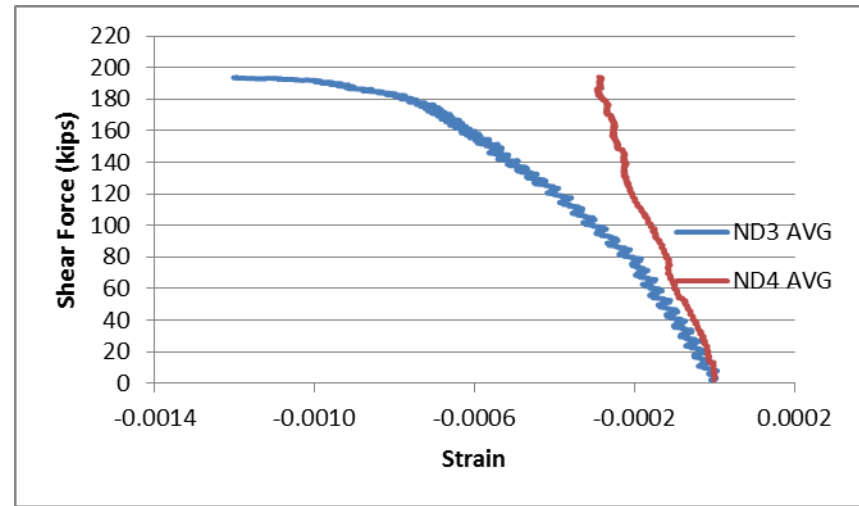


d - South strain gauges located at 45°

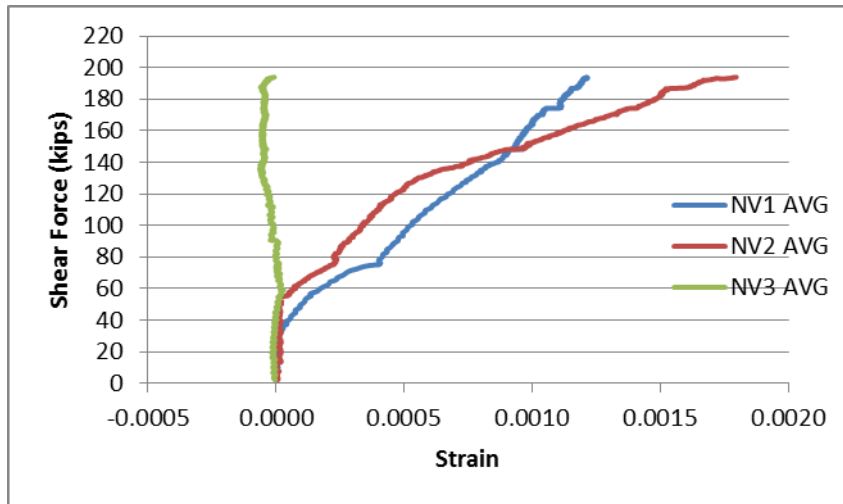
Fig. 4.55 Shear Force vs. Local Transverse Tensile Strain of Girder C4 – First Run



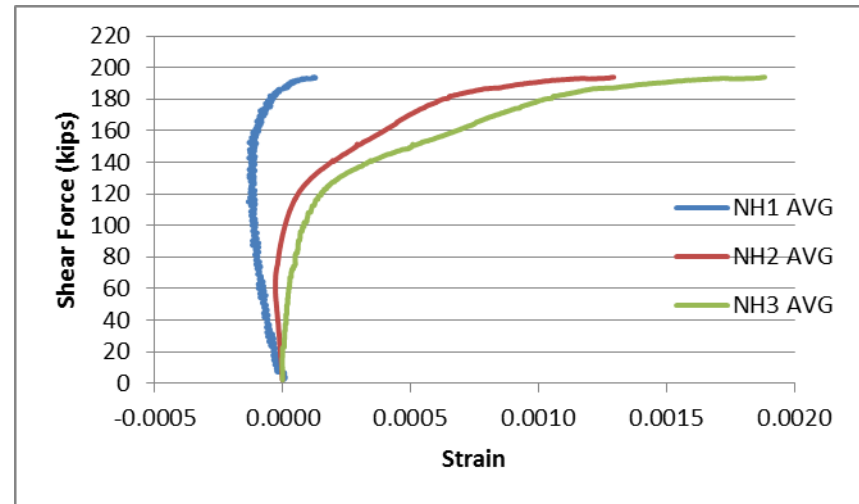
a - Average smeared tensile strain across Cracks



b - Average smeared compressive strain in concrete struts

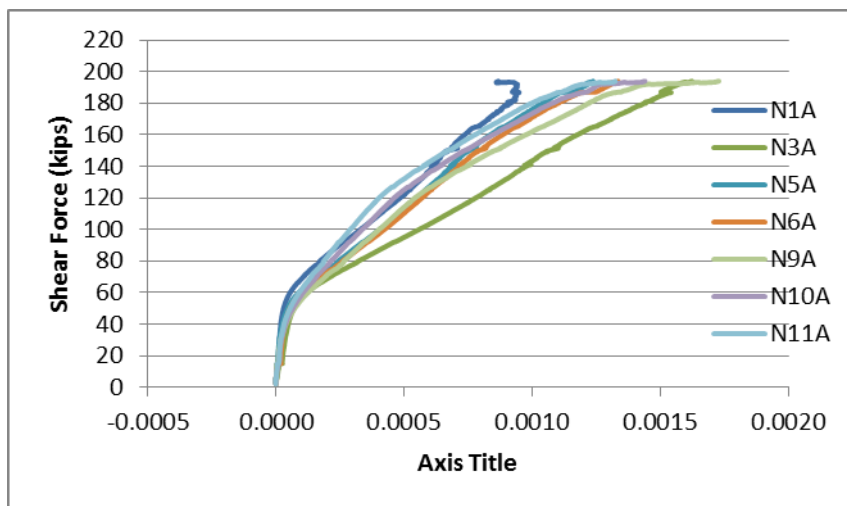


c - Average transverse smeared strain

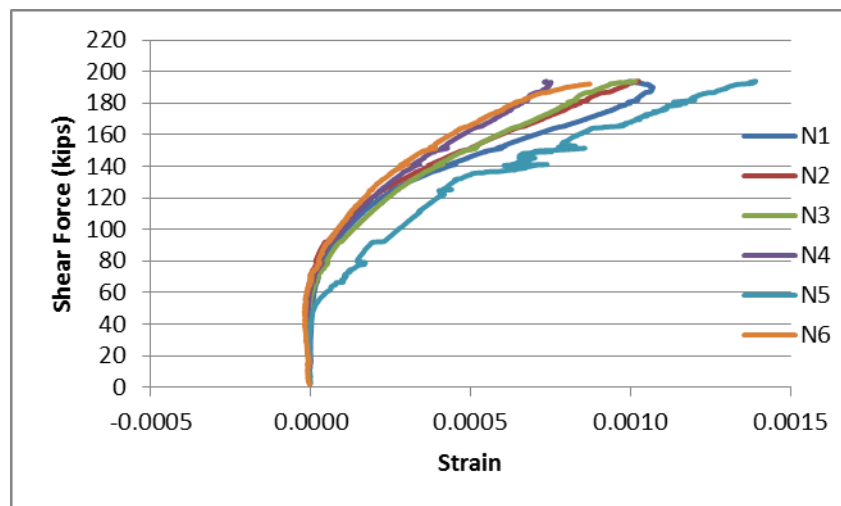


d - Average longitudinal smeared strain

Fig. 4.56 Shear Force vs. Concrete Smeared Strains Curves for Girder C4 – Second Run



a - North strain gauges located at AASHTO angle



b – North strain gauges located at 45°

Fig. 4.57 Shear Force vs. Local Transverse Tensile Strain of Girder C4 –Second Run

4.5. Maximum Shear Strength for High Strength Concrete Prestressed Girders

Table 4.1 summarizes the ultimate shear strength for each end of the girders as well as the test variables and mode of failure. The ultimate strength of each end shown in this table includes half of the self-weight of the girder. Figure 4.58 shows the variation of the normalized ultimate shear strength versus the concrete strength. This figure shows that the ultimate shear strength of the prestressed girders of Bennett and Balasooriya (1971), Rangan (1991), Ma et al. (2000), and the two Girders (A1 and A2) of group A in this experimental program are closely predicted by all the available code provisions.

Table 4.1 Test Variables and Ultimate Shear Strength of Girders

Girder	a/d	Concrete strength f'_c (psi)	Failure Mode	Experimental Ultimate Shear Strength, (Kips)	
A1	1.77	7,000	Web Shear	North South	142.11 116.86
A2	3.00	7,200	Web Shear	North South	129.50 123.23
F1	1.77	13,200	Web Shear	North South	207.67 201.59
F2	2.25	13,000	Web Shear	North South	199.14 189.25
F3	1.77	13,300	Web Shear	North South	202.07 203.45
F4	2.25	13,100	Web Shear	North South	162.70 176.73
C1	1.77	15,700	Web Shear	North South	191.40 172.40
C2	3.00	15,000	Flexure Shear	North South	193.00 167.50
C3	1.77	16,900	Web Shear	North South	218.34 232.14
C4	3.00	15,300	Flexure Shear	North South	196.90 174.40

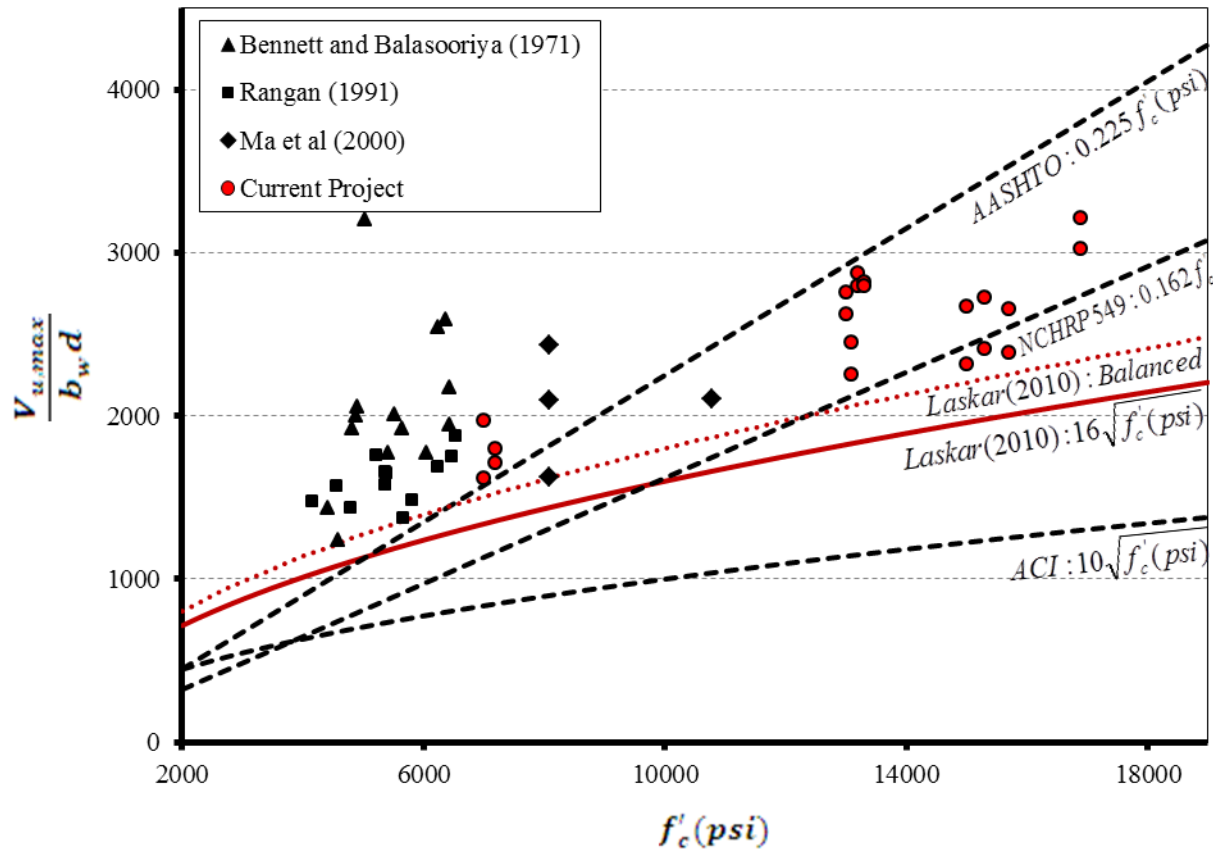


Fig. 4.58 Variation of Normalized Ultimate Shear Strength with Concrete Strength

Although the AASHTO (2010) formula has the minimum margin of safety in predicting the maximum shear strength for PC girders with low strength concrete, NCHRP 549 (2005) reduced the maximum shear strength by 28% to be safe in the higher range of concrete strength. This has been done because of the high possibility of having a local failure in the end zone (D-region) before reaching the ultimate shear strength in the B-region in the case of using high strength concrete.

The comparison of the different shear provisions with the test data from the current experimental program for the range of the high strength concrete is shown in Fig. 4.58. From this figure it can be seen that the equation proposed by Laskar et al. (2010) can closely predict the ultimate shear strength of girders for different concrete strength up to 17,000 psi. This equation is less conservative than the ACI (2011) equation. Also, comparing with the AASHTO LRFD

(2010) prediction, it can be seen that the AASHTO prediction is unsafe for high strength PC girders tested in this experimental program.

Figure 4.58 shows that the equation provided by NCHRP 549 (2005) can well predict the ultimate shear strength up to concrete strength 14,500 psi. However, it is able to predict only 93% of the test data in the range of high strength concrete. This is different from Laskar's equation (2010), which has almost the same margin of safety for different concrete strength. It should be noticed that AASHTO and NCHRP 549 equations shown in Fig. 4.58 are function of d instead of d_v as it is previously mentioned. To make them comparable to the ACI and Laskar's equations, it was assumed that $d_v = 0.9 d$.

4.6. Steel and Concrete Shear Contributions

The steel contribution V_s to the ultimate shear strength can be calculated based on the method proposed by Laskar et al. (2010), (as discussed in Chapter 2) by simply assuming the failure shear crack to be inclined at an angle of 45° , similar to the ACI (2011) Code. By assuming the yielding of all transverse bars, the steel contribution can be calculated using:

$$V_s = A_v f_y \left(\frac{d}{s} - 1 \right), \text{ if } \varepsilon_{avg} \geq \varepsilon_y \quad (4.1)$$

In the case of over-reinforced girders in the transverse direction, it is expected that some of the transverse bars cutting the 45° crack might not reach the yielding point. From the strain gauge readings, the local strain in these bars can be known and the average strain can be calculated. If the average strain is less than the yield strain, the steel contribution V_s to the ultimate shear strength can be calculated as:

$$V_s = A_v \varepsilon_{avg} E_s \left(\frac{d}{s} - 1 \right), \text{ if } \varepsilon_{avg} < \varepsilon_y \quad (4.2)$$

In Table 4.2, the steel contribution, V_s , is calculated based on the yield stress of the mild steel of 60,000 psi and the modulus of elasticity of 30,000 ksi. Knowing the steel

contribution, V_s , the concrete contribution, V_c , can be calculated by subtracting the steel contribution, V_s , from the ultimate shear strength of the tested girders, V_{test} .

Fig. 4.59 shows that the experimental normalized concrete contribution values for all tested girders in this research work with shear span to depth ratio greater than 1.6 lie above the conservative curve proposed by Laskar et al. (2010) for predicting the concrete contribution. It demonstrates that the proposed UH method (Laskar et al. 2010) for predicting the concrete contribution of PC girders is conservative and valid for concrete strength up to 17,000 psi.

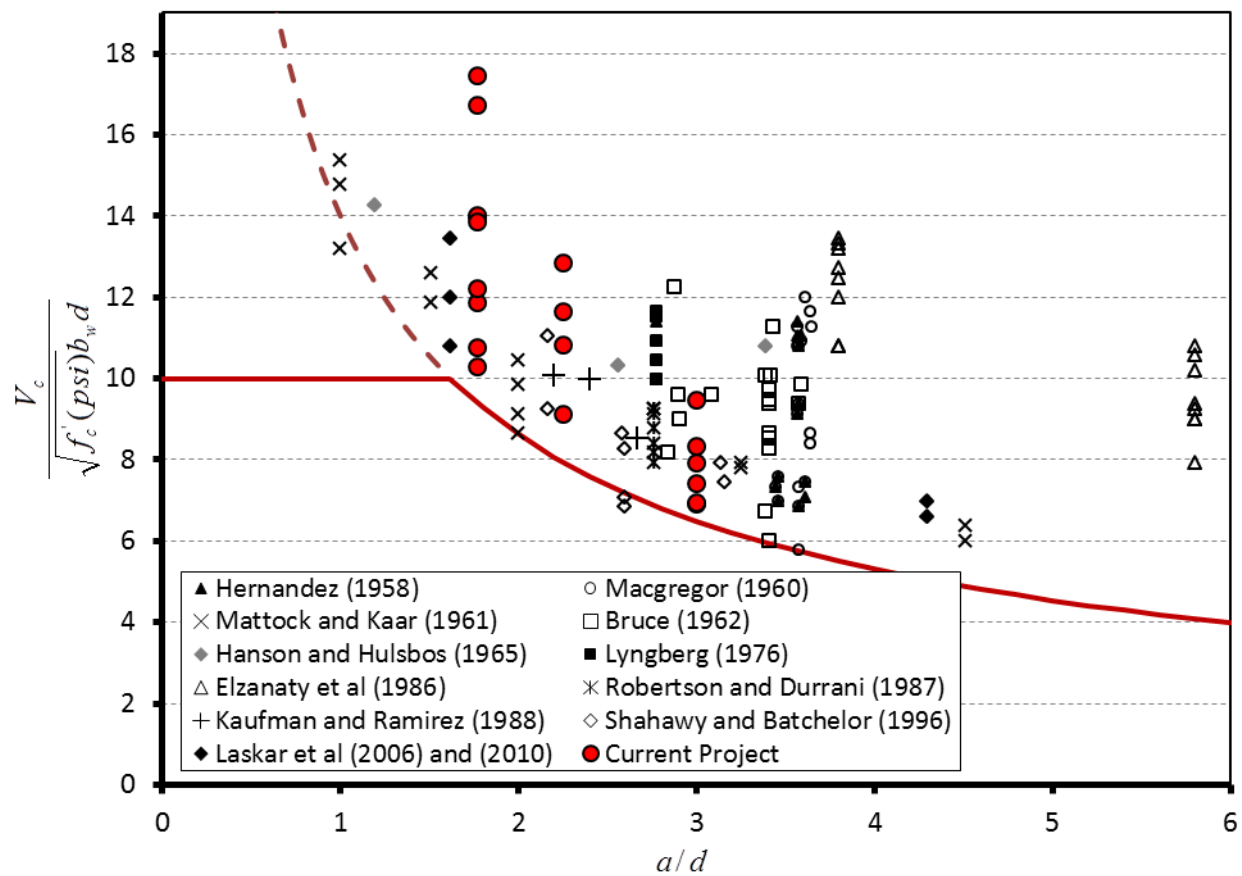


Fig. 4.59 Variation of the Normalized Concrete Shear Contribution with Shear Span to Effective Depth Ratio a/d for Girders

Table 4.2 Calculations of Steel and Concrete Shear Contribution

Girder I.D.	Ultimate Shear ($V_{test}, kips$)	a/d	f'_c (psi)	Transverse Steel						Concrete Contribution ($V_c, kips$)	Failure Mode
				(ρ %)	Balanced ($V_s, kips$)	Provided ($V_s, kips$)	Increasing (%)	Avg. Strain (ϵ_{avg})	Actual ($V_s, kips$)		
A1	North 142.11	1.77	7000	1.76	52.03	57.61	+ 10.72 %	ϵ_y	57.60	84.51	Web-shear
	South 116.86							-	-	-	
A2	North 129.50	3.00	7200	2.30	70.53	80.89	+ 14.69 %	ϵ_y	80.89	48.61	Web-shear
	South 123.23									42.34	
F1	North 207.67	1.77	13200	1.88	71.45	62.80	- 12.11 %	ϵ_y	62.80	144.87	Web-shear
	South 201.59									138.79	
F2	North 199.14	2.25	13000	2.58	82.86	93.33	+ 12.63 %	ϵ_y	93.33	105.81	Web-shear
	South 189.25									95.92	
F3	North 202.07	1.77	13300	2.43	71.72	86.74	+ 20.94 %	ϵ_y	86.74	115.33	Web-shear
	South 203.45									116.71	
F4	North 162.70	2.25	13100	3.31	83.18	124.66	+ 49.86 %	$0.70 \epsilon_y$	87.27	75.43	Web-shear
	South 176.73									89.46	
C1	North 191.40	1.77	15700	2.58	77.93	93.33	+19.76%	$0.90 \epsilon_y$	83.99	107.41	Web-shear
	South 172.40							$0.85 \epsilon_y$	79.33	93.07	
C2	North 193.00	3.00	15000	3.18	101.81	119.15	+17.03%	ϵ_y	119.15	73.85	Flexure-shear
	South 167.50							$0.85 \epsilon_y$	101.28	66.22	
C3	North 232.14	1.77	16900	3.44	80.85	130.63	+61.57%	$0.90 \epsilon_y$	117.57	114.57	Web-shear
	South 218.34									100.77	
C4	North 196.90	3.00	15300	4.13	102.82	160.48	+56.08%	$0.70 \epsilon_y$	112.34	84.56	Flexure-shear
	South 174.40									62.06	

CHAPTER 5 SIMULATION OF PRESTRESSED CONCRETE I- GIRDERS FAILED IN SHEAR

5.1. Introduction

Reinforced concrete structures can be visualized as assemblies of membrane elements, and their behavior can be predicted using the finite element method once the constitutive relationships of the elements are established. At the University of Houston, Zhong (2005) developed a nonlinear finite element program, called Simulation of Reinforced Concrete Structures (SRCS), for analysis of reinforced concrete structures. In SRCS, based on the Cyclic Softened Membrane Model (CSMM) (Mansour, 2001; Mansour et al. 2001a and 2001b; Mansour and Hsu, 2005a and 2005b), a two-dimensional reinforced concrete plane stress material module and three uniaxial material modules of steel and concrete were developed and implemented into an object-oriented finite element framework - OpenSees (Fenves 2001). SRCS is proven to successfully simulate the behavior of reinforced concrete plane stress structures subjected to static, reversed cyclic, and dynamic loading.

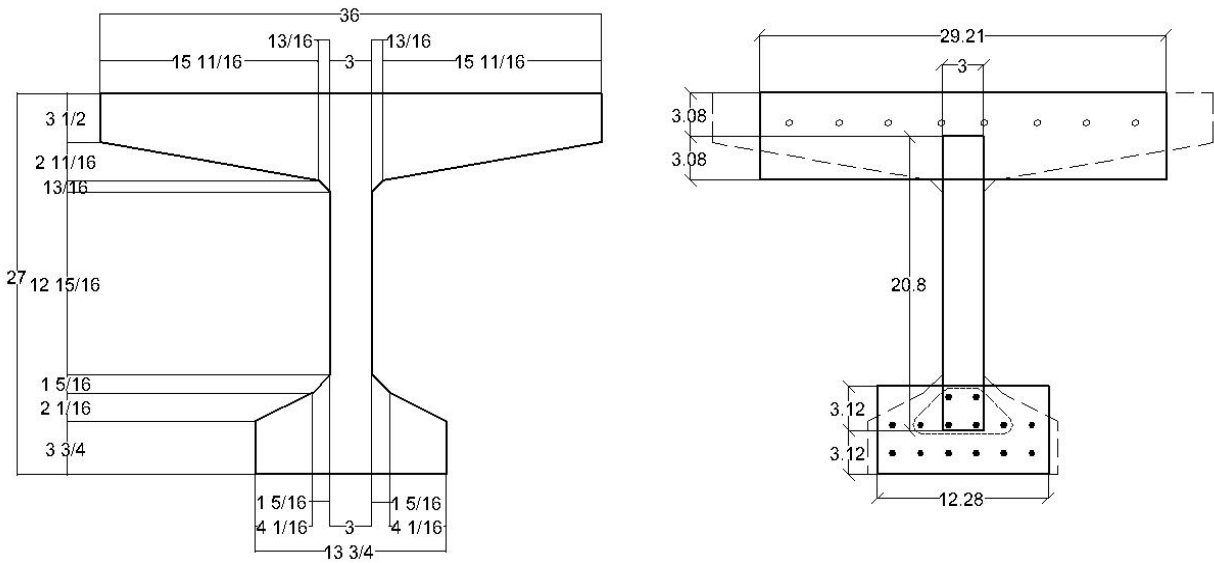
In recent years, research work at the University of Houston has been focused on developing the constitutive laws for Prestressed Concrete (PC) membrane elements and developing an analytical model for simulating the shear behavior of such elements. PC panels with normal strength concrete have been tested by Wang (2006) and the Softened Membrane Model for Prestressed Concrete (SMM-PC) has been developed to simulate the response of prestressed concrete membrane elements under monotonic shear loading. The main points of this model are: (1) new constitutive relationships of prestressing tendons embedded in concrete, and (2) revised constitutive relationships of concrete considering the effect of prestress. The SMM-PC model is based on stress equilibrium, strain compatibility, and constitutive laws of PC. Laskar (2009) extends the analytical model (i.e., SMM-PC) to Cyclic Softened Membrane Model for Prestressed Concrete (CSMM-PC), which is able to simulate the cyclic behavior of prestressed structural elements. Five PC girders were tested and used to validate the CSMM-PC analytical model to simulate behavior of PC girders under monotonic shear loading (Laskar 2009).

In this research, another 10 prestressed girders are tested under monotonic shear loading and will be used to validate the analytical model (CSMM-PC) to simulate the behavior of prestressed girders with different concrete strength and different percentage of transvers steel.

5.2. Analytical Model

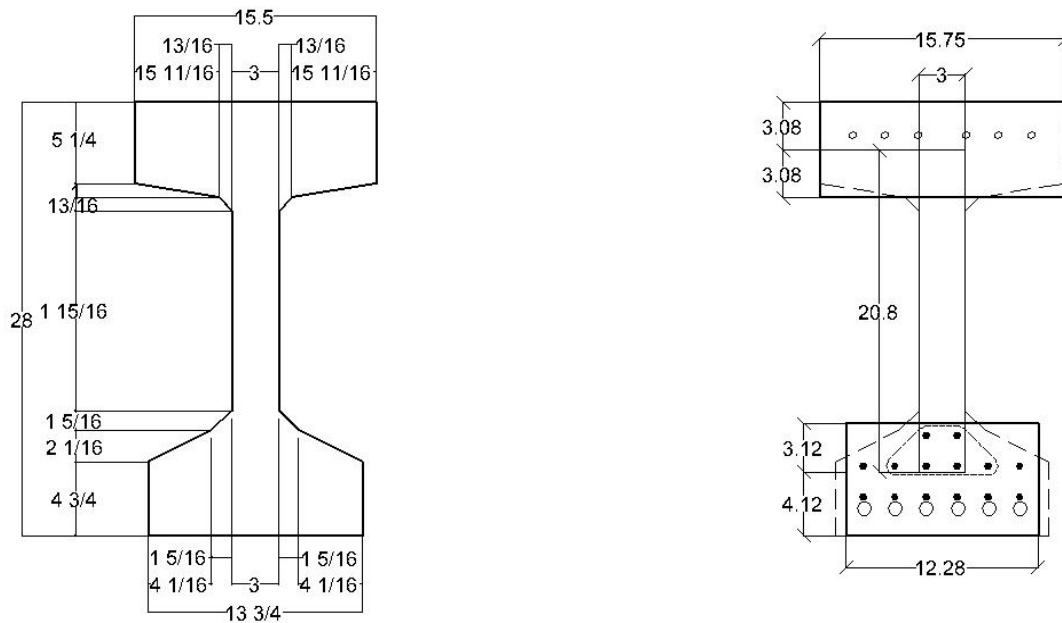
The finite element models of the prestressed girders created for analyzing the girders using Simulation of Concrete Structures (SCS) are described in this section. The web of the girders, which resists the shear forces acting on the girders, is defined by 16 PCPlaneStress Quadrilateral elements. Top and bottom flanges are modeled using 16 NonlinearBeamColumn at top and bottom of the PCPlaneStress Quadrilateral elements. The inclined top and bottom flanges are modeled using NonlinearBeamColumn elements having rectangular cross sections of an equivalent area. Each NonlinearBeamColumn element is defined with two control sections, one representing the concrete and the other representing the steel rebar or the prestressing tendon. It should be noted that the NonlinearBeamColumn elements were previously developed in OpenSees (Taucer et al. 1991). Figures 5.1 and 5.2 show the used sections in this model. Fig. 5.1 shows the section used to simulate group A Girders (A1 and A2), group F Girders (F1 to F4), and Girders C1 and C3 in group C. Fig. 5.2 shows the section used to simulate Girders C2 and C4.

Concrete02, Steel01, and Steel02 are previously defined in the OpenSees framework and are used to define the concrete and steel fibers in NonlinearBeamColumn elements in the top and bottom flanges. Concrete02 gives the opportunity to add the tensile strength of concrete, which is required to resist tensile stresses at the top flange due to prestressing force application or at the bottom flange due to flexure cracking in flexure-shear specimens. Steel01 was used to define the mild steel rebars used in the top flange and in the bottom flange as an additional reinforcement in Girders C2 and C4. Steel02 was used to define the prestressing tendons in the bottom flange. Steel02 gives the opportunity to define the prestressing force using an “initial stress” option. This initial stress is calculated by subtracting the prestressing losses due to concrete elastic shortening from the applied prestressing stresses at transfer ($0.75f_{pu}$).



(All Dimensions are in Inches)

Fig. 5.1 Experimental and Analytical Cross Section for Girders A1, A2, F1 to F4, C1, and C3



(All Dimensions are in Inches)

Fig. 5.2 Experimental and Analytical Cross Section for Girders C2 and C4

ConcreteL01, SteelZ01, and Tendon L01 (Laskar 2009) are uniaxial materials developed at the University of Houston, and they are used to define concrete, transverse steel, and prestressing tendons in the PCPlaneStress quadrilateral elements, respectively.

The constant k is used in Concrete02 and ConcreteL01 to impose an upper limit to the initial stress strain relationship of concrete in compression and thereby make the initial slope of the stress strain curve of concrete lower than $\frac{2f'_c}{\epsilon_c}$ and is taken as 1.4 for the analysis of all the girders in this research work.

The concentrated loads on the girders were actually applied through 6 inches wide high strength steel plates. Hence, while modeling these loads, it has been decided to distribute the loads equally among nodes adjacent to the location of load application. The nodal displacement and corresponding vertical forces were recorded at each converged displacement step.

5.3. Finite Element Model of Girders with Web Shear Failure

Seven girders of the experimental program presented and discussed in previous chapters have failed in web shear. Five of these girders had been tested using a shear span to depth ratio of 1.77, namely A1, F1, F3, C1, and C3. The other two girders had different shear span to depth ratio. Girder A2 has failed in web shear with shear span to depth ratio equal to 3.00, while Girder F4 has failed in web shear having a shear span to depth ratio equal to 2.25. Figs. 5.3 to 5.5 show the finite element mesh and the location of applied loads and supports used for these girder specimens.

The top flange in these girders is discretized into 84 fibers of concrete and 10 fibers of steel. The bottom flange is discretized into 60 fibers of concrete and eight fibers of prestressing tendons, as shown in Fig. 5.6. In fact, the real girders are reinforced in flexural using 14 prestressing tendons, eight of them are discretized as fibers in the NonlinearBeamColumn elements representing the bottom flange and the remaining six tendons are provided in the PCPlaneStress quadrilateral elements used to represent the webs of these specimens.

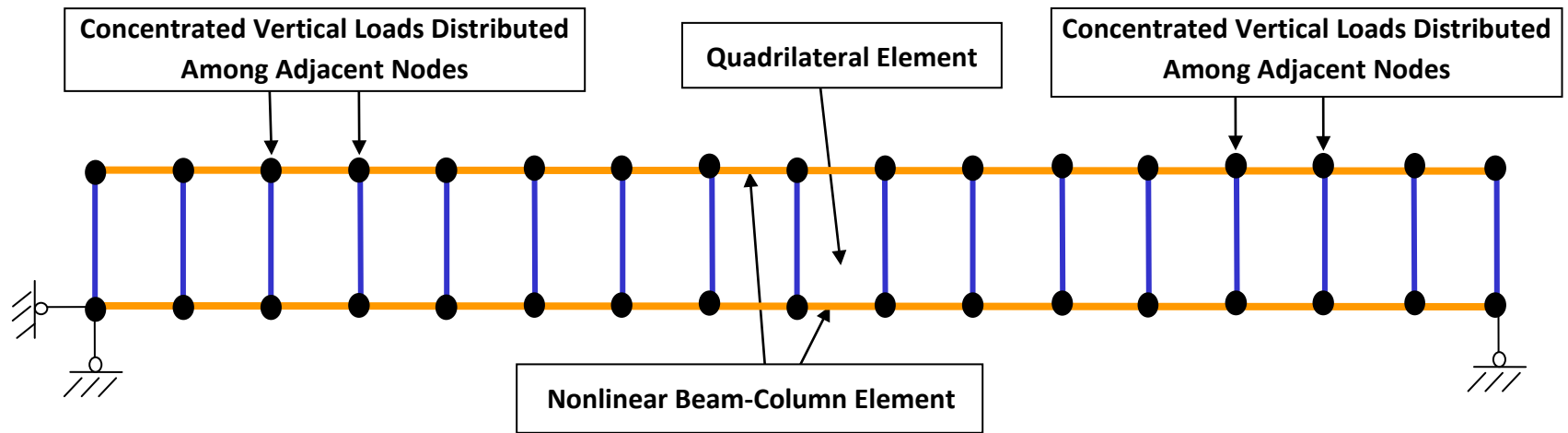


Fig. 5.3 Finite Element Mesh of Girder Specimens A1, F1, F3, C1, and C3

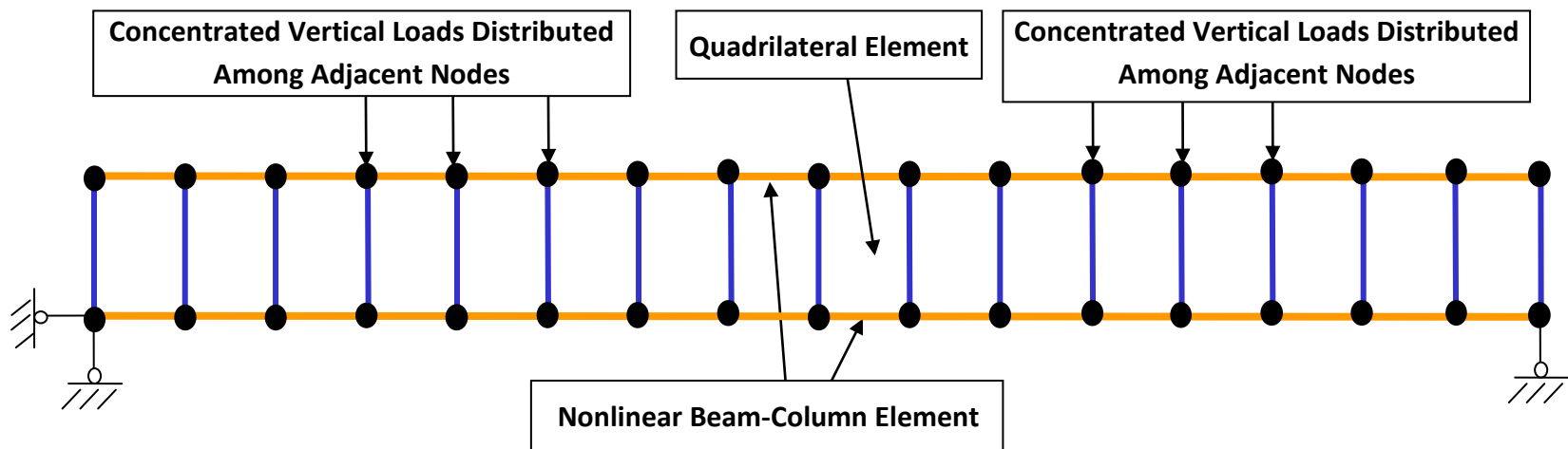


Fig. 5.4 Finite Element Mesh of Girder Specimens A2

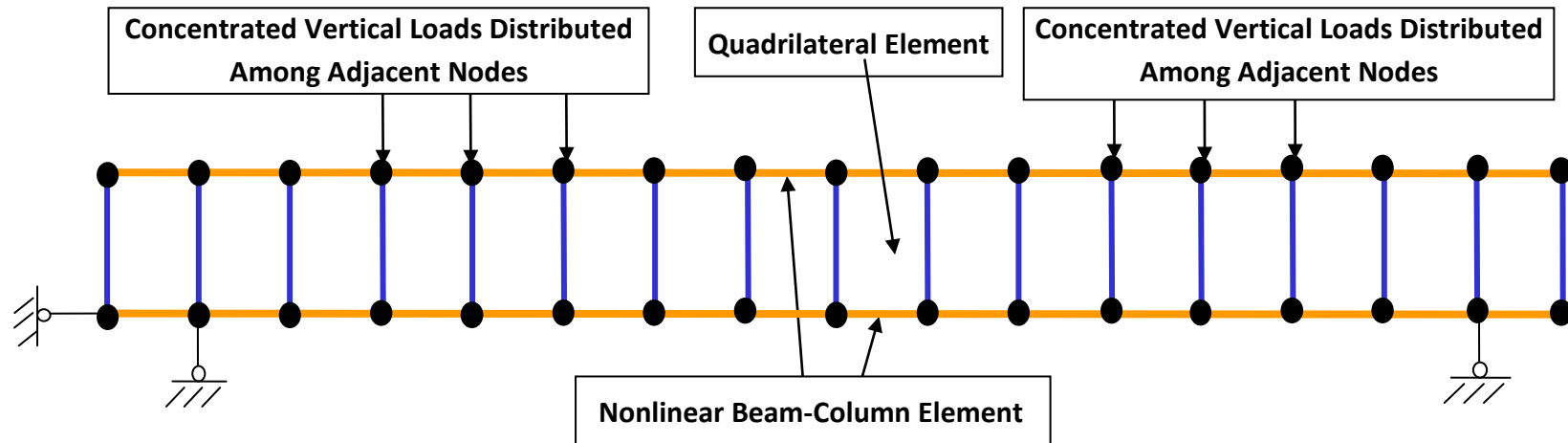


Fig. 5.5 Finite Element Mesh of Girder Specimen F4

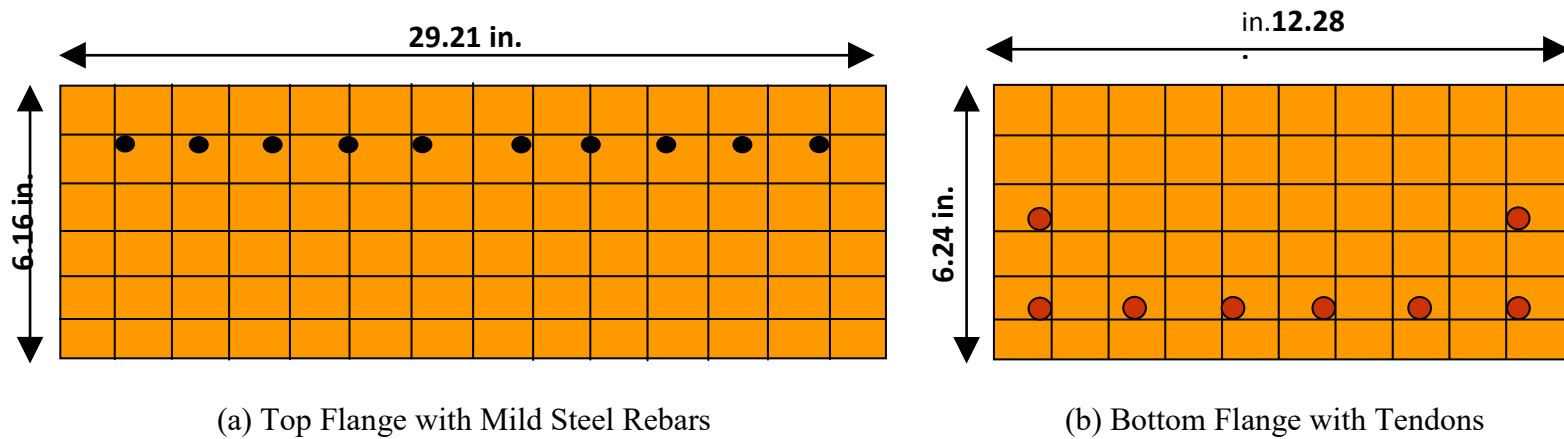


Fig. 5.6 Section Discretization of Nonlinear Beam-Column Elements for Web Shear Girder

Comparison between the analytical and experimental shear force versus net deflections are shown in Figs. 5.7 to 5.13. The comparison shows the capability of the SCS program to accurately predict the cracking shear load, and pre-cracking and post-cracking behavior. In general the predicted capacity is very close to the experimental capacity except in the case of Girder C1 where the experimental capacity is too low comparing to the predicted capacity for the given cylinder concrete strength, which means that the concrete strength of the girder was lower than expected, which might be due to lack of compaction during casting.

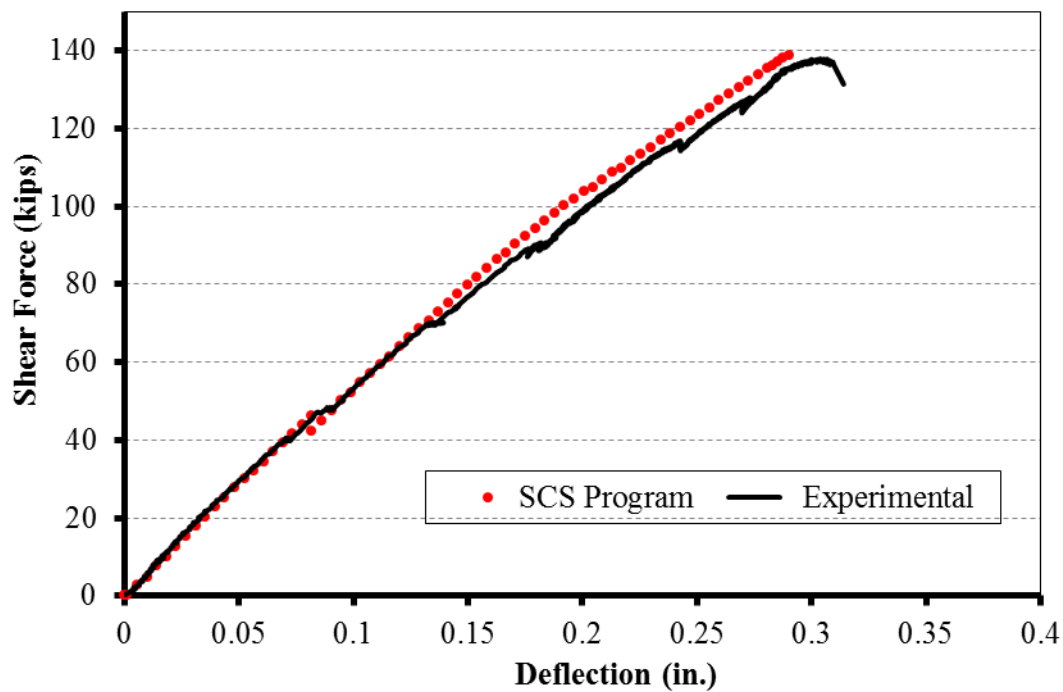


Fig. 5.7 Analytical and Experimental Load-Deflection Curves of Girder A1

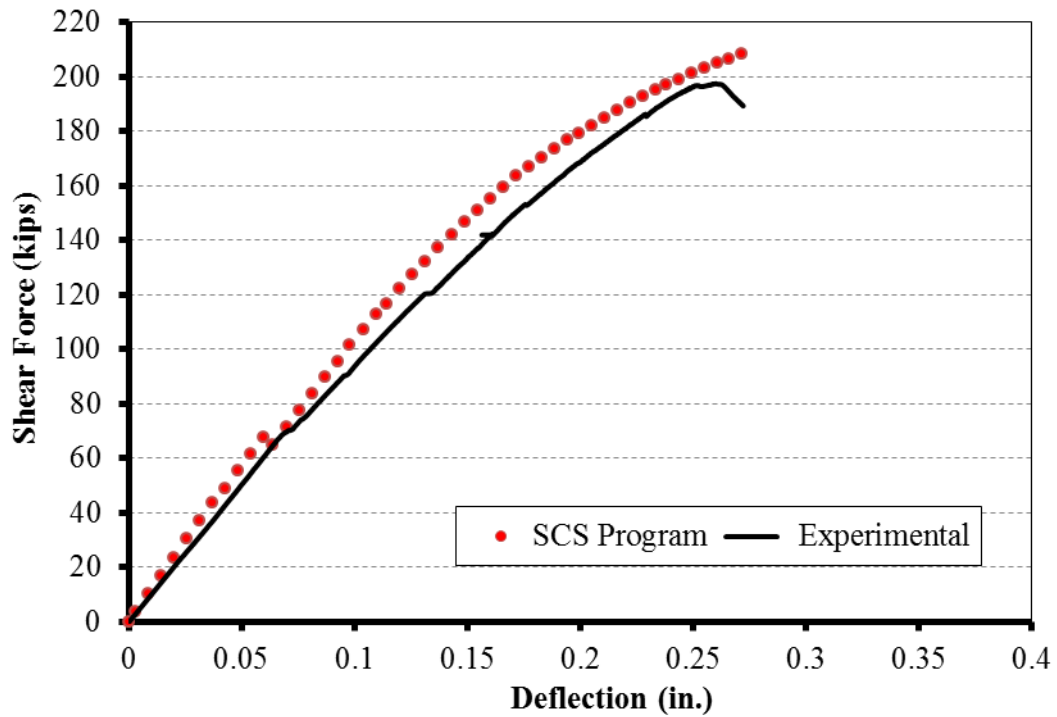


Fig. 5.8 Analytical and Experimental Load-Deflection Curves of Girder F1

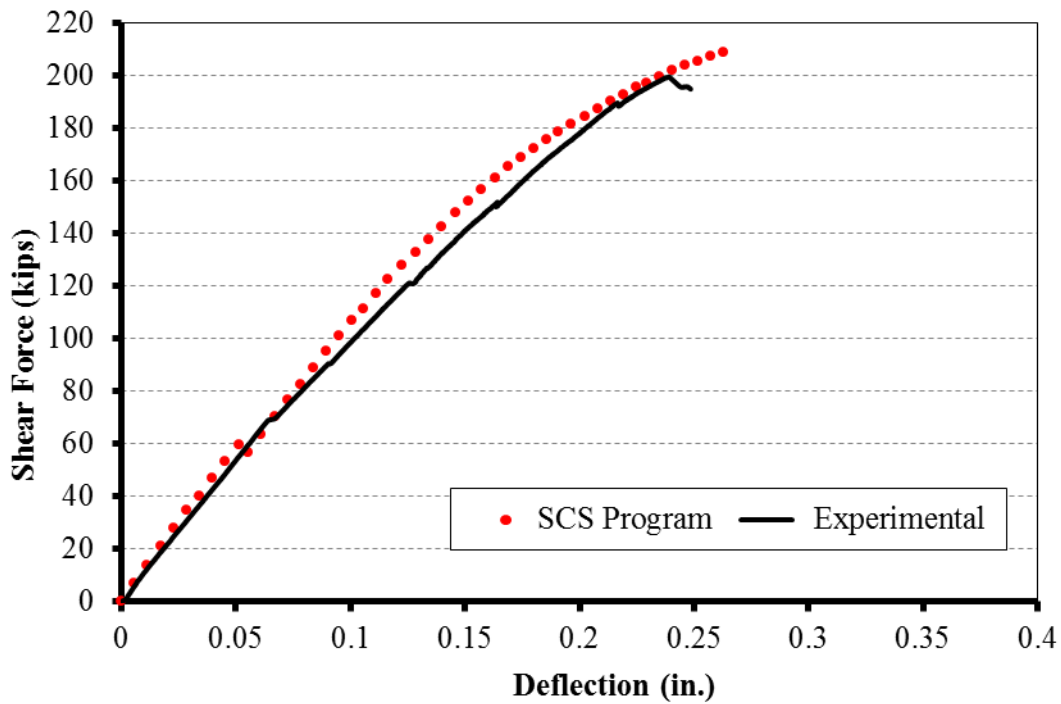


Fig. 5.9 Analytical and Experimental Load-Deflection Curves of Girder F3

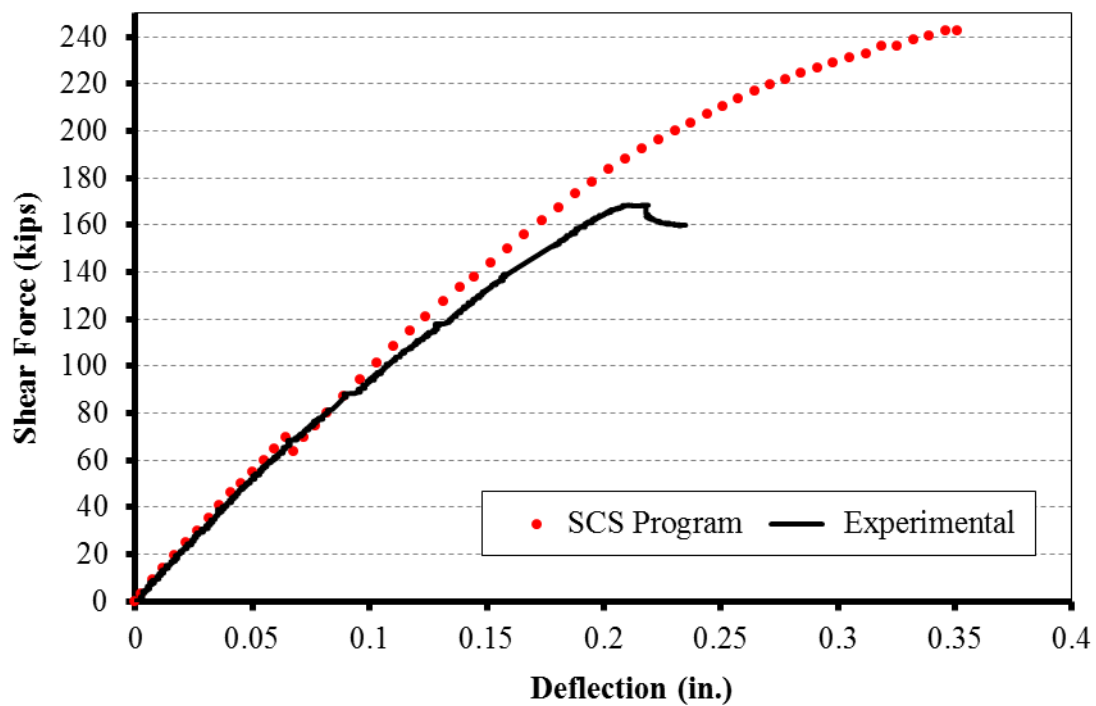


Fig. 5.10 Analytical and Experimental Load-Deflection Curves of Girder C1

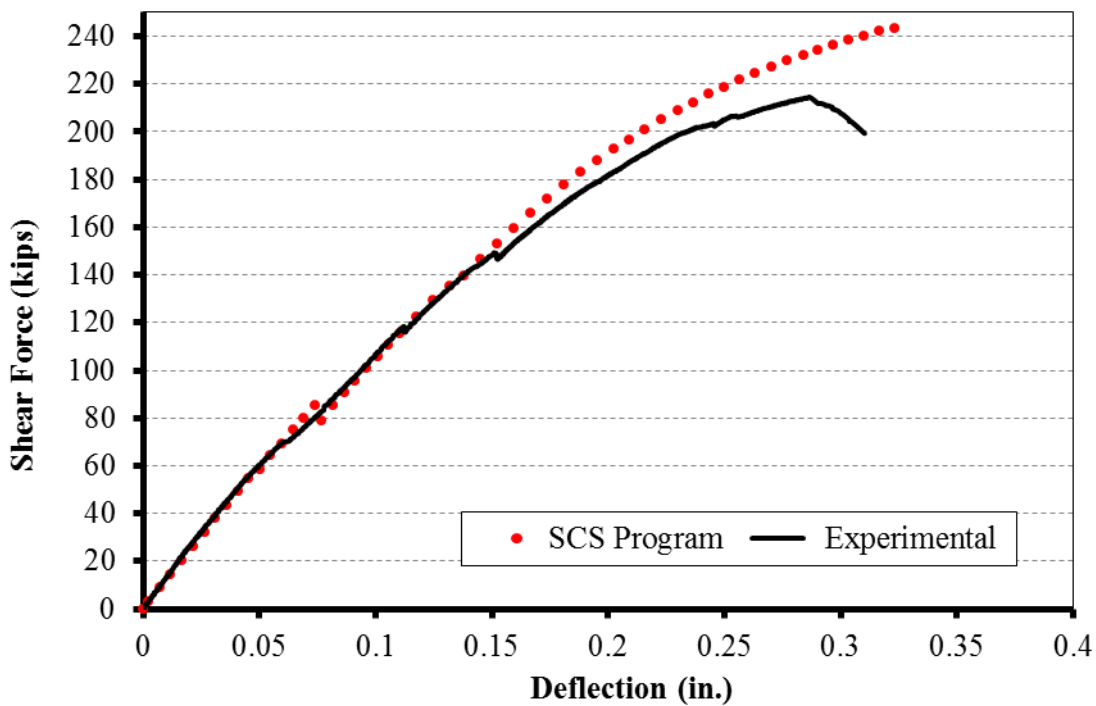


Fig. 5.11 Analytical and Experimental Load-Deflection Curves of Girder C3

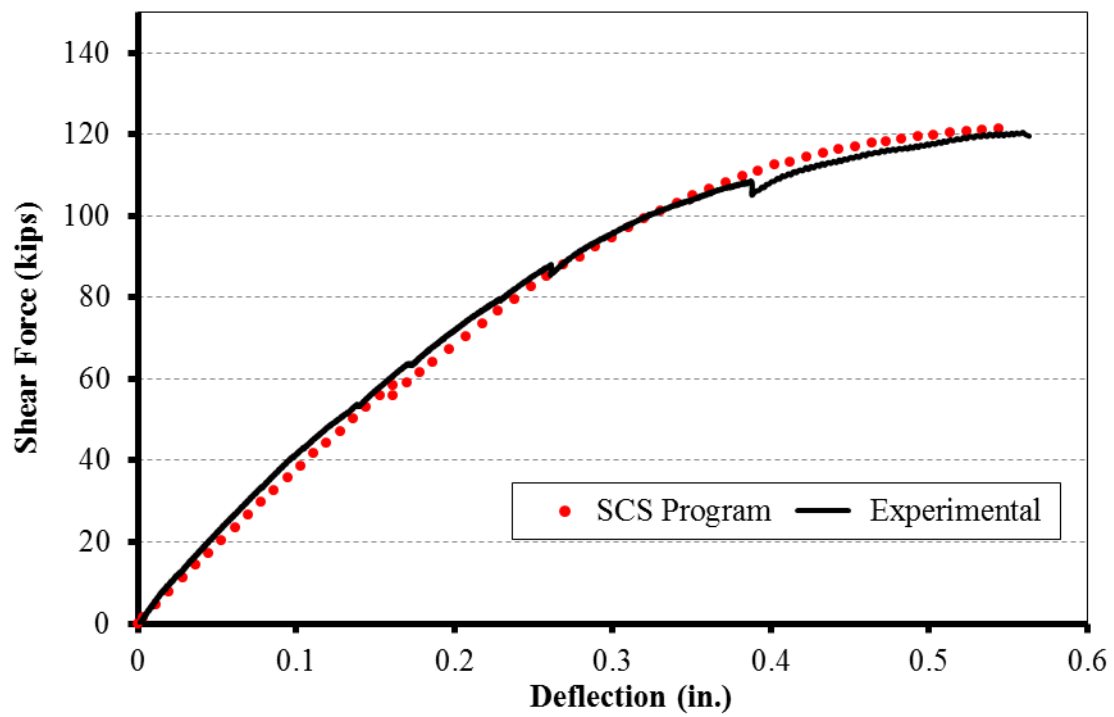


Fig. 5.12 Analytical and Experimental Load-Deflection Curves of Girder A2

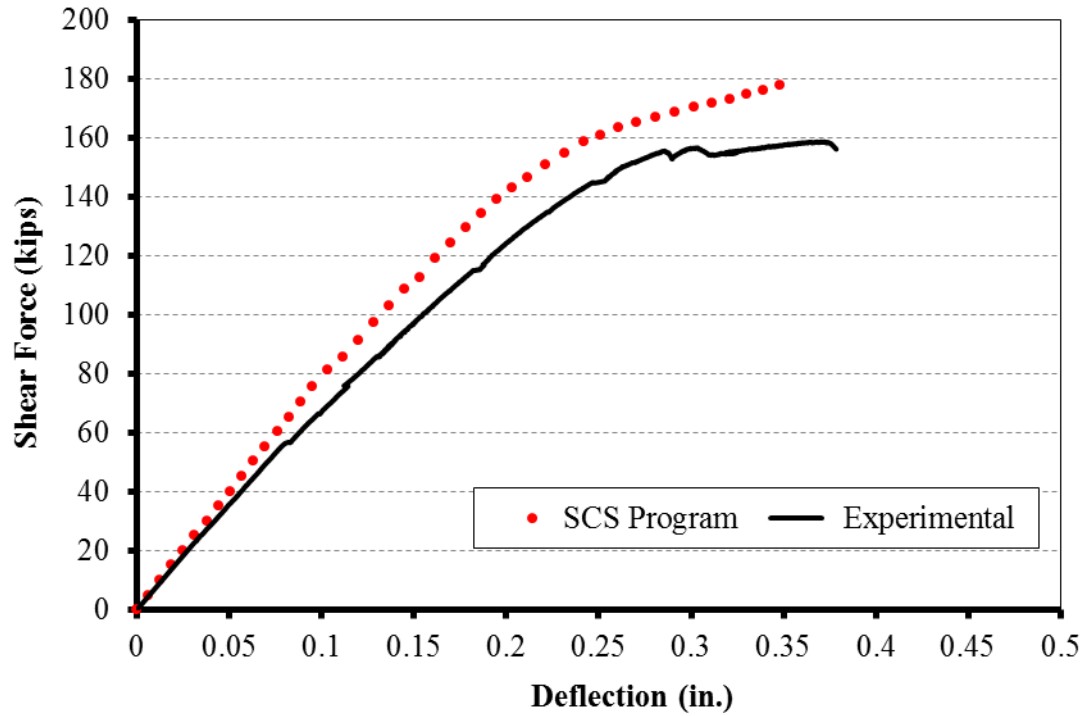


Fig. 5.13 Analytical and Experimental Load-Deflection Curves of Girder F4

5.4. Finite Element Model of Girders with Flexure Shear Failure

Two girders of the experimental program had been tested using shear span to depth ratio 3.00, namely C2, and C4. Fig. 5.14 shows the finite element mesh and the location of applied loads and supports used for these girder specimens.

The top flange in these girders was discretized into 60 fibers of concrete and 6 fibers of steel, as shown in Fig. 5.15. The bottom flange is discretized into 60 fibers of concrete and 8 out of 14 prestressing tendons are modeled as steel fibers in the bottom NonlinearBeamColumn in all the 4 girders. The additional flexure reinforcement has been modeled with six fibers of steel in the middle part of the girder, as shown in Fig. 5.15.

The comparison between the analytical and experimental shear force versus net deflections are shown in Figs. 5.16 and 5.17. These figures show that the used finite element program is able to accurately predict the behavior of prestressed girders with different concrete strength and different percentage of transverse steel with shear span to depth ratio equals 3.00.

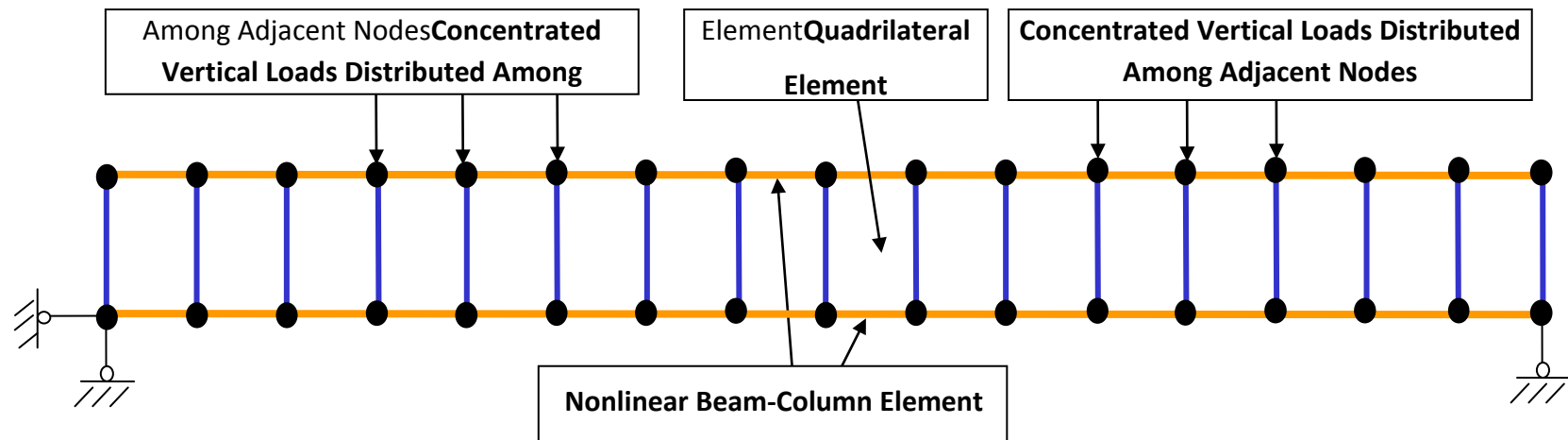


Fig. 5.14 Finite Element Mesh of Girder Specimens C2 and C4

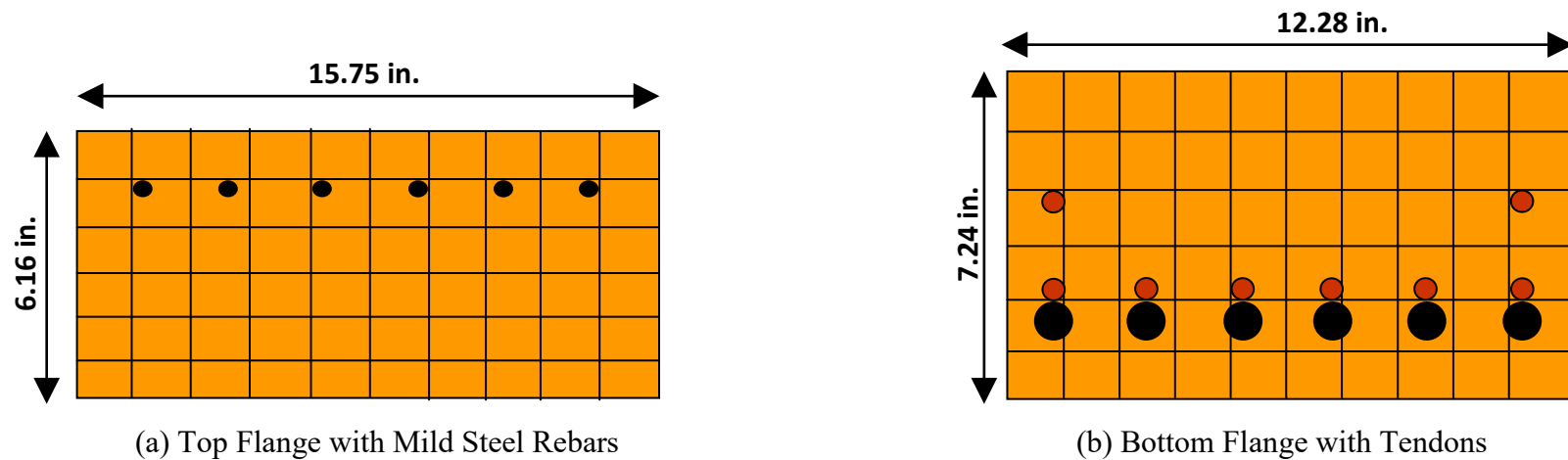


Fig. 5.15 Section Discretization of Nonlinear Beam-Column Elements for Girder Specimens C2 and C4

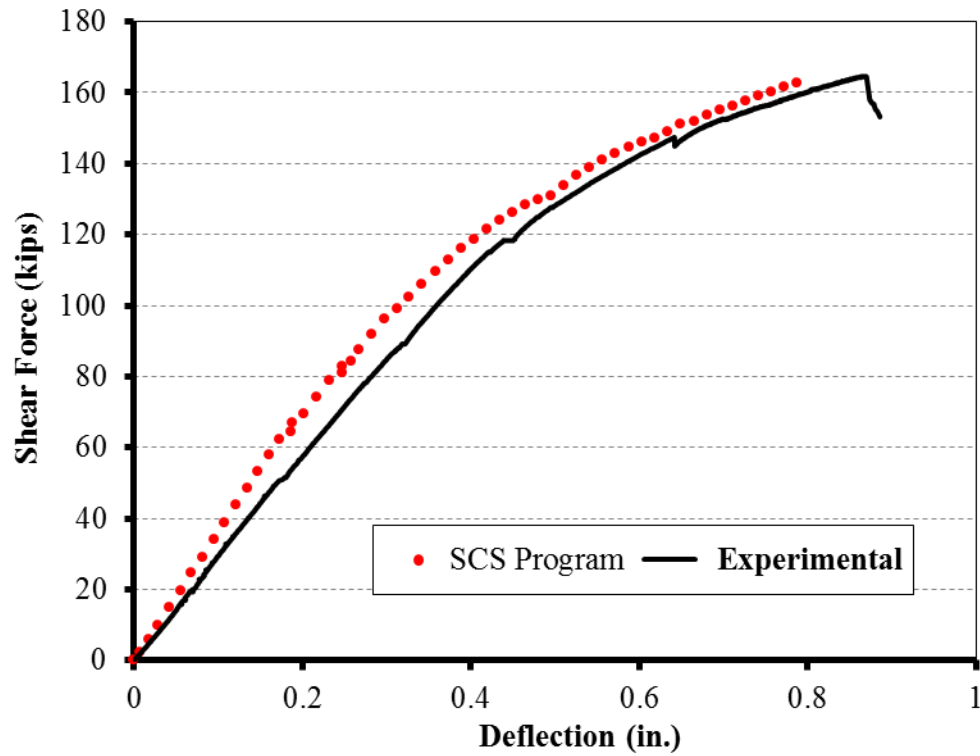


Fig. 5.16 Analytical and Experimental Load-Deflection Curves of Girder C2

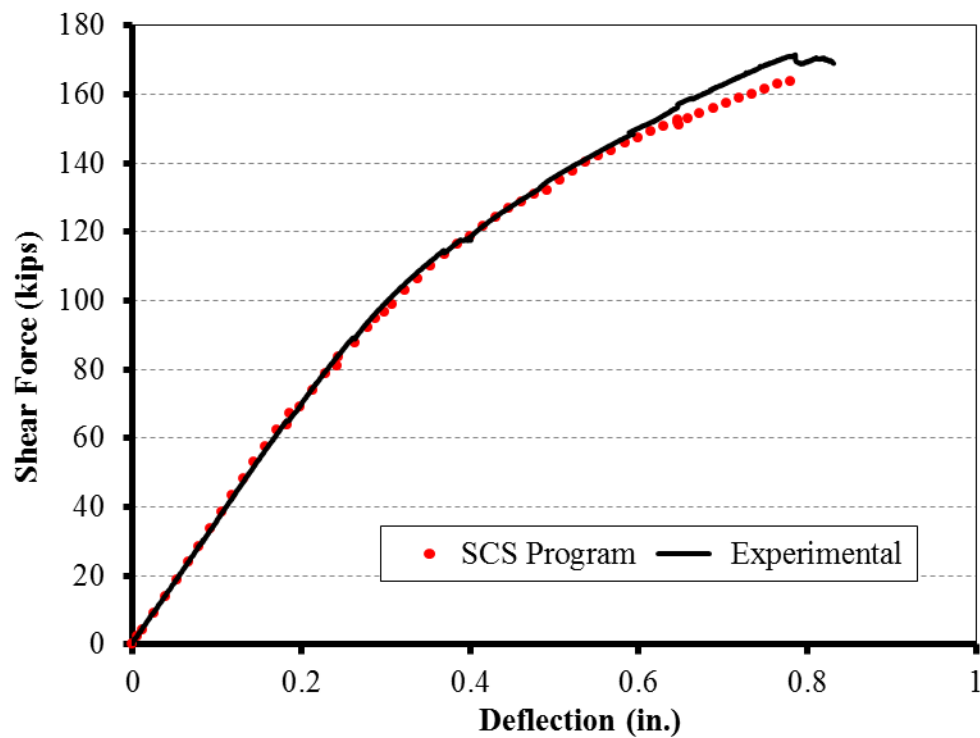


Fig. 5.17 Analytical and Experimental Load-Deflection Curves of Girder C4

5.5. Finite Element Model of Girders with Flexure Failure

Girder F2 had been tested using a shear span to depth ratio of 3.00. Fig. 5.18 shows the finite element mesh and the location of the applied loads and supports used for this girder. The top and bottom flanges had the same discretization as the first seven girders. The top flange is discretized into 84 fibers of concrete and 10 fibers of steel, as shown in Fig. 5.19. The bottom flange is discretized into 60 fibers of concrete and 8 out of 14 prestressing tendons are modeled as steel fibers in the bottom NonlinearBeamColumn

The comparison between the analytical and experimental shear force versus net deflections are shown in Fig. 5.20. It can be seen that SCS could not simulate the entire behavior of the girder and stopped earlier, because this girder was going to fail in flexure, which cannot be fully simulated using the current membrane element.

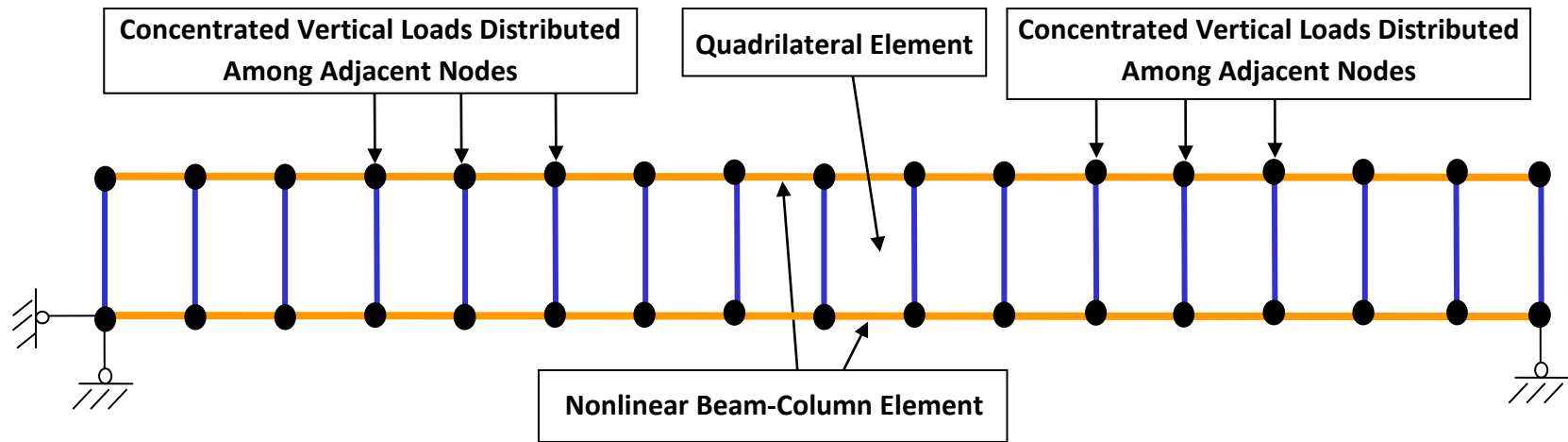


Fig. 5.18 Finite Element Mesh of Girder Specimen F2

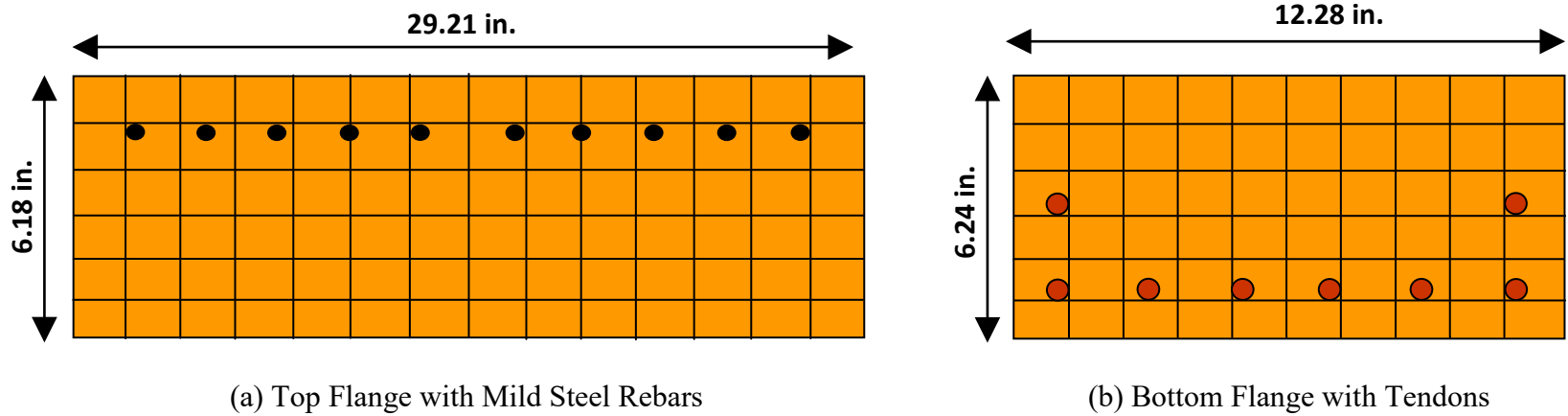


Fig. 5.19 Section Discretization of NonlinearBeamColumn Elements for Girder Specimen F2

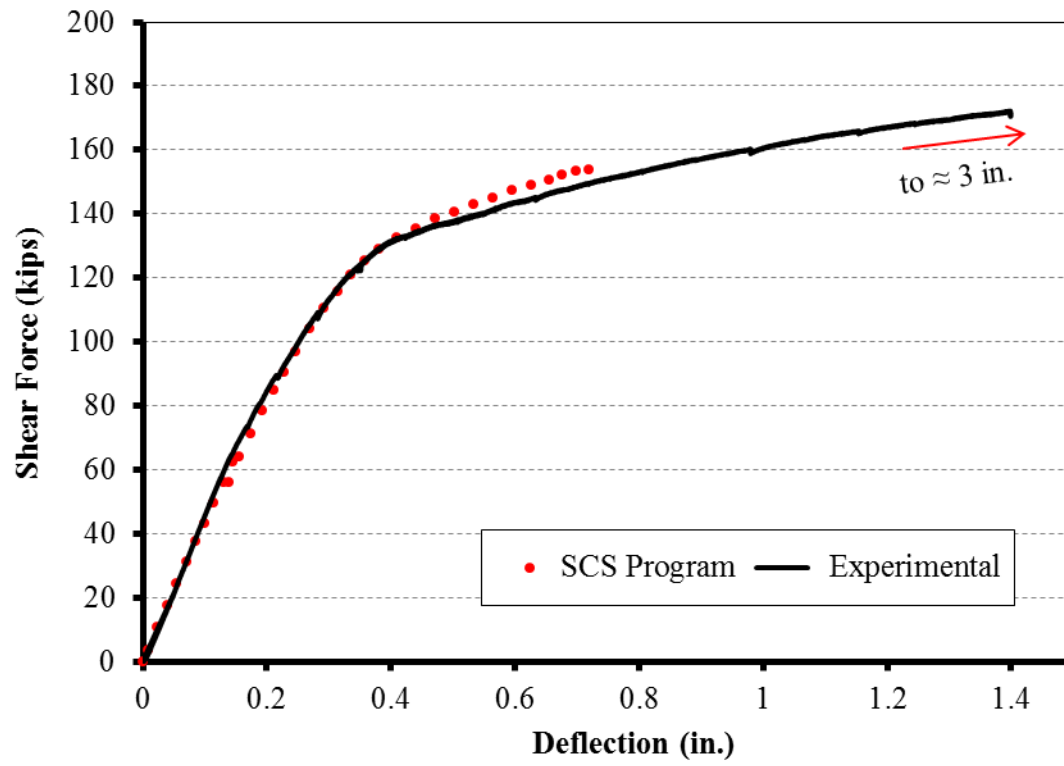


Fig. 5.20 Analytical and Experimental Load-Deflection Curves of Girder F2

PART II: STUDY OF SHEAR BOND FAILURE

CHAPTER 6 EXPERIMENTAL PROGRAM TO STUDY SHEAR- BOND FAILURE

6.1. Introduction

If a girder has been tested using a small span-to-depth ratio, the web-shear capacity may be less than the recommended capacity if inadequate tendon anchorage length is provided at the end of the girders. The girder may fail at a reduced load due to crushing at the intersection of the web to the bottom flange, or splitting of the bottom flange due to tendon pullout. The maximum capacity is achieved if the stirrups yield prior to the crushing of concrete in the web.

The behavior of the end regions is affected by the dimension of the cross-section, the percentage of transverse steel, the amount of prestressing force, the layout of the tendons and the anchorage length next to the support. This experimental program is studying the effect of the cross-section dimension and the percentage of transverse steel. The most important aspect in the cross-section dimension is the web's depth-to-thickness ratio. A larger ratio means more chance to have a premature failure in the end region. Two different percentage of transverse steel are studied to investigate the validity of Laskar's (2010) equation for predicting the concrete contribution to prevent the premature failure in the end zone of the pretensioned PC girders. The layout of the tendons and the location of the support will be typically according to TxDOT specification. The maximum allowed amount of prestressing force is used.

6.2. Tested Girders and Studied Objective

Three different sizes of Tx-series are selected to study the effect of the cross-section's dimensions, i.e., the web's depth-to width ratio, the end region behavior and in turn the shear capacity of the girder. These girders are Tx28, Tx46, and Tx62. These three girders have the same web thickness equal to seven inches and almost the same dimensions of the top and bottom flanges. This results in a compacted web in girder Tx28, a proportional web in girder Tx46, and a slender web in girder Tx62.

This chapter is mainly concerned with studying shear in end regions. The middle part of the girder does not affect the shear capacity or the shear behavior of the end region. The girder

length should be sufficient to apply load at both ends of the girder independently. Thus, the total length of the studied girders was decided to be 25 ft.

Two girders of each size are tested. Both girders have the same number and layout of tendons, amount of confinement steel in the bottom flange and longitudinal and lateral reinforcement in the top flange. The maximum number of tendons that satisfies the maximum allowable compressive stresses on the bottom flange at release is used as the flexural reinforcement. Forty, fifty-four, and sixty-two tendons are used in both Tx28 girders in Group G, both Tx46 girders in Group D, and both Tx62 girders in Group E, respectively. All of the tendons in the six studied girders are seven-wire, low-relaxation straight tendons with 0.5-in. diameter and a cross-section area 0.153 in^2 . The confinement steel in the bottom flange and the longitudinal and the lateral reinforcement in the top flange are chosen according to TxDOT standard specifications. The longitudinal reinforcement in the top flange has been checked to ensure its ability to resist the tensile stresses in the top fiber due to the application of the prestress force. The main difference between each two girder group is the amount of the transverse reinforcement and existence of the top slab.

The first girder of each size is typically reinforced in the transverse direction according to TxDOT standard specifications and has a top slab, as shown in Figs. 6.1 to 6.6. The main target of testing these three groups of girders is to investigate if the proposed design by TxDOT is sufficient to prevent shear-bond failure with a top slab. In other words, the objective of the first set of girders is to study the possibility of having a premature failure in the new Tx-series due to the slippage of the tendons in the end zone using TxDOT design specifications.

The top slab has a typical thickness of 8 inches. Because, only the shear behavior of the end regions are studied in this experimental program, and based on the fact that the web dimensions are the most effective dimension on the shear capacity, a top slab with the same width as the top flange was casted regardless of the practical spacing between girders.

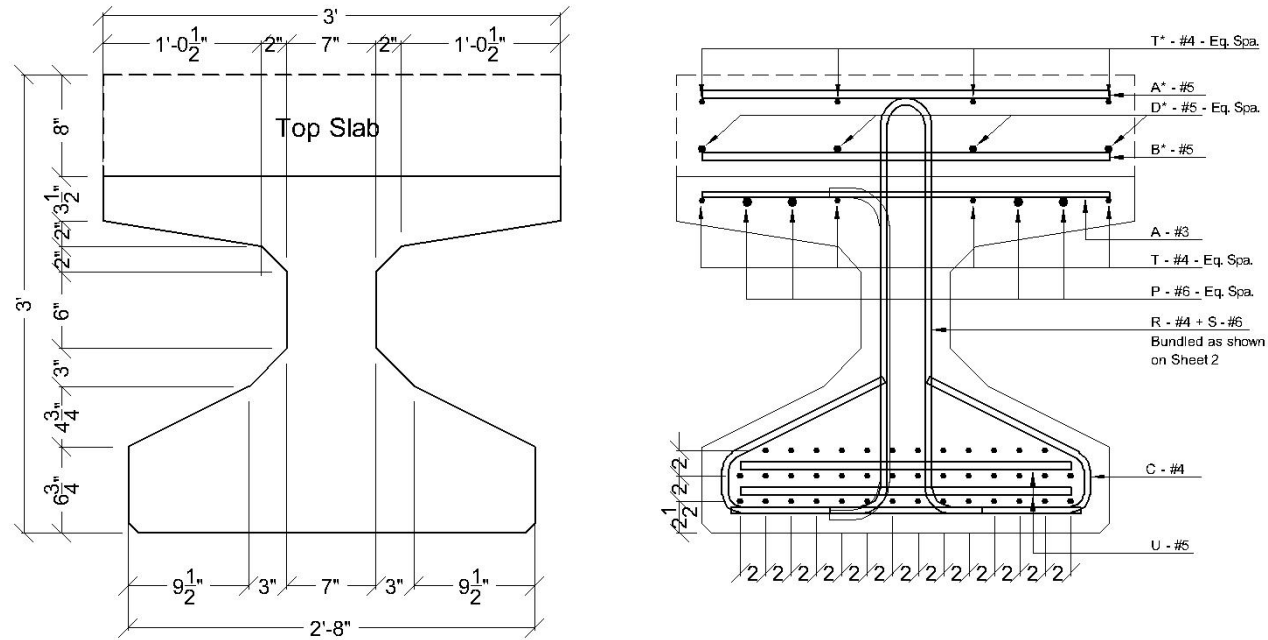
The second girder of each size is reinforced in the transverse direction only with the minimum reinforcement according to AASHTO LRFD (2010), as shown in Figs. 6.7 to 6.12. Because this amount of reinforcement seems critical in resisting end zone cracks at release due to bursting forces, the girder end was additionally reinforced with additional transverse reinforcement to resist these forces.

The additional reinforcement at the girder end for each girder was taken as the higher of AASHTO LRFD (2010) requirements and Marshall and Mattock (1962) recommendations, recently widely known as the Portland Cement Association (PCA) recommendations. Table 6.1 summarizes the required additional reinforcement for each girder calculated by both methods and the corresponding recommended distance from the girder end. The distance from the girder end is taken to be within the recommended distance by AASHTO LRFD (2010) to have practical spacing between the stirrups and the same cover at the girder end recommended in the TxDOT specifications.

Table 6.1 Additional End Zone Reinforcement

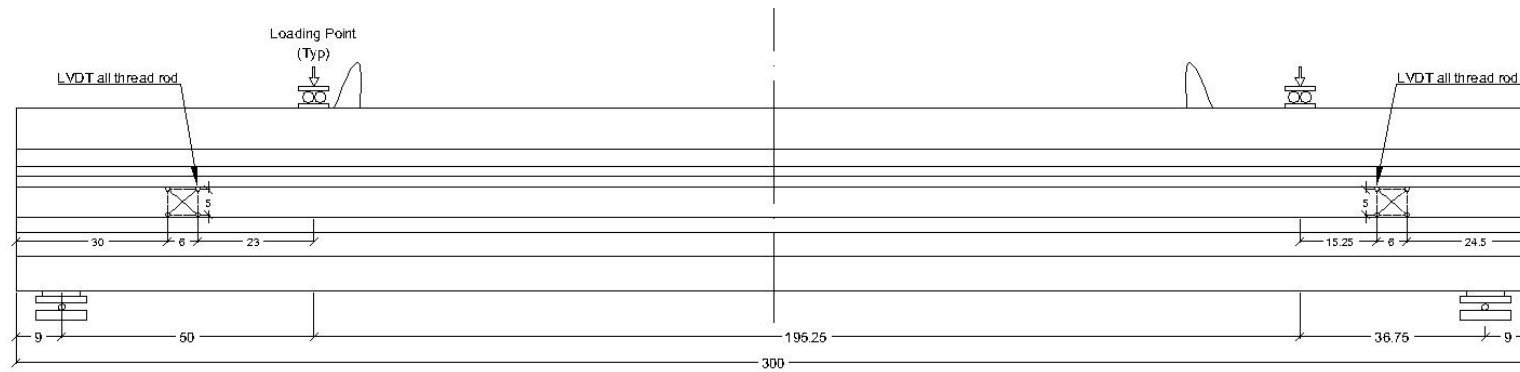
		Tx28	Tx46	Tx62
AASHTO LRFD	Required reinforcement (2 legs each)	2#4 + 2#6	3#4 + 3#6	4#4 + 4#5
	Distance from Girder End	7	11.5	15.5
Marshall and Mattock (1962)	Required reinforcement (2 legs each)	2#6	3#4 + 3#6	4#4 + 4#6
	Distance from Girder End	5.6	9.2	12.4
Used	Required reinforcement (2 legs each)	2#4 + 2#6	3#4 + 3#6	4#4 + 4#6
	Distance from Girder End	6.5	10.5	14.5

The detailed concrete dimensions of the tested girders' cross-sections, flexural reinforcement layout and fully detailed longitudinal cross-sections for the tested girders are shown in Figs. 6.1 to 6.12. These longitudinal sections show the desired locations for the Linear Variable Displacement Transformer (LVDT) rods and the locations of supports and loading points.

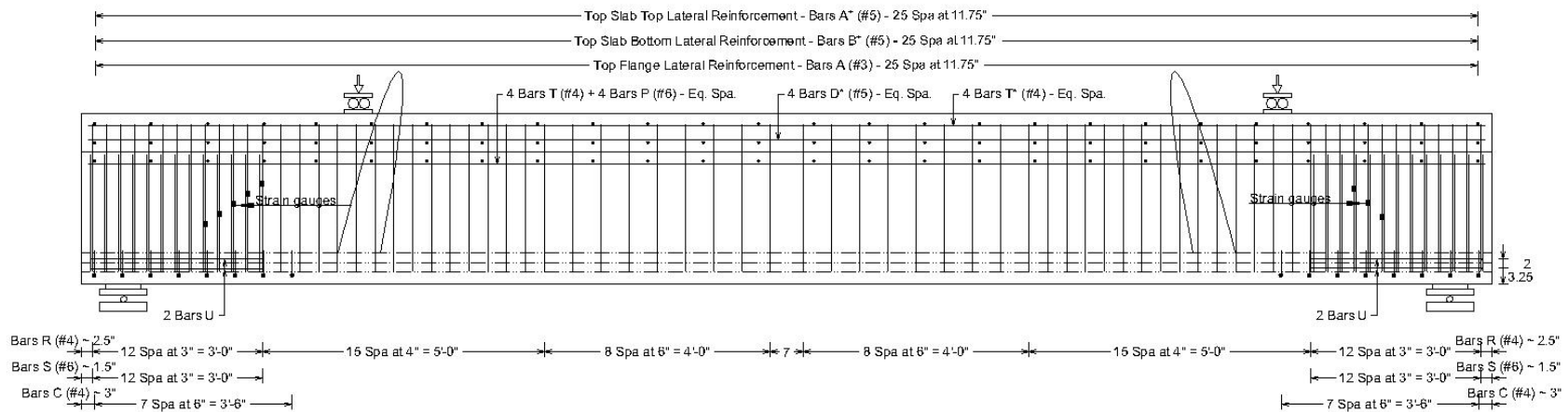


(All Dimensions are in Inches)

Fig. 6.1 Concrete Dimensions and Reinforcement Details for Girder G1



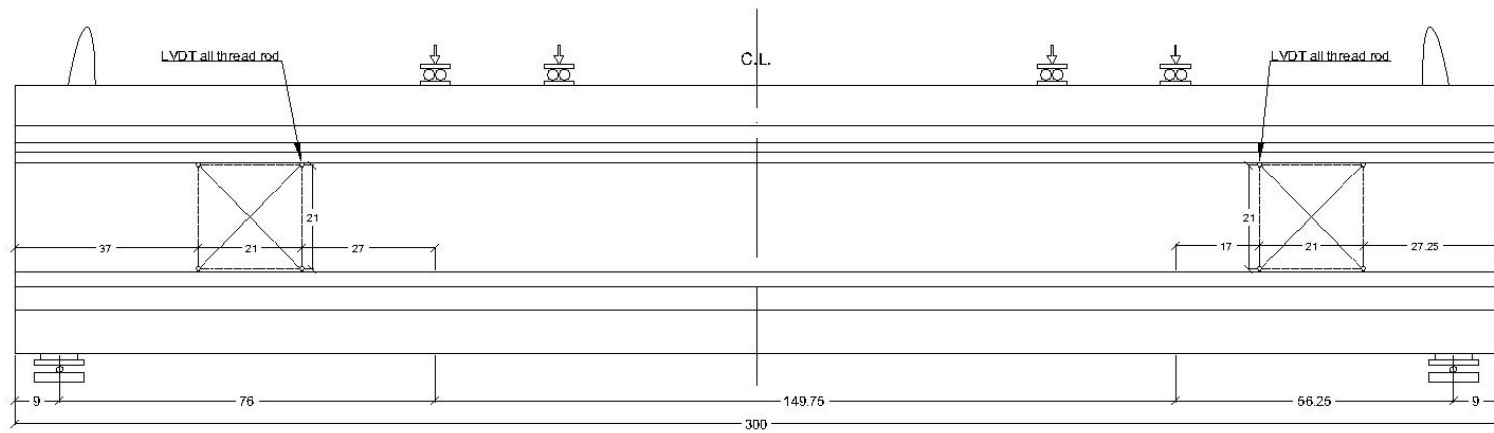
(a) Locations of LVDTs' rods, Supports, and Actuators



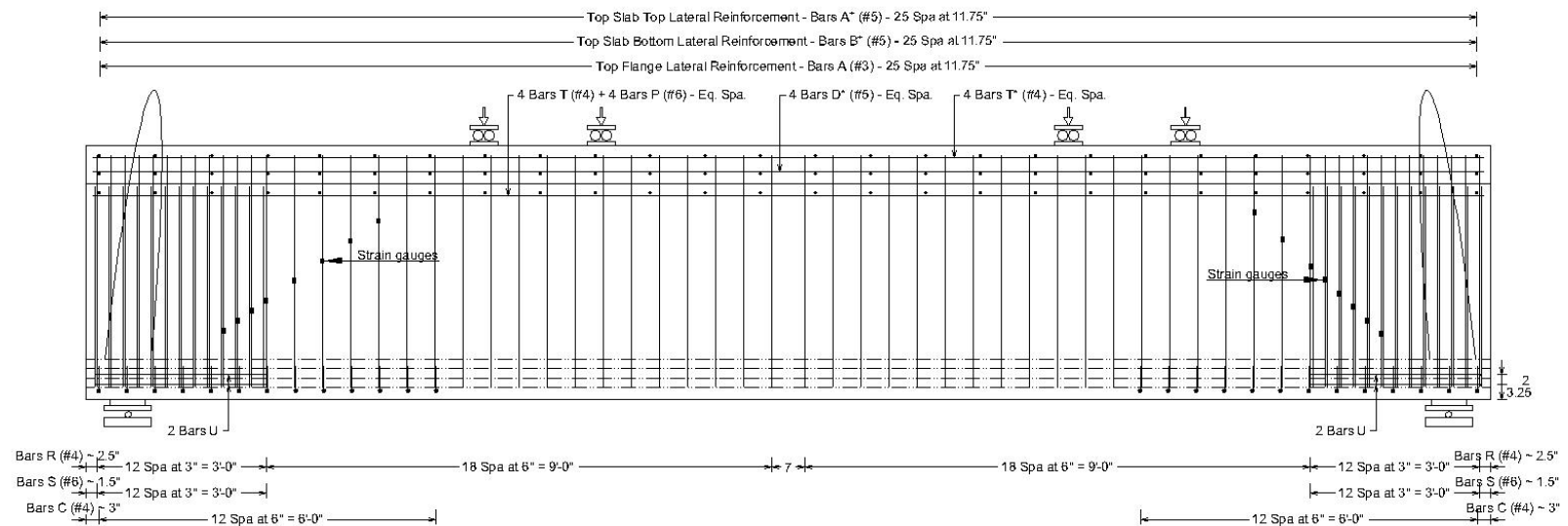
(b) Reinforcement Detailed Longitudinal Cross-section

(All Dimensions are in Inches)

Fig. 6.2 Detailed Longitudinal Cross-Sections for Girder G1



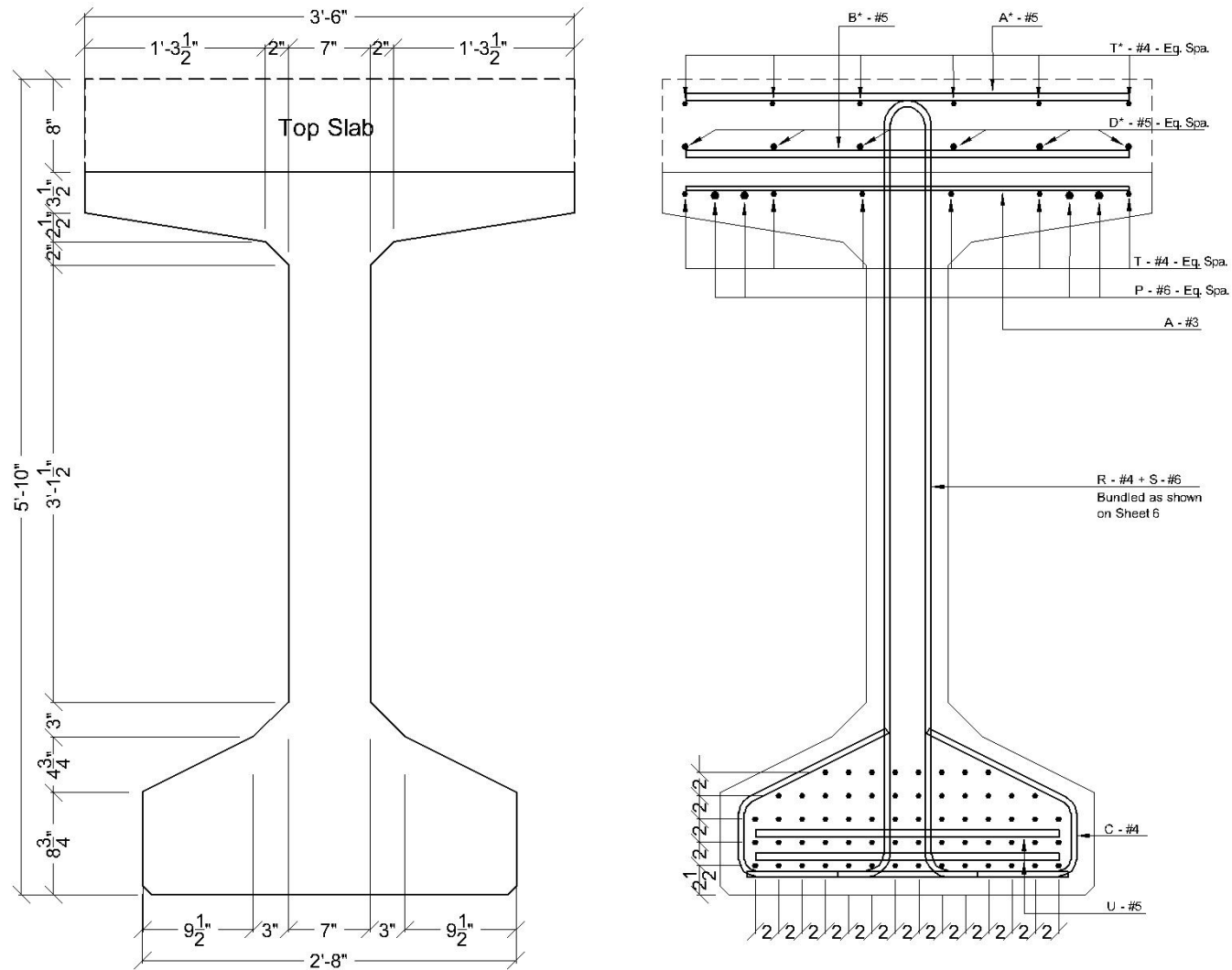
(a) Locations of LVDTs' rods, Supports, and Actuators



(b) Reinforcement Detailed Longitudinal Cross-Section

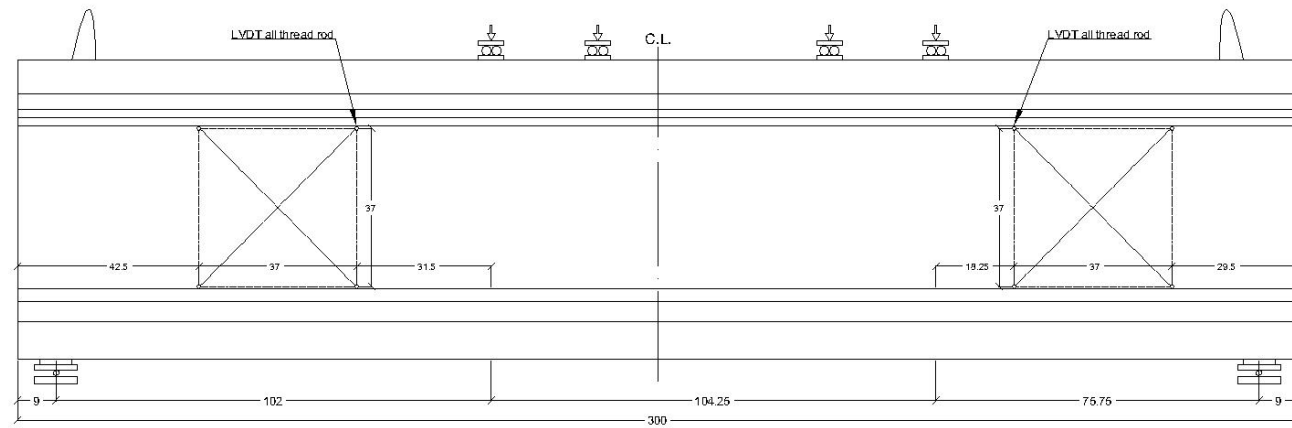
(All Dimensions are in Inches)

Fig. 6.4 Detailed Longitudinal Cross-Section for Girder D1

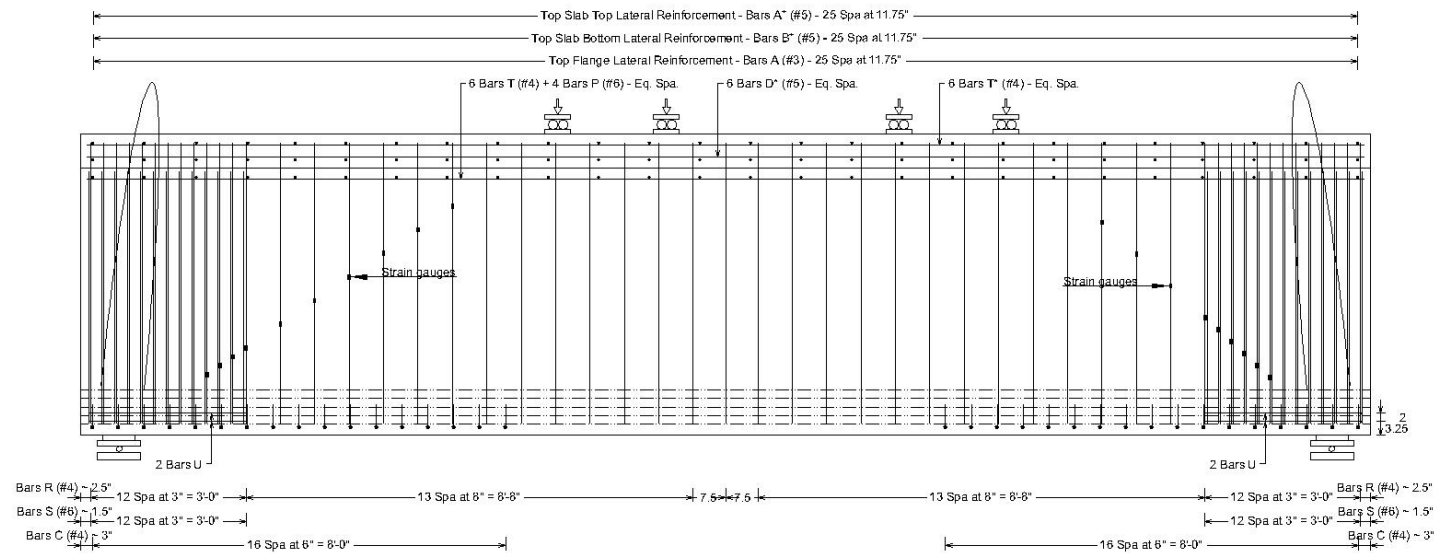


(All Dimensions are in Inches)

Fig. 6.5 Concrete Dimensions and Reinforcement Details for Girder E1



(a) Locations of LVDTs' rods, Supports, and Actuators



(b) Reinforcement Detailed Longitudinal Cross-section

(All Dimensions are in Inches)

Fig. 6.6 Detailed Longitudinal Cross-Section for Girder E1

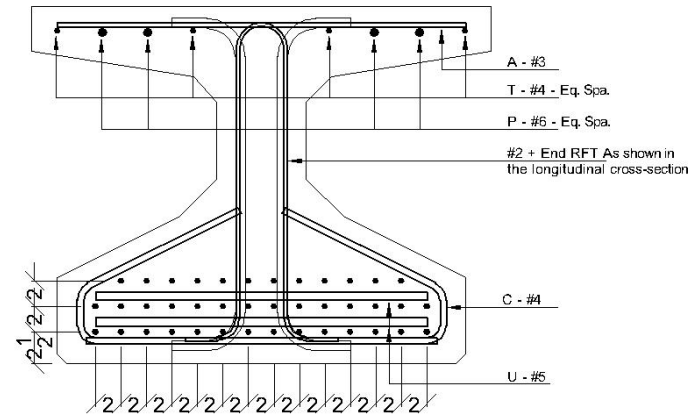
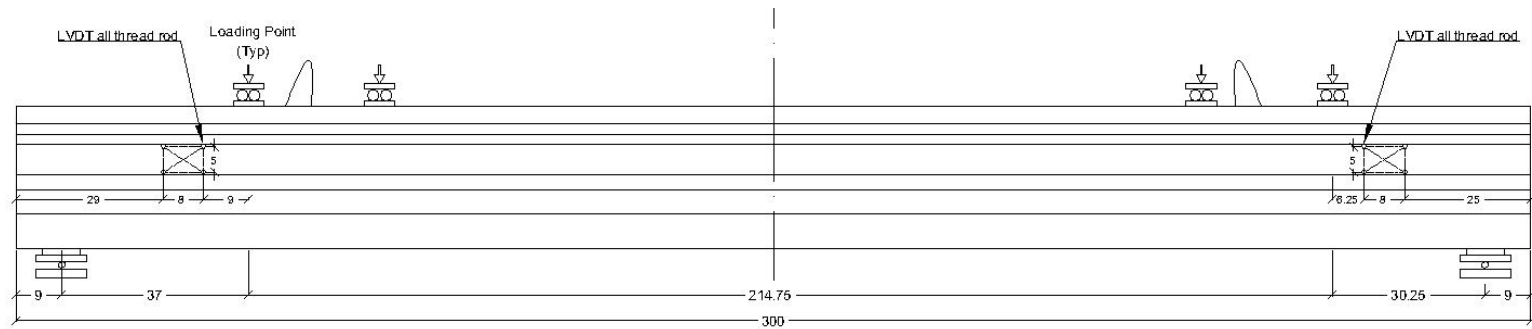
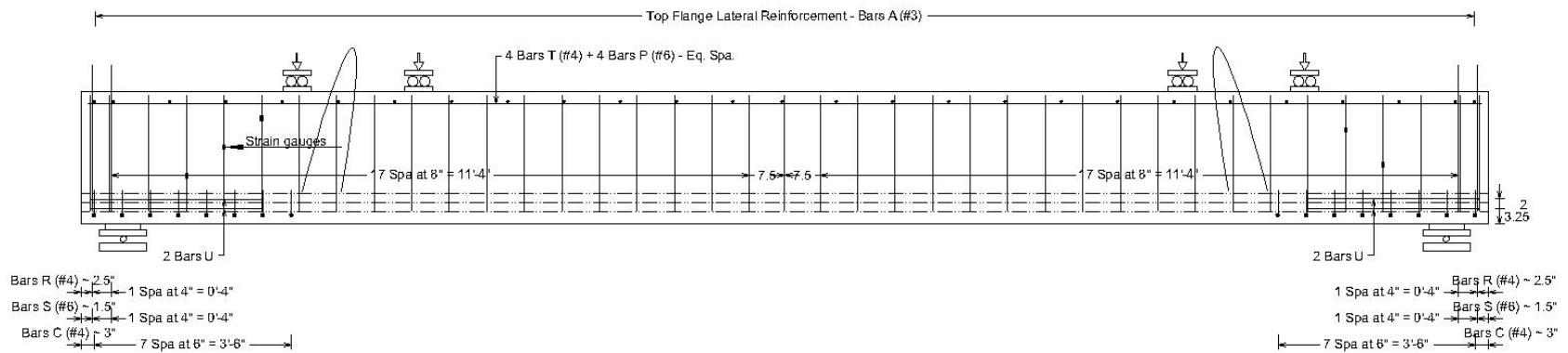


Fig. 6.7 Concrete Dimensions and Reinforcement Details for Girder G2



(a) Locations of LVDTs' rods, Supports, and Actuators



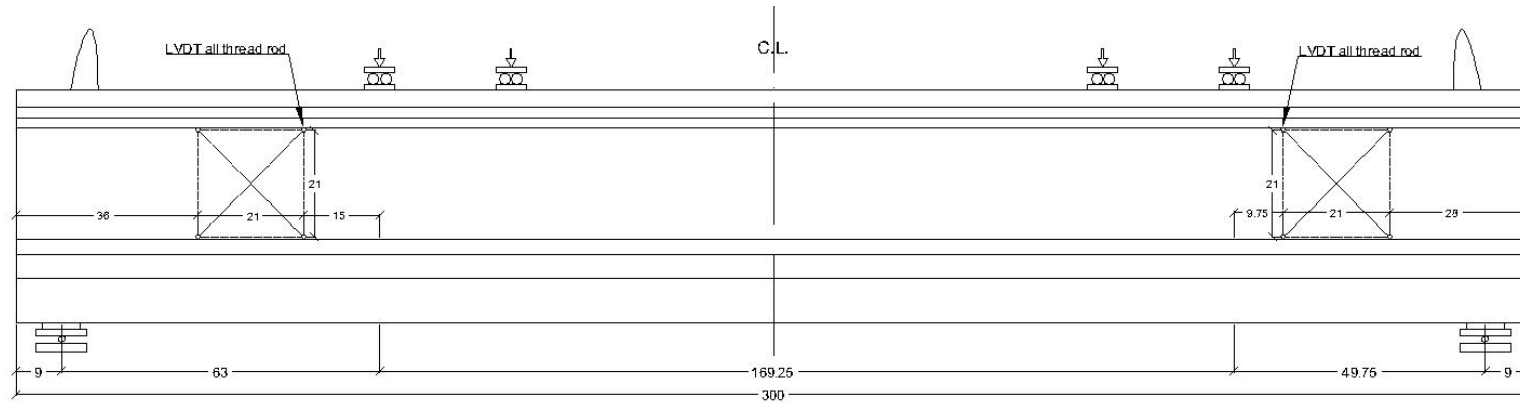
(b) Reinforcement Detailed Longitudinal Cross-section

(All Dimensions are in Inches)

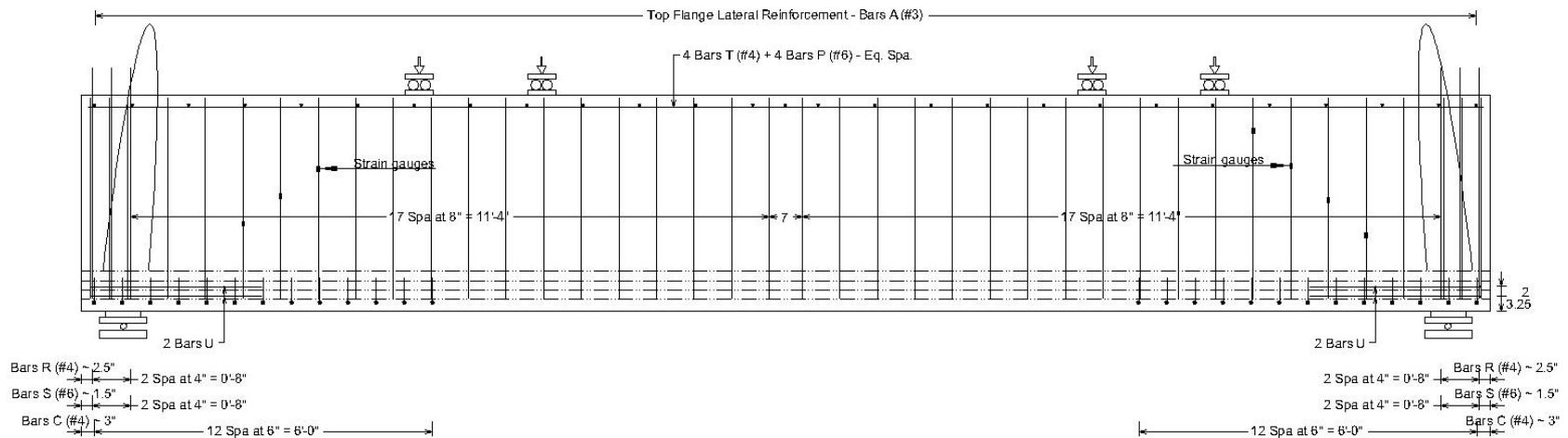
Fig. 6.8 Detailed Longitudinal Cross-section for Girder G2

[illegible]

Fig. 6.9 Concrete Dimensions and Reinforcement Details for Girder D2



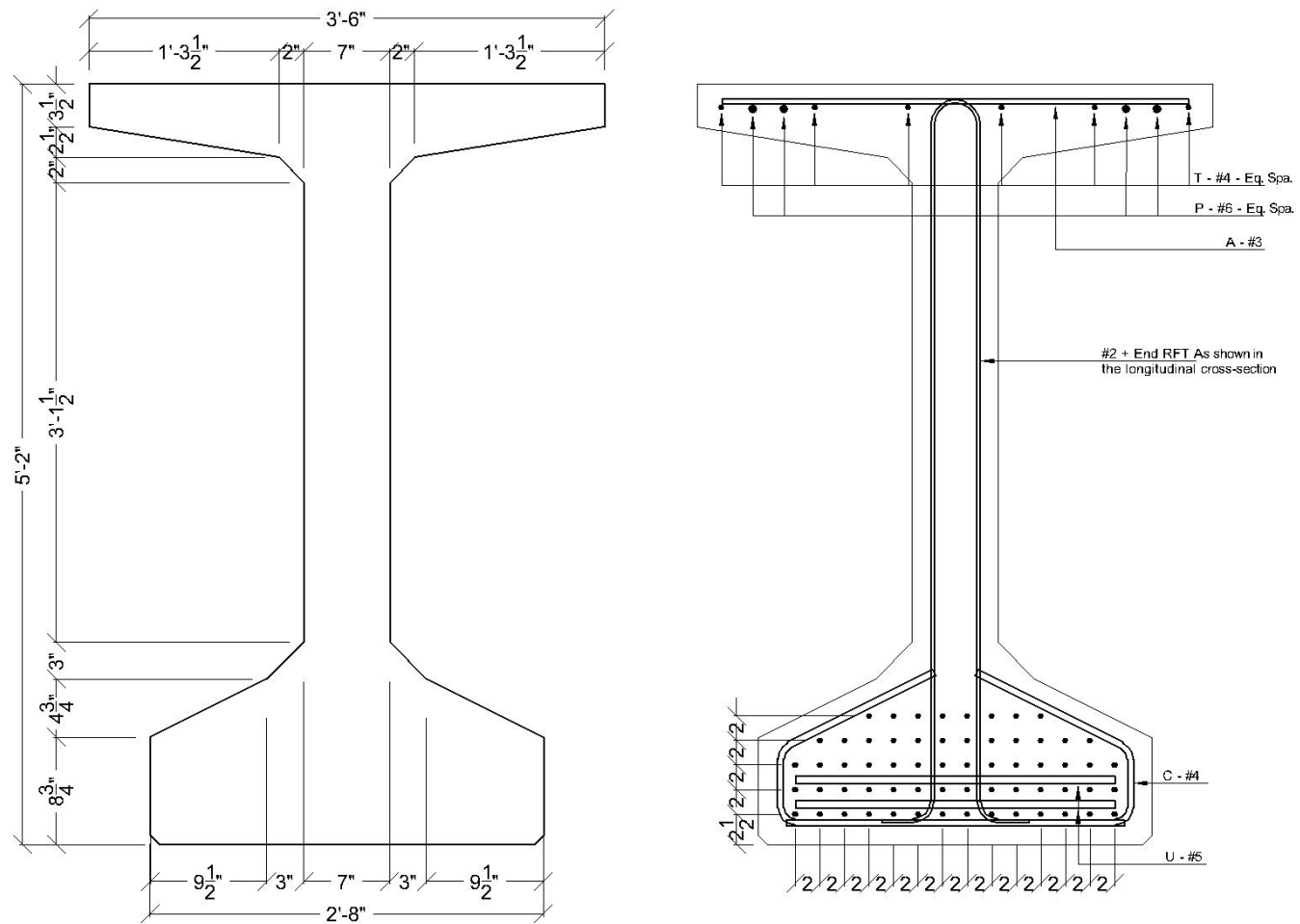
(a) Locations of LVDTs' rods, Supports, and Actuators



(b) Reinforcement Detailed Longitudinal Cross-section

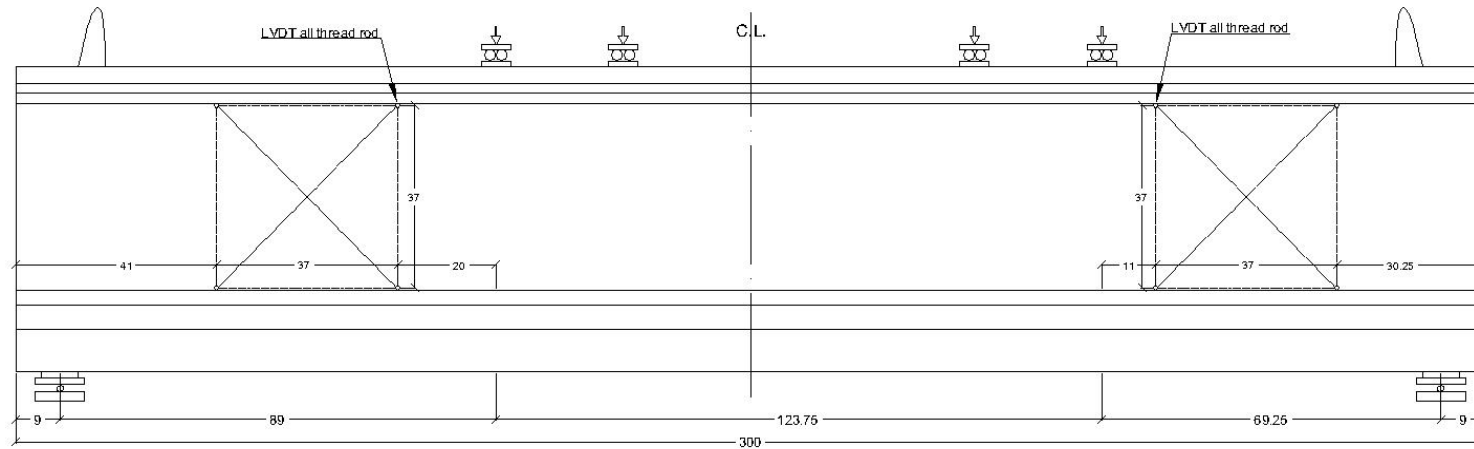
(All Dimensions are in Inches)

Fig. 6.10 Detailed Longitudinal Cross-Section for Girder D2

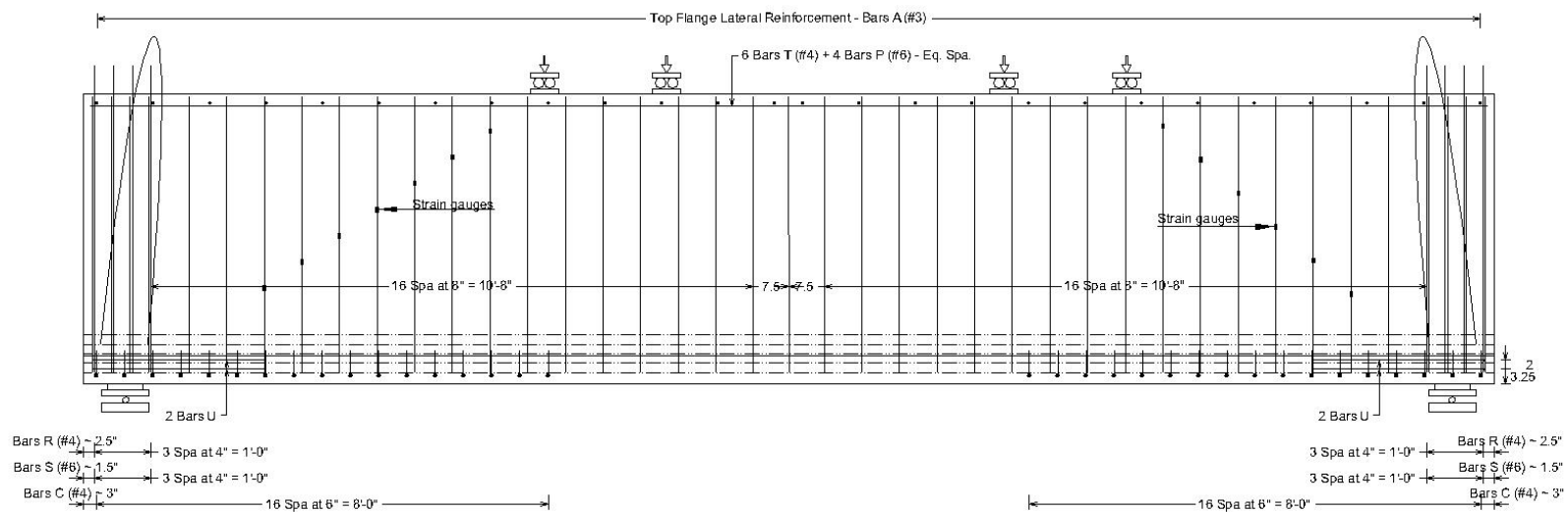


(All Dimensions are in Inches)

Fig. 6.11 Concrete Dimensions and Reinforcement Details for Girder E2



(a) Locations of LVDTs' rods, Supports, and Actuators



(b) Reinforcement Detailed Longitudinal Cross-Section

(All Dimensions are in Inches)

Fig. 6.12 Detailed Longitudinal Cross-Section for Girder E2

6.3. Manufacturing of Test Girders

The first set of three Girders, G1 (Tx28), D1 (Tx46), and E1 (Tx62), was cast at the Texas Concrete Company in Victoria, Texas, in July 2011. Two girders of the second set of three girders, namely Girders D2 (Tx46), and E2 (Tx62), were also cast at the Texas Concrete Company in Victoria, Texas, in April 2012. Because of the steel form availability, Girder G2 (Tx28) was cast at Texas Concrete Partners in Waco, Texas, in May 2012. Because there was a different number of tendons in each girder, one girder had to be cast at a time. The prestressing tendons were pretensioned by hydraulic jacks placed in a prestressing steel platform/bed. Transverse steel, including the rebars instrumented with strain gauges, along with all the other confining and flexural reinforcements were installed in the girders. Fig. 6.13 shows the reinforcement cage of a typical girder.

Coupling nuts of 2 in. length were installed in the web of each girder on the steel sides at pre-determined locations as depicted in Fig. 6.14 by drilling holes in the steel form with a diameter of 3/8 inch. These steel rods were used to mount the LVDT, which served as instrumentation to measure the average or smeared strains in the girders during the load testing.

The concrete mix was prepared in a plant mixer, transported to the casting site, and deposited into the formworks using a mobile hopper, as shown in Fig. 6.15. The average slump for the girders was 8.50 inch. During casting, spud vibrators were used to compact the concrete as well as bed vibrator fixed on the side forms, as shown in Fig. 6.16. Seven standard concrete cylinders six inches in diameter and twelve inches in height were cast per girder. Just prior to the actual girder tests, the concrete cylinders were tested to get the representative concrete compressive strength of the girder.

One day after casting the girders, the prestressing tendons were slowly released, when the girder reached the required strength. The release strength was 6,240, 6,200, and 6,950 psi for Girders G1 (Tx28), D1 (Tx46), and E1 (Tx62), respectively, and 7,100, 6,340, and 6,200 psi for Girders G2 (Tx28), D2 (Tx46), and E2 (Tx62), respectively. After release, girders were transported to the storage yard.



Fig. 6.13 Reinforcement Cage for a Typical Girder



Fig. 6.14 Coupling Nuts Fixed in Steel Forms



Fig. 6.15 Concrete Placement Using a Hopper



Fig. 6.16 Bed Vibrator Attached to Steel Forms

Then the formwork and the reinforcement cage for the top slab were prepared for the first three girders, as shown in Fig. 6.17. Then the concrete was prepared and placed as explained before and compacted using the spud vibrators. Four standard concrete cylinders four inches in diameter and eight inches in height were cast per each girder's slab. Just prior to the actual girder tests, the concrete cylinders were tested to get the representative concrete compressive strength of the top slab.



Fig. 6.17 Reinforcement Cage for Top Slab

6.4. Test Set-up

The girders were subjected to vertical loading up to their maximum shear capacity in a specially built steel loading frame, as shown in Fig. 6.18. Two actuators each attached to a vertical steel frame were used to apply the vertical loads on the girders. Each of these two actuators had a capacity of 600 kips in compression. The two actuator frames were installed on each end of the girder to break one end at a time. These two actuator frames were sitting on top of two WF30×173 girders, bolted securely to the strong floor. The two WF30×173 girders were 25 ft. long and spaced at 87 in. center to center. The girder was positioned in the middle of this spacing width on top of two load cells placed at the north and south ends.

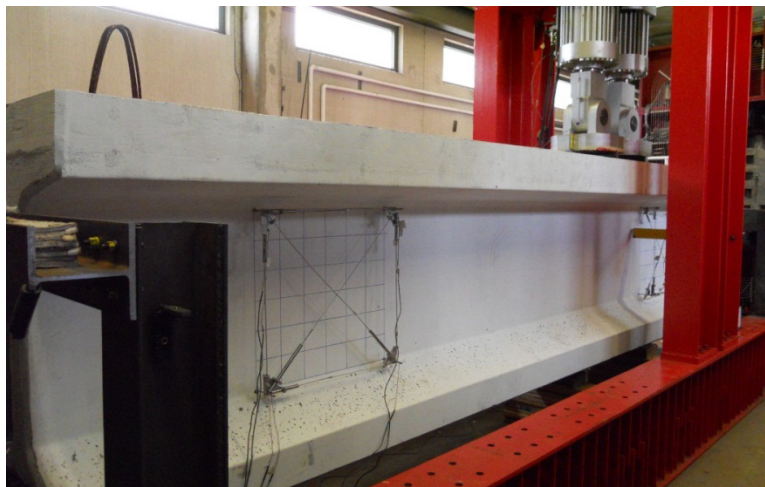


Fig. 6.18 Test Setup for Girders

Each hydraulic actuator shown in Fig. 6.18 has one horizontal pin that allows the bottom head to rotate due to the girder's curvature, which corresponds to the specimen deflection. The rotation of the bottom head of the actuator results in horizontal force at the top surface of the girder. To compensate this horizontal force, one high strength rod $2\frac{3}{8}$ inches in diameter was used between the actuator and the top surface of the girder. This single rod has been used with two thin lead sheets at top and bottom to minimize the rod's rolling, as shown in Fig. 6.19. This setup works as another hinge at the top of the girder's surface, which helps in transferring the load vertically to the girder and minimizing the horizontal force.



Fig. 6.19 Details of Loading Set-up

Theoretically due to the girder's curvature, the bottom fibers expand toward the support resulting in horizontal force acts on the support. This horizontal force should be eliminated by allowing the support to move with the bottom fiber's expansion, otherwise this horizontal force may result in losing stability because of the girder sliding over the load cell.

To allow the support to move, the load cell of 1000 kips capacity was placed on top of a square steel plate 18 in. x 18 in. This steel plate is resting on eight high strength pre-heat-treated rods with two in. diameter. These rods are connected together having almost 1/8 in. gap in between to prevent locking each other and to let them roll freely. In turn, the top plate can roll smoothly over another long steel plate which works as a fixed pedestal to the strong floor, as shown in Fig. 6.20.

On top of the load cells, bearing plates to support the girder were placed with a hinge on both ends of the girder. Thus, the girder is allowed to rotate freely at both supports and to expand freely along its length.

The bearing plate right underneath the girder has typical dimensions used by TxDOT. For all girders, this plate is 21 inches in length. The plate is 8 inches in width for Tx28 and Tx46 while it is 9 inches in width for Tx62. The thickness of this plate depends on the vertical available clearance. In addition to the precaution taken regarding vertical and longitudinal stability, lateral supports were attached to actuators' frames to provide a lateral stability for the girder in the case of emergency during loading.



Fig. 6.20 Details of Support

6.5. Instrumentation

Strains in transverse steel were measured as load was applied on the girders. Electrical-resistance foil-type strain gauges were installed on transverse steel rebars to measure local maximum strains at critical locations in the girders during the load tests. The strain gauge data obtained during the load tests were used to ascertain the average strain of transverse steel rebars at the failure shear force. Because the girders were designed to fail in web-shear, the strain gauges had been installed on transverse rebars along the line joining the points of applied load and the load cell support. In first three Girders G1 (Tx28), D1 (Tx46), and E1 (Tx62) where #4 rebars and #6 rebars are bundled together according to TxDOT specifications, the strain gauges had been installed on the #4 rebars. Because each stirrup has two legs, it was decided to post the strain gauges in staggered (one on the east side and one on the west side) in order to have the average strain of rebars on both sides. Table 6.2 shows the names and locations for the used strain gauges at each end of each girder.

Table 6.2 Strain Gauges Names and Locations

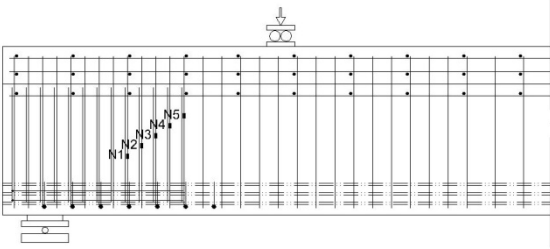
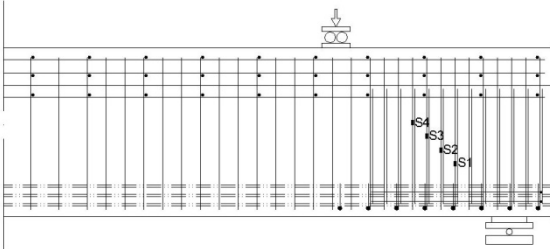
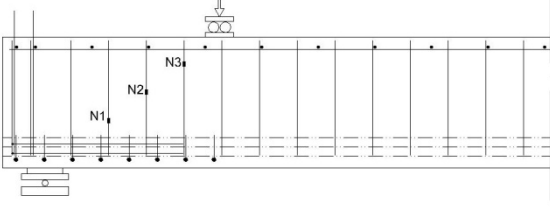
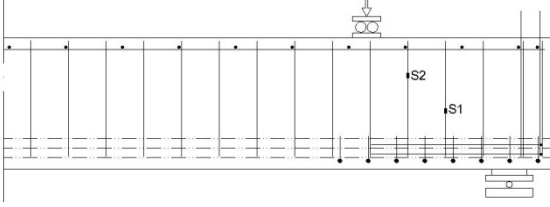
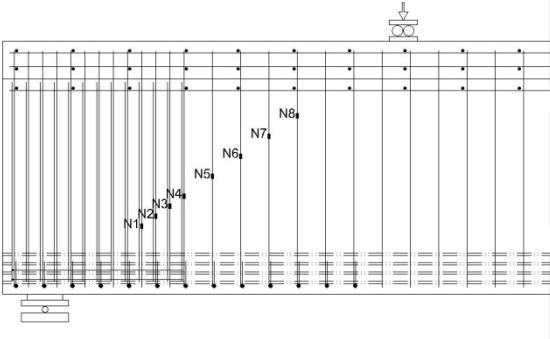
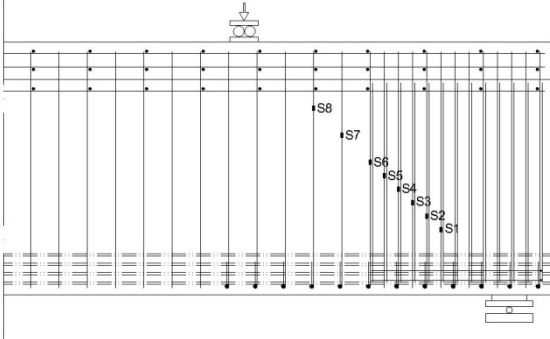
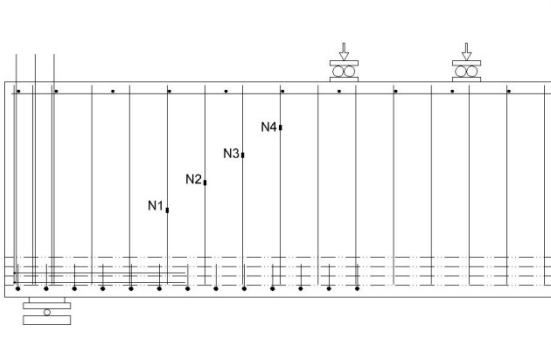
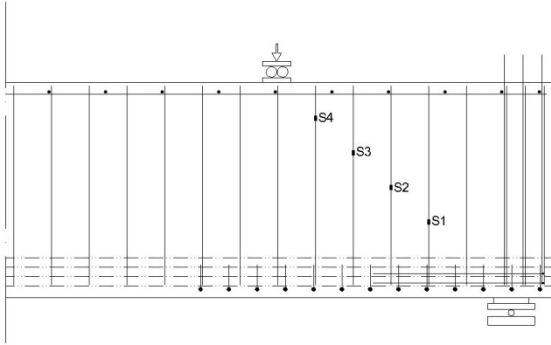
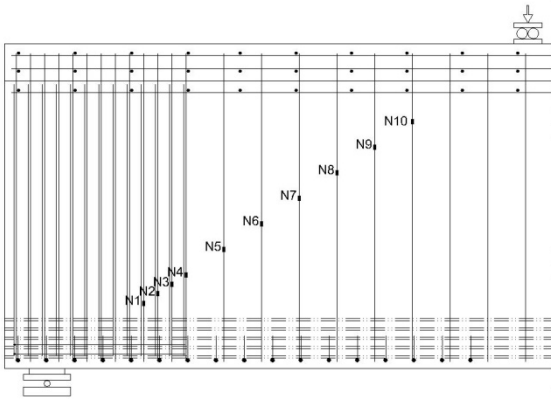
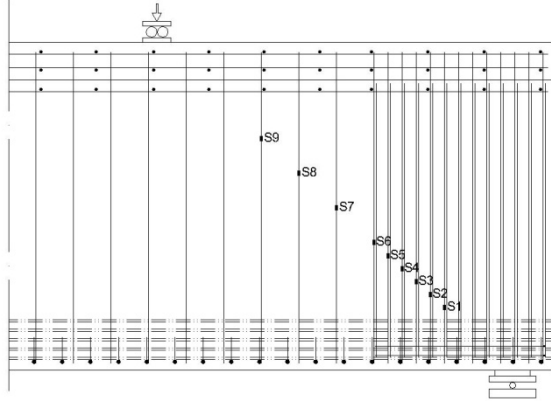
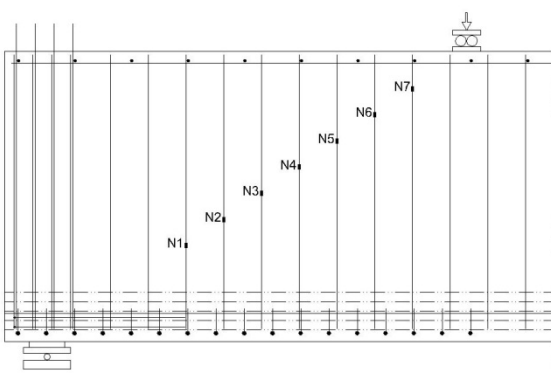
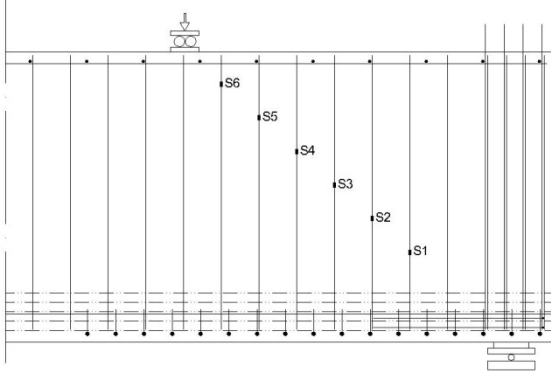
	North	South
G1	 <p>Diagram of the North side of girder G1. The diagram shows a cross-section of the girder with a central downward load. Strain gauges are labeled N1, N2, N3, N4, and N5, positioned along the bottom reinforcement bars. N1 is at the left end, N2 is slightly right of N1, N3 is further right, N4 is to the right of N3, and N5 is at the far right end.</p>	 <p>Diagram of the South side of girder G1. The diagram shows a cross-section of the girder with a central downward load. Strain gauges are labeled S1, S2, S3, and S4, positioned along the bottom reinforcement bars. S1 is at the right end, S2 is slightly left of S1, S3 is further left, and S4 is at the far left end.</p>
G2	 <p>Diagram of the North side of girder G2. The diagram shows a cross-section of the girder with a central downward load. Strain gauges are labeled N1, N2, and N3, positioned along the bottom reinforcement bars. N1 is at the left end, N2 is slightly right of N1, and N3 is further right.</p>	 <p>Diagram of the South side of girder G2. The diagram shows a cross-section of the girder with a central downward load. Strain gauges are labeled S1 and S2, positioned along the bottom reinforcement bars. S1 is at the right end, and S2 is slightly left of S1.</p>
D1	 <p>Diagram of the North side of girder D1. The diagram shows a cross-section of the girder with a central downward load. Strain gauges are labeled N1, N2, N3, N4, N5, N6, N7, and N8, positioned along the bottom reinforcement bars. N1 is at the left end, N2 is slightly right of N1, N3 is further right, N4 is to the right of N3, N5 is to the right of N4, N6 is to the right of N5, N7 is to the right of N6, and N8 is at the far right end.</p>	 <p>Diagram of the South side of girder D1. The diagram shows a cross-section of the girder with a central downward load. Strain gauges are labeled S1, S2, S3, S4, S5, S6, S7, and S8, positioned along the bottom reinforcement bars. S1 is at the right end, S2 is slightly left of S1, S3 is further left, S4 is to the left of S3, S5 is to the left of S4, S6 is to the left of S5, S7 is to the left of S6, and S8 is at the far left end.</p>

Table 6.2-Cont. Strain Gauges Names and Locations

	North	South
D2		
E1		
E2		

A set of six LVDTs were used in a rosette formation as shown in Fig. 6.21 to measure the average or the smeared strain in concrete within the expected failure region of the girder-web on

both faces (i.e., west and east) and on both ends of the girder. The strain in the web in certain direction is calculated by taking the average of the readings giving by the pair of LVDTs on both faces (i.e., west and east) of the web. Table 6.3 summaries the names of each LVDT and location of the LVDTs rosset for both ends of each girder.

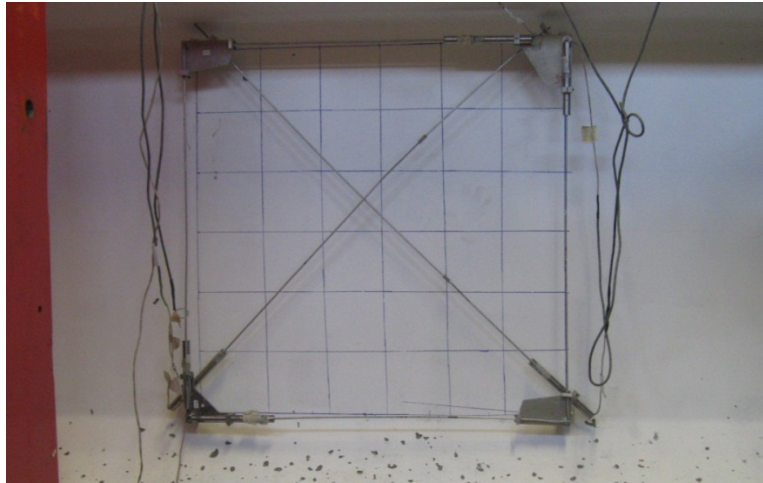


Fig. 6.21 LVDT Rosette Installed on Girders

Eight LVDTs were positioned on selected tendons against the concrete surface to measure their slip. Because the shear bond failure is known for the crushing of concrete at the intersection between the bottom flange and the web, which indicates that the most effective tendons are the closest ones to that location, six LVDTs were posted on selected tendons of the closest row to the web against the concrete surface. Two additional LVDTs were posted on the closest two tendons to the web center in the bottom row. Fig. 6.22 shows the LVDTs' location on both the north and south ends for each girder. These LVDTs were leveled and tied mechanically to the selected tendons against the concrete surface to ensure their free movement with the tendons in the case of any slippage, as shown in Fig. 6.23.

Table 6.3 LVDTs Names and Locations

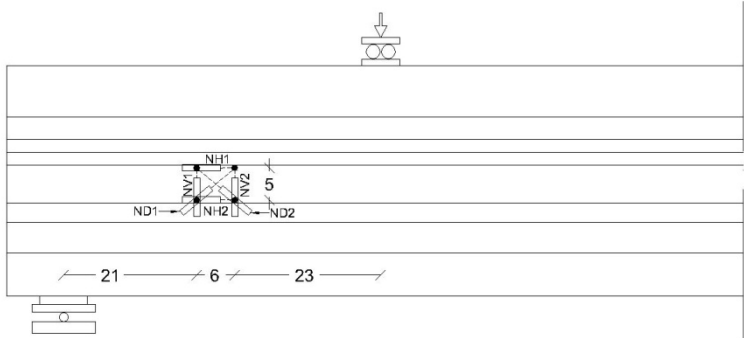
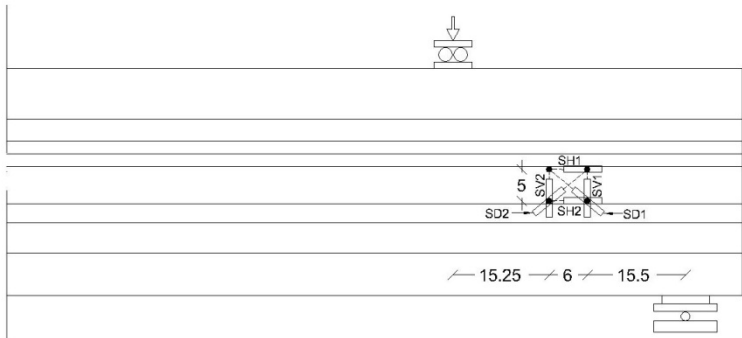
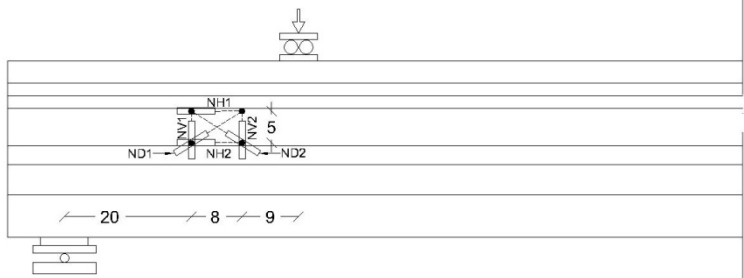
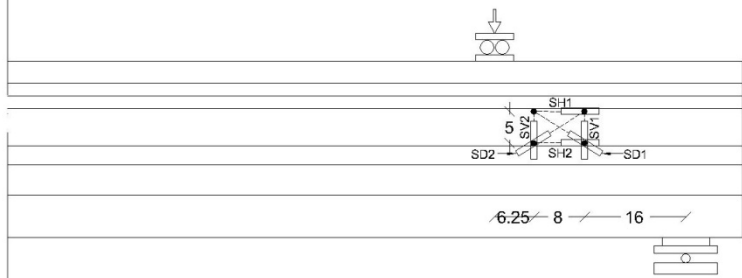
Girder	North	South
G1		
G2		

Table 6.3-Cont. LVDTs Names and Locations

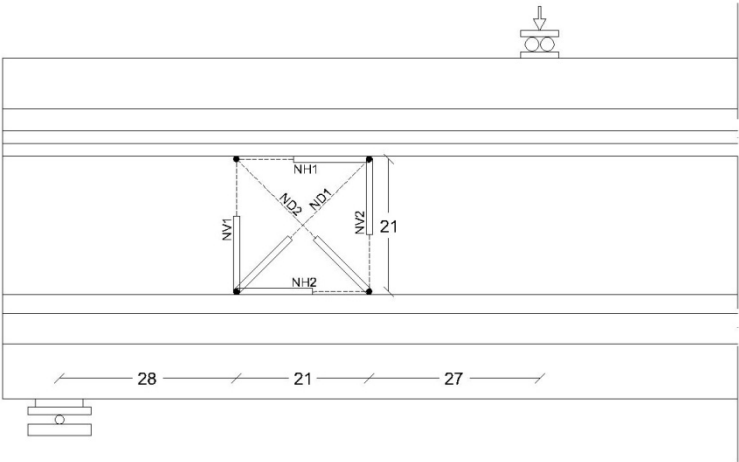
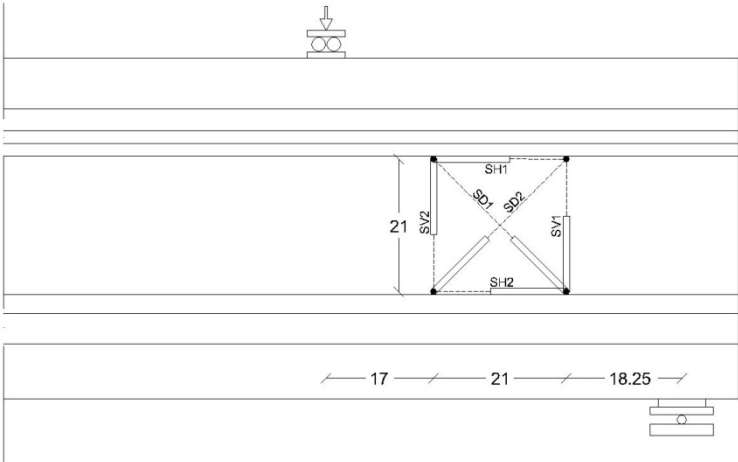
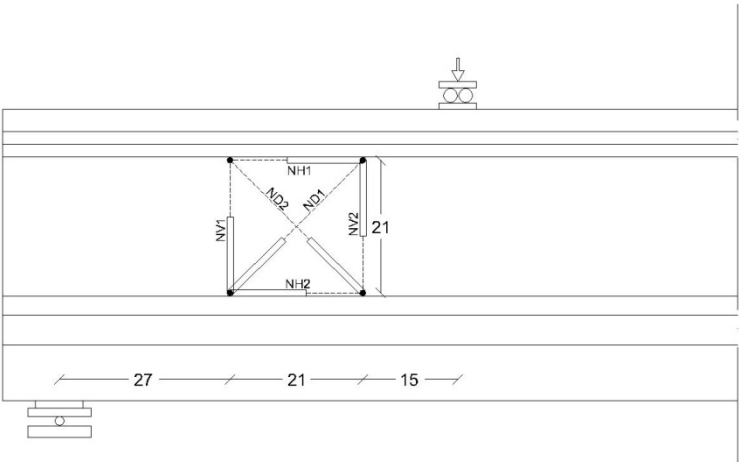
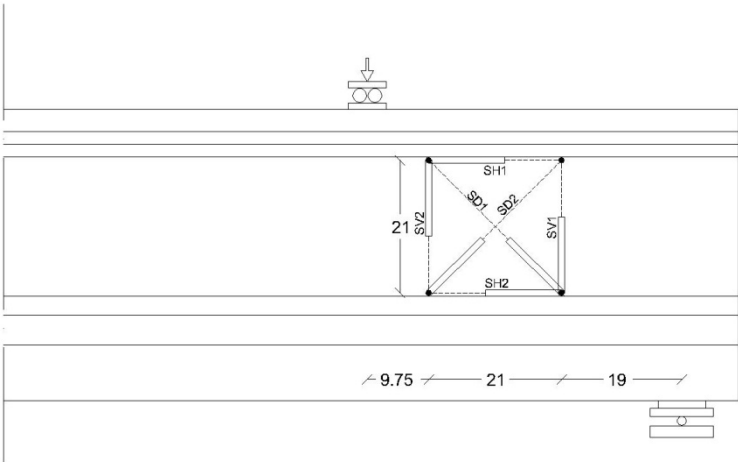
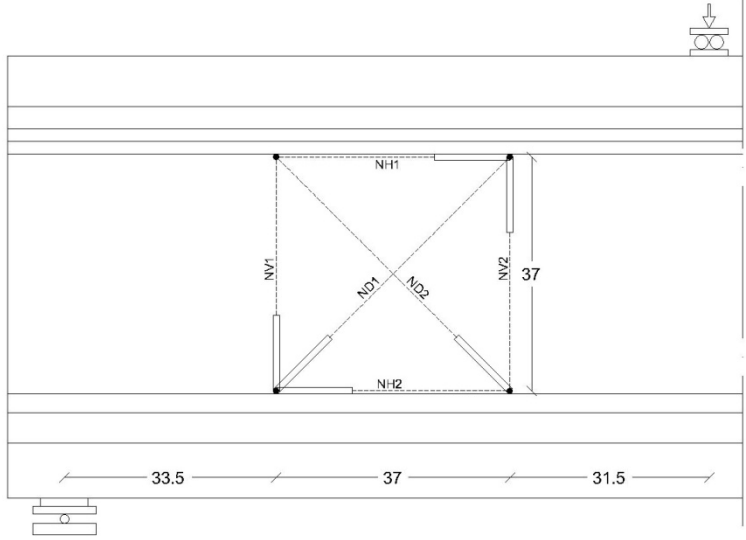
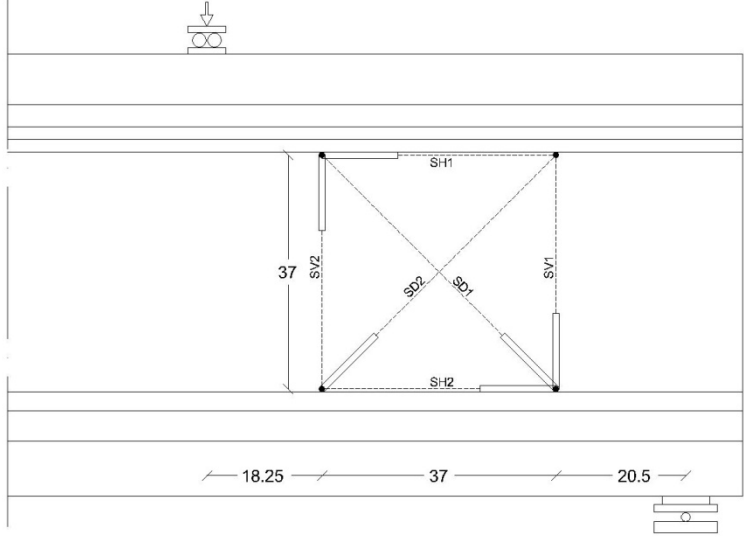
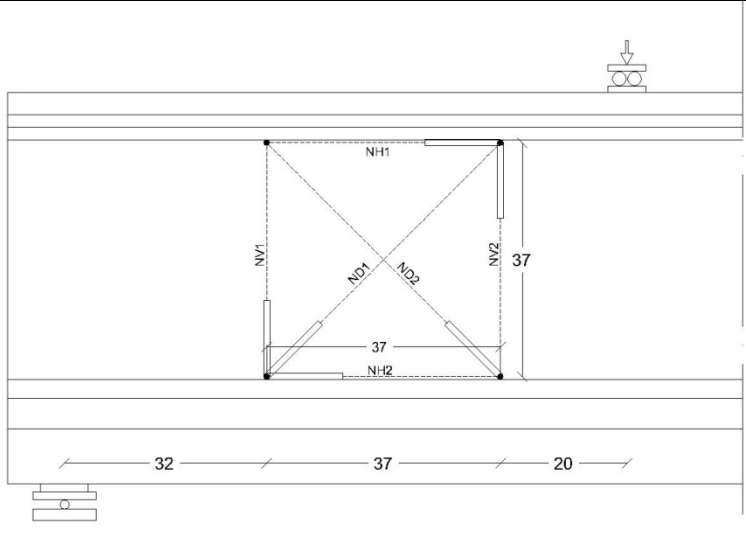
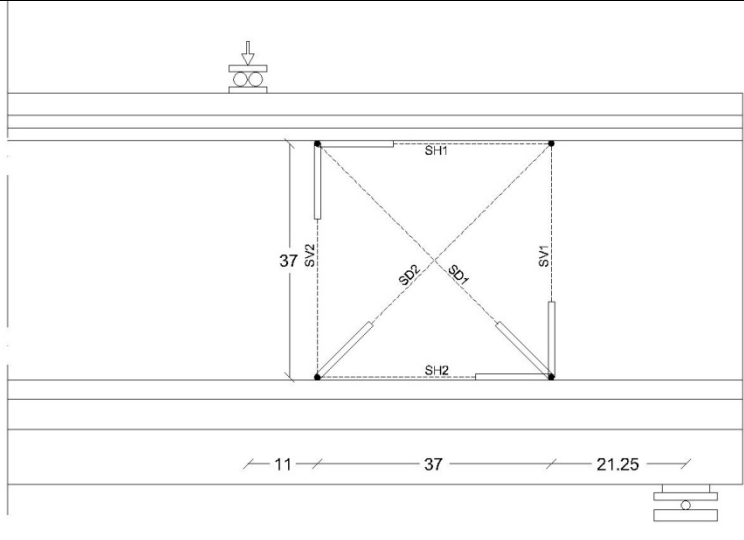
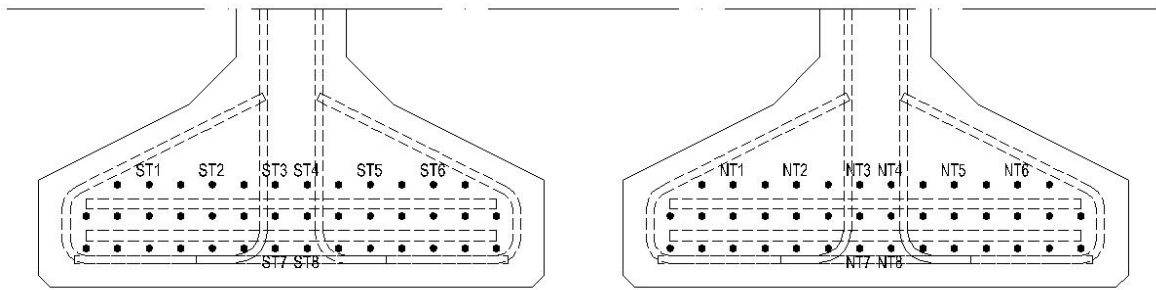
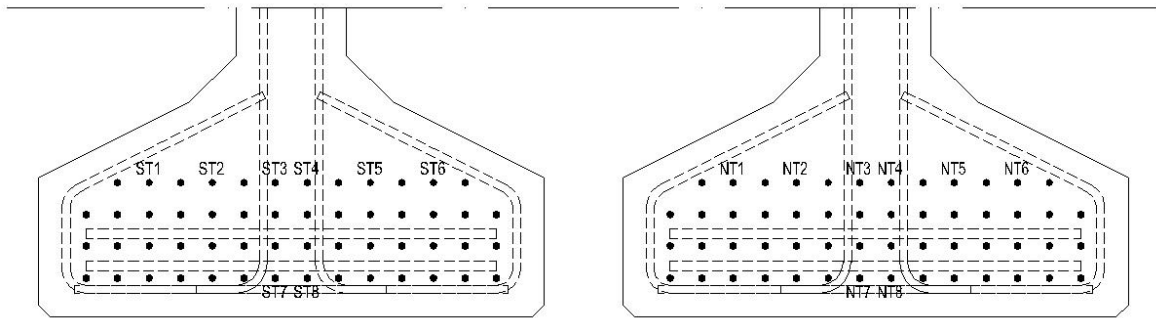
Girder	North	South
D1		
D2		

Table 6.3-Cont. LVDTs Names and Locations

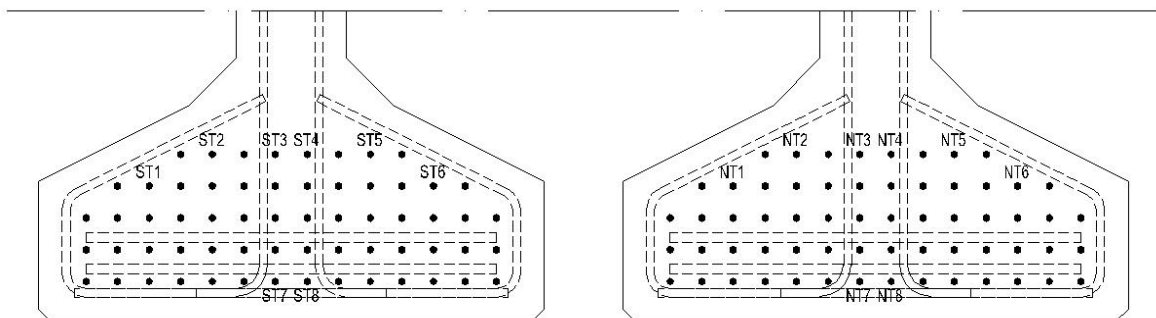
Girder	North	South
E1		
E2		



(a) Girder Tx28



(b) Girder Tx46



(c) Girder Tx62

Fig. 6.22 LVDTs Names on Selected Tendons to Measure Slip

Six LVDTs placed under the girder were used to measure the vertical displacement, i.e., deflection of the girder during the test. Two of the six LVDTs were positioned under the applied load on the east and west sides to measure the average total deflection of the girder as the load increases while the other four were located next to the north and south supports, i.e., two on both sides (i.e., west and east) of each support, to measure the average settlement of each support as the load increases. Thus the net deflection of the girder can be calculated by subtracting the average settlement of the supports of the total average deflection under actuator.

On an average, each girder was instrumented with 38 LVDTs and several strain gauges. Data from all the above discussed sensors was continuously monitored and stored by HBM ‘Spider-8’ Data Acquisition System. Shear and flexure cracks formed on the girder during the load test were regularly marked on a grid.



Fig. 6.23 LVDTs to Measure Slip

CHAPTER 7 SHEAR-BOND FAILURES VERSUS WEB-SHEAR FAILURE

7.1. Introduction

Six girders with three different sizes were manufactured and tested as discussed in Chapter 6. This chapter presents the experimental results of each girder. This includes the shear force versus net deflection curves, the average local strain in the transverse steel, and the bond slip recorded by LVDTs attached previously to selected tendons. Also, the test procedure and the mechanism of failure for each girder will be discussed in detail. In addition, photos for the final failure for each end of each girder are presented.

The experimental data presented in this chapter will be used to validate Laskar's (2010) maximum shear strength equation for different sizes of prestressed girders and the concrete contribution equation for shear span to depth ratio less than 1.6.

7.2. Experimental Results of Group G Girders

As reminder, this group of girders consists of two girders Tx28. The first girder named G1 was reinforced in transverse direction according to TxDOT specifications. The second girder named G2 was reinforced in the transverse direction with the minimum reinforcement according to AASHTO (2010). Girder G1 had a top slab with eight inch thickness while Girder G2 did not.

7.2.1. Girder G1

The north end of Girder G1 was tested first with shear span to depth ratio (a/d) 1.58. Because the failure affected the stability of the girder, it was decided to retest the girder on the south end after moving north support after the zone of failure resulting in a net span of 16 ft. The girder was loaded on the south end having shear span to depth ratio (a/d) 1.15. Fig. 7.1 shows the shear force versus the net deflection for both ends. It can be seen that the south end had a stiffer curve due to using shorter span and smaller shear span to depth ratio.

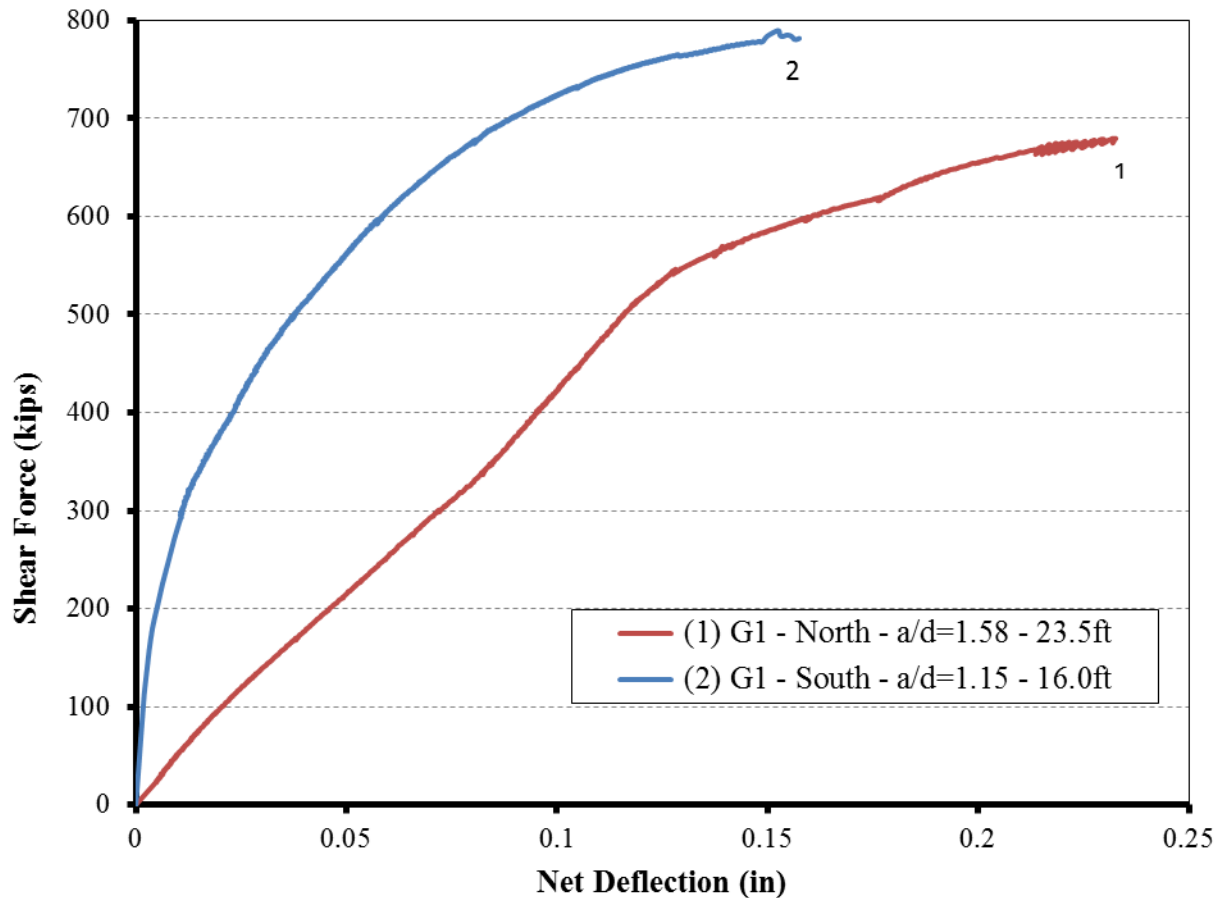


Fig. 7.1 Shear Force vs. Beam Deflection Curves for Girder G1

The first shear crack has been seen at the north end at shear load 206 kips, Fig. 7.2 (a). With increasing the load, cracks were observed on the south end at a shear force on the north end around 500 kips while the corresponding shear force at the south end was around 120 kips. With increasing the applied load on the north end shear cracks were seen at the south end, as shown in Fig. 7.2 (b). After the failure of the north end and moving the north support, the south end was reloaded to have the first new crack at shear force 213 kips. Fig. 7.2 (c) and (d) shows the final crack pattern at each end before failure.

Figs. 7.3 and 7.4 show the measured slip at selected tendons. It can be seen that the maximum value at the north end was 0.019 inch at NT4, while at the south end it was 0.026 inch at ST6. This small slip did not contribute to the failure either of them, and both north and south ends failed finally due to concrete crushing in the web exhibiting a very clear web shear failure under a total shear load of 679.65 and 789.66 kips, respectively.

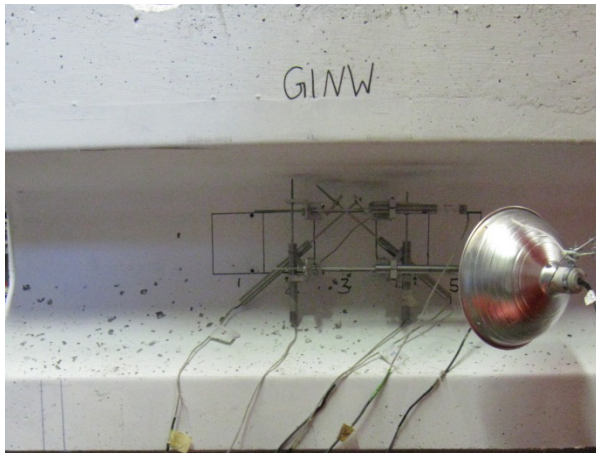
Fig. 7.5 shows the smeared strains in concrete at the north end. It shows that the actual cracking of the web happened under a shear load around 150 kips. The delay in showing the crack at the surface may be due to the huge volume of the flanges comparing to the web and because the crack was passing through heavily reinforced region in the transverse direction.

Also, the existence of these huge flanges and the huge percentage of transverse steel helped in strengthening the concrete struts allowing the girder to reach higher smeared compressive strains. Figs. 7.5 (a) and (b) show that the smeared tensile strain across the shear cracks at the north end reached 0.0094 while the corresponding smeared compressive strain in the concrete struts reached 0.0023. The maximum smeared tensile strain in the transverse and longitudinal directions was 0.0099 (measured by LVDT NV1), and 0.0034 (measured by LVDT NH1) respectively, as shown in Figs. 7.5 (c) and (d). Generally, the values of smeared tensile strains are higher than what was expected. This is due to the bulky top and bottom flanges. The depth of these flanges, especially the top flange, contributes toward the shear strength. Their huge width prevents the propagation of shear cracks resulting in a concentration of tensile strains in the web.

The smeared strains at the south end were collected during testing the north end. Fig. 7.5 shows that, in general, strains at the south end were minor. Fig. 7.6 shows the smeared strains in the web at the south end during testing. Because of some cracks due to testing the north end and the compacted web, only the transverse smeared tensile strain could reflect the appearance of the new shear crack at a shear force of 242 kips crossing LVDT SV1, as shown in Fig. 7.6 (c). The higher smeared tensile strain at the peak across shear cracks of 0.0124 softened the concrete struts resulting in crushing at lower smeared compressive strain of 0.0018, as shown in Fig. 7.6 (a) and (b). Fig. 7.6 (c) and (d) shows that the maximum smeared tensile strain in transverse and longitudinal directions was 0.0155 (measured by LVDT SV1) and 0.002 (measured by LVDT NH2), respectively.

Fig. 7.7 shows the local strain in the transverse reinforcement at both ends. Fig. 7.7 (a) shows that the average local strain at the north end measured by strain gauges was only $0.8 \varepsilon_y$. Fig. 7.7 (c) shows that the average local strain at the south end measured by strain gauges was $0.75 \varepsilon_y$.

North End



(a) First shear crack at 206 kips

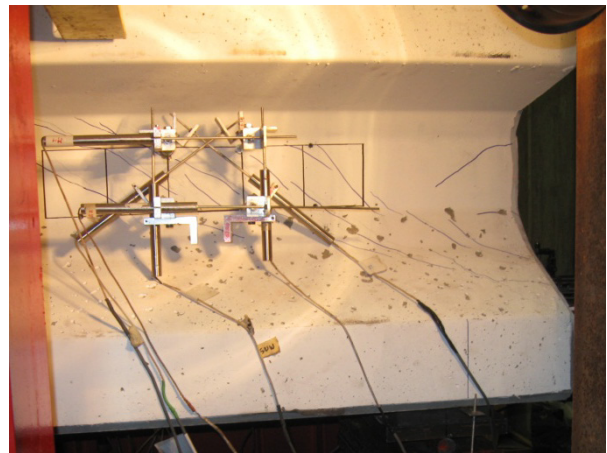
South End



(b) First shear crack at 213 kips



(c) Shear crack pattern before failure



(d) Shear crack pattern before failure



(e) Shear failure at 679.65 kips



(f) Shear failure at 789.66 kips

Fig. 7.2 Shear Crack Pattern and Failure Mode of Girder G1

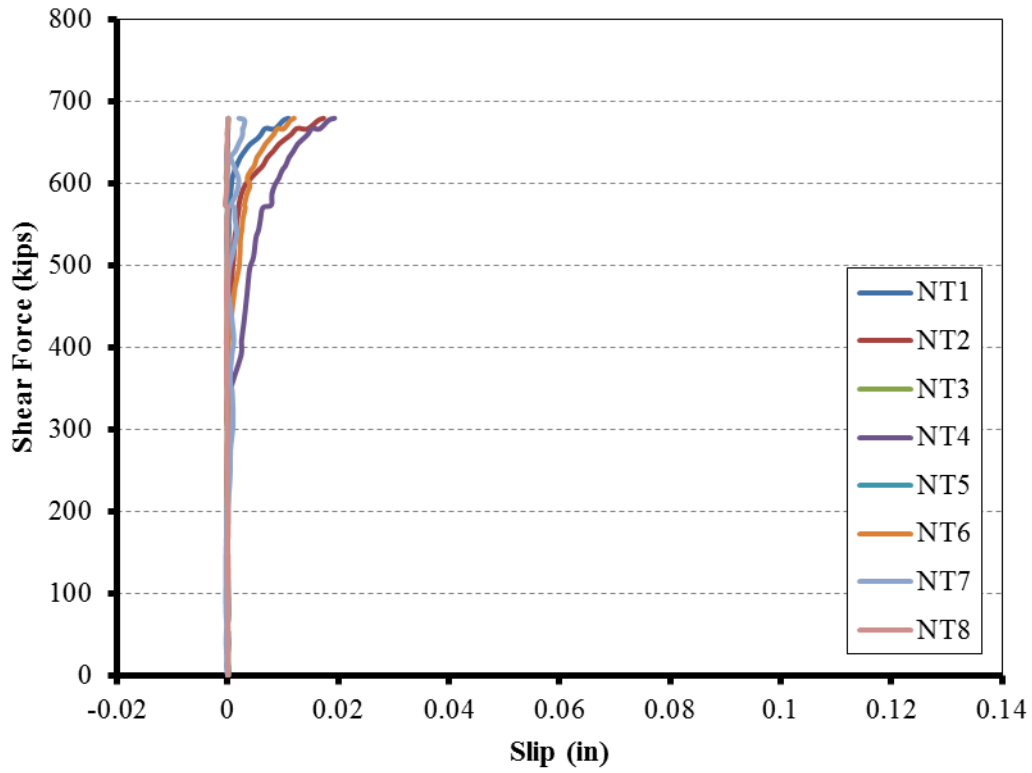


Fig. 7.3 Shear Force vs. Tendons Slip Curves for Girder G1-North

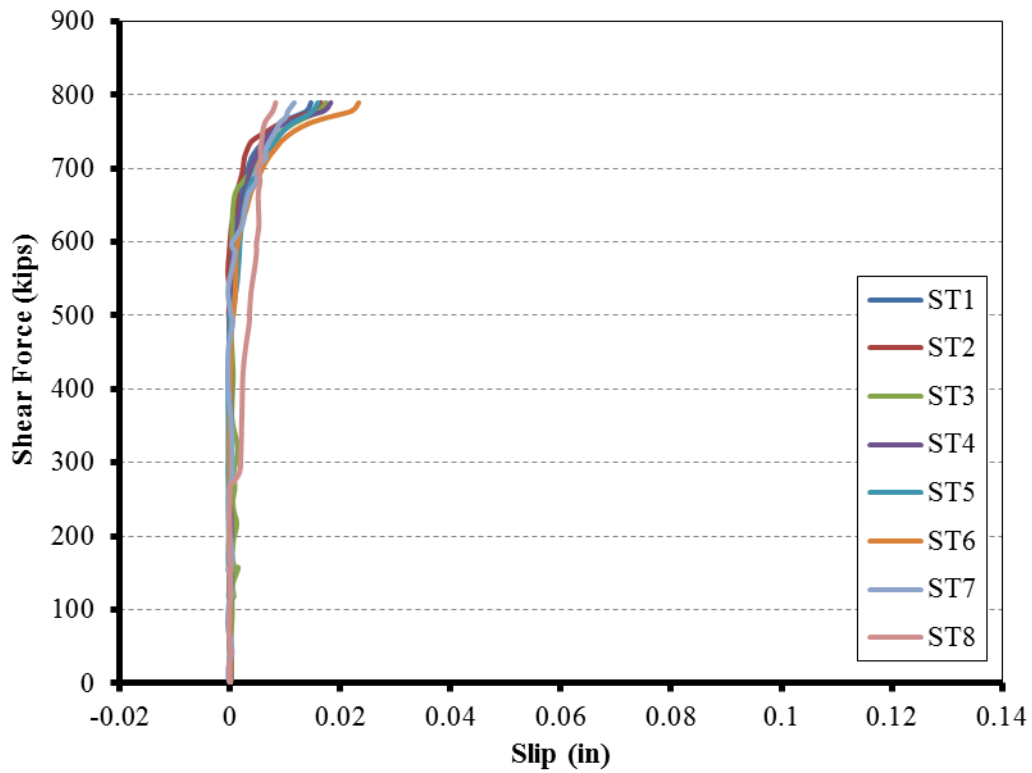
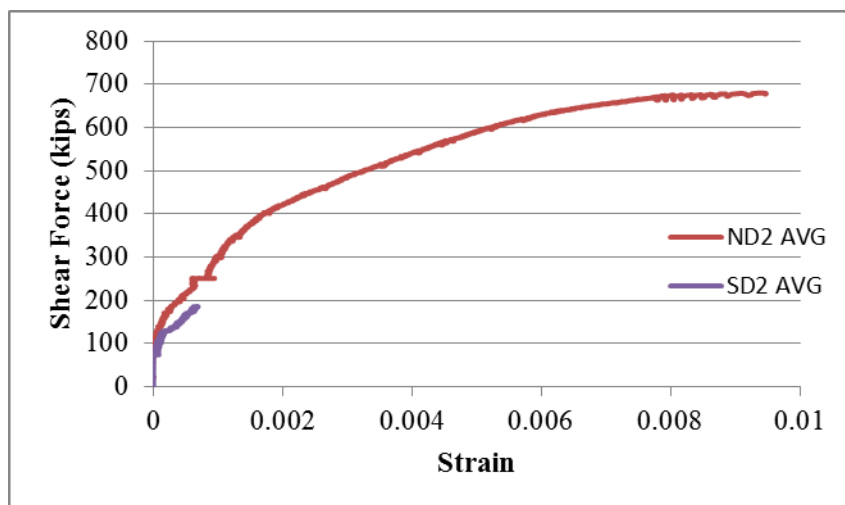
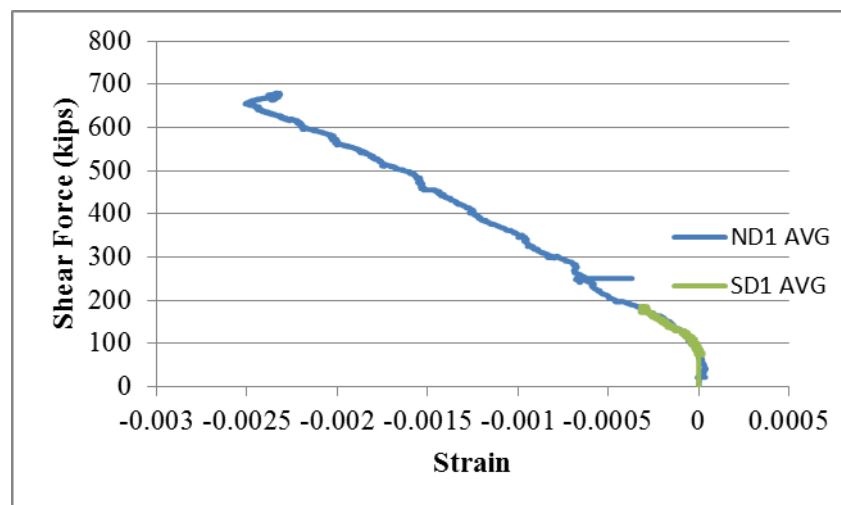


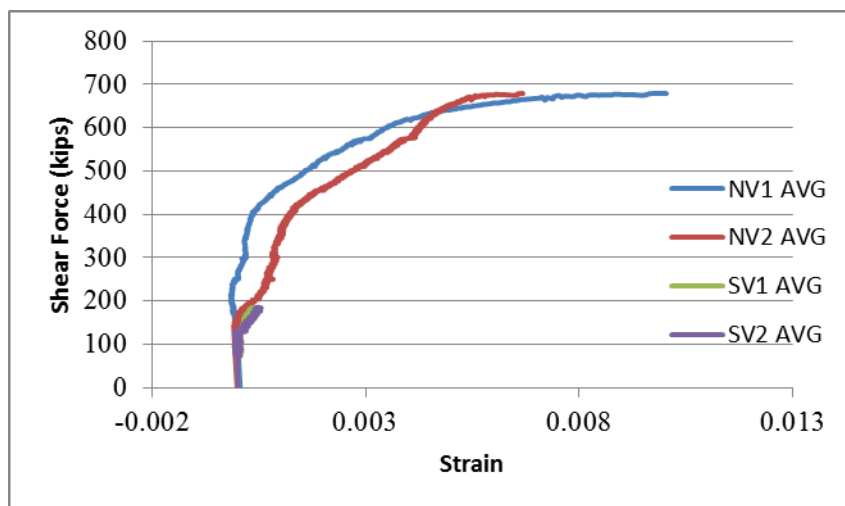
Fig. 7.4 Shear Force vs. Tendons Slip Curves for Girder G1-South



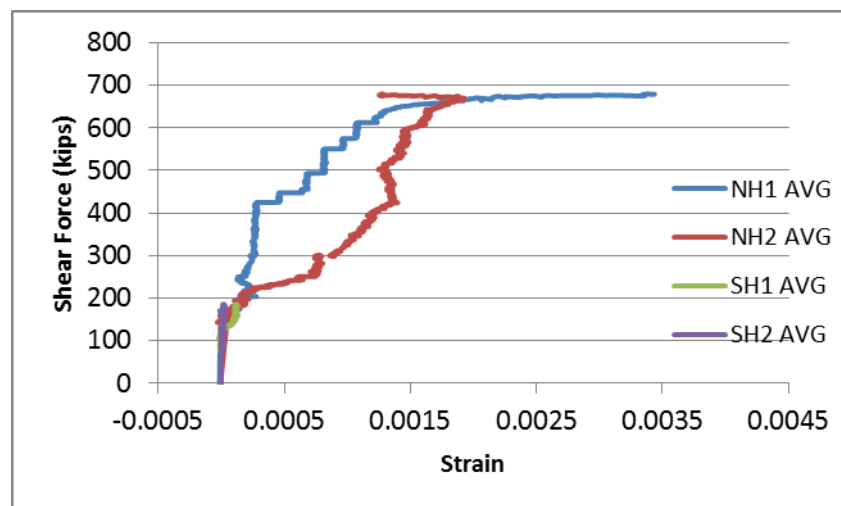
a - Average smeared tensile strain across Cracks



b - Average smeared compressive strain in concrete struts

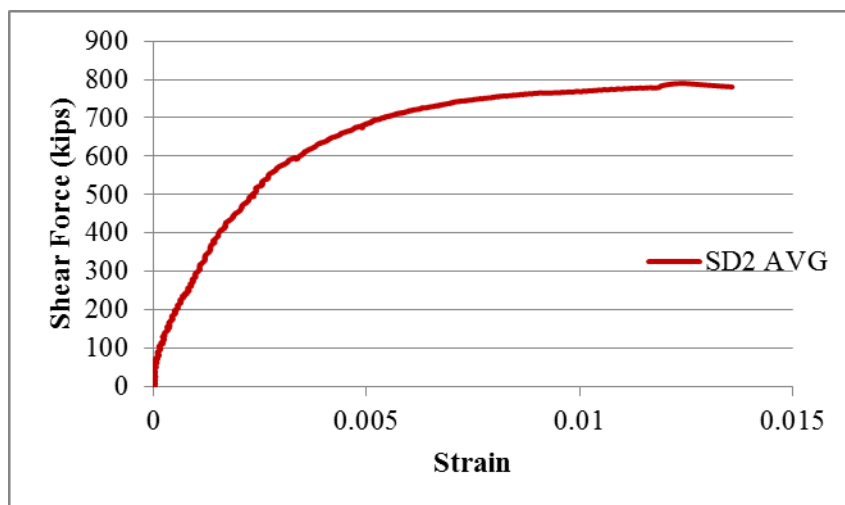


c - Average transverse smeared strain

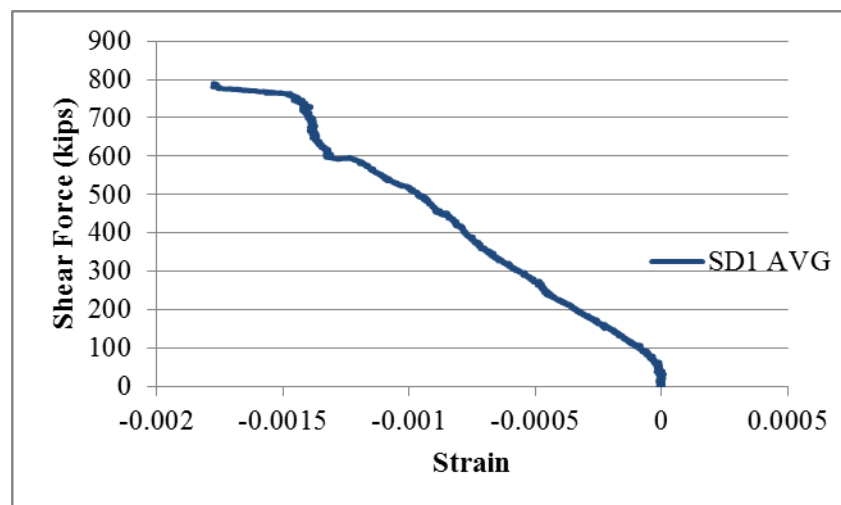


d - Average longitudinal smeared strain

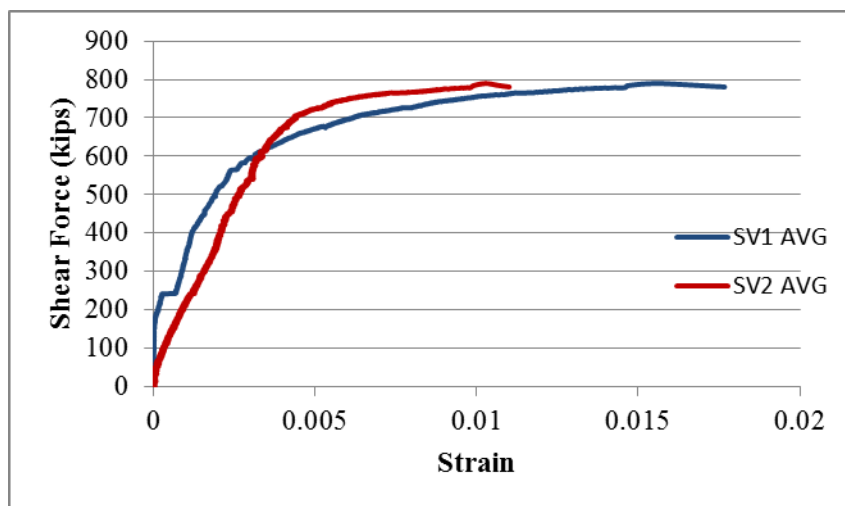
Fig. 7.5 Shear Force vs. Concrete Smeared Strains Curves for Girder G1 (North End Test)



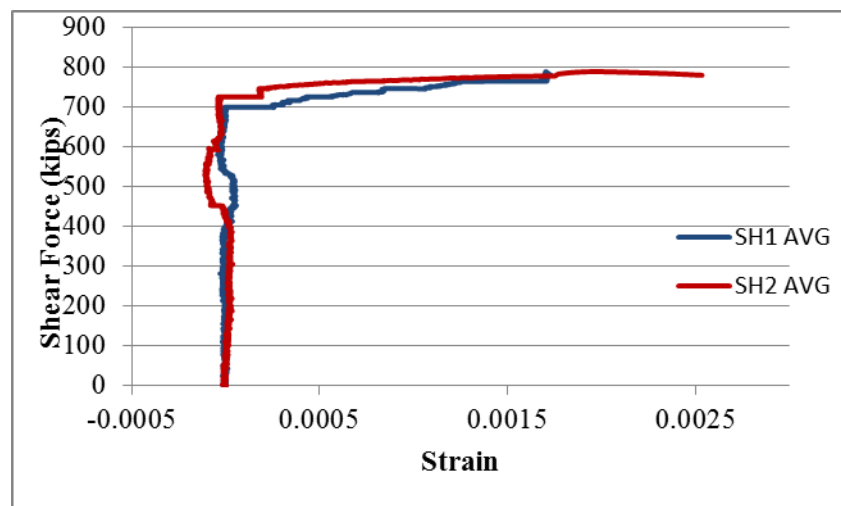
a - Average smeared tensile strain across Cracks



b - Average smeared compressive strain in concrete struts

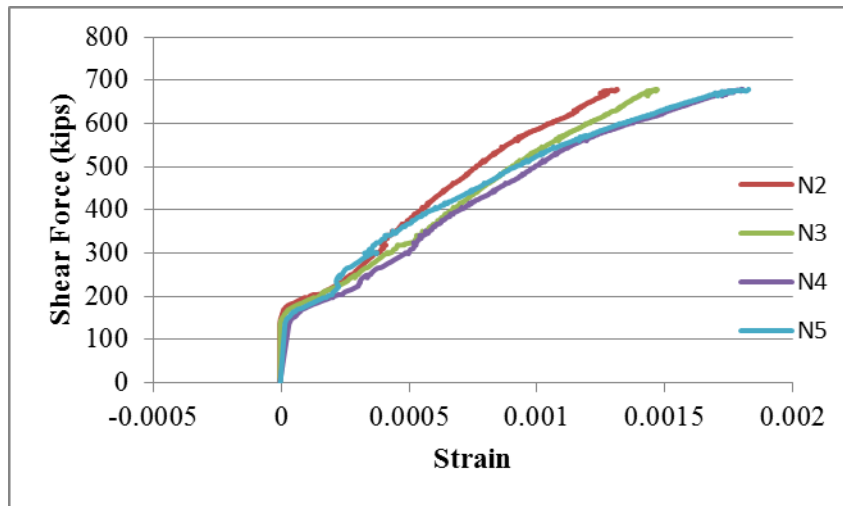


c - Average transverse smeared strain

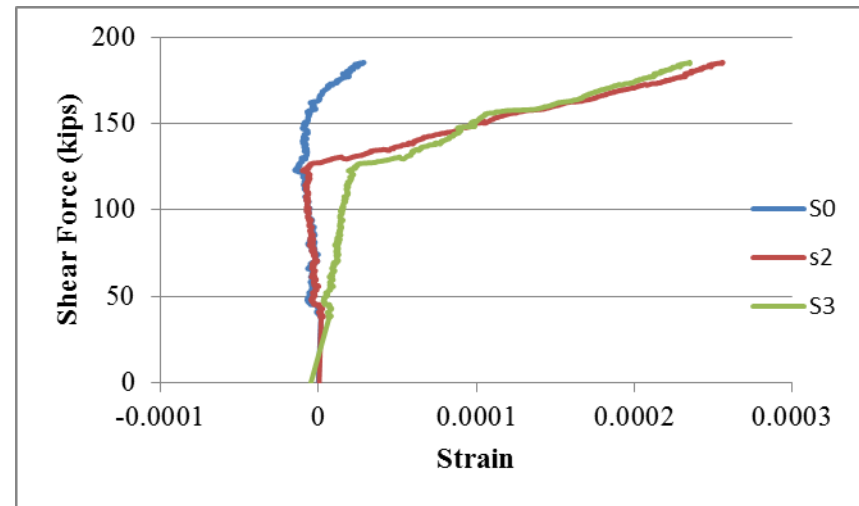


d - Average longitudinal smeared strain

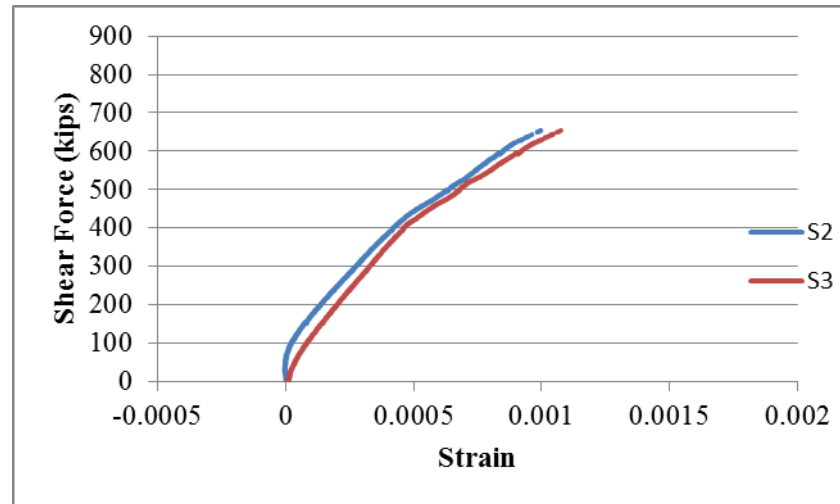
Fig. 7.6 Shear Force vs. Concrete Smeared Strains Curves for Girder G1 (South End Test)



(a) North strain gauges during testing north end



(b) South strain gauges during testing north end



(c) South strain gauges during testing south end

Fig. 7.7 Shear Force vs. Local Transverse Tensile Strain of Girder G1 (South End Test)

7.2.2. Girder G2

The north end of Girder G2 was tested first with shear span to depth ratio (a/d) 1.57. Because the failure did not affect the stability of the girder, it was decided to continue retesting the south end having the same net span without moving the north support. The girder was loaded on the south end with a shear span to depth ratio (a/d) 1.28. Fig. 7.8 shows the shear force versus the net deflection for both ends. It can be seen that the south end had a stiffer curve due to using a smaller shear span to depth ratio.

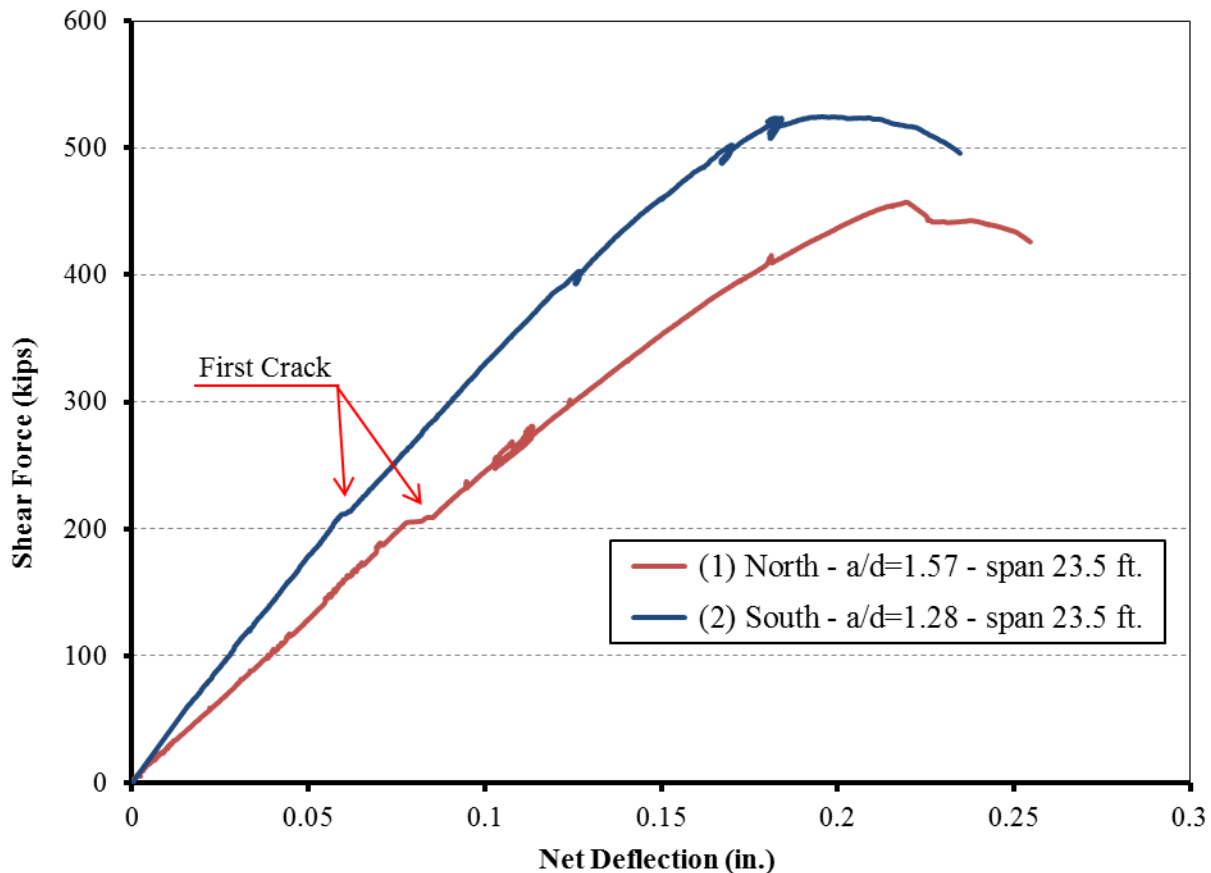


Fig. 7.8 Shear Force vs. Beam Deflection Curves for Girder G2

The first shear crack was seen at the north end at a shear load 206 kips, as shown in Fig. 7.9 (a). With increasing load, more cracks were developed in the web as seen in Fig. 7.9 (c) until the girder failed in web-shear at a shear load of 457.22 kips, as shown in Fig. 7.9 (e). During loading the north end no cracks were observed on the south end, which had a first crack at shear load of 213 kips while loading it. With increasing load at the south end, more cracks were developed in

the web as seen in Fig. 7.9 (d) until the girder failed in web-shear at a higher shear load of 524.64 Kips, shown in Fig. 7.9 (f), due to having a smaller shear span to depth ratio.

The measured slip at selected tendons, shown in Figs. 7.10 and 7.11, show that the maximum slip at the north end was 0.051 inch at NT4 comparing to 0.019 inch in Girder G1 at the same tendon, while at the south end it was 0.050 inch at ST3. This slip did not contribute to the failure at either end, and both north and south ends failed finally due to crushing of concrete struts in the web. Figs. 7.12 (a) and (b) show that the smeared tensile strain across the shear cracks at the north end reached 0.0068 while the smeared compressive strain in the concrete struts reached 0.0023. Figs. 7.13 (a) and (b) show that at the south end the smeared tensile strain across the shear cracks reached 0.0095 while the smeared compressive strain in the concrete struts reached 0.0022.

Fig. 7.12 (c) shows the smeared tensile strain in the transverse direction at the north end was higher closer to the support having a maximum value of 0.0038. Fig. 7.14 (a) shows the local strain in the transverse reinforcement at north end. The strain gauge readings indicated that the average local strain was only $0.8 \epsilon_y$. The fact that minimum reinforcement was used implies that the strain gauges have missed the main cracks and hence missed the peak strain. The assumption of yielding of transverse steel will be used in calculating the steel and concrete contribution later.

Fig. 7.13 (c) shows the smeared strains in the web at the south end. It can be seen that it had a higher smeared transverse tensile strain of 0.0048 than that at the north end. Fig. 7.14 (b) shows the local strain in the transverse reinforcement at south end. The strain gauges stopped working before reaching the failure point. Based on the trend of the plotted curves, it can be confidently presumed that the transverse reinforcement was approaching the yielding strain at the failure point.

Fig. 7.12 (d) shows the smeared strain in the longitudinal direction at the north end. It shows a minor smeared strain at the top of the web, while the bottom of the web had a higher tensile strain about 0.003. The difference in the behavior can be explained by the flexure behavior effect. Fig. 7.13 (d) shows the smeared strain in the longitudinal direction at the south end. The top of the web had a very minor smeared strain until before the failure. Then tensile strains developed due to many cracks crossing LVDT SH1 reaching a maximum smeared tensile strain of 0.0054 at the peak.

North End



(a) First shear crack at 206 kips



(c) Shear crack pattern before failure



(e) Shear failure at 457.22 kips

South End



(b) First shear crack at 213 kips



(d) Shear crack pattern before failure



(f) Shear failure at 524.64 kips

Fig. 7.9 Shear Crack Pattern and Failure Mode of Girder G2

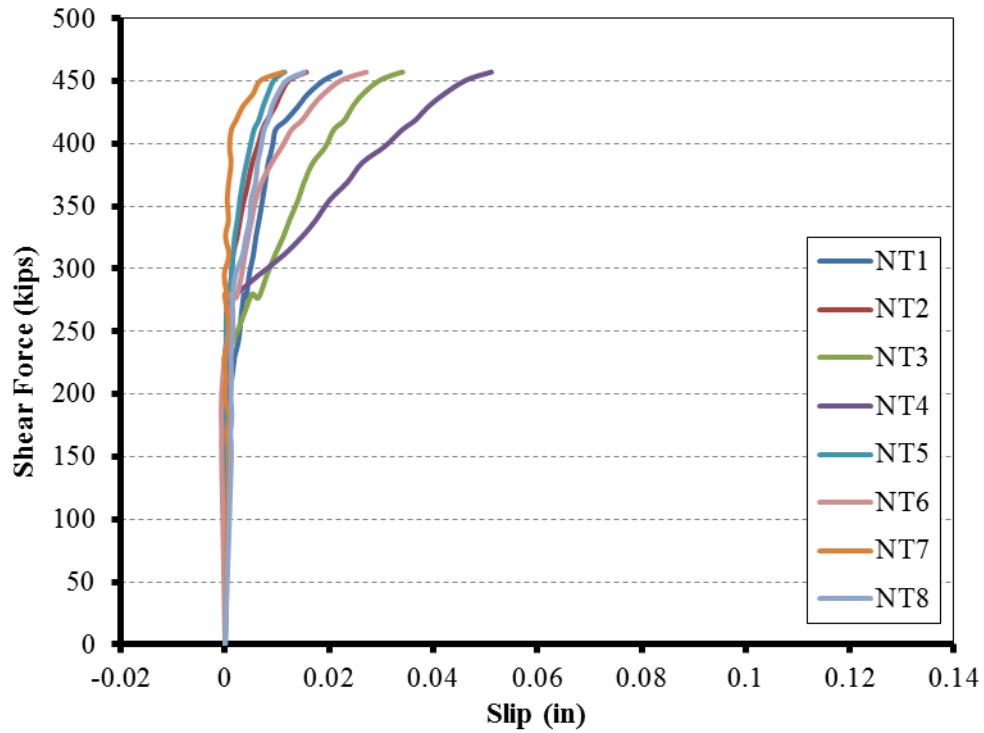


Fig. 7.10 Shear Force vs. Tendons Slip Curves for Girder G2-North

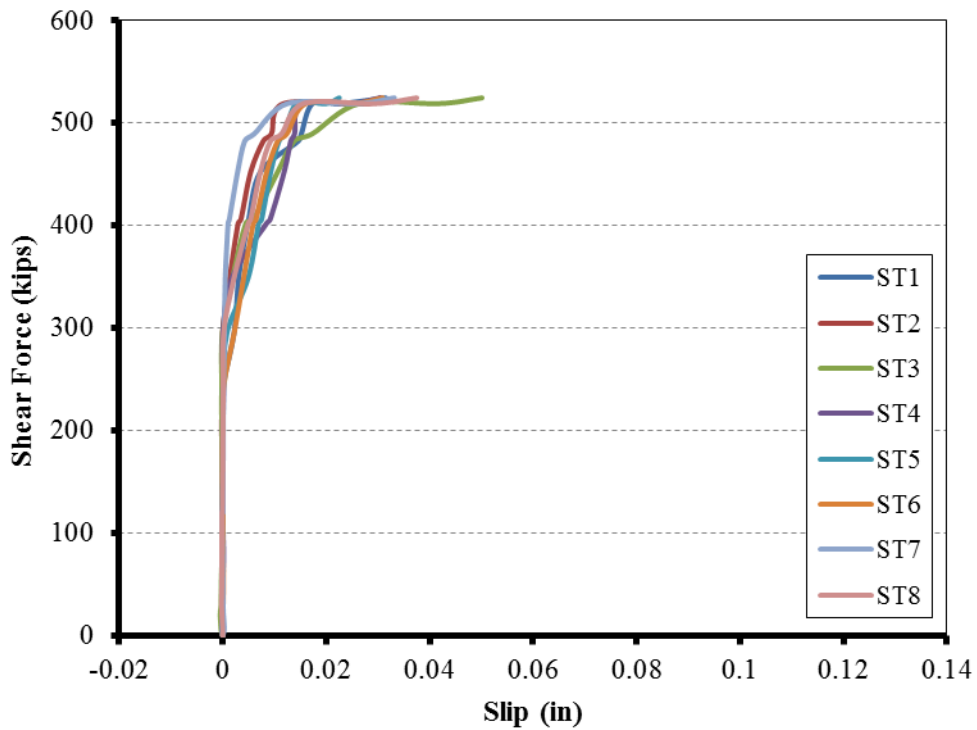
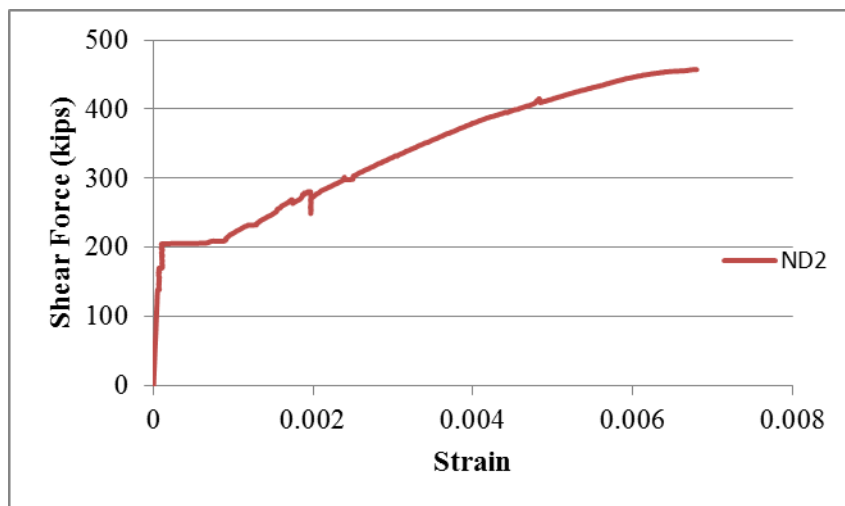
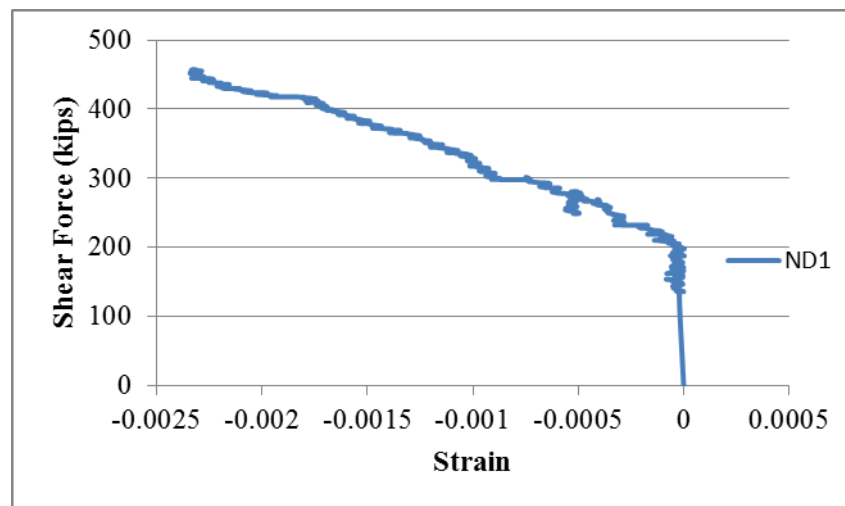


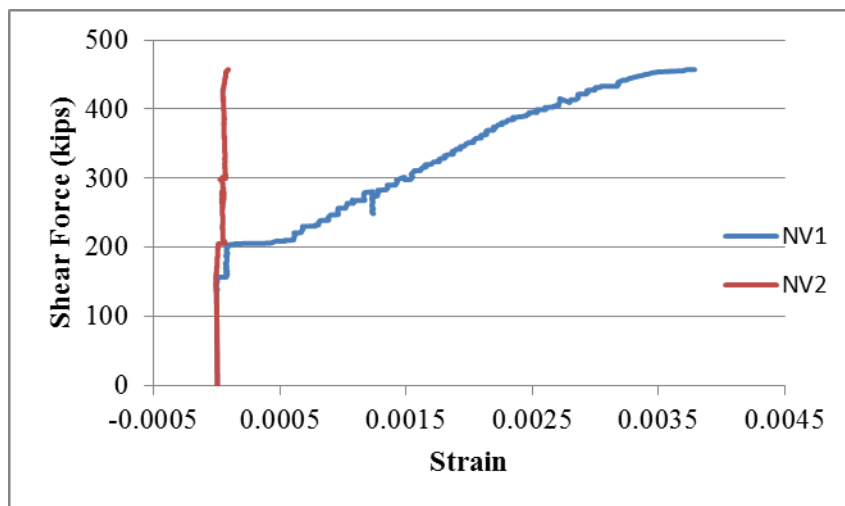
Fig. 7.11 Shear Force vs. Tendons Slip Curves for Girder G2-South



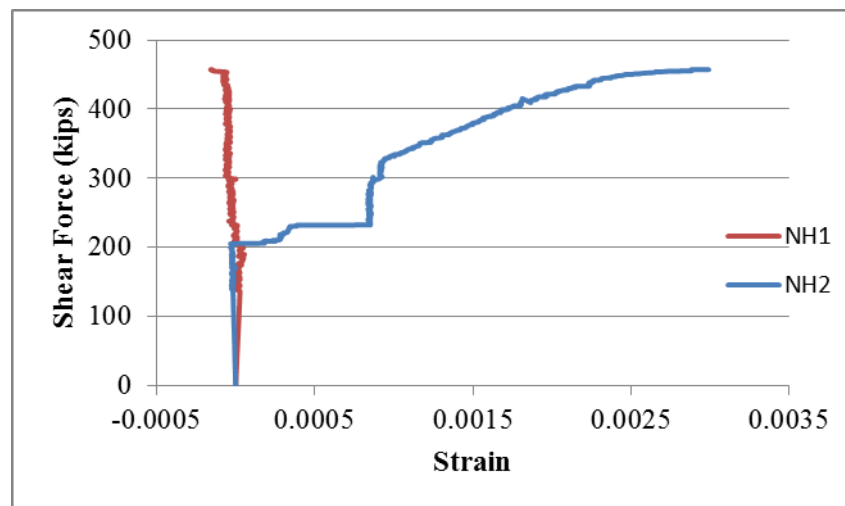
a - Average smeared tensile strain across Cracks



b - Average smeared compressive strain in concrete struts

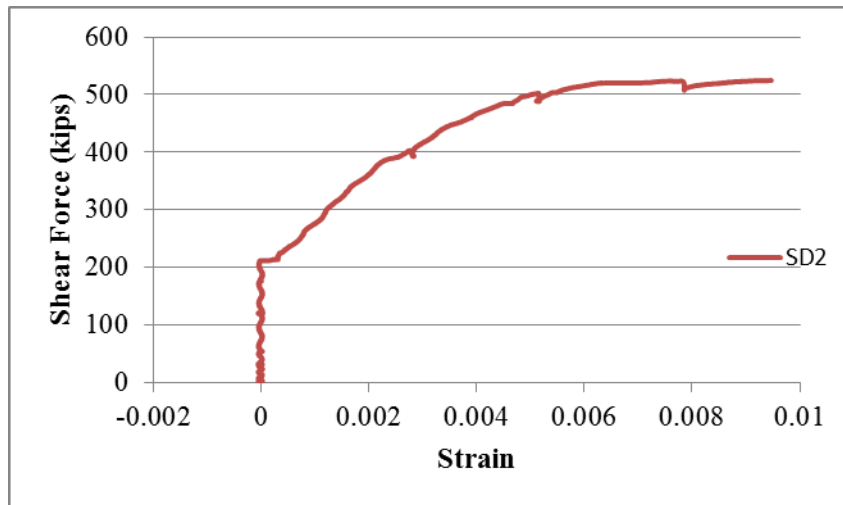


c - Average transverse smeared strain

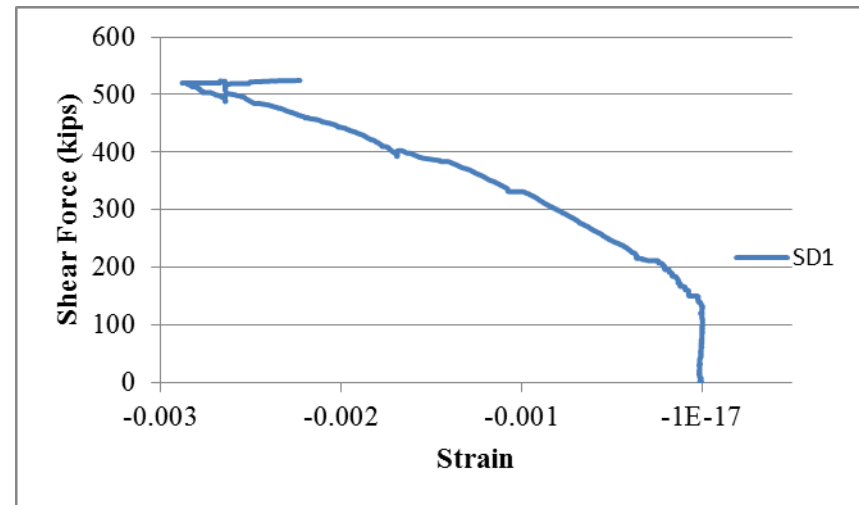


d - Average longitudinal smeared strain

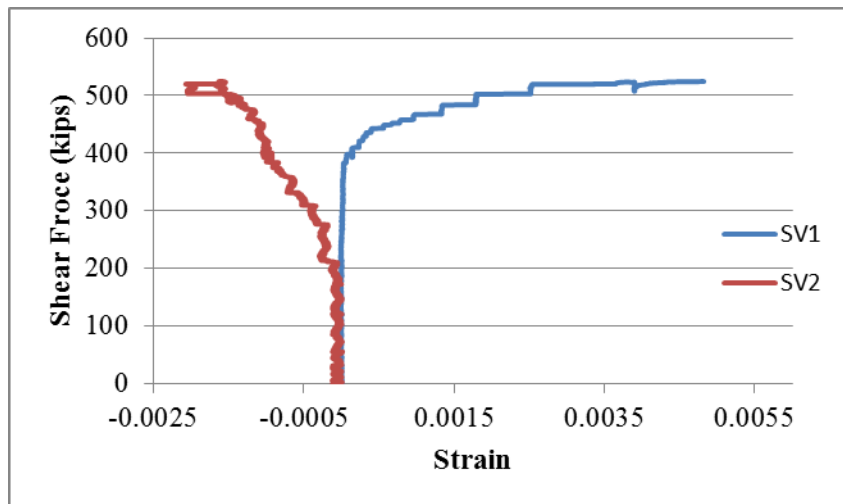
Fig. 7.12 Shear Force vs. Concrete Smeared Strains Curves for Girder G2 (North End Test)



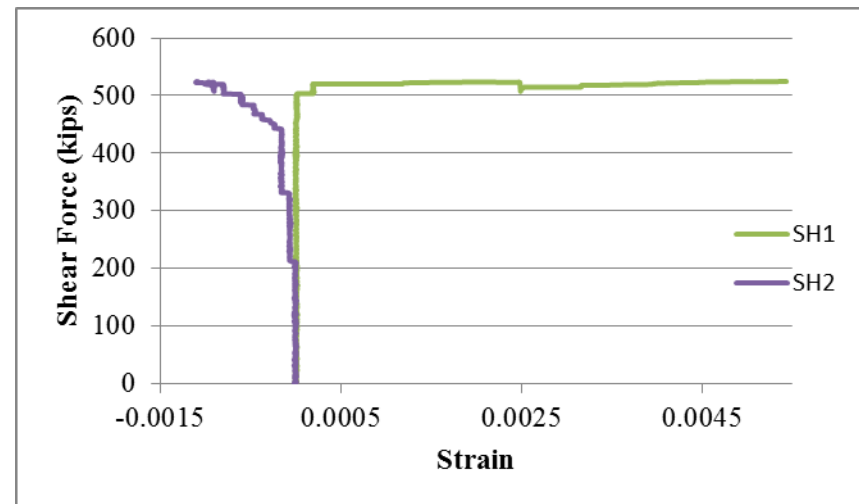
a - Average smeared tensile strain across Cracks



b - Average smeared compressive strain in concrete struds

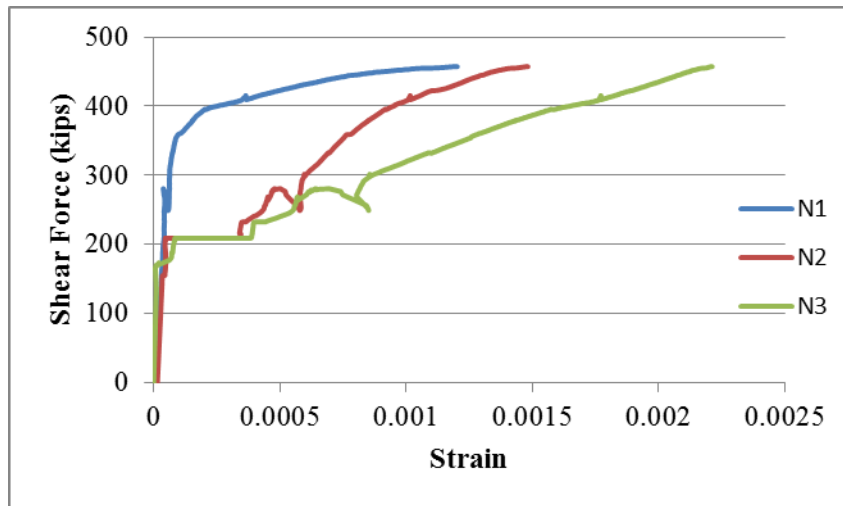


c - Average transverse smeared strain

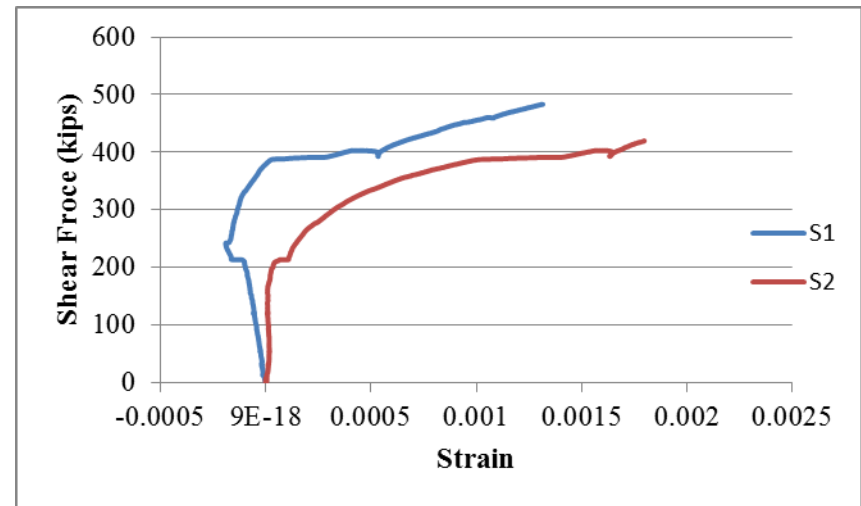


d - Average longitudinal smeared strain

Fig. 7.13 Shear Force vs. Concrete Smeared Strains Curves for Girder G2 (South End Test)



(a) North strain gauges during testing north end



(b) South strain gauges during testing south end

Fig. 7.14 Shear Force vs. Local Transverse Tensile Strain of Girder G2

7.3. Experimental Results of Group D Girders

Two girders Tx46 are studied in this group. The first girder named D1 was reinforced in transverse direction typically according to TxDOT specifications. The second girder named D2 was reinforced in the transverse direction with the minimum reinforcement according to AASHTO (2010). Girder D1 had a top slab with eight inch thickness while Girder D2 did not.

7.3.1. Girder D1

The south end of Girder D1 was tested first with a shear span to depth ratio (a/d) 1.16. Because the failure did not affect the stability of the girder, The girder was reloaded on the north end with a shear span to depth ratio (a/d) 1.56 without moving south support. Fig. 7.15 shows the shear force versus the net deflection for both ends. It can be seen that the north end had less stiffness due to using larger shear span to depth ratio and due to the failure at the south end.

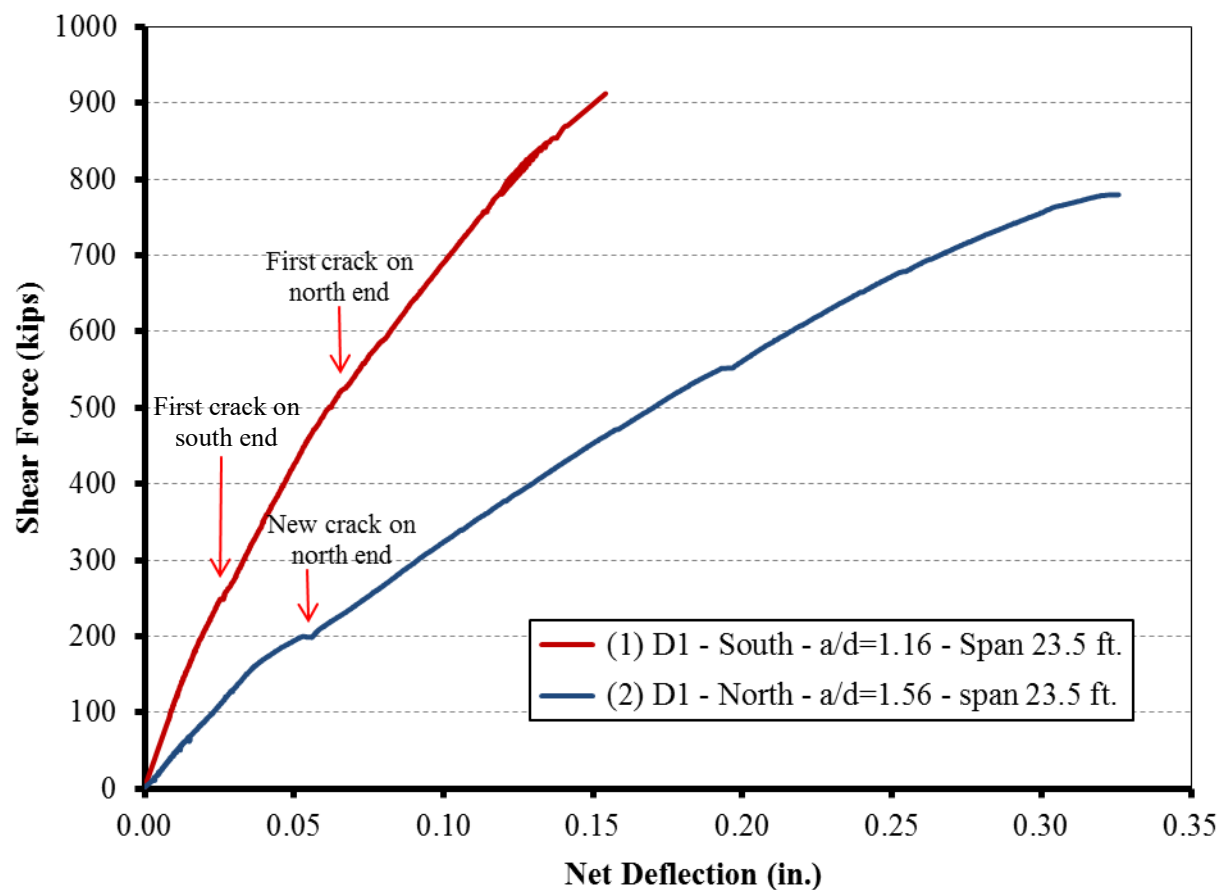


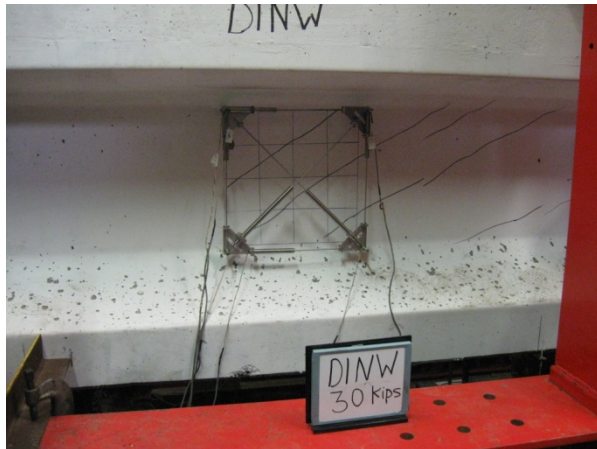
Fig. 7.15 Shear Force vs. Beam Deflection Curves for Girder D1

The first shear crack was seen at the south end at a shear force of 241 kips, as shown in Fig. 7.16 (b). With increasing the applied loads, new cracks were shown at the north end at a shear force of 170 kips on the north load cell. Fig. 7.16 (c) shows the final crack pattern the south end before the failure happen at a shear force of 912.78 kips. Then the girder was reloaded at the north end; new shear cracks were observed at a shear force of 190 kips, as shown in Fig. 7.16 (f). Fig. 7.16 (a) shows the old cracks due to the south end testing in black and the new crack due to the north end testing in red. Fig. 7.16 (c) shows the final crack pattern at the north end before the web crushing at shear force of 779.80 kips, as shown in Fig. 7.16 (e).

The measured slip at selected tendons, as shown in Figs. 7.17 and 7.18, show that the maximum slip at the failure of the south end was 0.010 inch at ST2 comparing to 0.008 inch at NT6 at the failure of the north end. This slip did not contribute to the failure at either end, and both north and south ends failed finally in web shear, at a maximum smeared compressive strain in concrete struts equals 0.0017 and 0.0016 at the south and north ends, respectively, as shown in Figs. 7.19 (b) 7.20 (b). The corresponding maximum smeared tensile strain across cracks equals 0.0030 and 0.0033 at south and north end, respectively, as shown in Figs. 7.19 (a) and 7.20 (a). Fig. 7.19(c) shows the smeared tensile strain in the transverse direction at the south end was higher closer to the support at the peak having a maximum value of 0.0016 while the maximum smeared transverse strain at north end was 0.0008. During reloading the girder at the north end, the smeared transverse strain on the north side reached 0.0029 closer to the loading point (measured by LVDT NV2), as shown in Fig. 7.20 (c). Fig. 7.19 (d) and Fig. 7.20 (d) shows the smeared strain in the longitudinal direction at the south and north ends, respectively. It shows that the behavior at the top and the bottom of the web is the same, although there was higher compressive smeared strain at the bottom of the web, which had a maximum value of 0.0012 at the peak load at both ends.

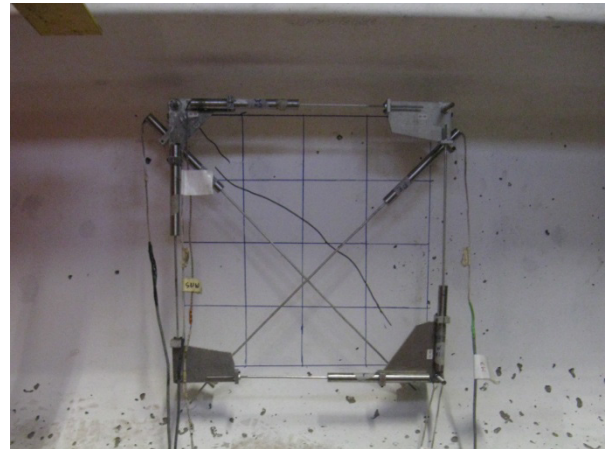
Fig. 7.21 (a) shows that the average local strain in the transverse reinforcement at south end was $0.7 \epsilon_y$. Fig. 7.21 (c) shows the strain gauge readings at the south end. By predicting the maximum local strain measured from strain gauges N5 to N8, which stopped before reaching the peak, based on the recorded trend, it can be concluded that the average local strain in the transverse reinforcement reached the yielding strain.

North End

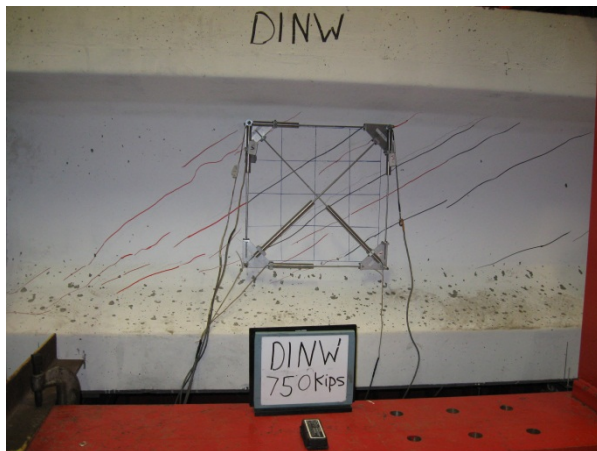


(a) Crack pattern at the start of north end testing

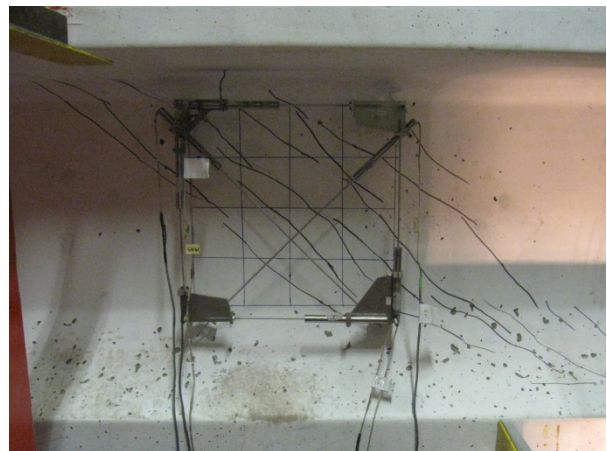
South End



(b) First shear crack at 241 kips



(c) Shear crack pattern before failure



(d) Shear crack pattern before failure



(e) Shear failure at 779.80 kips



(f) Shear failure at 912.78 kips

Fig. 7.16 Shear Crack Pattern and Failure Mode of Girder D1

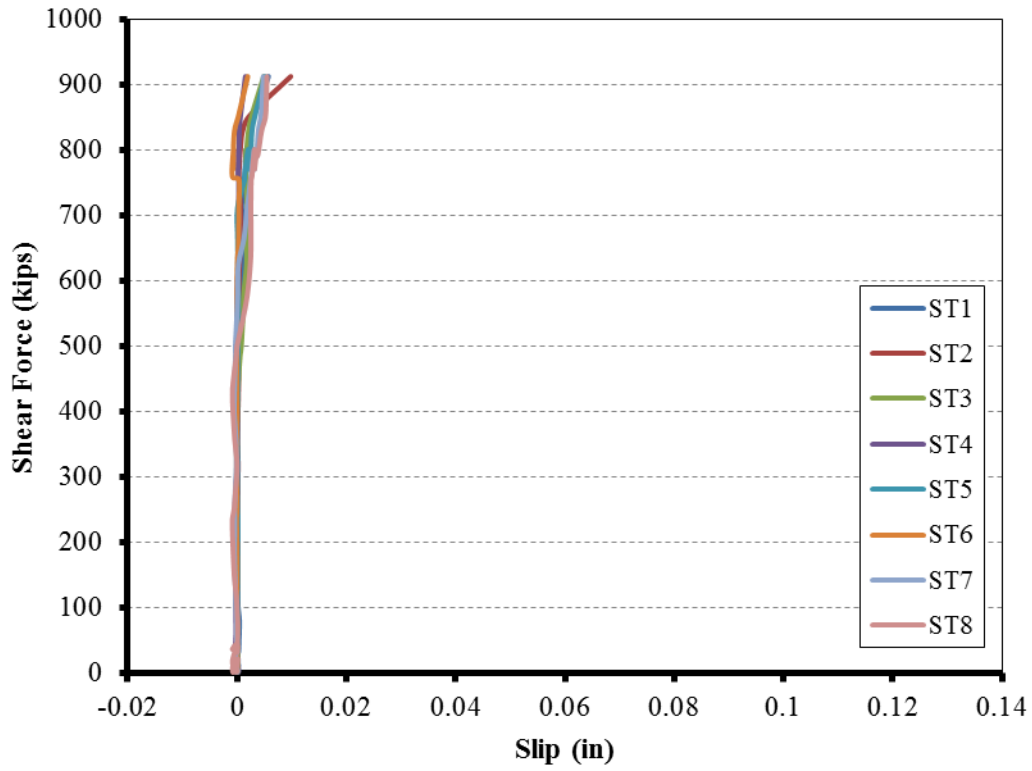


Fig. 7.17 Shear Force vs. Tendons Slip Curves for Girder D1-South

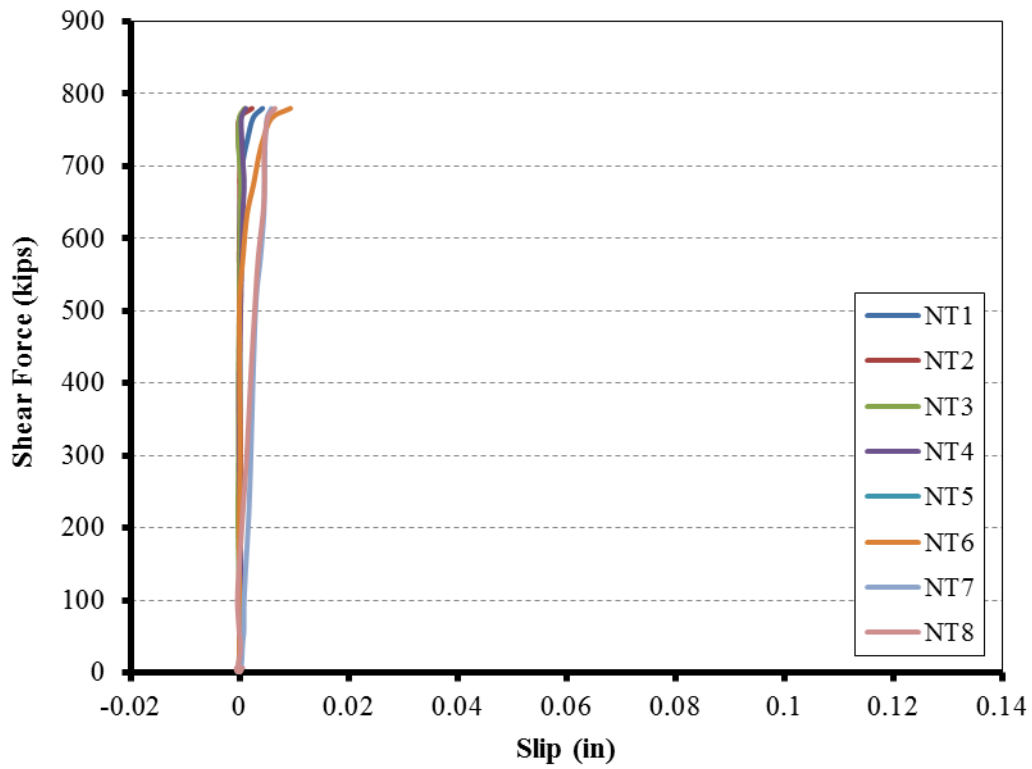
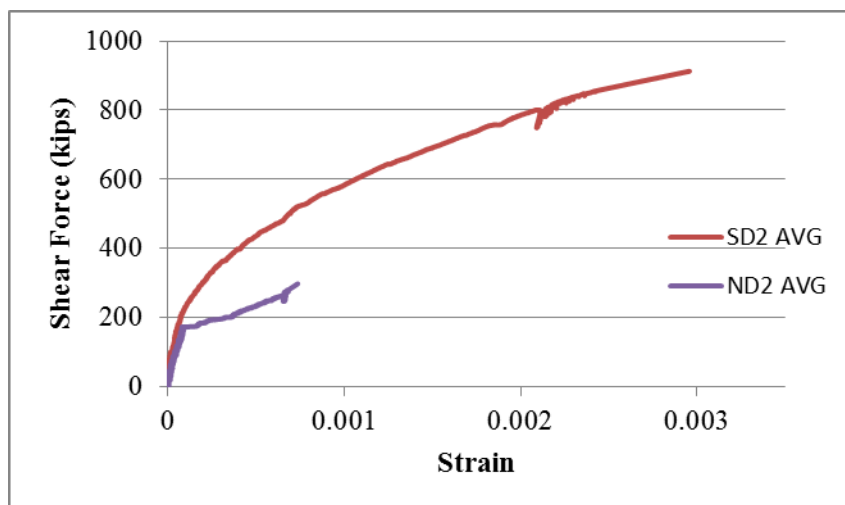
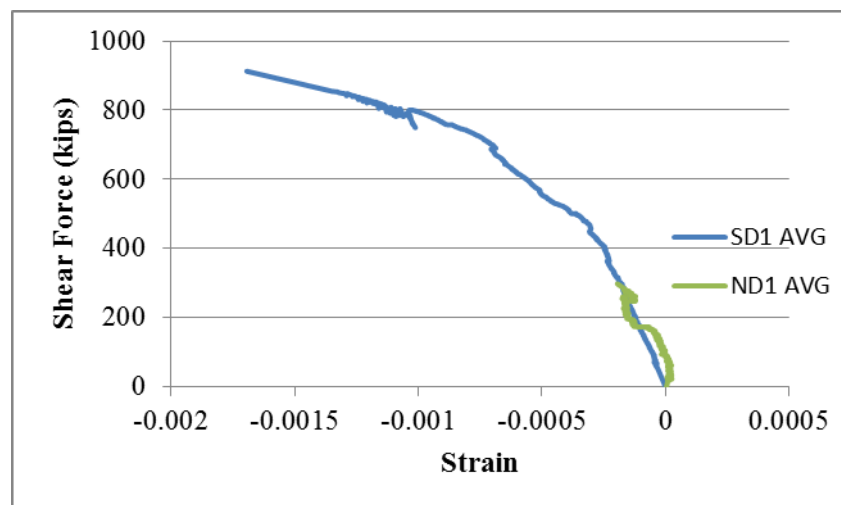


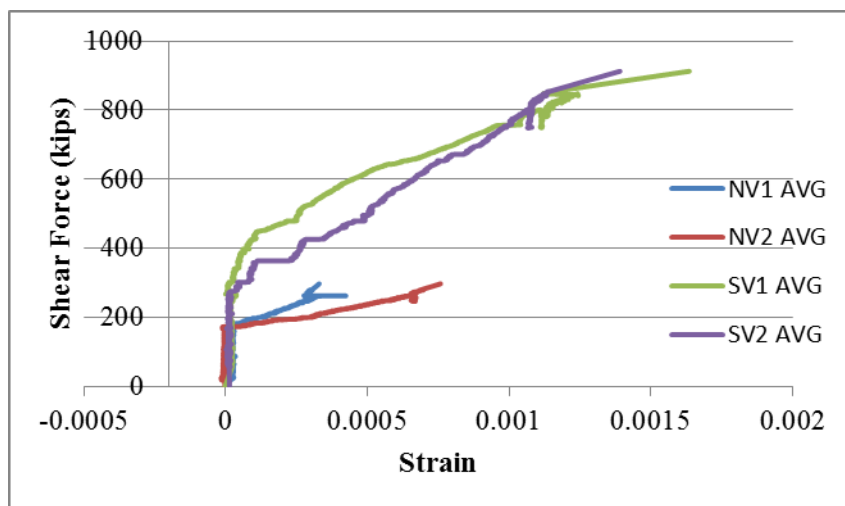
Fig. 7.18 Shear Force vs. Tendons Slip Curves for Girder D1-North



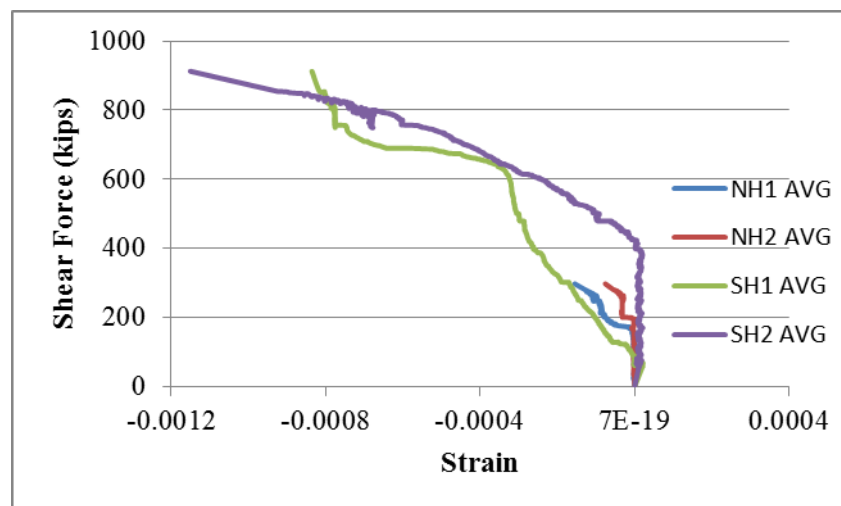
a - Average smeared tensile strain across Cracks



b - Average smeared compressive strain in concrete struts

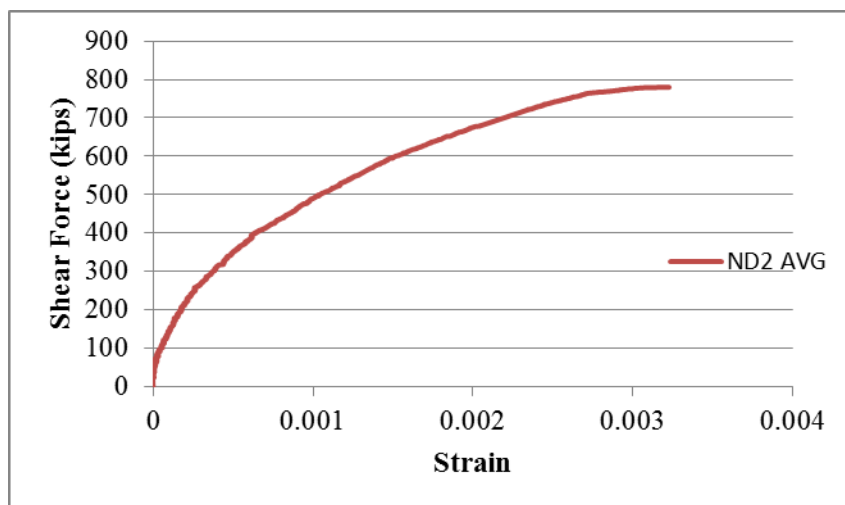


c - Average transverse smeared strain

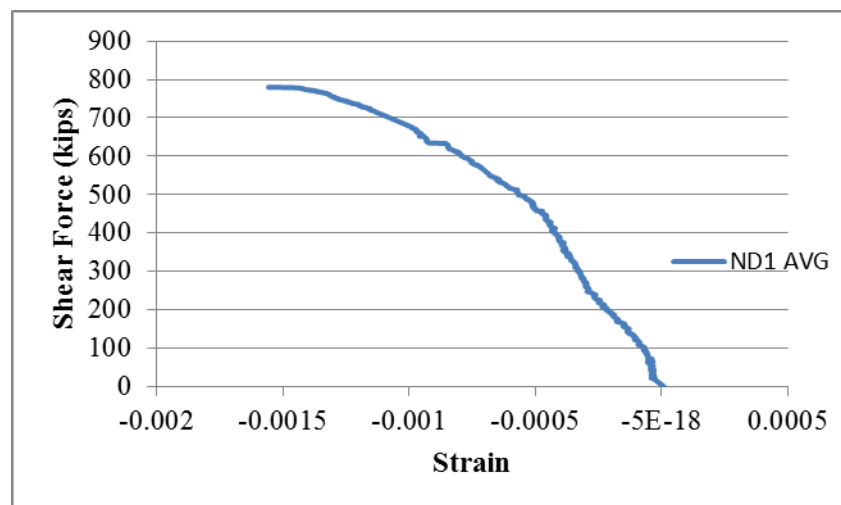


d - Average longitudinal smeared strain

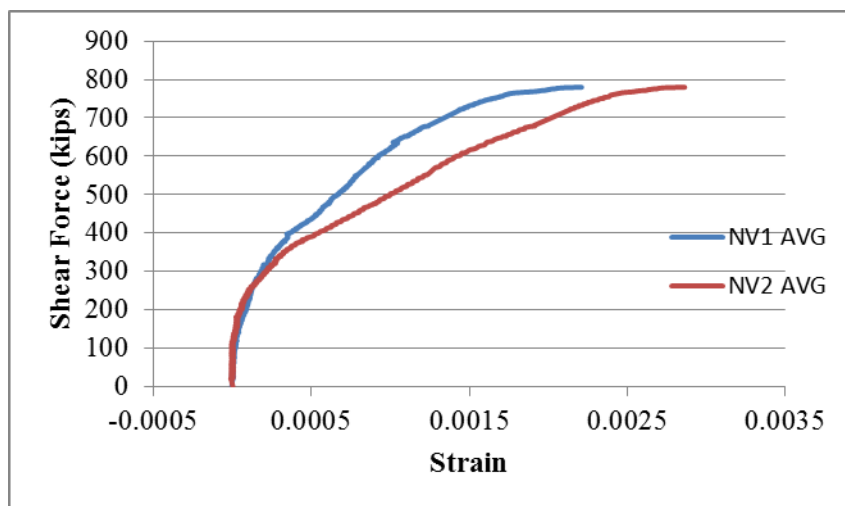
Fig. 7.19 Shear Force vs. Concrete Smeared Strains Curves for Girder D1 (South End Test)



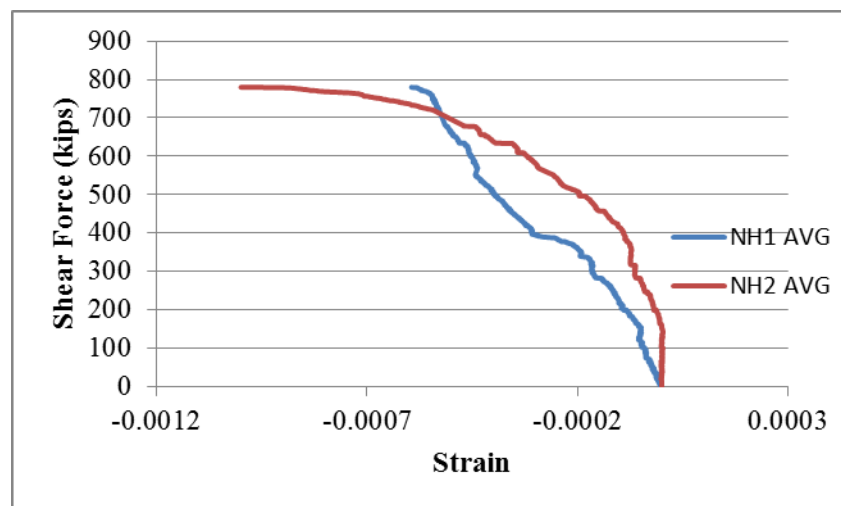
a - Average smeared tensile strain across Cracks



b - Average smeared compressive strain in concrete struts

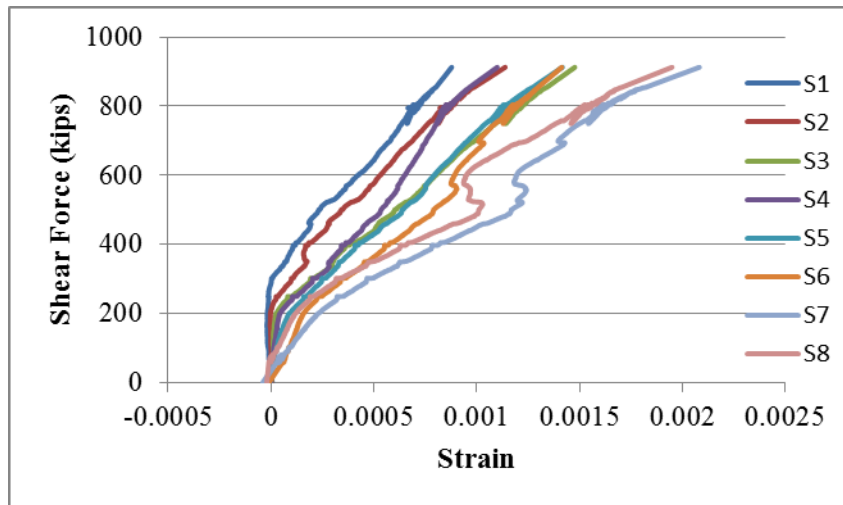


c - Average transverse smeared strain

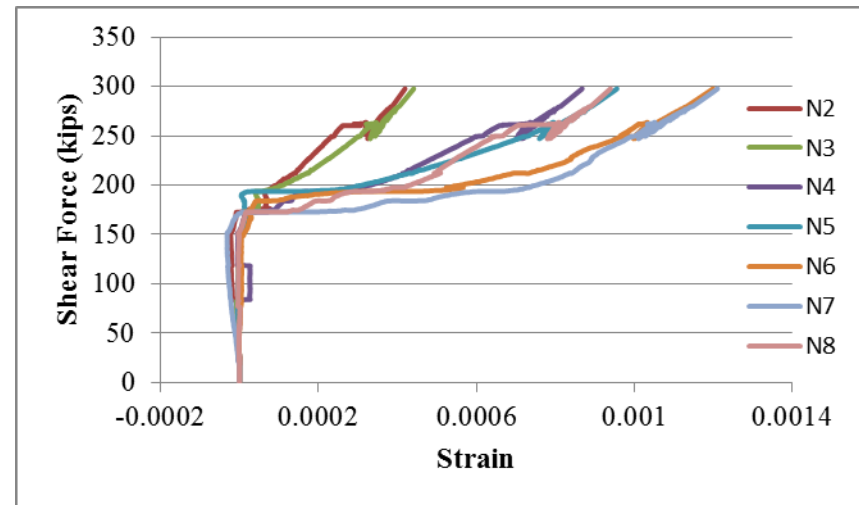


d - Average longitudinal smeared strain

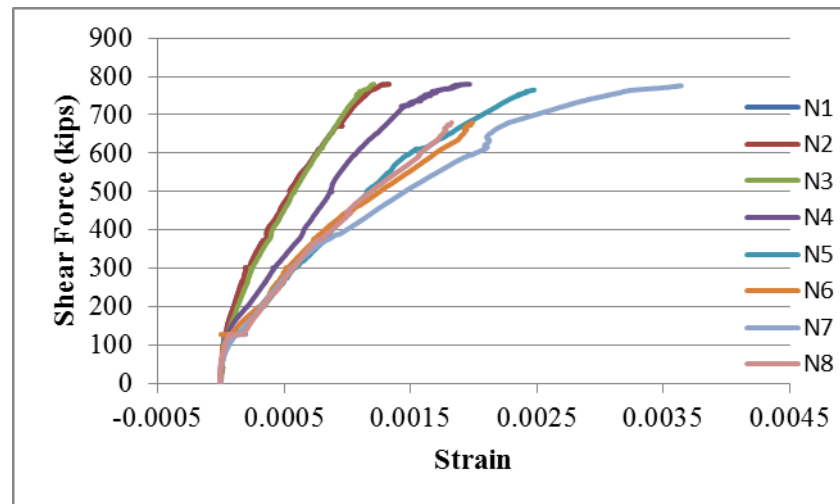
Fig. 7.20 Shear Force vs. Concrete Smeared Strains Curves for Girder D1 (North End Test)



(a) South strain gauges during testing south end



(b) North strain gauges during testing south end



(c) North strain gauges during testing north end

Fig. 7.21 Shear Force vs. Local Transverse Tensile Strain of Girder D1

7.3.2. Girder D2

The south end of Girder D2 was tested first with shear span to depth ratio (a/d) 1.23. Because the failure did not affect the stability of the girder, it was decided to continue retesting the north end with the same net span without moving the south support. Girder D2 was reloaded on the north end with a shear span to depth ratio (a/d) 1.56. Fig. 7.22 shows the shear force versus the net deflection for both ends. It can be seen that the north end had less stiffness due to using a larger shear span to depth ratio and due to the failure at the south end.

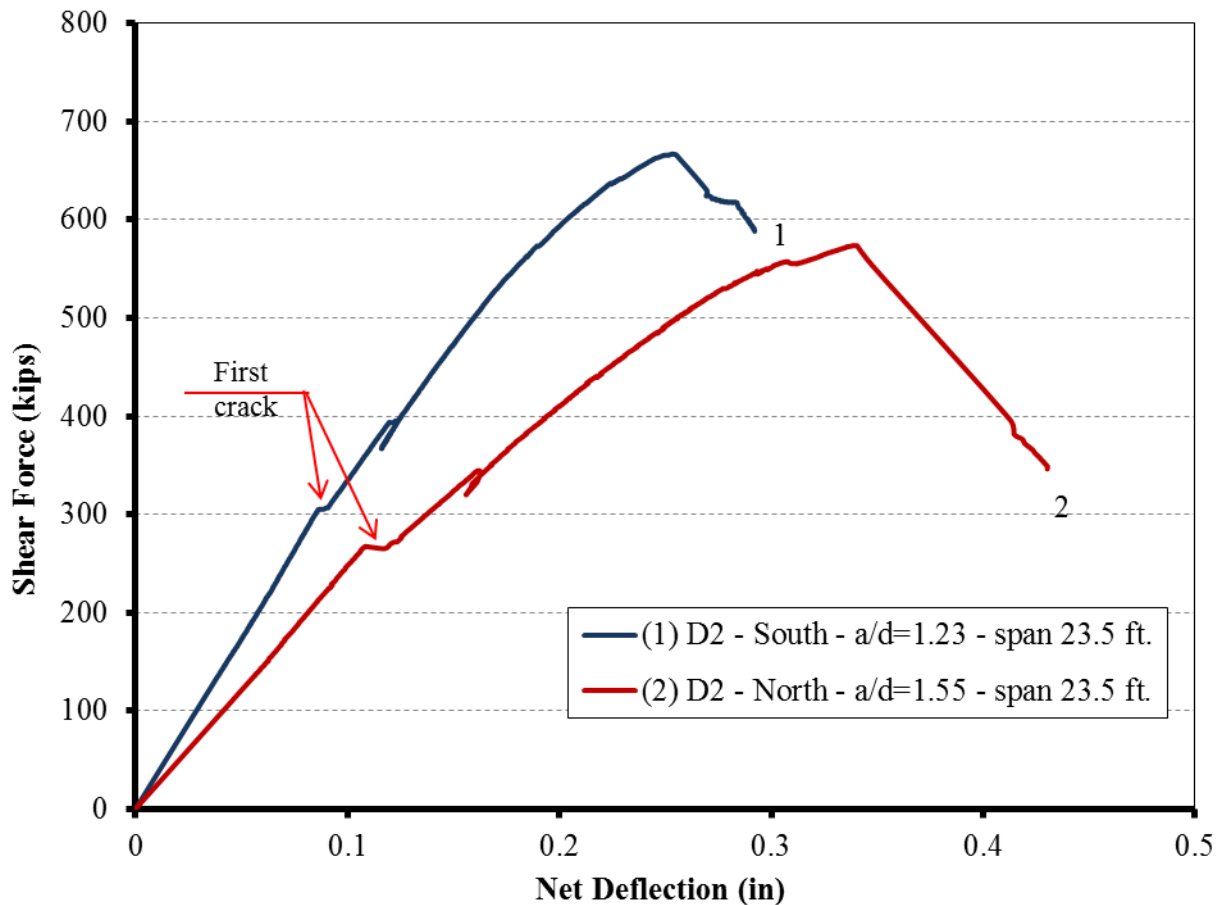


Fig. 7.22 Shear Force vs. Girder Deflection Curves for Girder D2

The first shear crack was seen at the south end at a shear force of 314 kips, as shown in Fig. 7.23 (b). With increasing the applied loads, new cracks developed. Fig. 7.23 (d) shows the final crack pattern at the south end before the failure happened at a shear force of 673.74 kips. Then the girder was reloaded at the north end to have the first shear crack at a shear force of

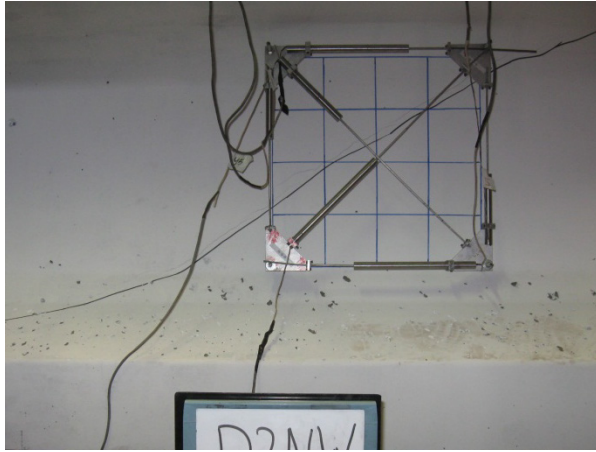
274 kips, as shown in Fig. 7.23 (a). Fig. 7.23 (c) shows the final crack pattern at the north end before the web crushing at a shear force of 578.67 kips, as shown in Fig. 7.23 (e).

The measured slip at selected tendons, as shown in Figs. 7.24 and 7.25, show that the maximum slip at the failure of the south end was 0.055 inch at ST4 comparing to 0.077 inch at NT3 at the failure of the north end. In spite of having this significant slip, the beam failed in web crushing at the south end having a maximum smeared tensile strain across the cracks equal to 0.0042 and a maximum smeared compressive strain equal to 0.0021, as shown in Fig 7.26 (a) and (b).

Unfortunately, the available data from the north end could not provide the smeared compressive strain in the concrete struts at failure because of the huge tensile deformation in the transverse direction where the smeared transverse tensile strain was 0.0082, which is almost twice the transverse smeared strain at the south end, which was 0.0047. This huge transverse strain let the diagonal LVDT ND1 go in tension instead of going in compression and increased the smeared tensile strain across the cracks to be 0.0053.

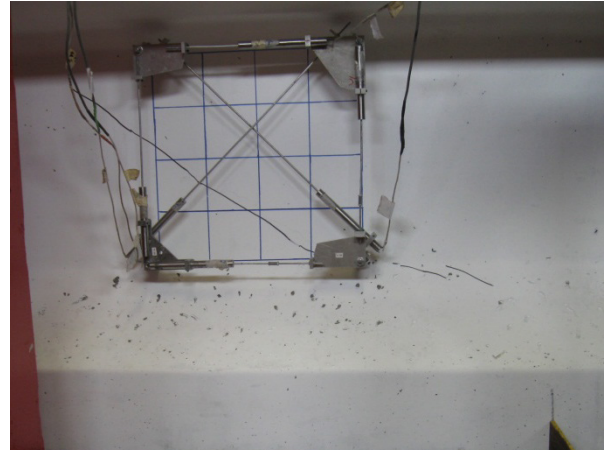
Fig. 7.28 shows the local strains in the transverse steel measured by strain. It shows that the transverse steel at both ends reached the yielding strain. It also shows that the strain in transverse steel at the south end jumped to the yield strain at the moment of cracking.

North End

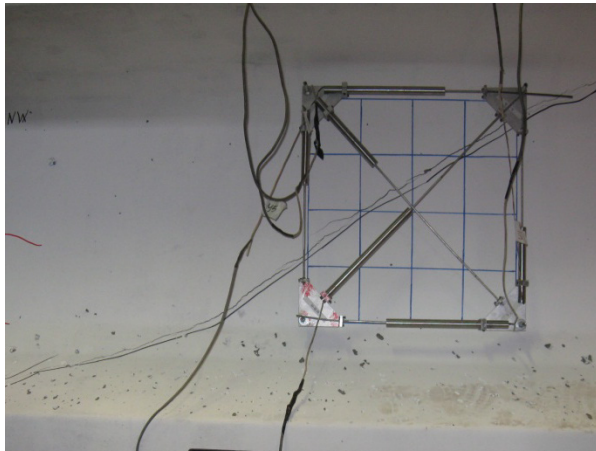


(a) First shear crack at 274 kips

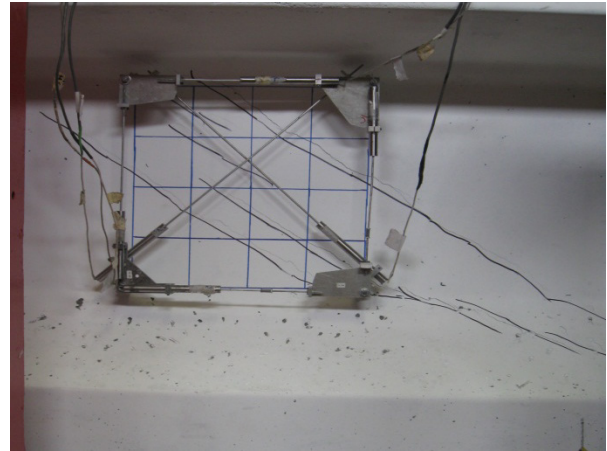
South End



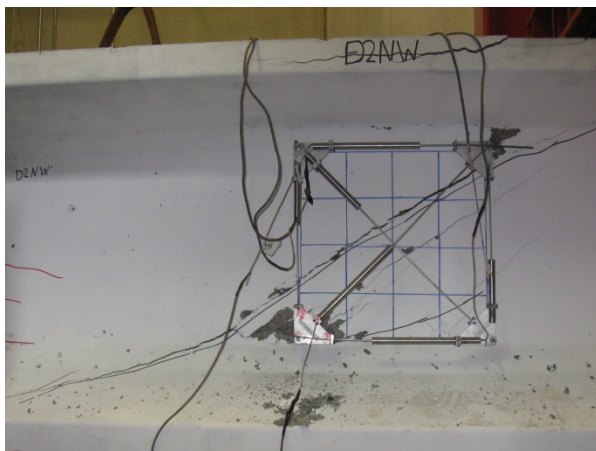
(b) First shear crack at 314 kips



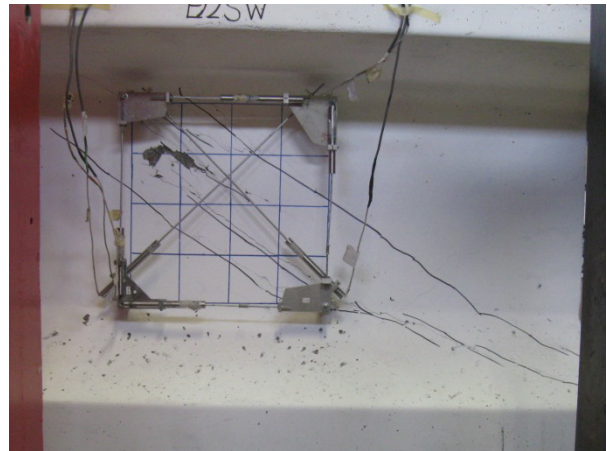
(c) Shear crack pattern before failure



(d) Shear crack pattern before failure



(e) Shear failure at 578.67 kips



(f) Shear failure at 673.74 kips

Fig. 7.23 Shear Crack Pattern and Failure Mode of Girder D2

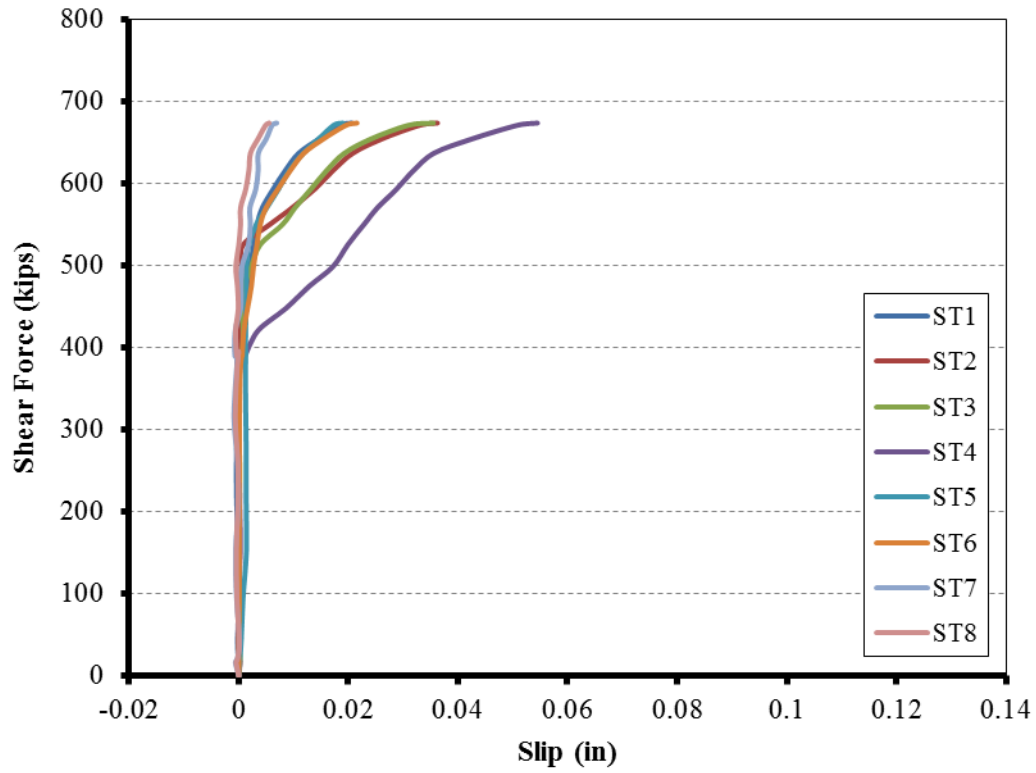


Fig. 7.24 Shear Force vs. Tendons Slip Curves for Girder D2-South

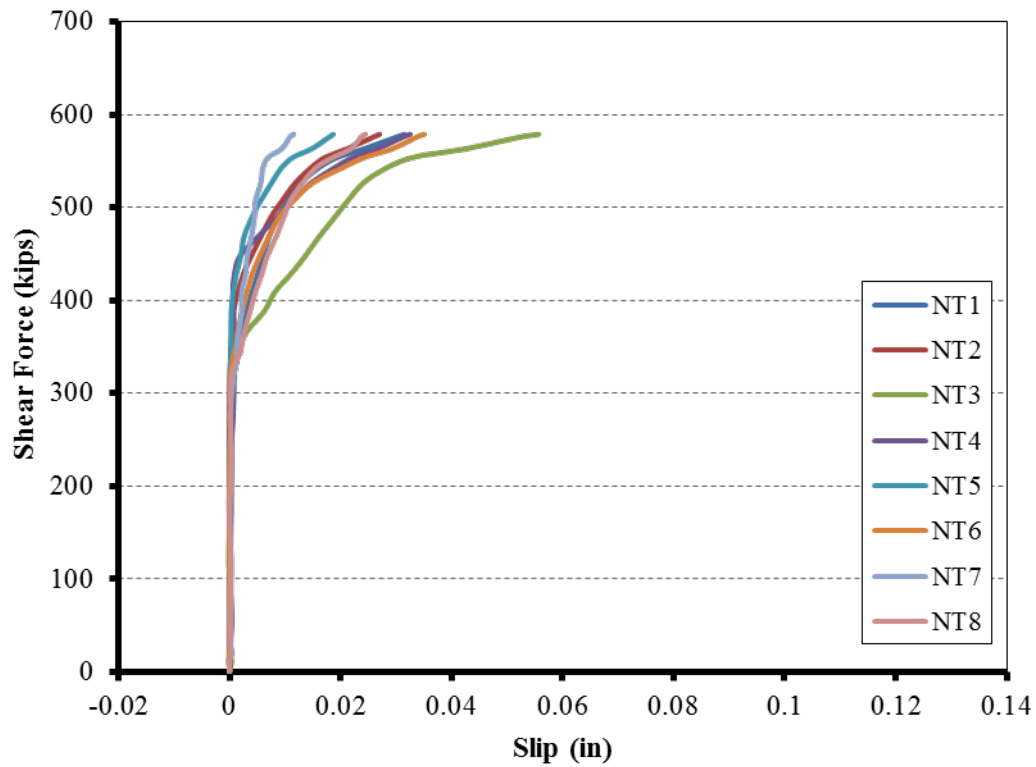
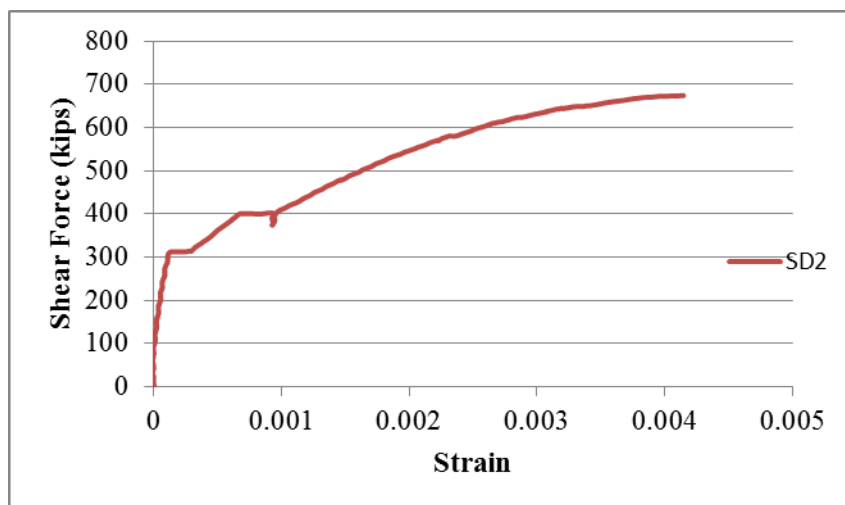
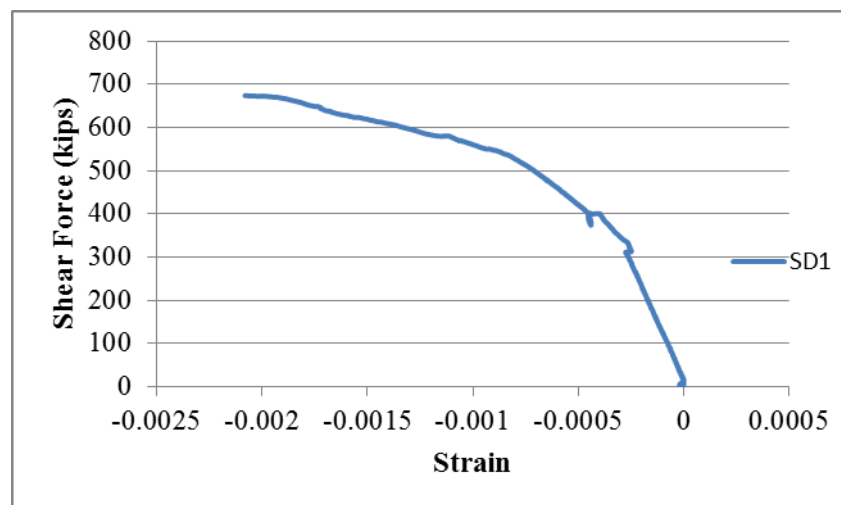


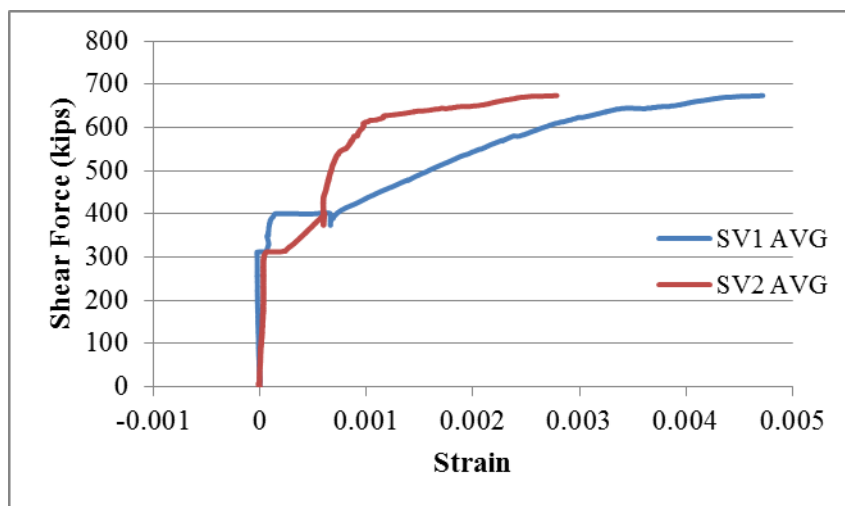
Fig. 7.25 Shear Force vs. Tendons Slip Curves for Girder D2-North



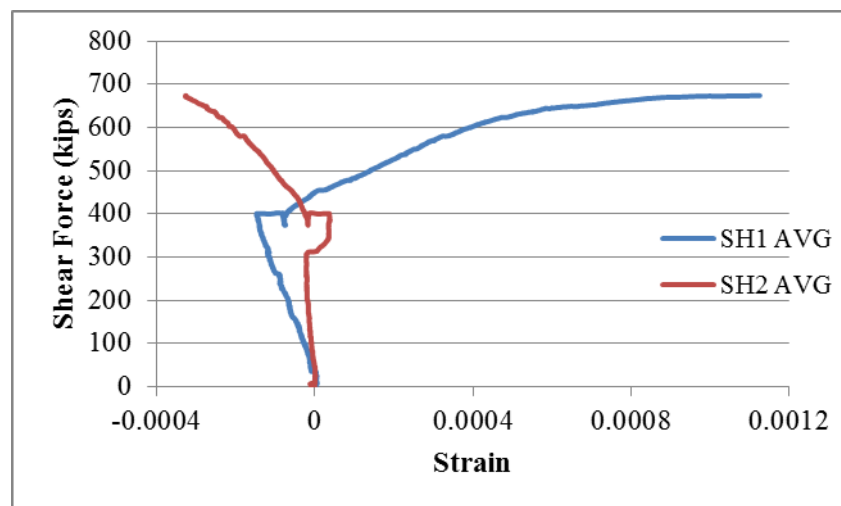
a - Average smeared tensile strain across Cracks



b - Average smeared compressive strain in concrete struts

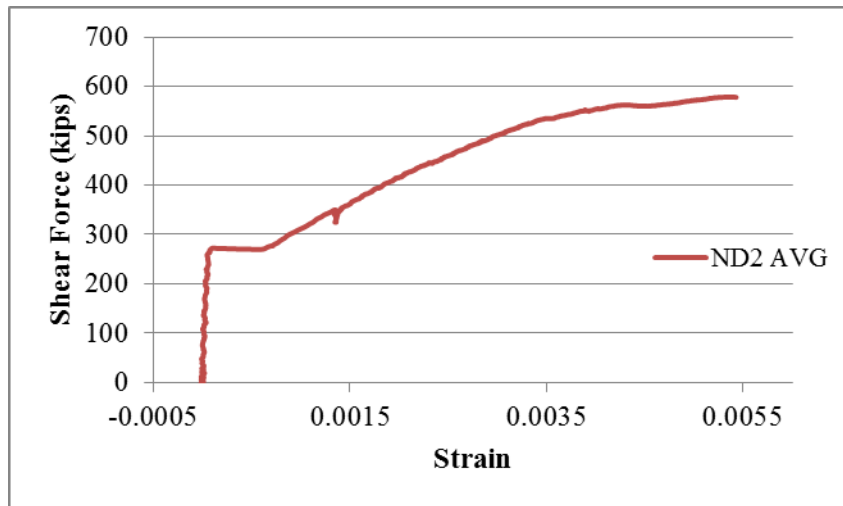


c - Average transverse smeared strain

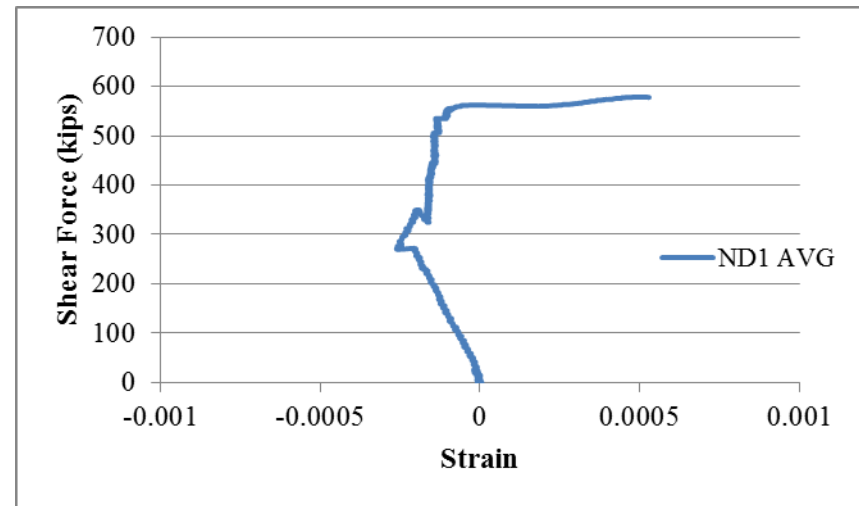


d - Average longitudinal smeared strain

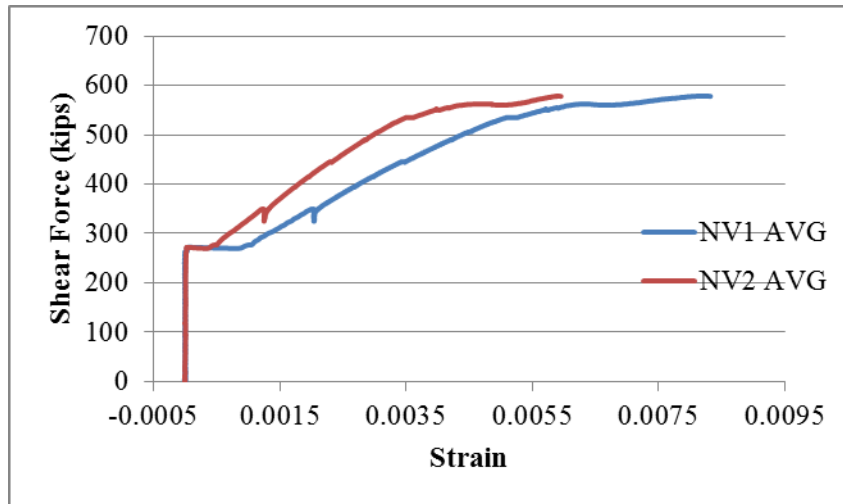
Fig. 7.26 Shear Force vs. Concrete Smeared Strains Curves for Girder D2 (South End Test)



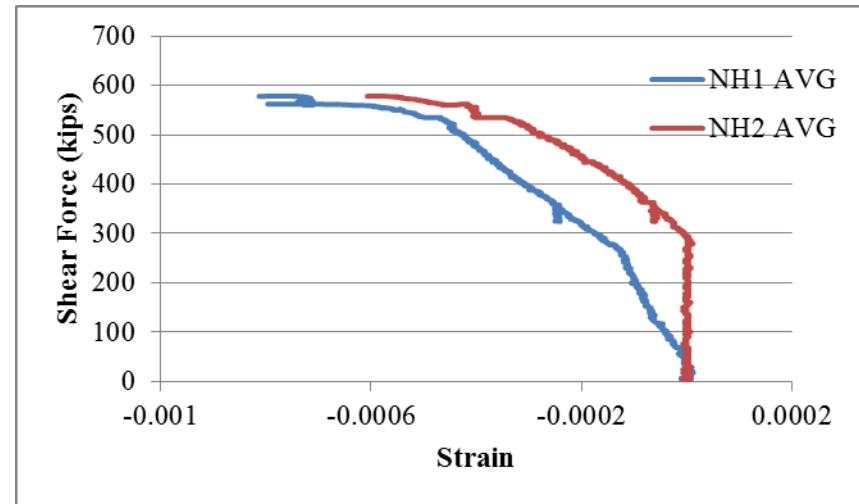
a - Average smeared tensile strain across Cracks



b - Average smeared compressive strain in concrete struts

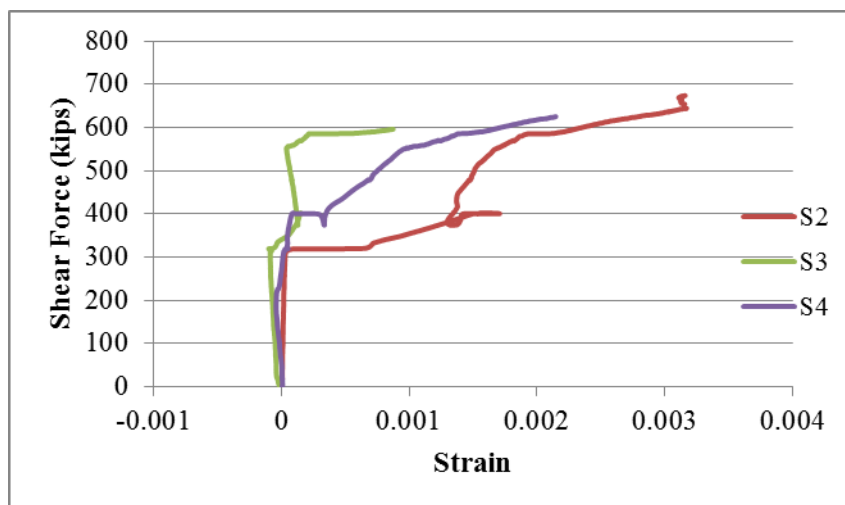


c - Average transverse smeared strain

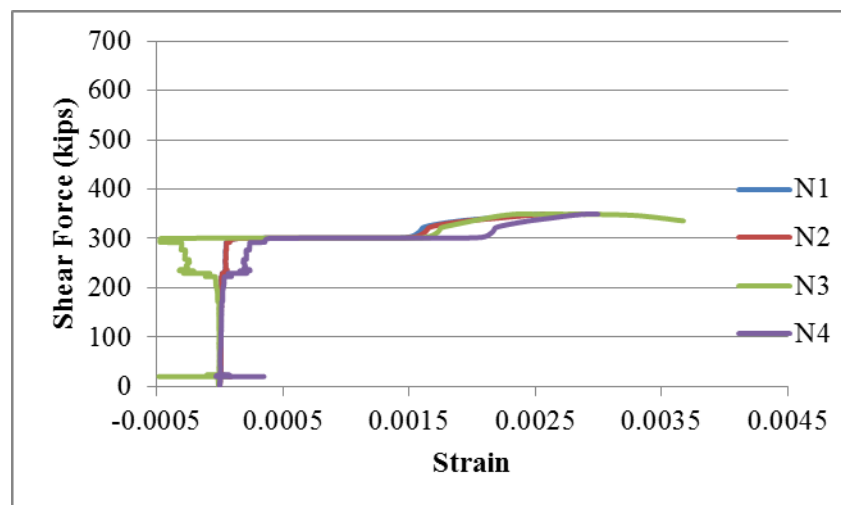


d - Average longitudinal smeared strain

Fig. 7.27 Shear Force vs. Concrete Smeared Strains Curves for Girder D2 (North End Test)



c - Average transverse smeared strain



d - Average longitudinal smeared strain

Fig. 7.28 Shear Force vs. Local Transverse Tensile Strain of Girder D2

7.4. Experimental Results of Group E Girders

Similar to groups G and D, this group of girders consists of two Tx62 girders. The first girder named E1 was reinforced in the transverse direction according to TxDOT specifications. The second girder named E2 was reinforced in the transverse direction with the minimum reinforcement according to AASHTO (2010). Girder E1 had a top slab with eight in. thickness while Girder E2 did not.

7.4.1. Girder E1

Girder E1 was loaded first on the south end with a shear span to depth ratio (a/d) 1.18, and then on the north end using a shear span to depth ratio (a/d) 1.59. Due to the huge shear capacity of the girder and the limited capacity of hydraulic jacks, the test was stopped at a shear force of 853.74 and 747.46 kips at south and north ends, respectively, as shown in Fig. 7.29.

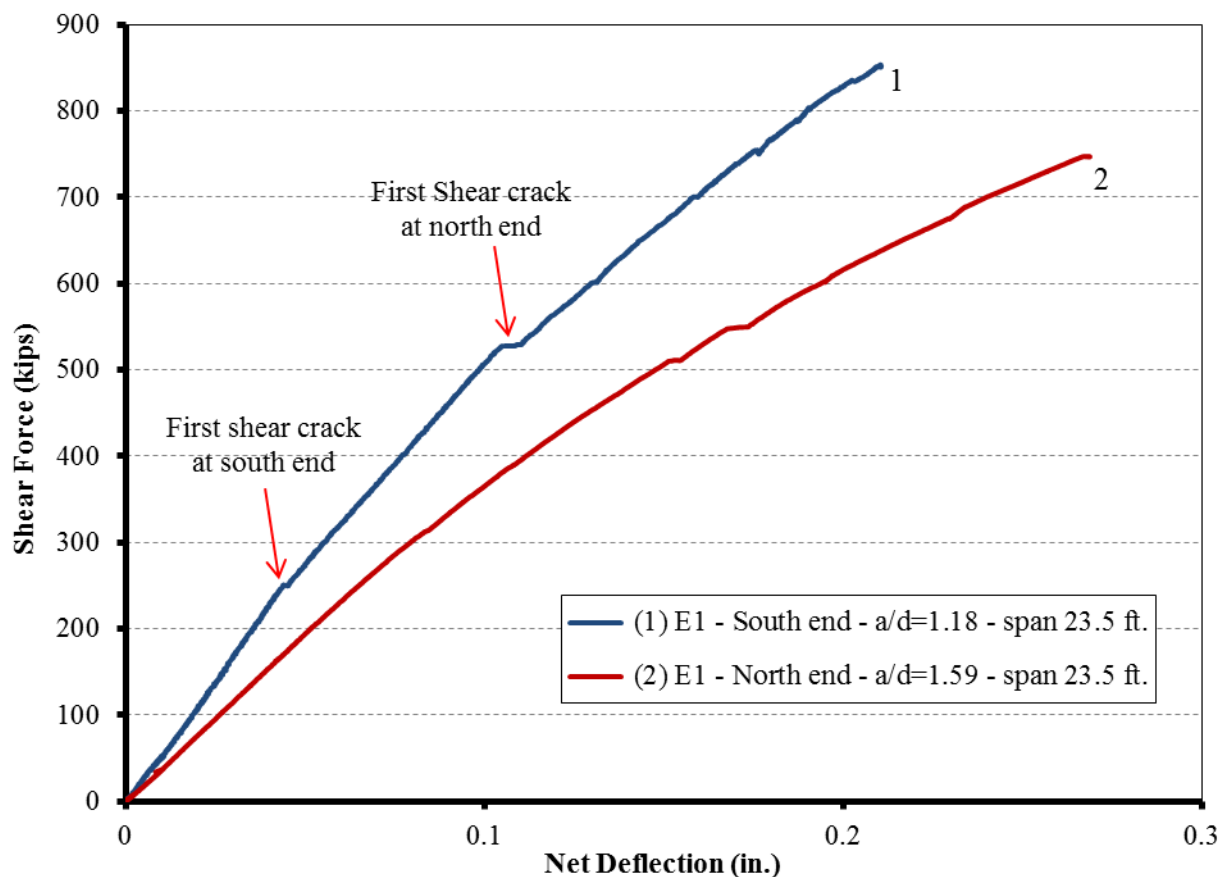


Fig. 7.29 Shear Force vs. Girder Deflection Curves for Girder E1

The first shear crack was seen at the south end at a shear load of 250 kips, as shown in Fig. 30 (b). As the applied load increased, the north end of the girder had the first crack at a shear load on the north load cell of 241 kips. Fig. 30 (d) shows the final crack pattern on the south end at the end of the test. During the reloading of the north end, new cracks appeared at both the north and south ends. Fig. 30 (a) shows the crack pattern at the start of loading the north end, which resulted from loading the south end. Fig. 30 (c) shows the final crack pattern on the north end at the end of the test. Figs. 7.31 and 7.32 show that the maximum measured slip at the end of the test at the south end was 0.004 inch at ST2 comparing to 0.005 inch at NT2 at the end of the north end test.

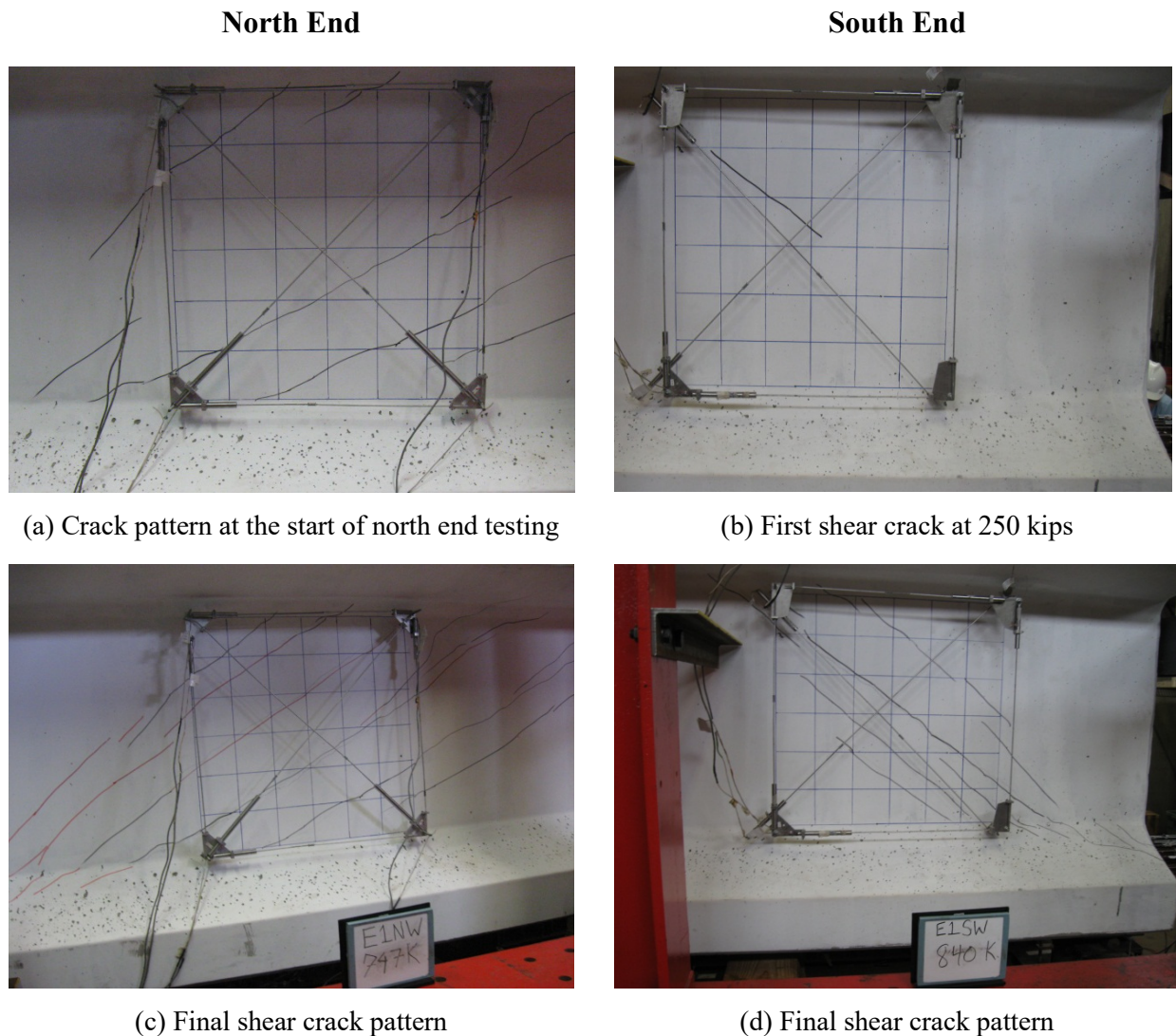


Fig. 7.30 Shear Crack Pattern and Failure Mode of Girder E1

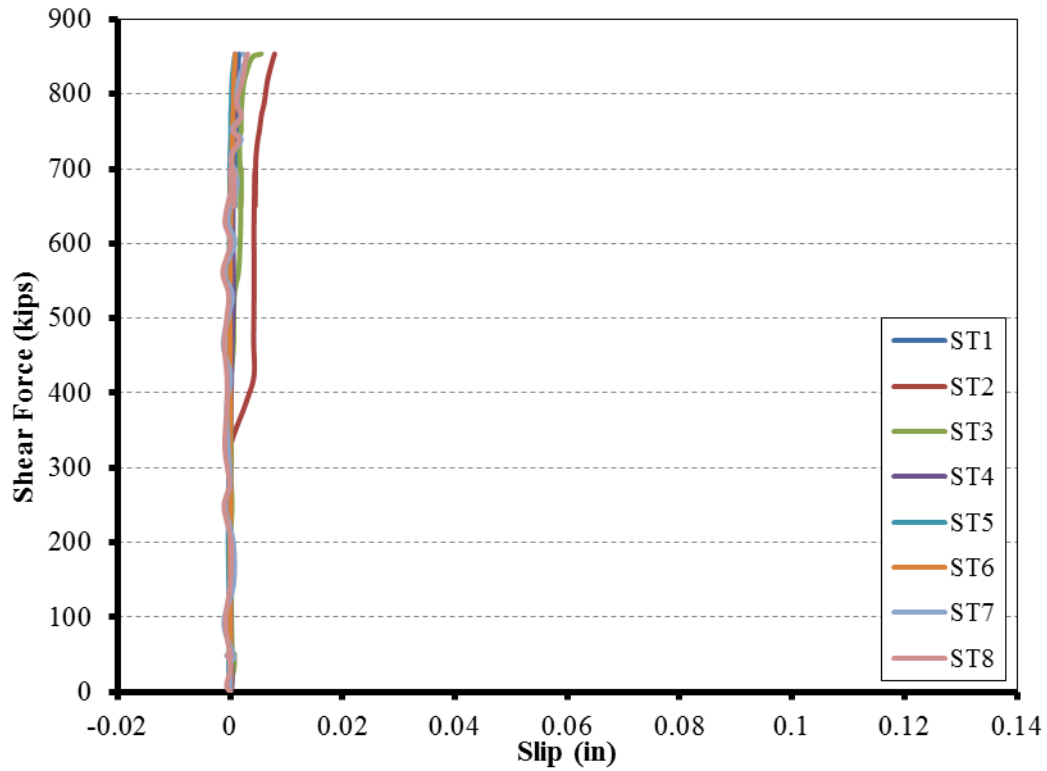


Fig. 7.31 Shear Force vs. Tendons Slip Curves for Girder E1-South

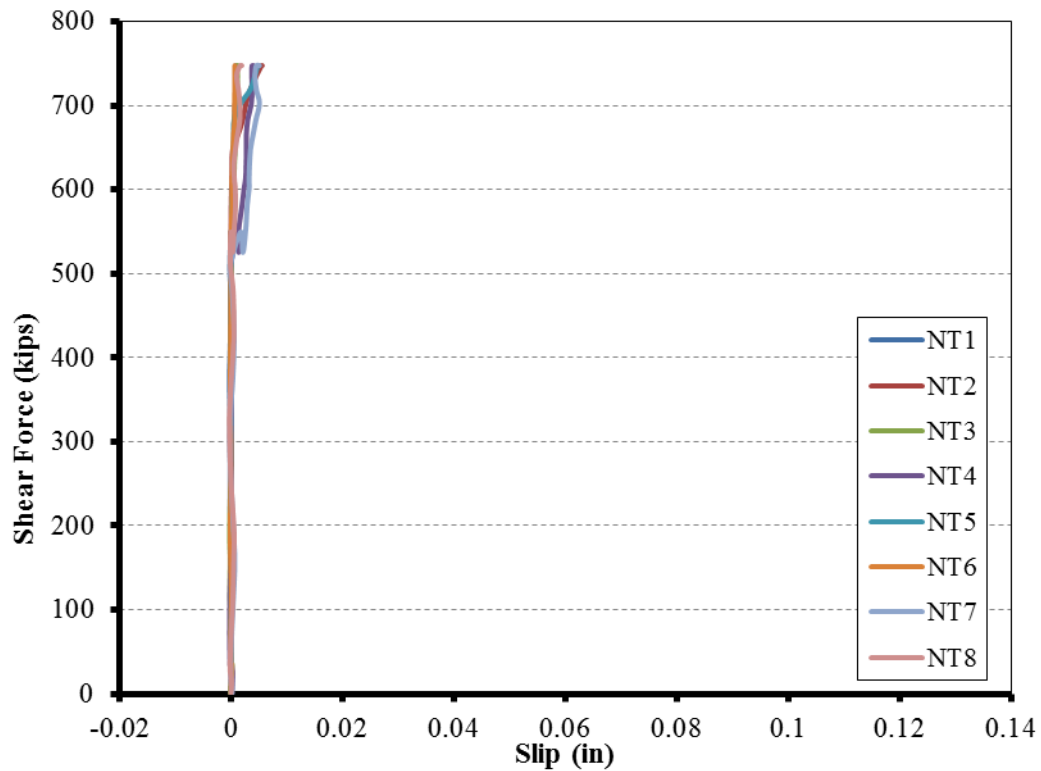
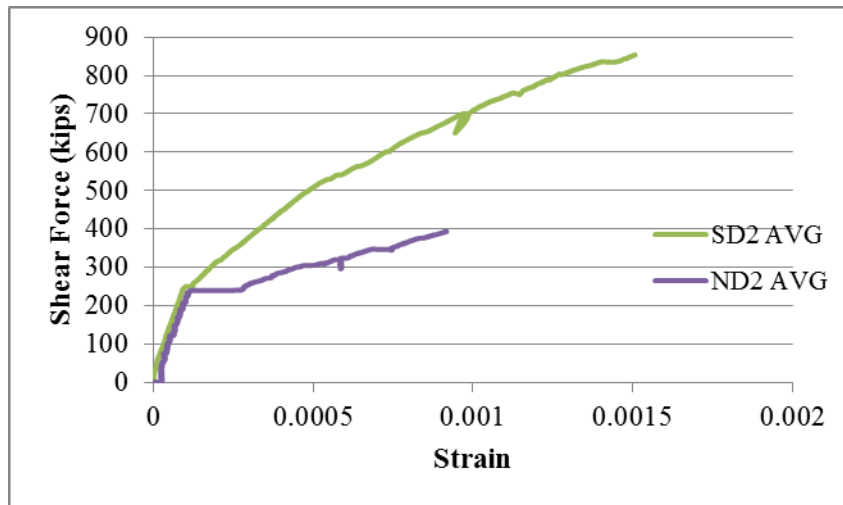


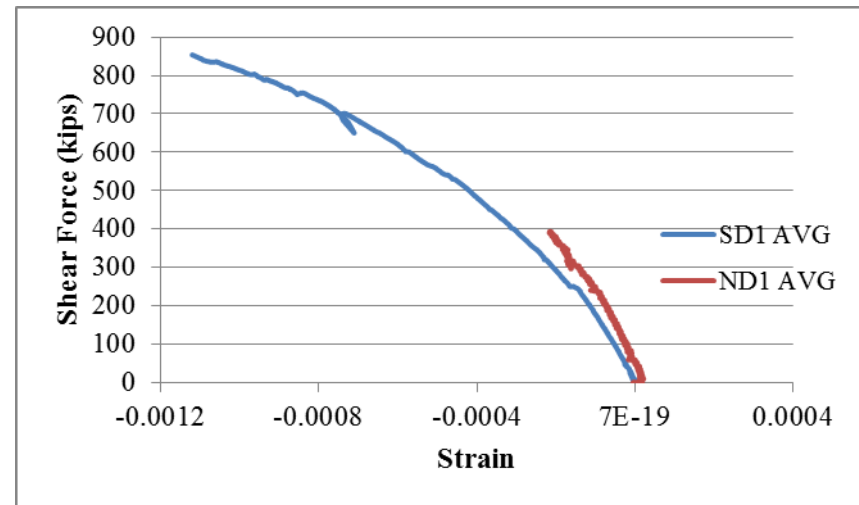
Fig. 7.32 Shear Force vs. Tendons Slip Curves for Girder E1-North

At the end of the south end testing, the smeared tensile strain across shear cracks was only 0.0015, while the smeared compressive strain in concrete struts was only 0.0011, as shown in Fig. 7.33 (a) and (b). At the end of the north end testing, the smeared tensile strain across shear cracks was only 0.0016, while the smeared compressive strain in concrete struts was only 0.0010, as shown in Fig. 7.34 (a) and (b).

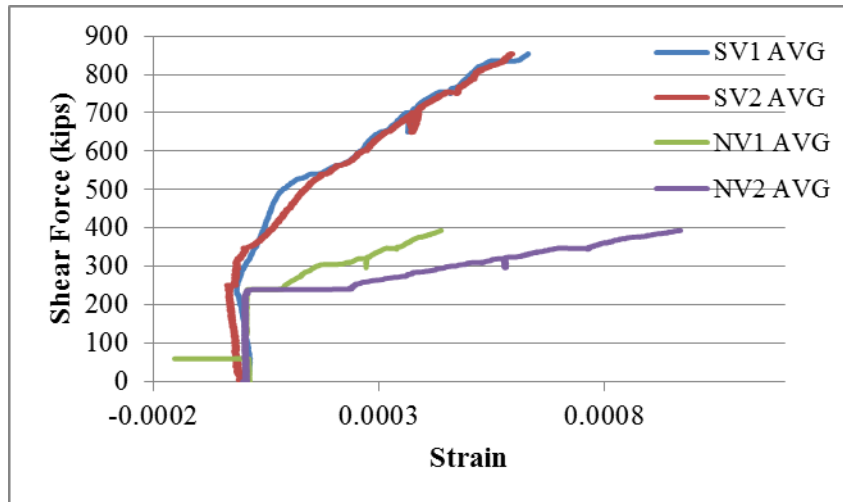
Figs. 7.33 (c) and 7.34 (c) show the maximum smeared transverse strain was 0.0006 and 0.001 at the south and north ends, respectively. Fig. 7.35 (a) and (b) show that the average local strain in the transverse steel measured by strain gauges during testing of the south end was $0.7\varepsilon_y$ and $0.4\varepsilon_y$ at the south and north ends, respectively. The residual strain at the north end after unloading the girder was found to be $0.18\varepsilon_y$. Fig. 7.33 (c) shows the average local strain in the transverse steel measured by strain gauges at the north end was $0.45\varepsilon_y$. The final average local strain in the transverse steel at the north end will be taken by adding the residual strain due to testing the south side to the final local strain measured during testing the north end test. An average value of $0.63\varepsilon_y$ will be used to calculate the steel and concrete contribution.



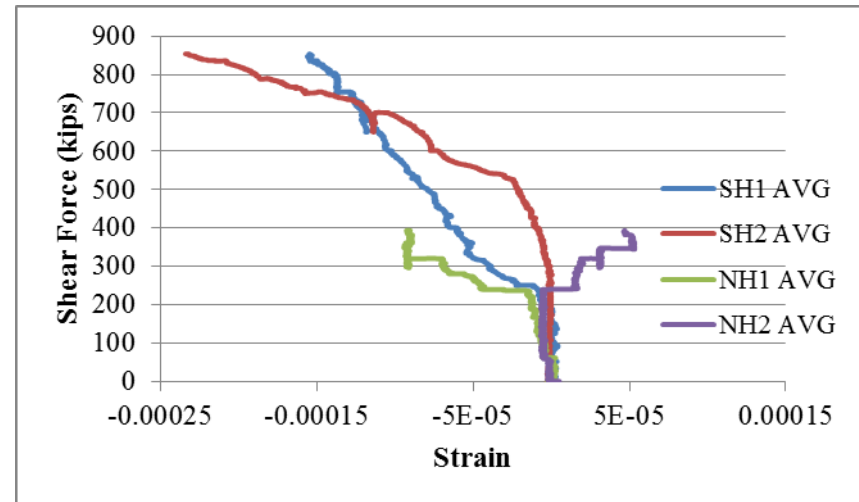
a - Average smeared tensile strain across Cracks



b - Average smeared compressive strain in concrete struts

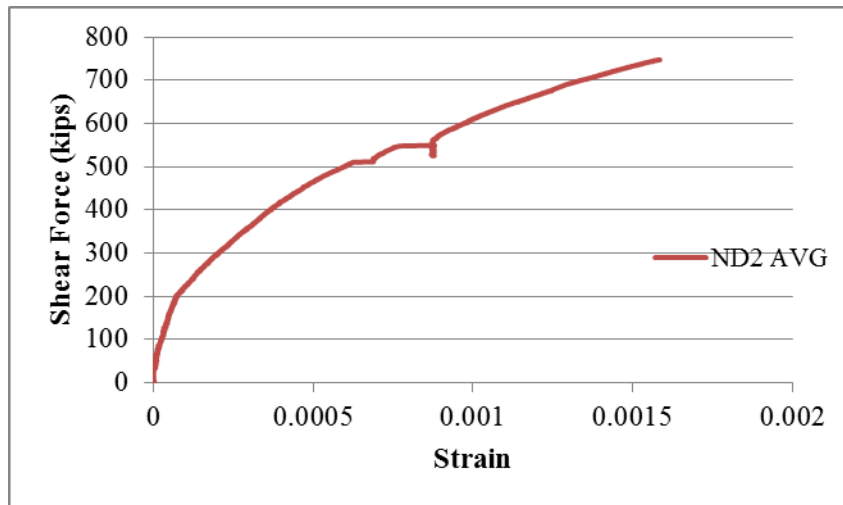


c - Average transverse smeared strain

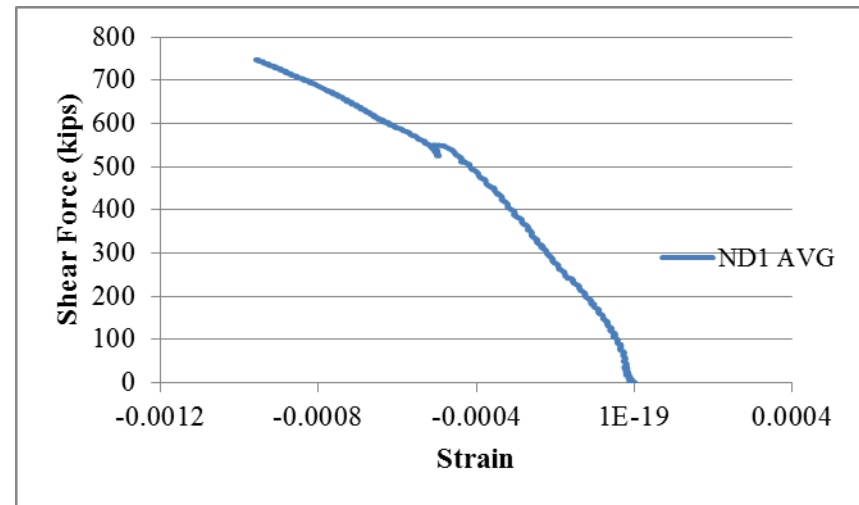


d - Average longitudinal smeared strain

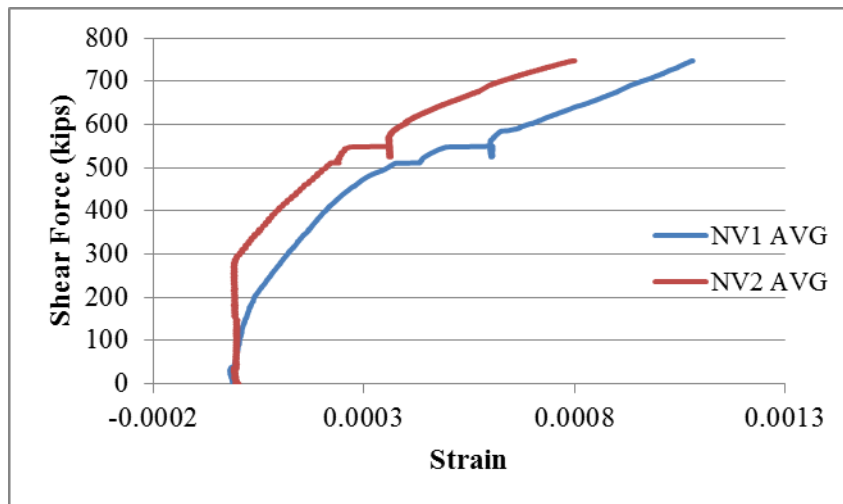
Fig. 7.33 Shear Force vs. Concrete Smeared Strains Curves for Girder E1 (South End Test)



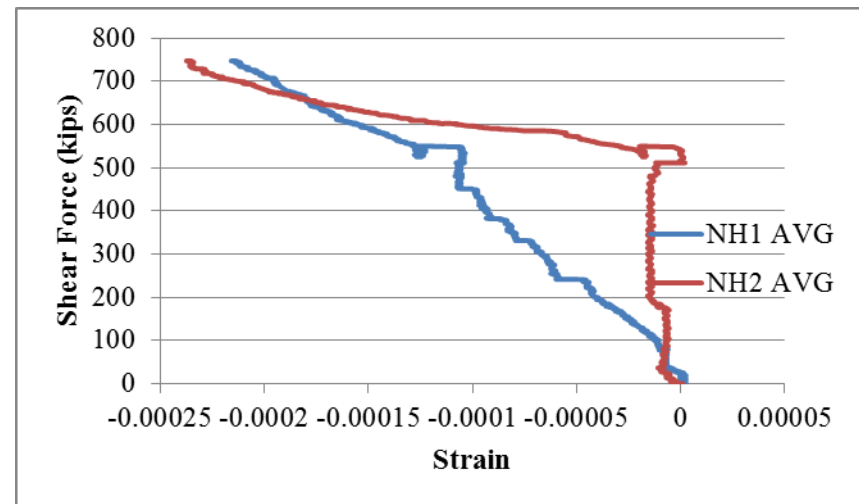
a - Average smeared tensile strain across Cracks



b - Average smeared compressive strain in concrete struts

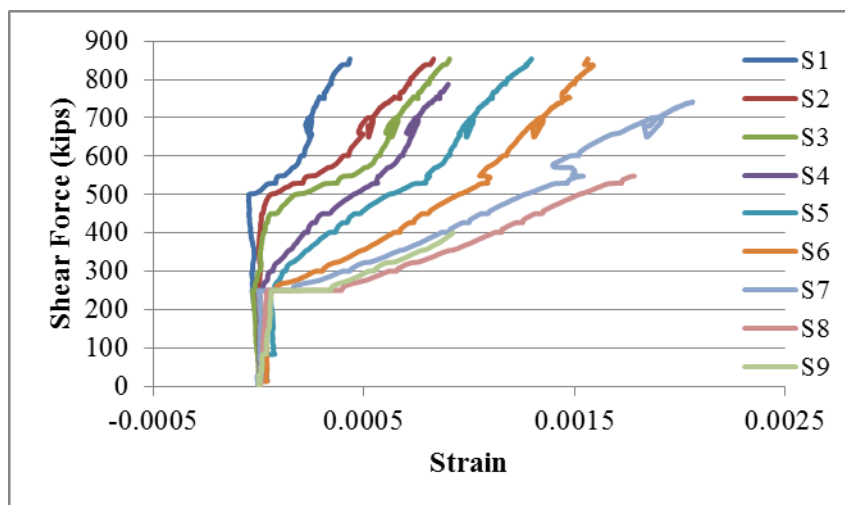


c - Average transverse smeared strain

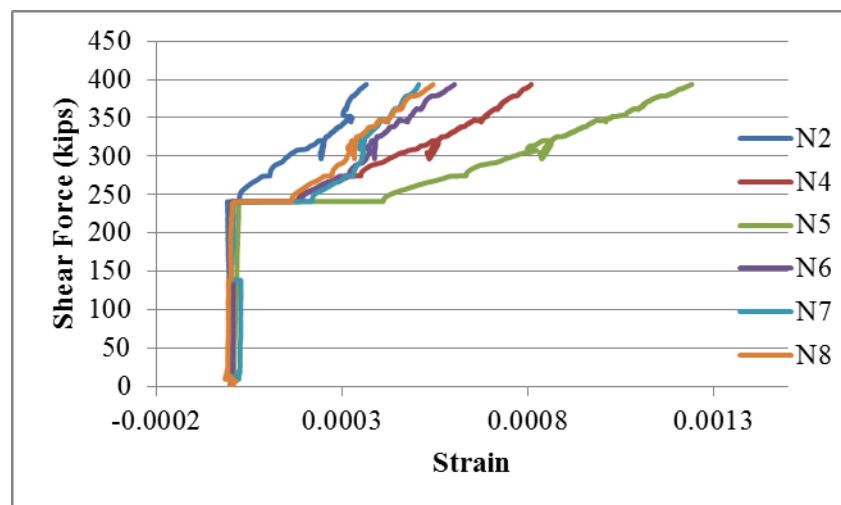


d - Average longitudinal smeared strain

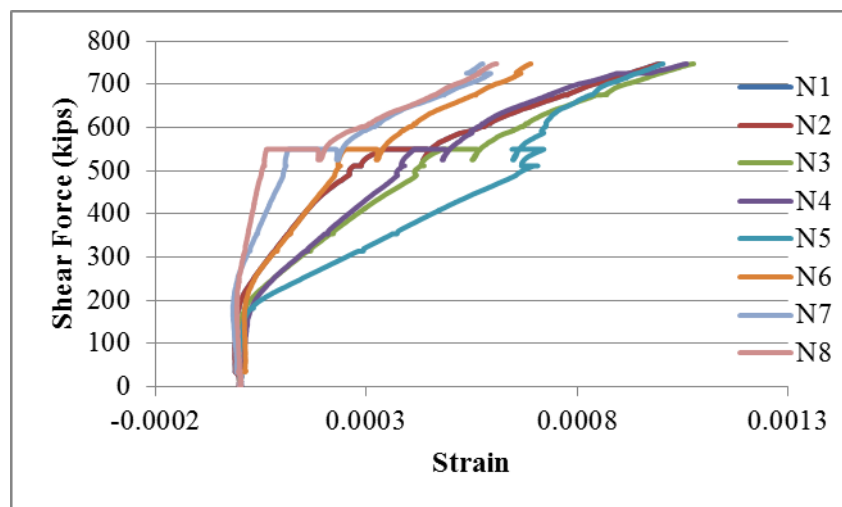
Fig. 7.34 Shear Force vs. Concrete Smeared Strains Curves for Girder E1 (North End Test)



a - Average transverse smeared strain



b - Average longitudinal smeared strain



c - Average transverse smeared strain

Fig. 7.35 Shear Force vs. Local Transverse Tensile Strain of Girder E1

7.4.2. Girder E2

The Girder E2 was tested next. The south end was tested first using a shear span to depth ratio (a/d) 1.23. Fig. 7.36 shows the shear force versus net deflection curve for the south end of Girder E2. The first crack was seen at the south end at a shear load of 416 kips, as shown in Fig. 7.37 (a), which caused a sudden increase in the recorded deflection, Fig. 7.36. As the applied load increased, the north side of the girder had the first crack at a shear load on the north load cell of 305 kips while the corresponding shear force at the south load cell was 739 kips. Fig. 7.38 (b) shows the cracks pattern just before failure, and Fig. 7.38 (c) shows an obvious web-shear failure at a shear force of 756.42 Kips. Because the failure affected the girder stability and because it was very hard and risky to move the support after the failure zone, it was decided to not test the north side.

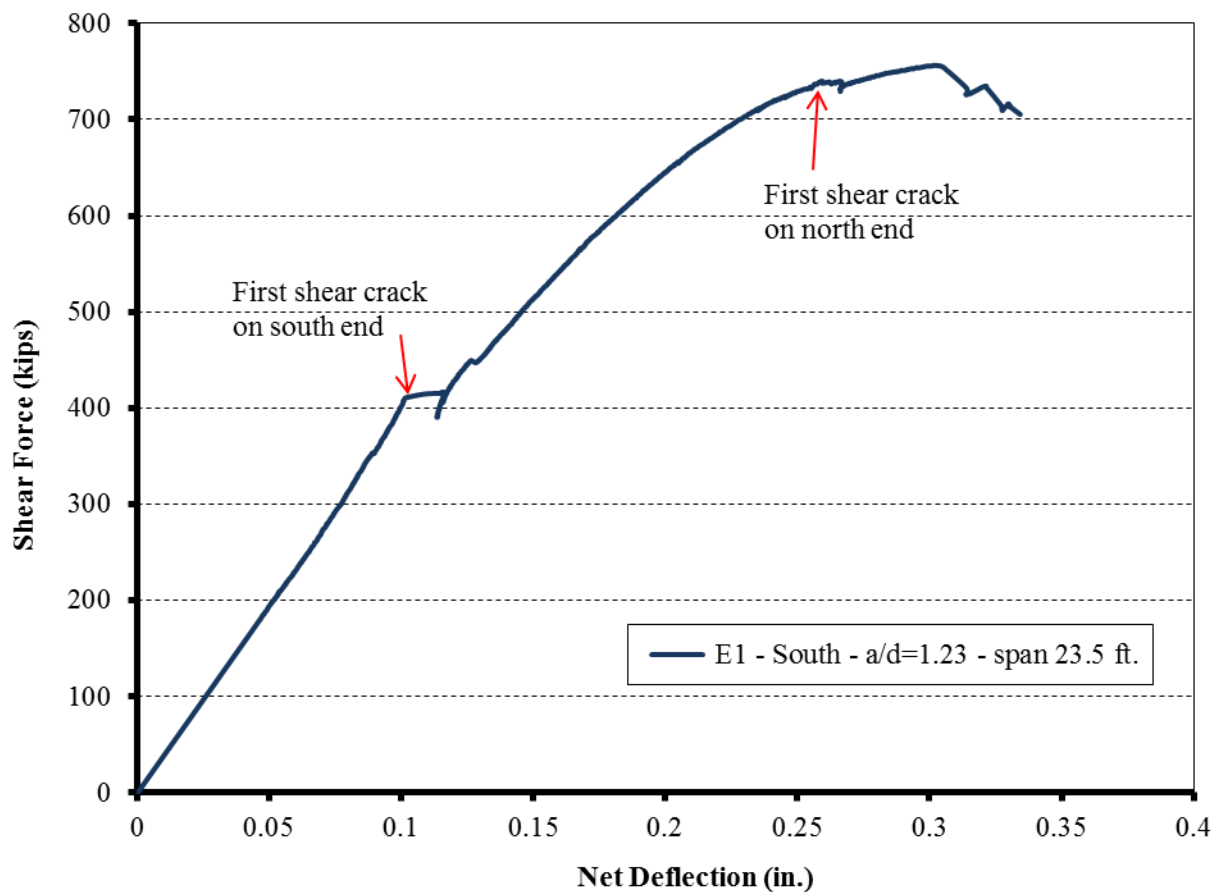
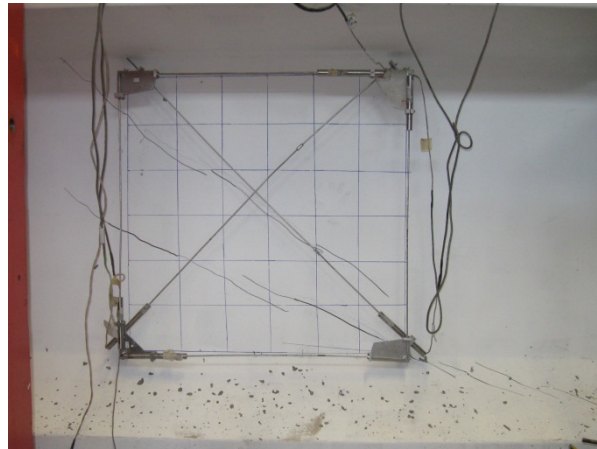


Fig. 7.36 Shear Force vs. Girder Deflection Curves for Girder E2

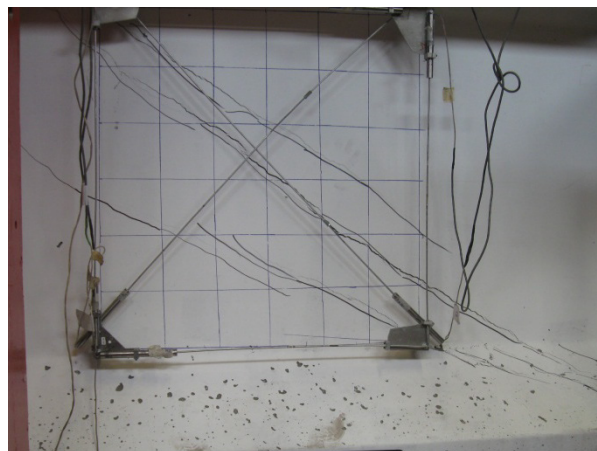
South End

South End



(a) First shear crack at 416 kips

(b) First shear crack during north end testing



(b) Shear crack pattern before failure

(d) Shear crack pattern before failure



(c) Shear failure at 756.42 kips

(f) Shear failure at 201.59 kips

Fig. 7.37 Shear Crack Pattern and Failure Mode of Girder E2

The measured slip at selected tendons, Fig. 7.38, show that the maximum slip at the south end was 0.113 inch at ST4. In spite of having this significant slip, the beam failed in web crushing at the south end having a maximum smeared tensile strain across the cracks equal to 0.0033 and a maximum smeared compressive strain equal to 0.0014, as shown in Fig 7.39 (a) and (b).

Fig. 7.39 (c) shows that the maximum smeared tensile strain in transverse direction was 0.0027 measured by LVDT V1. Fig. 7.39 (d) shows that the web had a compressive strain in the longitudinal direction at the intersection with both the top and bottom flanges with a maximum strain of 0.0008 at the peak at the intersection with the bottom flange.

Fig. 7.40 shows the local strains in the transverse steel measured by strain gauges. It shows that the transverse steel at the south end reached the yielding strain at the moment of cracking.

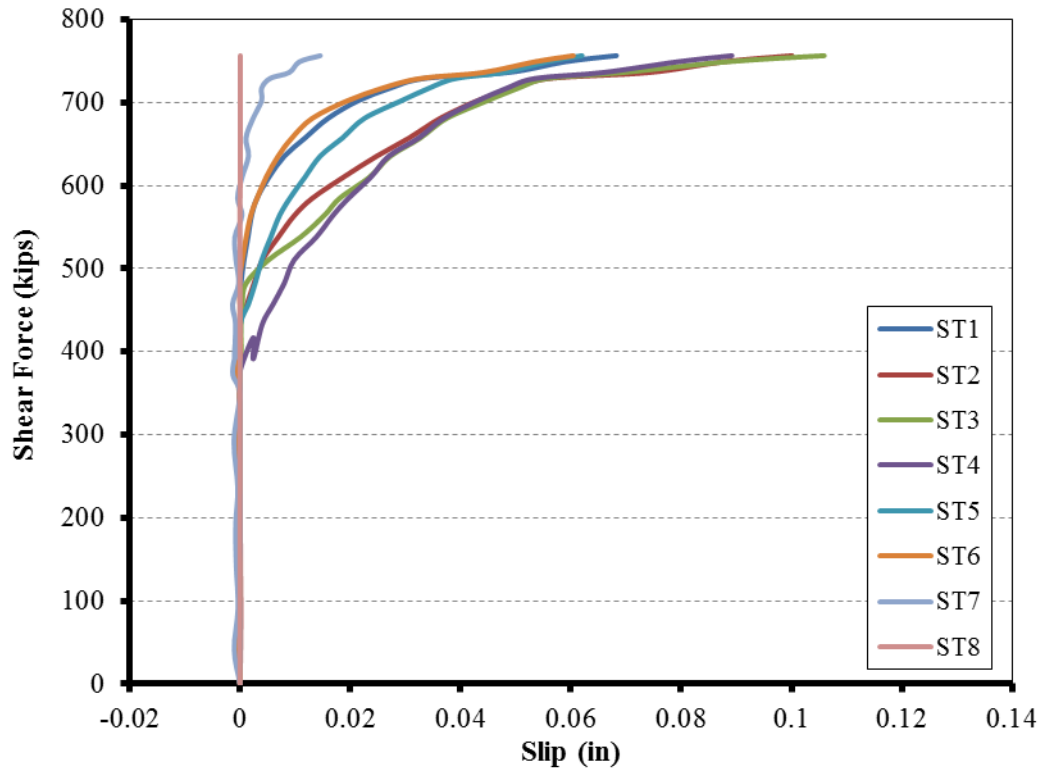
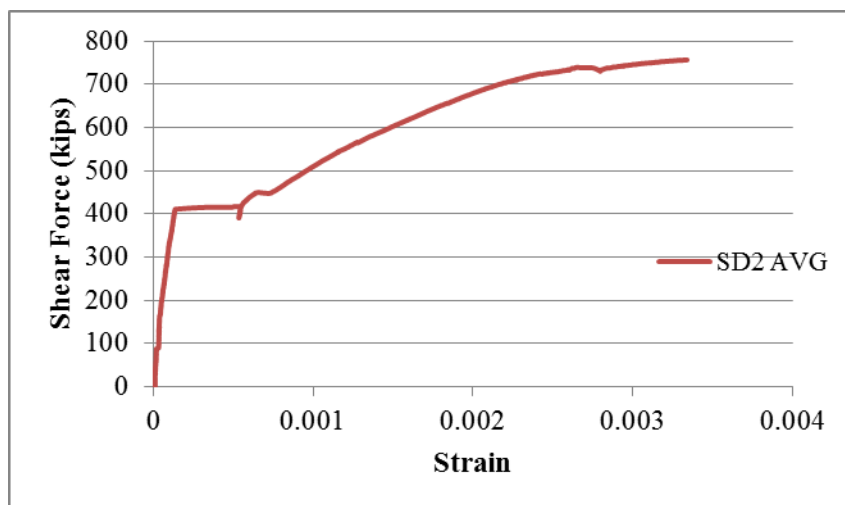
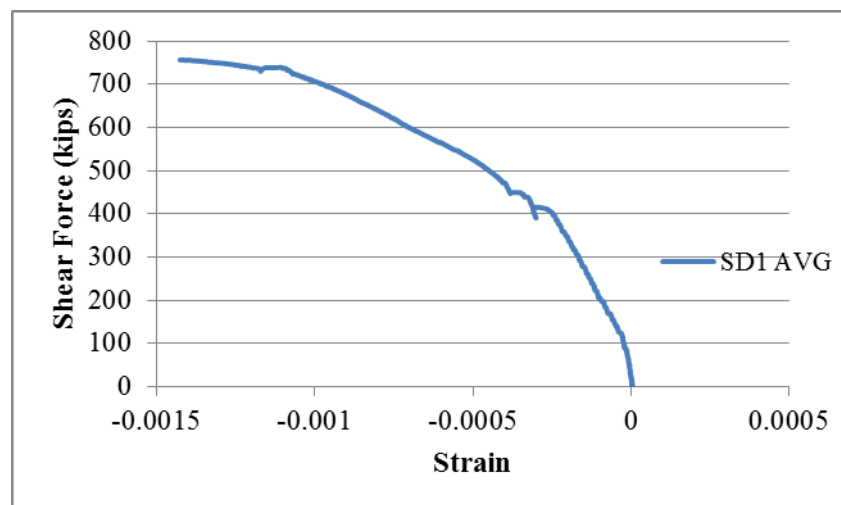


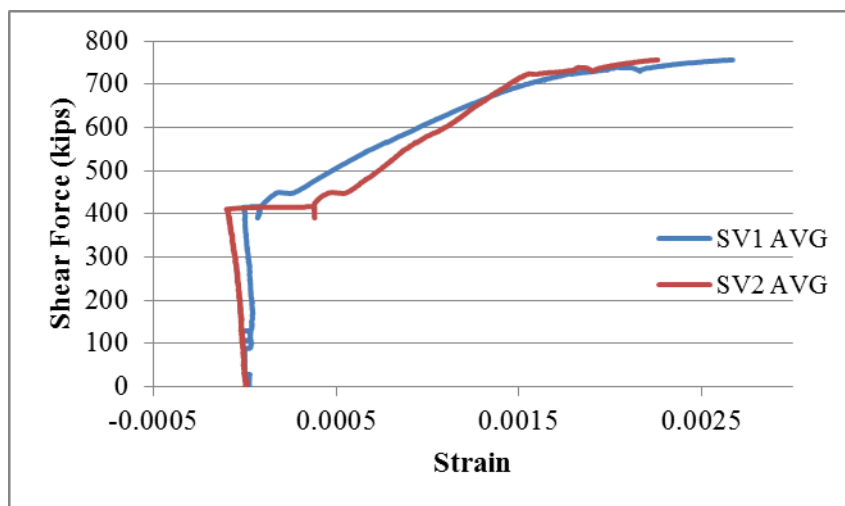
Fig. 7.38 Shear Force vs. Tendons Slip Curves for Girder E2-South



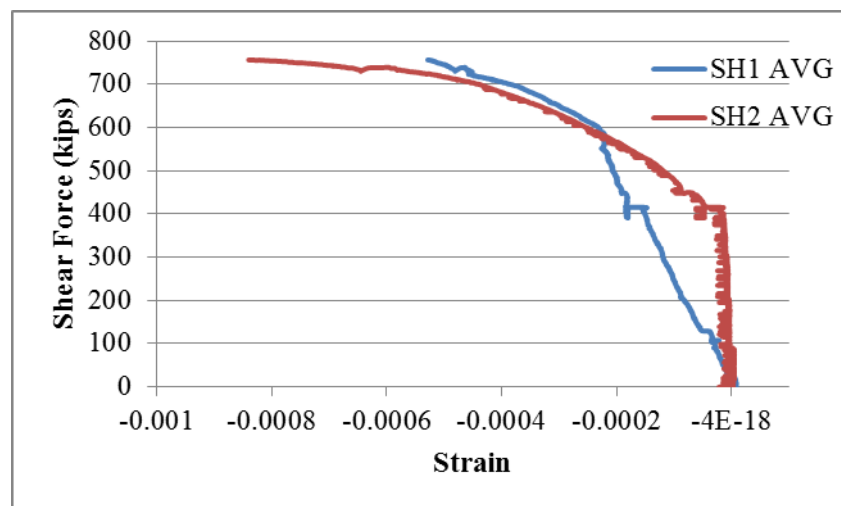
a - Average smeared tensile strain across Cracks



b - Average smeared compressive strain in concrete struts

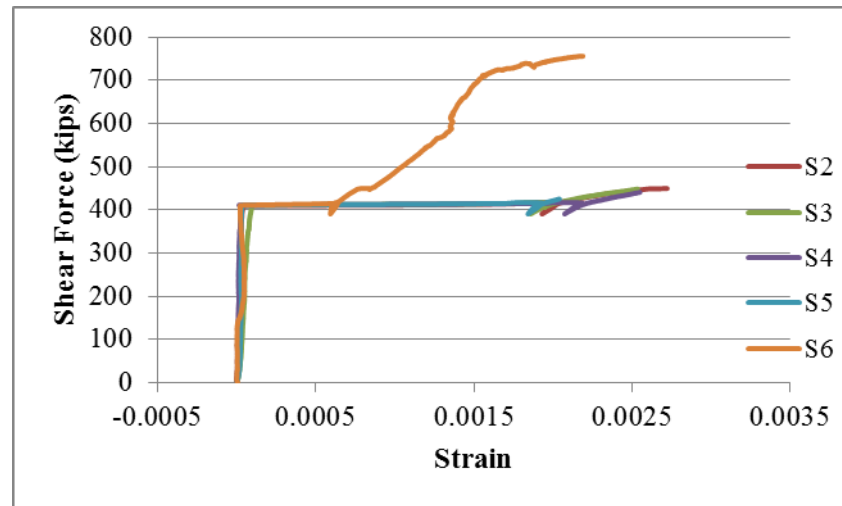


c - Average transverse smeared strain



d - Average longitudinal smeared strain

Fig. 7.39 Shear Force vs. Concrete Smeared Strains Curves for Girder E2 (South End Test)



a - Average transverse smeared strain

Fig. 7.40 Shear Force vs. Local Transverse Tensile Strain of Girder E2

7.5. Service Load vs. Cracking Load

In this section, the experimental cracking load for the girders designed according to TxDOT specifications recorded during experiments is compared to the service cracking load according to AASHTO LRFD (2010). The cracking load of the first tested side of each girder is used in this comparison.

The weights and spacing of axles and wheels for design tandem consisting of two 25 kips wheels with 4 feet apart, in addition to a lane load of 0.64 kip/ft assumed to cover 10 ft in the transverse direction according to HL-93 Load Pattern was used to calculate the live loads. The dynamic effect is taken by increasing the tandem weight by 33%. The maximum spacing (9.333 ft) between girders was used to calculate the maximum self-weight of the top slab and the maximum lane load (0.60 kip/ft) required to be carried by each girder. The maximum span corresponding to the used number of tendons is employed. Table 7.1 shows the comparison between the experimental cracking load and the service load. The comparison shows that the Tx-girders have no cracks under service loads.

Table 7.1 Experimental Cracking Load vs. Service Load

Beam I.D.	Cracking Load (kips)	Service Load (kips)
G1 (Tx28)	206	141
D1 (Tx46)	241	183
E1 (Tx62)	250	228

7.6. Discussion of Shear Force vs. Tendon Slip Curves

By comparing the shear force versus tendon slip presented before, a few points can be concluded. First, three girders that have a high percentage of transverse steel according to TxDOT standards exhibited minor slip until the test stopped because of failure occurrence or reaching the limited capacity of the hydraulic jacks. The highest measured slip belonged to

girder G1 (Tx28). Although the measured slip in both ends is very minor, around 0.02 inch, it was relatively higher at the south side where the shear span to depth ratio is less. Not all the tendons in the north end exhibited a slip. For example it can be seen that no slip has been recorded for tendons NT7 and NT8, as shown in Fig. 7.3. On the south side all of the tendons exhibited the same amount of slip, as shown in Fig. 7.4. On both ends, the recorded slip did not affect the shear capacity of the girder and the girder finally failed in web shear.

The measured slip at selected tendons of girder G2, as shown in Figs. 7.10 and 7.11, show that the maximum slip at the north end was near 0.05 inch at both ends, which is higher than that recorded in Girder G1.

Figures 7.17 and 7.18 show the shear force versus slip curves for girder D1 (Tx46). At both ends of this girder, a negligible slip was measured by the LVDTs posted on the selected tendons. The maximum value recorded during testing both ends of this girder is less than 0.02 inches. All tendons on the south side exhibit the same trend as the load increases, as seen in Fig. 7.17. At the north side, tendons NT7 and NT8 show a sudden increase in measured slip at a shear force near 540 kips, as shown in Fig. 7.18. From Figs. 7.24 and 7.25, it is very obvious that the slip is higher than that in girder D1. Comparing the data from girder D2 with the data available from the girder D1 shows the effect of the transverse reinforcement percentage on the amount of slip.

Figures 7.31 and 7.32 show the shear force versus slip curves for girder E1 (Tx62). As it was mentioned before, due to the limitation of the hydraulic jacks' capacity, this girder could not be failed. Until the test stopped, the data recorded from the selected tendons show a very minor slip at both ends. The south end exhibits a relatively higher trend than the north end.

Figure 6.38 shows the shear force versus slip curves for girder E2 (Tx62). The recorded slip is very high. If the girder E1 could be failed, it is not expectable to have such high slip. Comparing Figs. 7.24 and 7.38 show the effect of the cross-section proportionality, or the web depth to thickness ratio, on slip magnitude. This ratio and the measured slip in the case of girder E2 (Tx62) are higher than girder D2 (Tx46).

7.7. Maximum Shear Strength

Table 7.2 summarizes the ultimate shear strength for each end of the six tested girder as well as the test variables corresponding to each end. It should be noticed that the ultimate strength of each end shown in this table includes half the girder's own weight.

Table 7.2 Test Variables and Ultimate Shear Strength of Girders

Girder	d	a/d	Concrete strength f'_c (psi)	Experimental Ultimate Shear Strength, (kips)		Failure Mode
G1	31.60	1.58	11000	North	691.02	Web Shear
		1.15		South	801.03	Web Shear
G2	23.60	1.57	13000	North	464.84	Web Shear
		1.28		South	532.26	Web Shear
D1	48.61	1.56	11200	North	793.46	Web Shear
		1.16		South	926.44	Web Shear
D2	40.61	1.55	11200	North	588.58	Web Shear
		1.23		South	683.65	Web Shear
E1	63.95	1.59	11000	North	763.68	Web Shear
		1.18		South	869.96	Web Shear
E2	55.95	-	10600	North	-	-
		1.23		South	768.27	Web Shear

7.8. Maximum Shear Strength vs. AASHTO LRFD (2010)

The maximum shear strength of the first girder of each size, G1, D1, and E1, with a top slab and transverse steel according to TxDOT specifications will be used to evaluate the ability of the used cross-sections to reach the maximum shear strength proposed by AASHTO LRFD (2010) without having premature failure in the end zone due to shear bond failure.

Table 7.3 summaries the ratio between the shear strength reached during the test V_{Test} to the ultimate shear strength V_u . According to AASHTO LRFD (2010) for the girder only excluding the top slab, where:

$$V_u = \phi 0.25 f'_c b_w d_v \quad (7.1)$$

For simplicity the effective shear depth d_v will be taken as 90% of the depth of the flexure reinforcement measured from the top of the top flange d , and the resistant factor ϕ will be taken equal to 0.9.

Table 7.3 Test Variables and Ultimate Shear Strength of Girders

Girder	d	Concrete strength f'_c (psi)	Experimental Ultimate Shear Strength, (kips)		Ultimate shear strength	$\frac{V_{Test}}{V_u}$
G1	31.60	11000	North	691.02	367.98	1.88
			South	801.03		2.18
D1	48.61	11200	North	793.46	644.72	1.23
			South	926.44		1.44
E1	63.95	11000	North	763.68*	872.09	0.88*
			South	869.96*		1.00*

*Maximum shear force reached during the test due to the limitations of jack capacity

Table 7.2 ensures that the used cross section having the specified amount and arrangement of transverse reinforcement according to TxDOT specifications can reach the maximum shear strength according to AASHTO LRFD (2010) without having a premature failure in the end zone.

7.9. Proposed Equation for Concrete Contribution in End Zone

The local strain in the transverse rebars measured by pre-posted strain gauges presented and discussed before is used in calculating the average strain in transverse rebars. This average strain is used to evaluate the forces in transverse rebars, which simply represents the steel contribution V_s . By subtracting this value of the total shear strength applied to the girder, the concrete contribution can be calculated. Table 7.4 shows full detailed calculations of steel and concrete contribution for the six tested girders.

Figure 7.41 shows the variation of the normalized concrete contribution versus shear span to depth ratio. The data from the tested girders shows that the equation proposed by Laskar et al. (2010) is able to accurately predict the concrete contribution in the end region of prestressed girders. The only point lying under the horizontal line equation proposed by Laskar et al. (2010) is for the south side of the girder E1 (Tx62), which could not be failed. It is expected that with increasing the applied load the concrete contribution will increase to be higher than the proposed horizontal line. Although the data at the shear span to depth ratio a/d around 1.2 is more scattered than that data available at the shear span to depth ratio a/d around 1.6, the equation overall has been proved to be applicable for different girder sizes. Also, it has been proved that UH-equation can be used to well predict the concrete contribution to the shear-bond capacity of the girders tested by Kuchma et al. (2008) except for girders G5E, G5W, and G6W. For these girders, the concrete contribution comes out to be less than what is predicted by the UH-equation.

Table 7.4 Calculations of Steel and Concrete Shear Contribution

Girder I.D.	Ultimate Shear Capacity ($V_{u,exp}, kips$)	d (in.)	a/d	fc' (psi)	Average Strain (ϵ_{avg})	Actual ($V_s, kips$) (kips)	Concrete Contribution ($V_c, kips$)
G1	North 691.02	31.60	1.58	11000	$0.80 \epsilon_y$	364.80	326.22
	South 801.03		1.15		$0.75 \epsilon_y$	439.20	361.83
G2	North 464.84	23.60	1.57	13000	ϵ_y	11.70	453.14
	South 532.26		1.28				520.56
D1	North 793.46	48.61	1.56	11200	ϵ_y	297.60	495.86
	South 926.44		1.16		$0.70 \epsilon_y$	534.24	392.20
D2	North 588.58	40.61	1.55	11200	ϵ_y	24.46	564.12
	South 683.65		1.23				659.19
E1	North 763.68	63.95	1.59	11000	$0.63 \epsilon_y$	105.84	657.84
	South 869.96		1.18		$0.70 \epsilon_y$	443.52	426.44
E2	South 768.27	55.95	1.23	10600	ϵ_y	35.96	732.31

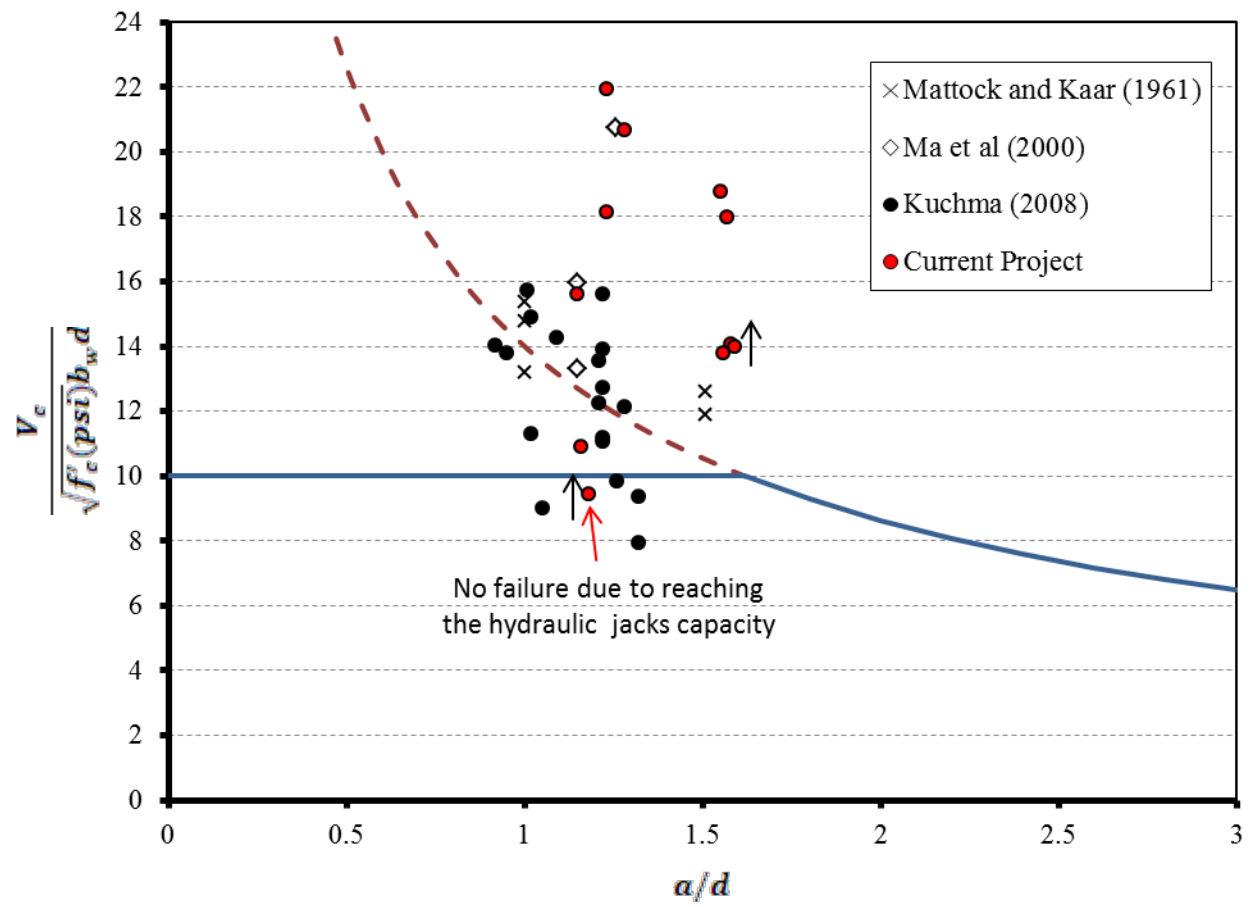


Fig. 7.41 Variation of the Normalized Concrete Shear Contribution with Shear Span to Effective Depth Ratio a/d for Girders

CHAPTER 8 SIMULATION OF FULL SCALE PRESTRESSED CONCRETE I-GIRDERS FAILED IN SHEAR

8.1. Introduction

The experimental data presented before in Chapter 7 will be used to validate the capability of the Simulation of Concrete Structures (SCS) finite element program to simulate different sizes of prestressed girders. The same technique used before in Chapter 5 will be used in simulating the behavior of these six girders.

8.2. Analytical Model

The finite element models of the prestressed girders created for analyzing the girders using SCS are described in this section. The web of each girder, which resists the shear forces acting on the girder, is defined by 16 PCPlaneStress Quadrilateral elements in the longitudinal direction. The number of membrane elements in the transverse direction is decided based on the depth of the web.

The top and bottom flanges are modeled using 16 NonlinearBeamColumn elements at the top and bottom of the PCPlaneStress Quadrilateral elements. The inclined top and bottom flanges are modeled using rectangular cross-sections of an equivalent area. Each NonlinearBeamColumn element is defined with two control sections, one representing the concrete and the other representing the steel rebar or the prestressing tendon. It should be noted that the NonlinearBeamColumn elements were previously developed in OpenSees (Taucer et al. 1991).

Concrete02, Steel01 and Steel02 are previously defined in the OpenSees framework and are used to define the concrete and steel fibers in NonlinearBeamColumn elements in the top and bottom flanges. Concrete02 gives the opportunity to add the tensile strength of concrete, which is required to resist tensile stresses at the top flange due to prestressing force application. Steel01 was used to define the mild steel rebars used in the top flange. Since Steel02 gives the opportunity to define the prestressing force as an “initial stress,” it was used to define the prestressing tendons in the bottom flange. This initial stress is taken approximately equal to 80% of the applied prestressing stresses at transfer ($0.75f_{pu}$).

ConcreteL01, SteelZ0, and Tendon L01 (Laskar 2009) are uniaxial materials developed at the University of Houston, and they are used to define concrete, transverse steel, and prestressing tendons in the PCPlaneStress quadrilateral elements, respectively. The constant k is used in Concrete02 and ConcreteL01 to impose an upper limit to the initial stress strain relationship of concrete in compression and thereby make the initial slope of the stress strain curve of concrete lower than $\frac{2f'_c}{\epsilon_c}$. The constant k is taken as 1.4 for the analysis of all the girders in this research work.

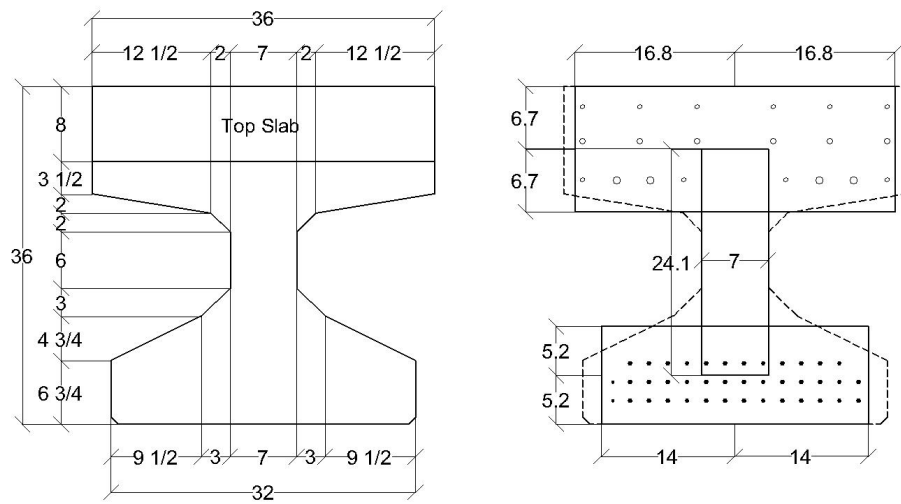
8.3. Finite Element Model of Group G Girders

The two Girders G1 and G2 in this group had been tested first at the north end using a shear span to depth ratio of 1.58 and 1.57, respectively. After the failure of the north end, the south end was loaded using a smaller shear span to depth ratio. In this section the behavior of the north end only will be simulated using SCS and compared to the experimental results. Figs. 8.1 and 8.2 show the real tested cross-section and the analyzed cross-section. Figs. 8.3 and 8.4 show the finite element mesh and the location of the applied loads and supports used for these two girder specimens.

The top flange in these girders was discretized into a different number of fibers due to having different sizes. In Girder G1, the flange was discretized into 450 fibers of concrete and 20 fibers of mild steel, as shown in Fig. 8.5(a), while Girder G2 was discretized into 300 fibers of concrete and 8 fibers of mild steel, as shown in Fig. 8.5(b).

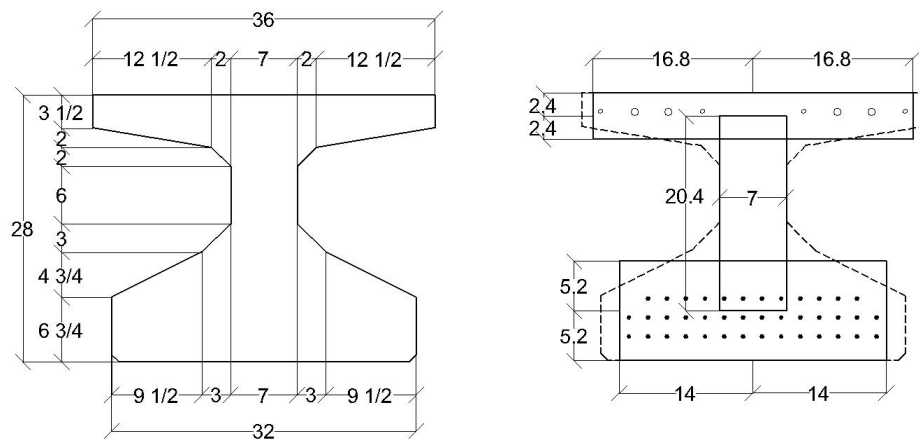
In fact, the real girders are reinforced in flexure using 40 prestressing tendons, 36 of them are discretized as fibers in the NonlinearBeamColumn elements representing the bottom flange and the remaining 4 tendons are provided in the PCPlaneStress quadrilateral elements used to represent the webs of these specimens. In addition, the concrete section of the bottom flange of both girders is discretized into 450 fibers of concrete, as shown in Fig. 8.5(c).

Figs. 8.6 and 8.7 show that the analytical model for both girders could well simulate the behavior of both girders. The initial stiffness of both girders could be captured accurately. The predicted ultimate strength is very close to the experimental strength in Girder G1 but it is around 13% higher than the experimental strength in Girder G2.



(All Dimensions are in Inches)

Fig. 8.1 Experimental and Analytical Cross Section for Girder G1



(All Dimensions are in Inches)

Fig. 8.2 Experimental and Analytical Cross Section for Girder G2

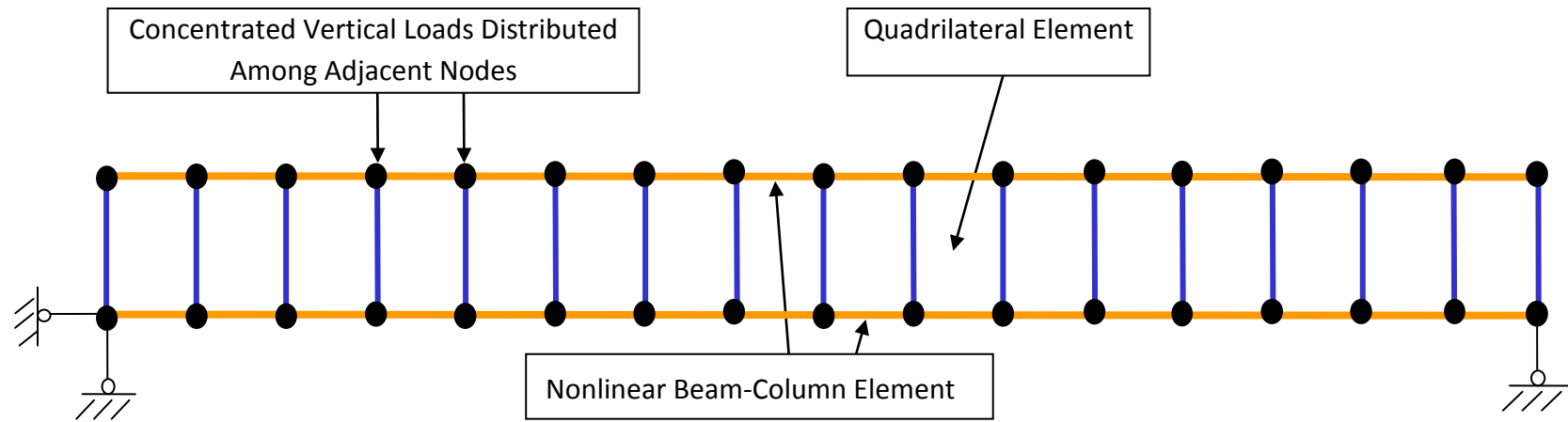


Fig. 8.3 Finite Element Mesh of Girder Specimen G1

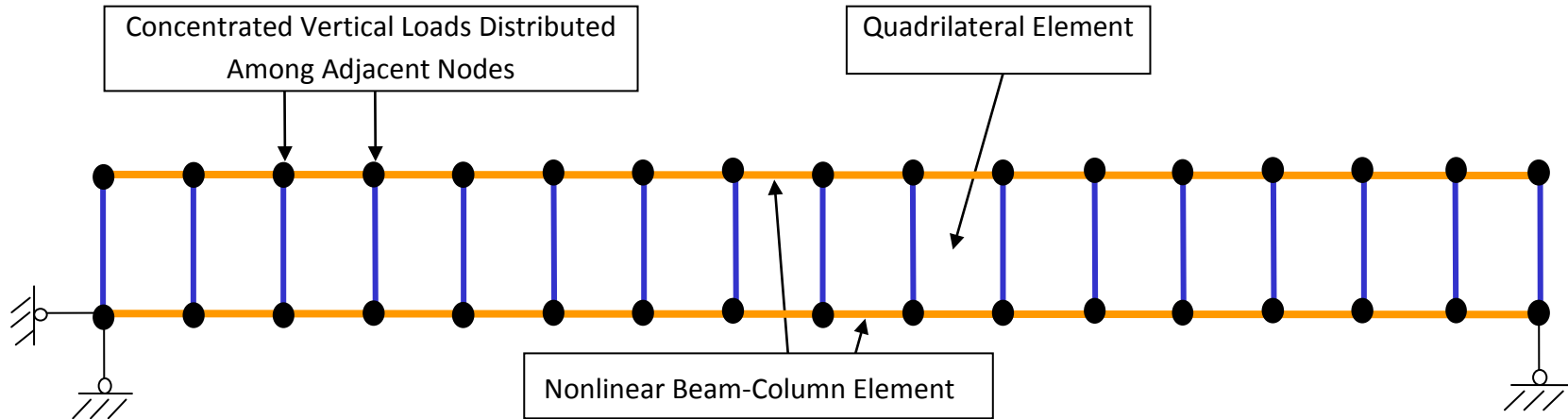
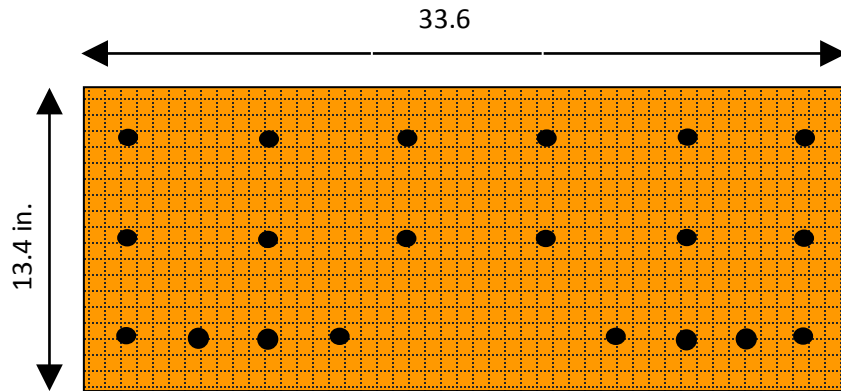
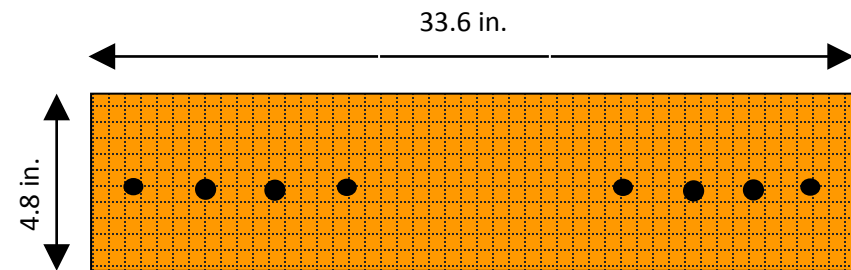


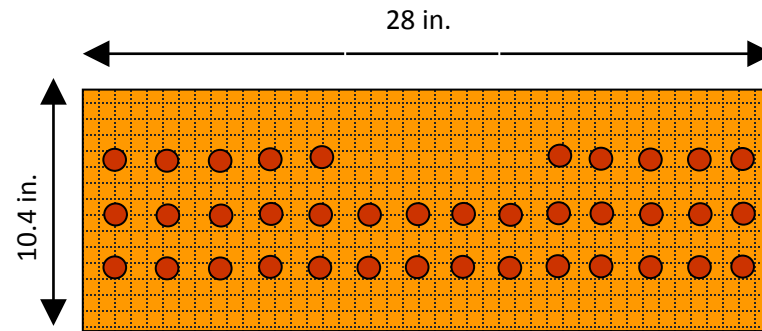
Fig. 8.4 Finite Element Mesh of Girder Specimen G2



(a) Top Flange with Mild Steel Fibers for Girder G1



(b) Top Flange with Mild Steel Fibers for Girder G2



(c) Bottom Flange with Tendons for Girders G1 and G2

Fig. 8.5 Section Discretization of NonlinearBeamColumn Elements for Girder Specimens G1 and G2

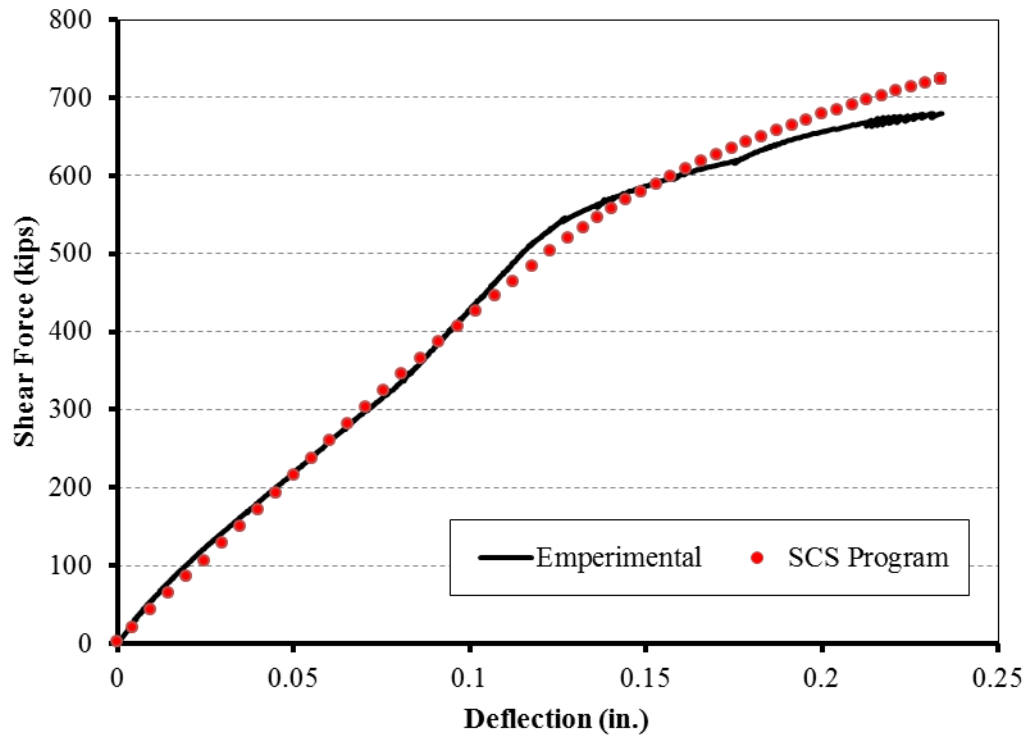


Fig. 8.6 Analytical and Experimental Load-Deflection Curves of Girder G1

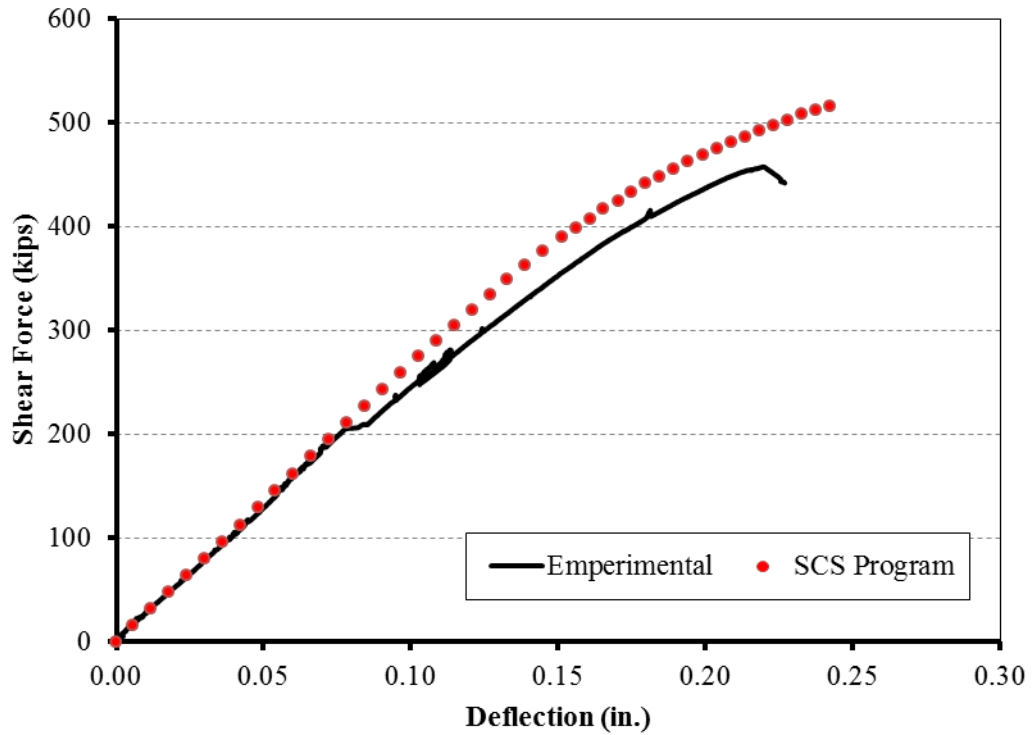


Fig. 8.7 Analytical and Experimental Load-Deflection Curves of Girder G2

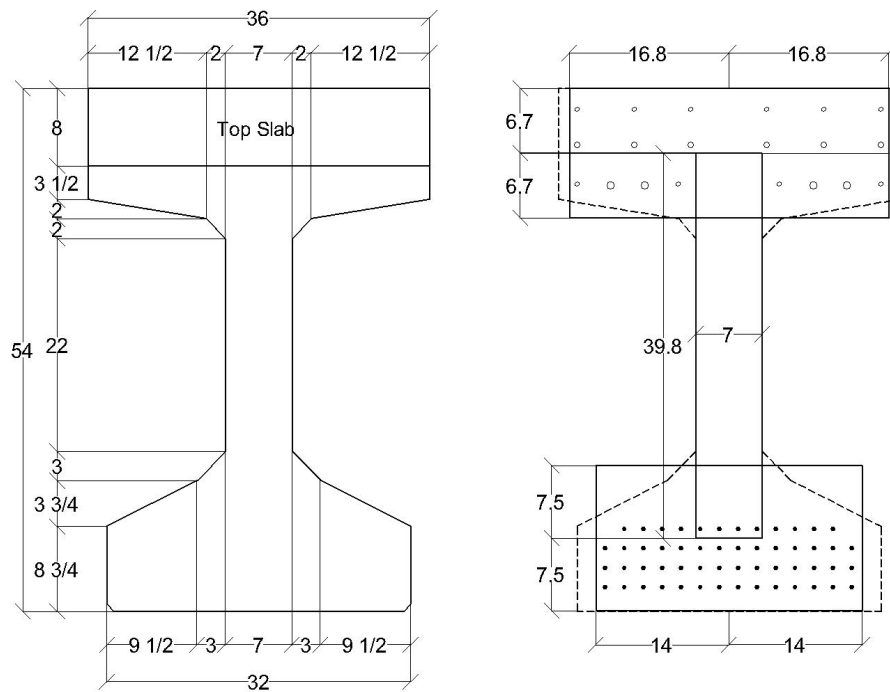
8.4. Finite Element Model of Group D Girders

This group consists of two Tx46 girders namely D1 and D2. Figs. 8.8 and 8.9 show the real tested cross-section and the analyzed cross-section for Girders D1 and D2, respectively. Fig. 8.10 shows finite element mesh and the location of the applied loads and supports used for these girder specimens.

Although having different depth due to existence of the top slab in Girder D1, the top flange in both girders was discretized into 300 fibers of concrete. In Girder D1, the top flange had 20 fibers of mild steel, as shown in Fig. 8.11(a), while in Girder D2 it had only 8 fibers of mild steel, as shown in Fig. 8.11(b).

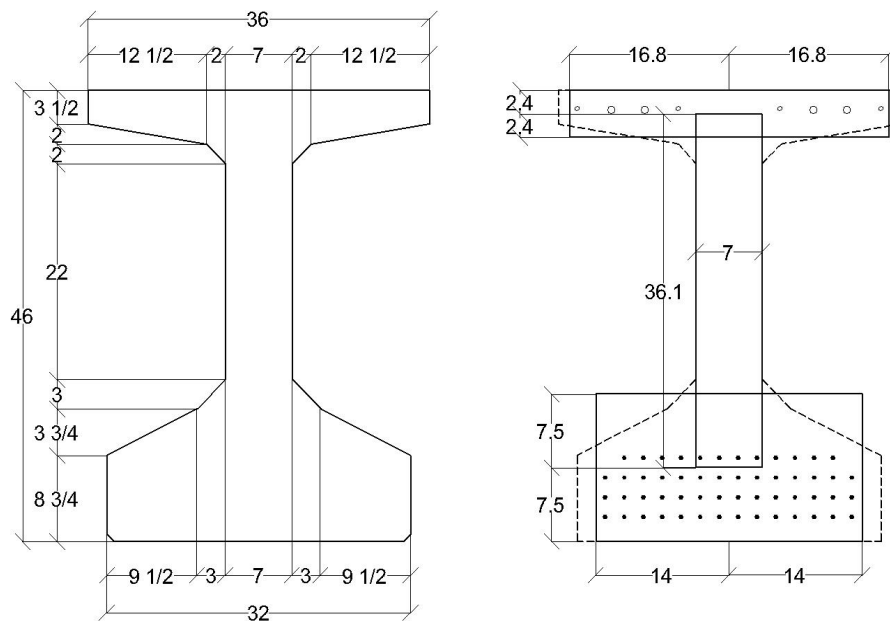
The real girders are reinforced in flexure using 54 prestressing tendons, 50 of them are discretized as fibers in the NonlinearBeamColumn elements representing the bottom flange and the remaining 4 tendons are provided in the PCPlaneStress quadrilateral elements used to represent the webs of these specimens. In addition, the concrete section of the bottom flange of both girders is discretized into 600 fibers of concrete, as shown in Fig. 8.5(c).

Figs. 8.12 and 8.13 show that the analytical model for both girders could well simulate the entire behavior of both girders. The initial stiffness of both girders could be captured accurately. The predicted ultimate strength is very close to the experimental strength in both girders, but the experimental result of Girder D1 was not ductile at the peak like the analytical results. This is due to the sudden increase in applied loads during the experiment, which resulted in a sudden failure; otherwise the girder would likely have the same ductility shown in the finite element results.



(All Dimensions are in Inches)

Fig. 8.8 Experimental and Analytical Cross Section for Girder D1



(All Dimensions are in Inches)

Fig. 8.9 Experimental and Analytical Cross Section for Girder D2

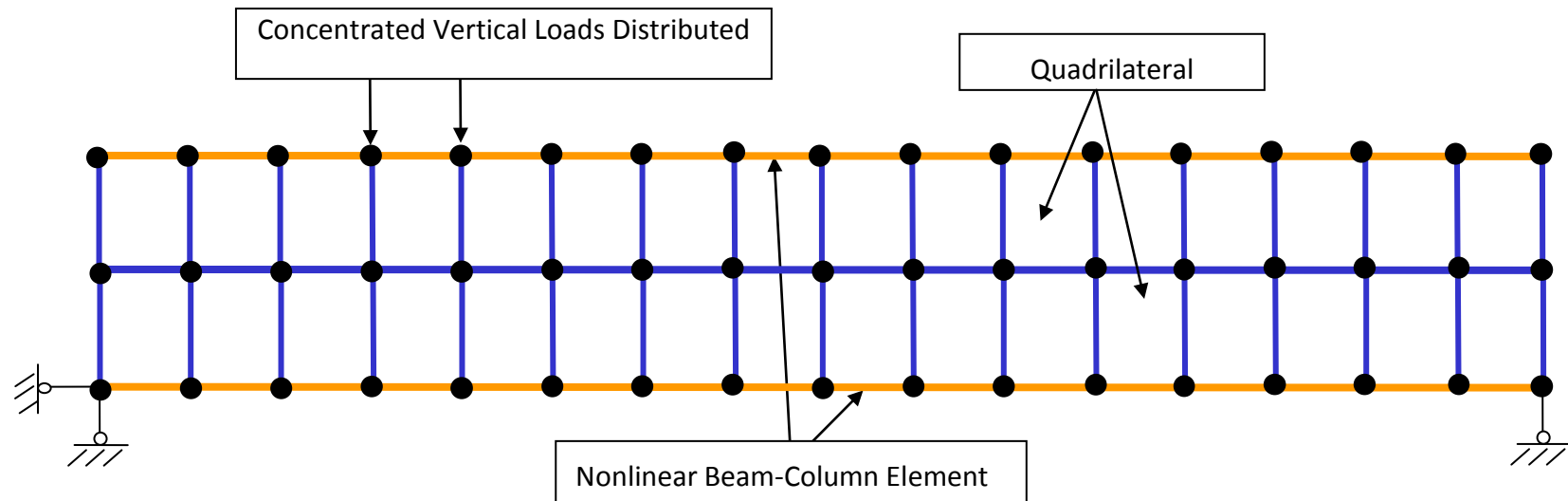
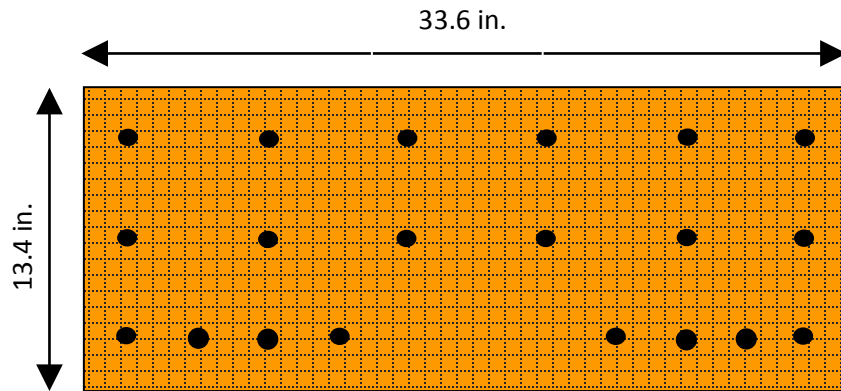
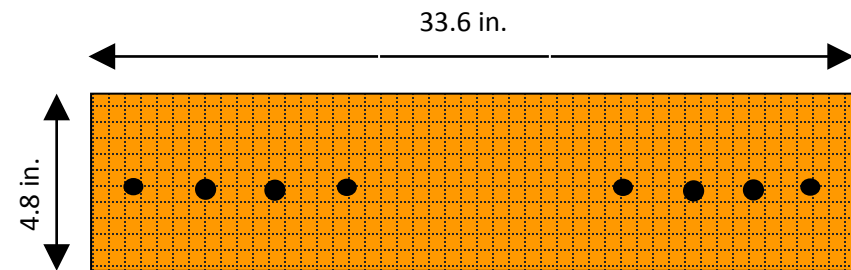


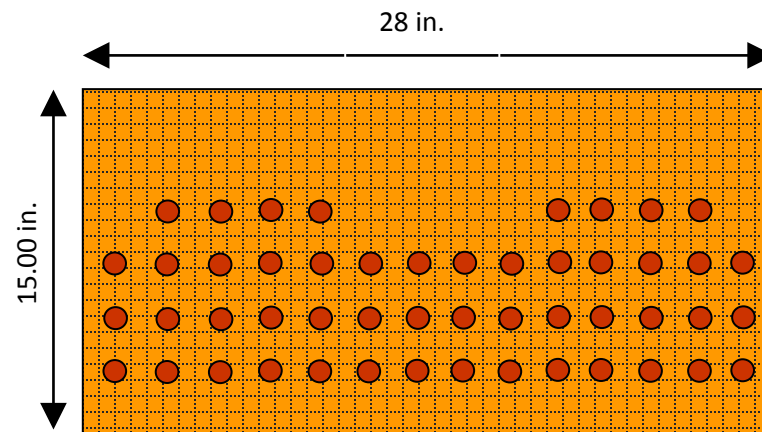
Fig. 8.10 Finite Element Mesh of Girder Specimens D1 and D2



(a) Top Flange with Mild Steel Fibers for Girder D1



(b) Top Flange with Mild Steel Fibers for Girder D2



(c) Bottom Flange with Tendons for Girders D1 and D2

Fig. 8.11 Section Discretization of NonlinearBeamColumn Elements for Girder Specimens D1 and D2

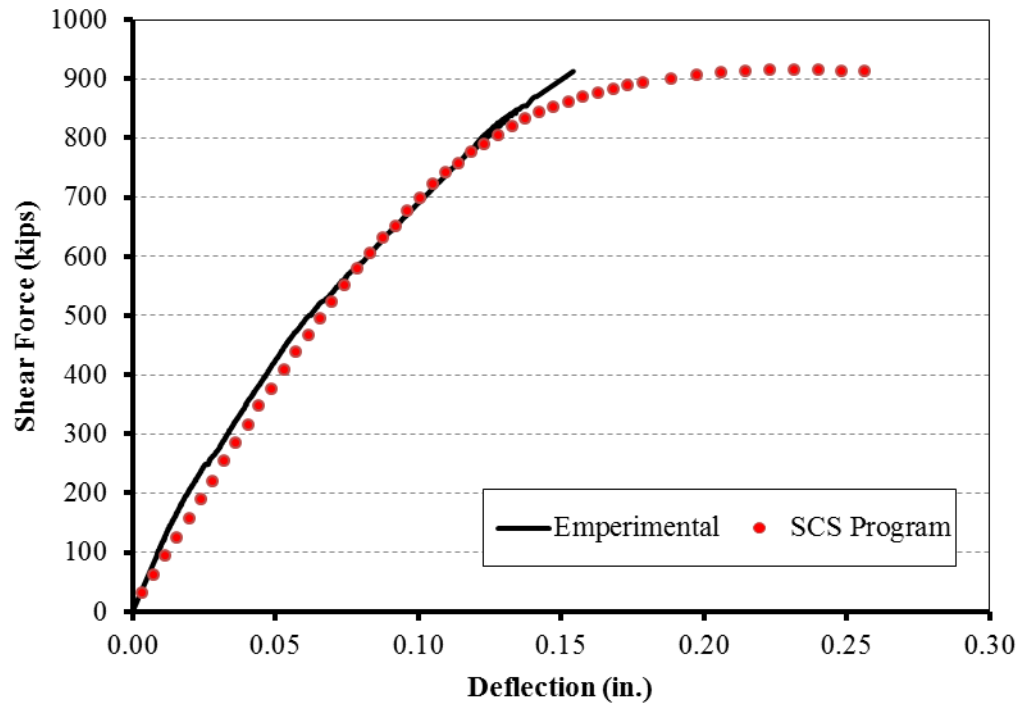


Fig. 8.12 Analytical and Experimental Load-Deflection Curves of Girder D1

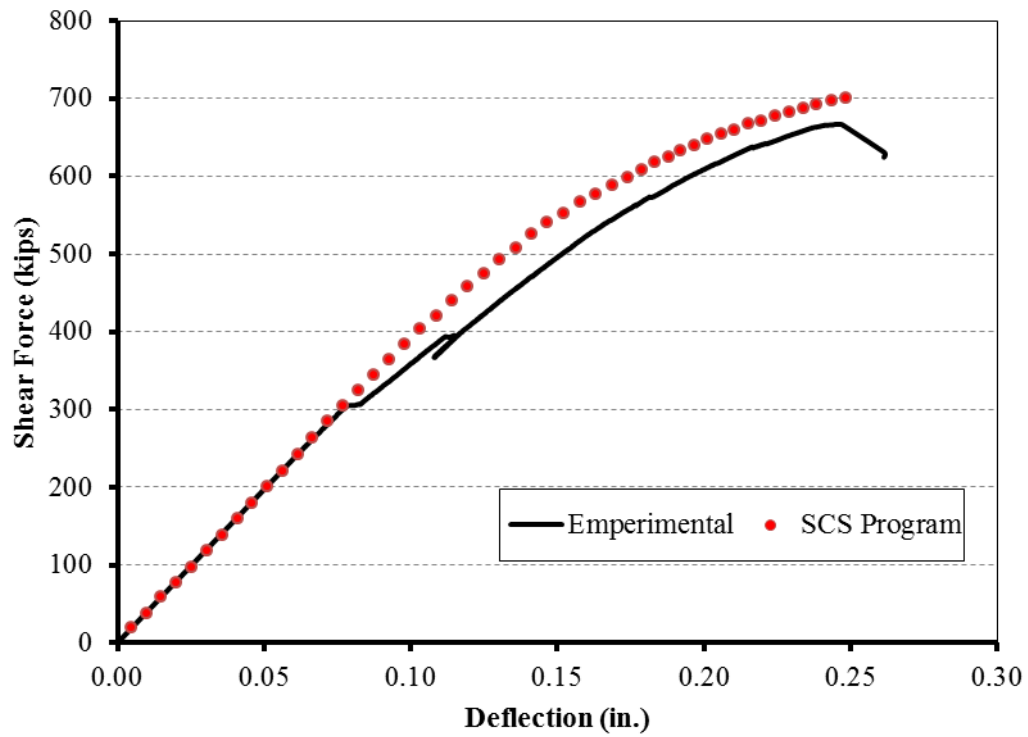
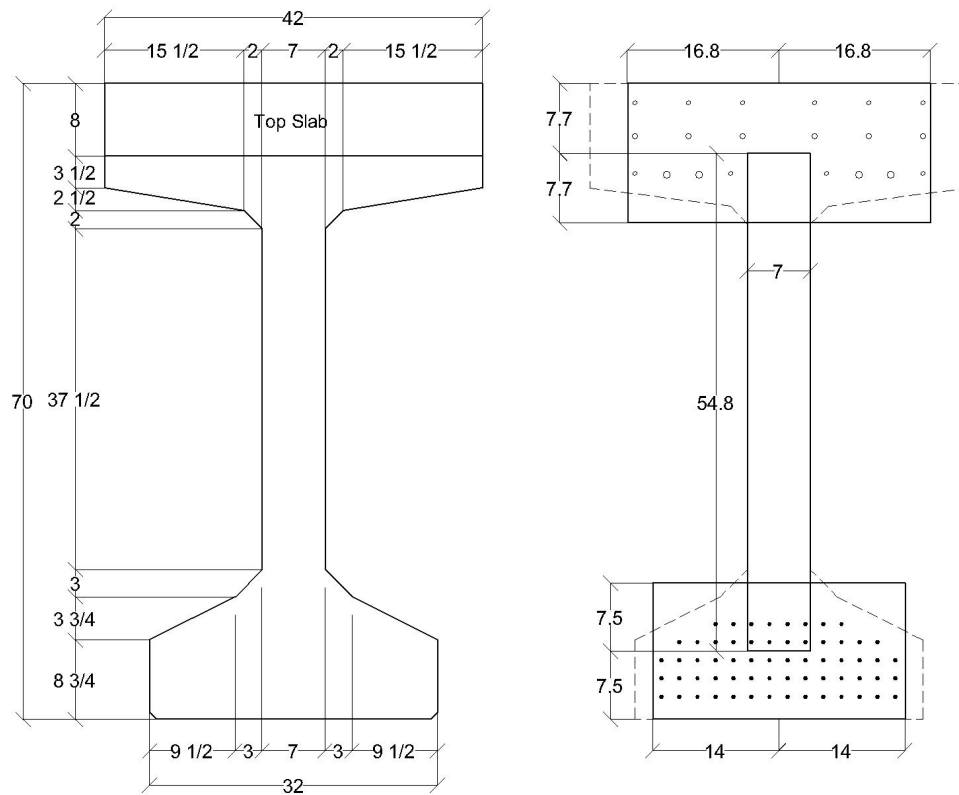


Fig. 8.13 Analytical and Experimental Load-Deflection Curves of Girder D2

8.5. Finite Element Model of Group E Girders

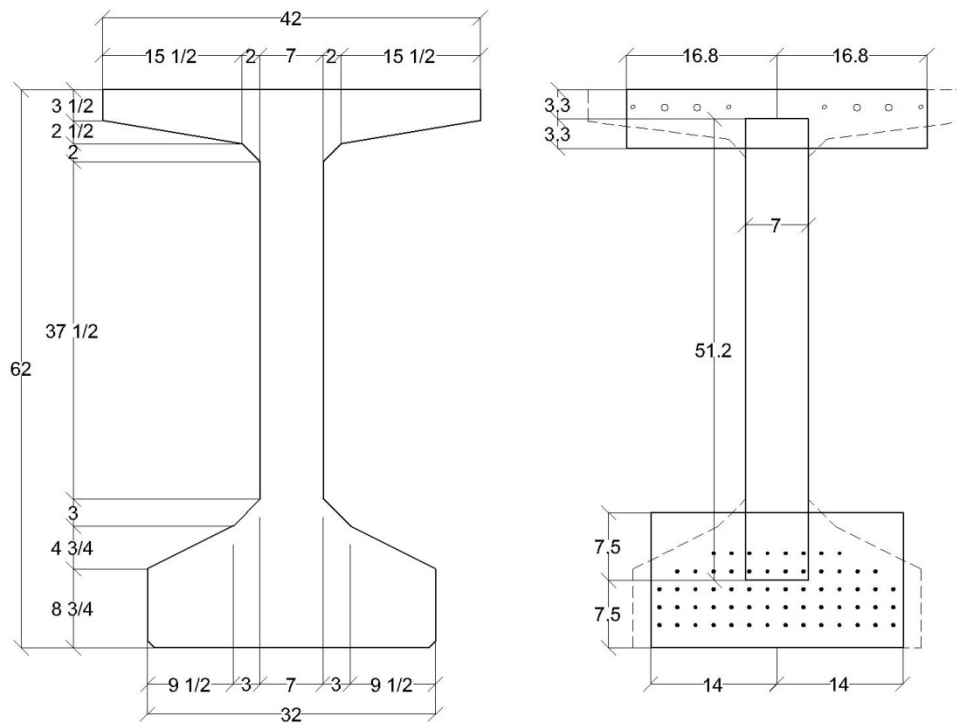
This group consists of two Tx62 girders namely E1 and E2. Figs. 8.14 and 8.15 show the real tested cross-section and the analyzed cross-section for Girders E1 and E2, respectively. Fig. 8.16 shows the finite element mesh and the location of the applied loads and supports used for these girder specimens.

The top flange in these girders was discretized into a different number of fibers due to having different sizes. In Girder E1 it was discretized into 450 fibers of concrete and 20 fibers of mild steel, as shown in Fig. 8.17(a). In Girder E2 it was discretized into 240 fibers of concrete and 8 fibers of mild steel, as shown in Fig. 8.17(b). The bottom flange is discretized into 450 fibers of concrete and 44 fiber of steel representing 44 prestressed tendons out of 62 tendons used in the real cross-section, as shown in Fig. 8.17(c). The remaining 18 tendons are simulated as smeared longitudinal reinforcement in the web.



(All Dimensions are in Inches)

Fig. 8.14 Experimental and Analytical Cross Section for Girder E1



(All Dimensions are in Inches)

Fig. 8.15 Experimental and Analytical Cross Section for Girder E2

The comparison between the analytical and experimental shear force versus net deflections are shown in Figs. 8.18 and 8.19. These figures show that the used finite element program is able to accurately predict the behavior of deep prestressed girders with total depth up to 70 inches. It should be noticed that Girder E1 did not fail in the experiment due to reaching the maximum capacity of the hydraulic jacks. The dashed line show that the expected experimental behavior of the girder at peak would be very close to the predicted behavior using the finite element program SCS.

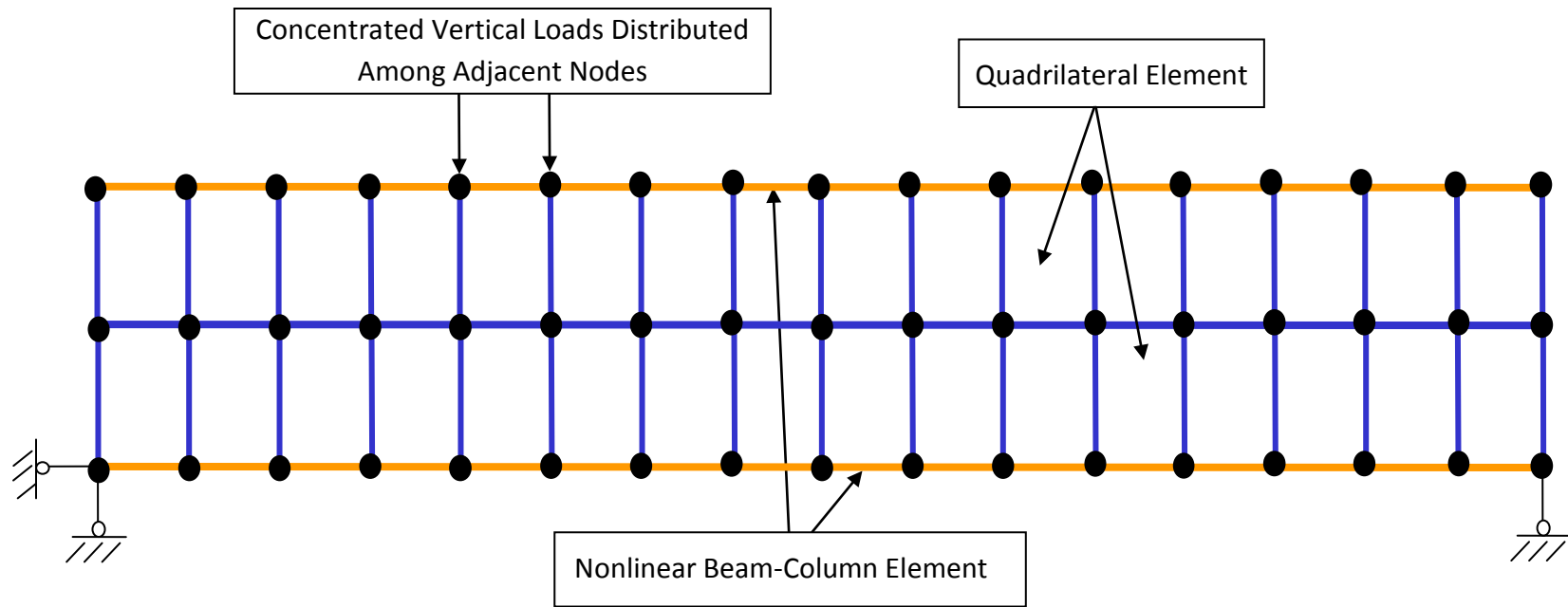


Fig. 8.16 Finite Element Mesh of Girder Specimens E1 and E2

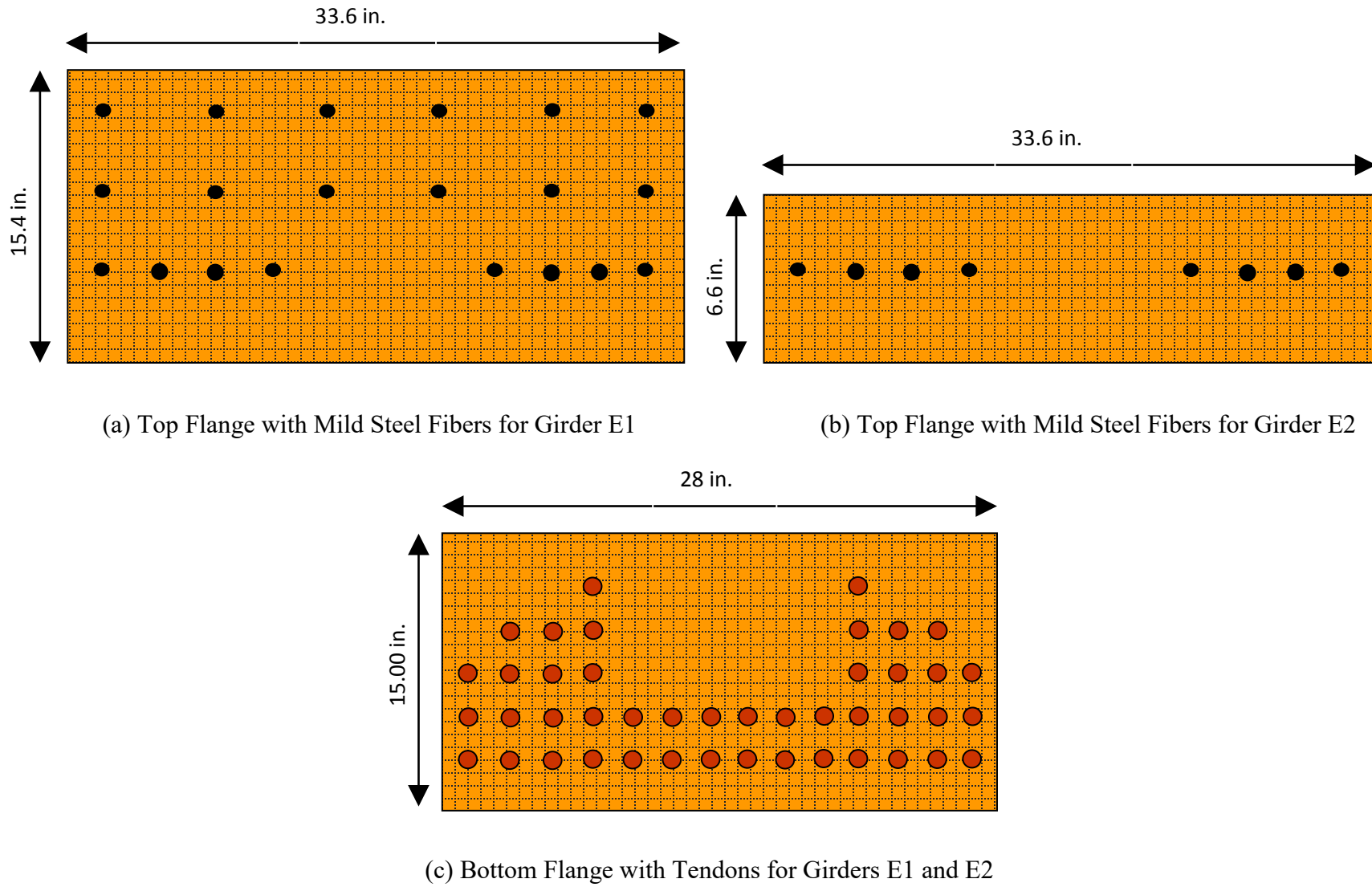


Fig. 8.17 Section Discretization of NonlinearBeamColumn Elements for Girder Specimens E1 and E2

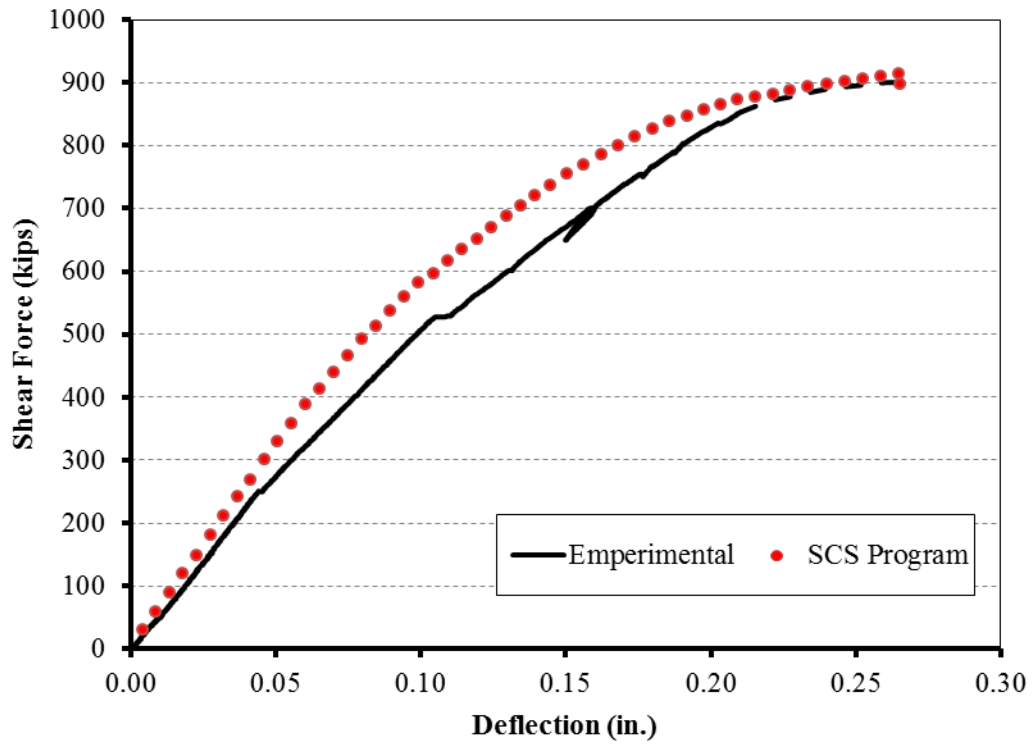


Fig. 8.18 Analytical and Experimental Load-Deflection Curves of Girder E1

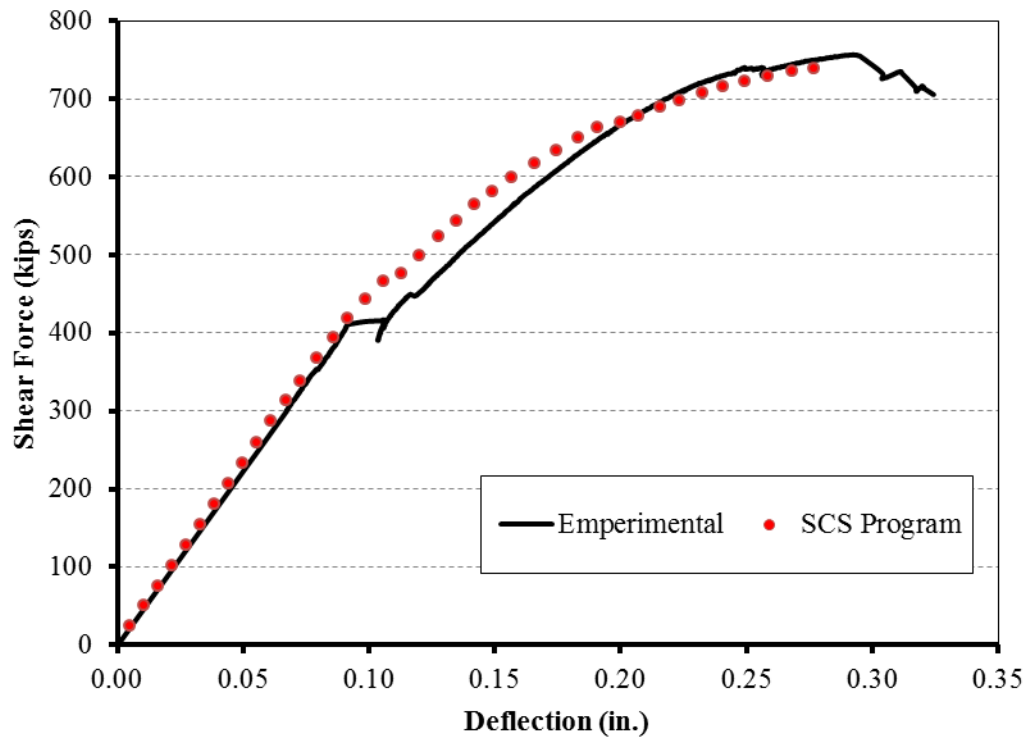


Fig. 8.19. Analytical and Experimental Load-Deflection Curves of Girder E2

8.6. Finite Element Analysis Using Fiber Elements

Another attempt to simulate the shear behavior of the six tested girders was done by discretizing the entire section into fibers with hysteretic material models for the constituent materials. The finite element model used is based on a smeared crack concrete model within a fiber beam-column element formulation. A Timoshenko beam theory was adopted in the model to account for shear deformation effects. The Softened Membrane Model (Hsu and Zhu 2002) was used to evaluate the concrete constitutive law at each fiber. To predict the descending branch of the shear stress-strain curves of membrane elements, Hsu/Zhu ratios (Poisson ratios of cracked reinforced concrete) (Hsu and Zhu 2002) were taken into effect. The work was developed using the finite element program FEAP described in Zienkiewicz and Taylor (1989). The model was implemented based on the numerically efficient force formulation (Mullapudi 2010) and (Mullapudi and Ayoub 2010).

CHAPTER 9 DESIGN RECOMMENDATION AND DESIGN EXAMPLES

9.1. Introduction

The use of the new set of design equations developed and validated for different concrete strength at the University of Houston for shear designing of PC girders are summarized and illustrated with design examples in the following sections. These design examples demonstrate that the new set is unified and applicable at any cross section along the length of the girder. The next section summarizes the design recommendation following UH-Design equations.

9.2. Design Recommendation

By knowing the ultimate shear force and the corresponding ultimate bending moment acting at a given cross section, the concrete contribution to the shear force can be evaluated and hence an adequate amount of transverse steel (stirrups) can be provided to ensure that the steel yields before concrete crushes giving enough warning. The design steps can be summarized as follows:

- (1) Calculate V_u and M_u at the desired section.
- (2) Calculate the maximum shear strength $V_{u,max}$ of the cross section, where:

$$V_{u,max} = \phi 16 \sqrt{f'_c} b_w d$$

If $V_{u,max} < V_u$, the dimension of the cross section needs to be increased

- (3) Calculate the concrete contribution to shear force acting at the desired cross-section:

$$V_c = 14 \left(\frac{V_u d}{M_u} \right)^{0.7} \sqrt{f'_c} b_w d$$

But not greater than $V_{c,max} = 10 \sqrt{f'_c} b_w d$

- (4) Calculate the steel contribution to shear force:

$$V_s = V_u - \left(\text{Smaller of } V_c \text{ or } V_{c,max} \right)$$

(5) Calculate the cross-sectional area of single stirrup A_v :

$$A_v = A_b \times n \quad (9.4)$$

where A_b = cross sectional area of one leg

n = number of legs

(6) Calculate the required spacing between stirrups s :

$$s = \frac{d}{\left(\frac{V_u}{A_v f_y} + 1\right)} \quad (9.5)$$

But not greater than the smallest of:

$$s_{max} = \frac{A_v f_y}{0.75 \sqrt{f'_c} b_w} \quad for \quad \begin{array}{l} \frac{V_u d}{M_u} \leq 0.25 \\ \frac{V_u d}{M_u} \geq 0.50 \end{array} \quad (9.6.1)$$

$$s_{max} = \frac{A_v f_y}{1.5 \sqrt{f'_c} b_w} \quad for \quad 0.25 \leq \frac{V_u d}{M_u} \leq 0.50 \quad (9.6.2)$$

$$s_{max} = \frac{d}{2} \quad (9.6.3)$$

Figure 9.1 simplifies and summarizes UH shear design procedure and all previous equations in a simple flowchart.

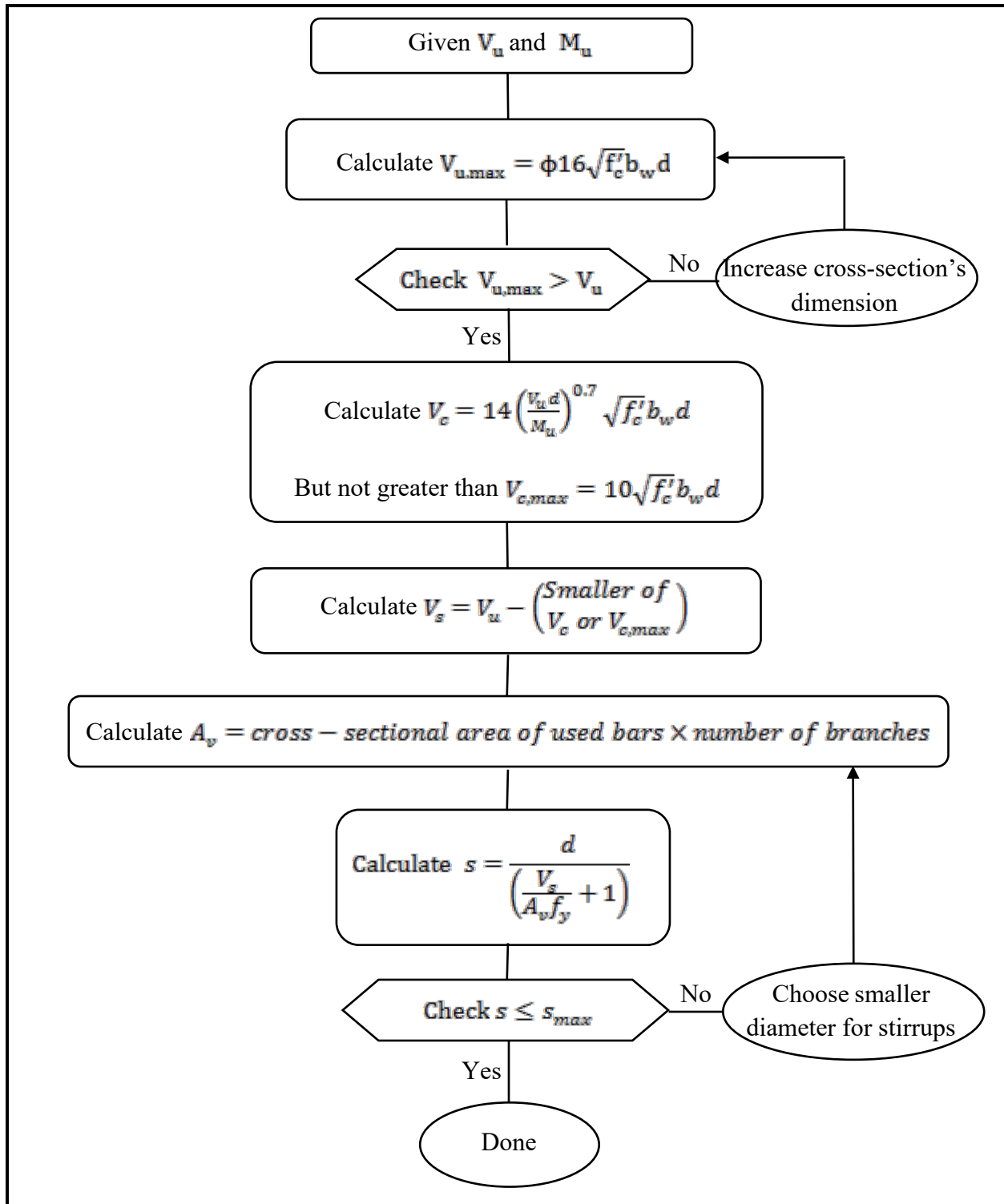


Fig. 9.1. Flowchart for UH Shear Design Procedure

9.3. Design Examples

9.3.1. Example 1

In this example the shear design for a Tx28 girder supporting a span with 40 feet is performed. The beam is reinforced in flexure with 14 tendons with half inch diameter. Top slab with total thickness 8 inches is considered. Assuming the beam supports a total load 20 kips/ ft.

The values of various quantities required for design is:

Distance of C.G. of beam cross section from top fiber = 15.02 in.

Eccentricity of tendons from C.G. = 10.48 in.

Thickness of deck slab = 8 in.

The effective depth $d = 15.02 + 10.48 + 8 = 33.50$ in.

Maximum shear capacity of the beam is,

$$V_{u,max} = \phi 16 \sqrt{f'_c} b_w d = 0.9 \times 16 \times \sqrt{11000} \times 7 \times 33.50 \times 10^{-3} = 354.2 \text{ kips}$$

Maximum concrete shear capacity of the beam;

$$V_{c,max} = 10 \sqrt{f'_c} b_w d = 10 \times \sqrt{11000} \times 7 \times 33.50 \times 10^{-3} = 245.9 \text{ kips}$$

- Shear force at critical section of the beam is:

Assuming the critical section of the beam in shear to be at a distance d from the support,

$$V_u = w_u \left(\frac{l}{2} - d \right) = 20 \times \left(\frac{40}{2} - \frac{33.50}{12} \right) = 344.2 \text{ kips} < V_{u,max} \dots\dots O.K.$$

$$M_u = \frac{w_u d}{2} (l - d) = \frac{20 \times 33.50}{2 \times 12} \times \left(40 - \frac{33.50}{12} \right) = 1039 \text{ kips.ft}$$

$$\frac{V_u d}{M_u} = \frac{344.2 \times 33.50}{1039 \times 12} = 0.9248$$

$$V_c = 14 \left(\frac{V_u d}{M_u} \right)^{0.7} \sqrt{f'_c} b_w d = 14 \times 0.9248^{0.7} \times \sqrt{11000} \times 7 \times 33.50 \times 10^{-3} \\ = 326.0 \text{ kips} > V_{c,max}$$

$$V_s = \frac{V_u}{\phi} - V_{c,max} = \frac{344.2}{0.9} - 245.95 = 136.5 \text{ kips}$$

Using two-legged #4 rebars as shear reinforcement, the spacing required to provide the required V_s has been calculated,

$$s = \frac{d}{\left(\frac{V_s}{A_v f_y} + 1 \right)} = \frac{33.50}{\left(\frac{136.5}{2 \times 0.2 \times 60} + 1 \right)} = 5.009 \text{ in.}$$

Provide two-legged #4 rebars @ 5.000 in. c/c

- Shear force at 5 ft from the support is;

$$V_u = w_u \left(\frac{l}{2} - x \right) = 20 \times \left(\frac{40}{2} - 5 \right) = 300.0 \text{ kips} < V_{u,max}$$

$$M_u = \frac{w_u x}{2} (l - x) = \frac{20 \times 5}{2} \times (40 - 5) = 1750 \text{ kips.ft}$$

$$\frac{V_u d}{M_u} = \frac{300.0 \times 33.50}{1750 \times 12} = 0.4786$$

$$V_c = 14 \left(\frac{V_u d}{M_u} \right)^{0.7} \sqrt{f'_c} b_w d = 14 \times 0.4786^{0.7} \times \sqrt{11000} \times 7 \times 33.5 \times 10^{-3} \\ = 205.6 \text{ kips} < V_{c,max}$$

$$V_s = \frac{V_u}{\phi} - V_c = \frac{300}{0.9} - 205.6 = 127.7 \text{ kips}$$

Using two-legged #4 rebars as shear reinforcement, the spacing required to provide the required V_s has been calculated,

$$s = \frac{d}{\left(\frac{V_s}{A_v f_y} + 1\right)} = \frac{33.50}{\left(\frac{127.7}{2 \times 0.2 \times 60} + 1\right)} = 5.300 \text{ in.}$$

Provide two-legged #4rebars @ 5.000 in. c/c

- Shear force at 10 ft from the support is;

$$V_u = w_u \left(\frac{l}{2} - x\right) = 20 \times \left(\frac{40}{2} - 10\right) = 200.0 \text{ kips} < V_{u,max}$$

$$M_u = \frac{w_u x}{2} (l - x) = \frac{20 \times 10}{2} \times (40 - 10) = 3000 \text{ kips.ft}$$

$$\frac{V_u d}{M_u} = \frac{200 \times 33.50}{3000 \times 12} = 0.1861$$

$$V_c = 14 \left(\frac{V_u d}{M_u}\right)^{0.7} \sqrt{f'_c} b_w d = 14 \times 0.1861^{0.7} \times \sqrt{11000} \times 7 \times 33.5 \times 10^{-3} \\ = 106.1 \text{ kips} < V_{c,max}$$

$$V_s = \frac{V_u}{\phi} - V_c = \frac{200}{0.9} - 106.1 = 116.1 \text{ kips}$$

Using two-legged #4rebars as shear reinforcement, the spacing required to provide the required V_s has been calculated,

$$s = \frac{d}{\left(\frac{V_s}{A_v f_y} + 1\right)} = \frac{33.5}{\left(\frac{116.1}{2 \times 0.2 \times 60} + 1\right)} = 5.739 \text{ in.}$$

Provide two-legged #4rebars @ 5.000 in. c/c

- Shear force at 15 ft from the support is;

$$V_u = w_u \left(\frac{l}{2} - x\right) = 20 \times \left(\frac{40}{2} - 15\right) = 100.0 \text{ kips} < V_{u,max}$$

$$M_u = \frac{w_u x}{2}(l - x) = \frac{20 \times 15}{2} \times (40 - 15) = 3750 \text{ kips.ft}$$

$$\frac{V_u d}{M_u} = \frac{100 \times 33.50}{3750 \times 12} = 0.0744$$

$$V_c = 14 \left(\frac{V_u d}{M_u} \right)^{0.7} \sqrt{f'_c} b_w d = 14 \times 0.0744^{0.7} \times \sqrt{11000} \times 7 \times 33.5 \times 10^{-3} \\ = 55.86 \text{ kips} < V_{c,max}$$

$$V_s = \frac{V_u}{\phi} - V_c = \frac{100}{0.9} - 55.86 = 55.25 \text{ kips}$$

Using two-legged #4rebars as shear reinforcement, the spacing required to provide the required V_s has been calculated:

$$s = \frac{d}{\left(\frac{V_s}{A_v f_y} + 1 \right)} = \frac{33.5}{\left(\frac{55.25}{2 \times 0.2 \times 60} + 1 \right)} = 10.15 \text{ in}$$

Provide two-legged #4rebars @ 10.00 in. c/c

Table 9.1 shows the full design at different sections along half-span of the girder.

Table 9.1 Full Design of Tx28

Shear Span	V_u (kips)	M_u (kips.ft)	$\frac{V_u d}{M_u}$	V_c (kips)	V_s (kips)	s_{req}	s_{prov}
2.79	344.2	1039	0.9248	245.9	136.5	5.009	5.000
5	300.0	1750	0.4786	205.6	127.7	5.300	5.000
7.5	250.0	2438	0.2863	143.5	134.3	5.079	5.000
10	200.0	3000	0.1861	106.1	116.1	5.739	5.000
12.5	150.0	3438	0.1218	78.87	87.80	7.191	5.000
15	100.0	3750	0.0744	55.86	55.25	10.15	10.00
17.5	50.00	3938	0.0354	33.21	22.35	17.35	10.00
20	0	4000	0	0	0.00	33.50	10.00

9.3.2. Example 2

In this example the shear design for a Tx62 girder supporting a span with 60 feet is performed. The beam is reinforced in flexure with 14 tendons with half inch diameter. Top slab with total thickness 8 inches is considered. Assuming the beam supports a total load 28 kips/ ft.

The values of various quantities required for design is

Distance of C.G. of beam cross section from top fiber = 33.72 in.

Eccentricity of tendons from C.G. = 25.78 in.

Thickness of deck slab = 8 in.

The effective depth $d = 33.72 + 25.78 + 8 = 67.50$ in.

Maximum shear capacity of the beam is,

$$V_{u,max} = \phi 16 \sqrt{f'_c} b_w d = 0.9 \times 16 \times \sqrt{11000} \times 7 \times 67.50 \times 10^{-3} = 713.6 \text{ kips}$$

Maximum concrete shear capacity of the beam;

$$V_{c,max} = 10 \sqrt{f'_c} b_w d = 10 \times \sqrt{11000} \times 7 \times 67.50 \times 10^{-3} = 495.6 \text{ kips}$$

- Shear force at critical section of the beam is:

Assuming the critical section of the beam in shear to be at a distance d from the support,

$$V_u = w_u \left(\frac{l}{2} - d \right) = 28 \times \left(\frac{60}{2} - \frac{67.50}{12} \right) = 682.5 \text{ kips} < V_{u,max} \dots\dots O.K.$$

$$M_u = \frac{w_u d}{2} (l - d) = \frac{28 \times 67.50}{2 \times 12} \times \left(60 - \frac{67.50}{12} \right) = 4282 \text{ kips.ft}$$

$$\frac{V_u d}{M_u} = \frac{682.5 \times 67.50}{4282 \times 12} = 0.8966$$

$$V_c = 14 \left(\frac{V_u d}{M_u} \right)^{0.7} \sqrt{f'_c} b_w d = 14 \times 0.8966^{0.7} \times \sqrt{11000} \times 7 \times 67.50 \times 10^{-3} \\ = 642.8 \text{ kips} > V_{c,max}$$

$$V_s = \frac{V_u}{\phi} - V_{c,max} = \frac{682.5}{0.90} - 495.6 = 262.7 \text{ kips}$$

Using two-legged #5 rebars as shear reinforcement, the spacing required to provide the required V_s has been calculated,

$$s = \frac{d}{\left(\frac{V_s}{A_v f_y} + 1 \right)} = \frac{67.50}{\left(\frac{262.7}{2 \times 0.31 \times 60} + 1 \right)} = 8.373 \text{ in.}$$

Provide two-legged #5 rebars @ 8.000 in. c/c

- Shear force at 10 ft from the support is;

$$V_u = w_u \left(\frac{l}{2} - x \right) = 28 \times \left(\frac{60}{2} - 10 \right) = 560.0 \text{ kips} < V_{u,max} \dots\dots O.K.$$

$$M_u = \frac{w_u x}{2} (l - x) = \frac{28 \times 10}{2} \times (60 - 10) = 7000 \text{ kips.ft}$$

$$\frac{V_u d}{M_u} = \frac{560 \times 67.50}{7000 \times 12} = 0.4500$$

$$V_c = 14 \left(\frac{V_u d}{M_u} \right)^{0.7} \sqrt{f'_c} b_w d = 14 \times 0.4500^{0.7} \times \sqrt{11000} \times 7 \times 67.50 \times 10^{-3} \\ = 396.7 \text{ kips} < V_{c,max}$$

$$V_s = \frac{V_u}{\phi} - V_c = \frac{560}{0.9} - 396.7 = 225.5 \text{ kips}$$

Using two-legged #5 rebars as shear reinforcement, the spacing required to provide the required V_s has been calculated,

$$s = \frac{d}{\left(\frac{V_s}{A_v f_y} + 1\right)} = \frac{67.50}{\left(\frac{225.5}{2 \times 0.31 \times 60} + 1\right)} = 9.558 \text{ in.}$$

Provide two-legged #5 rebars @ 9.500 in. c/c

- Shear force at 20 ft from the support is:

$$V_u = w_u \left(\frac{l}{2} - x\right) = 28 \times \left(\frac{60}{2} - 20\right) = 280.0 \text{ kips} < V_{u,max} \dots\dots O.K.$$

$$M_u = \frac{w_u x}{2} (l - x) = \frac{28 \times 20}{2} \times (60 - 20) = 11200 \text{ kips.ft}$$

$$\frac{V_u d}{M_u} = \frac{280 \times 67.50}{11200 \times 12} = 0.1406$$

$$V_c = 14 \left(\frac{V_u d}{M_u}\right)^{0.7} \sqrt{f'_c} b_w d = 14 \times 0.1406^{0.7} \times \sqrt{11000} \times 7 \times 67.50 \times 10^{-3} \\ = 175.7 \text{ kips} < V_{c,max}$$

$$V_s = \frac{V_u}{\phi} - V_c = \frac{280.0}{0.9} - 175.7 = 135.4 \text{ kips}$$

Using two-legged #5 rebars as shear reinforcement, the spacing required to provide the required V_s has been calculated,

$$s = \frac{d}{\left(\frac{V_s}{A_v f_y} + 1\right)} = \frac{67.50}{\left(\frac{135.4}{2 \times 0.31 \times 60} + 1\right)} = 14.55 \text{ in.}$$

Provide two-legged #5 rebars @ 14.5 in. c/c

Table 9.2 shows the full design at different sections along half-span of the girder.

Table 9.2 Full Design of Tx62

Shear Span	V_u (kips)	M_u (kips.ft)	$\frac{V_u d}{M_u}$	V_c (kips)	V_s (kips)	S_{req}	S_{prov}
5.625	682.5	4282	0.8966	495.6	262.8	8.370	8.000
10.00	560.0	7000	0.4500	396.7	225.5	9.560	9.500
12.50	490.0	8313	0.3316	320.4	224.1	9.610	9.500
15.00	420.0	9450	0.2500	262.9	203.8	10.42	9.500
17.50	350.0	10413	0.1891	216.2	172.7	11.97	9.500
20.00	280.0	11200	0.1406	175.7	135.4	14.55	14.50
22.50	210.0	11813	0.1000	138.4	94.90	19.01	14.50
25.00	140.0	12250	0.0643	101.6	53.94	27.55	14.50
27.50	70.00	12513	0.0315	61.67	16.11	47.10	14.50
30.00	0.000	12600	0.0000	0	0	67.50	14.50

CHAPTER 10 CONCLUSIONS

10.1. Final Summary

The work presented in this report with regard to the study of the shear behavior and design of prestressed concrete members can be summarized as follows:

- (1) Ten modified Tx28 PC girders were designed, cast, and tested to evaluate their ultimate shear strength using different concrete strength. The modified cross-section is derived by scaling down Tx54 with 80 inches wide top slab by around 43%. The girders were divided into three groups (namely Groups A, C and F) based on the concrete compressive strength. Group A consisted of two girders with a concrete compressive strength of 7000 psi. Group F had four girders with a concrete compressive strength of 13000 psi and Group C included four girders with a compressive strength 16000 psi. The study included their behavior at different shear-span-to-depth ratio (a/d) and with different ratios of transverse steel.
- (2) Six full-scale prestressed concrete I-girders were designed, cast, and tested with three different sizes of the Tx-series to study their end zone behavior and if prestressing tendon slip affects the web shear capacity. The girders were divided into three groups based on their sizes. Group G consisted of two Tx28 girders. Group D had two Tx46 girders and Group E included two Tx-62 girders. The two girders in each group had a different design as follows:
 - a. The first girder in each group was designed and cast with transverse reinforcement according to TxDOT specifications. Top slab with the same width as the top flange was added after tendon releasing. These girders were tested at different shear-span-to-depth ratio (a/d) to check if the studied cross-sections designed and cast according to current specifications can reach their web shear capacities without having a shear bond failure.
 - b. The second girder in each group was designed and cast with minimum transverse reinforcement to check the minimum web shear capacity of the studied cross-sections at the end zone according to AASHTO LRFD provisions (2010).
- (3) A simple and accurate shear design provision that was developed recently at the University of Houston was validated for high strength concrete and different girders sizes based on the results of the current experimental research work. The new provision consists of three

equations. The first equation was derived for the maximum shear strength ($V_{n,max}$) to ensure the yielding of transverse steel before the crushing of concrete. $V_{n,max}$ is a function of the square root of the concrete strength ($\sqrt{f'_c}$) and the web dimensions ($b_w d$). The second equation was derived to predict the “concrete contribution” (V_c) which is also proportional to the square root of the concrete strength ($\sqrt{f'_c}$) and the web dimensions ($b_w d$) and inversely proportional to the shear span to depth ratio $(a/d)^{0.7}$. The third equation is for estimating the “steel contribution” (V_s) based on the minimum number of transverse steel bars intersecting a 45° crack.

- (4) Recently, the constitutive models of prestressed concrete were developed at the University of Houston and implemented into OpenSees to develop a computer program called Simulation of Concrete Structures (SCS). The tested PC girders in this research work were used to validate the capability of SCS to simulate the shear behavior of different sizes of prestressed concrete girders with different concrete strength f'_c , shear-span-to-depth ratio (a/d), and transverse steel ratio.

10.2. Major Conclusions

Based on the experimental and analytical results of the PC girders, the following conclusions can be derived:

- (1) The experimental data shows that the real Tx-girders designed according to the current specifications have no cracks under service loads.
- (2) The shear behavior of ten Mod. Tx28 and six full-scale Tx-series I-girders with different concrete strength was tested until either web-shear or flexure-shear failure. From the experimental results of ten Mod. Tx28 I-girders and six full scale Tx girders, the UH equation can accurately predict the ultimate shear strength of PC girders having concrete strength up to 17,000 psi. The proposed UH equation is not as overly conservative as the ACI 318 (2011) code provisions. On the other hand, shear design provisions of AASHTO LRFD (2010) code overestimate the ultimate shear strength for PC girders with high strength concrete. From the experimental results of six full-scale Tx-series I-girders, no shear bond failure was found.

- (3) The tested girders either according to TxDOT current design specifications or with the minimum transverse reinforcement according to AASHTO LRFD (2010) have no shear bond failure.
- (4) The experimental results of 16 PC I-girders shows that the UH equation for predicting the concrete shear contribution (V_c) in a PC girder remains valid for high strength concrete up to 17,000 psi with different shear span to depth ratio and different ratios of transverse steel. Also it is applicable for girders with different depths and web depth to thickness ratios.
- (5) The experimental results of 16 PC I-girders shows that the UH equation for predicting the ultimate shear strength is not affected by the girder size. It is applicable for girders with different depths and web depth to thickness ratios.
- (6) The minimum amount of shear reinforcement recommended by AASHTO LRFD (2010) is sufficient to prevent immediate and sudden failure of large PC girders up to 62 inches in depth. Also the end zone reinforcement available in current provisions to resist the bursting forces and to prevent the end zone cracks is applicable for PC girders with depths up to 62 inches.
- (7) The experimental results shows that UH method ensures adequate ductility at the estimated ultimate shear strength, which is required to provide warning before failure.
- (8) The computer program SCS developed recently at the University of Houston using the constitutive models of prestressed concrete derived by the Universal Panel Tester is able to accurately predict the shear behavior of prestressed concrete girders with concrete strength up to 17,000 psi and with depth up to 70 inches under monotonic loads.

10.3. Suggestions for Future Work

Several ideas for future studies could be suggested based on the work presented in this research:

- (1) Review of the tests by other researchers in this study indicates that the shear strengths of PC girders is not affected by the amount of prestressing force, but the behavior in terms of pre-cracking and post-cracking stiffness is affected. More experimental work need to be done to ensure the validity of the University of Houston design provision as well as the SCS finite element program for partially prestressed concrete girders.

- (2) This study shows that the SCS program is capable of predicting the behavior of prestressed high strength concrete structures under monotonic loading. Further experimental work needs to be conducted to validate its capability of predicting the behavior of high strength concrete structures under cyclic loading.

REFERENCES

- AASHTO (1994), "AASHTO LRFD Bridge Design Specifications," 1st Ed., American Association of State Highway and Transportation Officials (AASHTO), Washington, D. C.
- AASHTO (1996), "Standard Specification for Highway Bridges" 16th Ed., American Association of State Highway and Transportation Officials (AASHTO)
- AASHTO (2007), "AASHTO LRFD Bridge Design Specifications," 4th Ed., American Association of State Highway and Transportation Officials (AASHTO), Washington, D. C.
- AASHTO (2010), "AASHTO LRFD Bridge Design Specifications," 4th Ed., American Association of State Highway and Transportation Officials (AASHTO), Washington, D. C.
- Abrishami, H. and Mitchell, D. (1993), "Bond Characteristics of Pretensioned Strand," ACI Structural Journal, Vol. 90, No. 3, pp. 228-235.
- ACI 363R-92 (1997) "State-of-The-Art Report on High Strength Concrete," ACI Committee Report, 55 PP.
- ACI-318, (2011) "Building Code Requirements for Structural Concrete Commentary," American Concrete Institute, Farmington Hills, Michigan.
- Arthur, P.D. (1965), "The Shear Strength of Pretensioned I Girders with Unreinforced Webs," Magazine of Concrete Research, Vol. 17, No. 53, Dec., pp 199-210.
- Barnes, R. W., Grove, J. W., and Burns, N. H. (2003), "Experimental Assessment of Factors Affecting Transfer Length," ACI Structural Journal, Vol. 100, No. 76, pp. 740-748.
- Belarbi, A. and Hsu, T. T. C. (1994), "Constitutive Laws of Concrete in Tension and Reinforcing Bars Stiffened by Concrete," ACI Structural Journal, Vol. 91, No. 4, pp. 465-474.
- Belarbi, A. and Hsu, T. T. C. (1995), "Constitutive Laws of Softened Concrete in Biaxial Tension-Compression," ACI Structural Journal, Vol. 92, No. 5, pp. 562-573.
- Bennett, E.W. and Balasooriya, B.M.A (1971), "Shear Strength of Prestressed Girders with Thin Webs Failing in Inclined Compression," ACI Journal, Proceedings, Vol 69, No. 3, pp 204-212.
- Billet, D.F. and Appleton, J.H. (1954), "Flexural Strength of Prestressed Concrete Girders," ACI

- Journal, Vol. 25, No. 10, pp 837-854.
- Bruce, R.N. (1962), "An Experimental Study of the Action of Web Reinforcement in Prestressed Concrete Girders," PhD Dissertation, University of Illinois Urbana.
- Elzanaty, A. H., Nilson, A. H., and Slate, F. O. (1986), "Shear Capacity of Prestressed Concrete Girders Using High-Strength Concrete," ACI Journal, Vol. 83, No. 3, pp. 359-368.
- Evans, R.H. and Schumacher, E.G. (1963), "Shear Strength of Prestressed Girders without Web Reinforcement," ACI Journal, Proceedings, Vol. 60, No. 11, Nov., pp 1621-1642.
- Fenves, G. L. (2005), "Annual Workshop on Open System for Earthquake Engineering Simulation," Pacific Earthquake Engineering Research Center, UC Berkeley, <http://opensees.berkeley.edu/>.
- Giaccio. C., Al-Mahaidi, R., and Taplin, G., (2002) "Experimental study on the effect of flange geometry on the shear strength of reinforced concrete T-beams subjected to concentrated loads" Can. J. Civ. Eng. Vol. 29, 2002.
- Hanson, N. W., and Kaar, P. H.. (1959). "Flexural bond tests of pretensioned prestressed beams". ACI Journal. Proceedings 55(7): 783–802.
- Hanson, J.M. and Hulsbos, C.L. (1965), "Overload Behavior of Pretensioned Prestressed Concrete I-Girders with Web Reinforcement," Highway Research Record 76, Highway Research Board, pp 1-31.
- Hawkins, N. M., and Kuchma, D. A. (2005), "Application of LRFD Bridge Design Specifications to High-Strength Structural Concrete: Shear Provisions," Final Report to National Cooperative Highway Research Program, University of Illinois, Urbana, IL, USA, 283 pp.
- Hernandez, G. (1958), "Strength of Prestressed Concrete Girders with Web Reinforcement," Report, The Engineering Experiment Station, University of Illinois, Urbana, Illinois.
- Hicks, A.B. (1958), "The influence of Shear Span and Concrete Strength upon the Shear Resistance of Pretensioned Prestressed Concrete Girders," Thesis submitted to the University of London for the degree of M.Sc. (Eng.), pp 119.
- Holmberg, Åke, and Lindgren, S. (1970). Anchorage and prestress transmission. Document D1.

Stockholm: National Swedish Institute for Building Research.

- Hoyer, E., and E. Friedrich. (1939). Beitrag zur frage der haftspannung in eisenbetonbauteilen
“Contribution to the question of bond stress in reinforced concrete elements”. Beton und
Eisen 38(March 20).
- Hsu, T. T. C. and Zhang, L. X. (1996), “Tension Stiffening in Reinforced Concrete Membrane
Elements,” ACI Structural Journal, Vol. 93, No. 1, pp. 108-115.
- Hsu, T. T. C. and Zhu, R.R.H. (2002), “Softened Membrane Model for Reinforced Concrete
Elements in Shear,” ACI Structural Journal, Vol. 99, No. 4, pp. 460-469.
- Janney, Jack R. (1963). “Report of stress transfer length studies on 270 k prestressing strand”.
PCI Journal 8(1): 41–45.
- Kar, J. N. (1969), “Shear Strength of Prestressed Concrete Girders Without Web
Reinforcement,” Magazine of Concrete Research, Vol. 21, No. 68, pp. 159-170.
- Kaufman, M.K. and Ramirez, J.A. (1988), “Re-evaluation of Ultimate Shear Behavior of High-
Strength Concrete Prestressed I-Girders,” ACI Structural Journal, Vol. 85, No. 3, pp 295-
303.
- Kuchma, D., Kim, K. S., Nagle, T. J., Sun, S., and Hawkins, N. M., (2008), “Shear Tests on
High-Strength Prestressed Bulb-Tee Girders: Strengths and Key Observations,” ACI
Journal, V. 105, No. 35, pp. 358-367.
- Laskar, A., Wang, J., Hsu, T.T.C., and Mo, Y.L. (2007), “Rational Shear Provisions for
AASHTO LRFD Specifications,” Technical Report 0-4759-1 to Texas Department of
Transportation, Department of Civil and Environmental Engineering, University of Houston,
Houston, TX, USA, 216 pp.
- Laskar, A., (2009), “Shear Behavior and Design of Prestressed Concrete Members,” PhD
dissertation, Department of Civil and Environmental Engineering, University of Houston,
Houston, TX, 322 pp.
- Laskar, A., Hsu, T.T.C., and Mo, Y.L. (2010), “Shear Strength of Prestressed Concrete Beams
Part 1: Experiments and Shear Design Equations” ACI Journal, V. 107, No. 3, pp. 330-339.
- Loov, R. E. (2002), “Shear Design of Uniformly Loaded Girders,” Presented at the Sixth

International Conference on Short and Medium Span Bridges, Vancouver, Canada, July 31 – August 2, 2002.

- Lyngberg, B. S. (1976), “Ultimate Shear Resistance of Partially Prestressed Reinforced Concrete I-Girders,” *ACI Journal*, V. 73, No. 4, pp. 214-222.
- Ma, Z. J., Tadros, M. K. and Baishya, M. (2000), “Shear Behavior of Pretensioned High-Strength Concrete Bridge I-Girders,” *ACI Structural Journal*, Vol. 97, No. 1, Jan.-Feb., pp. 185-193.
- MacGregor, J. G., Sozen, M. A., and Siess, C. P. (1960), “Strength and Behavior of Prestressed Concrete Girders with Web Reinforcement”, Report, The Engineering Experiment Station, University of Illinois, Urbana, Illinois.
- Mahgoub, M.O. (1975), “Shear Strength of Prestressed Concrete Girders without Web Reinforcement,” *Magazine of Concrete Research*, Vol. 27, No. 93, Dec., pp. 219-228.
- Mansour, M. (2001), “Behavior of Reinforced Concrete Membrane Elements under Cyclic Shear: Experiments to Theory,” PhD dissertation, Department of Civil Engineering, University of Houston, August 2001.
- Mansour, M. and Hsu, T. T. C. (2005a), “Behavior of Reinforced Concrete Elements under Cyclic Shear: Part 1 – Experiments,” *Journal of Structural Engineering*, ASCE, Vol. 131, No. 1, January, 2005, pp. 44-53.
- Mansour, M. and Hsu, T. T. C. (2005b), “Behavior of Reinforced Concrete Elements under Cyclic Shear: Part 2 - Theoretical Model,” *Journal of Structural Engineering*, ASCE, Vol. 131, No. 1, January, 2005, pp. 54-65.
- Mansour, M., Hsu, T. T. C., and Lee, J. Y., (2001a), “Pinching Effect in Hysteretic Loops of R/C Shear Elements,” *ACI Special Publication 205: Finite Element Analysis of Reinforced Concrete Structures*, K. William and A. Tanabe (eds), American Concrete Institute, Farmington Hill, MI, pp. 293-321.
- Mansour, M., Lee, J. Y., and Hsu, T. T. C. (2001b), “Constitutive Laws of Concrete and Steel Bars in Membrane Elements under Cyclic Loading,” *Journal of Structural Engineering*, ASCE, Vol. 127, No. 12, Dec. 2001, pp. 1402-1411.

- Marshall, W. T., and Mattock, A. H. (1962), "Control of Horizontal Cracking in the Ends of Pretensioned Prestressed Concrete Girders," PCI JOURNAL, V. 7, No. 5, October 1962, pp. 56-74.
- Mattock, A.H. and Kaar, P.H. (1961), "Precast-Prestressed Concrete Bridges – 4: Shear Tests of Continuous Girders," Journal of the PCA Research Development Laboratories, pp 19-47.
- McClarnon, F.M.; Wakabayashi, M; and Ekberg, C.C. Jr. (1962), "Further Investigation into the Shear Strength of Prestressed Concrete Girders without Web Reinforcements," Report No. 223.22, Fritz Engineering Laboratory, Lehigh University, Bethlehem, Pennsylvania.
- Mullapudi, T.R.S., (2010), "Seismic Analysis of Reinforced Concrete Structures Subjected to Combined Axial, Flexure, Shear and Torsional Loads," PhD dissertation, Department of Civil and Environmental Engineering, University of Houston, Houston, TX, 328 pp.
- Mullapudi, T.R.S., Ayoub, A.S., (2010) "Modeling of the Seismic Behavior of Shear-Critical Reinforced Concrete Columns," Journal of Engineering Structures, Vol. 32, No.11, pp. 3601-15.
- Myers, J.J., and Carrasquillo, R.L., (1999), "Mix Proportioning for High-Strength HPC Bridge Girder," American Concrete Institute, Detroit, MI, Special Publication 189, Fall 1999, pp. 37-54
- NCHRP 579 (2007). "Application of LRFD Bridge Design Specifications to High-Strength Structural Concrete: Shear Provisions," NCHRP Report 579, Transportation Research Board, sponsored by ASSHTO and FHWA.
- NCHRP 603 (2008). "Transfer, Development, and Splice Length for Strand/Reinforcement in High-Strength Concrete" NCHRP Report 603, Transportation Research Board, sponsored by ASSHTO and FHWA.
- Pang, X. B. and Hsu, T. T. C. (1995), "Behavior of Reinforced Concrete Membrane Elements in Shear," ACI Structural Journal, Vol. 92, No. 6, pp. 665-679.
- Pang, X. B. and Hsu, T. T. C. (1996), "Fixed-Angle Softened-Truss Model for Reinforced Concrete," ACI Structural Journal, Vol. 93, No. 2, pp. 197-207.
- Pansuk, W., and Sato, Y., (2007), "Shear Mechanism of Reinforced Concrete T-Beams with

- Stirrups,” *Journal of Advanced Concrete Technology*, Vol. 5, No. 3, pp. 395-408.
- Rangan, B. V. (1991), “Web Crushing Strength of Reinforced and Prestressed Concrete Girders,” *ACI Journal*, Vol. 88, No. 1, pp. 12-16.
- Rizkalla, S., Zia, P., Mirmiran, A., Russell, H. G., and Mast, R. (2009) “Proposal for Concrete Compressive Strength Up to 18 ksi (124 MPa) for Bridge Design,” *Journal of the Transportation Research Record*, No. 2131, pp. 59-67.
- Robertson, I.N. and Durrani, A.J., (1987) “ Shear Strength of Prestressed Concrete T Girders with Welded Wire Fabric as Shear Reinforcement,” *PCI Journal*, Vol.32, No. 2, pp. 46-61.
- Shahawy, M. A. and Batchelor, B. (1996), “Shear Behavior of Full-Scale Prestressed Concrete Girders: Comparison Between AASTHO Specifications and LRFD Code,” *PCI Journal*, Precast/Prestressed Concrete Institute, Vol. 41, No. 3, pp. 48-62.
- Stocker, M.F., and Sozen, M.A. (1970). “Investigation of prestressed concrete for highway bridges, part v: bond characteristics of prestressing strand. ” Bulletin 503. Urbana: University of Illinois Engineering Experiment Station.
- Taucer, F.T., Spacone, E., and Filippou, F.C. (1991), “A Fiber Girder-Column Element for Seismic Response Analysis of Reinforced Concrete Structures,” Report No. UCB/EERC-91/17, University of California Berkeley.
- Teoh, B.K., Mansur, M.A., and Wee, T.H. (2002), “Behavior of High Strength Concrete I-Girders with Low Shear Reinforcement,” *ACI Structural Journal*, Vol 93, No 3, May-June 2002, pp 299-307.
- Tuan, C. Y., Yehia, S. A., Jongpitaksseel, N., and Tadros, M. K. (2004) “End Zone Reinforcement for Pretensioned Concrete Girders”, *PCI Journal*, May-June 2004
- Wang, J. (2006), “Constitutive Relationships of Prestressed Concrete Membrane Elements,” Ph.D. Dissertation, Department of Civil and Environmental Engineering, University of Houston, Houston, TX.
- Yerlici, V. A., and Özturan, T., (2000), “Factors Affecting Anchorage Bond Strength in High-Performance Concrete”, *ACI Structural Journal* vol. 97, pp 499-507
- Zararis, L. P., Karaveziroglou, M. K., and Zararis, P. D. (2006), “Shear Strength of Reinforced

Concrete T-Beams”, ACI Structural Journal vol. 103, pp 693-700

Zhang, L. X. and Hsu, T. T. C. (1998), “Behavior and Analysis of 100Mpa Concrete Membrane Elements,” Journal of Structural Engineering, ASCE, Vol. 124, No. 1, Jan. 1998, pp. 24-34.

Zhong, J. X. (2005), “Model-Based Simulation of Reinforced Concrete Plane Stress Structures,” Ph.D. Dissertation, Department of Civil and Environmental Engineering, University of Houston, Houston, TX.

Zienkiewicz, O. C., and Taylor, R. L. (1989), “The Finite Element Method Volume 1. Basic Formulation and Linear Problems”, Fourth Edition. McGraw Hill, London.

Zwoyer, E.M. and Siess, C.P. (1954), “Ultimate Strength in Shear of Simply-Supported Prestressed Concrete Girders Without Web Reinforcement,” ACI Journal, Proceedings, Vol. 51, No. 2, pp 181-200.

